

AN EXPERIMENTAL STUDY ON MECHANICAL PROPERTIES OF FLY-ASH-GYPSUM BRICKS

T. U. Ahmed, M. Ashikuzzaman* & Z. Alam

*Department of Civil Engineering, Rajshahi University of Engineering & Technology,
Rajshahi-6204, Bangladesh*

E-mail: ashik.amjr120116@yahoo.com

**Corresponding author*

ABSTRACT

Bricks are such an element that can't be thought of to construct a house. Usually, burnt clay bricks is using to meet the ambition but to do so, a large amount of soil is removing for the production of clay bricks. This paper reveals the mechanical properties of fly ash bricks taking different proportions of fly-ash, gypsum, sand and a fixed amount of cement. To perform this research a varieties of tests were conducted i.e., compressive strength, water absorption, unit volume weight, apparent porosity, open pore, and impervious pore in the laboratory. Ingredients were being used to produce the bricks at four proportions of using fly-ash (50%, 55%, 60%, 65%), gypsum (12%, 9%, 6%, 3%), sand (28%, 26%, 24%, 22%) respectively and 10% of cement in each and every proportions. All the weighted materials were mixed in a mixing pan until the homogeneous mixture attained and then added 80 ml of water considering the total volume of the brick mold. Then the mortar was placed to a mold of 9.5cm x 4.5cm x 2.75cm which is the ratio in cm scale of traditional brick using in Bangladesh. ASTM code of practice was followed to conduct the tests of this research. From the study, it is concluded that proportion no. 1 shows the good quality of bricks which can be employed as an alternative to the conventional burnt clay bricks.

Keywords: Fly-ash bricks, compressive strength, water absorption, unit volume weight, apparent porosity, open pore, impervious pores and apparent specific gravity.

INTRODUCTION

Brick is one of the most widely used construction materials, now a days. Manufacturing of bricks consume larger amount of clay which leads to top soil remover and land degradation. In brick kilns, the firing of bricks causes serious environmental pollution and health problem. Environmental value is the people's cognition on belief, attitude, rational consideration and value of the environment. In 1995 O. Brien and Guerrier pointed that environmental value is advisory and supportive activities of environmental concern and responsibility. McMilln et al. (2004) investigated that fly ash is a byproduct which is generated from thermal power plants and industries and its disposal causes a serious environmental problem. Fly ash brick is a building material, specifically masonry units, containing class C and class F fly ash and water. Fly ash is generally evaluated in cement and concrete production as an inexpensive pozzolanicblending material, Pei-wei et al. (2007). Lingling et al. (2005) conducted a scientific study to find out the effect of wet fly ash in burnt clay brick replacing a high volume of ratio. They finally got a conclusion that the plasticity index for both fly ash and clay had the proportional relationship in nature. They also made conclusion replacing clay by high amount of fly ash can improve compressive strength as well as gave low water absorption, no cracking and high strength during the melting of the frost. Gourav and Reddy (2018) tried to reveal the causes behind the clay-fly ash-gypsum-lime masonry. They also experimented their materials i.e., SEM, XRD, and TGA for the investigation. In the conclusion, chemical bonding took place among those materials. Cultrone and

Sebastian (2008) conducted a research to develop strength of solid bricks using fly ash in five proportions. Naganathan et al. (2015) conducted to search the performance of traditional bricks using fly ash and bottom ash together. They concluded that compressive strength was a range from 7.13 to 17.36 MPa and UPV was from 2.2 to 2.96 km/s. They also found that at the time of increasing the percentage of fly ash resulted the decreased of the water absorption. Tayfun and Yasin (2015) conducted to find the possibility of the production of light weight bricks considering fly ash and lime, and they concluded that it can be utilized as an alternative means of the conventional burnt clay bricks. Fly ash bricks are lighter and stronger than clay bricks. Now a days it has become more popular than clay bricks in most of the country like India, China. In India, The Ministry of Environment and Forests issued directives for proper utilization of fly ash discharged from coal or lignite-based thermal power plants (Gazette of India). In Bangladesh, it is estimated that 1.3 million cubic feet of fly ash is produced per annum for dumping from thermal power plants. There are 6 potential coal fields which have been identified till date, out of which only one, Barapukuria coal field is in production.

MATERIALS AND METHODOLOGY OF TESTING PROGRAM

Raw Materials

Fly Ash

Fly ash is collected after the combustion of coal in almost every portion of the kilnker. The chemical composition of the fly ash were tested and presented in table 1. Class “F” fly ash was used to make mortar for the production of the bricks. Fly ash was collected from Noapara, Jessore to do the research.

Table 1. Chemical composition of fly-ash

Compound	SiO ₂	Al ₂ O ₃	Fe ₂ O ₃	CaO	MgO
Mass fraction, %	62.45	21.4	6.58	1.25	0.55

Gypsum

Hydrated calcium sulphates are called gypsum (CaSO₄.2H₂O). Basically, gypsum doesn't create any adverse effect to the environment, human beings, animals, and plants. It is moderately water soluble. Gypsum blocks are used like concrete blocks in building construction. Gypsum was also collected from Noapara, Jessore to do the research

Sand

Locally available sands were used in this study. To perform the research sands were collected from the construction site of Architectural Building of RUET. Specific gravity and fineness modulus were tested in the laboratory to see the physical properties, and the specific gravity and fineness modulus of sand were 2.78 and 2.34 respectively.

Cement

Cement is a binder, a substance used for construction that sets, hardens and adheres to other materials, binding them together. Ordinary Portland Cement was used in this study. The physical properties used are given in table 2.

Table 2. Physical properties of ordinary Portland cement

No	Characteristics	Value obtained experimentally
1	Specific gravity	3.14
2	Setting time(minutes)	
	Initial	75
	Final	610

Mixing of Raw Materials

Raw materials including fly ash, gypsum, sand, cement and water were prepared for mixing to make mortar blocks in certain proportion of weight. For each proportion, the required materials were calculated correctly and the materials were weighted properly. The percentages of materials required for fly-ash bricks and weight of the materials are given in table no 3 according to brick sample no.

Table 3. Mixing proportion of raw materials and brick sample no.

Proportion no.	Brick Sample No.	Fly ash (%)	Gypsum (%)	Sand (%)	Cement (%)	Water (ml)
		Weight (gm)	Weight (gm)	Weight (gm)	Weight (gm)	
1	A	50	12	28	10	80
		119	31	88	35	
2	B	55	9	26	10	80
		131	24	82	35	
3	C	60	6	24	10	80
		143	16	76	35	
4	D	65	3	22	10	80
		155	8	70	35	

Preparation of Brick Sample

For the preparation of brick sample, a brick mould was used which inner diameter was 9.5cmX4.5cmX2.75cm. After preparation of the mixing raw materials following the raw materials proportion chart, they were placed in the mould and a compaction procedure was done. The mortar was compacted using digitec concrete compression machine. The load was applied with average load of 35-40 KN. Sixteen specimens were prepared, four samples of each proportion. After that the brick forming load from the screen of the digitec concrete compression machine was recorded.

Curing Procedure

After compaction, the brick samples were taken out from the mould after 2 minutes. Air curing is the process of preserving or drying by exposure to air and water curing is the process of controlling the rate of moisture loss from concrete during cement hydration. So some of the samples were kept in air for 14 days and others were kept in water for 14 days including 3 days kept in air before curing.

Table 4 Curing process and curing period of brick sample

Proportion No.	Brick sample	Brick No.	Curing process (Air)	Brick No.	Curing Process (Air)	Curing Process (Water)
1	A	A ₁	14	A ₃	3	14
		A ₂		A ₄		
2	B	B ₁	14	B ₃	3	14
		B ₂		B ₄		
3	C	C ₁	14	C ₃	3	14
		C ₂		C ₄		
4	D	D ₁	14	D ₃	3	14
		D ₂		D ₄		

Method of Testing

Compressive Strength Test

Compressive strength was determined by applying load on the specimen using a digitec concrete compression machine. No factor was applied to attain the actual compressive load and actual compressive strength.

Water Absorption Test

The specimens were dried in a ventilated oven at a temperature of 105°C to 115°C for 24 hours. Then these were cooled at room temperature and obtained its weight (M_1). These were immersed in clean water for 24 hours. Finally, the specimens were removed and wiped out and obtained the weight (M_2). Water absorption test, (%) by mass were conducted by following IS:3495 and the formula is given in Eq (1),

$$x = \frac{M_2 - M_1}{M_1} \times 100 \quad (1)$$

The value of the test results were taken carefully.

Unit Volume Weight

After curing, the bricks were then dried at oven maintain the temperature of about 110 degree centigrade for 24 hours and kept them t make the room temperature. After that the bricks were put to the water to make immersed maintain room temperature and at that time the suspended weight was also recorded. Then the bricks removed from the water and by using a cloth the water was wiped off and saturated weight was measured. Dry weight, D gm, Suspended weight, S gm, Saturated weight, W gm were noted in a note book. Unit volume weight B, gm/cm³ = D/ V, where volume V, cm³ = (W - S) was evaluated.

Apparent Porosity, Open Pore and Impervious Pore

To calculate the apparent porosity, open pore and impervious pore, ASTM code of practice (C 67-00) was used. The following equations were employed to determine the Apparent porosity P, % = [(W - D)/ V], Open pore volume, cm³ = W - D and impervious pore volume, cm³ = D - S.

RESULTS AND DISCUSSION

The mechanical properties of the specimen such as compressive strength, water absorption, unit volume weight, apparent porosity, open pore volume and impervious pore volume were determined by following standard laboratory test method. From the calculation, test results and graph figure, the optimum values were found showing in the Figs 1, 2, 3, 4, 5 and 6.

For air dried curing, the optimum value of compressive strength, average value of each sample was found in proportion no. 1 from the Table 3, shown in Fig 1. For water curing, the optimum value of compressive strength, average value of each sample was found in proportion no. 1 from the Table 3, shown in Fig 1(a). For water absorption test, the lower average value of each sample was found in proportion no. 1 from the Table 3, shown in Fig 1(b).

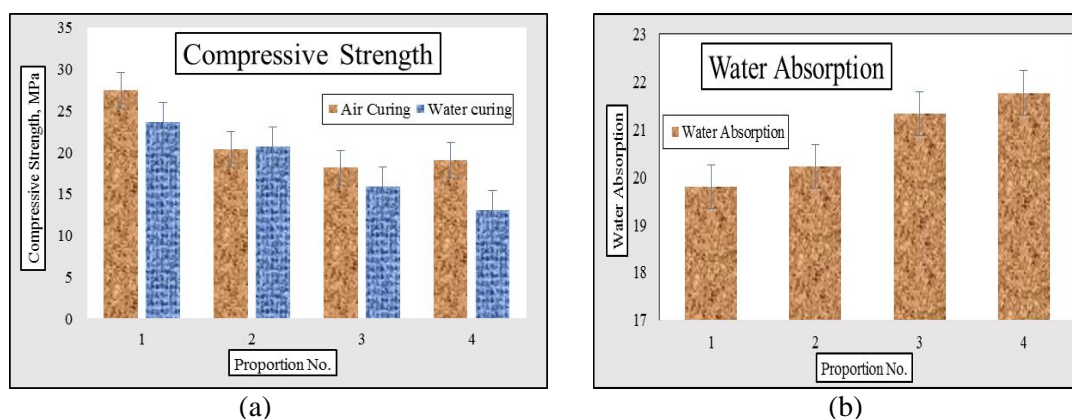


Fig. 1 Mechanical Properties, (a) Compressive strength test result in air dried and water curing condition; (b) Water absorption test result in various proportion

For unit weight volume test result, the maximum average value of each sample was found in proportion no. 1, shown in Fig. 2(a). For Apparent porosity test result, the maximum average value of each sample was found in proportion no. 3, shown in Fig. 2(b).

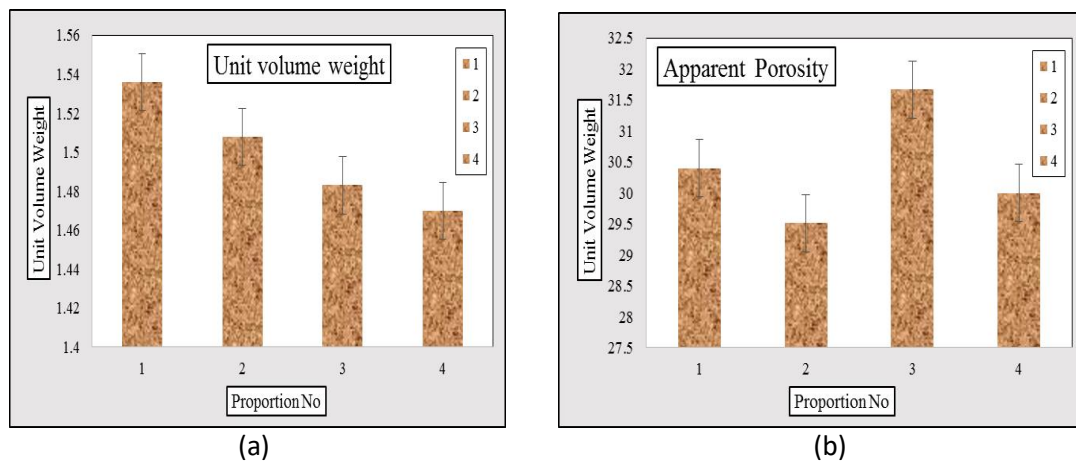


Fig. 2 Mechanical Properties, (a) Unit volume test results; (b) Apparent Porosity results of fly ash bricks

For open pore volume tests result, the value of each proportion is shown in Fig. 3(a). For impervious pore volume tests result, the value of each proportion is shown in Fig. 3(b).

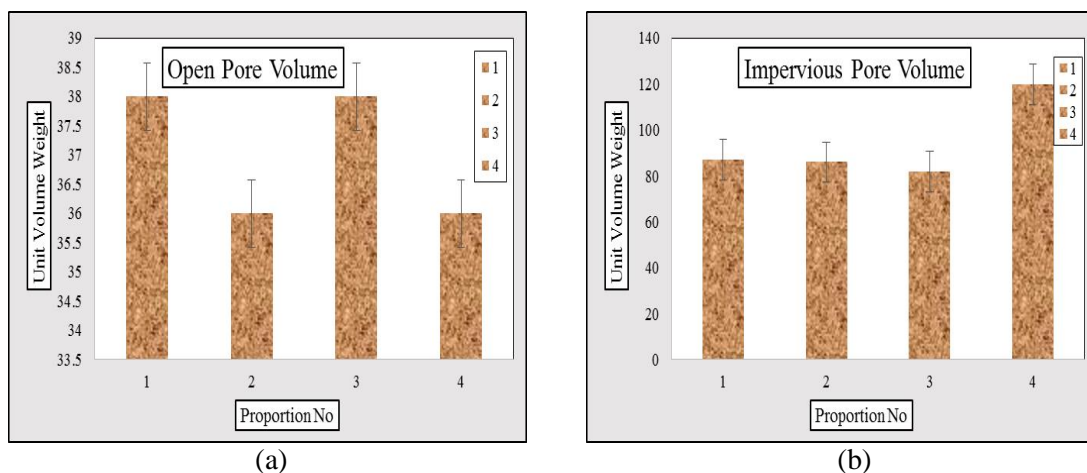


Fig. 2 Mechanical Properties, (a) Open pore volume test results; (b) Impervious pore volume test results in various proportions

CONCLUSIONS

The chemical composition shows a very high amount sandy properties in fly ash (62.45% SiO₂) and also a high amount Alumina (21.4%). The chemical reactions were taken place to form a harder block among fly-ash, gypsum, sand, and cement. At the wet stage, fly ash reacts very quickly with gypsum. But attaining the full hydration, generally it takes lot of time. From figure 1(a), it is shown that compressive strength of water curing is higher than air curing but in proportion no. 3 and 4, compressive strength in air curing is higher than water curing. This was happened because of the early time hydration. It can be also seen from figs 2 and 3 that proportion no. 1 relatively god results from the other proportions of the fly ash bricks mixture. More bricks also should be checked to find relationships among the properties. Considering all the test results, it can be said that fly ash brick can be used as a building material to reduce the deduction of soil from the earth.

REFERENCES

- Cultrone, G and Sebastian, E. (2008). Fly ash addition in clayey materials to improve the quality of solid bricks. *Construc. Bulid. Mate.* 23, 1178-184.
- Gazette of India, Part II. (1999). sub section (ii), vide S.O.763(E).
- Gourav, K and Reddy, BVV. (2008). Bond development in burnt clay and fly ash-lime-gypsum brick masonry. *Jour. Mate. Civ. Engr.* 30(9), 04018202.
- Lingling, X; Wei, G; Tao, W and Nanru, Y. (2005). Study on fired bricks with replacing clay by fly ash in high volume ratio. *Construc. Build. Mate.* 19, 243-247.
- McMillan, EE; Wrught, T and Beazley K. (2004). Impact of a university-level environmental studies class on students' values. *Journal Environ. Educ. HDREF.* 35(3), 19–21.
- Naganathan, P; Mohemed, AYO and Mustapha, KN. (2015). Performance of bricks made using fly ash and bottom ash. *Construc. Biuld. Mate.* 96, 576-580.
- Pei-wei, G; Xiao-li, L; Hui, L; Xiaoyan, L and Jie, H. (2007). Effects of the fly ash on the properties of environmentally friendly dam concrete. *Fuel.* 86, 1208–11.
- Tayfun, C and Yasin, C. (2015). Use of fly ash in production of light-weight building bricks. *Construc. Biuld. Mate.* 94, 521-527.

AN EXPERIMENTAL INVESTIGATION ON THE PERFORMANCE OF BACTERIAL CONCRETE

S. N. Priyom*, M. Islam, and S. Islam³

Department of Civil Engineering, Chittagong University of Engineering & Technology, Chittagong, Bangladesh

Email: sudiptonathpriyom@gmail.com

**Corresponding Author*

ABSTRACT

Concrete is the most used building material composed of cement, sand, stone and aggregate. Tiny micro-crack is the main reason to cause failure in concrete structure. A noble technique has been developed in recent years to remediate these cracks by incorporating special species (*bacillus*) of bacteria in concrete. These types of bacteria have the capability to secret calcite precipitation and eventually repair the cracks. This paper investigates the performances of bacterial concrete exposed to plain water. Concrete specimens of 100 mm cubical size were cast and cured for 120 days with and without using bacteria. Using spectrophotometer to determine optical density has always been a central technique in microbiology. Concrete specimens having OD₆₀₀ 0.107, 0.20, 0.637 and 1.221 have been studied in plain water. The specimens were taken out periodically and subjected to compressive & tensile strength tests. From the investigation, it has been revealed that microbial concrete having OD₆₀₀ 0.637 shows better resistance against strength deterioration under all curing conditions and curing ages. Later on the concrete specimens were subjected to Ultrasonic Pulse Velocity (UPV) tests. This study proposes the UPV and strength relationship curves for different microbial ratios used in concrete. From this test, it has been observed that specimens having OD₆₀₀ 0.637 shows better pulse velocity. The higher pulse velocity can therefore be used to assess the quality and uniformity of the concrete material.

Keywords: OPC; Microbial Concrete; *Bacillus subtilis*; Optical Density; MICP; UPV test

INTRODUCTION

Concrete is one of the most widely used construction materials by mankind and it is the main material used for the infrastructure development of every country. It has an ultimate load bearing capacity under compression but the material is weak in tension. That is why steel bars are embedded in the concrete for the structures to carry tensile loads. The steel reinforced bars take the tensile load when the concrete cracks in tension. The elasticity of concrete is relatively constant at low stress levels but starts decreasing at higher stress levels as matrix cracking develop. That why concrete is a high maintenance material that cracks and suffers serious wear and tear over the decades of its expected term of service.

Repair of conventional concrete structures usually involves applying a concrete mortar which is bonded to the damaged surface. Sometimes, the mortar needs to be keyed into the existing structure with metal pins to ensure that it does not fall away. Repairs can be particularly time consuming and expensive because it is often very difficult to gain access to the structure to make repairs, especially if they are basements or at a great height. An advance technique has been developed in remediating cracks and fissures automatically

in concrete by utilizing Microbiologically Induced Calcite or Calcium Carbonate (CaCO_3) Precipitation (MICP) which will ultimately increase the durability of concrete structure. By incorporating special species (*bacillus*) of bacteria in concrete these cracks can be repaired as natural healing process. These types of microbes can secrete calcite precipitations which will ultimately repair the cracks and increase the durability of structure.

Ultrasonic pulse velocity (UPV) test is a non-destructive test technique to monitor the post construction performance of concrete. This technique was first introduced by Long, Kurtz and Sandenaw (1945) for evaluating the non destructive method of testing for quality of concrete by transmitting an irrational pulse to travel a known distance through a concrete. In this study, cylindrical specimens of dia 100 mm and height 200 mm were used. Curing period for test was taken as 28 days. 5 different microbial groups having OD_{600} 0, 0.107, 0.20, 0.637 and 1.221 had been studied.

EXPERIMENTAL DETAILS

The experimental work was carried out to study the different aspects of strength development of microbial concrete in plain water over a period of 28 days. The variable parameters studied and the materials involved were as follows:

Materials

(i) Bacteria :

Bacillus subtilis strain 121 has been used in the following study. It was obtained from Micro-biology Department, Chittagong University. Media used was nutrient broth for *B. subtilis* growth. Four different OD_{600} (0.107, 0.20, 0.637 and 1.221) has been used to investigate the performances of bacteria. Absorbance of the cell suspension is also being measured by using 'Spectrophotometer'. The cell concentration varies with optical density and could be roughly determined by following formula:

$$Y = 8.59 \times 10^7 X^{1.362}$$

where,

X = reading at OD 600 nm

Y= concentration of bacterial cells per ml

(ii) Cement :

Ordinary Portland Cement (OPC) ASTM Type-1, conforming to ASTM C-150 was used as binding material. Its physical properties and chemical compositions are given in Table 1.

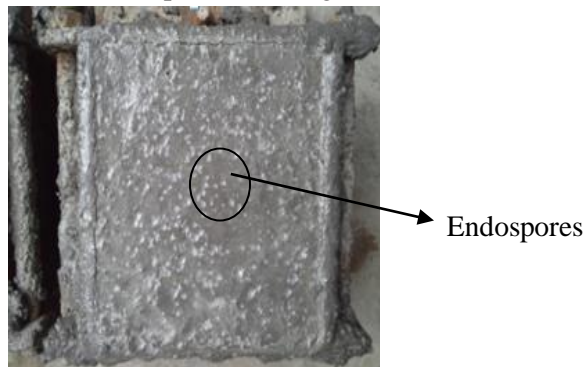


Fig. 1: Microbial Concrete

(iii) Aggregate :

Locally available natural sand passing through 4.75 mm sieve and retained on 0.075 mm sieve was used as fine aggregate. The coarse aggregate was crushed stone with nominal size of 12.5 mm. The properties of aggregates are given in Table 2.

(iv) Water :

Water conforming to the requirements of IS456-2000 was taken with pH value 7 and at zero turbidity.

Table 1: Physical properties and chemical composition of OPC

SL. No	Characteristics	Value
1	Blaine's Specific surface (cm ² /gm)	2900
2	Normal Consistency	26%
3	Soundness by Le Chatelier's Test (mm)	4.5 mm
4	Specific gravity	3.15
5	Setting Time	
	(a) Initial (min)	70
	(b) Final (min)	175
6	Compressive Strength	
	(a) 3 Days (MPa)	16.2
	(b) 7 Days (MPa)	21.2
	(c) 28 Days (MPa)	31.4
7	Calcium Oxide (CaO)	64%
8	Silicon Dioxide (SiO ₂)	21%
9	Aluminum Oxide (Al ₂ O ₃)	6%
10	Ferric Oxide (Fe ₂ O ₃)	3.5%
11	Magnesium Oxide (MgO)	1.2%
12	Sulfur Trioxide (SO ₃)	2.5%
13	Loss on ignition	1.2%
14	Insoluble matter	0.6%

Table 2: Physical properties of aggregate

Properties	Coarse Aggregate	Fine Aggregate
Specific Gravity	2.59	2.55
Unit Weight	1560 Kg/m ³	1580 Kg/m ³
Fineness Modulus	6.77	2.57
Absorption Capacity	0.6%	1.45%
Moisture Content	0.57%	1.12%

Table 3: Properties of microbial water (Absorbance reading: T60 UV-VIS Spectrophotometer @ RT & Absorbance at 600 nm wave length)

Group	Control	Bacterial Treatment	Optical Density
A	0.089	0.196	0.107
B		0.289	0.20
C		0.762	0.637
D		1.31	1.221

Variables

(i) Concrete Quality :

Three different grades of microbial concrete having OD₆₀₀ 0.107, 0.20, 0.637, 1.221 were used. OPC plain concrete was cast for comparing its properties with that of microbial concrete.

(ii) Exposure Period :

Specimens were tested periodically after the specified curing period of 28 days in plain water.

(iii) Size of Specimens :

Cylindrical specimens of 100 mm dia and 200 mm high were used following ASTM standard procedure.

(iv) Curing Environment :

A total of 45 cylindrical concrete specimens were cast in the laboratory. After casting, the specimens were kept at 27°C temperature and 90% relative humidity for 24 hours. After demoulding, all the specimens were cured in plain water for curing at room temperature.

(v) Mix Proportion :

Concrete was designed on the basis of material properties. For a mix design of 20 MPa concrete, the ratio of cement, fine aggregate, coarse aggregate was obtained as 1.0: 2.57: 2.71 with water cement ratio of 0.592 by mass. For 30 MPa concrete the mix ratio was 1.0: 1.68: 2.04 with water cement ratio of 0.45 and for 40 MPa concrete it was 1.0: 1.28: 1.73 with water cement ratio of 0.38 by mass. 100% water by mass

was used for conventional concrete and a water cement ratio of 50% and microbial culture of 50% by mass was used for microbial concrete.

RESULT & DISCUSSION

The ultrasonic pulse velocity of a material can be determined by placing a pulse transmitter on one face of a sample of the material and a receiver on the opposite face. A timing device measures the transit time of the ultrasonic pulse through the material. If the path length is known, then the UPV can be calculated from the path length divided by the transit time. In UPV test, an appropriate coupling agent of petroleum jelly is applied to the transducer diaphragms and over the test surface to avoid air entrap between the contact surfaces of the transducers diaphragms and the surface of concrete. Then the transducers are pressed against the surfaces of the concrete for reasonably good contact between two surfaces and then the transit time is measured. Measurements are repeated at same location to minimize erroneous readings due to poor contact (Ref. Figure: 2).

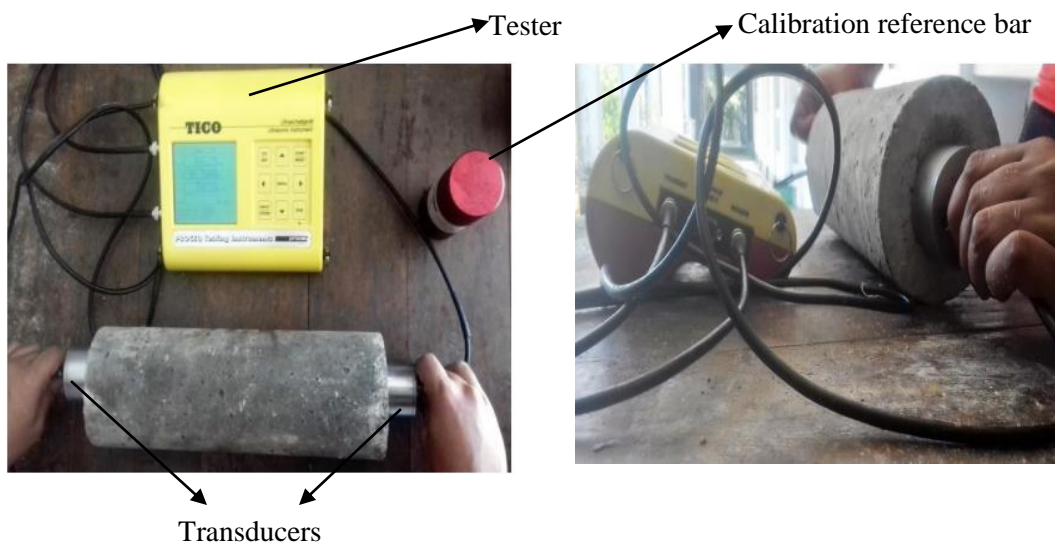


Fig. 2: Ultrasonic Pulse Velocity Measurement Process

It can be seen that concrete specimens having OD_{600} 0.637 have the higher velocity. That means that specimens having OD_{600} 0.637 are denser and more compact than other microbial groups. UPV values for different grades of concrete have been presented in Figure 3.

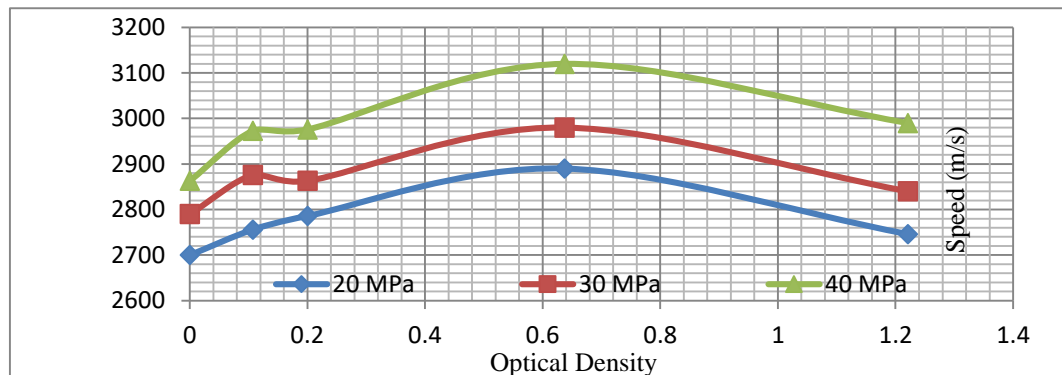


Fig. 3: UPV Values for different grades of concrete specimens with various optical density

Many scientists have studied and mentioned how UPV can be correlated with concrete strength. According to previous research by **Tharmaratnam**, the compressive strength and ultrasonic pulse velocity UPV values are related by the following equation (Non-linear model is suggested):

$$F_c = ae^{bv}$$

Here,

F_c = Compressive strength

V = Pulse velocity (km/s)

a and b are empirical constants

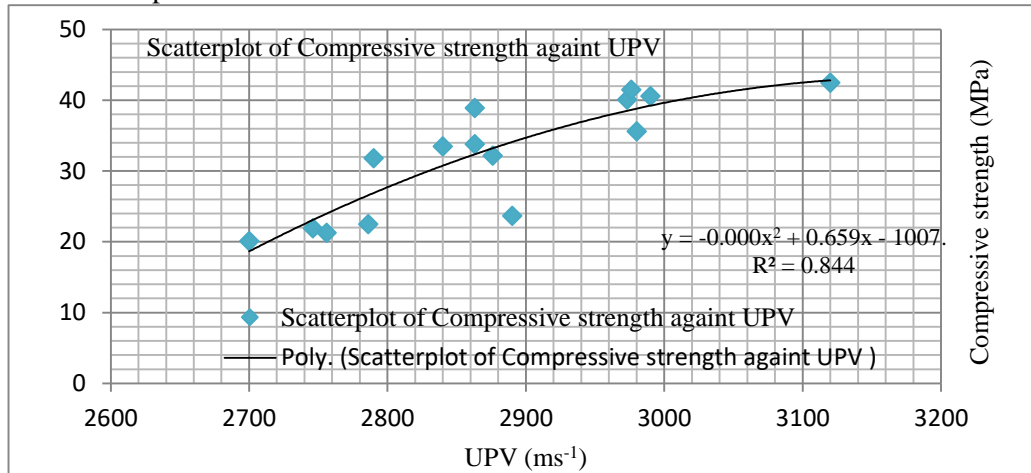


Fig. 4: Correlation between compressive strength against UPV

Considering the test result, the following expression relating compressive strength (F_c in MPa) to UPV (V in m/s) was established:

$$y = -0.000x^2 + 0.659x - 1007$$

$$R^2 = 0.844$$

It was an acceptable polynomial relationship between UPV and compressive strength. Because of $R^2 = 0.844$, it can be said that 84.4% of the variation in the values of compressive strength is accounted for by polynomial relationship with UPV.

CONCLUSION

Based on the limited number of test variables including different concrete grades, the following conclusions can be drawn.

- (i) Bacterial concrete technology has been proved to be better than many conventional technologies because of its eco-friendly nature, self-healing abilities and increase in durability of structural concrete as building materials.
- (ii) Cementation by this method is very easy and convenient for usage. This will soon provide the basis for high quality structures that will be cost effective and environmentally safe but, more work is required to improve the feasibility of this technology from both an economical and practical viewpoints
- (iii) Mix proportion of microbial water with plain water has a significant effect on strength development of microbial concrete. Among the microbial concretes, concrete with OD_{600} 0.637 is found to be most effective in increasing the strength and pulse velocity.
- (iv) It can be seen from the above Figure 4 that 84.4% of the variation in the values of compressive strength is accounted for by polynomial relationship with UPV.
- (v) If the spectrophotometer technique is adequately controlled and the sample is properly calibrated, the estimation of microbial numbers by optical density can be considered sufficiently accurate for use in preparing inoculate for QC testing.

(vi) The study may provide some necessary information related to the use of microbial concretes for the construction of marine onshore / offshore reinforced concrete structures.

REFERENCES

- Anagnostopoulos, C., and Spizzen, J.,(1961)**, Requirements for Transformation in *Bacillus Subtilis*. *J. Bacteriol*, 81:741-746
- Anderson, S., Appanna, V. D., Huang, J., and Viswanatha, T.,(1992)**, A Novel Role for Calcite in Calcium Homeostasis, *FEBS Lett*, 308:94-96
- Barabesi, C., Tamburini, E., Mastromei, G., and Perito, B.,(2003)**, Mechanisms of Microbial Calcium Carbonate Precipitation, p. 472-485, In Koestler, R. J., Koestler, V. R., Charola, A. E., and NietoFernandez, F. E. (ed.), *Art, Biology, and Conservation: Bio-Deterioration of Works of Art*. Metropolitan Museum of Art, New York, NY
- Barabesi, C., Galizzi, A., Mastromi, G., Rossi, M., Tamburini, E., Peritto, B.,** *Bacillus subtilis* Gene Cluster Involved in Calcium Carbonate Biomineralization, Accepted manuscript posted online 3 November 2006, doi: 10.1128/JB.01450-06 *J. Bacteriol.* January 2007 vol. 189 no. 1 228-235
- Bäuerlein, E.,(2003)**, Biomineralization of Unicellular Organisms: Unusual Membrane Biochemistry for the Production of Inorganic Nano- and Microstructures, *Angew. Chem. Int. Ed.*42:614-641
- Douglas, S., and Beveridge, T. J.,(1998)**, Mineral Formation by Bacteria in Natural Microbial Communities, *FEMS Microbiol. Ecol.* 26:79-88
- Ehrlich, H. L.,(1996)**, *Geomicrobiology*. Marcel Dekker, New York
- Ehrlich, H. L.,(1999)**, Microbes as Geologic Agents: Their Role in Mineral Formation, *Geomicrobiol. J.* 16:135-153
- Fortin, D., Ferris, F. G., and Beveridge, T. J.,(1997)**, Surface-Mediated Mineral Development by Bacteria, *Rev. Mineral. Geochem.* 35:161-180
- Gavimath, C. C., Mali, B. M., Hooli, V. R., Mallpur, J. D., Patil, A. B., Gaddi, D. P., Ternikar, C.R., Ravishankera, B.E.,** Potential Application of Bacteria to Improve The Strength of Cement Concrete, *International Journal of Advanced Biotechnology and Research*, ISSN 0976-2612, Vol 3, Issue 1, 2012, pp 541-544
- Geymayr, August, G. W.,(1980)**, Repair of Concrete in Tropical Marine Environment, Performance of Concrete in Marine Environment, ACI Publication, SP-65, pp. 527-556
- Meldrum F. C., (2003)**, Calcium Carbonate in Biomineralisation- Biomimetic Chemistry, 48, 187-224
- Mohini P. Samudre, M. P., Mangulkar, M. N., Saptarshi, S. D.,** A Review of Emerging Way to Enhance the Durability and Strength of Concrete Structures: Microbial Concrete. Vol. 3, Issue 2, February 2014
- Neville, A.,** Autogenous healing – A concrete miracle?, *Concrete International*, November 2002
- Ramos-Cormenzana, A.,(1975)**, Formation of Calcite Crystals by Bacteria of the Genus *Bacillus*, *Microbios* 13:61-70
- Ravindranatha, Kannan, N., Likhit M. L.,** Self-healing Material Bacterial Concrete, *IJRET: International Journal of Research in Engineering and Technology*, eISSN: 2319-1163 | pISSN: 2321-7308
- Reddy, S., Rao, M. V. S., Satya, A. , Azmatunnisa, M.,** A Biological Approach to Enhance Strength And Durability in Concrete Structure, *International Journal of Advances in Engineering & Technology*, Sept 2012 ©IJAET, ISSN: 2231-1963
- Santhosh K. R., Ramakrishnan V., Duke E. F., and Bang S.S.,** SEM Investigation of Microbial Calcite Precipitation in Cement, *Proceedings of the 22nd International Conference on Cement Microscopy*, pp. 293-305, Montreal, Canada, 2000

EVALUATION OF IN-SITU MECHANICAL PROPERTIES AND QUALITY OF CONCRETE STRUCTURES BY NON-DESTRUCTIVE TESTING

M. M. Ali^{1*}, M. Z. Ali², A. A. Saeem³ & M. S. Ahmed²

¹*Department of Civil Engineering, Bangladesh Army University of Engineering & Technology, Qadirabad Cantonment, Natore-6431, Bangladesh.*

E-mail: mmali19bd@gmail.com

²*Department of Civil Engineering, Chittagong University of Engineering & Technology (CUET), Chittagong-4349, Bangladesh. E-mail: mdzobaearali8630@gmail.com*

³*Bangladesh Army*

**Corresponding Author*

ABSTRACT

The non-destructive testing (NDT) of various components of reinforced cement concrete structures is becoming increasingly important for both economic and safety reasons in Bangladesh perspective. The modern NDT methods have received growing attention during recent years, especially to study the mechanical properties and quality characterization of damaged constructions made of concrete. There are many non-engineered constructions of reinforced concrete (RC) buildings which have been constructed without any consideration to resist earthquake forces or without following current code of earthquake resistance design. A quick NDT assessment could be a good approach for safety measurement of buildings within considerable cost for such type of seismically deficient buildings. In this study, a five (5) storied RCC building was selected and assessed its mechanical properties and quality of concrete through NDT. To investigate the mechanical properties of existing concrete structures against different loading patterns, several non-destructive tests such as Ferro-scanner, Rebar detector, Ultrasonic device, rebound hammer have been introduced. The present work deals with different NDT techniques for the assessment of the quality of existing old concrete structures and key findings obtained from the analysis of the surveyed data.

Keywords: RCC; NDT; Ferro-Scanner; Ultrasonic Device; Rebound Hammer Test.

INTRODUCTION

Non-destructive testing is the process by which the inspection or evaluation of materials and structural components are performed without destroying the serviceability of the structural system. Due to their simple operating system NDT are widely used to determine uniformity, strength, durability and other properties of concrete structures. The modern NDT techniques have a much more authenticity to integrity assessment of existing structures before re-strengthening work. According to the international norms and regulations any building that are going to be designed should have sufficient physical and strength properties to meet the required ultimate strength during their full design life (Samia, 2012). The modern NDT are widely accepted to diagnose the strength properties, quality, surface absorption, surface hardness and reinforcement details (location, size and spacing) embedded in concrete without damaging any part of the concrete structures (IS 13311, 1992, Jones 1969, IAEA, 2002). NDT techniques also determine the lack of bonding with reinforcing bars, location of in-built piping, wiring, ducting and the extent of defects such as cracks, corrosion, honeycombing, voids etc. (IS 13311, 1992, IAEA 2002). NDT is carried out to determine the suitability of existing concrete structures for its intended use. The major applications of NDT are to investigate the mechanical properties or checking

adequacy of structural elements for old existing concrete structures (IS 13311, 1992). For new concrete structures, the quality control of construction are the principal applications of NDT. The main objectives of this study were to study the mechanical properties of existing old concrete structural elements, to determine the reinforcement details (location, size and spacing) in the members of concrete structure and to evaluate the quality of in built concrete.

MATERIALS AND METHODS

Basic Information of Assessed Building

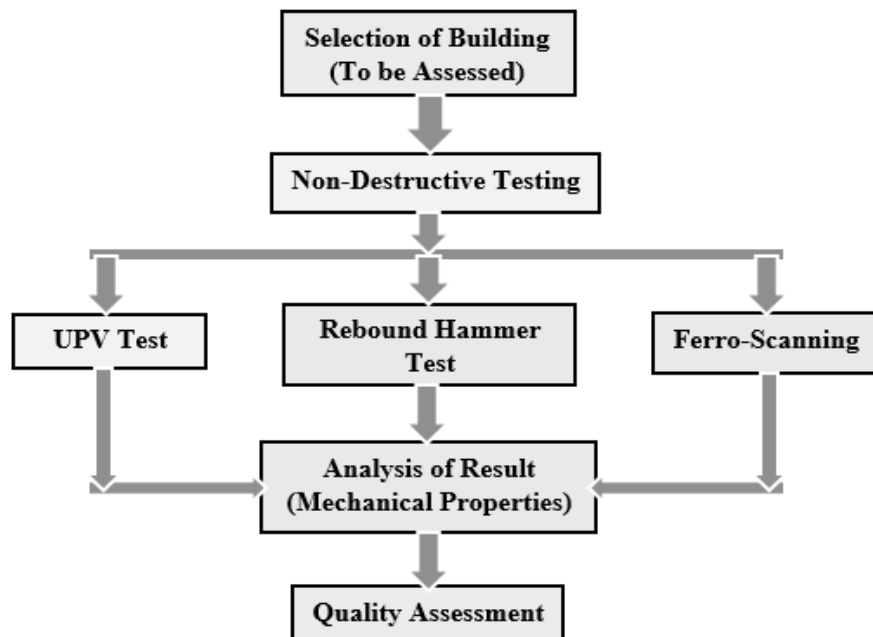
The assessed building was a garments factory building located in Dhaka, the capital of Bangladesh. The basic information of the assessed building are given in Table 1.

Table 1: Basic Information of Assessed Building

Information	Description
Structural System	The structural system of main production building is RCC Beam-Column frame system and foundation system is isolated column footing.
Area of Floor	Total building area: 30,000 sft.
Number of Stories	Five storied RCC building
Year of Construction	2005
Construction Materials	Concrete (with brick chips and steel)

Methodology

The step by step approaches for evaluation of mechanical properties and quality of in built concrete are given as follows:



Application of Schmidt RH Test

Standard Schmidt rebound hammer (RH) test is the most widely applied surface hardness procedure. Swiss engineer Ernst Schmidt developed the test in 1948 and is known to as the Schmidt RH (Kolek, 1969). While testing the rebounded hammer counts a rebound number under the impact of concrete surface and the compressive and flexural strength of concrete can be determined from the established empirical correlations between the rebound number and the strength of concrete. Small rebound number (RN) indicates the weak concrete surface at which corrosion may occur. However, several key factors affect the test results of concrete such as surface smoothness, type of coarse aggregate and cement, geometric properties, age and moisture condition of concrete and carbonation of the concrete surface (Malek and Kaouther, 2014). While conducting hammer test, it is necessary to place the

hammer in perpendicular direction to the concrete surface to be tested (Malek and Kaouther 2014, IS 13311, 1992). Fig. 1 shows the details of the equipment.

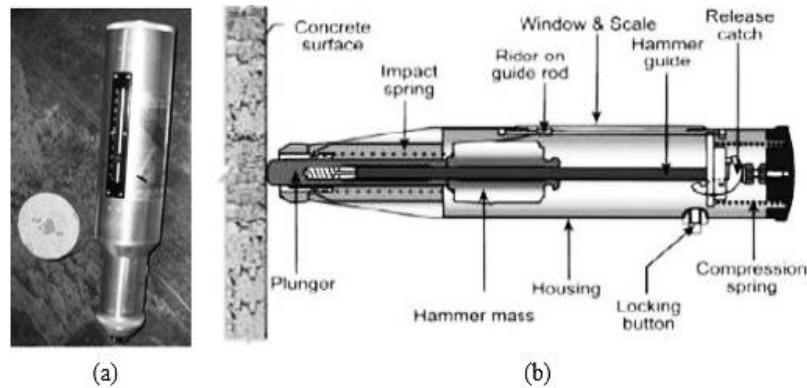


Fig. 1: (a) Schmidt Hammer (b) Different Parts of Schmidt Hammer.

Application of UPV Test

The modern ultrasonic pulse velocity (UPV) techniques provides an easy means of estimating the strength, quality and the uniformity of in built concrete by measuring the propagation speed of ultrasonic waves. The location of defects, cavity inside structures, depth of fractures and the strength of old concrete can also be determined by UPV test (Alexandre et Al., 2013). This ultrasonic device essentially consists of an amplifier, time measuring device, electrical pulse generator and two transducers (Jones 1969, Alexandre et Al., 2013). Fig. 2(a) shows an ultrasonic concrete testing instrument.



Fig. 2: (a) Ultrasonic Concrete Testing Instruments (b) Hilti PS 200 Monitor and Scanner Device.

Ferro Scan

Ferro scan is portable, non-destructive steel reinforcement detection system using electromagnetic pulse. It can reduce costly effort to drill, cut or physically break concrete surface to find out the bar. The position, depth and diameter of rebar in existing concrete structure can be determined using Ferro scan. The key elements of the system are the scanner and the monitor. After scanning a structure data has been transferred to the monitor. Collected data can be analyzed by monitor or in a PC using PS 200 software's. Maximum depth of scanning is 180 mm (at 36 mm rebar diameter) where rebar diameter range 6 - 36 mm. Depending on the mode of scan used and the range of depth, the accuracy of the measurement of depth for reinforcement is ± 1 mm. Fig. 2(b) shows monitor and scanning device produced by Hilti Corporation, 2011.

RESULTS AND DISCUSSIONS

The evaluation of in-place mechanical properties and quality of concrete structures were performed by UPV, Hammer test and Ferro scanning of structural members along with checking of foundations,

taking dimensions and removing plasters at different locations of the building for conforming reinforcement details.

Test result of UPV

Total UPV test at 16 points in different locations of the selected structure was performed to examine the strength of concrete. The data obtained from the UPV test are given in Table 2.

Table 2: Data of UPV Test

ID	Member		UPV Results		V (m/s)
	Type	Location	Size/Distance (mm)	Time (micro second)	
1.	Column	4F	343.5	94.2	3646
2.	Beam	4F	345.1	87.4	3949
3.	Column	3F	331.4	89.6	3699
4.	Beam	3F	332.6	85.9	3872
5.	Column	2F	326.9	91.6	3569
6.	Column	2F	355.6	85.4	4164
7.	Beam	2F	341.2	86.6	3940
8.	Beam	2F	341.8	87.8	3893
9.	Beam	1F	339.2	87.4	3881
10.	Column	1F	340.5	91.5	3721
11.	Beam	1F	338.5	88.6	3821
12.	Column	1F	342.5	83.4	4107
13.	Column	GF	342.5	87.3	3923
14.	Column	GF	340.5	91.2	3734
15.	Beam	GF	336.6	89.6	3757
16.	Column	GF	336.8	90.4	3726

The quality of concrete based on UPV value may be interpreted by the general guidelines for concrete quality as shown in Table 3 (Nikhil et al., 2015, CPWD Handbook 2002, IS 13311, 1992). Generally, higher pulse velocity represents the higher quality and durability of concrete and lower pulse velocity represents the lower quality concrete (Alexandre et Al., 2013).

Table 3: Quality interpretation of Concrete based on UPV Value

Concrete Quality	V (m/s)
Very Good	> 4000
Good, But May Be Porous	= 3500 to 4000
Poor	= 3000 to 3500
Very Poor	= 2500 to 3000
Very Poor and Low Integrity	= 2000 to 2500
No Integrity, Large Voids Suspected	< 2000 and Reading Fluctuating

From the assessment, the UPV value was found above 3500 m/sec for beams and columns at different locations of the selected structure and ranged from 3569 m/sec to 4164 m/sec (as shown in Table 2). So, the quality of concrete was found to be good based on UPV value (from Table 3).

Test result of Rebound Hammer

Rebound hammer was used in columns & beams located at different floors to evaluate the elastic properties or strength of concrete. Rebound hammer test was performed at 16 points in different locations of the selected structure. An average of 12 impacts was considered for each concrete surface. The data obtained from the rebound hammer test are given in Table 4.

Table 4: Data of Rebound Hammer Test

ID	Member		12 Values of Rebound	Average R Value
	Type	Location		
1.	Column	4F	37, 31, 31, 35, 34, 30, 32, 30, 31, 36, 37, 38	33
2.	Beam	4F	45, 43, 49, 42, 38, 45, 36, 42, 38, 42, 48, 40	42
3.	Column	3F	38, 36, 49, 37, 40, 40, 46, 43, 42, 38, 40, 39	40
4.	Beam	3F	40, 38, 35, 42, 38, 49, 38, 39, 47, 32, 37, 41	40
5.	Column	2F	34, 32, 36, 29, 30, 28, 32, 26, 27, 30, 29, 37	31
6.	Column	2F	38, 40, 34, 36, 35, 42, 26, 46, 28, 40, 40, 38	38
7.	Beam	2F	32, 29, 40, 42, 42, 32, 32, 40, 40, 32, 34, 35	36
8.	Beam	2F	42, 42, 28, 48, 29, 38, 48, 28, 32, 28, 30, 38	36
9.	Beam	1F	30, 28, 35, 32, 30, 27, 38, 35, 34, 33, 31, 35	32
10.	Column	1F	35, 29, 34, 35, 31, 40, 36, 36, 30, 42, 38, 28	34
11.	Beam	1F	28, 32, 36, 38, 38, 28, 35, 39, 40, 35, 34,33	35
12.	Column	1F	40, 44, 32, 42, 38, 44, 38, 43, 49, 45, 42, 39	42
13.	Column	GF	34, 35, 31, 31, 38, 32, 40, 50, 32, 34, 30, 31	34
14.	Column	GF	32, 28, 34, 39, 18, 18, 32, 34, 30, 36, 30, 36	31
15.	Beam	GF	32, 31, 32, 32, 32, 35, 37, 34, 33, 40, 36, 41	33
16.	Column	GF	38, 38, 52, 38, 32, 32, 39, 42, 33, 39, 38, 34	37

The quality of concrete based on average rebound number may be interpreted as shown in Table 4. For the concrete made with the same coarse aggregate, higher RN value represents higher compressive strength of concrete while the lower RN value represents lower compressive strength of concrete.

Table 5: Average Rebound Number and Quality of Concrete (CPWD Handbook, 2002).

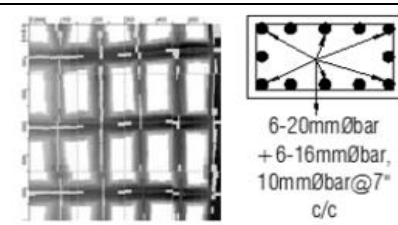
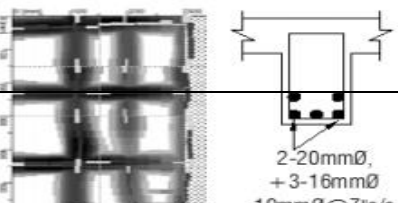
Quality of Concrete	RN (average)
Very Good Hard Layer	Greater than 40
Good Layer	From 30 to 40
Fair	From 20 to 30
Poor Concrete	Less than 20
Very Poor and/or Delaminated	0

From the assessment it was found that average rebound value ranged from 31 to 42 (as shown in Table 4) for beams and columns at different locations of the selected structure. So, the quality of concrete was found good to very good hard layer (from Table 5).

Ferro-Scanning

The reinforcement details using Ferro-scanner for beam and column are shown in Table 6.

Table 6: Details of Reinforcement using Ferro-Scanner

Location and Member Type	Reinforcement Details	Image from Ferro-Scanner
GF Column (22" X 12")	Along 22" face: Main Reinforcement: 3-Ø20mm + 2- Ø16mm Tie Bar: Ø10 mm @ 7" c/c	 <p>6-20mmØbar + 6-16mmØbar, 10mmØbar@7" c/c</p>
	Along 12" face: Main Reinforcement: 2-Ø20mm + 1- Ø16mm Tie Bar: Ø10 mm @ 7" c/c	
	Column Strip: Main Reinforcement: 2-Ø20mm + 3- Ø16mm Tie Bar: Ø10 mm @ 7" c/c	 <p>2-20mmØ, + 3-16mmØ 10mmØ@7" c/c</p>

GF Beam (12" X 15")	Middle Strip: Main Reinforcement: 2-Ø20mm + 3- Ø16mm Tie Bar: Ø10 mm @ 7" c/c	
1 th Floor Slab (6")	Slab (Bottom): Ø12 mm @ 4" c/c	
	Slab (Top): Ø10 mm @ 4" c/c	

The detail Ferro-scanning was performed to evaluate reinforcement details (to know the existing rebar diameter, quantity & spacing) of column, beam & slab. As built analysis was performed by remodeling the structure using powerful finite element based structural design software package CSI Etabs V9.7.4. It was found from the analysis results that the selected structure had sufficient structural strength to resist BNBC loadings and load combinations.

CONCLUSIONS

In this study, an overview of NDT and the evaluation of the in situ mechanical properties of reinforced concrete structures by NDT are presented in a simple. To ensure safety and credibility of concrete structures NDT plays an extreme role in each stage of construction. The integrity of structure throughout its design life can also be determined by NDT techniques. A series of non-destructive tests have been performed to evaluate the in situ mechanical properties of concrete structures due to its easy execution system and minor disruption to the occupants. The NDT has a great technical importance for quality and condition assessment of existing concrete structures and evolved in great savings of cost and time. However, the optimal in situ NDT techniques must be routinely adopted to diagnose and evaluate the concrete structures which enable accurate, reliable and cost-effective inspection of buildings during its whole useful life.

REFERENCES

- Alexandre, B J, Gloria, G M, and Augusto, G (2013). Compressive strength evaluation of structural lightweight concrete by non-destructive ultrasonic pulse velocity method. 2013.
- Handbook on Repair and Rehabilitation of RCC Buildings. CPWD, Government of India, New Delhi. 2002.
- IAEA (International Atomic Energy Agency, 2002). Guidebook on non-destructive testing of concrete structures. Training Courses Series, Vol.17, Vienna.
- IS 13311(1992). Code of Practice for Non Destructive Testing of Concrete – Methods of Test Part: 1 Ultrasonic Pulse Test, Bureau of Indian standards (BIS), New Delhi, January 1992.
- IS 13311(1992). Code of practice for Non Destructive Testing of concrete – methods of test part: 2 Rebound Hammer test, Bureau of Indian standards (BIS), New Delhi, January 1992.
- Jones, R. (1969). A review of the non-destructive testing of concrete. London: Institution of Civil Engineers.
- Malek, J and Kaouther, M (2014). Destructive and Non-destructive Testing of Concrete Structures. *Jordan Journal of Civil Engineering*, Volume 8, No. 4, 2014.
- Nikhil L. Jagtap, Mehetre P R (2015). Study on Retrofitted RCC Building by Different NDT Methods. *IOSR Journal of Mechanical and Civil Engineering (IOSR-JMCE)*. Volume 12, Issue 3 Ver. I (May - Jun. 2015), PP 85-89.
- Samia H, Mohamed NG, (2012). Application of the Combined Method for Evaluating the Compressive Strength of Concrete on Site. *Open Journal of Civil Engineering*, 2012, 2, 16-21.

EFFECTS OF DIFFERENT SIZES OF CRUSHED STONES ON MECHANICAL STRENGTH OF CONCRETE

S. Rahman* & A. Ullah

*Department of Civil Engineering, Port City International University, Chittagong
Bangladesh*

E-mail: sajedurrahman.ce@gmail.com

**Corresponding Author*

ABSTRACT

The mechanical strength of concrete depends on well-graded coarse aggregates used in construction. The strength can be increased by increasing the sizes of coarse aggregates. However, excessive increase in size of coarse aggregates can cause internal bleeding due to water being trapped on the underside of a large sized aggregate, which will reduce strength, and crack may occur early. This study is intended to inspect the impact of sizes of crushed stones of diameter of 14 mm, 19 mm and 28 mm on compressive and split tensile strength of concrete. Three separate mix designs were conducted targeting 3000 psi concrete for these three sizes of crushed stones. Total nine cubes for compressive strength test and nine cylinders for split tensile strength test were casted by using ordinary Portland cement. For each size, three samples were casted for different curing period of 7, 14 and 28 days. Overall, concrete with 19 mm crushed stone showed improved result in both the tests compared to others. The compressive strength was found as 3142 psi for concrete with 19 mm crushed stone, which was 7.96% more than 14 mm and 4.93% more than 28 mm and the split tensile strength was established as 1920 psi for concrete with 19 mm crushed stone that was 6.35% more than 14 mm and 2.92% more than 28 mm. Both the strengths were found less than the target strength for concrete with 14 mm and 28 mm stones.

Keywords: Concrete; Crushed stone; Compressive strength; Split tensile strength.

INTRODUCTION

Concrete usually consists of cement, sand and aggregates. Aggregate occupies most of the volume of the concrete. It acts as structural filler in concrete. The larger the aggregate percentage in concrete mix makes it to contribute a lot to its strength (Waziri et al., 2011). The workability, durability, strength, weight, and shrinkage of the concrete depend on composition, shape, and size of the aggregate. According to Patel et al. (2013), aggregate shape and grading can significantly influence concrete workability. Aggregate size and gradation are the most important factors when aggregates are selected for concrete casting. Aggregate can be large or small, being fist-sized rocks to fine sand.

Vilane et al. (2016) studied the effect of aggregate size on the compressive strength of concrete. The experiment had three treatments, which were the aggregate sizes (9.5 mm, 13.2 mm and 19.0 mm) and the control. It was concluded that concrete workability (slump) was directly proportional to aggregate size. The mean concrete compressive strength increased with increasing aggregates size. Sneka et al. (2018) conducted the utilisation of three sizes of aggregate for concrete work. The experiment had three treatments, which were the aggregate sizes (19mm, 25mm, and 37.5mm) and the control. The mean concrete compressive strength and split tensile strength increased with increasing aggregates size. According to Adishesu et al. (2011), larger aggregates demand lower water on its mix thus reducing the workability and increasing the compressive strength of concrete. So, in this

study the effects of aggregates sizes as of 14 mm, 19 mm and 28 mm (Fig. 1) on compressive and split tensile strength of concrete were investigated to find out the aggregate size impact on concrete strength.

METHODOLOGY

Materials

Ordinary Portland cement was used for casting of concrete. Specific gravity of cement was tested. Locally available sand collected for Sylhet, Bangladesh was used as fine aggregate (FA). Specific gravity, absorption tests and gradation were conducted on FA as illustrated in Fig. 2 and Fig. 3. Crushed stones of three different sizes having diameter of 14 mm, 19 mm and 28 mm were used as coarse aggregates (CA). Specific gravity, absorption, dry rodded unit weight tests and gradation were performed separately on all three sizes of CA as shown in Fig. 4, Fig. 5 and Fig. 6. All the test results on materials are given in Table 1. Specific gravity increased here as the particle size decreased. Because as the aggregate particles get smaller, the fraction of pores exposed to the aggregate surface increases.



Fig. 1: Different sizes of coarse aggregates.



Fig. 2: Specific gravity and absorption capacity tests of FA.



Fig. 3: Gradation of FA.



Fig. 4: Specific gravity and water absorption capacity tests of CA.



Fig. 5: Dry rodded unit weight test of CA.



Fig. 6: Gradation of CA.

Table 1: Test results of different materials.

Materials	Name of tests	Results		
Cement	Specific gravity (ASTM C188-16)	2.82		
Fine aggregates	Specific gravity (ASTM C128-15)	2.1		
	Absorption capacity (ASTM C128-15)	2.25%		
	Gradation (ASTM C778-13)	Fineness Modulus = 3.1		
Coarse aggregates	Sizes →	14 mm	19 mm	28 mm
	Specific gravity (ASTM C127-15)	2.56	2.33	2.11
	Absorption capacity (ASTM C127-15)	1.63%	1.54%	1.42%
	Dry rodded unit weight (ASTM C29-C29M-17)	112.13 lb/ft ³	107.24 lb/ft ³	101.53 lb/ft ³
	Gradation (ASTM C33-C33M-16e1)	Fineness Modulus = 6.1	Fineness Modulus = 6.7	Fineness Modulus = 7.1

Mix Design

Concrete mix design was done to find out the right proportions of cement, sand and coarse used for concrete casting. Three ACI mix designs were done for three sizes of coarse aggregates targeting 3000 psi compressive strength of concrete. From the results of materials tests, ACI mix design was conducted and the ratio among cement (C), FA and CA and water-cement ratio (W/C) were found as given in Table 2. The detailed mix amount according to different sizes of CA is shown in Table 3. The slump value was also found satisfactory.

Table 2: Mix design results.

Diameter of CA	14 mm	19 mm	28 mm
C: FA: CA	1: 2.31: 2.92	1: 2.33: 3.57	1: 2.44: 3.74
W/C	0.59	0.59	0.59

Table 3: Detailed mix amount according to different sizes of CA.

Sizes of CA →	14 mm	19 mm	28 mm
Water (lb)	190.48	215.15	234.14
Cement (lb)	396.83	398.43	396.85
Coarse Aggregate (lb)	1158.74	1422.4	875.68
Fine Aggregate (lb)	916.68	928.34	571.3
Total	2662.73 lb/yd ³ or, 98.62 lb/ft ³	2964.32 lb/yd ³ or, 109.79 lb/ft ³	2077.97 lb/yd ³ or, 76.96 lb/ft ³

Casting and Curing

Total 9 cubes and 9 cylinders were casted (Fig. 7) for compressive strength test and split tensile strength test respectively. Appropriate mix proportion was maintained during the construction. After 24 hours of casting, the cylinders were demolded and submerged under water for curing.



Fig. 7: Casting of concrete.

Compressive and Split Tensile Strength Test

The cubes were tested for compressive strength with respective ages of curing as 7, 14 and 28 days. Compressive strength test helps to determine concrete grading. A compressive axial load was applied to the cubes at a rate which is within a prescribed range until failure occurred (ASTM C39-C39M-17). Again, the cylinders were also tested for split tensile strength test with respective ages of curing as 7, 14 and 28 days. It is a method to determine the tensile strength of concrete. A diametral compressive force along the length of the cylinders was applied at a rate which is within a prescribed range until failure occurred. This loading generated tensile stresses on the plane containing the applied load (ASTM C496-C496M-11). Split tensile strength test of concrete was done to find out the load at which crack occurs, because concrete is weak in tension due to its brittle nature. Tensile strength of concrete greatly affects the extent and size of cracking in concrete. Universal Testing Machine (UTM) of capacity of 1000 KN was used for both compressive strength and split tensile strength tests as shown in Fig. 8 and Fig. 9.



Fig. 8: Compressive strength test of concrete cube.



Fig. 9: Split tensile strength test of concrete cylinder.

RESULTS AND DISCUSSIONS

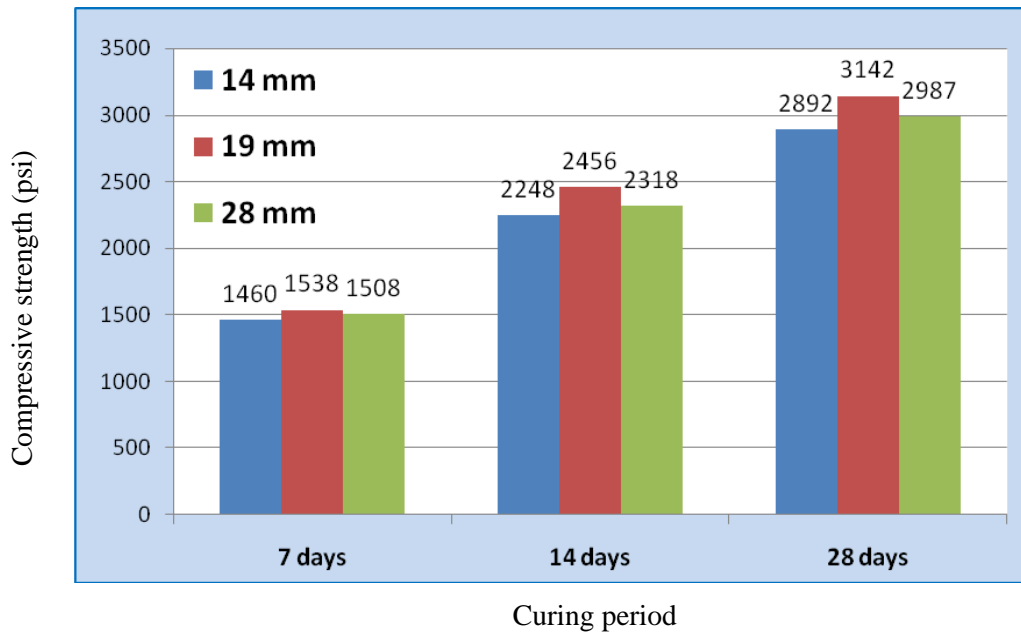


Fig.10: Comparison between compressive strength of concrete with 14 mm , 19 mm and 28 mm CA with respect to curing periods.

Fig. 10 shows the comparison between compressive strength of concrete with 14 mm, 19 mm and 28 mm CA with respect to curing periods. The compressive strengths were measured in 7, 14, and 28 days of curing respectively for all the specimens and compared. It was seen that, compared to 14 mm CA concrete in 7 days, the 19 mm CA concrete compressive strength was increased by 5.34% being maximum and 28 mm CA concrete compressive strength was also increased by 3.29%. In 14 days, the 19 mm CA concrete compressive strength was increased by 9.25% being maximum and 28 mm CA concrete compressive strength was also increased by 3.11%. Finally, in 28 days, the 19 mm CA concrete compressive strength was increased by 8.64% being maximum again and 28 mm CA concrete compressive strength was increased by 3.28%.

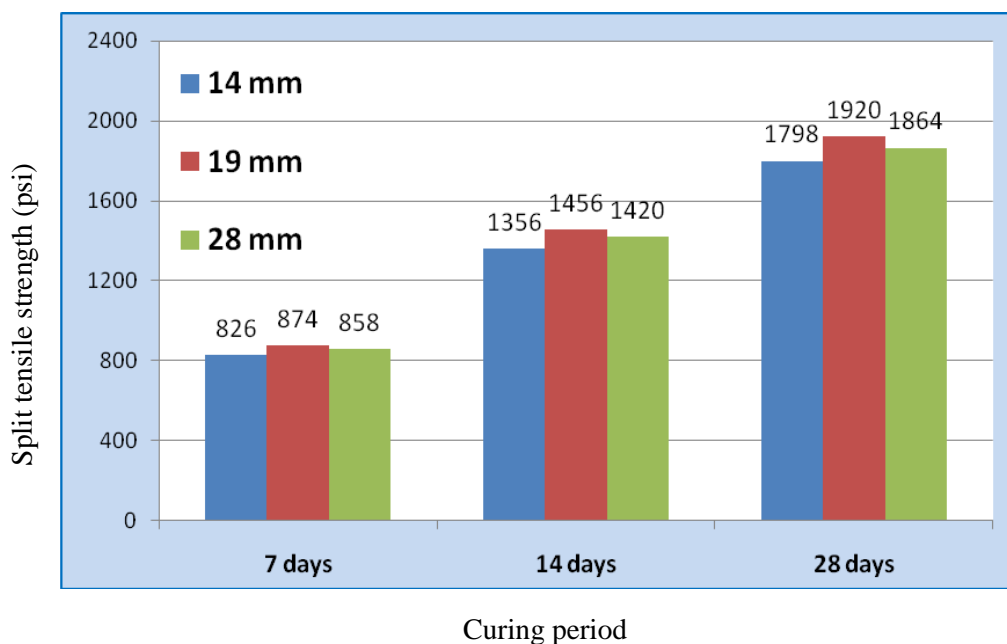


Fig. 11: Comparison between split tensile strength of concrete with 14 mm , 19 mm and 28mm CA with respect to curing periods.

Fig. 11 shows the comparison between split tensile strength for concrete with 14 mm, 19 mm and 28 mm CA with respect to curing periods. The split tensile strengths were calculated in 7, 14, and 28 days respectively for all the specimens and compared. It was found that, compared to 14 mm CA concrete in 7 days, the 19 mm CA concrete split tensile strength was increased by 5.81% being maximum and 28 mm CA concrete split tensile strength was increased by 3.87%. In 14 days, the 19 mm CA concrete split tensile strength was increased by 7.37% being maximum again and 28 mm CA concrete split tensile strength was increased by 4.72%. Finally, in 28 days, the 19 mm CA concrete split tensile strength was increased by 6.78% and 28 mm CA concrete split tensile strength was also increased by 3.67%.

CONCLUSIONS

Result states that both compressive strength and split tensile strength of concrete were strongly influenced by aggregate size distribution. The strengths increased as the size of the aggregates increased but again decreased with over size of aggregates. Because an addition of excessive sized coarse aggregates resulted in surplus mixing water that resulted in slight segregation that reduced the overall strengths. Again the tensile strength of concrete became about 60% of the compressive strength because of different shape and surface texture of CA and slow progression of tensile strength compared to compressive strength.

ACKNOWLEDGMENTS

The authors are grateful to Department of Civil Engineering, Port City International University, Chittagong, Bangladesh for giving the opportunity to use the Engineering Materials Laboratory facilities for the experimental works.

REFERENCES

- Adishesu, S. and Ganapati, N. P. 2011. Influence of coarse aggregates on the strength of asphalt concrete mixtures. *International Journal of Engineering Research and Application*, 1(4): 2013-2014.
- ASTM C29-C29M-17 Standard test method for bulk density ("unit weight") and voids in aggregate.
- ASTM C33-C33M-16e1 Standard Specification for Concrete Aggregates.
- ASTM C39-C39M-17 Standard test method for compressive strength of cylindrical concrete specimens.
- ASTM C127-15 Standard test method for density, relative density (specific gravity), and absorption of coarse aggregate.
- ASTM C128-15 Standard test method for relative density (specific gravity) and absorption of fine aggregate.
- ASTM C188-16 Standard test method for density of hydraulic cement.
- ASTM C496-C496M-11 Standard test method for splitting tensile strength of cylindrical concrete specimens.
- ASTM C778-13 Standard specifications for standard sand.
- Haque, M.B.; Tuhin, I.A. and Farid, M.S.S. Effect of aggregate size distribution on concrete compressive strength. *SUST Journal of Science and Technology*, 19(5): 35-39.
- Kumar, R. and Rao, K. 2012. A study on the effect of size of aggregate on the strength and sorptivity characteristics of cinder based light weight concrete. *Research Journal of Engineering Sciences*, 1(6): 27-35.
- Oritola, S.; Saleh, A.L. and Sam, A.R.M. Comparison of different forms of gravel as aggregate in concrete. *Leonardo Electronic Journal of Practices and Technologies*, 2(25): 135-144.
- Patel, P.J.; Patel, M.A. and Pate, H.S. 2013. Effect of coarse aggregate characteristics on strength properties of high performance concrete using mineral and chemical admixtures. *International Journal of Civil Engineering and Technology*, 4(2): 89-95.
- Sneka, S.; Nirmala, M. and Dhanalakshmi, G. 2018. Size effect of aggregate in the mechanical properties of concrete. *International Research Journal of Engineering and Technology*, 5(2): 2093-2096.
- Vilane, B.R.T. and Sabelo, N. 2016. The effect of aggregate size on the compressive strength of concrete. *Journal of Agricultural Science and Engineering*, 2(6): 66-69.
- Waziri, B.S.; Bukar, A.G and Gaji, Y.Z.A. 2011. Applicability of quarry sand as a fine aggregate in the production of medium grade concrete. *Continental J. Engineering Science*, 6(2): 1-6.

EXPERIMENTAL INVESTIGATION AND FINITE ELEMENT ANALYSIS OF REINFORCED CONCRETE RECTANGULAR BEAM

S. Rahman*, E. Kabir, M. M. Hossain, M. Haque, K. Das, A. Rahman & A. A. Akhie

*Department of Civil Engineering, Port City International University, Chittagong
Bangladesh.*

E-mail: sajedurrahman.ce@gmail.com

**Corresponding Author*

ABSTRACT

The response of reinforced concrete (RC) rectangular beam under loading both experimentally and by Finite Element Analysis (FEA) were observed in this study which is crucial for efficient structure. Mix design was conducted by the data collected from materials test and total three beams were casted by using ordinary Portland cement (OPC) for three consecutive curing periods of 7, 14 and 28 days. The beams were loaded in Universal Testing Machine (UTM) of 1000 KN capacity. The flexural strength of beam was found as 8889.3 psi in 7th days of curing which increased to 16061.5 psi in 28th days. Again, the beam was modelled in SolidWorks v13 and analyzed in ANSYS v16 platform. From Finite Element Analysis (FEA), total deformation was found as 0.77986 mm and normal strain as 0.0027214. The normal stress was also witnessed and found as 0.52 psi experimentally which increased in FEA and became 8.88 psi.

Keywords: Concrete; Rectangular beam; Finite Element Analysis; Flexural strength; Deformation; Normal stress; Normal strain.

INTRODUCTION

Reinforced concrete (RC) is one of the most important building materials and is widely used for various types of constructions and structural elements. The economy, the efficiency, the strength and the stiffness of reinforced concrete make it an attractive material for a wide range of structural applications (Dawari et al., 2014). Understanding the response of the structural elements during loading is vital to the development of an effective structure.

Experimental investigation is widely popular for evaluating the behaviour of RC structure under loading. It is an efficient method but it consumes a lot of time. To help in this regard, Finite Element Analysis (FEA) is a method that can be used to analyse these structural components. Finite element method is a numerical analysis method that divides the structural element into smaller parts and then simulates static loading conditions to evaluate the response of concrete (Logan, 2011). Flexural strength of concrete is the theoretical maximum tensile stress reached in the bottom fibre of a test beam during a flexural strength test (Ajamu et al., 2015). It is one of the important parameters for computing deflection in reinforced concrete structures (Anbuvelan et al., 2014). The flexural behavior of RC beams was studied experimentally and the results were compared with analytical values (Buckhouse, 1997). Wolanski (2004) has verified and validated the experimental test results provided by Buckhouse (1997) using the finite element software ANSYS. Dahmani et al. (2010) studied the crack propagation in RC beams using ANSYS software modelled with Solid65 element with smeared reinforcement approach. Vasudevan et al. (2011, 2012) explored the advantages of batch mode approach and non-linear FE analysis has been carried out by creating a single batch file from modelling to complete post processing.

In this study, RCC beam was constructed to evaluate by both experimental works and finite element method.

METHODOLOGY

Materials

Ordinary Portland cement was collected for this study for quick curing and specific gravity was tested as shown in Fig. 1. Sand as fine aggregate (FA) collected from Sylhet, Bangladesh was used for its granular shape. Specific gravity, absorption capacity and gradation test were carried out as shown in Fig. 2 and Fig. 3. Crushed stones as coarse aggregates (CA) passing 19 mm sieve were used and also tested for specific gravity, water absorption capacity, dry rodded unit weight and gradation as shown in Fig. 4, Fig. 5 and Fig. 6. The results of the various tests on materials are given in Table 1.



Fig.1: Specific gravity test of ordinary Portland cement.



Fig. 2: Specific gravity and absorption capacity test for FA.



Fig. 3: Gradation of FA.



Fig. 4: Specific gravity and water absorption capacity test of CA.



Fig. 5: Dry rodded unit weight test of CA.



Fig. 6: Gradation of CA.

Table 1: Test results of different materials.

Materials	Name of tests	Results
Cement	Specific gravity ASTM C 188-16	2.82
Fine aggregates	Specific gravity	2.1
	Absorption capacity	2.25%
	Gradation	Fineness Modulus = 3.1
Coarse aggregates	Specific gravity	2.56
	Absorption capacity	1.63%
	Dry rodded unit weight	112.13 lb/ft ³

	Gradation	Fineness Modulus = 6.1
--	-----------	------------------------

Mix Design

ACI mix design was conducted based on the materials test results targeting 3000 concrete compressive strength as shown in Table 2. The slump value was established as 25 mm.

Table 2: Mix design ratio.

Compressive strength	3000 psi
C:FA:CA	1 : 2.39 : 3.17
W/C	0.59

Table 3: Detailed mix amount.

Materials	Amount
Water (lb)	222.35
Cement (lb)	376.86
Coarse Aggregate (lb)	1194.65
Fine Aggregate (lb)	900.7
Total	2694.56 lb/yd ³ or, 99.8 lb/ft ³

RCC beam preparation

Total 3 RCC beams were designed as in Fig. 7. The shuttering and the steel frameworks were prepared as shown in Fig. 8. The beams were then casted (Fig. 9) and immersed under water (Fig. 10) for respective curing period as 7, 14 and 28 days.

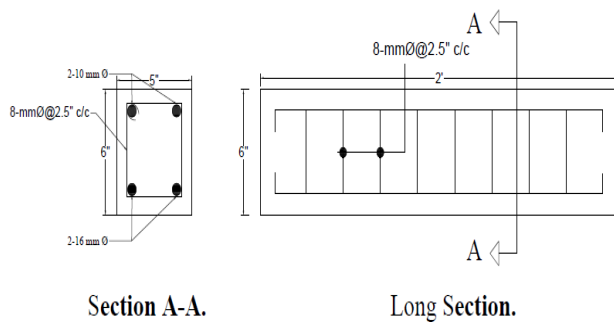


Fig. 7: Reinforcement detailing of RCC beam.



Fig. 8: Steel framework of RCC beam.



Fig. 9: RCC beam casting on prepared mould.



Fig. 10: RCC beam immersed under water for curing.

Loading of RCC beam

The beams were loaded with respective ages of curing as 7, 14 and 28 days. Universal Testing Machine (UTM) of 1000 KN capacity was used as shown in Fig. 11.



Fig. 11: Loading on RCC beam by UTM.

Finite Element Analysis

The RCC beam was modelled in SolidWorks v13.0 platform (Fig. 12) and then analyzed in ANSYS v16.0 by finite element method. From ANSYS the total deformation (Fig. 13, 14, 15), normal strain (Fig. 16, 17, 18) for respective 7, 14 and 28 days of curing and normal stress (Fig. 19) were observed.

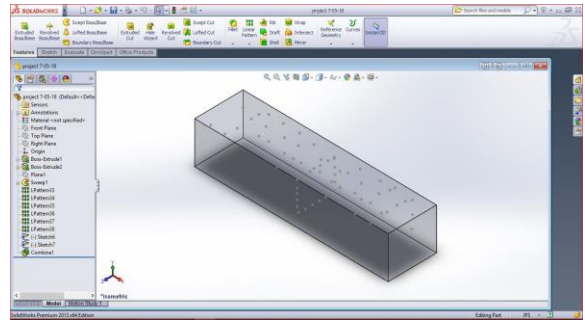
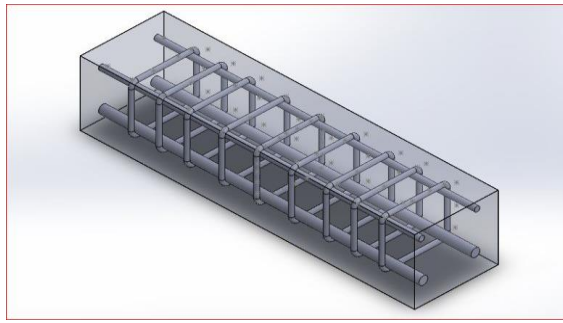


Fig. 12: Modelling of RCC beam.

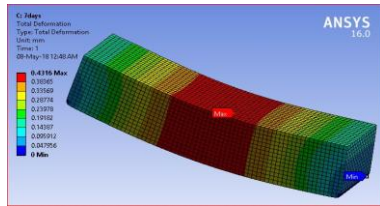


Fig. 13: Total deformation (at 7 days curing period).

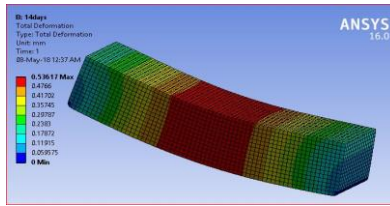


Fig. 14: Total deformation (at 14 days curing period).

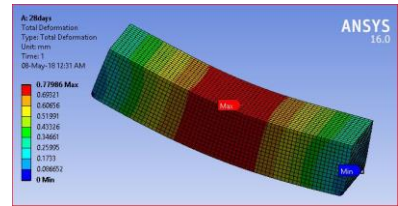


Fig. 15: Total deformation (at 28 days curing period).

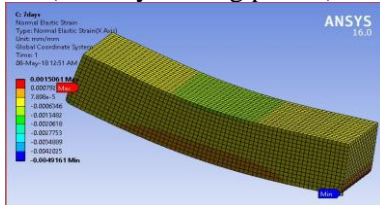


Fig. 16: Normal strain (at 7 days curing period).

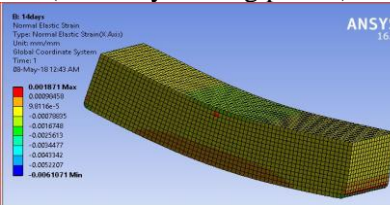


Fig. 17: Normal strain (at 14 days curing period).

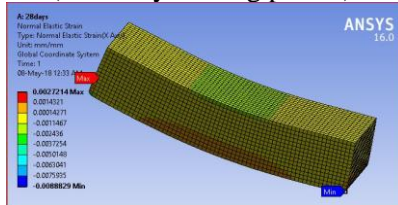


Fig. 18: Normal strain (at 28 days curing period).

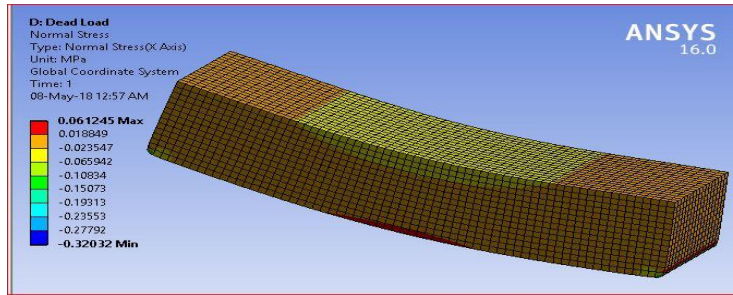


Fig. 19: Normal stress.

RESULTS AND DISCUSSIONS

The flexural strength was calculated according to ASTM C78/C78M-18. From Fig. 20 it can be seen that, the flexural strength was found 8889.3 psi in 7th days of curing and gradually increased by 8.68% to 16061.5 psi in 28th days of curing. The total deformation was also increased gradually from 0.4316 in 7th days to 0.77986 in 28th days (Fig. 21). The normal strain was also observed and found to be 0.001 in 7th days which increased to 0.002 in 28th days of curing (Fig. 22). Finally, the normal stress found by both experimental investigation and FEA was compared (Fig. 23). The experimental normal stress was less than the FEA by large amount.

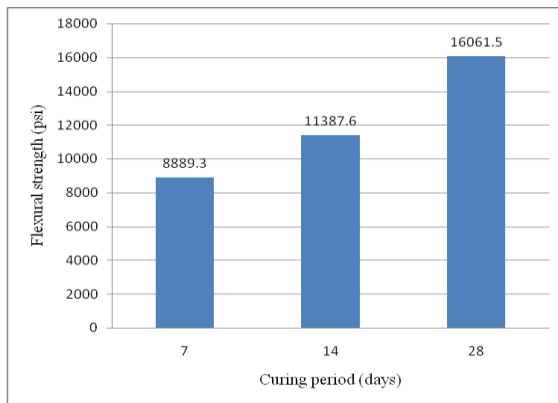


Fig. 20: Comparison between flexural strength of RCC beam with respect to curing periods.

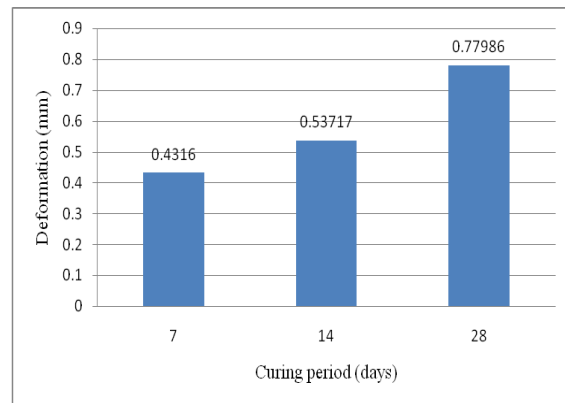


Fig. 21: Comparison between total deformation of RCC beam with respect to curing periods.

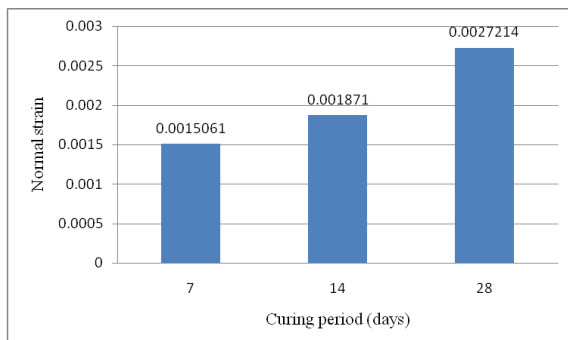


Fig. 22: Comparison between normal strain of RCC beam with respect to curing periods.

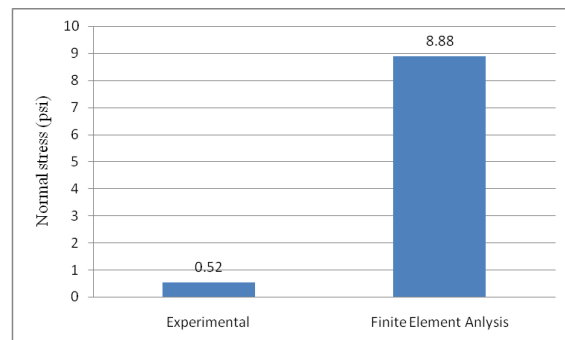


Fig. 23: Comparison between experimental and FEA value of normal stress of RCC beam with respect to curing periods.

CONCLUSIONS

A small scale experimental investigation and finite element method was carried out in this study to observe the behavior of RCC beam under loading with respect to curing periods. The flexural strength, total deformation and normal strain were increased as the curing periods increased, being maximum in 28th days of curing. But, the experimental value of normal stress was not close to FEA value. It caused due to sensitivity of finite element method to mesh size, materials properties, load increments, etc. The

analysis procedure used in this paper and various output plots constructed by FEA would provide a deeper insight for future application of finite element software for the non-linear analysis of RC beams.

ACKNOWLEDGMENTS

The authors would like to acknowledge Department of Civil Engineering, Port City International University, Chittagong, Bangladesh for giving the opportunity to use the Engineering Materials Laboratory facilities for the experimental works.

REFERENCES

- Ajamu, S.O. and Ige, J.A. 2015. Effect of coarse aggregate size on compressive strength and flexural strength of concrete beam. *International Journal of Engineering Research and Applications*, 5(1): 67-75.
- Anbuvelan, K. and Subramanian, K. 2014. An empirical relationship between modulus of elasticity, modulus of rupture and compressive strength of M60 concrete containing metakaolin. *Res. J. Appl. Sci. Eng. Technol*, 8(11): 1294-1298.
- ASTM C29-C29M-17 Standard test method for bulk density (“unit weight”) and voids in aggregate.
- ASTM C33-C33M-16e1 Standard specification for concrete aggregates.
- ASTM C78/C78M-18 Standard test method for flexural strength of RCC beam.
- ASTM C127-15 Standard test method for density, relative density (specific gravity), and absorption of coarse aggregate.
- ASTM C128-15 Standard test method for relative density (specific gravity) and absorption of fine aggregate.
- ASTM C187-16 Standard test method for amount of water required for normal consistency of hydraulic cement paste.
- ASTM C188-16 Standard test method for density of hydraulic cement.
- ASTM C191-13 Standard test methods for time of setting of hydraulic cement by Vicat needle.
- ASTM C778-13 Standard specifications for standard sand.
- Buckhouse, E.R. 1997. External flexural reinforcement of existing reinforced concrete beams using bolted steel channels. Master of Science Thesis, Marquette University, USA
- Dahmani, L.; Khennane, A. and Kaci, S. 2010. Crack identification in reinforced concrete beams using ANSYS software. *Strength of Materials*, 42(2): 232-240.
- Dawari, V. B. and Vesmawala, G. R. 2014. Application of nonlinear concrete model for finite element analysis of reinforced concrete beams. *International Journal of Scientific & Engineering Research*, 5(9): 776-782.
- Logan, D.L. 2011. *A first course in the finite element method*. USA: Cengage Learning. 1p.
- Vasudevan, G. and Kothandaraman, S. 2012. Behaviour prediction of RC beams - comparison of experimental, FEA and analytical methods. *Proc. of the IEEE Int. Conf. on Advances in Engineering, Science, and Management*, Nagapattinam, India, pp. 365-370.
- Vasudevan, G. and Kothandaraman, S. 2013. Study on non-linear flexural behavior of reinforced concrete beams using ANSYS by discrete reinforcement modeling. *Strength of Materials*, 45(2): 231-241.
- Wolanski, A.J. 2004. Flexural behavior of reinforced and prestressed concrete beams using Finite Element Analysis. Master of Science Thesis, Marquette University, USA

MECHANICAL PROPERTIES OF RUBBERIZED NORMAL WEIGHT AGGREGATE CONCRETE - AN EXPERIMENTAL STUDY

M. M. Kamal¹, S. K. Adhikary² & M. A. Islam^{2*}

¹*Department of Civil Engineering, Dhaka International University, Dhaka-1212, Bangladesh.*

E-mail: mkrabbi13@gmail.com

²*Department of Civil Engineering, Khulna University of Engineering & Technology, Khulna-9203, Bangladesh. E-mail: sajal@ce.kuet.ac.bd; ashiq.civil13@gmail.com**

**Corresponding Author*

ABSTRACT

In this study, an attempt is made to investigate mechanical properties of rubberized normal weight aggregate concrete, wherein rubber content is used as a volumetric replacement of coarse aggregate. The mechanical properties including compressive strength, splitting tensile strength, flexural strength and flexural toughness are tested in order to study the effect of rubber content on concrete strength. For experimental investigation, five batches of concrete specimens are prepared with 0%, 25%, 50%, 75% and 100% rubber contents. Cylindrical specimens are casted to investigate the compressive strength and the splitting tensile strength properties whereas beam specimens are prepared to study the flexural strength and the flexural toughness properties. Test results indicate that there is a significant reduction in the compressive, splitting tensile and flexural strengths of concrete with increasing rubber content. It is found that the compressive strength is reduced by 87% of initial strength with 100% rubber content whereas with the same rubber content, the splitting tensile and flexural strengths are decreased by 82% and 70% of initial strength, respectively. However, the flexural toughness of concrete is increased by 86% with 100% rubber content, which indicates such concrete could be adopted in special construction where vibration mitigation is a major concern.

Keywords: Rubberized normal weight aggregate concrete; Rubber content; Splitting tensile strength; Tire derived aggregated; Toughness.

INTRODUCTION

Globally, the waste tires have been increasing with an alarming rate and nowadays is a major concern to the researchers and environmentalists. According to the Environmental Protection Agency (EPA), the annual production of scrap tires in the United States is about 289 Million (Miller and Tehrani, 2017). Recycling of rubber materials from waste tires has become a vital concern across the world. The closed loop recycling technique is regarded as the most appropriate practice for recycling waste materials. However, the closed loop technique of waste rubber cannot be applied in recycling process because of high cost associated with this processes of waste rubber materials (Taha and Nounu, 2009). So, waste rubber could be a suitable option to be used as the coarse aggregate in concrete.

Concrete is the single most widely used artificial material on the earth owing to its remarkable versatility as a construction material (Crow, 2008). Accordingly, the annual production of concrete exceeds about 2 Billion metric tons per year across the world. A major weakness of the concrete as a construction material is the harmful effects on the environment posed by the production of its components (Roskos et al., 2015). In Bangladesh, the generation of rubber waste has been substantially

increased due to increase of use of rubber materials. Therefore, it is important to devise viable options in order to convert rubber wastes into resources for the sustainable development of the country.

The objective of this study was to investigate the mechanical properties of rubberized normal weight concrete. Rubberized normal weight aggregate concrete is a concrete prepared by using rubber (waste rubber material) as aggregate in the concrete mix. Numerous researches have been conducted since the early 1990s to study the rubberized normal weight aggregate concrete. Some studies have shown that an increase in rubber content enhances durability, while some investigations have found that compression strength is decreased with the increasing rubber content (Topçu, 1994; Ganjian et al, 2008; Zheng et al, 2008; Xue et al, 2013). Other common properties of concrete such as the splitting tensile strength (Li et al, 2004) and static flexural strength (Khatib et al, 1999) have also been found to decrease with the increased rubber content in the concrete. However, no studies have been found in the past to investigate several mechanical properties of the rubberized normal weight aggregate concrete including compressive strength, splitting tensile strength, flexural strength and flexural toughness. Therefore, an attempt has been made in this study to study the aforementioned mechanical properties of the rubberized normal weight aggregate concrete.

MATERIALS AND METHODS

In this study, several mechanical properties of the rubberized normal weight aggregate concrete were investigated. This includes compressive, splitting tensile and flexural strengths, and flexural toughness properties. Test setup was developed according to the ASTM specifications for each of the aforementioned tests. Five batches of concrete mix were used, which contains 0%, 25%, 50%, 75%, and 100% of tire derived aggregate (TDA) as a volumetric replacement of coarse aggregate.

TDA was extracted from the auto-mobile's tyre and crumbled for using it as the coarse aggregate. It was found that TDA had specific gravity of 1.74 and unit weight of 652 kg/m³. According to the ASTM C150 specification for using binding materials, Ordinary Portland Cement (OPC) was used in the current study. Black stone was used as the coarse aggregate with a specific gravity of 2.70 whereas Kushtia sand was used as the fine aggregate having a specific gravity of 2.52. The concrete mix was designed for a slump value of 100 mm, maximum aggregate size of 19 mm for 21 MPa of concrete with a water-cement (w/c) ratio of 0.48. The mixing ratio of concrete was 1:1.7:2.7 by weight whereas the ratio was 1:2:3 by volume.

Experimental set up to test mechanical properties of the rubberized normal weight aggregate concrete is shown in Fig 1. As can be seen from the figure, four tests (e.g., compressive, splitting tensile and flexural strength tests, and flexural toughness test) were undertaken in this study. The compressive strength test was performed according to the ASTM C39 standard test procedure. A total of 15 cylindrical samples (4" diameter x 8" height) were prepared with the aforementioned five different rubber contents (RC). Samples were kept in curing for 28 days before carrying out the test. The experimental set up for this test is shown in Fig 1a. For the splitting tensile strength test, the ASTM C496 standard test procedure was followed. Fig 1b shows the experimental set up for this test. A total of 15 cylindrical samples (4" diameter x 8" height) were made in this test with five different RC like the compressive strength test procedure. The specimens were also kept under curing for 28 days before performing the test.

In order to undertake the flexural strength test, 5 beam specimens (6" width x 6" height x 24" length) were casted for 5 different concrete mixes with different RC as indicated above starting from 0% to 100%. In this test, the ASTM C78 specifications were used. Samples were kept in curing for 28 days before undertaking the test. Samples were tested using the Universal Testing Machine (UTM). The experimental set up is shown in Fig 1c. In this test, 5 beam specimens were casted with the same specifications detailed in the flexural strength test. To perform this test, the ASTM C1018-97 standard test procedure was adopted. It is important to mention that this test calculation is based on an experiment for which deflection against load data are necessary. Accordingly, the same setup of the flexural strength test with dial gauge deflections were used in this test. The experimental set up for this test is shown in Fig 1d.



Figure 1. Experimental set up for (a) compressive strength test, (b) splitting tensile strength test, (c) flexural strength test, and (d) flexural toughness computation.

RESULTS AND DISCUSSIONS

Compressive Strength Properties of Rubberized Normal Weight Aggregate Concrete

The compressive strength test results indicate that there is a reduction in the compressive strength with the increasing rubber content, which is shown in Fig 2. It is seen from the figure that the strength reduction takes an exponential pattern for the rubberized normal weight aggregate concrete in the current study. The control mix (standard case with 0% rubber content) strength was found as 19.4 MPa, which is less than the estimated 21 MPa, decreased to 2.5 MPa for 100% replacement of coarse aggregate by the rubber content. The reason behind this could be the fact that the surfaces of the rubber aggregate were not rough enough to create proper bonding with the binding materials.

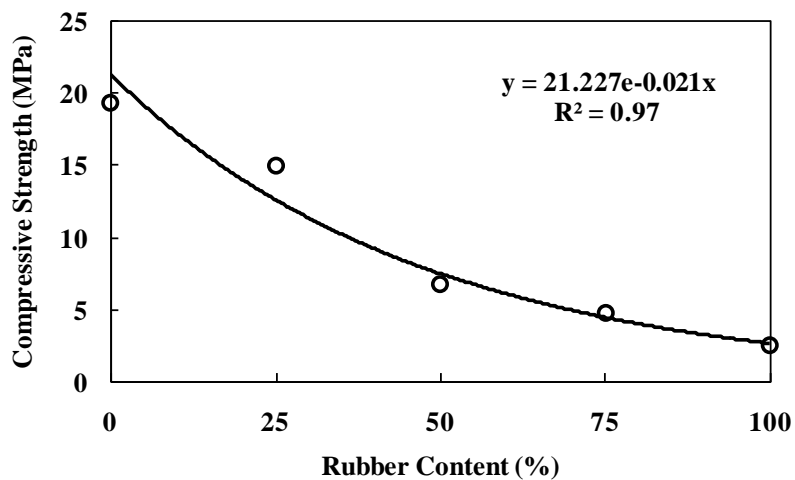


Figure 2. The compressive strength of rubberized normal weight aggregate concrete at 28 days

Failure mode of the test specimens was also investigated for all the replaced quantity of rubber. Three different types of failure patterns were observed following the ASTM C 39 specification to identify the failures. The observed failure patterns were shear, cone and shear, and columnar. For the control mix, failure occurred with taking sufficient time. However, failure occurred with less time compared to the control mix with the increasing rubber content in the concrete mix.

Splitting Tensile Strength Properties of Rubberized Normal Weight Aggregate Concrete

In this test procedure, load was applied at the perimeter of concrete cylinder block. It was found from the test results that the splitting tensile strength value for the control mix (standard case with 0% rubber content) was 2.60 MPa. However, the strength values were decreased exponentially with the increasing rubber content. Fig 3 shows the variation of splitting tensile strength for the rubberized normal weight concrete for different rubber contents. As can be seen from the figure, the strength reduction is exponential with the increasing rubber content. It is important to note that the characteristic splitting-tensile mode of failure was observed for all specimens in this test, which was followed by a single crack formed down the centre of the cylinder prior to failure. It is worth mentioning that with the reduction in splitting tensile strength, failures were more rapid compared to the control mix but the failure was occurred similarly at the middle of the cylindrical specimens.

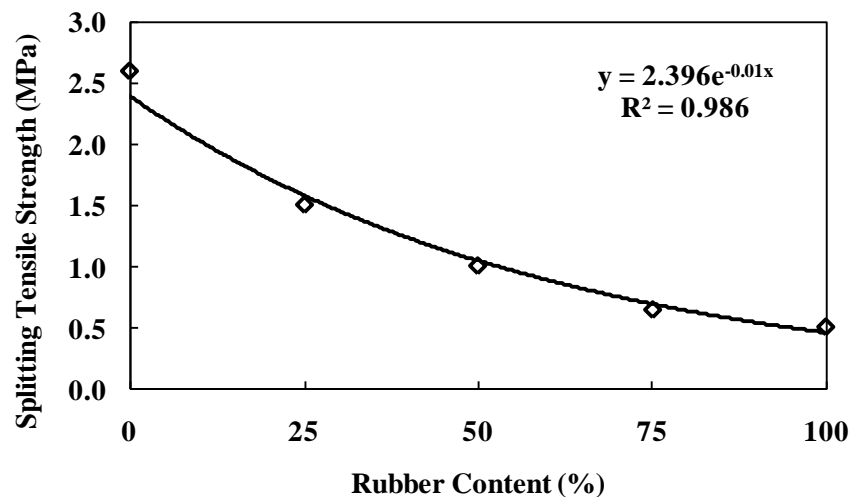


Figure 3. The splitting tensile strength of rubberized normal weight aggregate concrete at 28 days

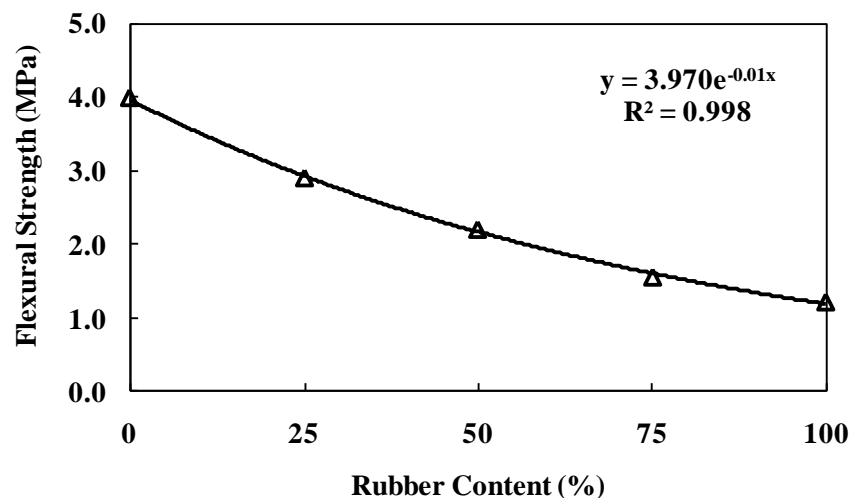


Figure 4. The flexural strength of rubberized normal weight aggregate concrete at 28 days

Flexural Strength Properties of Rubberized Normal Weight Aggregate Concrete

In order to investigate the flexural strength behaviour of the rubberized normal weight concrete, the specimens were tested under a simply supported loading orientation. The test results indicated that the flexural strength for the control mix was 4 MPa. The flexural strength obtained for the rubberized normal weight concrete with different rubber contents is shown in Fig 4. The figure reveals that the flexural strength also decreases with the increasing rubber content in the rubberized normal weight concrete and the strength reduction follows an exponential pattern. The reason could be the loose bonding between the aggregates due to inadequate roughness of the aggregates.

Flexural Toughness Properties of Rubberized Normal Weight Aggregate Concrete

Toughness usually refers to the ability to absorb energy comes from the external sources. Toughness is often represented by an index named Toughness Index. Toughness Index can be defined as the ratio of area under load-deflection curve up to 3.0 times first crack deflection to the area under load-deflection curve up to first crack deflection, which is often noted as I_5 (Miller and Tehrani, 2017). Fig 5 shows the variation of Toughness Index for different rubber contents. As can be seen from the figure, initially after an unexpected slight decrease in index value from 7.41 for 0% to 7.31 for 25%, the values are increasing with the increasing rubber content in the rubberized normal weight concrete. The noticeable fact is that the index value is the highest for 100% coarse aggregate replacement by the rubber content in rubberized normal weight concrete. The toughness index value for 100% rubber content was found as 13.8. This gives an important insight regarding the potential utilization of the rubberized normal weight concrete for the cases where shock absorption is more important rather than the concrete strength.

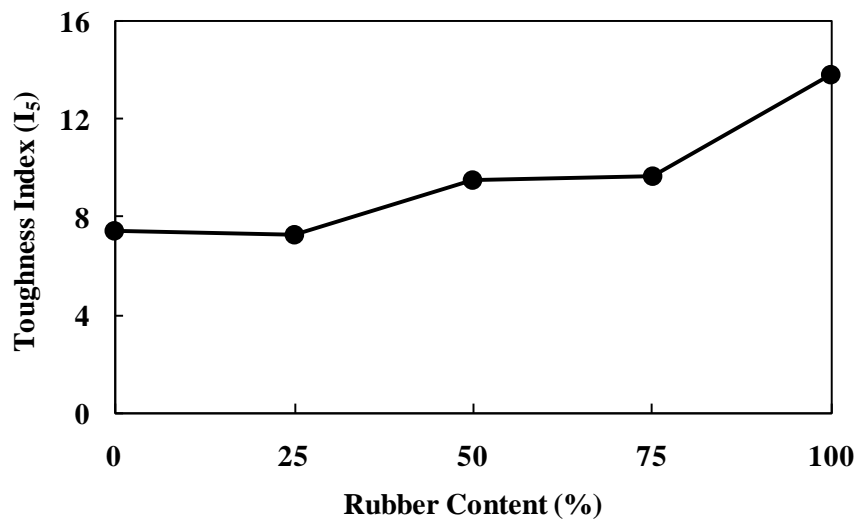


Figure 5. The flexural toughness of rubberized normal weight aggregate concrete at 28 days.

CONCLUSIONS

The conclusions and specific findings of the research are summarized as follows:

- Rubber reduces the compressive strength, splitting tensile strength and flexural strength up to 87%, 81.7% and 70%, respectively for 100% rubber content with respect to normal concrete (standard case with 0% rubber content as a volumetric replacement of coarse aggregate).
- Most impressive part of this study is that there is an increase in the flexural toughness with increasing rubber content in the concrete mix. It was found that rubber increases the flexural toughness by 28.9%, 31%, and 86% for a rubber content of 50%, 75%, and 100%, respectively. Increased flexural toughness demonstrates that the energy absorbing capacity of concrete increases with increasing rubber content.
- The results of the current study suggest that the rubberized normal weight aggregate concrete could be used for applications where absorption of excessive energy or mitigation of vibration is a key concern at high rubber replacement values rather than achieving higher strength.

REFERENCES

- Crow, JM. 2008. The concrete conundrum. *Chem. World*, 5(3): 62–66.
- Ganjian, E; Khorami, M and Maghsoudi, AA. 2008. Scrap-tyre-rubber replacement for aggregate and filler in concrete. *Constr. Build. Mater.*, 23(5): 1828–1836.
- Khatib, ZK and Bayomy, FM. 1999. Rubberized Portland cement concrete. *J. Mater. Civ. Eng.*, 11(3): 206–213.
- Li, G; Garrick, G; Eggers, J; Abadie, C; Stubblefield, MA and Pang, SS. 2004. Waste tire fiber modified concrete. *J. Compos. Part B: Eng.*, 35(4): 305–312.
- Miller, N. M and Tehrani, F. M. 2017. Mechanical properties of rubberized lightweight aggregate concrete. *Constr. Build. Mater.*, 147: 264–271.
- Roskos, C; White, T and Berry, M. 2015. Structural performance of self-cementitious fly ash concrete with glass aggregates. *J. Struct. Eng.*, 141(3): B4014010-1-10.
- Taha, B and Nounu, G. 2009. Utilizing waste recycled glass as sand/ cement replacement in concrete. *J. Mater. Civ. Eng.*, 21(12): 709-721. DOI: 10.1061/(ASCE)0899-1561 (2009)21:12(709).
- Topçu, IB. 1994. The properties of rubberized concretes. *Cement Conc.. Res.*, 25(2): 304–310.
- Xue, J and Shinozuka, M. 2013. Rubberized concrete: a green structural material with enhanced energy-dissipation capability. *Constr. Build. Mater.*, 42: 196–204.
- Zheng, L; Huo, XS and Yuan, Y. 2008. Strength, modulus of elasticity, and brittleness index of rubberized concrete. *J. Mater. Civ. Eng.*, 20(11): 692–699.

EXPERIMENTAL INVESTIGATION OF COMPRESSIVE STRENGTH OF 12.5 mm PLASTERED UNREINFORCED BRICK MASONRY WALL

A. F. Mazumder^{1*}, S. Hossain², M. R. Rana² & M. S. Ali²

¹*Department of Civil and Construction Engineering, Western Michigan University, Michigan, USA.*

E-mail: abul.f.mazumder@wmich.edu

²*Department of Civil Engineering, Presidency University, Dhaka, Bangladesh.*

E-mail: hossainsaddam426@yahoo.com; rasel.rana222@gmail.com; ahmedmdsujan@gmail.com

**Corresponding Author*

ABSTRACT

Plaster is a mix of cement, sand, and water. Plaster is applied on the masonry surface to cover rough surfaces of the wall. The key purposes of providing plaster are to protect the masonry surfaces from environmental exposure to hide defective joints, to prevent moisture entrance, and to obtain clean, smooth, and durable surface. Besides these advantages, plaster increases the axial capacity of the wall. The main objective of this paper is to investigate experimentally the increase of axial load bearing capacity of a plastered masonry wall. To accomplish the objective, six specimens ($234.95 \times 114.3 \times 63.5$ mm) are constructed. Among these specimens, three specimens are plastered with 12.5 mm thick plaster. The cement-sand ratio of the plaster is 1:2.5 and water-cement ratio is 0.6. After 28 days wet curing period, all the specimens are tested under axial compressive load. The average compressive strength of the masonry walls without and with plaster is 3.48 and 3.85 MPa, respectively. Therefore, the 12.5 mm plaster could increase the axial capacity by 10.63% and the efficiency of the plaster is 17.29%.

Keywords: Brick; Masonry; Plaster.

INTRODUCTION

Masonry wall is one of the most popular and common type of structural component which is made from individual units laid in and bonded together using mortar. For many years, masonry wall is being used because of its aesthetic appearance, cost effectiveness, and ease of construction. The key advantages of masonry wall include increase of thermal mass and fire protection of the building, reduced life cycle cost, and 30 to 100 times higher useful life cycle than structural steel. Masonry walls are most commonly used as partition wall, structural wall, retaining wall, and even in heritage structures. Masonry walls are constructed usually as unreinforced. These unreinforced masonry (URM) walls are vulnerable to high axial load and earthquake load. URM walls can be used as load-bearing wall, if proper strengthening materials are used. Some researchers used CFRP, GFRP sheet and bars, tensile reinforced mortar, ultra high performance concrete, and ordinary mortar for strengthening (Basaran et al., 2013; Vasconcelos et al., 2012; Mahmood et al., 2008; ElGawady et al., 2006; Zhao et al., 2003; Mazumder, 2017; Mazumder et al., 2017) and found out axial capacity of masonry wall with and

without strengthening schemes. Some researchers investigated the axial capacity of masonry wall using numerical simulations (Mazumder and Sarfin, 2017; Mazumder and Nishat, 2017).

URM wall is more useful for load-bearing type of wall with proper strengthening techniques and cementitious material could be one of the possible solutions. Usually, cement-sand mortar is used to plaster a wall. Plaster is provided to protect the masonry wall surface from rough environmental exposure, to hide defective joints, to prevent moisture entrance, and to obtain clean, smooth, and durable surface. A 12.5 mm thick plaster is provided for inner surface and 18.75 mm plaster is provided for outer surface of the wall. This plaster makes the wall stronger, durable, and increases the load bearing capacity of the wall as well. The main objective of this study is to investigate experimentally the increase of load bearing capacity of unreinforced masonry wall with the use of 12.5 mm thick plaster on both sides.

METHODOLOGY

The load bearing capacity of unreinforced concrete masonry wall prisms are evaluated using axial load tests. In this test, incrementally increased compressive load is applied to the prisms. Six specimens are tested in two categories – i) three unreinforced masonry prisms (UMP) and ii) three 12.5 mm thick plastered masonry prisms (UMPP). The compressive strength of brick and mortar is also investigated. Six specimens are constructed and wet cured. Specimens are tested under compressive load after curing period.

Material properties

Mechanical properties of wall components, concrete masonry brick and mortar, are investigated experimentally. Compressive strength of concrete masonry bricks is obtained following test procedure of Barbosa (2009). The average compressive strength of bricks is 957.75 psi. The compressive strength of mortar is tested following ASTM C39. The 28-day compressive strength of mortar is obtained and average value is 2688.35 psi. The water-cement and cement-sand ratio of mortar are 0.6 and 1:2.5, respectively.

Construction of prisms

Six prisms are constructed with concrete masonry bricks and Portland cement mortar is used as head and bed joints. The nominal size of a brick is $235 \times 110 \times 70$ mm, approximately. Three layers of bricks, containing one and a half bricks in each layer, are cast to form the prisms. 12.5 mm thick plaster is applied on the both sides of the three prisms. The aspect ratio for all walls is 0.9 and height to thickness of the wall is 2.10, approximately. After casting, specimens are wet cured for 28 days. After curing period, the specimens are tested.

Experimental setup, instrumentation, and procedure

According to ASTM C1314 and European Standard EN1052-1(1999), masonry prisms (UMP and UMPP) are tested under uniaxial compressive load. To avoid eccentricity, the prisms are placed vertically and horizontally perfectly aligned on Universal Testing Machine (UTM). The axial compression forces are exerted on the prism through steel plate and rubber sandwich. The steel plate and rubber sandwiches are attached on the top and bottom of the prisms to ensure uniform distribution of the axial force without any stress localization. Fig. 1 shows the test setup for UMP and UMPP.



a) Experimental setup of UMP



b) Experimental setup of UMPP

Figure 1: Specimen and experimental setup of UMP and UMPP

RESULTS

Six prisms are tested to evaluate compressive strength using UTM. An incrementally increased compressive load is applied on the prisms until failure. Table 1 shows the compressive strength of UMP prisms. The average compressive strength of UMP is 504.73 psi. Compressive strength of each UMPP is presented in Table 2. The average compressive strength of UMPP is 557.65. The 12.5 mm plaster could successfully increase the compressive strength of UMP by 10.63%. The efficiency of the plaster is 17.29%.

Table 1: Compressive strength of UMP

Serial no.	Dimension (L × B × H) (mm × mm × mm)	Load (kN)	Stress (psi)	Average stress (psi)
1	360 × 112.33 × 219	140	502.12	504.73
2	363 × 111 × 214.33	148	532.74	
3	365 × 111.67 × 219	135	480.38	

Table 2: Compressive strength of UMPP

Serial no.	Dimension (L × B × H) (mm × mm × mm)	Load (kN)	Stress (psi)	Average stress (psi)
1	370 × 110 × 225	150	534.54	557.65
2	365 × 112.67 × 220.67	152	536.07	
3	323 × 110.33 × 225.33	148	602.35	

CONCLUSIONS

Ordinary Portland cement mortar is used to plaster the inner and outer surface of an unreinforced masonry wall. The main purpose of plastering is to protect the wall from deleterious moisture ingress and provide a smooth, clean, and durable surface. Plaster increases the axial capacity of the masonry wall. To evaluate the increase in axial capacity, six prisms are constructed and three of them are plastered. All the specimens are tested under compression in universal testing machine after 28 days wet curing period. The average compressive strength is 504.73 and 557.65 psi for UMP and UMPP prisms, respectively. Therefore, the axial capacity of masonry wall is increased by 10.63% approximately due to 12.5 mm plaster. The efficiency of the plaster is 17.29%.

ACKNOWLEDGMENT

The research work presented in this paper was carried out at the Civil Engineering laboratory of Presidency University (PU). The authors would like to thank PU for the continuous support.

REFERENCES

- Basaran, H; Demir, A and Bagci, M. 2013. The Behavior of Masonry Walls with Reinforced Plaster Mortar. *Advances in Material Science and Engineering*, 1-9.
- Barbosa, CS and Hanai, JB. 2009. Strength and Deformability of Hollow Concrete Blocks: Correlation of Block and Cylindrical Sample Test Results. *Ibracon Structures and Materials Journal*.
- ElGawady, MA; Lestuzzi, P and Badoux, M. 2006. A Seismic Retrofitting of Unreinforced Masonry Walls Using FRP. *Science Direct, Composites: Part B* (37): 148-162.
- Mahmood, H; Russell, AP and Ingham, JM. 2008. Monotonic Testing of Unreinforced and FRP-Retrofitted Masonry Walls Prone to Shear Failure in an Earthquake. *The 14th World Conference on Earthquake Engineering*, 214-220.
- Mazumder, AF and Sarfin, MAA. 2017. Numerical Investigation of Axial Capacity Assessment of UHPC Plastered Wall using ABAQUS. *Proceedings of the ICEIRE 2017*, 4: 45-48.
- Mazumder, AF; Mahmud, A and Rafael, M. 2017. Investigation of the Contribution of the Plaster in Compressive Strength of Unreinforced Masonry Wall. *Proceedings of the ICEIRE 2017*, 4: 182-184.
- Mazumder, AF. 2017. Axial Load Bearing Capacity of Unreinforced Concrete Masonry Wall and UHPC Block Wall. *Proceedings of the ICEIRE 2017*, 4: 25-28.
- Mazumder, AF and Nishat, M. 2017. Numerical Investigation of Axial Capacity Assessment of UHPC Plastered Wall using ABAQUS. *Proceedings of the ICEIRE 2017*, 4: 33-36.
- Vasconcelos, G; Abreu, S; Figueiro, R and Cunha, F. 2012. Retrofitting Masonry Infill Walls with Textile Reinforced Mortar. *15 WCEE, LISBOA*, 178-187.
- Zhao, T; Xie, J and Li, H. 2003. Strengthening of Cracked Concrete Block Masonry Walls Using Continuous Carbon Fiber Sheet. *9th North American masonry conference, South Carolina, Clemson*, 9: 156-167.

PERFORMANCE OF RECYCLED AGGREGATE CONCRETE AS A FULLY REPLACEMENT OF NATURAL AGGREGATE

M. A. Rahman*, A. Rahman & M. Ahmed

Department of Civil and Environmental Engineering, Shahjalal University of Science and Technology, Sylhet-3114, Bangladesh.

E-mail: ashiq064@gmail.com

**Corresponding Author*

ABSTRACT

Use of recycled aggregate concrete (RAC) can be beneficial to environmental upkeep and waste management. Enormous amount of RAC are generated daily in developing countries like Bangladesh nowadays. Using this RAC can be an economical option hereafter. This paper highlights the scope of using RAC as a fully replacement of natural aggregate. In this study, physical properties, workability, compressive strength and splitting tensile strength of RAC are investigated deftly and discussed about their impacts on concrete. RAC has been used in two different concrete mix proportion (1:1.5:3 and 1:2:4) for four arbitrary w/c ratio of 0.4, 0.45, 0.5 and 0.55 to find out the 28 days compressive strength and splitting tensile strength of RAC. Portland composite cement (PCC) of CEM II and Sylhet sand (Sari River) having a constant F.M. of 2.81 are used to conduct the study. Experimental results show that the maximum compressive strength 18.70 Mpa of RAC is found for the mix proportion of 1:1.5:3 and w/c ratio of 0.45 and maximum splitting tensile strength 2.42 Mpa of RAC is found for the mix proportion of 1:1.5:3 and w/c ratio of 0.45. Thus, these results are satisfactory comparing to natural aggregate concrete. Furthermore, this practice can be a new aspect of using RAC to conserve the natural aggregate resources as well as uncover a cost effective approaches in concrete technology.

Keywords: Recycled Aggregate Concrete; Compressive strength; Splitting Tensile Strength; Water Cement Ratio; Demolished waste; Cost effective.

INTRODUCTION

As urbanization rate trend in Bangladesh is increasing day by day like other developing countries, the need for new buildings and infrastructure has also grown up. This has an influence on the storage of natural aggregates as they are depleted up rapidly. The way this matter is evolved which causes adverse environmental threat afterwards. Alternatively, a huge amount of construction wastes are continuously being generated daily which are being usually unloaded in landfills. So, it requires a large area to manage this waste (Kalpavalli and Naik, 2015).

Rather, if this waste can use as recycle aggregate which can be a probable way of replacement of natural aggregates in construction work. Thus, it opens a solution from running out of natural aggregate problem by preserving the natural resources of aggregate. In addition, it could solve the environmental phenomena and also maintain the sustainability of the construction work.

Common sources of recycled aggregate are outdated buildings, demolished concrete pavements, and pile cap from new construction site. Another source of these aggregates are destroyed buildings, concrete pavements, bridges, etc. due to natural disaster like earthquake, cyclone, floods or manmade disaster like war.

Recycled aggregate is lighter than natural aggregate which indicates its low density but having higher absorption capacity of recycled aggregate results less strength than natural aggregate. In that case, concrete made from recycle aggregate can be employed where less strength requires for instance in low rise building, in reinforced concrete pavement etc. (Somani et al., 2016)

Moreover, these large amounts of construction wastes can purchase in a very cheap cost which is normally considered as debris by most of the people. By using this debris, people can easily reduce the cost construction cost.

METHODOLOGY

Sand

Locally available coarse sand (Sari River Sand) was used as fine aggregate in concrete mix which fineness modulus value was 2.82.

Cement

Portland Composite Cement of CEM-II/B-M (ASTM C595) has been used from Seven Rings Cement brand of Bangladesh for using as binding material.

Recycled Aggregate Concrete

Recycle aggregate were collected from a demolished illegal commercial building near Kumar Para road, Sylhet. Demolished wastes were mostly taken from beams, slabs and columns portion. The demolished aggregate were mostly rock and were ash in color (see Fig. 1).

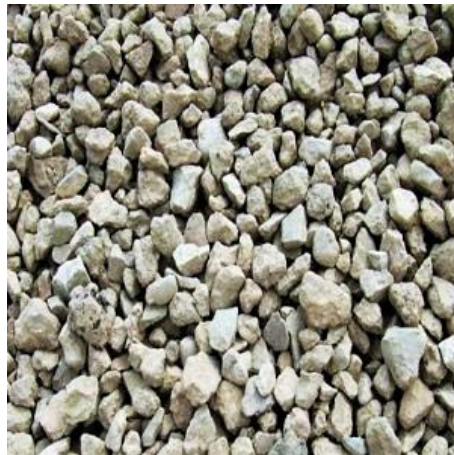


[Fig. 1] Recycled Aggregate

Processing of Recycled Aggregate

Collected demolished wastes were crushed through stone breaking machine. After completion of crushing, cementing mortar and other foreign materials are filtered out through screening, hand pickling and water flotation process and then mixing of different sizes of aggregate was done (see Fig. 2). The sizes of the recycled aggregate are kept between 6 mm to 12 mm.



[Fig. 2] Processing of Recycled Aggregate

Mixing process

Two arbitrary mix proportion of 1:1.5:3 and 1:2:4 (Cement: Fine aggregate: Coarse aggregate) by volume was chosen for the experimental work. These mix proportion was chosen because of their widespread application. Four water-cement ratios of 0.40, 0.45, 0.50 and 0.55 were used in this study.

For casting of concrete specimens, both coarse aggregate (RAC) and fine aggregate (sari sand) were kept in saturated surface dry (SSD) condition.

Specimen

A total number of 48 concrete cylinders were casted to perform compressive strength test and splitting tensile strength test. The mould size was 100 mm diameter X 200 mm height. Each Cylindrical specimen were set for 28 days curing and tested by universal testing machine (UTM).

Testing Procedures

The compressive strength test was carried out according to ASTM C39, 2003 method by using 100 mm X 200 mm concrete cylinders as specimen. The splitting tensile strength test was carried out according to ASTM C496 method by using 100mm X 200mm concrete cylinders as specimen.

RESULTS AND DISCUSSIONS

Relative Density (Specific gravity) and Absorption

According to ASTM C127, specific gravity and absorption capacity test were conducted for recycled aggregate. The specific gravity for recycled aggregate ranges between (2.13-2.23) which is slightly lower than the acceptance criteria of natural aggregate (see Table-1). Due to cement mortar attached to recycled aggregate, absorption capacity is much higher than the acceptance criteria of natural aggregate (see Table-1).

Bulk Density and Void

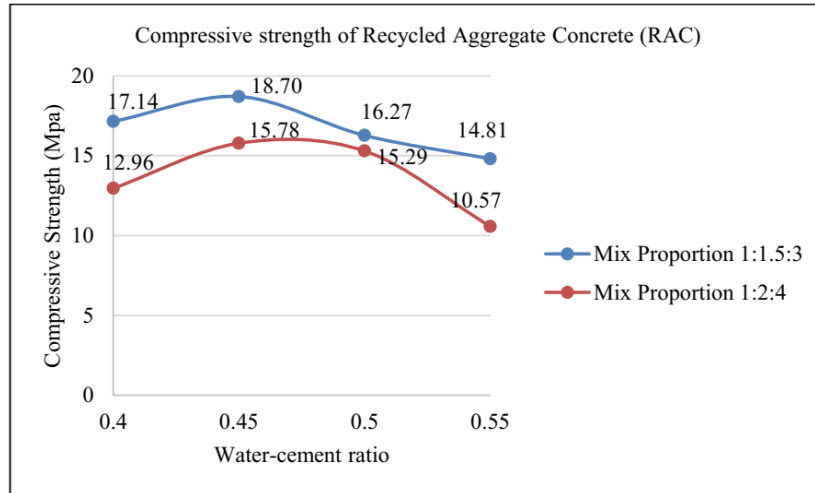
ASTM C29 followed to determine the bulk density (both rodding and shovelling) and void of recycled aggregate. Bulk density of recycled aggregate is slightly higher than the minimum criteria of the bulk density of natural aggregate (see Table-1) according to ACI EI-07. Void ratio of recycled aggregate is also satisfying the acceptance criteria of natural aggregate (see Table-1). Proper crushing and screening is necessary to maintain a uniform shape of recycled aggregate as it ensures the voids. Thus voids affect on some engineering properties like compressive strength (Kabir et al., 2016).

Table 1: Properties of Recycled Aggregate comparing with Natural Aggregate

Properties	Recycled Aggregate	Acceptance Criteria (For Natural Aggregate)
Oven dry Specific gravity- ASTM C127	2.13	2.30-2.90 (ACI EI-07)
Apparent Specific gravity - ASTM C127	2.23	2.30-2.90 (ACI EI-07)
Absorption Capacity (%) - ASTM C127	2.11	≤ 2, (IS 2386-Part 5)
Bulk Density (Shoveling) (lb/cft) – ASTM C29	83.4	80-120 (ACI EI-07)
Bulk Density (Rodding) (lb/cft) - ASTM C29	90.85	80-120 (ACI EI-07)
Void (Shoveling) (%) – ASTM C29	37.12	≥30
Void (Rodding) (%) - ASTM C29	31.52	≥30

Compressive Strength of RAC

As absorption is much higher in recycled aggregate, RAC consumes much water for mix proportion 1:2:4 than mix proportion 1:1.5:3. Thus, mix proportion 1:1.5:3 gives much higher compressive strength than mix proportion of 1:2:4 for four different water cement ratios of 0.4, 0.45, 0.5 and 0.55. Whereas water cement ratio containing of 0.45 gives the maximum compressive strength of 18.70 Mpa (See fig.3) for RAC for mix proportion 1:1.5:3 which is quite acceptable for construction or pavement works. Firstly, compressive strength relationship follows an increasing trend for both mix proportion. Compressive strength increases 9.1% (Mix proportion 1:1.5:3) and 21.76% (Mix proportion 1:2:4) for changing water cement ratio 0.4 to 0.45. But after the water cement ratio of 0.45, the relationship follows a decreasing trend. Compressive strength decreases 13% (Mix proportion 1:1.5:3) and 3.11% (Mix proportion 1:2:4) due to changing the water cement ratios from 0.45 to 0.5. And compressive strength again decreases 8.97% (Mix proportion 1:1.5:3) and 30.87% (Mix proportion 1:2:4) for 0.5 to 0.55 water cement ratio.



[Fig. 3] Compressive strength for RAC

Splitting tensile strength of RAC

Like compressive strength, splitting tensile strength also found maximum for mix proportion of 1:1.5:3 than mix proportion 1:2:4 for all the water cement ratios of 0.4, 0.45, 0.5 and 0.55. Here, water cement ratio containing of 0.45 gives the maximum splitting tensile strength of 2.42 Mpa (See fig.4) which is greater than the 10% compressive strength (18.70 Mpa) of same water cement ratio for mix proportion 1:1.5:3. Initially, splitting tensile strength relationship follows an increasing trend for both mix proportion. Splitting tensile strength increases 13.62% (Mix proportion 1:1.5:3) and 12.37% (Mix proportion 1:2:4) for changing water cement ratio 0.4 to 0.45. Then again, after water cement ratio of 0.45, the relationship follows a decreasing trend. Splitting tensile strength decreases 14.88% (Mix proportion 1:1.5:3) and 17.89% (Mix proportion 1:2:4) for changing the water cement ratios from 0.45 to 0.5. And decreases 20.87% (Mix proportion 1:1.5:3) and 5.59% (Mix proportion 1:2:4) for 0.5 to 0.55 water cement ratio.

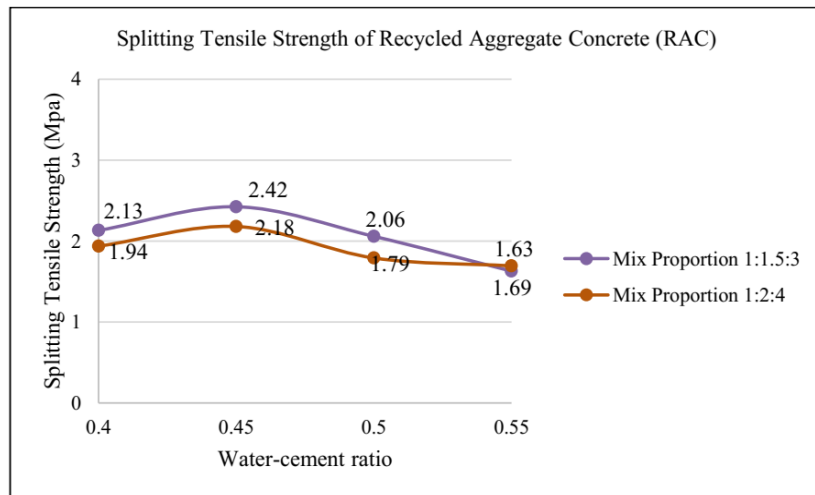


[Fig. 4] Splitting Tensile strength for RAC

Correlation between Compressive and tensile strength

Correlations between the compressive strength and splitting tensile strength of the different samples were calculated in order to determine the relevance of the results, based on the Pearson correlations calculations; in particular, the correlations between the results of the compressive strength tests and the results of the other tests were calculated for mix proportion 1:1.5:3 and Mix proportion 1:2:4.

Correlation between compressive strength and splitting tensile strength for mix proportion 1:1.5:3 are shown in “Fig. 5” and “Eq. 1”. A linear relationship is noted between these two properties ($R^2=0.9624$).

$$S_p = 0.1965f_c - 1.2316 \dots\dots\dots (1)$$

Where, S_p is the splitting tensile strength and f_c is the compressive strength

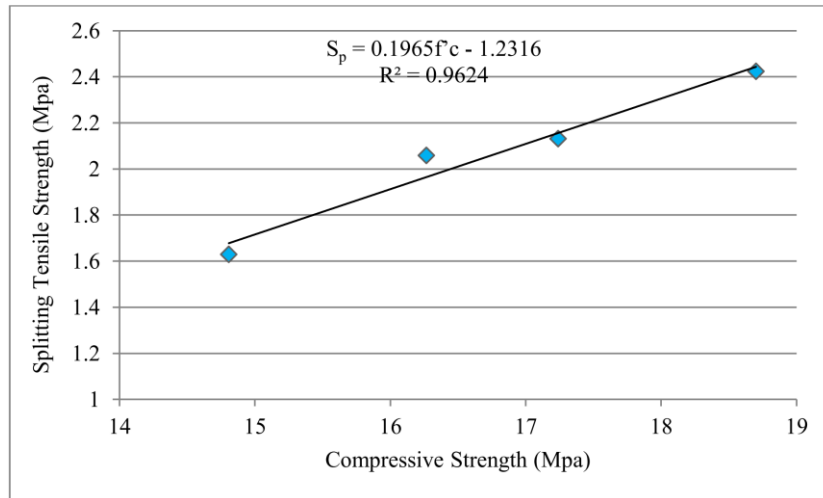


[Fig. 5] Correlation between compressive strength and splitting tensile strength for mix proportion 1:1.5:3

Correlation between compressive strength and splitting tensile strength for mix proportion 1:2:4 are shown in “Fig. 6” and “Eq. 2”. A linear relationship is noted between these two properties ($R^2=0.4568$). Here, R^2 values for mix proportion 1:2:4 depicts that “Eq. 2” doesn’t show a proper linear relationship. As the water cement ratio increases, the compressive and splitting tensile strength characteristics are becoming aberrant in mix proportion 1:2:4.

$$S_p = 0.0598f_c + 157.31 \dots\dots\dots (2)$$

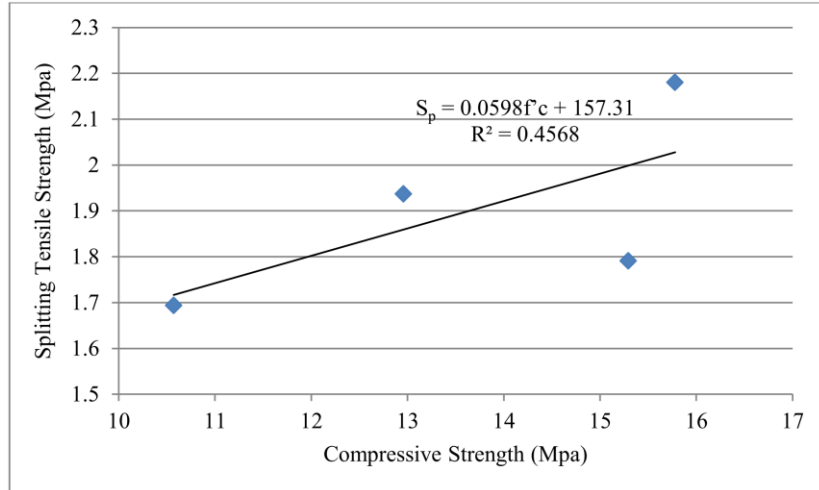


[Fig. 6] Correlation between compressive strength and splitting tensile strength for mix proportion 1:2:4

CONCLUSIONS

1. Physical properties of recycled aggregate satisfy the specific gravity and bulk density criteria of natural aggregate for both shoveling and rodding but absorption capacity found 2.11% which is higher than the natural aggregate.
2. For Mix proportion of 1:1.5:3, compressive and splitting tensile strength found maximum 18.70 Mpa and 2.42 Mpa respectively for water cement ratio of 0.45 which is quite satisfactory regarding natural aggregate concrete.
3. For Mix proportion of 1:1.5:3, compressive and splitting tensile strength shows a linear correlation with a high $R^2=0.9624$ whereas for mix proportion 1:2:4 correlation is very poor

having a low $R^2=0.4568$.

ACKNOWLEDGMENTS

Authors would like to acknowledge Ministry of Science & Technology, Bangladesh for funding the research work under ‘Concrete strengthening using natural fibers’– R&D project (2014-15). Also authors are very much grateful to Professor Dr. Mushtaq Ahmed, Civil and Environmental Engineering Dept., Shahjalal University of Science & Technology, Sylhet-3114 for his dear facilitation.

REFERENCES

- ACI EI-07. 2007 ACI committee education bulleting-aggregates for concrete. American Concrete Institute. Farmington Hills, USA: Author.
- ACI EI-07. 2007 ACI committee education bulleting-aggregates for concrete. American Concrete Institute. Farmington Hills, USA: Author.
- American Concrete Institute (2008). Building Code Requirements for Structural Concrete (ACI-318). Detroit, Michigan, USA: Author.
- ASTM C127-88, 1998. Standard test method for specific gravity and absorption of coarse aggregate. West Conshohocken, PA.
- ASTM C 33-3, 2003. Standard specification for coarse aggregate. West Conshohocken, PA.
- ASTM C 29/C 29M-97, 1997. Standard test method for bulk density and void in aggregate. West Conshohocken, PA.
- ASTM C 39-03, 2003. Standard test for compressive strength of Concrete aggregate. West Conshohocken, PA.
- ASTM C 496-04, 2004. Standard test method for splitting tensile strength of cylindrical concrete specimen. West Conshohocken, PA.
- IS 2386-Part V: 1997. Method of tests for aggregates of concrete mechanical properties. New Delhi, India: Bureau of Indian Standards
- Kabir, S.; Al-Shayeb, A. & Khan, I. M. 2016. Recycled concrete debris as concrete aggregate for sustainable construction materials. *International Conference on Sustainable Design, Engineering and Construction*. Procedia Engineering 145 (2016), 1518-1525.
- Kalpavalli, A., & Naik, D. 2015. Use of demolished concrete wastes as coarse aggregates in high strength concrete production. *International Journal of Engineering Research & Technology (IJERT)*, 4(7).
- McNeil, K. and Kang, T.H.K., 2013. Recycled concrete aggregates: A review. *International Journal of Concrete Structures and Materials*, 7(1), 61-69.
- Mr. Sonawane T. R. and Prof. Dr. Pimplikar S. S. 2009. Use of recycled aggregate concrete. *Journal of Mechanical and Civil Engineering (IOSR-JMCE)*, 52-5.
- Saidi, M., Ait-Medjber, F., Safi, B. and Samar, M., 2014. Recycling of aggregates from construction demolition wastes in concrete: study of physical and mechanical properties. *International Journal of Civil, Environmental, Structure, Construction and Architectural Engineering*, 8(12), 1307-1311.
- Shivakumar, M.N.; Nithin, K.S. and BM, G. 2014. Use of building demolished waste as coarse aggregate in porous concrete. *International Journal of Research and Engineering Technology*.
- Somani, P.; Dubey, B.; Yadav, L.; Kumar, J.; Kumar, A. & Singh, M. 2015. Use of demolished concrete waste in partial replacement of coarse aggregate in concrete. *International Journal of Civil Engineering (SSRG-IJCE)*, 3(5).

COMPARATIVE STUDY BETWEEN STRAIGHT BRIDGE AND CURVED BRIDGE USING STEEL CONCRETE COMPOSITE I SECTION

A. Roy^{1*} & M. Begum²

¹Department of Civil Engineering, World University of Bangladesh, Dhaka, Bangladesh.

E-mail: abhijitroy1204188@gmail.com

²Department of Civil Engineering, Bangladesh University of Engineering and Technology, Dhaka, Bangladesh. E-mail: shuma92@gmail.com

*Corresponding Author

ABSTRACT

Bridges with Steel-Concrete Composite I Section is a relatively new structural system for Bridges in Bangladesh. Number of studies regarding this particular type of bridge is very few. An attempt has been made in this research to conduct a comparative study between straight bridge and curved bridge using steel concrete composite I section. The analysis is carried under the dead load, live load of AASHTO LRFD 2007 vehicle load. This research is focussed on the comparative study of different girder sections with constant span keeping the cross-sectional shape and material properties constant. Finite element method has been employed for analysis using CSI Bridge (2016). The comparative investigations performed on different girders helps to evaluate the effects of change in girder section due to curvature. This study would enable bridge engineers to better understand the behaviour of steel-concrete composite I girder bridges and the results presented will be a valuable guidance to them in further studies regarding the topic or designing a bridge using similar type of girder.

Keywords: Steel Concrete Composite I Girder, Straight and Curved Bridge, CSI Bridge

INTRODUCTION

The main objective of this study is to conduct a comparative study of moment, shear force, axial force, torsional force and lateral shear force both for entire bridge section and girder section between straight bridges and curved bridges using Steel-Concrete Composite I Section to have an idea about the effect of curvature. This is an initial approach regarding selection of curvature in case of steel bridge design. This study will be helpful for those who want to do further studies on bridges using composite section. In this study, a straight bridge and a curved bridge are analysed using finite element software CSI Bridge 2016. The comparisons are done for a fixed span length and fixed degrees of curvature. Only dead loads and live loads are considered in this study. No lateral force is considered. Full composite action is considered. For further progression of this study, comparison for lateral forces can be done. The behaviour can be checked by changing the percentage of composite action too. Considering all the design considerations and cost analysis, an economic section can be designed and this study will be helpful for initial selection.

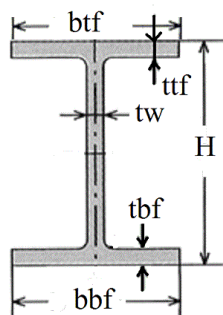
METHODOLOGY

Modelling of the Bridges:

The bridges to be analysed are modelled using frame and shell elements. CSI Bridge 2016 software is to generate nodes, elements, bearing line, lane, material properties, deck system, loading pattern, vehicle

class. The standard truck is HL 93 according to AASHTO LRFD 2007 design preference. The bridge modelling data are as follows-

1. Bridge Type:
 - a. Straight Bridge using Steel Concrete Composite I Girder
 - b. 90° Curved Bridge using Steel Concrete Composite I Girder (Left to Right Curve)
2. Bridge Layout Data: Length = 30 meter; Width = 12 meter; Lanes = 2
3. Material Properties: Concrete Yield Strength = 4 ksi; Steel Yield Strength = 50 ksi
4. Girder Properties:

Table 1: Girder Properties		
Properties	Dimension	Cross- Section of Girder
Height (H)	1 meter	
Top flange width (b_{tf})	400 mm	
Top flange thickness (t_{tf})	40 mm	
Web thickness (t_w)	20 mm	
Bottom flange width (b_{bf})	500 mm	
Bottom flange thickness (t_{bf})	50 mm	
Material Properties	50 grade steel	

5. Bent Properties: Depth = 1.52 meter; Width = 1.22 meter; Cap Beam Length = 9.15 meter; Number of Columns = 1
6. Super –Structure Properties: Top Slab Thickness = 304.8 mm; Concrete Haunch+ Steel Flange = 128.9 mm; Haunch Depth = 88.9 mm; Girder Spacing = 3.39 meter; Overhang Length = 1.19 meter; Overhang Distance to Fillet = 0.30 meter; Steel Flange = 40 mm.

Cross Section of the Super-structure along with necessary dimensions are given below-

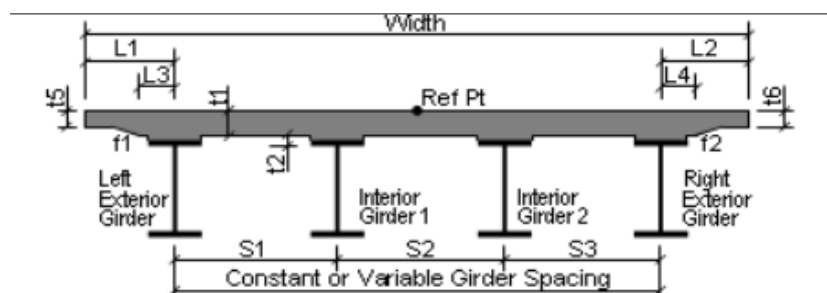


Fig.1: Cross-section of Bridge Super-structure

Width = 12 m; $L_1 = 1186.5$ mm; $L_2 = 1186.5$ mm; $L_3 = 305$ mm; $L_4 = 305$ mm; $S_1 = S_2 = S_3 = 3.39$ m; $t_1 = 305$ mm; $t_2 = 128.9$ mm; $t_5 = 305$ mm; $t_6 = 305$ mm; $f_1 = 305$ mm; $f_2 = 305$ mm.

7. Diaphragm Properties: Height= 1 meter; Top Flange Width = 400 mm; Top Flange Thickness = 18 mm; Web Thickness = 15 mm; Bottom Flange Width = 500 mm; Bottom Flange Thickness = 18 mm
8. Load Cases:
 - a. Dead Load: Self Weight of the Structure + 3" Wearing Surface + Railing
 - b. Live Load: HL 93 Live Load (Design Truck, Design Tandem, Design Lane)

The comparative study has been made separately for dead load and live load cases. The main focus of the study is to find out the change of forces for entire bridge section as well as girder section. Graphical representation has been shown to make the comparison. Comparison has been made for moment, shear force, axial force, torsional moment, lateral shear force.

Comparative Study for Dead Load Cases:

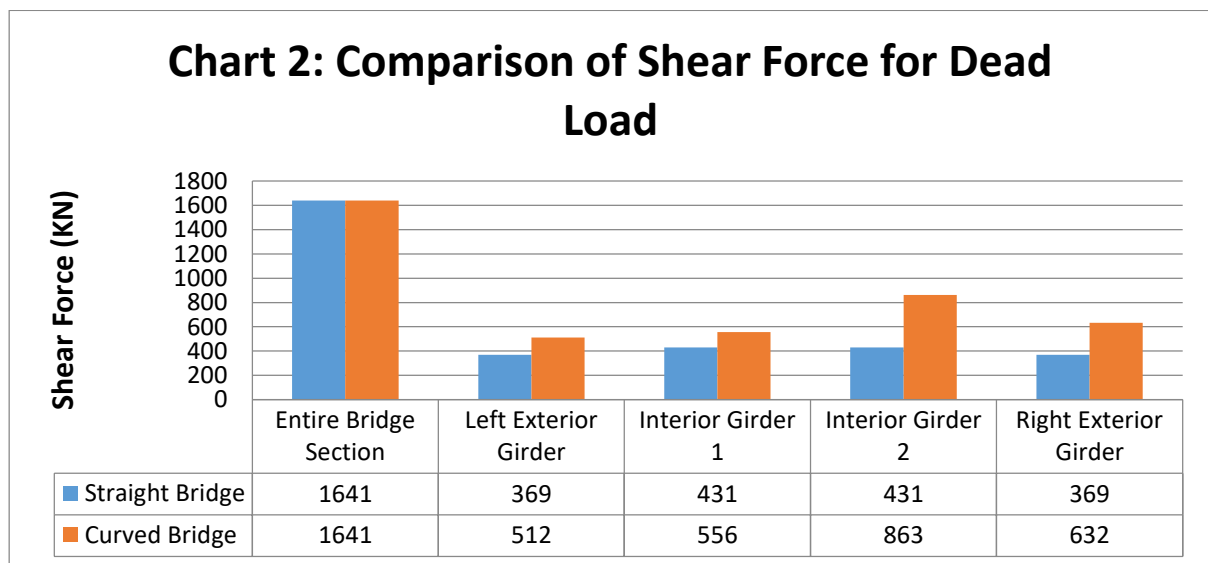
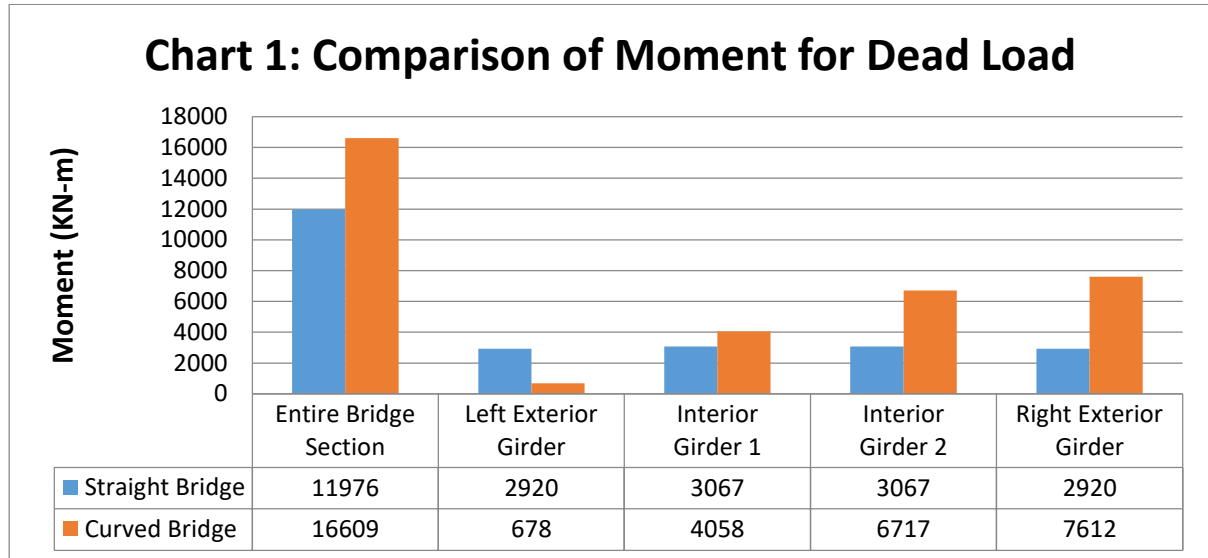


Chart 3: Comparison of Axial Force for Dead Load

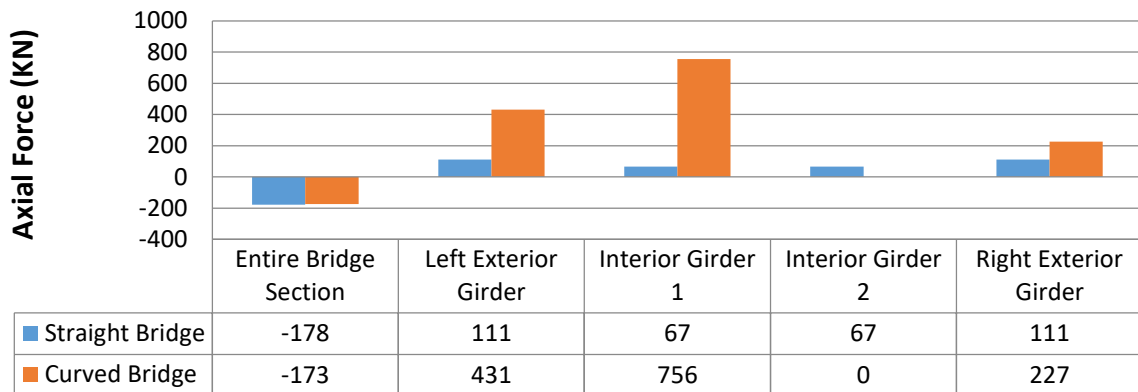


Chart 4: Comparison of Twisting Moment for Dead Load

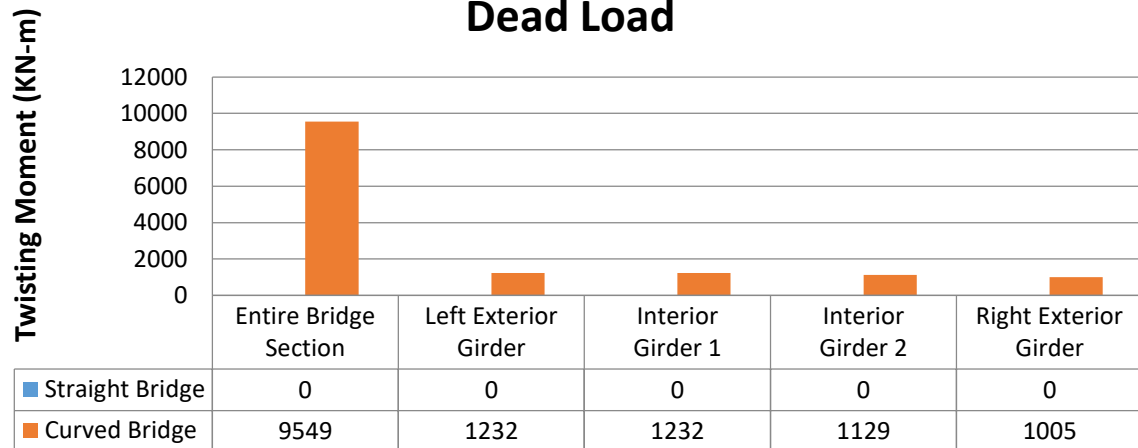
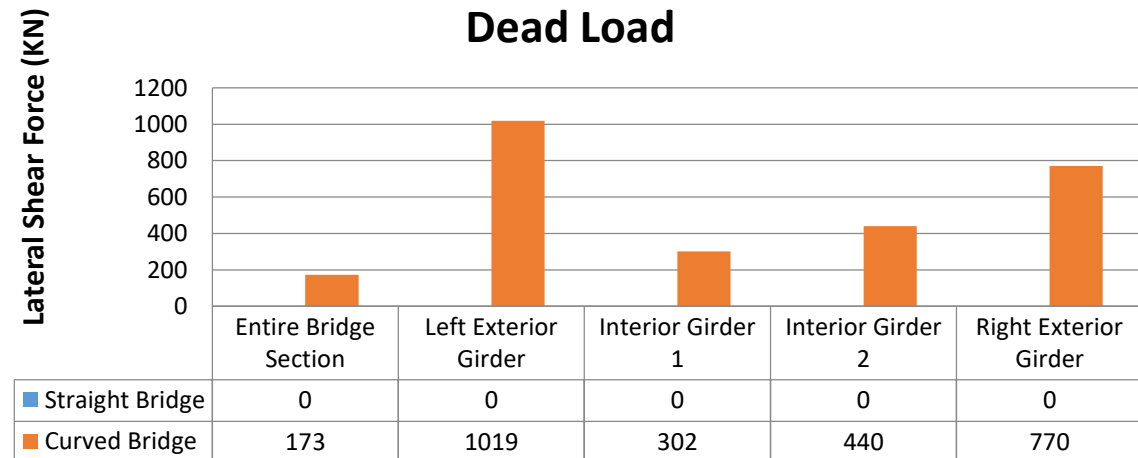


Chart 5: Comparison of Lateral Shear Force for Dead Load



Comparative Study for Live Load Cases:

Chart 6: Comparison of Moment for Live Load

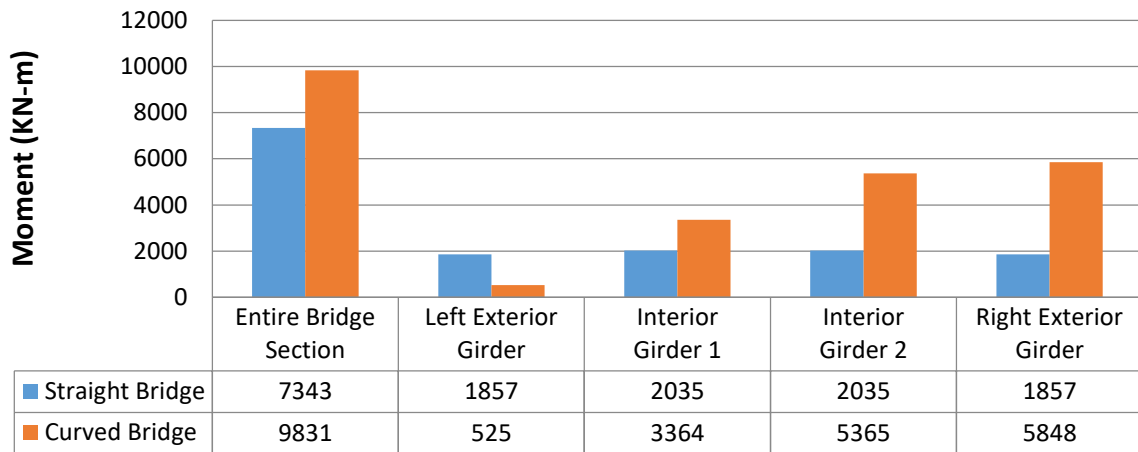


Chart 7: Comparison of Shear Force for Live Load



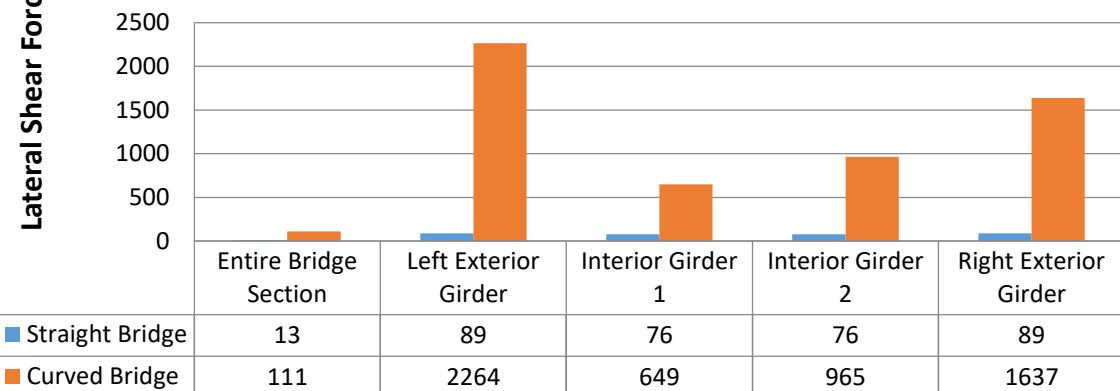
Chart 8: Comparison of Axial Force for Live Load



Chart 9: Comparison of Twisting Moment for Live Load



Chart 10: Comparison of Lateral Shear Force for Live Load



RESULTS AND DISCUSSIONS

From the above comparison curve, a certain change in forces due to curvature effect. The changes can be summarized as follows-

1. Bending Moment is 1.4 times more in case of Curved Bridge than Straight Bridge in case of Entire Bridge Section. This number is directly proportional to Degrees of Curvature. Moment will increase if Curvature Angle is increased. In case of Girder to Girder Comparison, we can see a gradual change of Moment in case of Curved Bridge from inner girder of the curved bridge to the outside girder of the curved bridge.
2. Development of Axial Force is constant throughout the entire span length in case of Straight Bridge, but in case of Curved Bridge, it varies along the length.
3. Development of Twisting Moment and Lateral Shear Force is quite large in case of Curved Bridge, but no Twisting Moment or Lateral Shear Force is developed in case of Straight Bridge. This large amount Twisting Moment and Lateral Shear Force must be considered in designing Curved Bridge.

Lateral Loads are not considered in this study. This study is done for a fixed radius of curvature. Full Composite Action is considered in this study. Further progress of this study can be done considering Lateral Loads, different radius of curvature and different composite action. The design can be done

considering all these things and cost analysis can be done. This analysis will be helpful in decision making.

CONCLUSIONS

A certain change in case of flexural moment is noticeable in case of curved bridge. Large amount of torsional force and lateral shear force is developed due to curvature effect. These cases must be considered in case of designing Curved I Section. This large moment and development of torsional force and lateral shear force make the curved I section heavier. Feasibility study can be made considering these effects.

ACKNOWLEDGMENTS

First of all the author would like to pay his deepest gratitude to Almighty for His graciousness, benevolence and unlimited blessing.

The author feels privileged to express his heartfelt indebtedness and sincere gratitude to his honourable and respected Professor, Dr. Mahbuba Begum of the Department of Civil Engineering, Bangladesh University of Engineering and Technology, for her invaluable suggestion, proper guidance, continual inspiration, encouragement, tolerance and leadership.

Finally the author would like to express his special thanks and gratefulness to his families and friends for their cordial cooperation and support, and also to others who were directly or indirectly related to this work.

A STUDY TO FIND THE MOST SIMILAR REAL EARTHQUAKE RESPONSE SPECTRUM TO THE RESPONSE SPECTRUM DEVELOPED FROM BNBC 2006 NORMALIZED RESPONSE SPECTRUM

S M Shafi^{*}, N. Tabassum¹ & F. A. Mazumder²

¹*Department of Civil Engineering, Stamford University, Dhaka, Bangladesh.*

E-mail: shafi@stamforduniversity.edu.bd

²*Department of Civil Engineering, Chittagong University of Engineering & Technology,
Chittagong, Bangladesh. E-mail: engrfaruk248@yahoo.com*

**Corresponding Author*

ABSTRACT

Earthquake is a natural phenomenon which has an adverse effect on human lives and natural resources. It is now a growing concern of our structural engineer to design an earthquake resisting structure. In this study, the comparison has been made between earthquake response spectra with our national building code provided response spectra. BNBC 2006 has provided us with a normalized response spectrum for 5% damping ratio. This is used in this study to develop a response spectrum for rock and stiff soil (soil type S1) and earthquake zone 2. With the help of Pacific Earthquake Engineering Research Centre (PEER) we have selected 5 earthquake response spectra named Friuli earthquake Italy, Gazli earthquake Uzbekistan, Imperial Valley 2 earthquake USA, Imperial Valley 6 earthquake USA, and Tabas earthquake Iran for the comparison. The analysis has been done by using SAP2000 on a steel structure. With some modification, the model structure has been developed from Federal Emergency Management Agency (FEMA) 355C report Appendix B which is a 9 storied building, square in plan and with 5 bays in each direction with one underground basement. The structural response like base reaction, joint reaction, and joint displacement has been considered for the comparison. Finally, it is found out that the response spectrum for earthquake Gazli of Uzbekistan which is a magnitude of 7.0 provides response close to BNBC response spectrum for soil type S1.

Keywords: Response Spectrum; BNBC 2006, PEER; FEMA; SAP2000

INTRODUCTION

Dhaka is the capital of Bangladesh which is a developing country facing the problem of overpopulation, environmental degradation, open space loss, and socio-economic tension. Due to centralization Dhaka controls the major portion of the Bangladesh economy. This growing economy leads to industrialization, which demands quicker and sustainable development of infrastructure to ensure accommodation and employment for new residents. Steel structures are now gaining more concentration due to its advantages over RCC structure. So almost every industry are now constructed by steel. Also, residential buildings are constructed using steel frame and RCC which we called composite structure. Though steel structure has many advantages over RCC structure it is not free from the risk of an earthquake. As Bangladesh is not free from the danger of earthquake so whatever the

building type is it should be sustainable and can withstand any danger posed by the earthquake. There are lots of techniques to study a building response when it is faced by earthquake and response spectrum analysis is one of them which is a fine tool to understand building behavior under earthquake.

In this study, response spectrum analysis has been done on a standard steel structure which is described in FEMA 355C article (FEMA 355C, 2000). For response spectrum analysis, BNBC provided normalized response spectrum has been used to develop response spectra for Dhaka city which is located at zone 2 according to BNBC 2006 earthquake zoning (BNBC, 2006). After that, this developed response spectrum has been used to find similar response spectrum of some real earthquake. Finally, the comparison has been made between the developed response spectrum and response spectrum of the different earthquake to find the most suitable response spectrum of an earthquake based on the structural response which can be used for future analysis.

The objectives of the study are:

1. To find some similar earthquake response spectrum to developed earthquake.
2. To compare the developed response spectrum with different earthquake response spectrum to find the most similar earthquake response spectrum based on structural response like base reaction, joint reaction, and joint displacement.

METHODOLOGY

Development of Response Spectrum for rock and stiff soil and zone 2 from the normalized response spectrum:

The ground acceleration S_a graph has been developed based on the normalized response spectrum provided in the BNBC 2006 (Shafi et al., 2015). Two conditions have been considered in order to calculate the ground acceleration. They are:

1. Zone 2 has been considered (where, $z=0.15$)
2. Ordinary Moment Resisting Frame OMRF for steel has been considered (where, $R=6$)

Calculation:

$$S_a/gZ = 2.48 \quad (1)$$

$$\text{Or, } S_a = 2.48 * g * Z$$

$$\text{Or, } S_a = 2.48 * 32.2 * 0.15$$

$$\text{Or, } S_a = 11.98$$

$$\text{Now, } S_a \text{ for OMRF} = 11.98/6 = 1.9964$$

Based on the above calculation following table has been prepared.

Table 1: Ground acceleration for different soil.

Time Period	S_a		
	Soil I	Soil II	Soil III
0.0	1.9964	1.9964	1.9964
0.4	1.9964	1.9964	1.9964
0.5	1.6020	1.9964	1.9964
0.9	0.9660	1.2880	1.9964
1.0	0.8855	1.1914	1.8515
1.5	0.5635	0.7970	1.2075
2.0	0.4347	0.6440	0.8855
2.5	0.3542	0.4830	0.6762
3.0	0.2737	0.4025	0.5796

Based on the above table following graph has been prepared which can be used for response spectrum analysis.

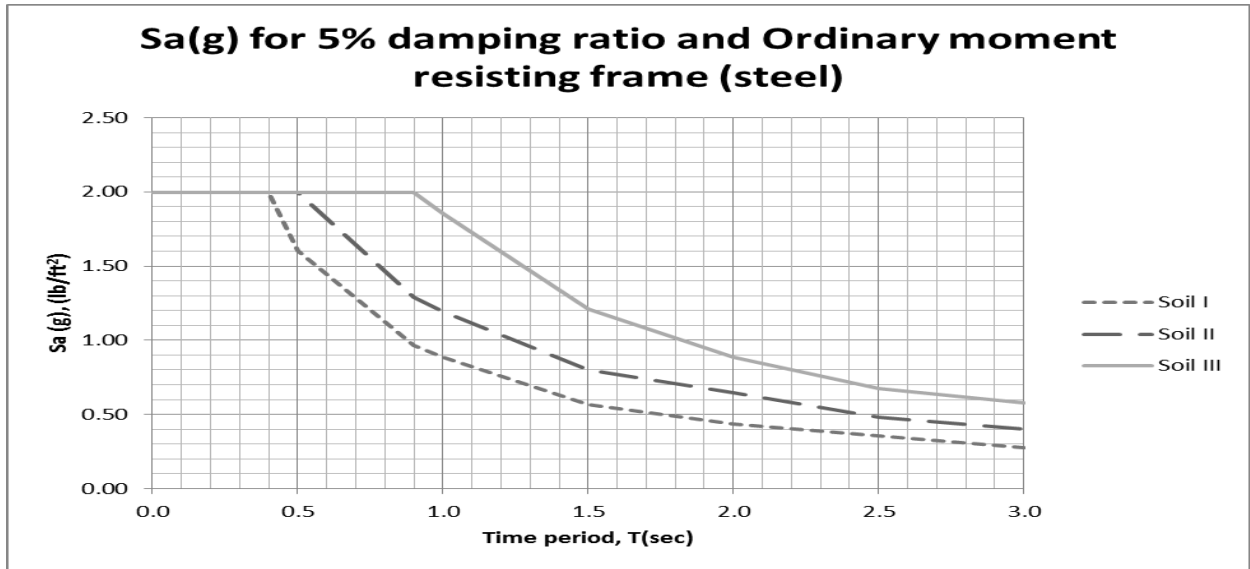


Fig 1: Response spectrum developed from BNBC normalized response spectrum.

A brief description of the development of building model in Etabs:

We have used the 9 stories SAC building for the analysis. The detail of the building has been described in FEMA 355C report appendix B. A brief summary has been described in this section.

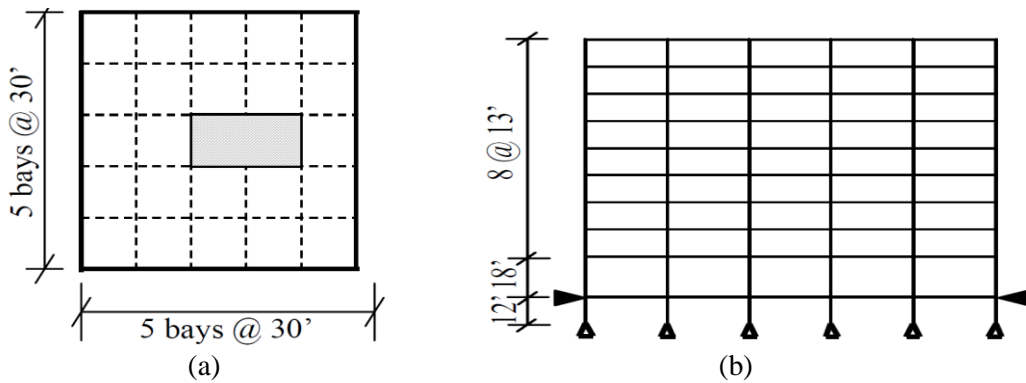


Fig 2: (a) plan view (b) elevation view

The orientation of the frame elements of the structures is given in the following table.

Table 2: Orientation of frame elements.

9-story Building				
Story/Floor	COLUMNS		DOUBLER PLATES (in)	GIRDER
	Exterior	Interior		
-1/1	W14X370	W14X500	0.0	W36X160
1/2	W14X370	W14X500	0.0	W36X160
2/3	W14X370, W14X370	W14X500, W14X455	0.0	W36X160
3/4	W14X370	W14X455	0.0	W36X135
4/5	W14X370, W14X283	W14X455, W14X370	0.0	W36X135
5/6	W14X283	W14X370	0.0	W36X135
6/7	W14X283, W14X257	W14X370, W14X283	0.0	W36X135
7/8	W14X257	W14X283	0.0	W30X99
8/9	W14X257, W14X233	W14X283, W14X257	0.0	W27X84
9/Roof	W14X233	W14X257	0.0	W24X68

The joint restraint has been defined as fixed support. The joint constraint has been provided as a rigid diaphragm. For this study auto meshed has been used. Mesh has been done by 5X5 area meshes. A mass

source has been defined as “From loads” where only the dead and super dead loads have been included. For modal load case, we have considered a maximum of 12 modes and minimum of 01 mode and the other parameters are as default. The response spectrum has been defined as RS1, RS Friuli, Italy RS Gazli, RS Imperial Valley 2, RS Imperial Valley 6 & RS Tabas.

Finding similar earthquake response spectrum using PEER (Pacific Earthquake Engineering Research Centre):

At first, the developed response spectrum data should be written file where one column contains the time period and another column contains the soil acceleration. After that, the file should be saved as CSV (Comma delimited). Then we logged into the PEER website and enter NGA west 2 database. Here we select user-defined spectrum model and use the previously developed CSV file to generate the spectrum. After that, we search the record to find the most suitable response spectrum that matched our response spectrum. The criteria’s has been shown in the following figure.

The screenshot shows a web-based search interface for the PEER database. It is divided into several sections:

- Search:** Contains a note: "These characteristics are defined in the NGA-West2 Flatfile. You need to re-run Search when any of these parameters are updated." Below this are input fields for "Record Characteristics": RSN(s), Event Name, and Station Name.
- Search Parameters:** Includes dropdowns for "Fault Type" (set to "All Types") and "Pulse" (set to "Any Record"). It also has input fields for "Magnitude" (6.5,7.5), "R_JB(km)", "R_rup(km)", "Vs30(m/s)", and "D5-95(sec)", each with "min,max" labels.
- Additional Characteristics:** Includes "Max No. Records" (30, with a note "<=100") and "Initial ScaleFactor" (0.5,2, with "min,max" label).
- Suite:** Includes "Spectral Ordinate" (H1), "Damping Ratio" (5%), and "Suite Average" (Arithmetic).
- Scaling:** Includes "Scaling Method" (No Scaling).
- Controls:** At the bottom, there are buttons for "Search Records" and "Rescale Only".

Fig 3: Search criteria for finding similar spectrum to developed spectrum.

Here spectral ordinate has been selected as H1 so that we could use the raw data of the earthquake in one direction. Finally, from the search result, we have selected 5 earthquake spectrums. The values for time period 0.01 sec to 0.032 sec have been shown in the following table.

Table 3: Response spectrum data of five earthquakes.

Period (sec)	Friuli_Italy-01 pSa (g)	Period (sec)	Gazli pSa (g)	Period (sec)	Imperial Valley 2 pSa (g)	Period (sec)	Imperial Valley-06 pSa (g)	Period (sec)	Tabas_Iran pSa (g)
0.01	0.4782703	0.01	1.2206390	0.01	0.352449	0.01	0.416275	0.01	0.531173
0.02	0.4874193	0.02	1.4793732	0.02	0.351271	0.02	0.455293	0.02	0.533529
0.022	0.4949621	0.022	1.4445406	0.022	0.351456	0.022	0.474753	0.022	0.562051
0.025	0.4928253	0.025	1.7216740	0.025	0.351738	0.025	0.541016	0.025	0.574011
0.029	0.4936260	0.029	2.0473408	0.029	0.352179	0.029	0.663627	0.029	0.569074
0.03	0.4996952	0.03	2.0434354	0.03	0.352315	0.03	0.6916	0.03	0.565956
0.032	0.5151942	0.032	2.0354354	0.032	0.352623	0.032	0.691264	0.032	0.541983

RESULTS AND DISCUSSIONS

The comparison has been discussed made on three outputs. They are base reaction, joint reaction, and joint displacement.

Comparison based on base reaction:

To perform the comparison based on base reaction two reactions have been considered. They are reaction force in global X direction and moment about global Y direction.

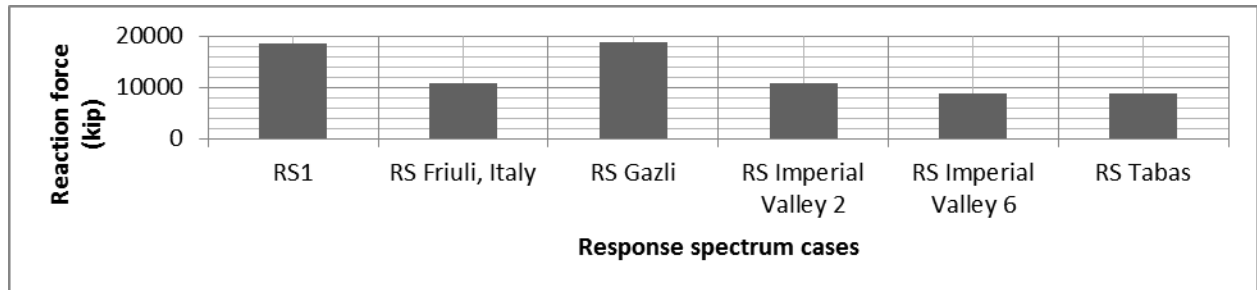


Fig 4: Base reaction force in the global x-direction for different earthquake response spectra.

The [Fig. 4] compare different earthquake response spectrum with BNBC response spectrum for soil type 1. The horizontal axis represents different response spectra cases and in the vertical direction, it represents the reaction force in kip. The RS Gazli has maximum reaction followed by RS1. Here the base reaction of RS1 is 18516.74 kip and of RS Gazli is 18846.58 kip. The least reaction was found for RS Tabas which is 8691.903 kip.

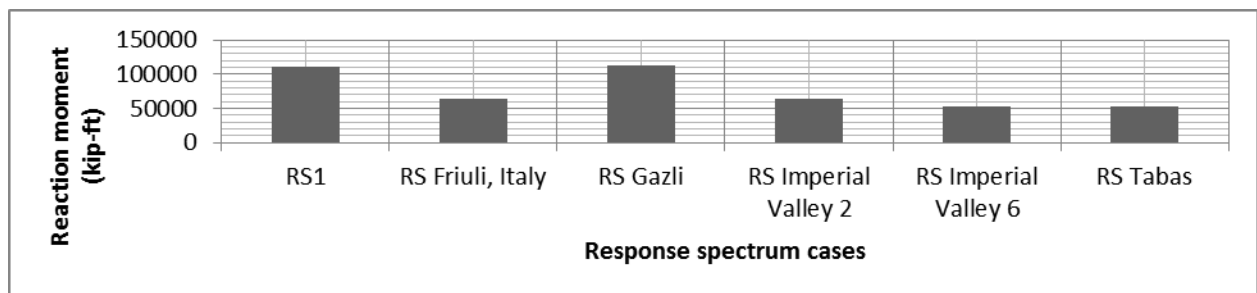


Fig 5: Base reaction moment about global Y direction for different earthquake response spectra.

The [Fig. 5] compare different earthquake response spectrum with BNBC response spectrum for soil type 1. The horizontal axis represents different response spectra cases and in the vertical direction, it represents the reaction moment in kip-ft. The RS Gazli has maximum reaction followed by RS1. Here, the base reaction moment of RS1 is 111100.42 kip-ft and of RS Gazli is 113079.49 kip-ft. The least reaction was found for RS Tabas which is 52151.41 kip-ft.

Comparison based on Joint reaction:

Joints of the bottom-most floor have been considered since it will provide maximum reaction.

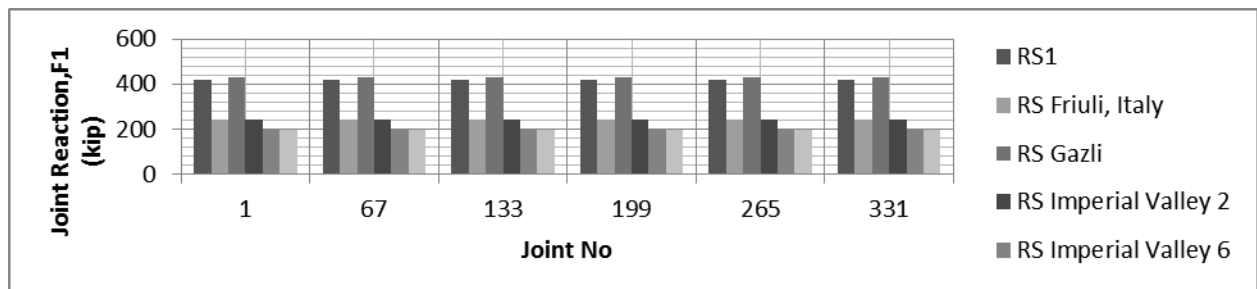


Fig 6: Joint reaction force about local 1 (red) direction for different earthquake response spectra.

The [Fig. 6] represents the comparison between different response spectra based on joint reaction force in local 1 direction. Since the structure is symmetric and the joints are in the same plane so the reaction

of each joint is similar. The joint reaction of RS Gazli is maximum followed by RS1 which is 429.05 kip and 421.54 kips respectively.

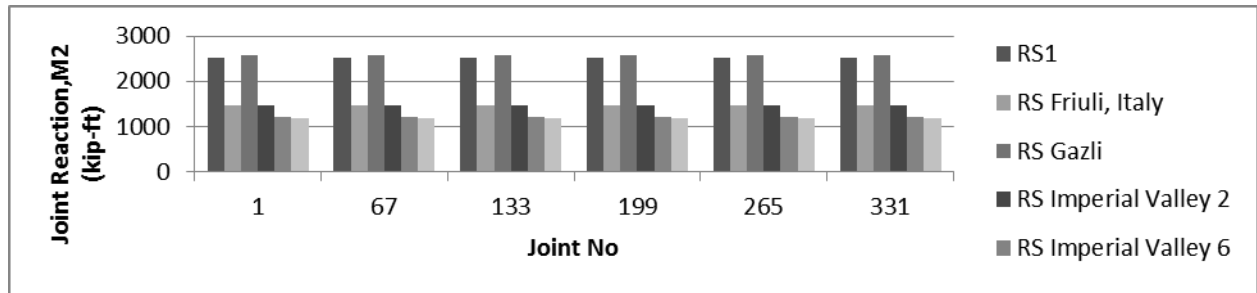


Fig 7: Joint reaction moment about local 2 (white) direction for different earthquake response spectra.

The [Fig. 7] represents the comparison between different response spectra based on joint reaction moment in local 2 direction. Since the structure is symmetric and the joints are in the same plane so the reaction of each joint is similar. Like the previous chart, it showed that the joint reaction of RS Gazli is maximum followed by RS1 and the value is 2574.33 kip-ft and 2529.27 kip-ft respectively.

Comparison based on joint displacement:

From left third column, joints have been selected for analysis.

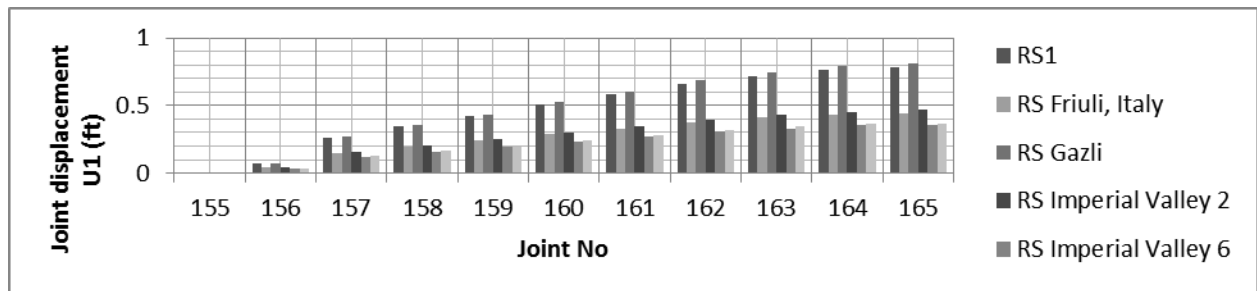


Fig 8: Joint displacement in U_1 direction for different earthquake response spectra.

The [Fig. 8] represents the comparison between different response spectra based on joint displacement in U_1 direction. In the horizontal axis, it represents joint number and in the vertical axis, it represents joint displacement in ft. The joint number 155 is at the base so it has no displacement and joint number 165 is at the top so it has maximum displacement. In every case except for the joint no 155, RS Gazli provide maximum displacement followed by RS1 and the values are almost the same.

CONCLUSIONS

Finally, it can be concluded that the response spectrum of Gazli earthquake which has a magnitude of 7.0 is the most identical to the response spectrum developed from BNBC normalized response spectrum. We can use this study to find more similar real earthquake response spectrum in order to analyze our structure against earthquake. Though this study only considers rock and stiff soil we can also use this study for the other two types of soil condition provided in the BNBC 2006.

REFERENCES

- Bangladesh National Building Code. (2006). "Earthquake load part 6 chapter 2 section 2.5". Institute of Building Research Institute and Bangladesh Standard & Testing Institute, Bangladesh.
- FEMA 355C. (2000). "A report prepared by SAC joint venture: A program to reduce earthquake hazards of steel moments-frames structure". September, Appendix-B, B1-7, and B15.
- Shafi, S. M., Navila, T., Bishu, D. N. & Shovona, K. (2015). Classification of soil types described in BNBC 2006 by analyzing the Los Angeles SAC model under BNBC response Spectrums. *IOSR Journal of Mechanical and Civil Engineering (IOSR-JMCE)*, September- October, 12, 5 (IV), 92-93.

PARAMETRIC STUDY OF RCC SQUARE COLUMN UNDER FIRE

S. I. G. Shuvo, M. N. Uddin & M. R. Hossain*

Department of Civil Engineering, Bangladesh University of Engineering & Technology, Dhaka, Bangladesh. Email: hmraquib@gmail.com

**Corresponding Author*

ABSTRACT

This paper demonstrates the parametrical analysis of RCC square columns under fire conditions. Proper resistance of column against fire hazards is crucial as column turns out to be one of the most vital load transferring members of a building. During a fire hazard, the rising of temperature in column is a time-dependent phenomenon. When it comes to susceptibility to fire damage, steel is more vulnerable than concrete. It is evident from the observation that the integrity of a column under fire hazard depends greatly on the exposure time of the reinforcement to fire. It indicates that the reinforcement of a column needs to be protected from fire exposure with adequate clear cover. For this study, three different sizes of column (12"X12", 16"X16" & 20"X20") with same steel percentage (3%) but having various clear covers are taken for analysis in three stages. The pre-processing is done by GID and the processing phase is executed by SAFIR while DIAMOND culminates the analysis through post-processing. Based on numerical analysis using these programs, an empirical relationship between clear cover required for square column and duration of fire exposure has been developed. BNBC code has been followed to establish the premise for the thermal resistivity of columns. Using the empirical formula, required clear cover of column can be directly computed for a particular duration of fire exposure which has significant value in planning and designing of a building.

Keywords: Fire on Column; Clear Cover Requirement; Relation between Clear Cover & Temperature; SAFIR; GiD.

INTRODUCTION

Concrete and Steel structures show different behavior to fire. Comparatively concrete structures are more sustainable under a longer period of fire attack. Steel losses its strength in a significant amount with the rise in temperature much earlier (Gillie, 2004). So structural steel shouldn't be exposed to fire at all for the safety issue. In RCC structure, reinforcement bars are kept safe providing adequate clear cover. So, the adequate clear cover should be provided for safety at various temperature (Awoyera et al., 2014). Sometimes design requirements against fire are less emphasized which may lead to an increase in the chance of loss of life and properties.

This parametrical study was aimed to observe the impact of fire on RCC square column visually and prescribe a solution to it. The definite objectives of the study were to observe the relation between the thickness of clear cover of the square column and the time of exposure to standard fire (Boström and Johansson, 2017) without significant damage and develop a simple empirical relation between them.

The question may arise, why column was chosen rather than other components of a structure. It's not unknown that column is considered to be the most critical component, as failure of the column eventually

leads to failure of the whole structure (Mills, 2011). So, the safety of the column during a fire event is of so much importance because of its inherent structural significance.

Norwegian Building Research Institute has studied that concrete has no threat up to 100°C and undergoes normal thermal expansion up to a temperature of about 300°C (Norwegian, 2001). Above 300°C, it starts to get pink color and different properties of concrete start to deteriorate. These characteristics should be demonstrated briefly in case of detailed study (Bilow and Kamara, 2008).

In this study, this 300°C temperature is considered as the benchmark for the safety of concrete. Under fire loading, behavior of both concrete structure (Fletcher et al., 2007) and steel structure (Mahale and Kandekar, 2016) should be analyzed for a better understanding of the study. SAFIR analysis and modeling of the structure under fire can be considered for future works (Franssen, 2003).

The standard fire applied in the simulation was according to ISO 834 fire curve (ISO, 1999) which represents a fully developed fire in a compartment with a constant rate of increase in temperature.

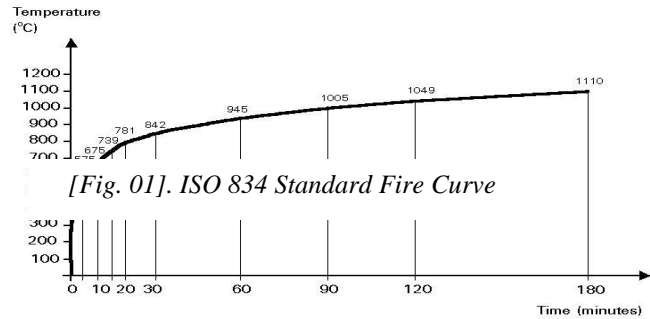


[Fig. 01]. ISO 834 Standard Fire Curve

SIMULATION

In this study, Simulation has been run to determine the temperature at different portions of an RCC square column section after the application of fire with the flow of time. Simulation process can be classified into 3 steps: i) Pre-processing, ii) Processing & iii) Post-processing

i) Pre-processing: GiD has been used for the pre-processing step. The objective of this segment is to create an INPUT (.in) file which contains the coding of a complete description of the RCC column section and its fire application. The Input file can be executed manually by coding.

The work segments can be stated in this step sequentially like these- Drawing the column section of actual size with proper reinforcement; Assigning concrete and steel in the proper portion; Applying fire in the frontier constraints; Meshing & Calculation Run. “FISO” is used as frontier constraints which indicates the side where ISO-834 fire curve was applied in.

ii) Processing: SAFIR has been used for processing the simulation whose objective is to process the input (.in) file and extract output which can be used in Post-processing. The thermal attack from the fire is given as input data to process. It computes the evolution of temperature in the section. It executes three kinds of file - TEM (Temperature Details) file, OUT (Output) file, XML document (.xml)

iii) Post-processing: DIAMOND is a post-processor for the finite element code SAFIR. It reads the XML file (.xml) and allows to read the temperature of any node after a certain time of fire application and also authorizes to save these temperature ranges in column section as an image file for further usage.

Material Properties: Various properties of used concrete and steel in the simulation are given below-

Table 01: Mechanical Properties of Concrete

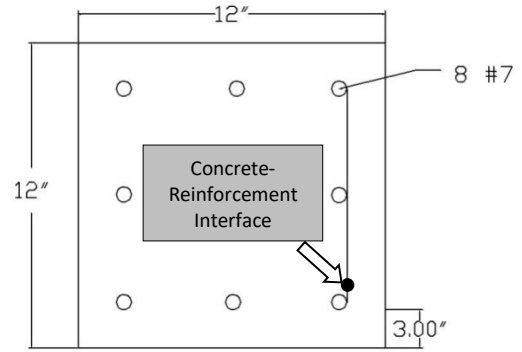
Properties	Value
Poisson's Ratio, σ	0.3
Compressive Strength, f_c	4.35 ksi
Tensile Strength, f_t	0.435 ksi
Specific Mass, ρ	2400 kg/m ³
Moisture Content	0
Convection Coefficient (Hot)	25
Convection Coefficient (Cold)	4
Relative Emission	0.8
Parameter of Thermal Conductivity	0.5

Table 02: Mechanical Properties of Steel

Properties	Value
Poisson's Ratio, σ	0.3
Yield Strength, f_y	3.55x 10 ⁸ N/m ²
Modulus of Elasticity	29X10 ⁶ psi
Convection Coefficient (Hot)	25
Convection Coefficient (Cold)	4
Relative Emission	0.7

RESULT & DISCUSSION

Simulation has been performed for 3 sets of RCC Column Section (12"X12", 16"X16", 20"X20") of 3% Steel Percentage and 13 different sizes of Clear Cover (from 1" to 4" with 0.25" interval) for variation of the result. The fire has been appointed at concrete reinforcement interface (shown in Figure 02) in two ways (4 sides, 2 Sides) and temperature data has been collected at eleven times (from 20 minutes to 2 hours with 10 minutes interval). Simulation result exhibited by using DIAMOND software demonstrates different temperature ranges on different points of the column section with the change of time.



[Fig. 02]. Section of 12"X12" Column (3.00" CC, 3% Steel percentage)

For example: 12"X12" column with 3" clear cover and 3% steel reinforcement.

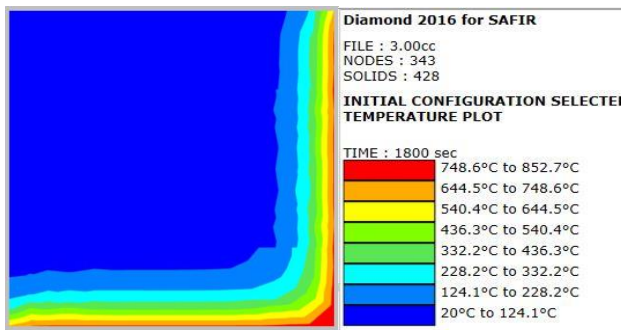


[Fig. 03]. 30 Minutes Fire applications on 2 Sides

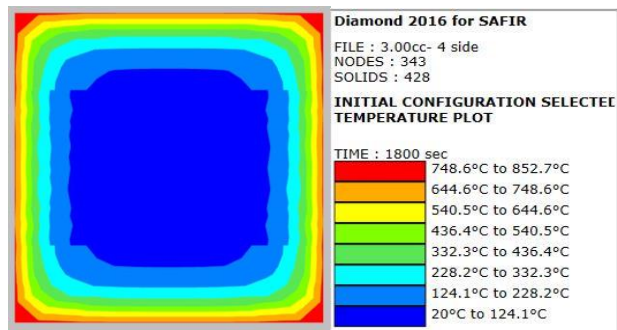


[Fig. 04]. 30 Minutes Fire applications on 4 Sides

Time vs. Clear Cover Graph: To understand the impact of temperature at concrete reinforcement interface by the clear cover particularly, six detailed Clear Cover vs. Temperature Curve has been constructed. We already know that the parts of a concrete structure that is exposed to temperatures above approximately 300 °C should be considered to fix. That's why a straight line has been constructed at 300°C temperature parallel to the X-axis (Clear Cover) in the graph. The 300°C temperature straight line intersects different time curves, and we get some intersection points. Then the corresponding clear cover data of the intersection points have been noted.

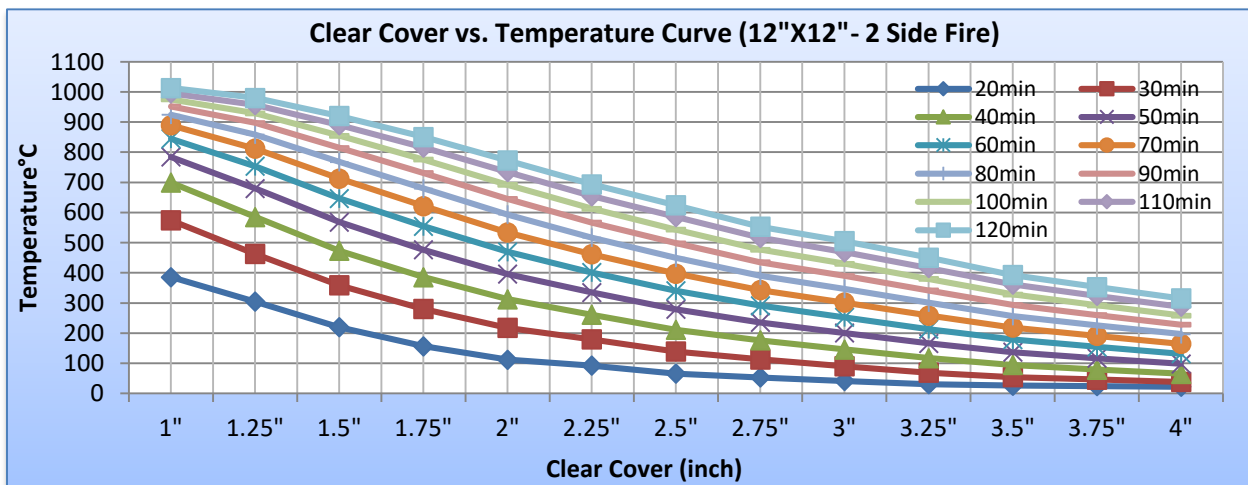


[Fig.05]. Clear Cover vs. Temperature Curve at different times (2 side fire at Concrete Reinforcement Interface, Steel percentage 3%)

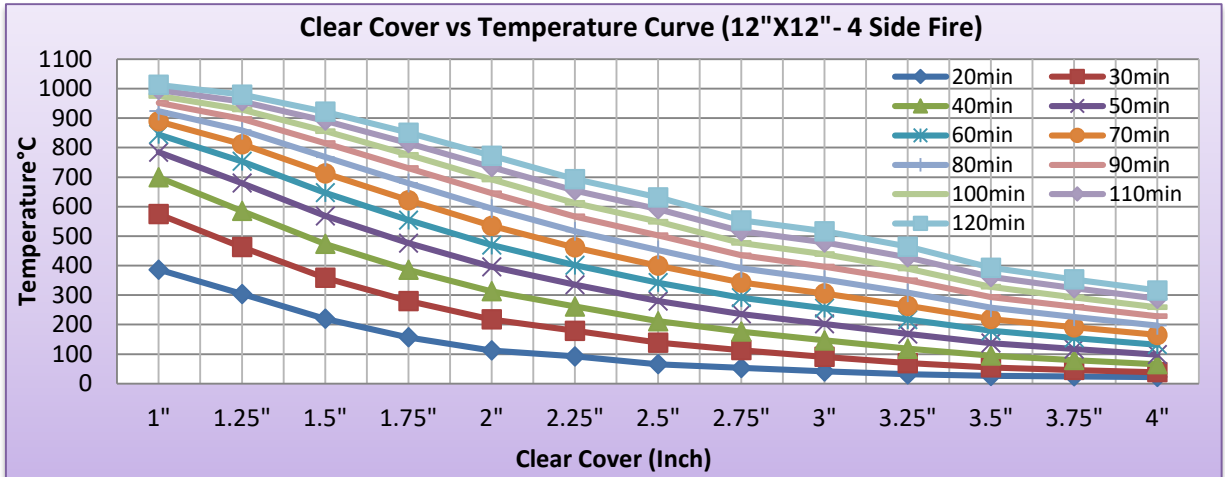


[Fig. 06]. Clear Cover vs. Temperature Curve at different times (4 side fire at Concrete Reinforcement Interface, Steel percentage 3%)

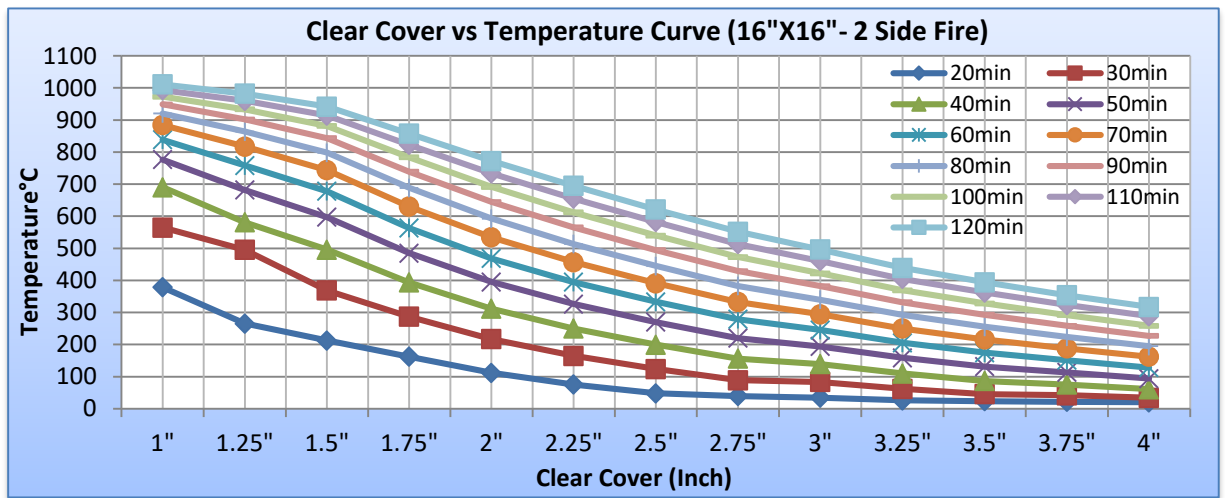


[Fig. 07]. Clear Cover vs. Temperature Curve at different times (2 side fire at Concrete Reinforcement Interface, Steel percentage 3%)

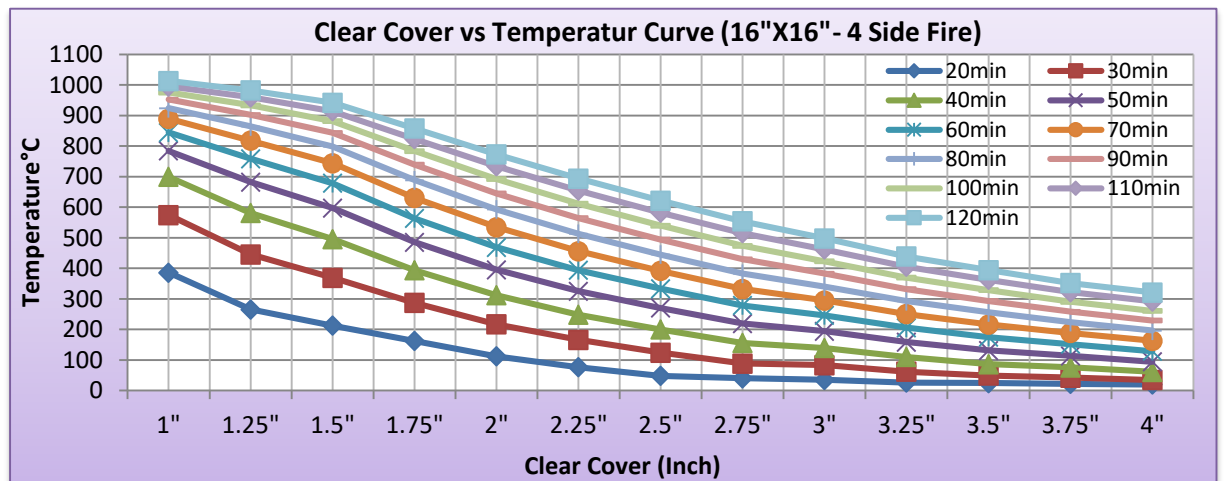


[Fig. 08]. Clear Cover vs. Temperature Curve at different times (2 side fire at Concrete Reinforcement Interface, Steel percentage 3%)

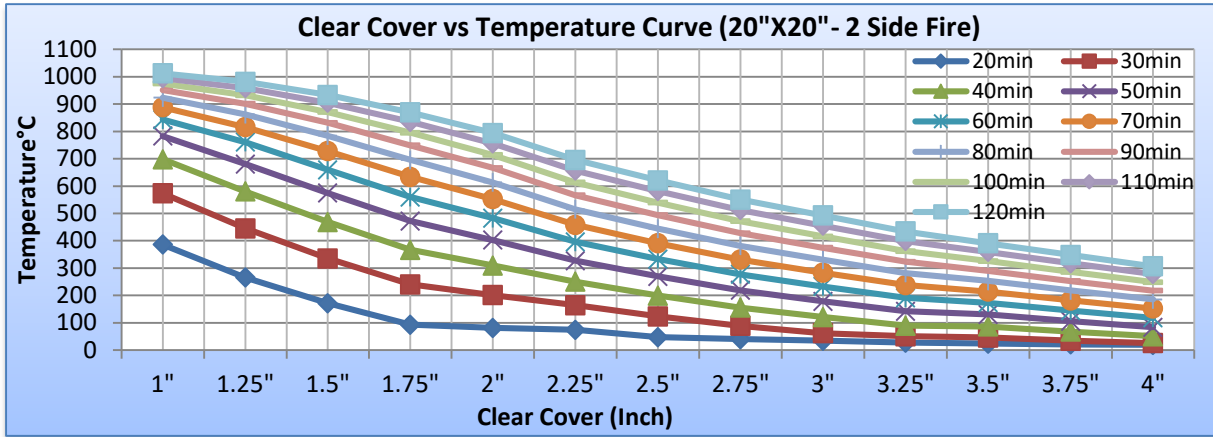


[Fig. 09]. Clear Cover vs. Temperature Curve at different times (2 side fire at Concrete Reinforcement Interface, Steel percentage 3%)

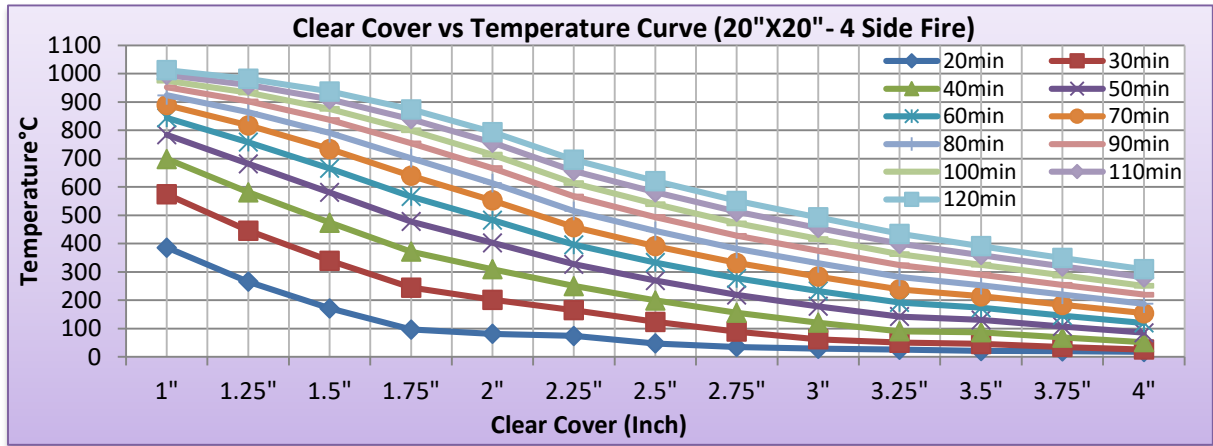


[Fig. 10]. Clear Cover vs. Temperature Curve at different times (2 side fire at Concrete Reinforcement Interface, Steel percentage 3%)

Formation of Empirical Relation between Time & Clear Cover: By using corresponding clear cover data of intersection points, another Time vs. Clear Cover graph has been sketched. A straight line-shaped figure has been noticed after plotting the data. A best fitted straight line has been constructed to represent the relation between Fire Resistant Time and Clear Cover.

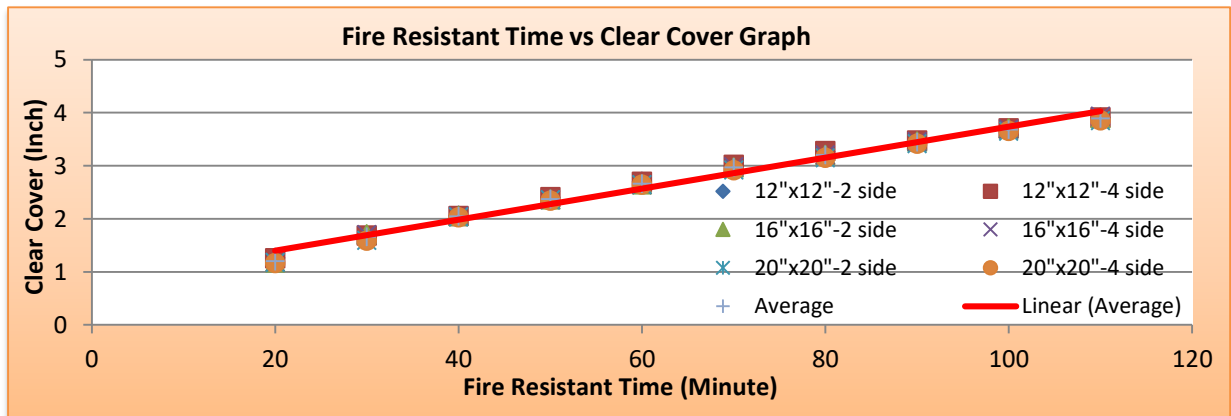


[Fig. 11]. Formation of Empirical Relation between Fire resistant time and Required Clear Cover for 300°C Temperature

The equation we get from the graph is-

$$C = 0.029 t + 0.817$$

Where, C= Required Clear Cover (Inch) and t= Fire Resistant Time (Minute). This empirical equation has notable significance to build a fire-resistant structure. It demonstrates us what should be the size of the clear cover of a square column if want to protect the column for a certain time from fire damage. For example, our traditional 2.5-inch clear cover in the column is safe till 58.034 minutes of fire application. After that, the column should be repaired.

CONCLUSION

In our Study, it was observed that whether the fire is applied in 2 sides or 4 sides, concrete reinforcement interface point at fire application side shows almost the same temperature for a definite time. While performing the study some limitations have arisen. The whole simulation was classified in pre, during and post-simulation. And they require individual software to perform. So, Simulation was much time-consuming. GiD is only compatible to work with SI (System International) unit system. It was a matter of extensive complication to convert every measurement of the traditional unit into SI unit as input in GiD. The software should be compatible with receiving input in various system of units so that it can be used by all types of user who use a different unit of measurements. In the post-processing, while using DIAMOND, the temperature can only be evaluated at the intersection of mesh lines. Since Auto mesh was used in GiD, the temperature of every point in the section couldn't be estimated. Manual meshing is encouraged so that the user can detect the temperature of their desired points.

An empirical equation has been evaluated to establish the relation between Fire Exposure Time & Required Clear Cover Size. But the equation won't be acceptable if any material property of the column has been changed. Those variations of the equation should be evaluated in the further study to be incorporated in codes for improving the safety of concrete structures under fire.

REFERENCES

- Awoyera, PO; Arum, C and Akinwumi, II. 2014. Significance of Concrete Cover to Reinforcement in Structural Element at Varying Temperatures. *Int. Journal of Scientific & Engineering Research.*, 5(6): 1120-21
- Bilow, DN and Kamara, ME. 2008. *Fire and Concrete Structures*. ASCE., Structures: Crossing Borders
- Boström, L; Johansson, P. 2017. Time-temperature curves. RISE Research Institutes of Sweden. [online]. available at: https://www.sp.se/en/index/services/firetest_building/fire_constructions/fireresist/time_temperature/Sidor/default.aspx [Accessed 17 July 2018]
- Fletcher, IA; Welch, S; Torero JL; Carvel, RO and Usmani, A. 2007. *The Behaviour of Concrete Structures in Fire*. Thermal Science. ResearchGate.
- Franssen, JM. 2003. SAFIR: A thermal/structural program for modeling structures under fire. North American Steel Construction Conference. *Engineering Journal.*, 3rd quarter: 143-158
- Gillie, M. 2004. *Fire Resistance of Structures*. School of Engineering and Electronics. The University of Edinburgh. UK: 1-11
- ISO 834-1. 1999. *Fire Resistance Tests – Elements of Buildings Construction*. International Organization for Standardization. Switzerland., General Requirements. Part-1.
- Mahale, HD; Kandekar, SB. 2016. Behaviour of Steel Structure Under the Effect of Fire Loading. *Int. Journal of Engineering Research and Applications.*, Vol. 6, 5(5): 42-46
- Mills, M. 2011. Column: Structural Importance & Requirement. *EzineMark*. [online]. Available at: <http://column.ezinemark.com/column-structural-importance-requirement-31eb92da58a.html> [Accessed 20 July 2018].
- Norwegian Building Research Institute. 2001. *Fire-damage to buildings*. Publication 24.

A STUDY ON THE PERFORMANCE OF FERROCEMENT RETROFITTED MASONRY WALL UNITS UNDER CYCLIC LOADING

M. Z. Alam, M. M. Asif* & R. Ahsan

*Department of Civil Engineering, Bangladesh University of Engineering and Technology,
Dhaka-1000, Bangladesh.*

E-mail: md.mahirasif92@gmail.com

**Corresponding Author*

ABSTRACT

Old masonry buildings are quite common in Bangladesh. One of the major drawbacks of these masonry buildings is their weakness to in plane and out of plane shear force. Besides, shear resistance of these buildings has decreased due to aging making them more vulnerable to earthquake. Furthermore, recent occurrences of earthquake in neighbouring countries have caused minor ground shaking in this country that can pose a threat to the safety of these structures. So, retrofitting of these buildings has become necessary. Considering the economic condition of Bangladesh ferrocement retrofitting technique can be both cost-effective and suitable among some available retrofitting techniques. This paper aims to investigate the performance of ferrocement retrofitted masonry wall units under cyclic compression. Total three masonry wall units (29 inch × 29 inch) have been prepared. Among them two wall units have been retrofitted with 18 gauge and 20 gauge woven wire mesh. Then these wall units have been tested by applying cyclic load along the diagonal of the specimens. The test results show that ultimate load carrying capacity of the ferrocement retrofitted specimens is 27%-46% greater than the reference specimen. Besides, ferrocement retrofitted specimens have experienced 33%-46% greater deformation before failure than the reference specimen.

Keywords: Earthquake, Masonry wall, Ferrocement retrofitting technique, 18 gauge and 20 gauge woven wire mesh, Cyclic load.

INTRODUCTION

Bangladesh is geographically a small country but every year visited by many devastating natural disasters. Among them earthquake is more lethal which has been threatening Bangladesh in the recent past (Al Zaman and Monira, 2017). Because, more people are killed by earthquakes than those by any other form of weather hazard lately (Roy, 2014). A huge portion of masonry buildings are located in Bangladesh. During extreme loading like an earthquake, these unreinforced masonry buildings are at high risk of failure (Nayak and Dutta, 2016). Weakness in resisting horizontal forces and heavy mass of these masonry structures make themselves more vulnerable to earthquake. Therefore, increasing seismic resistance of the masonry structures by using different retrofitting techniques has become an important issue. Among many retrofitting techniques ferrocement makes itself satisfactory and cost-effective (Tripathi et al., 1988).

Ferro- means iron although metal commonly used in ferro-cement is the iron alloy steel. Ferrocement is a system of reinforced mortar or plaster (lime or cement, sand and water) applied over layer of metal mesh. Ferrocement has become very popular in our country because of its cost-effective process, availability of raw materials and flexibility in construction (Kantharaju et al., 2001). It is found that, in

plane and out of plane strength and ductility of an unreinforced masonry wall can be enhanced by using thin ferrocement coating (Reinhorn and Prawel, 1985). Again, the effectiveness of Ferrocement as a rehabilitation material on masonry walls under gravity load was found satisfactory (Venkatesh, 2010).

The primary objective of the present study is to investigate the performance of ferrocement retrofitted (both with 18 gauge and 20 gauge wire mesh) masonry wall units under cyclic compression in terms of ultimate load carrying capacity, first cracking load and corresponding deformations. This study also includes different failure patterns of specimens.

METHODOLOGY

Three masonry wall specimens were investigated. One of them was control specimen (bare masonry wall) denoted as URMW whose final section size stood 29"×29"×5.5" as showed in Fig. 1. The other two were ferrocement retrofitted specimens denoted as FRSC-18 (wrapped with 18 gauge wire mesh) and FRSC-20 (wrapped with 20 gauge wire mesh) whose final section size stood 29"×29"×6.5" as showed in Fig. 2. All the bricks were connected by stretcher bond. 0.5" mortar was used between two adjacent layers of bricks. Between ferrocement layer and brick wall, 1.5" standard nails were placed at a spacing of 6" c/c at alternate brick layers and embedded to 1" into the wall.

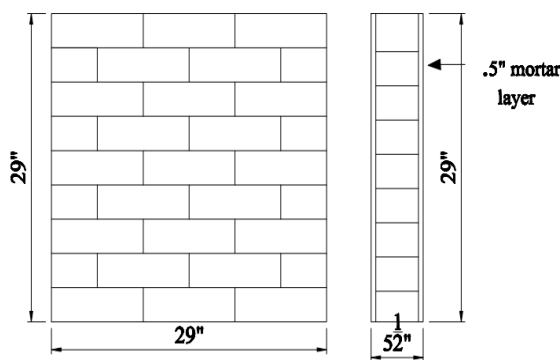


Fig. 1 Control specimen

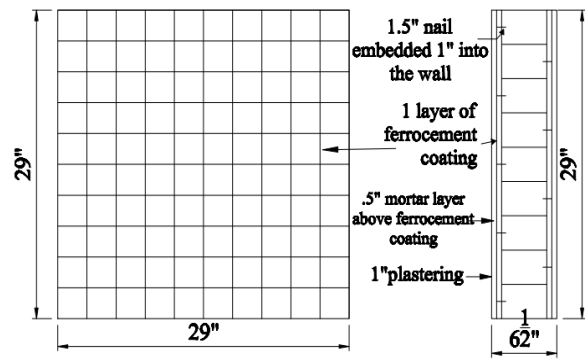


Fig. 2 Ferrocement retrofitted specimens

Proper preparation of specimens is essential for obtaining accurate results from structural tests. Three walls were prepared with brick and mortar as showed in Fig. 3. In case of brick jointing mixing ratio 1:4 (cement : sand) was used in mortar. But in case of plastering the ratio was 1:2 (cement : sand). Water cement ratio was maintained at 0.45 (BNBC, 2017). After that, two walls among them were coated with ferrocement as showed in Fig. 4. One of them was wrapped with 18 gauge wire mesh and another was wapped with 20 gauge wire mesh. Both wire meshes were woven and with 0.5" × 0.5" opening size. Eventually curing, grinding and painting were done to complete the preparation of specimens.



Fig. 3 Construction process of brick wall



Fig. 4 Brick wall with ferrocement coating

The summary of the specimens are showed in Table 1.

Table 1: Summary of the specimens.

Specimen	Dimension	Ferrocement coating			Mix proportion of mortar	
		Wire size(gauge)	Mesh size	No of layer	Masonry mortar	Ferrocement mortar
URMC	29"×29"×5.5"	-	-	-	1:4	-
FRSC-20	29"×29"×6.5"	20	.5"×.5"	1	1:4	1:2
FRSC-18	29"×29"×6.5"	18	.5"×.5"	1	1:4	1:2

After completion of preparation of the specimens, they were tested by testing machine. The experimental setup is showed in Fig 5. Two M-shaped steel frames were used as showed in Fig. 6 to hold the specimen. Pure epoxy binder was used to fix the wall with M-shaped steel frame.

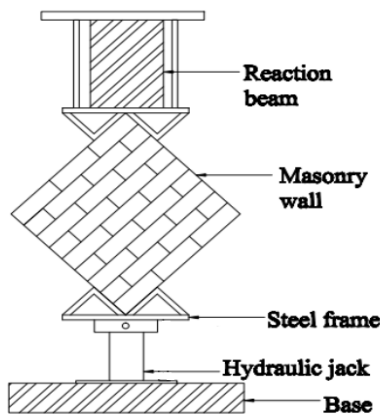


Fig. 5 Experimental setup

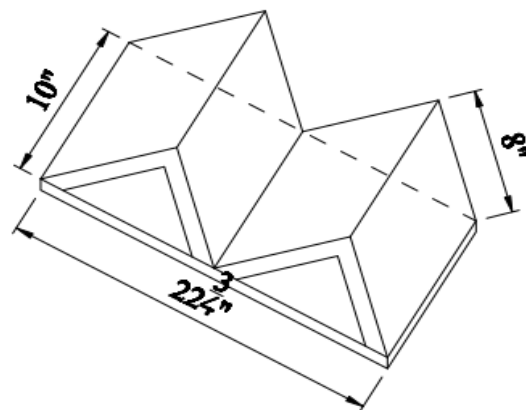


Fig. 6 M-shaped steel frame.

Cyclic load was applied by hydraulic jack as shown in Fig. 7. The load was applied by maintaining 51.5 KN of residual compression as shown in Fig. 8. The maximum value of compressive force per cycle was increased with the increment of cycle number.



Fig. 7 Hydraulic jack

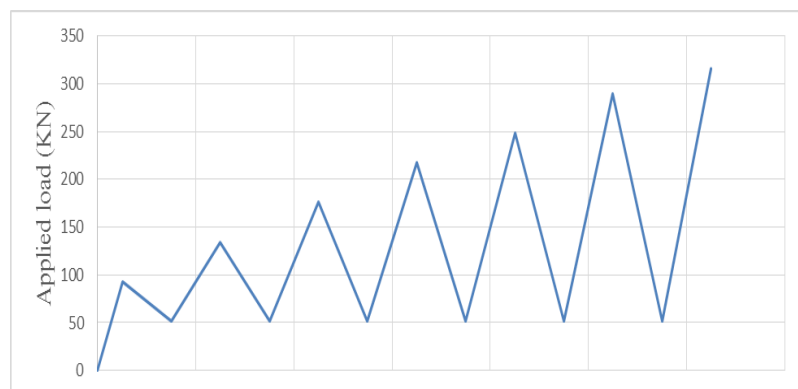


Fig. 8 Load history

RESULTS AND DISCUSSIONS

The performance of both ferrocement retrofitted specimens and control specimen were investigated under cyclic compression. First crack was appeared on the surface along the diagonal of the specimens for all cases. Gradually this crack extended further along the diagonal. For ferrocement retrofitted specimens this crack was accompanied by a series of cracks and finally complete failure occurred along the diagonal of the specimens as shown in Fig. 9. In case of bare masonry wall, failure was abrupt and failure occurred due to mortar joint failure. But for ferrocement retrofitted specimens, failure was gradual and failure occurred due to both mortar joint failure and brick failure.

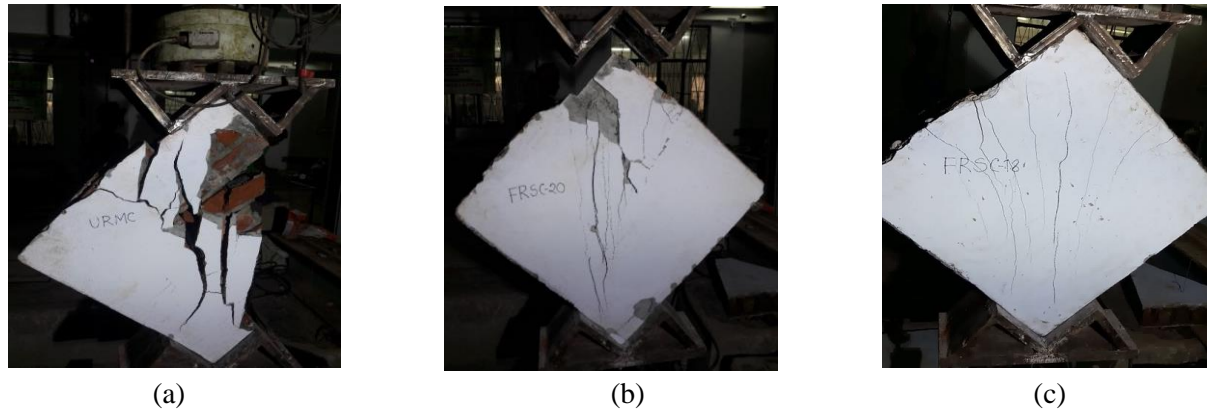


Fig. 9 Failure pattern of the specimens (a) URMC (b) FRSC-20 (c) FRSC-18

Load deformation curve for all specimens are provided in Fig. 10. It is clear from the graph that before failure, ferrocement retrofitted specimens experienced more deformation than the bare masonry wall. Besides, stiffness of the ferrocement retrofitted specimens were greater than the bare masonry wall and it decreased gradually with the increment of cycle.

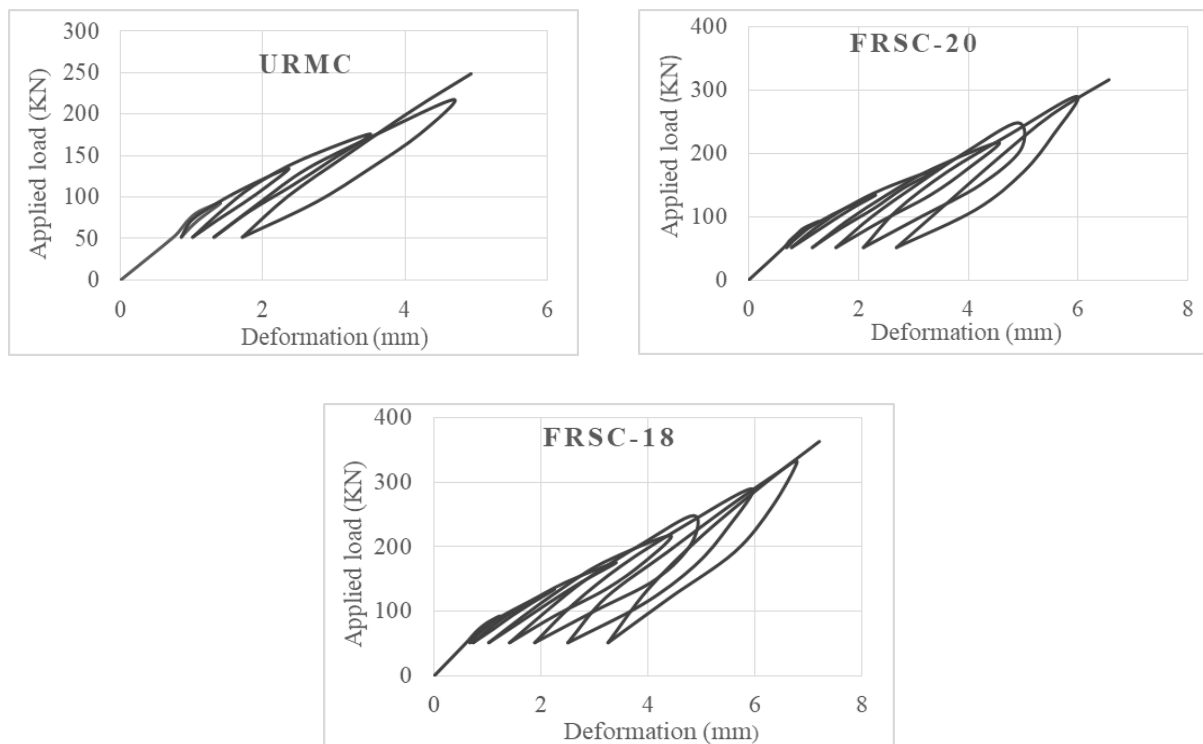


Fig. 10 Load deformation graph of the specimens URMC, FRSC-20 and FRSC-18

Table 2: Summary of the experimental results

Specimen	Compressive load at cracking(KN)	Ultimate load carrying capacity (KN)	Maximum deformation (mm)
URMC	217.49	248.61	4.93
FRSC-20	290.11	316.62	6.56
FRSC-18	331.6	363.55	7.2

CONCLUSIONS

The following conclusions may be drawn from the present study:

1. Under cyclic compression, ultimate load carrying capacity of the specimens retrofitted with 20 gauge and 18 gauge wire mesh were found 27% and 46% greater than that of bare masonry wall unit respectively. Before failure, the specimens retrofitted with 20 gauge and 18 gauge wire mesh experienced 33% and 46% greater deformation than the bare masonry wall respectively. Comparing the results, it is clear that retrofitting with 18 gauge wire mesh is more effective than 20 gauge wire mesh.
2. Large deformation before failure of the retrofitted specimens indicates that ductility of the specimens have been improved due to ferrocement coating. Besides, stiffness of the retrofitted specimens have also been improved as indicated by load deformation graphs.

ACKNOWLEDGMENTS

Financial support for the present study was provided under “Higher Education Quality Enhancement Project (HEQEP)” by University Grant Commission (UGC). The authors would also like to acknowledge the technical support of Bangladesh University of Engineering & Technology (BUET).

REFERENCES

- Al Zaman, MDA and Monira, NJ. 2017. A study of earthquakes in Bangladesh and the data analysis of the earthquakes that were generated in Bangladesh and its' very close regions for the last forty years (1976-2016). *Journal of Geology & Geophysics*, 6(4): 1000300: 1-5.
- BNBC. 2017. Bangladesh National Building Code, Volume 2, Part 6- Structural Design, chapter 12–Ferrocement structures. To be published by Housing and Building Research Institute, Bangladesh.
- Kantharaju; Vasudev, K; Kulkarni, S; Chandrashekar, CV; Rajappa, G and Malji, NG. 2001. Ferrocement components for low cost housing in developing countries. *26th Conference on Our World In Concrete & Structures*. Singapore.
- Nayak, S and Dutta, SC. 2016. Improving seismic performance of masonry structures with openings by polypropylene bands and l-shaped reinforcing bars. *Journal of Performance of Constructed Facilities (ASCE Library)*, 30(2): 04015003: 1-12.
- Reinhorn, AM and Prawel, SP. 1985. Seismic retrofit of structural masonry using a ferrocement overlay. *Proceedings of the Third North American Masonry Conference*.
- Roy, S. 2014. Probabilistic prediction for earthquake in Bangladesh: just how big does the earthquake have to be next years? *Open Journal of Earthquake Research*, 3(2): 108-114.
- Trikha, DN; Sharma, PC and Johnson, S. 1988. Rehabilitation of corrosion-damaged steel tanks by ferrocement at university of roorkee. *Proceeding of 3rd International Conference on Ferrocement, University of Roorkee*.
- Venkatesh, SV. 2010. Strength characteristics of brick masonry wall before and after encasing with ferrocement. *8th International Masonry Conference 2010 in Dresden*.

MINIMUM WEIGHT DESIGN OF A PLANE TRUSS IN MATLAB USING LINEAR PROGRAMMING

A. F. Mazumder^{*1}, T. Majumder², S. K. Rahul³, A. Mahmud⁴, and M. Rafael⁵

¹ Department of Civil and Construction Engineering, Western Michigan University, Michigan, USA.

E-mail: abul.f.mazumder@wmich.edu

² Department of Computer Science & Engineering, Metropolitan University, Sylhet, Bangladesh.

E-mail: majumdertanjiha21@gmail.com

³, Department of Electronic, Computing & Mathematics, University of Derby, Derby, UK.

E-mail: s.rahul1@unimail.derby.ac.uk

⁴ Bangladesh Water Development Board, Dhaka, Bangladesh. E-mail: asifmahmud1348@gmail.com

⁵ Department of Civil Engineering, Presidency University, Dhaka, Bangladesh.

E-mail: mdrafael7@gmail.com

**Corresponding Author*

ABSTRACT

Analysis of a truss is performed using joint method, section method, matrix method, and upper and lower bound theories of plasticity. Optimization of topography and cross-section are the main concerns of truss design. Many methods, algorithms, and software are available to perform analysis and minimum weight design. These tools are complicated and time consuming. Therefore, the need of a simple and time efficient tool still persist. The main objective of this paper is to develop a simple and time efficient tool that is capable of performing analysis and minimum weight design of truss. Therefore, a code is developed in MATLAB incorporating linear programming (LP). Users of the code need to input the nodal coordinates, nodes connecting elements, and support and loading conditions. With the given input, the MATLAB code performs truss analysis and minimum weight design by generating objective function and constraints. A truss was analysed by hand and minimum weight design was performed by commercially available software LINGO. Same truss was analysed and designed by the developed MATLAB code. Analysis results obtained from hand calculation, minimum weight design from LINGO, and analysis and minimum weight design results obtained from MATLAB show 100% congruency.

Keywords: Linear programming; MATLAB; Truss.

INTRODUCTION

The analysis of trusses is performed considering three basic assumption. The weight of the members is often insignificant compared to the applied loads and omitted or half of the weight is applied to both end joints of a member, moments transmitted through the joints are negligible, and nodes are treated as hinge or pin-joint as the members are long and slender. Under these simplified assumptions, every member of the truss is subjected to pure compression or tension forces. Therefore, shear, bending moment, and other complex stresses are considered to be zero. These simplification make the trusses stronger than other ways of arranging structural elements because nearly every material can resist a much larger load in pure tension or compression than in shear, bending, torsion, or other kinds of complex forces. These simplifications make trusses easier to analyse. Truss analysis is performed using joint method, section method, and a matrix method such as the direct stiffness method or flexibility method. Similarly, truss is analysed using upper and lower bound theories of plasticity (Charnes and Greenberg, 1951) which is also known as limit load analysis. Some researchers tried to use limit load

analysis to find out ultimate load carrying capacity (Petrovic et al., 2011) of a given truss. Limit load analysis measures the ultimate load carrying capacity of a truss before failure of any member.

Load calculation for a given truss is performed considering dead, live, snow, earthquake, and wind loads following national and international codes. Minimum weight design is required to perform as the number of members, topography, size, and shape are unknown to sustain a calculated load. Structural optimization has become a valuable tool for engineers and designers in recent years. Optimization in engineering has not been a commonly used design tool until high performance computing systems were widely available. Trusses are becoming lighter, stronger, and cheaper as industry adopts higher forms of optimization. Optimization of cross-section of truss members and topography are the main concerns before designing a truss. Different methodologies, algorithms, and genetic algorithm are adopted to optimize a given truss (Abo-Hamd, 1983; Romero et al., 2002; and Romero et al., 2004). These techniques consume a significant amount of time and require a high performance computer. As an example, genetic algorithm takes hours to perform optimization although time required to perform optimization depend on the configuration and type of truss and loading conditions. On the other hand, a simple and time efficient tool like linear programming is available to perform the analysis and minimum weight design of a truss.

Linear programming (LP) is used to perform truss analysis and minimum weight design. A MATLAB code is developed incorporating LP to analyse and perform minimum weight design of a given truss adopting upper and lower bound theories. Users of this code need to provide the nodal coordinates, nodes connecting elements, and support and loading conditions. With the given input, the code generates objective function and constraints of linear programming. A built-in tool (linprog) in MATLAB is used to perform minimum weight design. To check the result, hand calculation is performed to analyse the truss and minimum weight design is performed using commercially available software LINGO.

METHODOLOGY

LP is a mathematical model of achieving the best outcome. The equations of the mathematical model is formulated with linear equations. LP is a tool to optimize an linear objective fuction that is subjected to constraints. Constraints are composed of linear equality and inequility. The feasible region of LP is a convex polytope that is defined by the intersection of many finitely half-spaces. Each half-spaces are defined by a linear inequality. The objective function is a real-valued affine (linear) function defined on the polyhedron. The LP finds a point in the polyhedron where the objective function is optimized. A LP problems is expressed in a canonical form and presented below, where q represents the vector of variables that to be determined, R and S are vectors of known coefficients, and C is a known matrix of coefficients. R^Tq is the objective function and $Cq \leq S$ and $q \geq 0$ are the constraints. The inequalities specify a convex polytope and objective function is optimized over the polytope.

$$\begin{array}{ll} \text{Maximize} & R^Tq \\ \text{Constraints} & Cq \leq S \\ \text{And} & q \geq 0 \end{array}$$

LP tool is used to analyse and optimize a given truss. For any kind of truss members, let U_i are the member forces, n_{ij} are the direction cosines of the members, l_i are the lengths of the members, F_i are the forces in the nodes applied in global X and Y directions, A_i are the areas of the members, and σ is the compressive and tensile strength of the steel used in the truss. The main objective is to design a truss with minimum weight. Therefore, the volume of the truss members are required to be minimized. In case of plane truss, the volume is the product of length and cross-sectional area of each member. The full program to perform minimum weight design by using LP tool is presented below.

$$\begin{array}{ll} \text{Objective Function} & \text{Minimize, } \sum_{i=1}^n A_i l_i \\ \text{Constraints} & \sum_{i=1}^n U_i n_{ij} = F_i \\ & -\sigma A_i \leq U_i \leq \sigma A_i \\ & A_i \geq 0 \end{array}$$

FORMULATION

A truss presented in Fig. 1 consists of four nodes, five members, two supports, and one vertically downward applied force P at node 2. To optimize the truss using LP, the formulation is presented below. The cross-sectional areas of five truss members are denoted by A_1 to A_5 for member I to V, respectively. Length of the members is 1, $\sqrt{2}$, 1, $\sqrt{2}$, and 1 (unit of length) for members I to V, respectively. Tensile and compressive strength of the members is $\pm\sigma$. Member forces are denoted by U_{ij} , where i and j represents starting and ending node, respectively. Following equations are developed using nodal equilibrium conditions.

At node 2

$$U_{12} + \frac{\sqrt{2}}{2} U_{24} = 0$$

$$U_{23} + \frac{\sqrt{2}}{2} U_{24} = -P$$

At node 3

$$U_{23} + \frac{\sqrt{2}}{2} U_{13} = 0$$

$$U_{34} + \frac{\sqrt{2}}{2} U_{13} = 0$$

The LP is written for the truss as shown below.

Objective Function	Minimize $A_1 + \sqrt{2} A_2 + A_3 + \sqrt{2} A_4 + A_5$
Constraints	$U_{12} + \frac{\sqrt{2}}{2} U_{24} = 0$ $U_{23} + \frac{\sqrt{2}}{2} U_{24} = -P$ $U_{23} + \frac{\sqrt{2}}{2} U_{13} = 0$ $U_{34} + \frac{\sqrt{2}}{2} U_{13} = 0$ $-\sigma A_1 \leq U_{12} \leq \sigma A_1$ $-\sigma A_2 \leq U_{13} \leq \sigma A_2$ $-\sigma A_3 \leq U_{23} \leq \sigma A_3$ $-\sigma A_4 \leq U_{24} \leq \sigma A_4$ $-\sigma A_5 \leq U_{34} \leq \sigma A_5$ $A_i \geq 0$

The MATLAB code formulates the objective function, constraints for the truss. First, it performs the truss analysis then the minimum weight design.

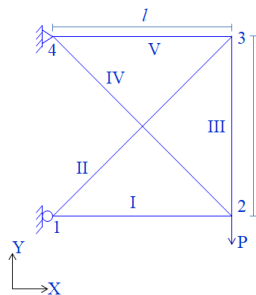


Figure 1: Example of a truss

ANALYSIS AND MINIMUM WEIGHT DESIGN

The analysis and minimum weight design are performed in three ways. First, the truss is analysed by hand calculation using joint method, and then the same truss is optimized by commercially available software LINGO. Then developed MATLAB code is used to find out member forces and minimum cross-sections.

Truss analysis using joint method

The reactions of the truss are calculated first. The reactions are found and shown in Fig. 2 a. Fig. 2 b shows equilibrium condition in nodes. Using joint method, member forces are calculated and presented below.

$$\begin{aligned} U_{12} &= P \\ U_{13} &= 0 \\ U_{23} &= 0 \\ U_{24} &= \sqrt{2}P \\ U_{34} &= 0 \end{aligned}$$

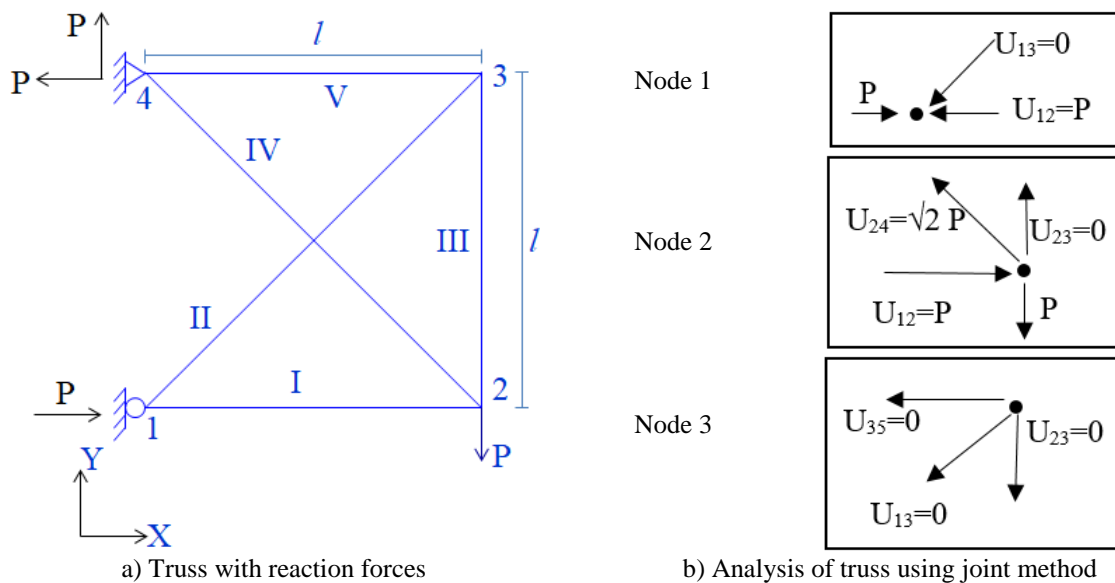


Figure 2: Truss with reaction forces

Optimization Using LINGO

The objective function and constraints are provided in LINGO software. Fig. 3 a and b shows the LINGO input code and output, respectively. LINGO result shows member U_{12} carries P and U_{24} carries $-1.414427 P$ force. The minimum cross-sectional area calculated by LINGO for members U_{12} and U_{24} are 0.02857143 and 0.0404122 , respectively. Other member carries zero load. Therefore, cross-sectional area is zero.

MATLAB result

Developed MATLAB code is used to analyse and optimize the truss presented in Fig. 1. Fig. 4 a shows the guideline for user to provide input and Fig. 4 b shows the input provided for the truss presented in Fig. 1. Result is obtained after the simulation and simulation time was approximately 2 seconds. Table 1 shows MATLAB result. Member forces in U_{12} and U_{24} are P and $\sqrt{2} P$, and cross-sectional area for both the members are 0.0286 and 0.0404 , respectively. Forces and cross-sectional area for other members are zero.

```

!Objective function;
Min=1*A1+1.414*A2+1*A3+1.414*A4+1*A5;

!Constraints;
!To ensure no negative value;
A1>=0;
A2>=0;
A3>=0;
A4>=0;
A5>=0;
U12>=0;
U13>=0;
U23>=0;
U24>=0;
U34>=0;

!Nodal equilibrium conditions;
U12+0.707*U24=0;
U23+0.707*U24=-1;
U23+0.707*U13=0;
U34+0.707*U13=0;

!Upper and lower bound theorems;
U12>=-A1*35;
U12<=A1*35;
U13>=-A2*35;
U13<=A2*35;
U23>=-A3*35;
U23<=A3*35;
U24>=-A4*35;
U24<=A4*35;
U34>=-A5*35;
U34<=A5*35;

```

a) LINGO input

Variable	Value	Reduced Cost
A1	0.2857143E-01	0.0000000
A2	0.0000000	1.414000
A3	0.0000000	1.000000
A4	0.4041220E-01	0.0000000
A5	0.0000000	1.000000
U12	1.000000	0.0000000
U13	0.0000000	0.0000000
U23	0.0000000	0.0000000
U24	-1.414427	176750.0
U34	0.0000000	0.0000000

b) LINGO output

Figure 3: LINGO input and output

Full history of the geometry				
n = total number of nodes	e = total number of elements	b = total number of supports	l = total number nodes where load is applied	σ = tensile and compressive strength of steel
Node history				
Node no.		X coordinate		Y coordinate
Element history				
Element no.		Starting node		Ending node
Support conditions history				
Node no. with supports				
Load history				
Node no.		Load along X direction		Load along Y direction

a) User input to MATLAB

Full history of the geometry				
n = 4	e = 5	b = 2	l = 1	$\sigma = 35$
Node history				
1	0		0	
2	1		0	
3	1		1	
4	0		1	
Element history				
1	1		2	
2	1		3	
3	2		3	
4	2		4	
5	3		4	
Support conditions history				
			1	
			4	
Load history				
	2	0		-1*

* Load P was applied as a multiplier of 1

b) MATLAB input for the truss presented in Fig. 1

Figure 4: MATLAB input

Table 1: MATLAB output

Member	Member Force	Cross-Sectional Area
U ₁₂	1 so P	0.0286
U ₁₃	0	0
U ₂₃	0	0
U ₂₄	$\sqrt{2}$ so $\sqrt{2}P$	0.0404
U ₃₄	0	0

CONCLUSION

A truss needs to be analysed first before designing. Many methods and software are available to perform the analysis. In case of design, several algorithm and software are available to perform minimum weight design. But, some softwares are limited to truss types and algorithms are complicated and consume a significant amount of time. As an example, genetic algorithm consumes hours to perform optimization of truss. On the other hand, linear programming (LP) is a time efficient tool that is used to perform minimum weight design. A MATLAB code is developed incorporating LP to perform analysis and minimum weight design. One truss (presented in Fig. 1) is analysed by joint method to know the member forces, and LINGO is used to perform minimum weight design. LINGO required user input of objective function and constraints that represents the equilibrium equations of unsupported nodes. Developing objective function and constraints required more time and it is easy to make a mistake, while performing hand calculation, although LINGO took less than two seconds to develop the result. On the other hand, the accuracy of the result is compromised since the decimal places are required to consider for trigonometric function of angle. The same truss is analysed by MATLAB. MATLAB simulation takes approximately two seconds to perform analysis and optimization. Conclusion can be drawn to the following points:

- The member forces obtained from MATLAB code is same as the member forces obtained from hand calculation and LINGO output.
- The minimum cross-sectional area obtained from MATLAB code is same as the result obtained from LINGO output.
- MATLAB code finds the unnecessary members with zero force and zero cross-sectional area.
- MATLAB code shows 100% congruency with hand calculation and LINGO.
- MATLAB code is less time consuming than LINGO in terms of formulation of the problem and there is minor chance of mistakes while using MATLAB code to perform truss analysis and minimum weight design.
- Hence, developed MATLAB code is recommended to use for performing truss analysis and minimum weight design of a plane truss.

REFERENCES

- Abo-Hamd, M. 1983. Minimum Weight Design of Trusses. *Applied Mathematics Modelling*, 7 (5): 374-376.
- Charnes, A and Greenberg, HJ. 1951. Plastic Collapse and Linear Programming. *Bulletin of the American Mathematical Society*, 57: 480.
- Romero, J; Mappa, PC; Herskotits, J and Soares, CM. 2002. An Efficient Technique for Optimal Truss Design. *Mecania Computational*, 21: 2752-2766.
- Romero, J; Mappa, PC; Herskotits, J and Soares, CM. 2004. Optimal Truss Design Including Plastic Collapse Constraints. *Structural Multidisciplinary Optimization*, 27: 20-26.
- Petrovic, Z; Milosevic, B; Mijalkovic, M and Brcic, S. 2011. Determination of the Limit Load of Statically Indeterminate Truss Girders. *Facta Universitatis*, 9 (2): 217-229.

EXPERIMENTAL INVESTIGATION OF COMPRESSIVE STRENGTH OF PLASTERED UNREINFORCED BRICK MASONRY WALL

A. F. Mazumder^{1*}, M. A. Obaida², A. T. Siddique² & A. Mahmud³

¹*Department of Civil and Construction Engineering, Western Michigan University, Michigan, USA.*

E-mail: abul.f.mazumder@wmich.edu

²*Department of Civil Engineering, Presidency University, Dhaka, Bangladesh. E-mail: abuobaida234@gmail.com; towhidsiddique@gmail.com*

³*Bangladesh Water Development Board, Dhaka, Bangladesh. E-mail: asifmahmud1348@gmail.com*

**Corresponding Author*

ABSTRACT

Plaster is a mix of cement, sand, and water that is applied on the masonry surface to cover rough surfaces of the wall. The key purposes of providing plaster are to protect the masonry surfaces from environmental exposure to hide defective joints, to prevent moisture ingress, and to obtain smooth and durable surfaces. Besides having these advantages, plaster also increases the axial capacity of the wall. The main objective of this paper is to investigate the increase of axial load bearing capacity of a plastered masonry wall. To accomplish the objective, six specimens ($234.95 \times 114.3 \times 63.5$ mm) are constructed. Among these specimens, three specimens are plastered with 18.75 mm thick plaster. The cement-sand ratio of the plaster is 1:2.5 and water-cement ratio is 0.6. After 28 days wet curing period, all the specimens are tested under axial compressive load. The average compressive strength of the masonry wall without and with plaster is 3.48 and 3.98 MPa, respectively. Therefore, the 18.75 mm plaster could increase the axial capacity by 14.37% and the efficiency of the plaster is 15.53%.

Keywords: Brick, masonry, plaster.

INTRODUCTION

Masonry wall is one of the most popular and common type of structural component which is made from individual units laid in and bonded together using mortar. For many years, masonry wall is being used because of its aesthetic appearance, cost effectiveness, and ease of construction. The key advantages of masonry wall include increase of thermal mass and fire protection of the building, reduced life cycle cost, and 30 to 100 times higher useful life cycle than structural steel. Masonry walls are most commonly used as partition wall, structural wall, retaining wall, and even in heritage structures. Masonry walls are constructed usually as unreinforced. These unreinforced masonry (URM) walls are vulnerable to high axial load and earthquake load. URM walls can be used as load-bearing wall, if proper strengthening materials are used. Some researchers used CFRP, GFRP sheet and bars, tensile reinforced mortar, ultra high performance concrete, and ordinary mortar for strengthening (Basaran et al., 2013; Vasconcelos et al., 2012; Mahmood et al., 2008; ElGawady et al., 2006; Zhao et al., 2003; Mazumder, 2017; Mazumder et al., 2017) and found out axial capacity of masonry wall with and without strengthening schemes. Some researchers performed experimental investigation of compressive strength of unreinforced masonry wall (Ravula and Subramaniam, 2017; Annamalai et al.,

1987). Some researchers investigated the axial capacity of masonry wall using numerical simulations (Mazumder and Sarfin, 2017; Mazumder and Nishat, 2017).

URM wall is more useful for load-bearing type of wall with proper strengthening techniques and cementitious material could be one of the possible solutions. Usually, cement-sand mortar is used to plaster a wall. Plaster is provided to protect the masonry wall surface from rough environmental exposure, to hide defective joints, to prevent moisture ingress, and to obtain smooth and durable surface. A 12.5 mm thick plaster is provided for inner surface and 18.75 mm plaster is provided for outer surface of the wall. This plaster makes the wall stronger, durable, and increases the load bearing capacity of the wall as well. The main objective of this study is to investigate experimentally the increase of load bearing capacity of unreinforced masonry wall with the use of 18.75 mm thick plaster on both sides.

METHODOLOGY

The load bearing capacity of unreinforced concrete masonry wall prisms are evaluated using axial load tests. In this test, incrementally increased compressive load is applied to the prisms. Six specimens are tested in two categories – i) three unreinforced masonry prisms (UMP) and ii) three 18.75 mm thick plastered masonry prisms (UMPP). The compressive strength of brick and mortar is also investigated. Six specimens are constructed and wet cured. Specimens are tested under compressive load after curing period.

Material properties

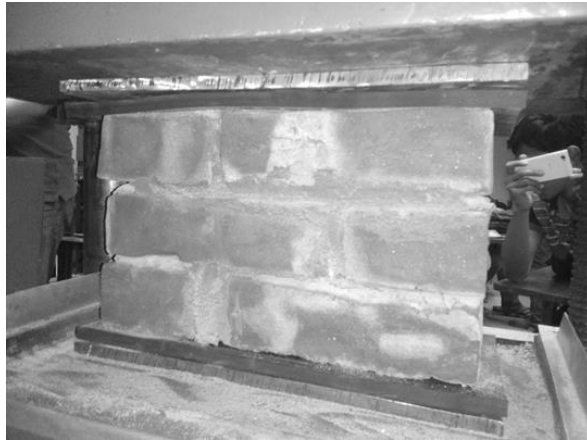
Mechanical properties of wall components, concrete masonry brick and mortar, are investigated experimentally. Compressive strength of concrete masonry bricks is obtained following test procedure of Barbosa (2009). The average compressive strength of bricks is 6.61 MPa. The compressive strength of mortar is tested following ASTM C39. The 28-day compressive strength of mortar is 18.54 MPa. The water-cement and cement-sand ratio of mortar are 0.6 and 1:2.5, respectively.

Construction of prisms

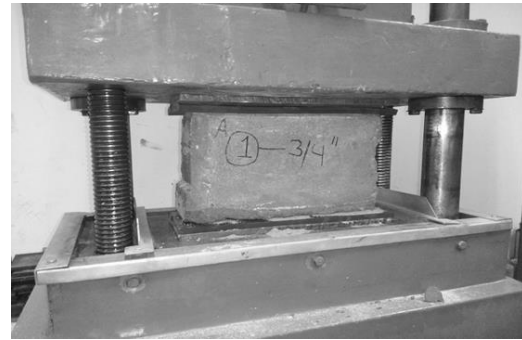
Six prisms are constructed with concrete masonry bricks and Portland cement mortar is used as head and bed joints. The nominal size of a brick is $235 \times 110 \times 70$ mm, approximately. Three layers of bricks, containing one and a half bricks in each layer, are cast to form the prisms. 18.75 mm thick plaster is applied on the both sides of the three prisms. The aspect ratio for all walls is 0.9 and height to thickness of the wall is 2.10, approximately. After casting, specimens are wet cured for 28 days. After curing period, the specimens are tested.

Experimental setup, instrumentation, and procedure

According to ASTM C1314 and European Standard EN1052-1(1999), masonry prisms (UMP and UMPP) are tested under uniaxial compressive load. To avoid eccentricity, the prisms are placed vertically and horizontally perfectly aligned on Universal Testing Machine (UTM). The axial compression forces are exerted on the prism through steel plate and rubber sandwich. The steel plate and rubber sandwiches are attached on the top and bottom of the prisms to ensure uniform distribution of the axial force without any stress localization. Fig. 1 shows the test setup for UMP and UMPP.



a) Experimental setup of UMP



b) Experimental setup of UMPP

Figure 1: Specimen and experimental setup of UMP and UMPP

RESULTS

Table 1 shows the compressive strength of UMP prisms. The average compressive strength of UMP is 3.48 MPa. Compressive strength of each UMPP is presented in Table 2. The average compressive strength of UMPP is 3.98 MPa. The 18.75 mm plaster could successfully increase the compressive strength of UMP by 14.37%. The efficiency of the plaster is 15.53%.

Table 1: Compressive strength of UMP

Serial no.	Dimension (L × B × H) (mm × mm × mm)	Load (kN)	Stress (MPa)	Average stress (MPa)
1	360 × 112.33 × 219	140	3.46	3.48
2	363 × 111 × 214.33	148	3.67	
3	365 × 111.67 × 219	135	3.31	

Table 2: Compressive strength of UMPP

Serial no.	Dimension (L × B × H) (mm × mm × mm)	Load (kN)	Stress (MPa)	Average stress (MPa)
1	365 × 110.67 × 217.33	159	3.94	3.98
2	371 × 115.67 × 228.33	156	3.64	
3	366 × 109.67 × 220	175	4.36	

CONCLUSIONS

Plaster increases the axial capacity of the masonry wall. To evaluate the increase in axial capacity, six prisms are constructed and three of them are plastered. All the specimens are tested under compression in universal testing machine after 28 days wet curing period. The average compressive strength is 3.48 and 3.98 MPa for UMP and UMPP prisms, respectively. Therefore, the axial capacity of masonry wall is increased by 14.37% approximately due to 18.75 mm plaster. The efficiency of the plaster is 15.53%.

ACKNOWLEDGMENT

The research work presented in this paper was carried out at the Civil Engineering laboratory of Presidency University (PU). The authors would like to thank PU for the continuous support.

REFERENCES

- Annamalai, G; Jayraman, R and Rao, AGM. 1982. Investigation on the Compressive Strength of Walls Built Using Local Chamber Burnt Bricks.
- Basaran, H; Demir, A and Bagci, M. 2013. The Behavior of Masonry Walls with Reinforced Plaster Mortar. *Advances in Material Science and Engineering*, 1-9.

- Barbosa, CS and Hanai, JB. 2009. Strength and Deformability of Hollow Concrete Blocks: Correlation of Block and Cylindrical Sample Test Results. *Ibracon Structures and Materials Journal*.
- ElGawady, MA; Lestuzzi, P and Badoux, M. 2006. A Seismic Retrofitting of unreinforced Masonry Walls Using FRP. *Science Direct, Composites: Part B (37)*: 148-162.
- Mahmood, H; Russell, AP and Ingham, JM. 2008. Monotonic Testing of Unreinforced and FRP-Retrofitted Masonry Walls Prone to Shear Failure in an Earthquake. *The 14th World Conference on Earthquake Engineering*, 214-220.
- Mazumder, AF and Sarfin, MAA. 2017. Numerical Investigation of Axial Capacity Assessment of UHPC Plastered Wall using ABAQUS. *Proceedings of the ICEIRE 2017*, 4: 45-48.
- Mazumder, AF; Mahmud, A and Rafael, M. 2017. Investigation of the Contribution of the Plaster in Compressive Strength of Unreinforced Masonry Wall. *Proceedings of the ICEIRE 2017*, 4: 182-184.
- Mazumder, AF. 2017. Axial Load Bearing Capacity of Unreinforced Concrete Masonry Wall and UHPC Block Wall. *Proceedings of the ICEIRE 2017*, 4: 25-28.
- Mazumder, AF and Nishat, M. 2017. Numerical Investigation of Axial Capacity Assessment of UHPC Plastered Wall using ABAQUS. *Proceedings of the ICEIRE 2017*, 4: 33-36.
- Rabula, MB and Subramaniam, KVL. 2017. Investigation of Compression Failure in Brick Masonry Assemblies Made with Soft Brick. *Proceedings of the ICACMS*, pp. 1-9
- Vasconcelos, G; Abreu, S; Figueiro, R and Cunha, F. 2012. Retrofitting Masonry Infill Walls with Textile Reinforced Mortar. *15 WCEE, LISBOA*, 178-187.
- Zhao, T; Xie, J and Li, H. 2003. Strengthening of Cracked Concrete Block Masonry Walls Using Continuous Carbon Fiber Sheet. *9th North American masonry conference, South Carolina, Clemson*, 9: 156-167.

STRUCTURAL STRENGTH AND BEHAVIOUR OF COMPOSITE PROFILED STEEL SHEET WITH PLASTIC BOARD AND PLYWOOD UNDER FLEXURE AND WEB CRIPPLING LOADING

S. M. Z. Islam*, A. E. Biswas & M. M. Rana

*Department of Civil Engineering, Rajshahi University of Engineering and
Technology, Rajshahi-6204, Bangladesh.*

E-mail: zahurul90@gmail.com

**Corresponding Author*

ABSTRACT

Profiled steel sheet is a ductile and lower stiffness material which is increasingly used as roofing elements in recent years. Structurally strong, efficient, lightweight and easily erected profiled steel sheet composite sandwich panel can be developed with non-ductile and stiffer materials plastic board and plywood. The composite panel system consist of the profiled steel sheet attached to top layer plastic board and bottom layer plywood by simple mechanical connector. Profiled steel sheeting plastic board with plywood (PSSPBP) system can be used as an alternative to traditional form of roof construction. The objective of this study is to develop composite sandwich roofing system of profiled steel sheeting plastic board with plywood (PSSPBP). The structural strength and behaviour of composite profiled steel sheet with plastic board and plywood are investigated in this study. A series of tests were performed on composite sandwich roofing system of profiled steel sheeting plastic board with plywood (PSSPBP) subjected to combined flexure and web crippling loading. The failure loads, failure modes and the load-web deformation behaviour of profiled steel sheeting with plywood are also presented. The experimental and analytical results were compared to validate and determine the structural strength and behaviour of profiled steel sheeting plastic board with plywood (PSSPBP). This PSSPBP composite sandwich roofing system helps to enhancing the stiffness and strength of the composite system. The proposed PSSPBP composite roofing system has a great potential to be exploited for the construction of housing as well as disaster relief shelter. The application of plywood as a load bearing structural component in PSSPBP system has the potential for disaster relief shelter. This system can reduce time and overall cost of construction and has the potential of opening up new composite system as disaster relief shelter as well as the building construction industry.

Keywords: Composite panel; profiled steel sheet; plywood; plastic board; structural behaviour.

INTRODUCTION

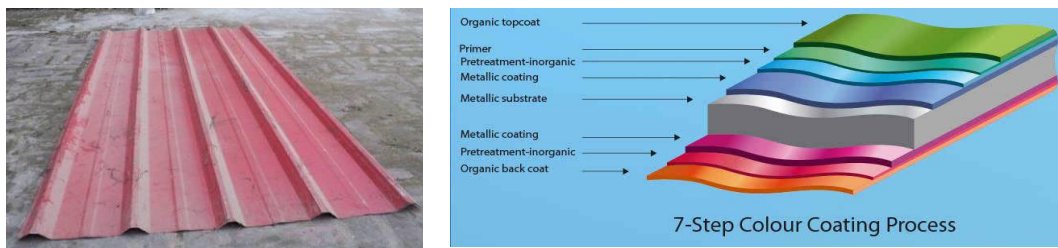
The growth rate of industrialization, urbanization and population is high now-a-days and for this housing necessity is also increasing. An emergency relief shelter is often required when sudden disaster takes place. Structurally strong, efficient, lightweight and easily erected construction material is needed for solve this problem. Profile steel sheet are used in roofing elements popularly due to aesthetic and economical use of materials. Experimental and numerical investigation on structural strength and behavior of self-supporting cylindrical profiled steel sheet proof roofing elements have been performed by (Islam et al. 2006). Rib of profiled steel sheet provided ten time's higher strength and stiffness than plain steel sheet. The profiled steel sheeting with plywood (PSSPW) can solve this problem. The main advantage of PSSPW is to reduce the internal trussing and supporting system is as traditional trussed

roof system. The PSSDB system was first invented in the United Kingdom by (Wright et al. 1989) as a replacement of timber joint flooring for low cost small scale domestic buildings. PSSDB is easily erectable and bear structural load described by (Wright et al. 1989). Structural behavior of profiled steel sheet dry board folded plate structure has been investigated by (Ahmed, 1999). The PSSDB is far better than others form construction system like reinforced concrete system from many aspects. These are described in other publications (Ahmed et al., 2000; Ahmed et al., 2002; Badaruzzaman et al., 2003). Ahmed and Badaruzzaman (Ahmed et al., 2005) conducted numerical investigations on structural performance of PSSDB and proposed as a disaster relief shelter. They were used dry board outside of the profiled sheet. However, it may easily damage due to rain, thunderstorm and weathering. It should be used inside of profiled steel sheet. Dry board should be provided inner site which will be provided better results. However they did not considered profiled steel sheeting and plywood (PSSPW) composite system in inner side. There is no research yet to be done with profiled steel sheet and plywood composite structure. The profiled steel sheeting connected to plywood and plastic board can be considered as an alternative to traditional forms of roof as well as floor construction. The main advantage of this system is to reduce the internal trussing and supporting system is as traditional trussed roof system thus adding to livable space in a building.

There is no research on profiled steel sheet, plywood and plastic board as sandwich composite structure either roof or flooring system. This proposed sandwich model can be used as a roof or floor surface to provide an efficient emergency shelter. The purpose of this study is to evaluate the structural strength and behavior of profiled steel sheeting plywood and plastic Board (PSSBPB) system. The failure loads, failure modes and the load-web deformation behavior of profiled steel sheeting with plywood and plastic board are also presented. Web crippling is one of the failure modes that can occur due to high local intensity of concentrated loads or reactions which should be considered. The structural strengths and behaviour of profiled steel sheet subjected to web crippling is also investigated in this study.

Material Properties of profiled steel sheet, Plywood and Connector and Plastic Board

The material properties of the profiled steel sheet were determined by tensile coupon tests following to the American Society for Testing and Materials Standard, (ASTM, 1997) and the Australian Standard (AS 1391, 1991) using Universal Testing Machine (UTM). Here 12.5 mm wide coupons were used. Deformation is measured by using deformation gauge. The test set-up and tested specimen after tensile test is shown in Fig. 2(a) and 2(b) respectively. Measured material properties obtained from tensile coupon tests are given in Table 1.



(a) Profile steel sheet

(b) Composition layer of profile steel sheet

Fig.1 Profile steel sheet and its composition



(a) Test set-up

(b) Tested specimen after tensile test

Figure 2: Profiled steel sheet tensile coupon test setup and failure mode

Table-1: Measured material properties obtained from tensile coupon tests

Specimen No.	Width b_c (mm)	Thickness t_c (mm)	Yield Stress σ_y (N/mm ²)	Ultimate Stress σ_u (N/mm ²)
1.	12.7	0.66	232.7	251.6
2.	12.6	0.65	238.6	261.5
3.	12.7	0.66	244.8	268.2

Plywood consists of numbers of thin sheets of wood (veneers) which are pressed and bonded together with some binding or cementing material like glue or synthetic adhesives. Plywood is also light in weight in comparison to those of cement-bonded boards, which is also very convenient for transporting and handling. Nominal thickness of plywood 15 mm, weight 7.55 kg/m², area of plywood 557418.24 mm² and Modulus of elasticity 6019 MPa as shown in Fig 3(b). Simple mechanical connectors, such as self-drilling, drilled screws have been used to connect the plywood & plastic board to the steel sheeting to form the composite unit as shown in Fig. 3. Mechanical properties of screw connectors which have carbon steel material, spacing 0.05-0.10 zinc Chromium, length 27.00 mm and diameter of thread 4.0mm. Thickness of plastic board is 7.7mm, area 2880000mm², tensile strength is 13.8ksi and Yield strength is 22.5ksi. Modulus of flexure is 783ksi.

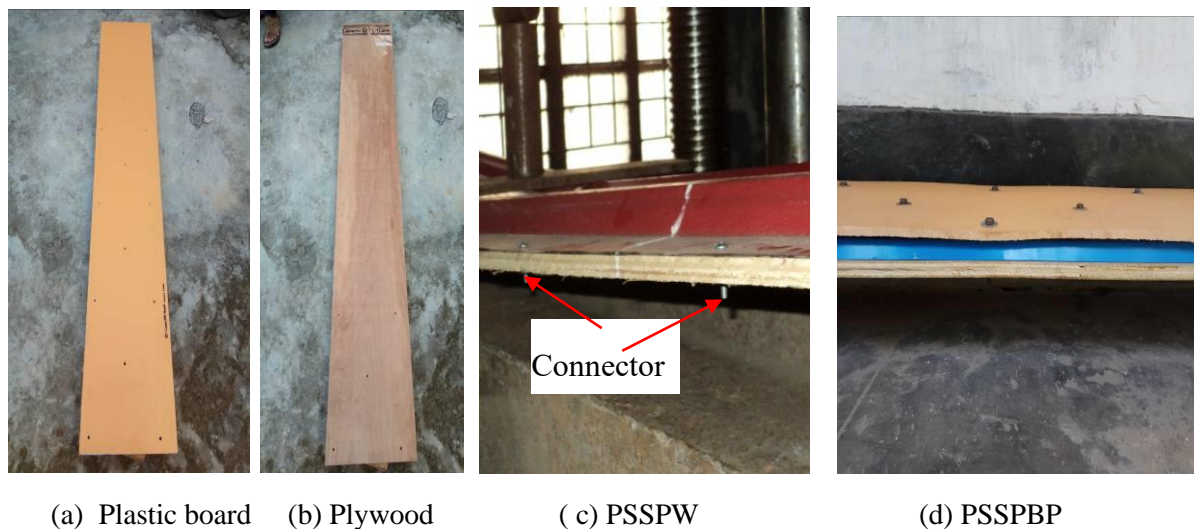


Fig-3: Plywood plastic board and connector

METHODOLOGY

Test specimens lying inside and outside of certain geometric profiled parameter ranges of the specifications were tested under concentrated load. Photograph of test specimen and test rig is shown in Fig. 3(c) and Fig. 3(d). Two rectangular identical small-scale specimens were prepared for the experimental investigations 0.56mm thick profiled steel sheeting 15mm thick plywood, 7.5 mm thick plastic board and self-tapping, drilled screws were selected for this purpose. All specimens one with plywood, plastic board the other one is single corrugated steel sheet dimensions of 1828.8mm by 304.8mm and were constructed. The connectors were arranged along PSSPBP with a spacing of 200mm. Testing specimen and plywood plastic board connected with profiled steel sheet using connectors is shown in Fig 3(d). Steel bearing plate was placed under the loading tool to distribute the loading. Fig 4: shows the loading arrangement. The PSSPBP panels were tested using an incremental loading procedure. For each increment of loading, the deflection at selected positions on the panels was

recorded by using deflection gauges. Fig. 4: Shows details of positions of strain gauges and their



Fig.4: Test setup of bending test



Fig.5: Failure of mode of bending test specimen

The web crippling tests were carried out under Interior-One-Flange (IOF) loading condition specified in the ASCE Specification (ASCE, 2002). Test setup and failure mode of web crippling test is shown in Fig. 6. The webs of the specimens were buckled outward.



Figure 6: Test setup and failure of mode of web crippling test specimen

RESULTS AND DISCUSSIONS

The results were obtained experimentally and analytically, which are then followed by the comparison of two results. The failure loads, failure modes and the load-web deformation behaviour of profiled steel sheeting with plywood and plastic board are also presented. It is found that the deflection of composite PSSPBP is lower and load carrying capacity is higher than the single profiled steel sheet as shown in Fig 7. The proposed system helps in enhancing the stiffness and strength of the composite system.

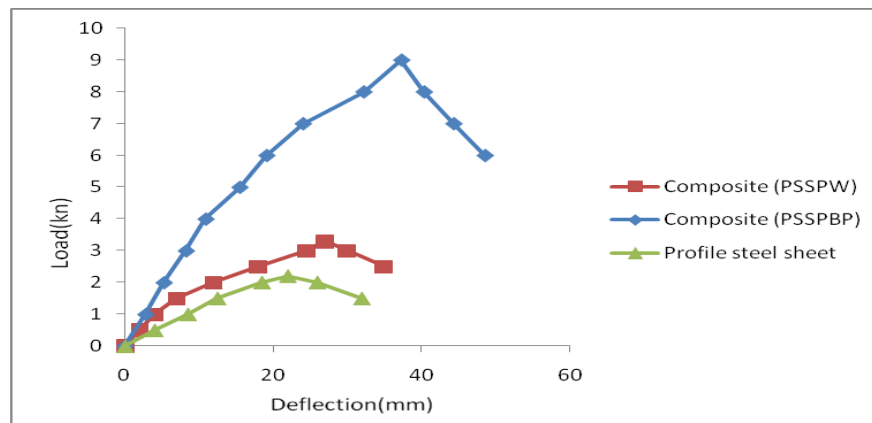


Fig. 7: Comparison load-deflection curve of profiled steel sheet, composite PSSPW and composite PSSPBP

Based on test results, it is observed that the structural strength and behaviour of composite PSSPBP under concentrated loading is better than the single plain profiled steel sheet. The experimental results were compared to validate and determine the structural strength and behaviour of profiled steel sheet and profiled steel sheet with plywood (PSSPW) and composite profiled steel sheet with plywood and Plastic Board (PSSPBP) as shown in Fig. 7. Fig-8 represents the result of web crippling test.

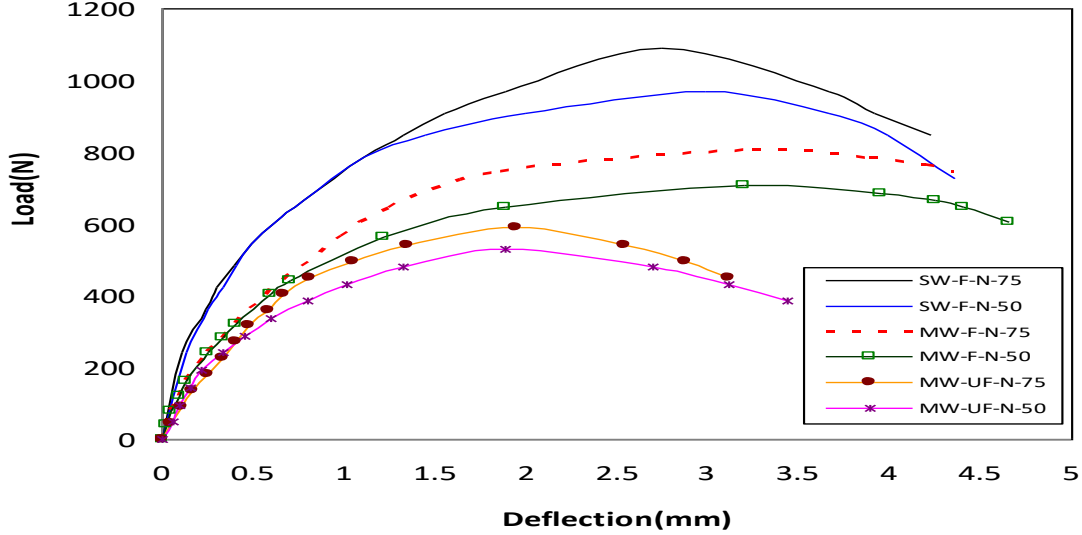


Figure 8: Comparison load-web deformation curves for under different condition

Table 2: Comparison of Analytical results with Experimental results for different condition

Condition/Case		Bearing length (mm)	Length (mm)	Thickness (mm)	Web crippling strength P_t (kN)	Web crippling strength P_n (kN)	P_t / P_n
Muli-web	Fasten	50	335.1	0.66	0.707	0.803	0.88
		75	460.0	0.66	0.805	0.956	0.84
	Unfasten	50	335.1	0.66	0.529	0.601	0.88
		75	460.0	0.66	0.592	0.704	0.84
Single web	Fasten	50	335.1	0.66	0.970	1.066	0.91
		75	460.0	0.66	1.090	1.267	0.86
	Unfasten	50	335.1	0.66	0.725	0.796	0.91
		75	460.0	0.66	0.817	0.950	0.86

According to the Canadian Specification and using North American coefficient the web crippling strength is determined. The unified North American (AISI S100, 2007) equation is provided in equation 1.

$$P_n = Ct^2 f_y \sin \theta \left(1 - C_R \sqrt{\frac{r_i}{t}} \right) \left(1 + C_N \sqrt{\frac{N}{t}} \right) \left(1 - C_h \sqrt{\frac{h}{t}} \right) \quad (1)$$

A comparison is carried out between the test value (P_t) and the design predicted value (P_n) as shown in Table 1. The web crippling capacity of profiled steel sheet may restrict the use of profiled steel sheet. It is recommended that the web crippling strength should be considered to achieve more effective designs of profile steel sheet.

CONCLUSIONS

The paper presents an experimental investigation on the structural strength and behaviour of composite profiled steel sheet with plywood and plastic board. The failure loads, failure modes and the load-web deformation behaviour of profiled steel sheeting with plywood and plastic board are also presented. It is found that for composite PSSPBP the deflection is lower and load carrying capacity is higher than the single profiled steel sheet. Its basic behaviour in the elastic range was investigated and checking deflection as the main controlling design factor. Based on test results, it is observed that the structural performance of composite PSSPBP is better than the simple single profiled steel sheet. The method of enhancing the structural stiffness and performance of the system is proposed. Based on experimental results, increasing load carrying capacity of PSSPBP is 309.09% for flexure test and 102% for web crippling test with respect to profiled steel sheet. Therefore, the proposed PSSPBP composite roofing system has a great potential to be exploited for the construction. The application of Plastic board as heat reducing and aesthetic component, plywood as a load bearing structural component in PSSPBP system has the potential to meet the demands of building construction. PSSPBP panel is light weight, easily erectable and flexible for handling which is suitable for disaster relief centre. This system can reduce time and overall cost of construction and has the potential of opening up new composite system in the building construction industry.

ACKNOWLEDGMENTS

The authors are grateful to Abul Khair Steel Mills, Dhaka, Bangladesh for supplying the test specimens.

REFERENCES

- Islam, SMZ; Abdullah, AAA and Jafor, MS. 2006. An Investigation on structural performance of profiled steel sheet to develop self-supporting roofing system." *Journal of Advance Steel Construction* 2006,2(2006), 87-108.
- Wright, HD; Evans, HR and Burt, CA. 1989. Profiled steel sheet/dryboarding composite floors. *Struct Eng* 1989,67(7/4),114–29.
- Ahmed, E. 1999. Behaviour of profiled steel sheet dry board folded plate structure. PhD thesis, Universiti Kebangsaan, Malaysia;1999.
- Ahmed, E; Badaruzzaman, WHW and Wright, HD. 2000. Experimental and finite element study of profiled steel sheet dry board folded plate structures. *Thin Wall Struct* 2000,38(2),125–43.
- Ahmed, E; Badaruzzaman, WHW and Wright, HD. 2002. Two-way bending behaviour of profiled steel sheet dry board composite panel system. *Thin Wall Struct* 2002,40(11), 971–90.
- Badaruzzaman, WHW; Zain, MFM and Akhand, AM. 2003. Dry boards as load bearing element in the profiled steel sheet dry board floor panel system—structural performance and applications. *Construction and Building Materials*, 2003, 17, 289–297.
- Ahmed, E and Badaruzzaman, WHW. 2005. Finite element prediction on the structural performance of profiled steel sheet dry board structural composite system proposed as a disaster relief shelter. *Construction and Building Materials*, 2005,19, 285–295.
- ASTM.AS. 1997. Standard test methods for tension testing of metallic materials, E 8M-97. West Conshohocken: American Society for Testing and Materials, 1997.

AS. 1991. Methods for tensile testing of metals, Australian standard AS 1391. Sydney, Australia: Standards Association of Australia, 1991.

COMPARATIVE STUDY OF STRUCTURAL PERFORMANCE USING SITE SPECIFIC RESPONSE SPECTRUM ANALYSIS

S. L. U. Islam & N. H. M. K. Serker*

*Department of Civil Engineering, Rajshahi University of Engineering & Technology,
Rajshahi, Bangladesh.*

E-mail: labib.ruet@gmail.com; kserker@yahoo.com

**Corresponding Author*

ABSTRACT

Response Spectrum Analysis (RSA) is a linear dynamic statistical analysis which measures the contribution from each natural mode of vibration to indicate the likely maximum seismic response of an essentially elastic structure. For taller buildings RSA is found to be more suitable for more accurate results in analyzing the building response to ground motion. In the BNBC 2015 (final draft), sites are classified in the code based on soil properties in the code. In this paper, a comparative study has been conducted in regards to storey drift for different site types, using RSA. ETABS has been used to conduct the analysis. Site type SD has been identified as the site most vulnerable to earthquake responses and finally a comparison of the storey drifts for buildings in different site classes has been quantified.

Keywords: Site specific Response Spectrum Analysis; BNBC 2015; Dynamic analysis.

INTRODUCTION

The modern construction has been dominated by high-rise buildings. The problem of limited space for use by a large number of people has been solved by the tall buildings. The development of different building systems has made it increasingly easier to construct skyscrapers.

But these developments of tall buildings have brought greater risk of loss of life in case the structure fails for any reason. The devastation caused by recent past earthquakes has been reminders of the importance of effective seismic analysis.

As Bangladesh lies close to a fault line, structural engineers practicing in Bangladesh need to design with proper seismic analysis to avoid earthquake hazard as much as possible.

The simplest method of seismic analysis is Equivalent Static Analysis. It is a linear static analysis method and it can predict the seismic response in an acceptable way for relatively short buildings. For taller buildings Response Spectrum analysis is a lot more effective. Moreover, many construction firms and government projects design similar types of building as a part of a package. The buildings are often designed for one place that is in a specific seismic zone and applied at various other places within that zone. According to the code however, the sites of construction have significant impact on the structural performance in RSA, irrespective of the seismic zones.

In this paper, in accordance with the BNBC 2015, a comparative study is conducted using Response Spectrum analysis with the software analysis to show and quantify the difference in building responses in different classes of sites.

METHODOLOGY

Spectral Acceleration (SA) is a unit measured in g (the acceleration due to Earth's gravity, equivalent to the g-force), that describes the maximum acceleration in an earthquake on an object – specifically, a damped, harmonic oscillator moving in one physical dimension. The spectral acceleration graphs were prepared using BNBC 2015 provisions for the five site types [Fig. 1].

Three different plans of buildings with different heights were chosen [Fig. 2], [Fig. 3] and [Fig. 3].

The 3d models of the buildings were created with ETABS. The height of the building 1 in the model was 142ft. The Building 2 and Building 3 were of 132ft and 122ft heights respectively. The plinth area of the Building 1 was 2218.84 sq. ft.; Building 2 was 6460 sq. ft. and Building 3 was 11907 sq. ft.

The dimensions of columns of the models were 12"x24" and 12"x30"; dimension of beams was 12"x18" and the thickness of slab was taken as 8". The material properties used for the models were – Compressive strength of concrete, $f'_c = 3.5$ ksi; tensile strength of steel = 60ksi.

The applied loads were as follows – Superimposed dead load = 30 psi; live load = 70 psi; wall load = 9 k/ft (exterior walls) and 4.5 k/ft (interior walls).

For lateral loads, load directions U1 and U2 were applied. U1 and U2 are defined as direction with a specified angle of rotation about Z axis. In the program UX, UY, UZ loads corresponds to unit transitional acceleration of the ground in X, Y, and Z directions respectively. Angle of rotation about Z axis in response spectrum case was specified zero, so U1, U2 and U3 were the same as UX, UY and UZ. The load combination used for the analysis was – 1.2DL + 1.0LL + 1.0E (BNBC 2015, page 6-141). CQC method was used for combination of the modal results and response spectrum case results were analysed.

The title of the section shall be in capitals bold face letters (11 pt). Methodology of the paper should provide the reader with all the information necessary to repeat the work. For a modification of published methodology, only the modification needs to be described, with reference to the original source. Statistical analysis of the data (where applicable) is mandatory, using appropriate methods, which must be cited.

Figures

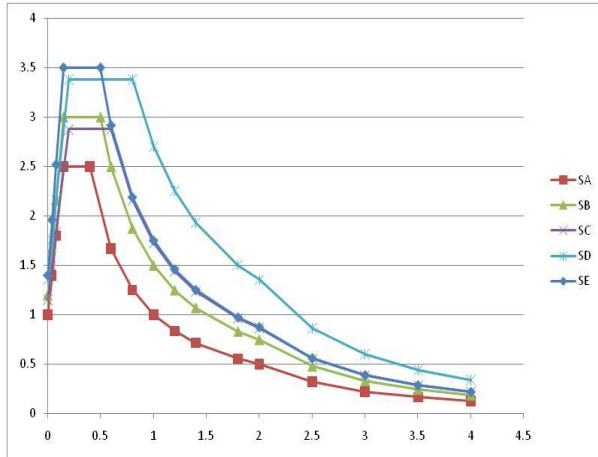


Fig. 1: Normalised Response Spectra

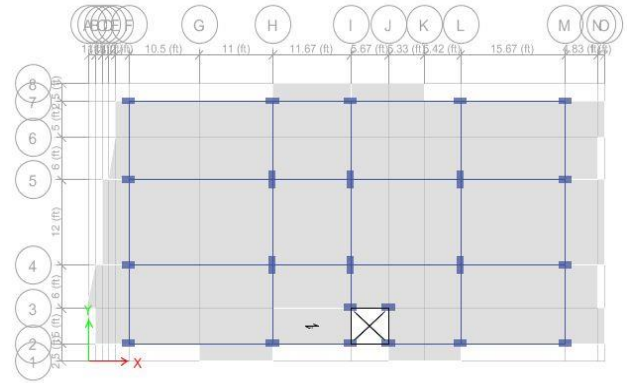


Fig. 2: Plan of building 1

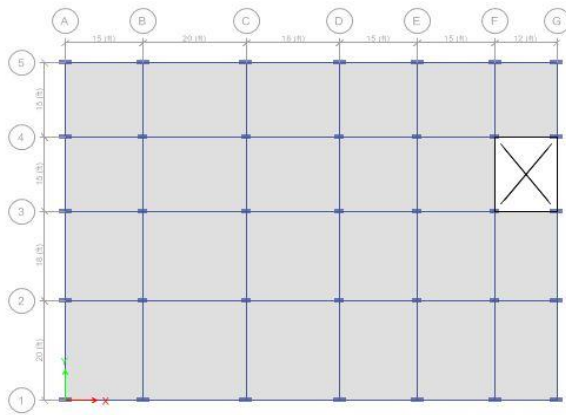


Fig. 3: Plan of building 2

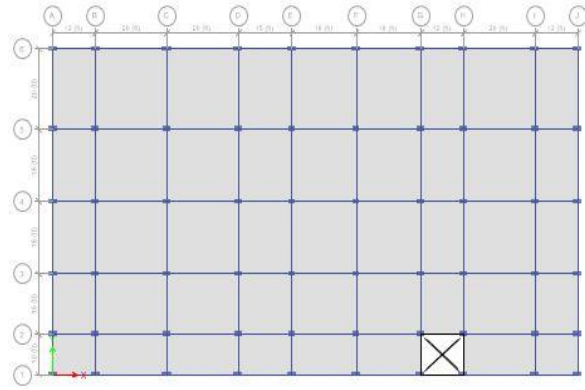


Fig 4: Plan of building 3

RESULTS AND DISCUSSIONS

After running the simulation, the maximum inter-storey drift was found to be at site type SD for all three buildings [Fig. 5]. The maximum base shear was also found to be at site type SD for all three buildings.

There was a 49.85% to 49.91% increase in inter-storey drift found in the analysis for site SB relative to site SA; a 14.87% to 14.95% increase in site SC relative to site SB; a 55.99% to 56.34% increase in site SD relative to site SC and a decrease of 34.88% to 35.06% in site SE relative to site SD.

As for base shears, there was a 46.72% to 48.54% increase in site SB relative to site SA; a 12.38% to 14.14% increase in site SC relative to site SB; a 50.88% to 53.61% increase in site SD relative to site SC and a decrease of 31.18% to 33.45% in site SE relative to site SD.

The values of the maximum inter-storey drift and maximum base shear are tabulated in Table 1 and Table 2.

These changes in inter-storey drifts and base shears were the result of the different non-linear normalized spectral acceleration graphs used for the site specific response spectrum analysis. The site properties stated on the code and the generated accelerations for particular site are the reasons for the

varying values of inter-storey drifts and base shears. The highest responses were found to be in the site type SD indicating the sensitivity of the particular site to seismic forces.

Furthermore it was found that the rate of relative change of inter-storey drift and base shear is fairly uniform for symmetrical buildings despite the difference in the building height and area. This signifies that the effect of earthquake on the building responses is broadly proportional in the different site types relative to each other, irrespective of their plinth area and height.

The site type SD is found to be the most vulnerable site type for seismic hazards by a long margin. Therefore the identification of this type of site in any construction project is of great importance and structures in such sites should be designed with greater care, instead of using similar structural elements for similar buildings irrespective of the site.

Figures

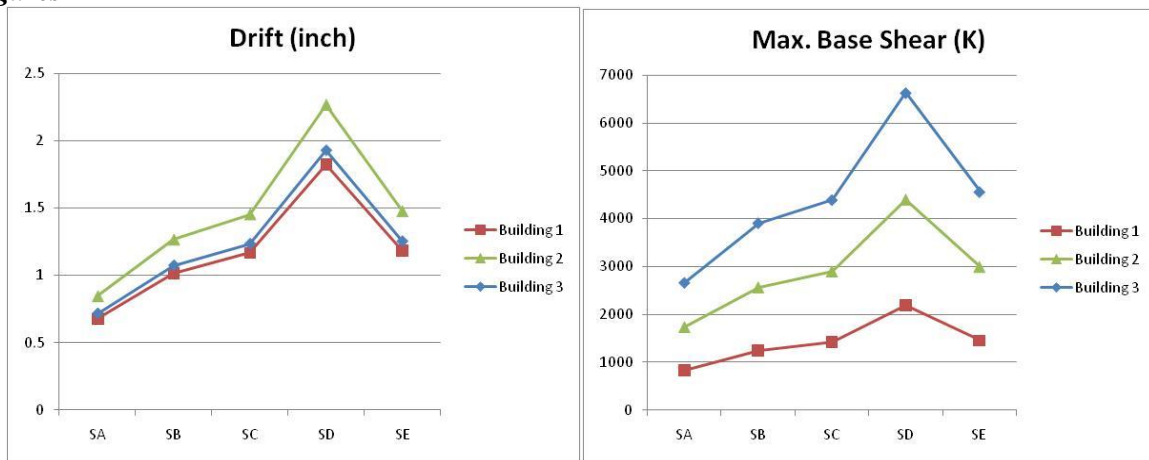


Fig 5: Maximum inter-storey drift in different sites for different buildings

Fig 6: Maximum base shear in different sites for different buildings

Tables

Table 1: Table for maximum drift for the buildings in different sites

<i>Building 1</i>		<i>Building 2</i>		<i>Building 3</i>	
<i>Soil type</i>	<i>Max. Drift</i>	<i>Soil type</i>	<i>Max. Drift</i>	<i>Soil type</i>	<i>Max. Drift</i>
SA	0.005634	SA	0.007031	SA	0.005962
SB	0.008446	SB	0.010537	SB	0.008934
SC	0.009709	SC	0.012104	SC	0.010268
SD	0.015174	SD	0.018881	SD	0.016053
SE	0.009856	SE	0.012296	SE	0.010425

Table 2: Table for maximum base shear for the buildings in different sites

<i>Building 1</i>		<i>Building 2</i>		<i>Building 3</i>	
<i>Soil type</i>	<i>Max. Base Shear (K)</i>	<i>Soil type</i>	<i>Max. Base Shear (K)</i>	<i>Soil Type</i>	<i>Max. Base Shear (K)</i>
SA	839.295	SA	1733.096	SA	2665.439
SB	1246.752	SB	2563.492	SB	3910.843
SC	1422.983	SC	2899.288	SC	4394.877
SD	2185.789	SD	4402.013	SD	6630.856
SE	1454.722	SE	2991.011	SE	4563.129

CONCLUSIONS

If the site characteristics are found to be consistent with the SD type as prescribed in the BNBC final draft (2015) – that is, shear wave velocity $\bar{V}_s < 180$; SPT value $\bar{N} < 15$ and undrained shear strength \bar{S}_u (kPa) < 70 – then special care needs to be taken to ensure the structural integrity and design against the increased drift.

Alternatively, some soil improvement techniques may be used to improve the characteristics of the soil, so as to reduce the inter-storey drift in structures.

In many construction firms or for official projects of the government, some specific types of buildings are prepared. At the same seismic zone, the same types of properties are used to construct the buildings. But the work here shows that there is a significant change in structural response in different site types even if the proposed buildings are in the same seismic zone.

Therefore, recommendations can be made that, the structures with similar physical properties - that are being built in the same seismic zone - cannot be considered safe without a proper site investigation and taking necessary considerations in the design according to the results of the investigation.

Many owners of the property are not willing to invest much in soil investigation - in some cases even no actual soil investigation is carried out. This study shows the importance of changing that attitude towards site classification through soil investigations. Classifying the site and then taking precautions for the earthquake hazards and the appropriate building response according to the BNBC 2015 is essential.

REFERENCES

- Alam, E. 2015. Earthquake and Tsunami Knowledge, Risk Perception and Preparedness in the SE Bangladesh. *Journal of Geography & Natural Disasters*, 5(3):154-161.
- Bangladesh National Building Code (Final Draft, 2015).
- Bangladesh National Building Code, 1993.
- Clough, RW. 1962. Earthquake Analysis by Response Spectrum Superposition. *Bull. Seism. Soc. Amer.*, 52(3):647-660.
- de Silva, CW. 2005. *Vibration and Shock Handbook*. Florida: Taylor & Francis Group. 3-1p.
- Dørheim, H. 2012. *Methods of Earthquake Analysis*. Master Thesis, Norwegian University of Science and Technology, Norway.
- Islam, BMS; Jameel, M; Ahmad, SI; Salman, FA and Jumaat, MZ. 2011. Engendering Earthquake Response Spectra for Dhaka Region Usable in Dynamic Analysis of Structures. *Scientific Research and Essays*, 6(16): 3519-3530.
- Joshi, RG and Gupta, ID. 1998. On the Relative Performance of Spectrum Superposition Methods Considering Modal Interaction Effects. *Soil Dynamics and Earthquake Engineering*, 17: 357-369.
- Kabir, MR; Sen, D and Islam, MM. 2015. Response of Multi-Storey Regular and Irregular Buildings of Identical Weight Under Static And Dynamic Loading in Context of Bangladesh. *International Journal for Computational Civil and Structural Engineering*, 5(3): 252-260.
- Penzien, J and Watabe, M. 1974. Characteristics of 3-dimensional Earthquake Ground Motions. *Earthquake Engineering & Structural Dynamics*, 3(4): 365-373.
- Wilson, EL; der Kiureghian, A and Bayo, ER. 1981. A Replacement for the SRSS Method in Seismic Analysis. *Earthquake Engineering & Structural Dynamics*, 9(2): 187-192.

PERFORMANCE TEST OF MICRO-CONCRETE REINFORCED WITH GI WIRE

A. Saha*, K. Nazneen & M. Faysal

Department of Civil Engineering, Bangladesh University of Engineering and Technology, Dhaka, Bangladesh.

E-mail: auditi.saha@gmail.com; kashfianazneen@gmail.com; arianfaysal@gmail.com

**Corresponding Author*

ABSTRACT

Micro-concrete is a special type of concrete which has high compressive strength. Micro-concrete, due to its greater strength over conventional concrete, has found an increasing use in construction work. It is mainly used for retrofitting purposes. In micro-concrete the size of coarse aggregate is reduced significantly without compromising the strength of concrete. Due to using higher ratio of cementitious material and smaller size of aggregate, it undergoes volume change during its service life. This is due to the loss of capillary water from the concrete, a phenomenon known as shrinkage. Thus cracks and fissures appear in the concrete structure. In this study we are mainly concerned with finding the right additive for micro-concrete. Currently, the best additive available is GI wire fiber. We have measured the drying shrinkage as well as the compressive strength for three different mix ratios. By using GI wire strength increases up to 19.2% and shrinkage decreases up to 47%. Considering strength and shrinkage, we find that 1:1:1.5 mix ratio with GI wire fiber content of 1.5% by weight is optimum.

Keywords: Micro-concrete, drying shrinkage, strength, GI wire

1. INTRODUCTION

Concrete is the most important material for RCC construction. Many researches have been done to improve the strength of concrete. Micro-concrete and fiber reinforced concrete are the results of such research. However, although there are examples of historical buildings constructed using micro-concrete (e.g. the Roman Coliseum); the properties of micro-concrete are not well understood. We do not find any combined research on these two types of concrete before. In this experiment property of micro-concrete with GI wire additive has been investigated. Fibers from GI wire can provide a viable low cost substitute for steel fibers, especially for Bangladesh since steel fiber for use in FRC is not available in local market and importing proves quite expensive. Main focus of this research is to find suitable fiber for micro-concrete and an optimum mixing ratio.

1.1 Objective

- To observe the variation of compressive strength of concrete with GI wire at different ratios of cement, fine aggregate, coarse aggregate, water and admixture.
- To find a mix ratio that will provide high early compressive and tensile strength.
- To find a mix ratio that will provide high flow ability.
- To observe the shrinkage behavior of MC with GI wire fiber.

1.2 Micro-concrete

Micro-concrete is a ready mix cementitious based composition formulated for use in repairs of areas where concrete is damaged or the area which is restricted in movement, making the placement of conventional concrete difficult (Shannag et al, 2002). Due to using higher ratio of cementitious

material and smaller size of aggregate, it undergoes volume change during its service life. This is due to the loss of capillary water from the concrete, a phenomenon known as shrinkage (Bazant, 1995).

1.3 Advantage of using micro concrete

The main advantage of using this micro-concrete is its capability of using in congested area where the spacing of reinforcement is kept smaller than usual spacing. Due to its flow ability it can be easily pumped to desired depth & areas. Rapid strength gain of micro concrete helps in early reinstatement & removal of shuttering. It makes repaired sections highly durable & compatible to parent. Micro concrete develops high initial and ultimate compressive strength.

1.4 Fibers used in concrete

Fiber reinforced concrete is a concrete mix containing water, cement, aggregate and discontinuous fibers of various shapes and sizes (Bentur and Mindess, 2006). Man-made fibers produced from steel, glass, synthetics, asbestos and natural fibers such as cellulose, sisal. Jute is example of material that is being used in contemporary FRC. According to origin there are four types of fiber-reinforced concrete: steel fiber, glass fiber, synthetic fiber and natural fiber reinforced concrete (Naaman, 2003). For architectural and decorative concrete products and for prevention of early age cracking, synthetic fibers may be used. Steel fibers are used for applications where properties of concrete in hardened stage have to be modified, namely, post crack flexural strength, abrasion resistance, impact resistance and shatter resistance of concrete. In this research we have used steel fibers only.

1.5 Specifications for steel fiber used in FRC

There are no specific specifications for steel fiber used in Micro-concrete. For normal concrete there are some specifications stated in ACI and ASTM. The length of the steel fiber to be used in FRC generally varies between 0.5 in. (12.7 mm) to 2.5 in. (63.5 mm) (Figure 1) and the most common fiber diameters are in the range of 0.017 in. (0.45 mm) to 0.04 in. (1.0 mm) (ASTM A820, 2004). Galvanized Iron (GI) wire is a slender strain like piece of filament of relatively rigid or flexible metal coated with Zinc to protect corrosion. The commonly available GI wires are either mild carbon or high carbon steel wires, which are coated with Zinc which impart the base wire with superior properties i.e. high resistance to moisture and mechanical damage and have a very bright and smooth surface finish.

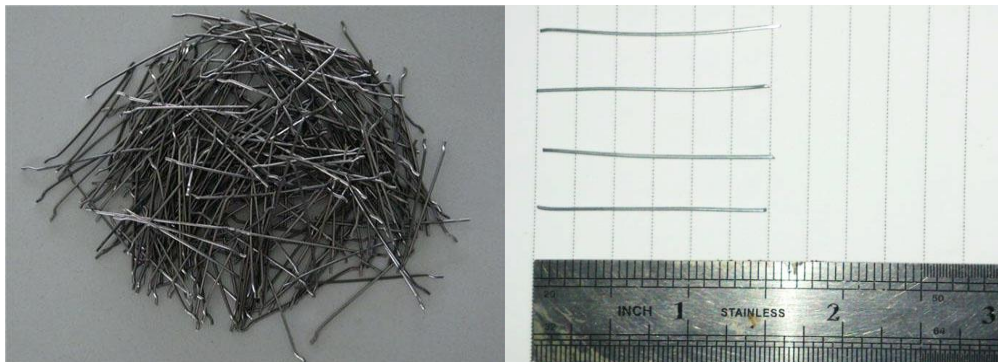


Figure 1.GI wire as steel fiber

1.6 Material used

For this experiment we have used 5mm downgraded crushed stone as coarse aggregate, Sylhet sand as fine aggregate, ordinary Portland cement (OPC) as binding material, 1 inch long GI wire (Figure 1) which is locally available as steel fiber. To improve the flow ability and reduce the water cement ratio of micro concrete an admixture called La adcrete GF has been used.

2. METHODOLOGY

The range of tests carried out was quite multi-dimensional and a carefully thought planning was required to accomplish the work in the stipulated time frame. For making micro concrete 1:1.1:1.4; 1:1:1.5; 1:1.1:1.6 mix ratios by weight and amount of admixture 3.33, 4.55, 6 ml/kg of cement have been used. we have taken optimum fiber content which has been found from research (1.5% GI wire)

for making GI wire reinforced micro concrete (GWRMC). All the tests were performed according to ASTM specification.

2.1 Slump test

The first phase of testing was for the determination of slump (Figure 2) which was done during the mixing and preparation of concrete for casting cylinders. This test method is intended to provide the user with a procedure to determine slump of plastic hydraulic-cement concretes according to ASTM (ASTM C143/143 M, 2010). Slump value is a important parameter for micro-concrete as it is used in congested places and joints.

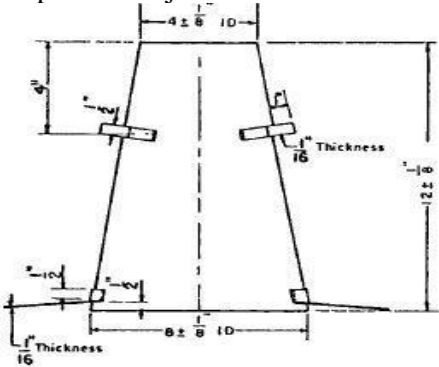


Figure 2.Test setup for slump test

2.2 Compressive Strength and tensile strength test

Compressive strength of cylindrical concrete specimens; for example, molded cylinders and drilled cores; is determined according to ASTM (ASTM C39/ C39M, 2003) (Figure 3). Compressive strength is measured after 28 days curing in lime water. The splitting tensile strength of cylindrical concrete specimens, such as molded cylinders and drilled cores, is determined by ASTM specification (ASTM C496, 2010) (Figure 4). According to the standard, a diametric compressive force is applied along the length of a cylindrical concrete specimen to conduct this test method at a rate that is within a prescribed range until failure occurs.



Figure 3.Test setup for compression test



Figure 4.Test setup for splitting tensile strength

2.3 Test for linear Shrinkage

Linear shrinkage test measure the volume change of concrete due to hydration. Shrinkage test was conducted as per ASTM specification (ASTM C 157, 2014) (Figure 5). This test method covers the determination of the length changes that are produced by causes other than externally applied forces and temperature changes. Linear Shrinkage is measured up to 84 days.

Calculation for shrinkage measurement: $DLx = \frac{CRD - \text{initial CRD}}{G} * 100\%$

Where: DLx = length change of specimen at any age, %,
 CRD = difference between the comparator reading of the specimen and the reference bar at any age,
 G = the gauge length (10 in. [250 mm])



Figure 5. Test set up for linear shrinkage

3. RESULTS AND DISCUSSIONS

3.1 Slump test

Slump gives an indication about the workability of concrete during placing and casting. Figure 6 summarizes the results obtained for the slump test. For mix ratio 1:1:1.5, the slump value for control sample (sample without fiber) is found to be the highest (8in). For mix ratio 1:1.1:1.4, the slump value was obtained to be lowest (5.5 inch). So from this research it can be said that workability decreases with addition of GI wire fiber.

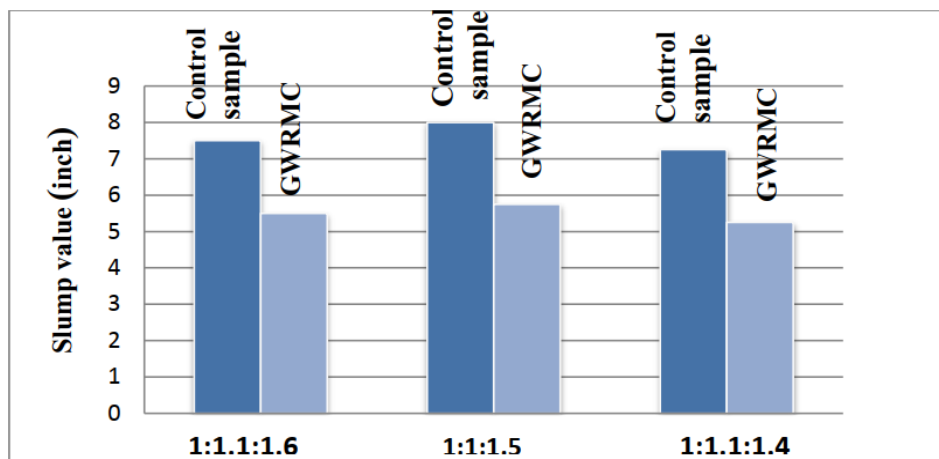


Figure 6. Variation in slump value with different mix ratio

3.2 Compressive strength and tensile strength

Strength is the capacity of a material or structure to withstand loads tending to reduce size. Characteristic compressive strength was determined with cylindrical concrete samples for 28 days of curing according to ASTM specification (ASTM C496, 2010). The results of compressive strength tests and tensile strength of all samples are presented in Table 1 for mix ratios 1:1.1:1.6; 1:1:1.5; 1:1.1:1.4. The maximum compressive strength of GWRMC and control sample is 7574 psi and 6357 psi respectively under ratio 1:1:1.5. From figure 7 we find that, increase in compressive strength is 19.14% for GWRMC with respect to control sample for mixing ratio 1:1:1.5. Tensile strength is about (7-8) % of compressive strength and tensile strength also increases with the addition of fiber. Increase in compressive strength is 13.48% for GWRMC with respect to control sample for mixing ratio 1:1:1.5. But the increment in tensile strength is not satisfactory.

Table 1.Determination of strength for different mix ratio

Trials	Types	Compressive strength(psi)	Tensile strength(psi)
1:1.1:1.6	Control sample	6039.96	442
	GWRMC	6433.66	501
1:1:1.5	Control sample	6356.98	460
	GWRMC	7574.01	522
1:1.1:1.4	Control sample	6152.38	455
	GWRMC	7086.57	512

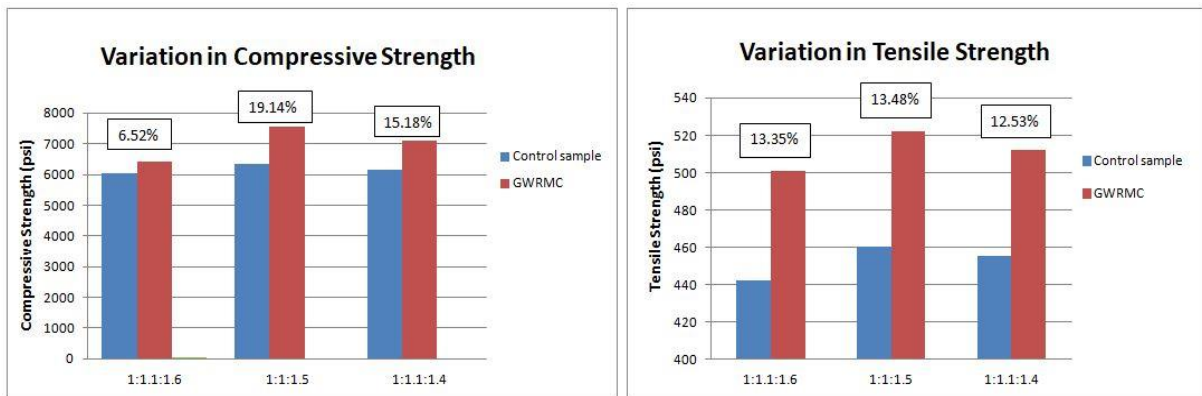


Figure 7.Variation in compressive and tensile strength due to adding fiber

3.3 Linear shrinkage

Knowledge of the shrinkage characteristics of micro concrete is a necessary parameter as it undergoes larger percentage of shrinkage comparing to normal concrete. Figure 8 shows the variation in drying shrinkage for control sample and GWRMC under different mix ratios after 28 days, 32 days, 35 days, 42 days, 56 days and 84 days respectively (ASTM C157, 2014). From this figure an initial swelling effect can be observed for all cases. This is due to the fact that specimens were kept submerged under water for the first 28 days and as a result no evaporation of mixing water occurred. It is also clear from the figures that after the initial swelling effect, the shrinkage of control sample increased with time. The shrinkage of GWRMC was less than that of control sample. Figure 9 shows that, for ratios 1:1.1:1.6 and 1:1:1.5 shrinkage is almost same around 45%, the decrease in shrinkage percentages being at 15.63% for GWRMC for ratio 1:1:1.4 with respect to control sample.

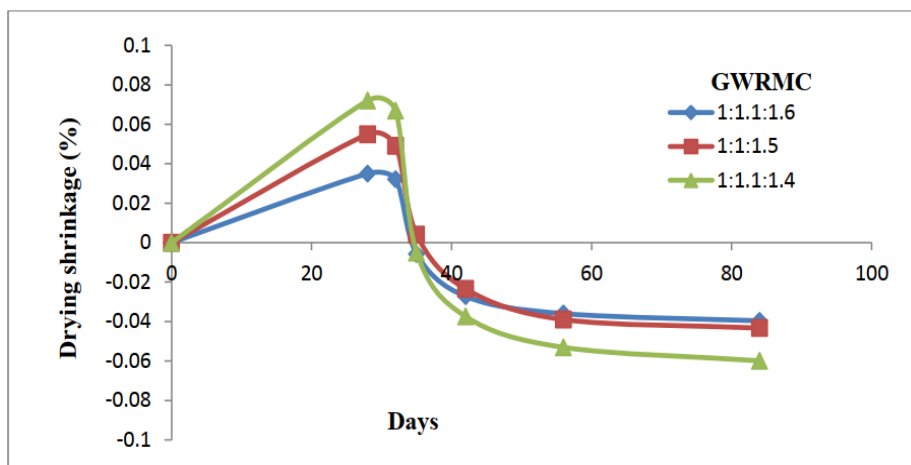


Figure 8.Variation in shrinkage due to adding fibers

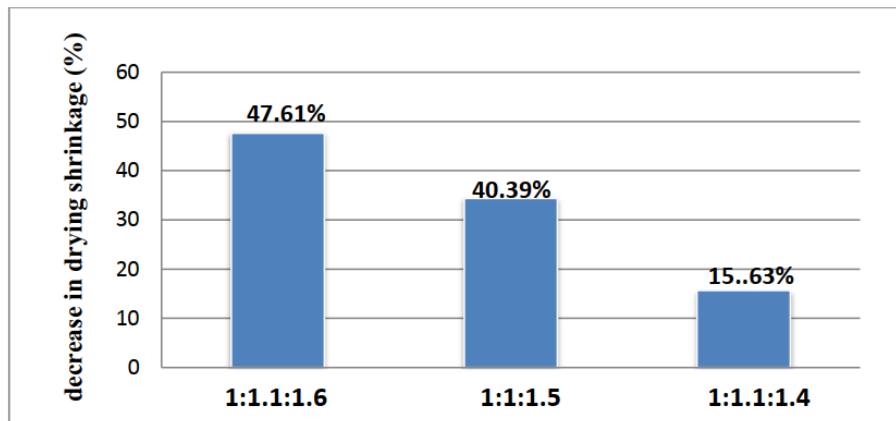


Figure 9. Decrease in drying shrinkage due to using fiber with respect to control sample

4. CONCLUSIONS

This research is an attempt for incorporating locally available GI wire fiber as a substitute for commercially available polyester fiber in Micro-concrete in Bangladesh. From the research we can conclude that-

- By analysis of all the experimental values mix ratio of 1:1:1.5 is considered as optimum mixing ratio with 1.5% GI wire.
- GI wire reduces shrinkage of micro concrete up to 45% and increases compressive strength up to 20%.
- However, the behavior and performance of such GI wire reinforced Micro-concrete (GWRMC) and other fiber are yet to be explored. Therefore, this research made an effort to discover several basic characteristics of GWRMC chiefly related to strength and durability.

ACKNOWLEDGEMENTS

The authors express their sincere gratitude to their supervisor Dr. Raquib Ahsan, Professor of the Department of Civil Engineering in BUET. Without his proper guidance this research work would have never progressed.

REFERENCES

- ASTM 307-03. 2012. *Standard Test Method for Tensile Strength of Chemical-Resistant Mortar, Grouts, and Monolithic Surfacing*. West Conshohocken, Pennsylvania: ASTM International.
- ASTM A820/A820M. 2004. *Standard Specifications for Steel Fibers for Fiber Reinforced Concrete*. West Conshohocken, Pennsylvania: ASTM International.
- ASTM C 157/C 157 M-08. 2014. *Standard test method for length change of hardened hydraulic-cement mortar and concrete*. West Conshohocken, Pennsylvania: ASTM International.
- ASTM C143/143 M. 2010. *Standard Test Method for Slump of Hydraulic-Cement Concrete*. West Conshohocken, Pennsylvania: ASTM International.
- ASTM C39/C39M. 2003. *Standard Test Method for compressive Strength of Cylindrical Concrete Specimens*. West Conshohocken, Pennsylvania: ASTM International.
- Bazant Z. P. 1995. Creep and Shrinkage Prediction Model for Analysis and Design of Concrete Structures Model B3. *Materials and Structures*, 28(6).
- Bentur A. and Mindess S. 2006. *Fibre Reinforced Cementitious composites*. New York: CRC Press, Taylor & Francis.
- Naaman A. E. 2003. Engineered steel fibers with optimal properties for reinforcement of cement composites. *Journal of advanced concrete technology*, 1(3): 241-252.
- Shannag M. J.; Barakat S. and Abdul-Kareem M. 2002. Cyclic Behaviour of HPFRC- Repaired Reinforced Concrete Interior Beam-column Joints. *Materials and Structures*, 35(6):348-356.

SEISMIC VULNERABILITY ASSESSMENT OF EXISTING BUILDINGS IN DINAJPUR CITY

M. I. Mostazid, R. Anjum*, & F. T. Jahara

Department of Civil Engineering, Hajee Mohammad Danesh Science & Technology University, Dinajpur, Bangladesh.

E-mail: mimostazid@hstu.ac.bd ; ramisa170297@gmail.com; nimmijahan4990@gmail.com

**Corresponding Author*

ABSTRACT

The suddenness of earthquakes constitutes one of the greatest hazards on earth. This paper reveals the seismic vulnerability of 10 No. ward of Dinajpur City with a goal of identifying whether the buildings can withstand the seismic force effect to avoid serious risk and to mitigate the corresponding earthquake impacts of earthquakes. The vulnerability assessment was conducted by adopting Modern Turkish method. Level I and Level II survey were performed by considering several parameters like storey, pounding effect, apparent quality, redundancy, strength index, etc. A total number of 340 buildings have been surveyed in the study area. Among these buildings 283 are found safe, 48 are moderate and nine numbers of buildings are unsafe. The main target of this study is to identify the damage category and reducing risk of Dinajpur City in a potential earthquake.

Keywords: Building; Dinajpur City; Seismic Vulnerability; Turkish Method.

INTRODUCTION

Due to geographic location, Bangladesh is in high seismic risk. A minor tremor can affect the major parts of the country. Bangladeshi people have significant experience of the earthquake and other natural disasters (Alam et al., 2014). This country is surrounded mostly by India, a small part with Myanmar and the south portion by the Bay of Bengal. In the west, the country is located near the boundary of the Indian plate and in the East with the Eurasian plate and North (figure 1). At present, the Indian plate is moving at a speed of approximately 6 cm per year in the northeast direction (Bilham, 2004). Furthermore, the Bogra Fault System (BGF), the Jamuna Fault (JF), the Madhupur Fault (MF) and the Sylhet Fault (SF) are lying inside Bangladesh (Alam, 2016). A right-lateral fault extending from Kakarbitta in Nepal to Saidpur in the northwest of Bangladesh (Nakata et Al., 2002). As reported by, CORONA photo interpretation, the low scarp is developed in the southwest of Saidpur Town (Figure 2). Any sudden release of energy throughout these fault systems may lead to a massive earthquake loss. Multistoried buildings are increasingly popular nowadays. In multistorey buildings for providing commercial or parking space, the ground floor is kept open which leads to form a soft storey. A building is considered to be having a soft storey if it's one floor is 70 percent less stiff than its upper floor (UBC-1997, ASCE-2002). A study by Fintel and Khan (1969) acknowledged this concept. Soft storey arises due to the presence of large open space either due to the large unobstructed commercial area or by windows, doors. Hejazi et al, (2011) reported that soft storey allows lower storey column to yield during seismic activity which reduces acceleration in a building and generates an energy-dissipation mechanism. The government of Bangladesh has developed earthquake-resistant building codes, with a few exceptions; these codes are rarely used for new building design (M.R. Sadat et al., 2010). That's why, the number of people living or working in unsafe structures is increasing (Paul, 2010).



Fig. 1: Plate Boundary between the Indian and Eurasian Plate (Dr. S.H. Akhter).

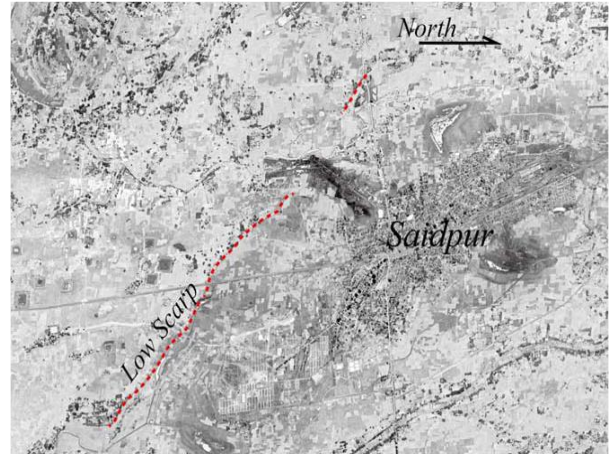


Fig. 2: Active fault in Saidpur.

METHODOLOGY

Dinajpur is the northern district of Bangladesh. It is surrounded by Thakurgaon and Panchagarh districts to the north, Joypurhat and Gaibandha districts to the south, Rangpur and Nilphamary districts to the east, West Bengal (Indian State) to the west (BBS, 2011). Although in the basic seismic zoning map of Bangladesh Dinajpur has been shown in the medium risk zone, earthquake risk of the Dinajpur Town is growing with every passing moment because of the unabated growth of human settlement and, administrative and other economic activities (CDMP, 2014). This paper aimed at identifying the riskiest structures, make a database with proper information about vulnerable buildings and emphasize the importance of seismic safety.

Study Area

The study area in Baluadanga ward no.10 of Dinajpur Municipality Area is situated near the banks of Kanchan River. The population of the ward is 17,686 (source: Dinajpur Municipality-general information 2016). A large amount of building in this area is old some are historic. Even a moderate earthquake can cause severe damage to these buildings and can lead to the loss of valuable lives (Ahmed et al. 2012). The location map of Dinajpur Town and the study area is shown in fig. 3 and 4. This study has been carried out to reveal an inventory of vulnerable structures so that highly vulnerable structures can be retrofitted on the priority basis and to develop an earthquake preparation program.



Fig. 3: Dinajpur Sadar Upazila map

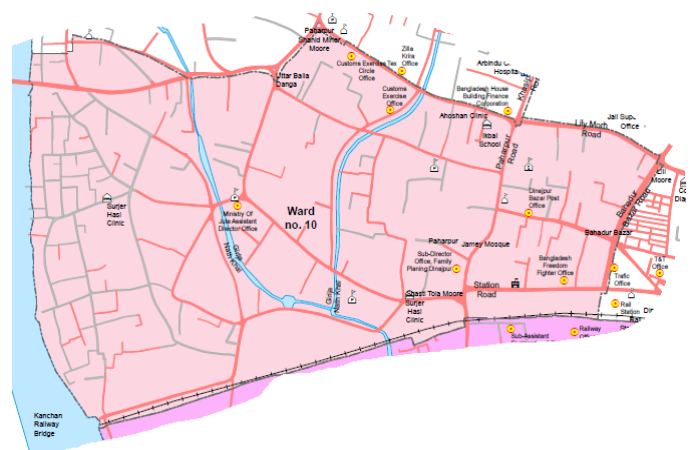


Fig. 4: Study area ward no. 10

Seismic Vulnerability Assessment

The seismic vulnerability is the inability of buildings to withstand the damaging effects of seismic forces. There are several techniques regarding the assessment of the seismic vulnerability of buildings. Some countries have their own seismic vulnerability assessment procedures considering local seismicity, local soil conditions, local building types, construction materials and quality practices, etc. In this study, depending on the complexity of seismic vulnerability evaluation methods can be classified into two main groups. Walk down Evaluation, is the first and the simplest level. The procedures in FEMA 154 (1988), FEMA 310 (1998) Tier 1 and the procedure developed by Sucuoglu and Yazgan (2003) are examples of the walk down survey procedures. In preliminary assessment methodologies (PAM), the simplified analysis of the building under investigation is performed based on a variety of methods. Data on the dimensions of the structural and non-structural elements in the most critical storey are required for these analysis. However, this paper only focuses on the Level-1 survey.

Walk Down Evaluation

The procedure developed by Sucuoglu and Yazgan (2003) has been used for level-I assessment. The trained observers collect data through walk-down visits. Simple structural and geotechnical parameters need for the street survey procedure which can be observed easily from the sidewalk. Following parameters are selected for representing building vulnerability:

1. The number of stories above ground
2. Presence of a soft story
3. Presence of heavy overhangs, such as balconies with concrete parapets
4. Apparent building quality
5. Presence of short columns
6. Pounding between adjacent buildings
7. Local soil conditions
8. Topographic effects

All of the above parameters are found to have a negative impact on a variant scale on the building under earthquake excitations.

Building Seismic Performance

Seismic performance is the identification of structure's ability to keep up its due functions, like safety and serviceability, at and after a particular earthquake. Once the vulnerability parameters of a building are obtained from the walk down surveys and its location is determined, the seismic performance score PS can be calculated by using Eq. (1). A performance scoring system is developed to rank the vulnerability assessment methodologies according to three different criteria namely, general description, physical vulnerable parameters and description of output (Hill and Rossetto, 2008). The base scores (BS), the vulnerability scores (VS) and the vulnerability score multiply (VSM) to be used in Eq. (1) are defined in Tables 1 and 2, respectively. The performance score (PS) can be calculated by the following general equation-

$$PS = (BS) - \Sigma (VSM) \times (VS) \quad (1)$$

Table 1: Vulnerability Parameters (VSM) (Yakut et al. 2003)

Soft story	Does not exist=0	Exists=1
Heavy overhangs	Does not exist=0	Exists=1
Apparent quality	Good = 0	Moderate = 1; Poor =2
Short columns	Does not exist=0	Exists=1
Pounding effect	Does not exist=0	Exists=1
Topographic effects	Does not exist=0	Exists=1

Several studies have been conducted in Bangladesh for vulnerability assessment by using the procedure developed by Sucuoglu and Yazgan (2003). The Base Scores (BS) and Vulnerability Scores (VS) used in some recent study in India also analogous with the procedure manifested by Sucuoglu and Yazgan though Indian method of evaluation consists of some other factors like frame action, water tank location in roof, basement (Jain et al., 2004, Srikanth et al., 2010). Based on their number of stories and the seismic hazard level at the site, buildings are assigned different base scores as shown in Table 2.

Table 2: Base Scores and Vulnerability Scores for Concrete Buildings (Yakut et al. 2003)

Number of Stories	Base Scores(BS)			Vulnerability Scores(VS)					
	Zone I (60<PGV<80)	Zone II (40<PGV<60)	Zone III (20<PGV<40)	Soft Story	Heavy Overhang	Apparent Quality	Short Column	Pounding Effects	Topography Effects
1or 2	100	130	150	0	-5	-5	-5	0	0
3	90	120	140	-15	-10	-10	-5	-2	0
4	75	100	120	-20	-10	-10	-5	-3	-2
5	65	85	100	-25	-15	-15	-5	-3	-2
6or 7	60	80	90	-30	-15	-15	-5	-3	-2

Buildings are classified into three risk groups in this study based on the calculated Seismic performance score (PS). Buildings are considered unsafe for $PS \leq 30$. The moderate and safe groups are categorized by the performance score range $31 < PS \leq 60$ and $61 < PS \leq 100$ respectively.

RESULTS AND DISCUSSIONS

The number of stories is the prime dominating damage instigating parameter which is observed after the recent earthquakes in Turkey. Reinforced concrete buildings are in the riskiest state due to storey numbers. The study defined this damage inducing parameter as the total number of particular floors over the ground level where the vertical cross-sectional areas and the moments of inertia are performed. The initial study reveals that various construction practices are carried out in Dinajpur, however, the predominant structures were made of RCC. Almost all structures in the study zone are residential. Some buildings are typical masonry construction types while large of them are made of moment resisting frame. A total of 340 RC buildings was surveyed in case of Level I survey. A significant number of these buildings are two-storied, 180 numbers to be exact. Of the 94 buildings are three-storied, 44 buildings are four-storied, 13 buildings are five storied and only 9 buildings are six storied [Fig. 5].

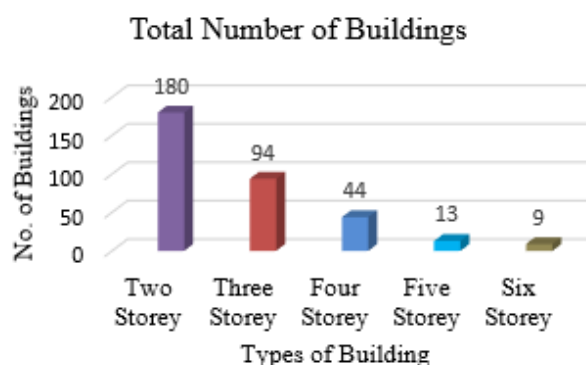


Figure 5 Total Number of Different Storied Buildings.

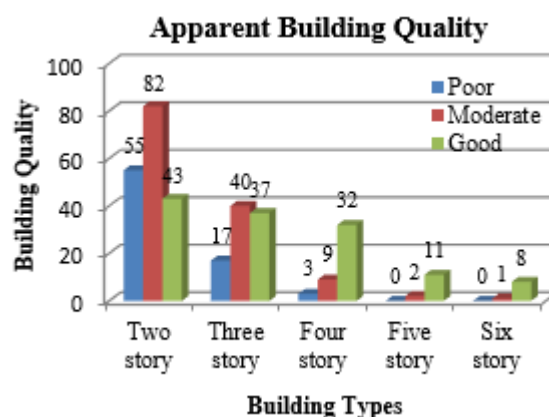


Figure 6 Apparent Building Quality

The apparent quality of buildings depends on material, workmanship quality and its maintenance. A well-trained surveyor is required to classify a building's apparent quality as good, moderate or poor. A

recent study of Turkey showed the existence of a close relationship between the damage categories due to an earthquake with the apparent quality of buildings. Poor apparent quality of buildings exhibits lower material strengths. Apparent building quality is classified into three categories poor, moderate and unsafe. For two storey buildings, 55 buildings are found poor, 82 numbers are moderate and 43 buildings are found in good condition. 18% buildings of three storey categories are found poor, 42.5% moderate and 39.5% buildings are in good condition. Only 3 buildings out of 44 buildings are in poor condition for four storey category, 9 buildings are in moderate and 32 buildings are surveyed in good quality. Five and six storey buildings have zero structures in poor condition, and most of them are in good condition [Fig. 6]. Overall survey parameters revealed that among 341 buildings 103 buildings have heavy overhangs, 157 buildings have short column problem, 100 buildings have soft story problem, 112 buildings have pounding possibilities and in terms of apparent quality 75 buildings are poor, 131 buildings are good and 134 buildings are average as shown in [Fig. 7].

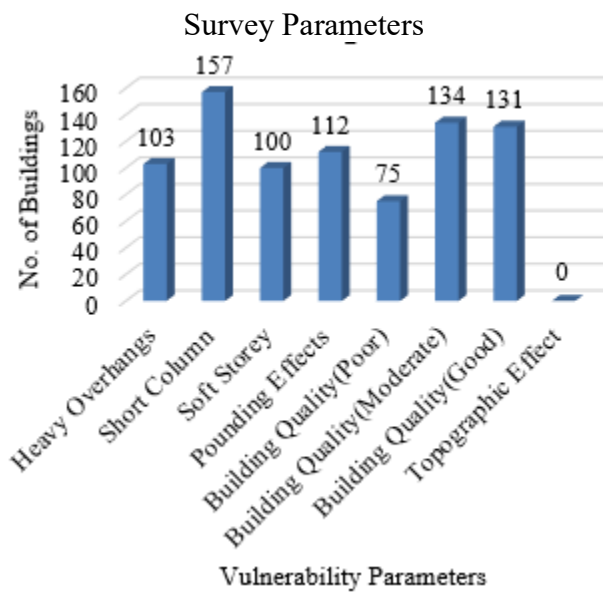


Fig. 7: Vulnerability Parameters after Walk down Evaluation.

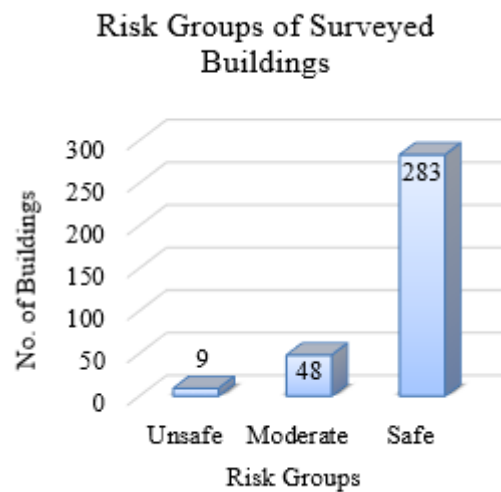


Fig. 8: Risk Groups after Level I Survey.

CONCLUSIONS

The focus of this study is to disclose the present scenario of Dinajpur City for an oncoming earthquake by seismic vulnerability assessment by the walk down evaluation. Numerous buildings (about 134 numbers) are subjected to the problem-related to pounding effect. Pounding is experienced up to separation gap between structures is six inches (Noman et al., 2016). If one of the soft buildings goes under liquefaction fails (Ahmed et al., 2013) it will affect the others easily because all the building structures are subjected to pounding effect. Among 340 buildings 283 (83%) buildings are found to be safe, 48 (14%) buildings are found to be moderate, and nine (2.6%) buildings are found to be unsafe in terms of their performance score (PS) value after level I survey. Based on this study the recommendations are marked below:

1. Engineers, architects, and the property owner should be aware of the earthquake and work simultaneously to minimize this threat.
2. The identified vulnerable buildings must be taken under retrofit as early as possible on the priority basis.

ACKNOWLEDGMENTS

The first author is obliged to the Department of Civil Engineering, HSTU for giving the opportunity to do this work. The first author is also grateful to Ramisa Anjum and Fatem-Tuz-Jahara, undergraduate students, for their assistance in the survey for the vulnerability assessment.

REFERENCES

Book

FEMA 310, 1988, Hand book of Seismic Evaluation of Buildings-A prestandard, *Federal Emergency Management Agency*, Washington DC, USA

Morino, M., 2009, Active Fault Mapping and Modeling in Bangladesh.

CDMP (2014), Scenario based Earthquake Contingency Plan of Dinajpur Pourashava Area, Comprehensive Disaster Management Programme, Dhaka, 2014.

Journal Article

Ahmed, M., Khaleduzzaman, K. M., Siddique, N.A., and Islam, S., 2012, Earthquake Vulnerability Assessment of Schools and Colleges of Sylhet, a North-eastern City of Bangladesh, *SUST Journal of Science and Technology*, Vol. 19(5):27-34

Ahmed Mohammad Mohinuddin, Md. Jahangir Alam, IngUwe.EDorka. Seismic Vulnerability Assessment of Concrete Pile Foundation. The 3rd International Conference on Engineering and Applied Sciences (ICEAS), 7-11-2013 to 9-11-2013, Osaka, Japan. pp. 1178-1184, 2013

Alam E, Howes DD (2014). An analysis of the AD1762 earthquake and tsunami in SE Bangladesh. *Natural Hazards* 70: 903-933.

Alam E. (2016). Earthquake and Tsunami Knowledge, Risk Perception and Preparedness in the SE Bangladesh. *Geogr Nat Disast* 2016, 6:1.

Bilham, R., 2004, Earthquakes in India and the Himalaya: tectonics, geodesy and history, *Annals of Geophysics*, Vol. 47 (2/3): 839-858.

F. Hejazi S. Jilani, J. Noorzaei, C. Y. Chieng, M. S. Jaafar, A. A. Abang Ali, 2011. Effect of Soft Story on Structural Response of High Rise Buildings, *Materials Science and Engineering* 17 (2011) 012034. doi:10.1088/1757-899X/17/1/012034

Hill, M., and Rossetto, R., 2008. Comparison of building damage scales and damage descriptions for use in earthquake loss modelling in Europe". *Bulletin of Earthquake Engineering*, 6(2): 335-365

M. Fintel and F. Khan 1969, "Shock-absorbing soft story concept for multistory earthquake structures ". Proceeding.

Nakata, T. and Y. Kumahara, 2002, Active faulting across the Himalaya and its significance in the collision tectonics. *Active Fault Research*, 20, 7-16.

Noman M., Alam B., Fahad M., Shahzada K., and Kamal M., 2016, Effects of pounding on adjacent buildings of varying heights during earthquake in Pakistan, *Cogent Engineering*, (2016), 3: 1225878.

Ozcebe, G., Yucemen, M. S., Aydogan, V., and A. Yakut, 2003, Preliminary Seismic Vulnerability Sucuoglu, H., and U. Yazgan, 2003, Simple Survey Procedures for Seismic Risk Assessment in Urban Building Stocks, *Seismic Assessment and Rehabilitation of Existing Buildings*, NATO Science Series IV/29, pp. 97-118.

Paul R. H. 2010. Urban earthquake hazard: perceived seismic risk and preparedness in Dhaka City, Bangladesh. *Disasters*. 34(2): 337-359.

Srikanth T., Kumar R. P., Singh, A. P., Rastogi, B. and Kumar, S., "Earthquake Vulnerability Assessment of Existing Buildings in Gandhidham and Adipur Cities Kachchh, Gujarat (India)", *European Journal of Scientific Research* , Vol.41 No.3, pp. 336-353 (<http://www.eurojournals.com/ejsr.html>), 2010.

Sudhir K Jain, Keya Mitra, Praseeda KI, "A Proposed Rapid Visual Screening Procedure for Seismic Evaluation of Buildings in India", January, 2004.

Wald, D. J, Quitariano, V., Heaton, T. H., Kanamori, H., Scrivner, C. W., and Worden, C. B., 1999, Trinet Shake Maps: Rapid Generation of Peak Ground Motion and Intensity Maps for Earthquakes in Southern California, *Earthquake Spectra*, 15(3): 537-555.

Yakut, A., Aydogan, V., Ozcebe, G., and M. S. Yucemen, 2003, Preliminary Seismic Vulnerability Assessment of Existing Reinforced Concrete Buildings in Turkey -Part II: Inclusion of Site Characteristics, *Seismic Assessment and Rehabilitation of Existing Buildings*, NATO Science Series IV/29, pp. 43-58.

STRENGTHENING OF REINFORCED CONCRETE BEAMS UTILIZING FERROCEMENT: ROLE OF EXTERNAL LOADING POSITIONS

M. J. Miah^{1*}, M. S. Miah^{1,2} and W. B. Alam¹

¹*Department of Civil Engineering, University of Asia Pacific, Dhaka-1215, Bangladesh.*

E-mail: jihad.miah@uap-bd.edu

²*Faculty of Civil Engineering, Technische Universität Dresden-TU Dresden, 01187 Dresden, Germany.*

E-mail: mshamim@uap-bd.edu; mohammad_shamim.miah@tu-dresden.de

**Corresponding Author*

ABSTRACT

The performances of retrofitted beam with ferrocement in comparison to un-retrofitted one is investigated herein by considering various loading positions. Over the last few decades, numerous research works have been focused on the level of stress, loading conditions, section size and shape, reinforcements detail, age and properties of concrete, confinement and so on. The scanty results are available in the literature on the effect of loading positions such as unsymmetrical loading distance on the deflection behavior of concrete beams. To this end, two simply supported reinforced un-retrofitted and retrofitted concrete beams having width 230 mm, height 230 mm, and length 2135 mm were subjected to four points incremental static loads on two different positions. Additionally, in order to a deeper understanding of the experimental results, a three-dimensional nonlinear finite element model was developed via the use of ABAQUS and SAP2000 v19.2. The experimental results have shown that the unsymmetrical loading distance decreases the load carrying capacity and deflection than symmetrical loading distance one. Ferrocement beams reinforced by steel wire mesh exhibited superior ultimate load carrying capacity and deflection compared to without ferrocement beams. It is noticed that the numerical results are in good agreement with the experimentally measured data.

Keywords: Reinforced concrete, Load-displacement relation; Retrofitting; Ferrocement; ABAQUS.

INTRODUCTION

The deflection characteristics of RC beams depends on many variables such as loads and their acting positions, supporting conditions, placement of main and shear reinforcements. Among the aforementioned issues, the position of the acting loads are immensely critical as it generates significant amount of shear forces and bending moments. In particular, when the loads are placed in symmetrical and un-symmetrical distance from the supports. For instance, the un-symmetrical loading from the supports may occur due to heavy machinery in industries, production factories (e.g. garment), storehouse and library building and so on. In such case, not only the vertical loads, earthquakes or any vibration from the machineries may intensify the effect of concentrated loads at different positions and may lead to partial-failure or fully-collapse of the structure, as beam works as a medium of transferring loads to column. Additionally, the increase in multi-purpose use of structures in recent years has created an interest in strengthening via retrofitting any existing structural (those are partially damaged) members to amplify its compatibility of carrying extra loads.

It is mentioned earlier that the strengthening of RC beams has taken serious attention, as structures are now used for multipurpose e.g. commercial cum residential/industrial. To minimize overall project cost, different retrofitting methods are used, for instance, the retrofitting with ferrocement is gaining more popularity for its cost effectiveness and inexpensiveness. A study by Al-Sulaimani et al., 1991 retrofitting with ferrocement wire mesh in web and flange of the beam and the improved shear resistance capacity by reducing tension cracks are reported. Also, several researches show that ferrocement channel beam's shear strength increases due to several reasons, such as the decrease of span to depth ratio and the amount of wire mesh or mortar strength increases (Ahmad et al. 1995; Desayi et al., 1992). Additionally, retrofitting by using Carbon fiber reinforced polymer (CFRP) laminates for shear and flexure, which shows an increase in its stiffness, maximum load and decrease in cracks width when compares with their corresponding control beam (Obaidat et al. 2011). It was also reported by many that the use of glass fiber reinforced polymer (GFRP) to strengthen RC beams resulted in better performance in the strength and load carrying capacity of the beams. It was also observed that a U-wrapping carried a greater load than the beams with GFRP stripes on sides alone (Sundarraja and Rajamohan, 2009). In existing literature, there are many alternatives are available for retrofitting such as Kevlar Fiber-epoxy Reinforced Plastic (KFRP) and steel plates to enhance the shear performance of partially damaged beams (Alam et al., 2016; Alam et al., 2014). Typically, the retrofitting materials e.g. CFRP, GFRP, KFRP are expensive to use due to the unavailability in the local market and the associated implementation technology might be expensive due to inexperienced labor and epoxy. Therefore, herein the locally available ferrocement technology is employed by considering local construction deficiencies such as proper mixed design. To do this end, the performance of both un-retrofitted and retrofitted beams with ferrocement subjected to symmetrical and un-symmetrical loading distance discussed herein. Finally, the experimentally observed behavior was compared with numerical results and quite good agreement was reported.

The rest of the paper contains the experimental investigation, finite element analysis via different software e.g. SAP2000, ABAQUS, results and discussions, and finally the paper was ended with conclusion and remarks.

EXPERIMENTAL INVESTIGATION

Preparation of the Beam Specimens

Two beams (2135 mm x 230 mm x 230 mm) were cast to evaluate the flexural performances under two different loading positions. The beams were made with first class burnt clay brick chips and natural river sand (locally called Sylhet sand). The volumetric mix ratio of 1:2:4 and water to cement ratio (by weight) of 0.45 were used for the mix. The average compressive strength of concretes are 13.0 MPa for Reference case beam and 13.3 MPa for Shear case beam, respectively. The beams were provided with 2 Ø 16 mm mild steel bars as tension reinforcements and 2 Ø 16 mm bars were used for anchorage. 10 mm bars @ 127 mm c/c (center to center) was used for shear reinforcements. The clear cover from the reinforcements in all the beams was 40 mm and the flexural tests were carried out after 28 days of curing. The un-retrofitted beams were loaded up to the initiation of major cracks.

In order to perform the retrofitting, the damaged concrete layer and loos materials from all sides of the beams were removed by using chipping hammers. Square welded wire steel mesh (an opening of 4 mm orthogonally) available in local markets was used as the reinforcing mesh. The beams were wrapped with a single layer of steel wire mesh around the beam surface. The joints of the wire mesh were secured by stitch all along length of the beam using thin steel wires that are commonly used in tying reinforcing bars. The sand to cement ratio by weight of 2 and water to cement ratio of 0.45 were used for the mortar mix of ferrocement. The mortar mix was poured around the beam specimens by hand plastering. Then the top surface of the specimens were finished and covered with double layer wet burlap in the laboratory temperature. The flexural tests were performed after 28 days of curing until collapse occurred. For the visualization purpose Figure 1 is given in the next section.

Instrumentation and test setup

Two beams were constructed and subjected to two different loading positions in order to observe the deflection behavior and the failure pattern of the beams due to the change of loading positions. The beams were loaded in four-point incremental static loads each on different positions, which were at $L/3$ interval (Reference case) and both close to the support (Shear case). More specifically, the Reference case of both un-retrofitted and with retrofitted was subjected at a uniformly spaced loads (660 mm). For the shear case, one load was placed 305 mm from the support and the other one at 530 mm from the first one. During the flexural tests, the deflections were monitored via three dial gauges positioned at mid-span of the beam (Gauge 2), two gauges at 305 mm of left and right sides of the Gauge 1 and Gauge 3, respectively. For the un-retrofitted beam tests, the beams were first loaded until major cracks (e.g. flexural and diagonal) appeared. While for the retrofitted beam tests, the load was increased until complete failure of the specimen was reached.

FINITE ELEMENT ANALYSIS USING SAP2000 AND ABAQUS

The FEA simulations were performed in SAP2000 v19.2 and ABAQUS/Standard 2017. To model the beams in SAP2000, the plasticity values acquired from the test samples were used in material non-linearity data. To model the beams in ABAQUS, a concrete damaged plasticity model was considered. Fig. 1 shows the un-retrofitted and retrofitted cross-section in ABAQUS and SAP2000. Value of the modulus of elasticity was also taken from the test samples and the poisson's ratio for the concrete and reinforcements was 0.2 and 0.3 respectively. For retrofitting, an additional layer of ferrocement with an embedded wire mesh was modeled. The loads were carefully positioned and the load-deflection values from both models were collected and compared with their corresponding beams experimental results.

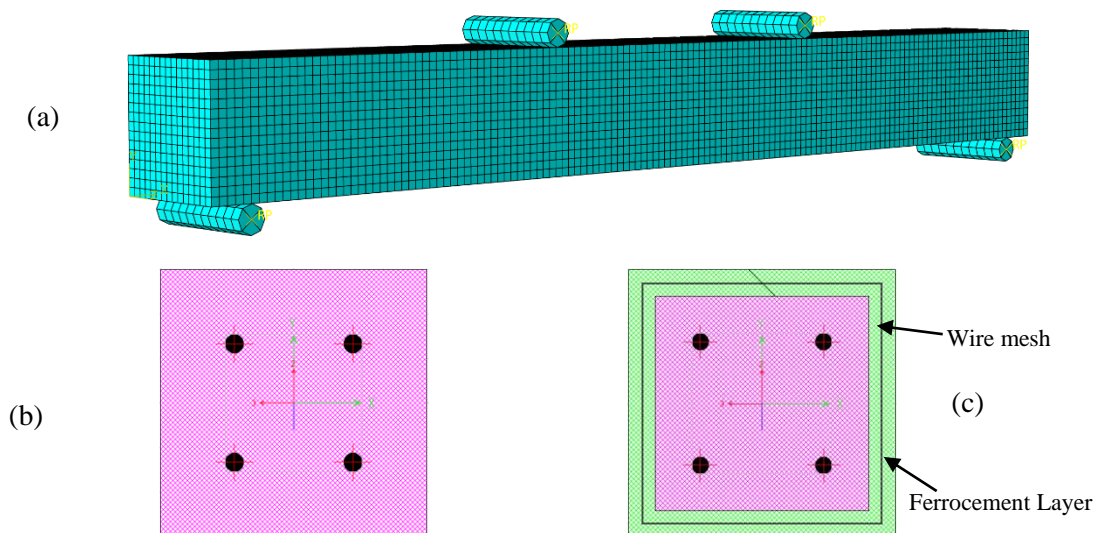


Fig. 1: A typical model of beam generated via FEM software: (a) the 3D view of beam, (b) un-retrofitted beam section, (c) retrofitted beam section.

RESULTS AND DISCUSSIONS

Load-deflection behavior

The load-deflection curves from three gauges of un-retrofitted and retrofitted beams are represented in Fig. 2. For the un-retrofitted beams, the Reference case (RC) experience significantly higher deflection than the Shear case (SC). For example, the maximum load and deflection are, respectively, 82.3 kN and 12.9 mm for RC and 52.4 kN and 4.9 mm for SC. This behavior could be due to the development of high concentration of shear stress in the SC beam than RC beam. Further, a thick crack was observed for Shear case close to the loading point at the end of the beam, while no similar cracking or damage of this type was observed for RC. From this observation, it implies that the beams with un-symmetrical loading distance (i.e. SC) decrease the load carrying capacity and deflection due to higher cracking than the symmetrical one which could be worst scenario and then can collapse of the structure which could increase the risk of human life.

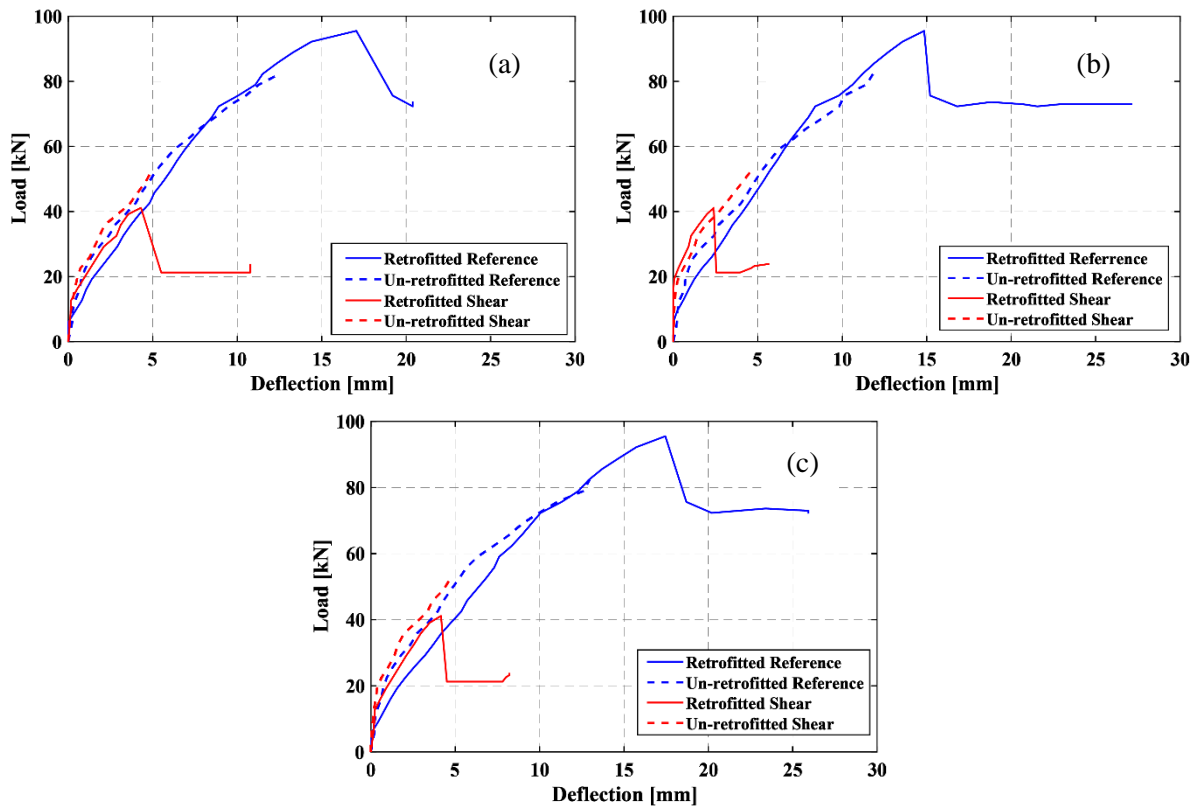


Fig. 2: Comparison of load-deflection behavior of retrofitted and un-retrofitted beams: at 305 mm left, Gauge 1 (a) and right, Gauge 3 (b) from the midpoint, (c) at midpoint (Gauge 2) of the beam.

As concern the retrofitted tests, Reference case exhibited superior load-deflection behavior compared to without ferrocement beams. This could be attributed to the fact that the steel wire mesh of the ferrocement prevented the propagation of micro-cracks and cracks and provided additional tensile strength in the tension face (i.e. bottom surface) of the specimens. While in the Shear case, the beam was damaged at the end of the beam close to the support due to higher concentration of shear stress. It was also observed that the retrofitted beam of Reference case has nearly 18% greater load carrying capacity than their un-retrofitted beams, while there was a decrease of about 20% for the Shear case due to early collapse of the beam. It can be seen that the deflections of the retrofitted beams are significantly higher than the un-retrofitted beams. For example, the maximum deflection measured at midpoint (Gauge 2) of the retrofitted and un-retrofitted beams are 25.92 mm and 12.95 mm for Reference case. Similar behavior was observed for the deflection measured by Gauge 1 and Gauge 2. This is in agreement with one of our test results on flat plate systems reported by Miah et al. (2018).

Failure pattern

Fig. 3 illustrates the cracking patterns of retrofitted beams at failure.

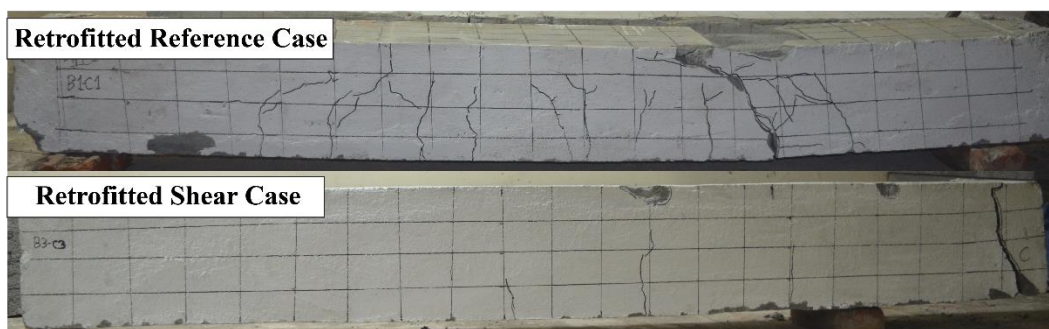


Fig. 3: Failure pattern of the retrofitted beams

In the Reference case, a well distribution of cracks was observed all along the whole length of the tension zone of the beam and then failed due to its bending and shear effect. While the Shear case, the beam was failed at the end of the beam just beneath of the load as it was failed in the un-retrofitted test condition due to its higher shear stress. However, the number of cracks observed in the Shear case was much lower than RC. Ductile mode of failure was observed for the Reference case, while a brittle failure was seen for the Shear case. The ductile failure mode of the beam can be explained in three steps: (i) Once the load is introduced on the beams, the load-deflection curve is quite linear, meaning that no crack in the tension zone and the specimen maintains its full flexural stiffness and rigidity. As the load increased gradually, the deflection of the beam increased. (ii) As load continues further, beam reaches in plastic stage, meaning that the initiation of cracks which reduce the slope of the load-deflection curve (see Fig. 2), resulting, lower bending stiffness. Therefore, a rapid propagation of cracks occurred from the tension side towards the compression side of the beam. (iii) In the final stage, as the load increase, the deflection increase, but in a significantly higher rate due to the opening of the cracks in the tension zone which allow beam move towards the loading direction. In that case, probably the steel wire mesh failed first by yielding of the steel wires, then deboned the mesh from the concrete surface, and then finally fails the concrete beam with significant higher deflection.

Predicted load-deflection behavior

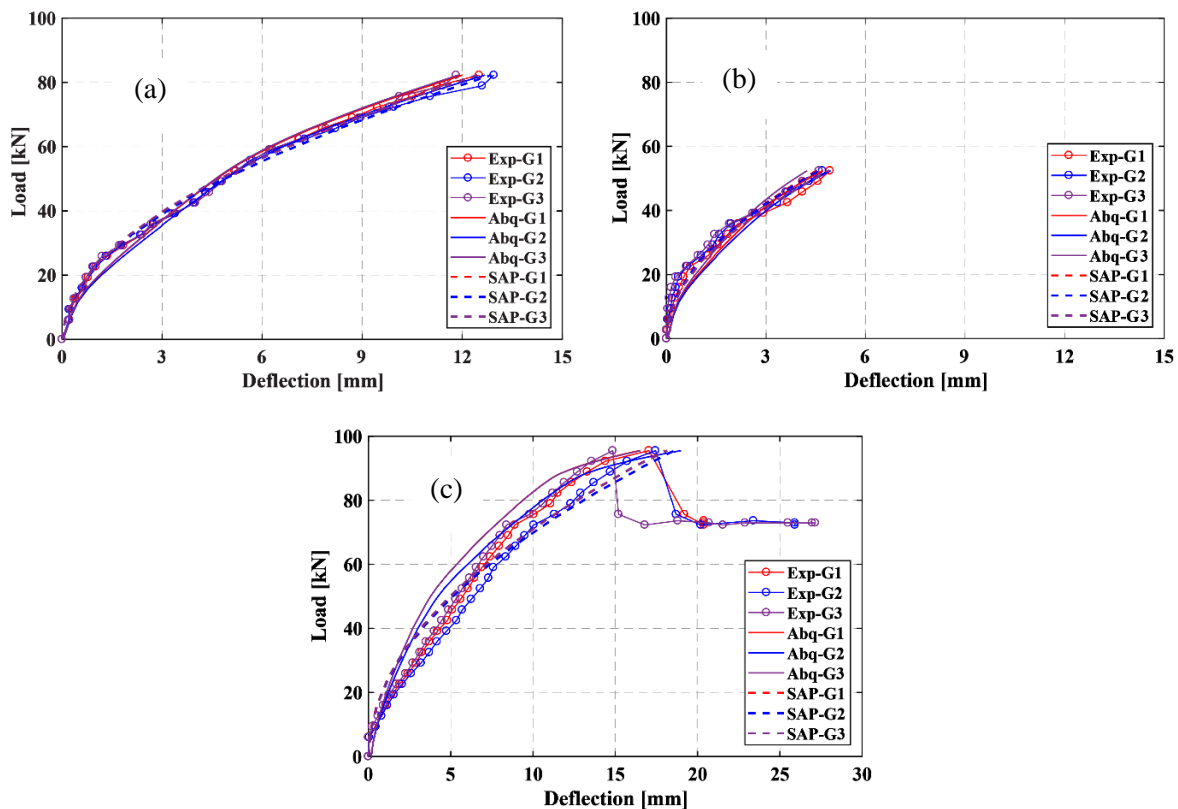


Fig. 4: Comparison of numerical and experimental result: un-retrofitted Reference case (a), un-retrofitted Shear case (b), retrofitted Reference case (c).

The predicted load-deflection behavior of the beams measured at three different locations of the un-retrofitted beams are presented in Fig. 4a-b. It can be seen that there is quite good agreement between the measured and the predicted (SAP2000 v19.2 and ABAQUS) deflections of the un-retrofitted beams. As concern the retrofitted beam test, since the Shear case beam was damaged, therefore, only load-deflection behavior of Reference case is compared with experimental results and presented in Fig. 4c. Both numerical results have some good agreement with the experimental results. It seems that the numerical deflection trend predicted via SAP2000 v19.2 is quite close to the experimental one than predicted via ABAQUS. The load-deflection curves predicted via ABAQUS are bit higher than that of experimental and via SAP2000. Actually, ferrocement behavior is a bit complicated than the

RC beam due to different role of different materials such as steel wire mesh, reinforced concrete, and cement mortar which could explain of this behavior. Also, since this test was performed till failure, hence the prediction of propagation and opening of cracks are quite complicated, which could explain the scatter of this behavior.

CONCLUSIONS

In this study, the beams are tested considering symmetrical and un-symmetrical loading distance. And the performances of the tested retrofitted and un-retrofitted beams are investigated experimentally and numerically. The poor performance of RC beam was observed for the case when shear forces are governing that leads to the formation of major crack at the end of the beams. Further, the retrofitted beams with ferrocement exhibited superior performances in terms of ultimate load carrying capacity and deflection compared to un-retrofitted beams. In a nutshell, the ultimate load carrying capacity of retrofitted beam is about 18% greater than without retrofitted beams. The ferrocement technique induced more ductility into the systems as a result the structural element can give warning to the peoples inside the building/structures to escape during an accident such as earthquake.

REFERENCES

- Ahmad, SF; Lodi, SH and Qureshi, J. 1995. Shear behavior of ferrocement thin webbed sections. *Cement and concrete research*, 25(5): 969-979.
- Al-Sulaimani, GJ; Basunbul, IA and Mousselhy, EA. 1991. Shear behavior of ferrocement box beams. *Cement and Concrete Composites*, 13(1): 29-36.
- Alam, MA; Hassan, A and Muda, ZC. 2016. Development of kenaf fibre reinforced polymer laminate for shear strengthening of reinforced concrete beam. *Materials and Structures*, 49(3): 795-811.
- Alam, MA; Jabbar, ASA; Jumaat, MZ; and Mustapha, KN. 2014. Effective Method of Repairing RC Beam Using Externally Bonded Steel Plate. In *Applied Mechanics and Materials*, 567: 399-404.
- Desayi, P; Kumar, NN and El-Kholy, SA. 1992. Strength and behaviour of ferrocement in shear. *Cement and Concrete Composites*, 14(1): 33-45.
- Hawileh, RA. 2012. Nonlinear finite element modeling of RC beams strengthened with NSM FRP rods. *Construction and Building Materials*, 27(1): 461-471.
- Kishi, N; Zhang, G and Mikami, H. 2005. Numerical cracking and debonding analysis of RC beams reinforced with FRP sheet. *Journal of Composites for Construction*, 9(6): 507-514.
- Obaidat, YT; Heyden, S; Dahlblom, O; Abu-Farsakh, G and Abdel-Jawad, Y. 2011. Retrofitting of reinforced concrete beams using composite laminates. *Construction and Building Materials*, 25(2): 591-597.
- Obaidat, YT; Heyden, S and Dahlblom, O. 2010. The effect of CFRP and CFRP/concrete interface models when modelling retrofitted RC beams with FEM. *Composite Structures*, 92(6): 1391-1398.
- Sundarraja, MC and Rajamohan, S. 2009. Strengthening of RC beams in shear using GFRP inclined strips—An experimental study. *Construction and building materials*, 23(2): 856-864.
- Zhang, K and Sun, Q. 2018. The use of Wire Mesh-Polyurethane Cement (WM-PUC) composite to strengthen RC T-beams under flexure. *Journal of Building Engineering*, 15: 122-136.
- Miah, MS; Miah, MJ; Hossain, MM and Paul, SC. 2018. Seismic Retrofit of Flat Plate and Flat Slabs Using Ferrocement, *Proceedings of 5th International Congress on Technology Engineering and Science*, February 01-02, Kuala Lumpur, Malaysia, 317-326.

DURABILITY PERFORMANCE OF FAIR-FACED CONCRETE

M. J. Miah^{1*} and M. S. Miah^{1,2}

¹Department of Civil Engineering, University of Asia Pacific, Dhaka-1215, Bangladesh.

E-mail: jihad.miah@uap-bd.edu

²Faculty of Civil Engineering, Technische Universität Dresden-TU Dresden, 01187 Dresden, Germany, E-mail: mshamim@uap-bd.edu, mohammad_shamim.miah@tu-dresden.de

*Corresponding Author

ABSTRACT

The durability performance of Fair-Faced Concrete (FFC) made with various percentage of White Portland Cement (WPC) under various exposure conditions such as water absorption porosity and capillary water absorption capacity tests are reported. The FFC was made with a combination of WPC and Ordinary Portland Cement (OPC). In order to optimize the durability performance of FFC, four different replacement percentage of OPC by WPC (0, 25, 75, and 100% for brick aggregate and 0, 30, 80, and 100% for stone aggregate) have been investigated. The volumetric mix ratio of 1:1:2 (cement: fine aggregate: coarse aggregate) and water to cement ratio (by weight) of 0.40 were used for all concretes. The water absorption porosity test was carried out according to the French standard NF P18-459 and capillary absorption capacity was followed by the French recommendations of the AFPC-AFREM. The experimental results showed that the FFC has lower apparent porosity and absorption capacity than normal concrete (made with 100% OPC). It is found that up to 75% WPC for brick aggregate and 80% WPC for stone aggregate could be suitably used to keep minimum porosity and absorption capacity of FFC which can provide maximum durability performance and can prevent the corrosion of steel bar.

Keywords: Fair-faced concrete; White Portland Cement; Porosity; Absorption capacity; Durability.

INTRODUCTION

The application of Fair-Faced Concrete (FFC) is receiving significant attention in the architectural/civil design of modern buildings due to its aesthetic qualities, infinite range of color tones, natural surface texture, lowering cost by avoiding plastering or veneered, and cladding as well as makes structures more sustainable and easier to recycle (PERI, 2002; Doka, 2013; Sun et al., 2012). In one of our recent study, it has been shown that the compressive strength and modulus of elasticity of FFC is higher than Normal Concrete (NC). It was also observed that the outer surface of FFC is smoother, impressive in color, and brighter than NC (Miah et al., 2018). Since the outer surface of the FFC specimens are smoother, hence, generally the plastering or painting are avoided to highlight the natural texture of the concrete surface. Though the FFC surface is smoother than NC, it does not mean that it can provide better prevention of penetration of water or any other effects that can decrease the durability performance of FFC. Therefore, it is essential to have exhaustive knowledge about the durability performance of FFC to guaranty the extra protection from the environmental actions at all seasons such as penetration of water to protect corrosion of steel bar, carbonization, penetration of chloride ion and so on.

In the literature, numerous research works have been conducted on the mechanical properties of fair-faced concrete or concrete made with white Portland cement. While comparatively, there are few

published data on the durability of FFC. Zhou et al., 2011 have investigated the durability performance of fair-faced lightweight aggregate concrete. Frost resistance test was carried out on the cubic specimen (100 x 100 x 100 mm³) which went through freezing-thawing cycles until their average mass loss is up to 5%. The results showed that the fair-faced lightweight aggregate concrete has better frost resistance than the normal lightweight aggregate concrete one. Dellinghausen et al., 2012 carried out the oxygen permeability and chloride ion penetration tests in concrete made with white Portland cement and blast-furnace slag. Authors concluded that the partial replacement of 70% of the white Portland cement by slag reduced chloride penetration by an average 37% and 47% when the concrete samples were cured for periods of 3 and 7 days, respectively. Lower permeability was observed for the concretes composed of white Portland cement and slag (50% and 70%) than those of similar mixtures composed of gray Portland cement. Öztürk and Kaplan 2017 investigated durability properties of mortars with white cement and Portland cement with different water to cement ratios. Authors concluded that the less expansion was observed on the mortars using Portland cement while the white cement gave the largest expansions. The mortars produced using white cement has less impact of higher temperatures in comparison with normal Portland cement. Durability tests also carried out by (Chengqiu et al., 2012 and Veiga and Gastaldini, 2012) and found quite similar observation as above mentioned authors.

It needs to be mentioned that almost no study has been done so far regarding the durability of FFC in Bangladesh. Therefore, this study investigates the durability performance of fair-faced concrete made with different replacement percentage of Ordinary Portland Cement (OPC) by White Portland Cement (WPC). Water absorption porosity and capillary absorption capacity tests are performed to analyze the durability performance of FFC.

EXPERIMENTAL INVESTIGATIONS

Preparation of the specimens

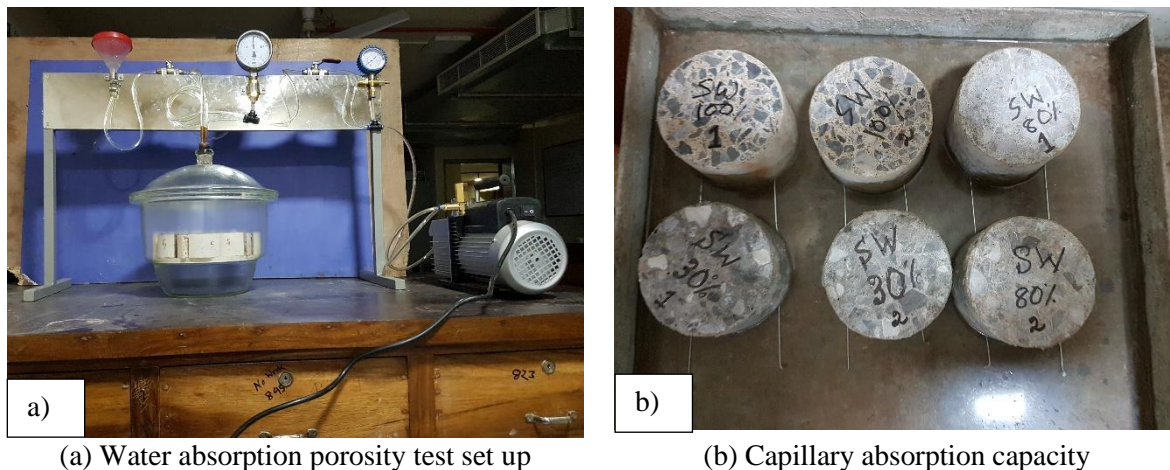
The durability tests were performed on different concretes made with different replacement percentage of OPC by WPC (0, 25, 75, and 100% for brick aggregate and 0, 30, 80, and 100% for stone aggregate). The same mix design was used for all concretes; the only difference is the percentage of WPC. For the simplification, the following shortened name such as FFCB for fair-faced concrete made with brick aggregate and FFCS for fair-faced concrete made with stone aggregate will be used throughout the paper. The control concrete (FFCB 0/FFCS 0, FFC denotes fair-faced concrete, B indicates brick and S for stone aggregate) was made with 100% OPC and the other concretes, named as, FFCB 25/FFCS 30, FFCB 75/FFCS 80, and FFCB 100/FFCS 100 were made with replacement percentage of OPC by WPC of (25/30)%, (75/80)%, and 100%, respectively. First class burnt clay bricks and locally available natural stones were used as coarse aggregates, while natural river sand (locally called Sylhet sand) was used as a fine aggregate. The volumetric mix ratio of 1:1:2 (cement: fine aggregate: coarse aggregate) and water to cement ratio (by weight) of 0.40 were used for all concretes. After completion of mixing, the cylindrical concrete specimens (104 mm in diameter and 300 mm long) were made for both durability tests.

Test procedures

The porosity of concrete was investigated by means of a technique based on water absorption porosity according to the French standard NF P18-459, see Fig. 1a. This technique was performed on a quarter-cylinder of 104 mm in diameter and 50 mm thickness concrete specimens. Three specimens were used for each concrete and then the final porosity was calculated by the arithmetic mean of three specimens. The specimens were dried in an oven at the temperature of 105 °C ± 5 °C until a constant value of mass was reached. Stabilization was considered achieved when the difference in terms of mass in an interval of more than 24 h was lower than 0.1%. The porosity (in %) of concrete is calculated by measuring the mass of concrete specimens in three states of saturation: (i) mass of dry (at 105 °C) test specimen, (ii) apparent mass of immersed test specimen, and (iii) mass of soaked test specimen.

The capillary water absorption capacity test was performed in accordance with the French recommendations of the AFPC-AFREM. The water capillary absorption capacity tests were performed on 104 mm diameter and 70 mm thickness concrete disc. The upper and lower discs were

not taken into account to avoid the edge effect which could influence the measurements of absorption capacity. Also, the concrete discs were cut very carefully by the diamond blade saw, meaning that not to damage the specimen which could allow faster migration of water from bottom to top. The curved surface of the specimen was sealed with epoxy so that the flow occurs uniaxially (from bottom to top) through the thickness of the specimen. First, the specimens dried in an oven at the temperature of 80 °C until a constant value of mass was reached. Then oven dried samples were placed vertically in water on average 3 mm diameter steel rods to allow free access of water to the inflow. The increased mass due to absorbed water was recorded up to 24 h. At the beginning of the test, readings were collected more frequently (least frequency of reading is done per 15 min) and after that, at least of one reading per hour was taken. The reading was determined by weighing specimens in each time step. It should be noted that the water depth along the 70 mm thickness of specimen was approximately 3 mm (see Fig. 1b), which was maintained throughout the test duration.



(a) Water absorption porosity test set up (b) Capillary absorption capacity
 Fig. 1: Test setup for porosity (a) and capillary water absorption capacity (b) according to French standard NF P18-459 and AFPC-AFREM, respectively.

RESULTS AND DISCUSSIONS

Effect of WPC on Porosity

Knowledge of porosity and capillary water absorption capacity will allow us to better understand the fluid transport behavior in concrete, which could influence the durability of concrete by directly influencing the corrosion of steel bar. The apparent porosity of concrete made with brick and stone aggregates are presented in Fig. 2a. The solid line represents the average value of three test data, while the three different symbols indicate each single test data. It can be clearly seen that the test data has some good repeatability especially for concrete made with brick aggregate. As the replacement percentage of OPC by WPC increased, the apparent porosity decreased up to 75% WPC for brick aggregate and 80% WPC for stone aggregate concrete, after that the increase in the percentage of WPC lead to increase in values of porosity. This behavior could be due to the higher percentage of the total silicates ($C_3S + C_2S$) and the higher percentage of dicalcium silicate (C_2S), leading to more CSH (calcium silicate hydrate) and less calcium hydroxide [CH or $Ca(OH)_2$] in the WPC concrete (Hamad 1995; Miah et al., 2018). Indeed, the higher the C_3S and C_2S , the higher the CSH gel, resulting in denser microstructure and higher compressive strength. As concern the 100% WPC concrete made with both brick and stone aggregates, a bit higher porosity was observed but not higher than 0% WPC concrete. Since those concretes containing a large amount of white cement, hence there is a possibility that hydration may not occur in all white cement with the mixed water which is also not so high ($w/c = 0.4$). Therefore, it can be believed that the concrete should be more porous due to un-hydrated cement particles than the other concrete made with low white cement.

Normalized porosity has been calculated to better analyze the durability performance of FFC. This was carried out with respect to reference porosity (i.e., porosity of 100% OPC), i.e., $p^{WPC(\%)} / p^{100\% OPC}$ for concrete containing brick and stone aggregates. The normalized apparent porosity is shown in Fig. 2b.

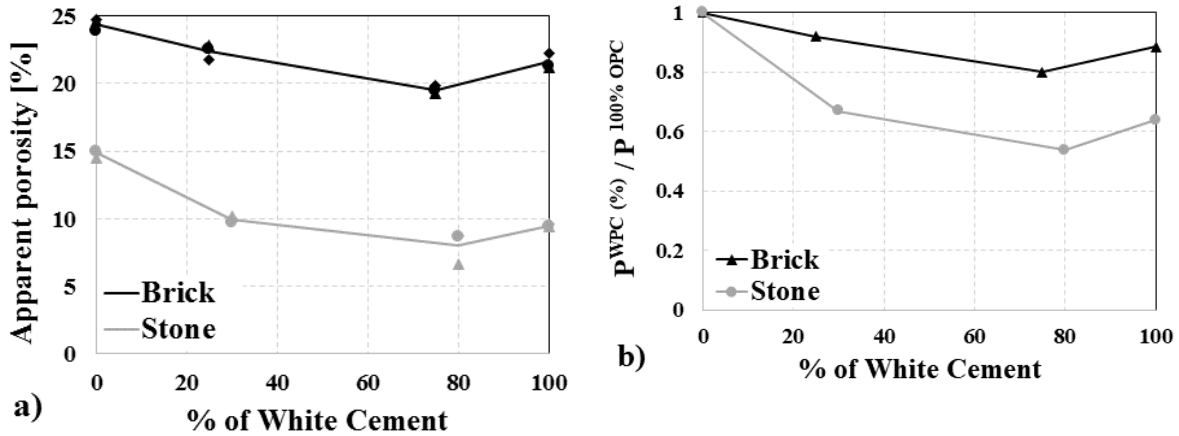


Fig. 2: Apparent water absorption porosity (a) and normalized apparent porosity (b) as a function of replacement percentage of OPC by WPC.

The experimental results showed that the porosity of FFC is about 20% for 75% WPC concrete made with brick aggregate and 46% for 80% WPC concrete made with brick aggregate lower than the 100% OPC concrete. From this observation, it can be concluded that up to 75% WPC for brick aggregate and 80% WPC for stone aggregate could be suitably used to obtain minimum porosity of FFC which can provide maximum durability performance. As concern the effect of aggregate on the porosity of concrete, concrete made with brick aggregate exhibited higher porosity (i.e. lower durability) than the concrete made with stone aggregate. These results are in good agreement with the mechanical properties of FFC carried out by Miah et al., 2018. Higher compressive strength and modulus of elasticity was observed for concrete made with stone aggregate than the concrete made with brick aggregate (Miah et al., 2018). This behavior could be due to the formation of a stronger interfacial transition zone (ITZ) around stone aggregates than brick aggregates as well as higher hardness properties of stone aggregates than brick aggregates. Hence, from this observation, it is clear that the permeability of concrete made with brick aggregate could be higher and can promote faster water and chloride penetration which could destroy the passivation film around the steel bar and then corrosion can start.

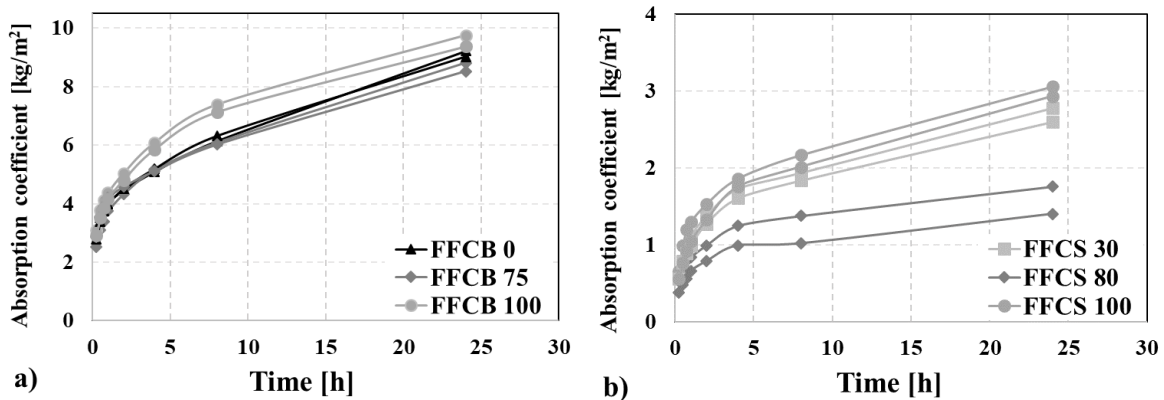


Fig. 3: Evolution of capillary water absorption coefficient of concrete made with brick (a) and stone (b) aggregate as a function of time.

The evolution of capillary water absorption coefficient of concrete is presented in Fig. 3. Except for 100% WPC, it can be noticed that the FFC concrete has lower absorption capacity than concrete made with 100% OPC. The concrete made with 100% OPC and stone aggregate (FFCS 0) test is not present in Fig. 3b due to technical problem in the lab. As mentioned earlier, white cement has higher amount of calcium silicate hydrate which creates denser microstructures as well as strong ITZ. Probably, this is the reason for the lower water absorption for mixes containing white Portland cement.

Moreover, a higher absorption capacity was observed for 100% WPC than 100% OPC concrete. Probably, this behavior could be explained by the formation of a porous paste structure and a poorer interfacial transition zone that lead to higher permeability than the 100% OPC concrete. The increase in capillary voids in the concrete microstructure with the addition of higher WPC in the mix results in higher absorption of water by capillary action. These results are in good agreement with the measurement of water absorption porosity. This higher water absorption capacity can induce higher corrosion than the other concretes. Also, as explained before that there is a possibility that hydration may not finish completely for 100% WPC due to lower amount of water (i.e. lower water to cement ration, $w/c = 0.4$) available for complete hydration. Probably, further hydration process may occur in the un-hydrated white cement particles when specimens were in contact with water during absorption capacity tests. Therefore, lower available water for higher amount of WPC due to lower w/c could be a reason for faster water absorption in the matrix. It can be also clearly seen in Fig. 3(a-b), a steep absorption capacity was observed for the concrete made with 100% WPC than other concrete. As seen before, brick aggregate has higher absorption capacity than the stone aggregate concrete. This is probably due to higher water absorption capacity of brick aggregate itself than the stone segregate. The absorption capacity of brick aggregate is about 30% higher than the stone aggregate. This higher absorption capacity of brick aggregate could explain the higher absorption of concrete made with brick aggregate.

The normalized relation between apparent porosity and absorption capacity measured at 4 h and 24 h of concretes made with different % of WPC and the results are analyzed and presented in Fig. 4. No clear relation between apparent porosity and water absorption capacity was observed. But in some cases, as the apparent porosity increased or decreased, the capillary water absorption capacity of concrete also increased or decreased. For example, at 75% WPC of brick aggregate and 80% WPC of stone aggregate, the porosity and absorption capacity was lower than 100% OPC concrete, see Fig. 4a-b.

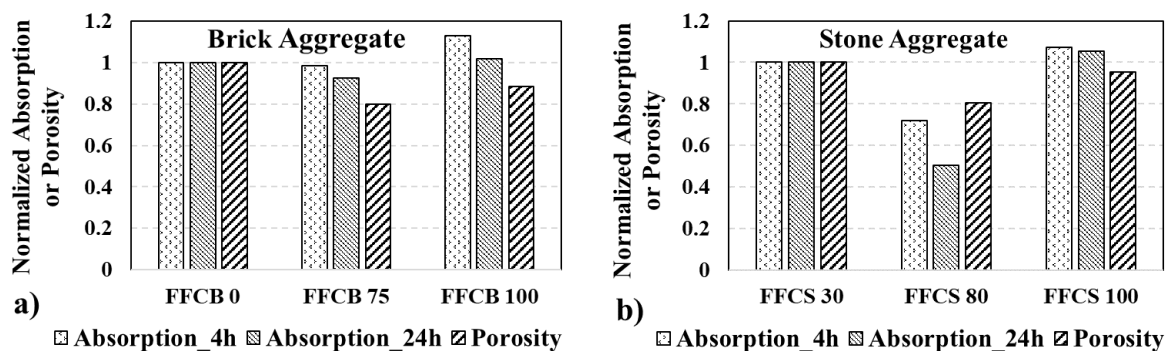


Fig. 4: The normalized relation between water absorption coefficient and apparent porosity of concrete made with brick (a), and stone (b) aggregates, respectively. Note: for stone aggregate, FFCS 30 has been considered as reference concrete since FFCS 0 is not present here.

CONCLUSIONS

In existing literature, many studies have shown that the porosity and absorption capacity of concrete is one of the important parameters that influence the migration of water and also can influence the durability performance of concrete. It is worth noting, however, that a number of studies have been conducted on the mechanical properties of FFC, while in contrast, there are very few works have been done on the durability of FFC. To this end, the apparent porosity and capillary water absorption capacity tests were carried out on FFC made with different percentage of WPC and the results were compared with 100% OPC concrete. The main findings regarding the partial replacement of OPC by WPC on the durability performance of FFC can be summarized as follows:

- The porosity of FFC is much lower than the normal concrete (100% OPC concrete). As the percentage replacement of OPC by WPC increased, the porosity decreased up to 75% WPC for brick aggregate and 80% WPC for stone aggregate concrete.

- Lower absorption capacity was observed for FFC than 100% OPC concrete, especially for concrete made with stone aggregate.
- The FFC made with 100% WPC of both brick and stone aggregates has little higher porosity and absorption capacity but not more than 100% OPC concrete for porosity.
- Though no clear relation between apparent porosity and absorption capacity was observed, in some cases, the porosity increased or decreased with the increase or decrease in absorption capacity of concrete.
- It has been found that up to 75% WPC for brick aggregate and 80% WPC for stone aggregate could be suitably used to obtain minimum porosity and absorption capacity of FFC which can provide maximum durability performance of FFC.

The results presented in this paper is from an ongoing project, and further work is currently underway such as behavior of FFC under fire made with different percentage of white cement.

ACKNOWLEDGEMENTS

The authors have appreciated the financial support of the Department of Civil Engineering of University of Asia Pacific. Authors also acknowledges the assistance of the lab attendee and students of the aforementioned department.

REFERENCES

- PERI. 2002. Reference Booklet Fair-face Concrete. *PERI GmbH*, 10/2002: 1–88.
- Doka G. 2013. Fair-faced concrete. *Doka GmbH*, [online]. Available at: www.doka.com [Accessed 18 August 2018].
- Sun, Y; Wang, Y; Cheng, L and Zhu, X. 2012. Construction technology and benefit analysis of fair-faced concrete in high-rise building. *Advanced Materials Research*. 446(449): 3690-3693.
- Miah, MS; Miah, MJ; Hossain, MM and Paul, SC. 2018. Experimental and numerical investigation on fair-faced concrete. *The proceedings of 5th International Congress on Technology Engineering and Science*, February 01-02, 2018, Kuala Lumpur, Malaysia, pp. 293–304.
- Zhou, J; He, M and Gu, Q. 2011. Fair-faced light weight aggregate concrete preparation and durability research. *Applied Mechanics and Materials*. 117(119): 1358-1360.
- Dellinghausen, LM; Gastaldini, ALG; Vanzin, FJ and Veiga, KK. 2012. Total shrinkage, oxygen permeability, and chloride ion penetration in concrete made with white Portland cement and blast-furnace slag. *Construction and Building Materials*. 37(2012): 652–659.
- Öztürk, AU and Kaplan, G. 2017. A study of some durability properties of mortars with white cement and Portland cement. *Romanian Journal of Materials*. 47(3): 315 – 321.
- Chengqiu, C; Qingsong, G and Xin, L. 2012. Experimental research on durability of fair-faced concrete. *Advanced Materials Research*. 535(537): 1693-1696.
- Veiga, KK and Gastaldini, ALG. 2012. Sulfate attack on a white Portland cement with activated slag. *Construction and Building Materials*. 34(2012): 494–503.
- NF P18-459. 2010. Essai pour béton durci-essai de porosité et de masse volumique. *French Standard*, NF P18-459, MARS 2010.
- AFPC-AFREM. 1997. Compte rendu des journées techniques AFPC-AFREM Durabilité des bétons. *Laboratoire Matériaux de Durabilité des Constructions, Institut national des sciences appliquées, Université Paul Sabatier*, Toulouse, Décembre 1997.
- Hamad, BS. 1995. Investigations of Chemical and Physical Properties of White Cement Concrete. *Advn Cem Based Mater J.*, 2: 161-167.
- Miah, MJ; Miah, MS; Paul, SC and Hossain, MM. 2018. Optimization of mechanical properties of fair-faced concrete: role of white Portland cement. *Proceedings of 111th IASTEM International Conference*, 2nd-3rd April 2018, Munich, Germany, pp. 54-59.

OPTIMIZATION OF MECHANICAL PROPERTIES OF HIGH PERFORMANCE CONCRETE MADE WITH FLY ASH AND BLAST-FURNACE SLAG

M. J. Miah^{1*}, M. S. Miah^{1,2}, M. A. Uddin¹ and M. Suzaudoula¹

¹Department of Civil Engineering, University of Asia Pacific, Dhaka-1215, Bangladesh.

E-mail: jihad.miah@uap-bd.edu

²Faculty of Civil Engineering, Technische Universität Dresden-TU Dresden, 01187 Dresden, Germany.

E-mail: mshamim@uap-bd.edu; mohammad_shamim.miah@tu-dresden.de

*Corresponding Author

ABSTRACT

This study presents an experimental investigation on the optimization of mechanical properties of High Performance Concrete (HPC) made with partial replacement of Ordinary Portland Cement (OPC) by fly ash and slag. In order to optimize the mechanical properties of HPC, initially, four different replacement percentage of OPC by fly ash or blast furnace slag (0, 10, 20, and 45%) have been investigated. Additionally, an unconstrained nonlinear optimization scheme known as Nelder-Mead Simplex Method was employed for modeling the stress-strain behavior of HPC and the predicted optimized results are also compared with existing model for better understanding. The experimental results have shown that the replacement of OPC by 20% fly ash (FA) and slag (SL) can increase the strength of HPC on average of about 3%, after that the increase in the percentage of FA and SL leads to decrease in values of concrete compressive strength. In contrast, lower reduction of compressive strength of HPC was observed for slag based concrete than fly ash concrete. From the experimental results, it is observed that 20% fly ash and slag can be incorporated in cement to maintain the maximum compressive strength of HPC. Finally, the stress-strain behavior is modeled by employing a nonlinear optimizer and a good agreement with the experimentally measured stress-strain curve for both fly ash and slag based concretes are observed.

Keywords: High performance concrete; Fly ash; Slag; Stress-strain relation; Optimization.

INTRODUCTION

There is a growing trend toward the use of supplementary cementitious materials (SCM) such as Fly Ash, Ground Granulated Blast-furnace Slag, Silica Fume, Rice-husk Ash, etc. in the production of Portland cement concrete. The application of such supplementary cementitious materials receiving serious attention in the scientific community and concrete industry due to significant reduction of carbon dioxide gas emissions arising from cement making, cost savings, energy savings, resource conservation as well as their very good durability performance (ACI Committee, 226; ASTM C618-05; Rashad, 2015; Gholampour and Ozbakkaloglu, 2017).

Rao et al., 2016 carried out the compressive strength of concrete made with five different replacement percentage of OPC by fly ash (0%, 10%, 20%, 30%, and 40%). A total number of 20 cubes (15 cm x 15 cm x 15 cm) were cast and tested at 3, 7, and 28 days. The author concluded that the maximum compressive strength of concrete is obtained at optimum dosage at 20% fly ash replacement with cement. Mohamed, 2011 investigated the effect of fly ash and silica fume on compressive strength of

self-compacted concrete made with partial replacement levels of 10%, 15%, 20%, 25%, 30%, 35%, 40%, and 50% of fly ash by weight of OPC. The compressive strength tests were performed on cylindrical specimens (100 mm in diameter and 200 mm in length) at 7 and 28 days. The experimental results showed that the compressive strength of concrete is increased up to replacement percentage of 30% of fly ash. Harison et al., 2014 studied that the effect of different percentage of fly ash (0%, 10%, 20%, 30%, 40%, 50%, and 60%) on compressive strength of concrete. It was observed that no significant changes of compressive strength occurred up to 30% replacement of OPC by fly ash as compared to reference concrete (without fly ash).

Shariq et al., 2008 investigated the strength development of cement mortar and concrete incorporating 20%, 40%, and 60% replacement of OPC by Ground Granulated Blast Furnace Slag (GGBFS). The compressive strength of concretes were carried out on cubic (150 mm x 150 mm x 150 mm) and cylindrical (150 mm in diameter and 300 mm in length) specimens at 3, 7, 28, 56, 90, 150, and 180 days. The authors concluded that a significantly higher compressive strength was observed in concrete incorporating 40% GGBFS after 56 days than 20% and 60% replacement. A study carried out by Sundaramoorthy and VimalBalaji, 2017 found that the compressive strength of concrete made with 20% slag cement gives higher strength than without slag cement. Shyamala et al., 2016 found that 10% to 20% replacement of cement by GGBS the compressive strengths are higher than the concrete made without GGBS. Awang and Aljournaily, 2017 observed that 30% blast furnace slag foam concrete mix exhibited higher compressive, flexural, and splitting tensile strengths than the control mix at all ages.

However, rapid growth in infrastructure is becoming the number one priority at the global level, particularly, in the developing countries like Bangladesh. Due to the aforementioned issues, the demand of High Performance Concrete (HPC) is increasing drastically. This paper provides insight on some of the mechanical properties of concrete containing different percentage of fly ash and slag. Additionally, an unconstrained nonlinear optimization scheme known as Nelder-Mead Simplex Method was employed for modeling the stress-strain behavior of HPC and the predicted optimized results are also compared with an existing model.

EXPERIMENTAL INVESTIGATION

Materials, mix design, and preparation of specimens

In this experimental campaign, locally available black stone was used as coarse aggregates whose specific gravity, density, and abrasion resistance are 2.74, 1550 kg/m³, and 12.01 % respectively. While natural river sand (locally called Sylhet sand) passing the standard No. 4 sieve (4.75 mm), clean and free of any deleterious substance, and of fineness modulus and specific gravity 3.29 and 2.56, respectively was used as a fine aggregate. The maximum size of coarse aggregate was 20 mm and the grading of the coarse aggregates was controlled as per ASTM C33. The weight basis mix design with water to binder ratio (w/b) of 0.3 and sand to total aggregate volume ratio (s/a) of 0.38 were used for all mixes, see Table 1. Ordinary Portland cement (OPC) with different percentage of fly ash and slag was used as binder. Since the w/b ratio is lower, hence superplasticizer is used (1.5% by mass of total binder) to maintain the workability of fresh concrete. In order to optimize the mechanical properties of HPC, four different replacement percentage of OPC by fly ash or slag (0, 10, 20, and 45%) have been investigated. In order to monitor the compressive strength of concrete, the cylindrical (100 mm in diameter and 200 mm long) concrete specimens were made and demolded after 24 hours of casting. Then all the concrete specimens were cured underwater (20 ± 2 °C) up to the day of the tests.

Test program and procedures

The compressive strength tests were performed at 14, 28, and 60 days to monitor the evolution of compressive strength as per ASTM C39 by using Universal Testing Machine (UTM) setup of UAP. Within the scope of the study, a total of 72 concrete cylindrical specimens (9 for each mix, means, 3 for each day) were tested. During the test, the deformation of concrete specimens was measured by a strain measurement setup with two dial gauges. The gauge length was 100 mm in the central part of the specimen. After crashing, the failure surfaces of concrete were also observed carefully. The overview of the experimental program for the compressive strength is presented in Table 1.

Table 1: Summary of the experimental program and mix design

ID	OPC (%)	Fly Ash (%)	Slag (%)	Binder	w/b	s/a	Superplasticizer
FA0	100	0	-	500 kg/m ³	0.3	0.38	1.5% by mass of binder
FA10	90	10	-				
FA20	80	20	-				
FA45	55	45	-				
SL0	100	-	0				
SL10	90	-	10				
SL20	80	-	20				
SL45	55	-	45				

Notations: FA – Fly ash, SL – Slag, OPC – Ordinary Portland Cement, w/b – water to binder ratio, s/a – sand to total aggregate volume ratio.

RESULTS AND DISCUSSIONS

Effect of supplementary cementitious materials on stress-strain curve of HPC

An example of stress-strain curves of HPC made with partial replacement of OPC by fly ash and slag are shown in Fig. 1. The stress-strain curve of fly ash and slag are based concrete measured at 60 and 28 days respectively. It is quite clear that after sudden percentage replacement of fly ash or slag can decrease the slope of the stress-strain curve (i.e., modulus of elasticity). This behavior is more pronounced for higher amount of fly ash or slag. Indeed, supplementary cementitious materials reduce the heat of hydration which provides lower compressive strength in the early age of concrete while a higher strength can be observed beyond a couple of months if the moisture is available for continued pozzolanic reaction. A significant difference of the slope of the stress-strain curve was observed with the increasing percentage of fly ash. While almost no significant change in the development of stress-strain curve has been observed for concretes made with different percentage of slag. Interestingly, higher modulus of elasticity can be seen for the concrete incorporating 10% and 20% of both fly ash and slag concrete than without fly ash and slag concrete.

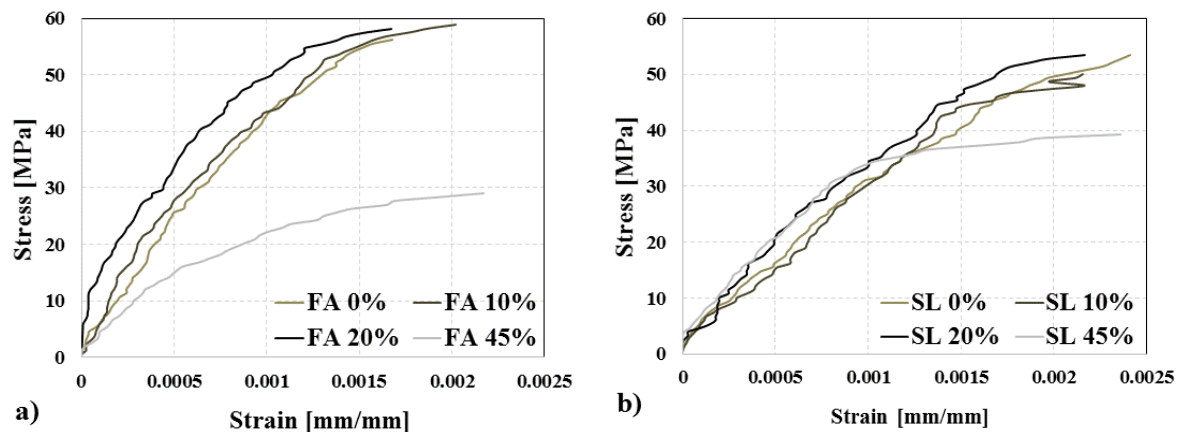


Fig.1: Stress-strain curve of HPC measured at 60 days for fly ash (a) and at 28 days for slag (b).

Effect of supplementary cementitious materials on compressive strength of HPC

The average compressive strength of HPC incorporating with different percentage of fly ash and slag measured at 14, 28 and 60 days are presented in Fig. 2. For every data set, three cylinders were tested and then the average value was calculated. It can be seen that in the addition of fly ash and slag, at 14 days the strength decreased at all replacement levels and this is more significant for fly ash concrete. However, it is significantly increased at 60 days for both fly ash and slag based concrete. As mentioned earlier that the decrease in strength could be due to slow heat of hydration process since fly ash is slow reactive pozzolan which delays the hydration process. These figures also indicate that an increasing trend of compressive strength was observed until 20% of fly ash and slag, after that the increase in the

percentage of FA and SL lead to decrease in values of concrete compressive strength. This behavior could be linked to the microstructure of the HPC made with FA and SL. Since the particle size of FA and SL is much smaller than the OPC which can fill the voids left by OPC (i.e. improve interfacial transition zone) and can provide very dense microstructure. Indeed, interfacial transition zone (ITZ) is the weakest path for failure of concrete during loading. And the supplementary cementitious materials can improve the ITZ and then can take more load than the OPC concrete. Likely, this is the reason why combined (both mortar and aggregate) failure was observed for all specimens made with fly ash and slag. Also, in the presence of water, pozzolan such as fly ash reacts with calcium hydroxide $[Ca(OH_2)]$ and produce second calcium silicate hydrate (CSH) which gives more compressive strength.

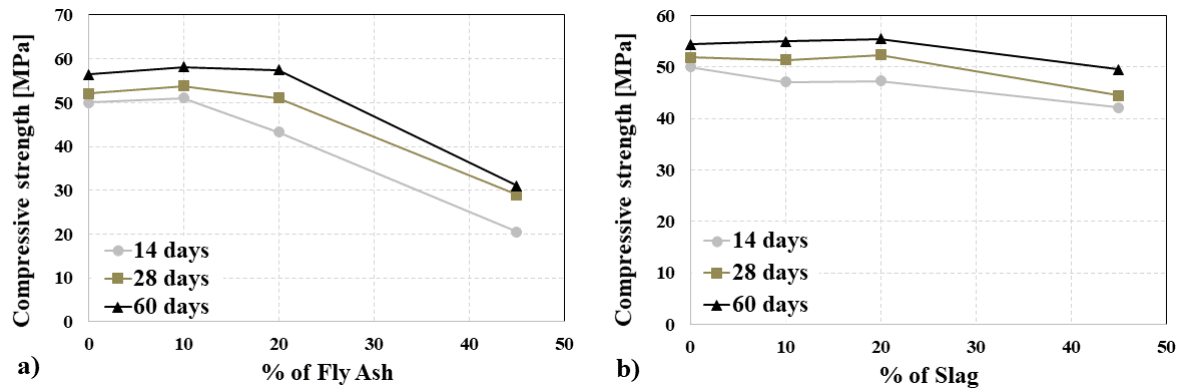


Fig. 2: Compressive strength of HPC made with different replacement percent of fly ash (a) and slag (b) by OPC measured at 14, 28 and 60 days.

For better understanding, normalized mechanical properties of HPC made with fly ash and slag are plotted in Fig. 3. The experimental results showed that the compressive strength of HPC containing 20% fly ash and slag is about on average 3% higher than without FA and SL concrete. This implies that without compromising the compressive strength, 20% clinker can be replaced by fly ash or slag which not only save the money and energy, it will also significantly reduce the carbon dioxide gas emission arising from the cement making industry. From this study, it has been found that up to 20% fly ash and slag could be suitably used to obtain maximum compressive strength of HPC. It is worth noting that the reduction rate of strength due to higher replacement percentage of OPC is comparatively higher for the fly ash based concrete than the slag based concrete. The maximum reduction of concrete compressive strength at 60 days of 45% fly ash and slag based concrete are 45% and 9% respectively.

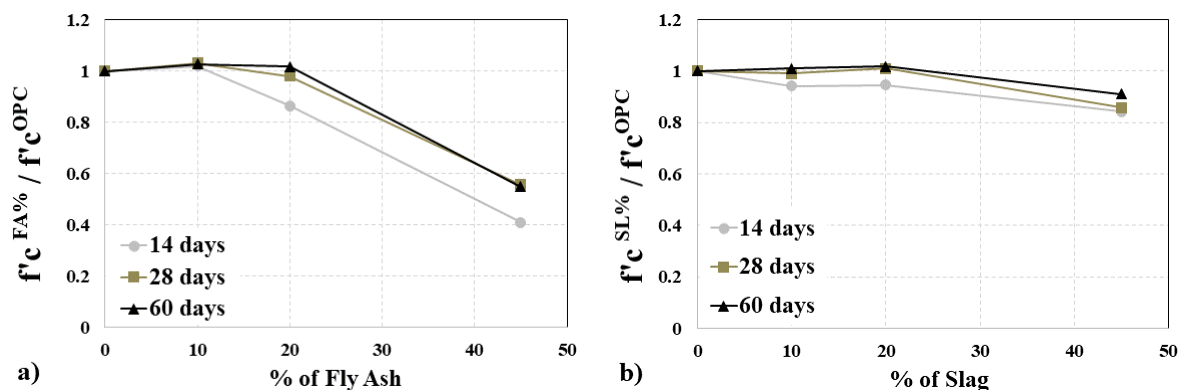


Fig. 3: Normalized compressive strength as a function of replacement percentage of OPC by fly ash (a) and slag (b).

Since Bangladesh is highly populated country and limited in land, hence the demand of high rise buildings and infrastructures are significantly increasing, as a result, the demand of HPC is also increasing. From the outcome of this research, it can be summarized that it is possible to make concrete strength of about 60 MPa ($\approx 9000 - 10000$ psi) with locally available stone aggregate and 20% fly ash or slag with cement. The HPC is not only capable of increasing the strength but also it will give dense

microstructure, lower porosity and permeability, higher durability, and lower risk of earthquake due to lower self-weight of the structure by reducing the size of the section.

Optimization of Stress-Strain Modeling

In order to model the stress-strain behavior of the investigated HPC an existing model proposed by Tsai in 1988 has been selected. Interested reader may get detail information regarding aforementioned model via Tsai, 1988. Further, an unconstrained nonlinear optimization so-called the Nelder-Mead Simplex (Lagarias et al., 1998) was employed for modeling the stress-strain behavior. The Nelder-Mead Simplex Method has been employed due to its superior performance among other alternatives Miah et al., 2015. The equation of Tsai was given as

$$\sigma_t^{tsai} = \frac{kx}{1 + \left(k - \frac{j}{j-1}\right)x + \frac{x^j}{j-1}} \times \sigma_c' \quad (1)$$

In the above equation, k and j are the scaling parameters. And for the optimization, the fitness function was defined as $\text{error} = \frac{\|\sigma^{exp} - \sigma_t^{tsai}\|}{\|\sigma^{exp}\|}$, where σ_t^{tsai} is the proposed model data, σ^{exp} means the true results. It needs to be noted that the existing model is not suitable for the HPC due to inherent properties of HPC such as aggregates type. However, the proposed (optimized) model shows a good match with the true data, see Fig. 4. It can be seen from the aforementioned figure that the proposed model is capturing the true results quite efficiently and the error is less than 2%.

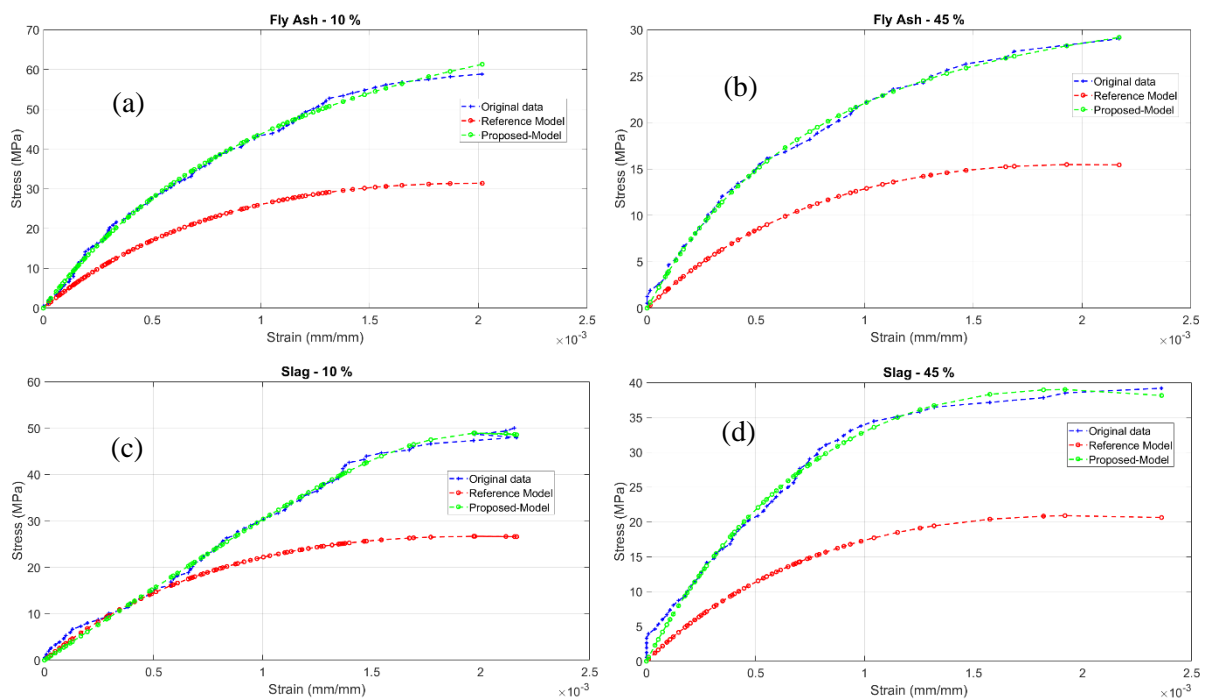


Fig. 4: Modeling of stress-strain behavior of HPC: with Fly-Ash 10% (a) and 45% (b) respectively, with Slag 10% (c) and 45% (d) accordingly.

CONCLUSIONS

This paper presents an experimental program to investigate the effect of incorporating of fly ash and slag in cement on the mechanical properties of HPC. Additionally, an optimization scheme for modeling the behavior of stress-stress is studied as well. The main findings regarding the partial replacement of OPC by fly ash and slag on the mechanical properties of HPC can be summarized as follows:

- The replacement of OPC by 20% fly ash and slag can increase the strength of HPC on average of about 3%, after that the increase in the percentage of FA and SL lead to decrease in strength.
- Comparatively lower reduction of compressive strength of HPC was observed for slag based concrete than concrete made with fly ash.

- Based on the experimental results, the optimum percentage replacement of OPC by fly ash and slag is about 20% that can maintain the maximum compressive strength of 100% OPC concrete.
- It is possible to make concrete strength of about 60 MPa (\approx 9000 – 10000 psi) with locally available stone aggregate and 20% fly ash or 20% slag with OPC which is economical and environmentally friendly since making clinker is more expensive and can increase the CO₂ emission.
- Even though, the data are limited to propose a generic model for HPC made with different replacement percentage of OPC by fly ash and slag, a very good agreement between the measured and the predicted stress-strain curves was observed.

Through quite good results have been observed, it is essential to study more percentage replacement of OPC by FA and SL and also need to study the durability performance of HPC to draw strong conclusion. This is an ongoing project, further work is currently underway and more percentage of FA and SL, additionally, the implementation of rice husk ash is outlined.

REFERENCES

- Committee 226, ACI. 1987. Ground Granulated Blast-Furnace Slag as a Cementitious Constituent in Concrete. *Materials Journal*, 84(4): 327-342.
- ASTM C618-05. 2005. Standard Specification for Coal Fly Ash and Raw or Calcined Natural Pozzolan for Use in Concrete. [online]. Available at: <https://www.astm.org/Standards/C618.htm> [Accessed 18 June 2018].
- Rashad, AM. 2015. A brief on high-volume Class F fly ash as cement replacement-A guide for Civil Engineer. *International Journal of Sustainable Built Environment*, 4: 278-306.
- Gholampour, A and Ozbakkaloglu, T. 2017. Performance of sustainable concretes containing very high volume Class-F fly ash and ground granulated blast furnace slag. *Journal of Cleaner Production*, 162: 1407-1417.
- Rao, GS; Kumar, GS and Ganesh, GL. 2016. Comparison of Compressive Strength of M25, M30 Grades of Concrete by Partially Replacement of Fly Ash with Normal and Accelerated Curing. *International Journal of Innovative Research in Technology*, 3(1): 164-172.
- Mohamed, HA. 2011. Effect of fly ash and silica fume on compressive strength of self-compacting concrete under different curing conditions. *Ain Shams Engineering Journal*, 2: 79–86.
- Harison, A; Srivastava, V and Herbert, A. 2014. Effect of Fly Ash on Compressive Strength of Portland Pozzolona Cement Concrete. *Journal of Academia and Industrial Research*, 2(8): 476-479.
- Shariq, M; Prasad, J and Ahuja, AK. 2008. Strength Development of Cement Mortar and Concrete Incorporating GGBFS. *Asian Jo. of Civil Engineering (Building and Housing)*, 9(1): 61-74.
- Sundaramoorthy, G and VimalBalaji, TK. 2017. Investigation of Strength in Concrete by Partial Replacement of Portland Slag Cement. *SSRG International Journal of Civil Engineering, Special Issue*, 439-442.
- Shyamala, K; Vinod, C and Manna, SA. 2016. Comparison of Strength for Concrete with GGBS and Cement Using Accelerated Curing Method. *International Journal of Engineering Research and Application (Part -2)*, 6(10): 96-100.
- Awang, H; Aljoumaily, ZS and Hussain, RR. 2017. Influence of granulated blast furnace slag on mechanical properties of foam concrete. *Cogent Engineering* 2017(4): 1409853.
- ASTM C33. 2003. *Standard Specification for Concrete Aggregates*. ASTM International, West Conshohocken, PA, USA, 11p.
- ASTM C39. 2005. *Standard Test Method for Compressive Strength of Cylindrical Concrete Specimens*. ASTM Standard, West Conshohocken, PA, USA, 16p.
- Tsai, WT. 1988. Uniaxial Compressional Stress-Strain Relation of Concrete. *Journal of Structural Engineering*, 14(9): 2133–2136.
- Lagarias, JC; Reeds, JA; Wright, MH and Wright, PE. 1998. Convergence Properties of the Nelder-Mead Simplex Method in Low Dimensions. *SIAM J. on Optimization*, vol. 9, no. 1, pp.112–47, 1998.
- Miah, MS; Chatzi, EN; Dertimanis, VK and Weber, F. 2015. Nonlinear modeling of a rotational MR damper via an enhanced Bouc–Wen mode. *Smart Mat. and Str*, vol. 24, no. 10: 105020, 2015.

EFFECT OF INTERNAL CURING ON CHLORIDE DIFFUSION COEFFICIENT OF CONCRETE

A. T. M. Masum*, M. F. A. Khan, T. Torsha & T. Manzur

Department of Civil Engineering, Bangladesh University of Engineering & Technology, Dhaka, Bangladesh.

E-mail:masum.ce08buet@gmail.com

**Corresponding Author*

ABSTRACT

Proper curing of concrete at early age is essential to obtain desired strength and durability. However, lack of knowledge and awareness and absence of strict supervision often result in inadequate curing of concrete. Such improper curing produces permeable concrete and eventually, reduces the service life of reinforced concrete (RC) structures. Some recent researches showed that saturated brick chips can be used as internal curing (IC) medium within concrete. It has been found that concrete mixed with optimum proportion of brick chip as IC agent was able to produce better concrete in the absence of proper curing or under adverse curing conditions. On the other hand, serviceability of concrete due to chloride induced corrosion primarily depends on chloride diffusion coefficient. It is expected that internal curing will increase the service life of concrete by reducing chloride ingress under harsh curing conditions. In this study, different adverse curing conditions have been simulated in the laboratory to determine the effect of internal curing on chloride diffusion coefficients of concrete. Samples (both control and internally cured) were exposed to the simulated conditions and tested for non-steady-state migration experiment to measure diffusion coefficients. It has been observed that internal curing significantly reduces the chloride diffusion rate under adverse conditions.

Keywords: Durability; Adverse Curing Condition, Internal Curing; Service Life; Chloride Diffusion Coefficient

INTRODUCTION

Bangladesh has been undergoing a boom in construction sector in recent years. Concrete is being used as main construction materials in most of the projects in the country [Manzur, 2017]. The reason of using concrete as main construction material is due to its wide spread availability and relative low cost. Proper curing of concrete at early ages is crucial to obtain design strength and maximum durability [Al-Gahtani, 2010]. The curing of concrete at the early age is usually done by supplying external water from outside after the casting [Manzur et al., 2015]. However, absence of proper curing is often observed in many construction site specially in small to medium scale projects at remote locations due to lack of knowledge and awareness among the workers [Afroz et al., 2015; Manzur et al., 2015; Iffat et al., 2017]. Moreover, strict supervision during construction is often not ensured. Such improper curing results in weaker and permeable concrete and eventually, reduces the service life of RC structures significantly particularly in aggressive environmental conditions. The primary cause for reduced service life is chloride induced corrosion resulting from ingress of chloride ion [Zhou et al., 2014]. The negative impacts caused by the lack of proper curing can be overcome by adapting the internal curing (IC) mechanism [Manzur et al., 2015]. In IC, additional water is supplied into the concrete from the internal source [Bentz et al. 2005]. In some recent studies, it is found that saturated brick chips (BC) can be used as internal curing (IC) medium within concrete [Iffat et al., 2017 and 2016]. Brick chip has the ability to absorb sufficient quantity of water during mixing and desorb it afterwards under favorable conditions [Manzur et al., 2015, Iffat et al., 2016]. Recent

research shows that optimum proportion (20 percent replacement of stone chips by saturated BC) of BC as IC agent produce more durable concrete compared to the conventional concrete with 100 percent stone chips [Iffat et al., 2017] in the absence of proper curing. On the other hand, chloride ingress within concrete primarily depends on chloride diffusion coefficient of the concrete. Chloride diffusion coefficient is defined by the resistance to chloride penetration of a particular concrete mix which can be evaluated by non-steady state migration test [Yang and Wang, 2004]. Concrete, mixed with optimum proportion of BC as IC agent is expected to produce reduced value of diffusion coefficient under harsh curing conditions. In this context, an attempt has been made to investigate the effect of internal curing on the chloride diffusion coefficient of concrete under varying curing conditions. The results obtained were compared with two sets of normal concrete; one of which was produced ensuring proper external curing (NC) and another without any curing (NC0W). For calculating the coefficients, Nordtest method [NT Build 492, 1999] was followed. Besides, in this study, a comparison is also made between compressive strength of conventional concrete and IC concrete for an in depth understanding of the positive impact of IC.

EXPERIMENTAL INVESTIGATION

Material Properties and Mix Proportions

Locally available stone chips (SC) as coarse aggregate (CA) and Sylhet sand as fine aggregate (FA) were used in this study to produce the concrete specimens (Fig. 1). Ordinary Portland Cement (OPC) produced by local industry was used as binding material. Saturated brick chips (BC), produced locally from burnt clay, was used as internal curing agent. Properties of mix ingredients were measured using relevant ASTM standards prior to the casting in order to confirm the quality of the ingredients.



Fig.1 Aggregates a) Sand b) Stone chips c) Brick chips

Adverse curing conditions

A total of 10 different adverse curing conditions were simulated in the laboratory. Concrete cylindrical specimens produced from 20% saturated BC as partial replacements of SC were kept under these simulated conditions [Fig.3]. Two sets of control samples (CS) were made by using only SC as coarse aggregate for comparison. One set of CS was kept under water for 28 days to represent the ideal curing condition which is termed as NC. Other set was exposed outside without any curing just after the casting (NC0W) to represent the most adverse curing condition. All the samples were prepared using a common mix ratio 1:1.5:3 (cement: FA: CA) on volume basis with a water cement ratio of 0.40. Details of different adverse curing conditions are shown in Table 1. Figure 3 shows example of three adverse curing conditions simulated in the laboratory.

Concrete compressive Strength Test

Concrete cylinders of 100 mm diameter and 200 mm height were made to carry out the compressive strength test [Fig.4]. After casting, samples were kept under different simulated curing conditions. At the age of 28 days, compressive strength test was performed for samples kept under each simulated curing condition as per ASTM C39 (2005).

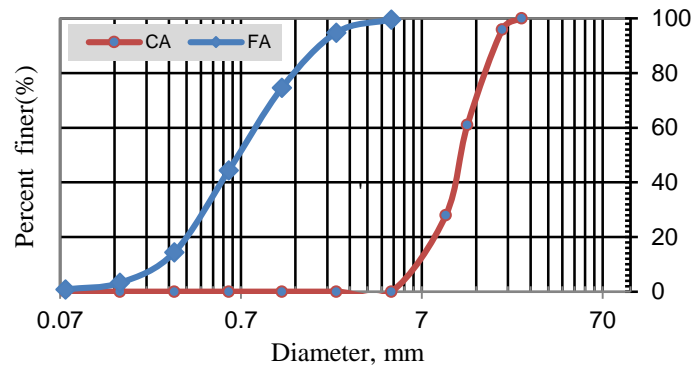


Fig. 2: Gradation Curves for Fine and Coarse aggregate

Table 1 : Simulated curing conditions in the laboratory

SL	Simulated curing conditions	Symbol
1.	Control sample curing under water for 28 days	NC
2.	Control sample exposed outside without covering just after casting	NC0W
3.	IC concrete exposed outside covered with polythene just after casting	IC0P
4.	IC concrete exposed outside without covering just after casting	IC0W
5.	IC concrete exposed outside covered with polythene after 3 days curing under water	IC3P
6.	IC concrete exposed outside without covering after 3 days curing under water	IC3W
7.	IC concrete exposed outside covered with polythene after 7 days curing under water	IC7P
8.	IC concrete exposed outside without covering after 7 days curing under water	IC7W
9.	IC concrete exposed outside having 3 days curing by wet gunny bag	IC3G
10.	IC concrete exposed outside having 7 days curing by wet gunny bag	IC7G
11.	IC concrete exposed outside having 28 days curing by wet gunny bag	IC28G

Chloride Migration Test

Test specimen

To carry out non steady state migration experiment as per NT Build 492(1999), concrete cylindrical specimens of 100 mm diameter and of 50 mm thickness were sliced out from previously cast cylinders (100 mm x 200 mm). Non- steady state migration experiment was carried out for each sample subjected to both normal and adverse curing conditions at the age of 65 days.

Preconditioning

Before conducting migration test, test specimens were taken for preconditioning. Sides of the specimen were coated with epoxy keeping only two end surfaces exposed [Fig.5]. The samples were then taken into SSD condition and put into the vacuum chamber [Fig.6]. The specimens were then made vacuum saturated with $\text{Ca}(\text{OH})_2$ for around 20 hours.



Fig. 3: IC samples exposed outside after 3 days curing under water

Test Procedure

After making vacuum saturated with $\text{Ca}(\text{OH})_2$, the specimen was immersed in an catholyte solution of NaCl and anolyte solution of NaOH. Applying an external voltage across the specimen, chloride ions

from catholyte solution were forced to migrate into the specimen through the exposed surface for 24 hours. The specimens were then split axially and silver nitrate solution was sprayed on the split section. Chloride penetration depths were then measured from visible white silver chloride precipitation. After that, chloride diffusion co-efficient of concrete samples kept under different simulated curing conditions were calculated from penetration depths, applied voltage and temperature using the equation provided in NT Build 492 (1999). Relevant figures of the test are shown in Fig.7.



Fig.4: Compressive strength test Fig. 5: Epoxy coated specimen Fig.6: Vacuum Chamber

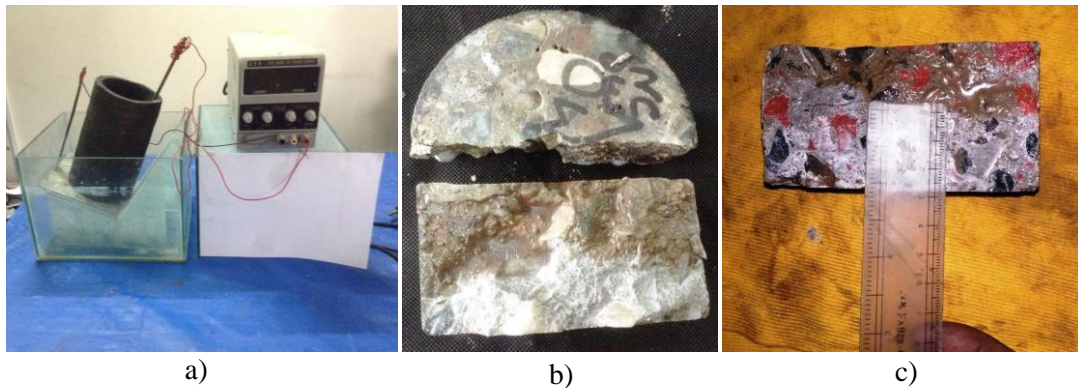


Fig.7: Chloride Migration Test a) Test set up b) Split surface of the tested specimen c) Measurement of Chloride penetration depth

RESULT AND ANALYSIS

Compressive strength

Effect of internal curing under different adverse curing condition on compressive strength at the age of 28 day is illustrated in Fig.8. Control samples under normal curing condition (NC) showed maximum compressive strength of 40.5 MPa. On the other hand, CS under NC0W condition produced minimum strength of 27.3 MPa which is around 33% less than that of NC sample. All internally cured samples exhibited higher strength (ranged from 8% to 42%) as compared to NC0W samples. This clearly indicates the supremacy of IC concrete over CS under adverse condition. From Fig. 8 it is seen that internally cured samples with covering produced better concrete than without covering. Moreover, it is observed that internally cured samples with 7 days curing under water (IC7P and IC7W) and 28 days curing by wet gunny bags (IC28G) produced relatively better performed concrete as compared to IC concrete subjected to other adverse curing conditions. Those samples showed around 40% higher strength than that of NC0W sample.

Chloride Diffusion Coefficient

Chloride diffusion coefficient values obtained from the chloride migration experiment are showed in Fig. 9. It is observed that control sample under proper curing exhibited minimum chloride diffusion coefficient value of $15.66 \times 10^{-12} \text{ m}^2/\text{s}$. Such observation was expected since it showed the lowest depth of penetration. On the other hand, control sample under adverse curing condition of NC0W

exhibited the maximum coefficient value of $37.43 \times 10^{-12} \text{ m}^2/\text{s}$. All the internally cured samples showed around 15-50% reduced coefficient value than that of NC0W samples according to the adversity of the curing condition. It should be noted that IC concrete produced around 15% less diffusion value than control sample under the most adverse curing condition where samples were exposed outside without covering just after casting (IC0W and NC0W). This clearly demonstrates the positive impact of internal curing over normal concrete when exposed to adverse curing condition.

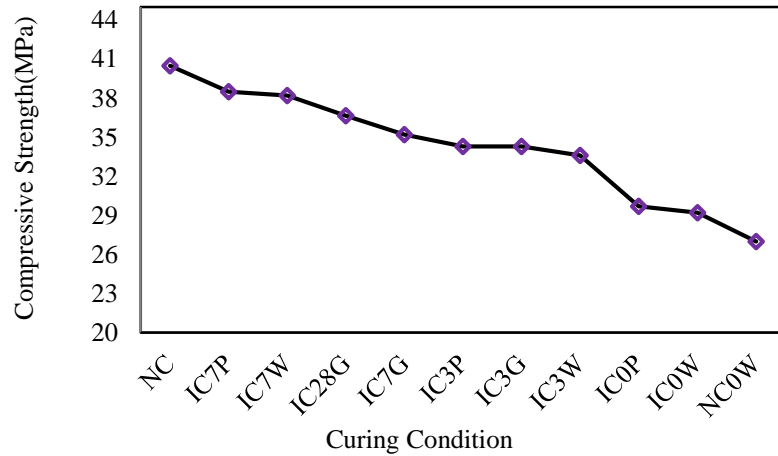


Fig.8 Effect of IC on the compressive strength of Concrete

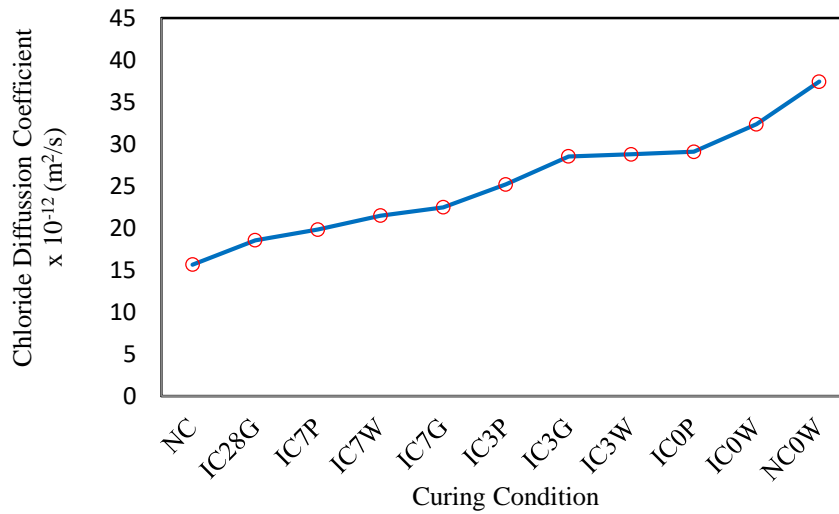


Fig. 9 Effect of internal curing on the chloride diffusion coefficient

The importance of curing on the chloride diffusion coefficient is clearly evident from Fig 9. Samples which were exposed to comparatively less adverse condition like IC7G, IC7W, IC7P and IC28G showed 40-50% lower diffusion values than NC0W. On the other hand, samples exposed to severe condition like IC0W, IC0P, IC3W, IC3G and IC3P showed around 15-30% lower value than control sample under NC0W condition. It is also quite evident that sample with covering (by both polythene and gunny bags) produced smaller value of chloride diffusion coefficient than that of sample without covering for all the adverse curing conditions.

CONCLUSION

This paper demonstrated the detrimental effects of adverse curing on chloride diffusion coefficient of concrete. The beneficiary aspect of using BC as internal curing under different simulated adverse

curing conditions is clearly evident from the study. The following conclusions can be drawn from the study performed:

- i. It is evident that internal curing with saturated BC under adverse curing condition can produce concrete with higher compressive strength as compared to conventional concrete with SC only.
- ii. The chloride diffusion coefficient of concrete can be significantly reduced through internal curing under harsh curing conditions.
- iii. It is also observed that covering of IC samples with polythene or gunny bags can improve the strength and durability in comparison with uncovered IC samples.
- iv. All IC samples exhibited significantly improved strength and diffusion coefficient properties as compared to control samples when subjected to most adverse curing condition of NC0W.

Therefore, it could be concluded that utilization of saturated BC as IC medium in concrete has immense potential to produce durable concrete in the absence of proper curing mechanism. The outcome of this paper will surely motivate the practicing engineers to explore the application of locally available brick chips as internal curing agent within concrete under adverse curing conditions.

ACKNOWLEDGEMENT

The authors of this paper sincerely acknowledge the assistance of personnel of the Concrete Laboratory of the Civil Engineering Department of Bangladesh University of Engineering and Technology for conducting the tests.

REFERENCES

- Afroz, S., Rahman, F., Iffat, S., and Manzur, T. 2015. Sorptivity and Strength Characteristics of Commonly Used Concrete Mixes of Bangladesh. *International Conference on Recent Innovation in Civil Engineering for Sustainable Development*, DUET, Gazipur, Bangladesh.
- Al-Gahtani, A. S. 2010. Effect of curing methods on the properties of plain and blended cement concretes. *Construction and Building Materials*, 24(3), 308-314.
- ASTM C39–14a. 2005. *Standard test method for compressive strength of cylindrical concrete specimens*. West Conshohocken, PA: ASTM International.
- Bentz, D. P., Lura, P., & Roberts, J. W. 2005. Mixture proportioning for internal curing. *National Institute of Standards and Technology, Concrete International*, 27(2), 35–40.
- Iffat, S., Manzur, T., Rahman, S., Noor, M. A., & Yazdani, N. 2017. Optimum Proportion of Masonry Chip Aggregate for Internally Cured Concrete. *International Journal of Concrete Structures and Materials*, 11(3), 513.
- Iffat, S., Manzur, T., & Noor, M. A. 2016. Durability performance of internally cured concrete using locally available low cost LWA. *KSCE Journal of Civil Engineering*, 21(4), 1256-1263.
- Manzur, T., Iffat, S., & Noor, M. A. 2015. Efficiency of sodium polyacrylate to improve durability of concrete under adverse curing condition. *Advances in Materials Science and Engineering*, Hindawi Publishing Corporation, Article ID: AMSE 685785.
- Manzur, T., Iffat, S., & Noor, M. A. 2015. Relation between properties of internally cured concrete and water cement ratio. *International Journal of Civil, Environmental, Structural, Construction and Architectural Engineering*, 9, 30326.
- Manzur, T. 2017. Adverse Curing Conditions and Performance of Concrete: Bangladesh Perspective. *World Academy of Science, Engineering and Technology, International Journal of Civil, Environmental, Structural, Construction and Architectural Engineering*, 11(4), 567-571.
- NT BUILD 492.1999. *Concrete, mortar and cement-based repair materials: Chloride migration coefficient from non-steady state migration experiments*. Nordtest, Espoo, Finland.
- Yang, C. C., & Wang, L. C. 2004. The diffusion characteristic of concrete with mineral admixtures between salt ponding test and accelerated chloride migration test. *Materials Chemistry and Physics*, 85(2-3), 266-272.
- Zhou, Y., Gencturk, B., Willam, K., & Attar, A. 2014. Carbonation-induced and chloride-induced corrosion in reinforced concrete structures. *Journal of Materials in Civil Engineering*, 27(9), 04014245.

SENSITIVITY ANALYSIS OF COST OPTIMIZED SOLUTION OF POST-TENSIONED PRE-STRESSED CONCRETE I-GIRDER BRIDGE SYSTEM

T. A. H. Nishat* & R. Ahsan

*Department of Civil Engineering, Bangladesh University of Engineering & Technology,
Dhaka, Bangladesh*

E-mail: tahsinbuet13@gmail.com

ABSTRACT

A new approach is presented for the sensitivity analyses of optimum design parameters of a post-tensioned pre-stressed concrete I-girder bridge system. The objective of this study is to determine the relative significance of each parameter of the I-girder bridge system optimized by “Evolutionary Operation Based Global Optimization Algorithm (EVOP)” for predicting structural adequacy as well as relative cost. This problem contains total 14 design variables along with 14 explicit constraints and 46 implicit constraints. To obtain the result, deviations of each of the 14 parameters on both the upper and lower sides of the optimum solution have been considered reflecting their realistic possible ranges of variation. In this process the remaining parameters have been held unchanged. For small fluctuations from the optimum design solution, compliance with the explicit and implicit constraints has been examined. Variation in the cost has also been estimated. Among 14 design parameters, deck slab thickness is found to be very sensitive for the 30m span bridge. It is observed that for only about 1 mm increase or 1mm decrease in slab thickness, structural adequacy of the bridge is affected. So the obtained result suggests that, for realistic design purpose, sensitivity analyses should be combined with optimum design methodology of a bridge system.

Keywords: Sensitivity analyses; optimum design; evolutionary operations; PC girder bridge.

1. INTRODUCTION

PC I-girder bridge system is an extensively used bridge system. During design procedure the bridge, structural adequacy and economy play the most important roles. A large number of design parameters are required while designing this type of concrete bridge. The parameters which are correlated with each other, lead to innumerable feasible designs of the bridge. Optimum design of bridge system is a significant design methodology which produces a cost effective solution ensuring structural safety. **Ghani (1989)** developed a global algorithm named EVOP (Evolutionary Operations) which can locate the global minima. The optimum method of design uses this algorithm to determine the optimum value of design parameters. Cost optimization for a post tensioned prestressed I-girder bridge system was done for bridge system with 14 design parameters (**Rana and Ahsan, 2010; Ahsan et al. 2012**). This optimization method gives the optimum solution for minimum cost of the bridge. Usually during design procedure, it is assumed that the optimum design parameters are kept unchanged at the time of construction. However, the optimum parameter values and assumptions derived from this method are subject to change due to constructional ease. Deviations in these parameters can affect structural adequacy. Therefore, sensitivity analyses should be combined with design methodology to determine the impact of design parameters.

Sensitivity analysis (SA) of any structure is the investigation of these potential changes of design parameters and their impacts on the structure. It allows the designers to assess the effects and sources of deviations during construction of any structure and facilitates structural modifications. The status of an optimum solution cannot be understood without such information. Over the years, sensitivity analysis is done for optimization problem in various discipline areas. **Seferlis and Hrymak (1996)** studied on sensitivity analysis for chemical process optimization. **Yue et al. (2008)** presented a sensitivity analysis and robust experimental design of a signal transduction pathway system. **Becker et al. (2011)** presented a Bayesian sensitivity analysis of a model of the aortic valve. **Chen and Yang (2017)** presented a sensitivity analysis and optimization of a typical passively designed residential building with hybrid ventilation in hot and humid climates. It can be recognized that there is a little research on combining sensitivity analysis and optimization in civil engineering field. Cost optimization method using EVOP for bridge structure is the most recent design method and sensitivity analysis for this type of method has not been attempted yet.

The main focus of the study is to analyze the sensitivity of 14 design parameters of pre-tensioned PC I-girder 30m span bridge in terms of structural safety and cost of bridge which was primarily optimized for minimum cost by “Evolutionary Operation Based Global Optimization Algorithm (EVOP)”. The focus is also to determine whether the structure is safe or not for small deviation of any parameter from optimum solution.

2. METHODOLOGY

In the present study a post-tensioned PC I-girder bridge system of 30m span is considered. The bridge system is simply supported and consists of cast-in place reinforced concrete deck with precast girders. A typical I-girder arrangement in the bridge is shown in [Fig. 1].

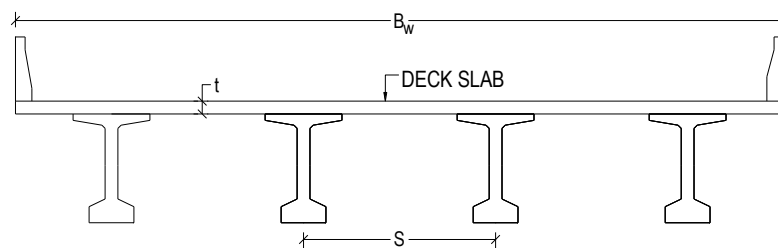


Figure 1: I-Girder arrangement in the bridge

The bridge system was primarily analysed for minimum cost for certain constant parameters using the computer program in C++ developed for minimum cost design of PC 30m span I-girder bridge system (**Rana and Ahsan 2010**). The optimization problem consists of 14 explicit and 46 implicit constraints with the objective function of cost minimization. The design parameters, explicit constraints and implicit constraints are tabulated in Table 1. By solving the problem, 14 optimum design parameters were obtained.

Finally sensitivity analyses were done on the obtained optimum solutions. The computer program, used for optimization, was modified to analyze the sensitivity of the design parameters. The design parameters used in optimization are considered as input parameters. For small deviation in input parameters (which reflect real life deflection) impacts on output parameters were investigated. The constraint parameter value and cost of bridge are considered as output parameters. The output contains the following information:

- If 14 explicit constraints are satisfied.
- If 46 implicit constraints are satisfied.
- The objective function value that is the total cost of the bridge.
- Value of any implicit constraint parameter.

After summarizing the results, whether the design is safe or not is determined. The main approach in the analysis is involves the following steps-

- a. Deviation of one input design variable at a time from its optimum value and assess the impacts.
- b. Repetition of this process for remaining parameters.
- c. Summarization of output results.

Table 1 Design parameters, explicit and implicit constraints

<i>Design parameters(14)</i>	<i>Explicit Constraints (14)</i>	<i>Implicit constraints (46)</i>
1. Girder spacing, S (mm)	$B_w/10 \leq S \leq B_w$	i. Flexural working stress constraint
2. Top flange width, TF_w (mm)	$300 \leq TF_w \leq S$	ii. Flexural ultimate strength constraints
3. Width of Bottom flange, BF_w (mm)	$300 \leq BF_w \leq S$	iii. Deck slab design constraint
4. Thickness of Bottom flange, BF_t (mm)	$a \leq BF_t \leq 600$	iv. Shear constraints (ultimate strength)
5. Depth of girder, G_d (mm)	$1000 \leq G_d \leq 3500$	v. Tendons eccentricity constraint
6. Number of strands per tendon, N_s	$1 \leq N_s \leq 27$	vi. Lateral stability constraint
7. Number of tendon per girder, N_T	$1 \leq N_T \leq 20$	vii. Deflection constraints
8. Lowest tendon position from bottom, y_l (mm)	$A_M \leq y_l \leq 1000$	viii. Ductility constraints
9. Prestress at initial stage, η (%)	$1\% \leq \eta \leq 100\%$	
10. Thickness of slab, t (mm)	$175 \leq t \leq 300$	
11. Main reinforcement ratio, ρ (%)	$\rho_{min} \leq \rho \leq \rho_{max}$	
12. Thickness of top flange, TF_t (mm)	$75 \leq TF_t \leq 300$	
13. Transition thickness of top flange, TFT_t (mm)	$50 \leq TFT_t \leq 300$	
14. Web thickness, W_w (mm)	$b \leq W_w \leq 300$	

a = sum of clear cover and duct diameter; b = sum of clear cover, web rebar diameter and duct diameter;
 A_M = Minimum vertical edge distance for anchorage

3. RESULTS AND DISCUSSIONS

Table 2 Cost Data Including Equipment and Labour

Cost Parameters	BDT
Cost of precast girder concrete (UP_{GC}) per m^3	12,500
Cost of girder formwork (UP_{GF}) per m^2	400
Cost of cast-in-place deck concrete (UP_{DC}) per m^3	6,000
Cost of deck formwork (UP_{DF}) per m^2	415
Cost of Girder post-tensioning tendon (UP_{PS}) per ton	90,000
Cost of anchorage set (UP_{ANC}) per set	4,500
Cost of metal sheath (UP_{SH}) per lin. meter	90
Cost of mild steel reinforcement (UP_{OS}) per ton	45,000

3.1. Optimization of the 30m span bridge

In this process 30m span bridge is designed for optimum cost. The cost data used in optimization are based on the data used for cost optimization for a post tension prestressed I-girder bridge system (**Rana and Ahsan 2010**). These data are listed in Table 2. For constant parameters listed in Table 3, the bridge is optimized and optimum parameter values are obtained. The optimum values the 14 design parameters and total cost of bridge are shown in Table 4. The cross section showing the values of design parameters of the bridge are given in [Fig. 2].

Table 3 Material Properties and Design Data

Material properties	$f_{pu} = 1861 \text{ MPa}$; $f_y = 410 \text{ MPa}$; $f_c = 40 \text{ MPa}$; $f_{cdeck} = 25 \text{ MPa}$ $f_{ci} = 30 \text{ MPa}$; $K = 0.005/\text{m}$; $\mu = 0.25$; $\delta = 6 \text{ mm}$;
Bridge design data	Girder Span = 30 m ($L = 29.25 \text{ m}$); Bridge Width, $B_w = 12.0 \text{ m}$ (3 Lane) Live Load= HS20-44 Diaphragm number = 2; Width of diaphragm = 250 mm; Wearing course thickness = 50 mm; Curb height = 600 mm; Curb width = 450 mm; 7 wire low-relaxation strand; Freyssinet anchorage system.

Table 4 Optimum Design Parameter Values and Variation Ranges for Sensitivity Analyses

<i>Design parameters</i>	Optimum Design	Variation Range for Sensitivity Analysis
1. Girder spacing, $S \text{ (mm)}$	4000	3975-4000
2. Top flange width, $TF_w \text{ (mm)}$	400	399-425
3. Bottom flange width, $BF_w \text{ (mm)}$	300	299-325
4. Bottom flange thickness, $BF_t \text{ (mm)}$	177	176-200
5. Girder depth $G_d \text{ (mm)}$	2000	1999-2025
6. Number of strands per tendon, N_s	8 (15.2mm dia)	7-9
7. Number of tendon per girder, N_T	4	3-5
8. Lowermost tendon position, $y_t \text{ (mm)}$	243	238-248
9. Initial stage prestress, $\eta \text{ (%)}$	29%	28.3-35
10. Slab thickness, $t \text{ (mm)}$	250	249-250
11. Slab main reinforcement ratio, $\rho \text{ (%)}$	0.633%	0.632-0.64
12. Top flange thickness, $TF_t \text{ (mm)}$	75	74-100
13. Top flange transition thickness, $TFT_t \text{ (mm)}$	50	49-75
14. Web thickness, $W_w \text{ (mm)}$	150	149-175
Objective function: Total cost of bridge (BDT)	2103960	

1.1. Sensitivity analyses of design parameters

In this process sensitivity of 14 design parameters is analysed in terms of design constraints and total cost of bridge. The variation ranges for this analysis are given in Table 4. Among the 14 parameters, if number of strand per tendon and number of tendons per girder are changed constraints are violated. Therefore further analyses are done for other 12 parameters.

1.1.1. Sensitivity with respect to design constraints

Sensitivity is analysed for both the explicit and implicit constraint parameters. There are total 14 explicit constraints and 46 implicit constraints for 30m span bridge system. Parameters are deviated from the optimum values. The results are summarized as follows-

- It is observed that the parameters are sensitive for some particular implicit constraints. Among 46 implicit constraints, bottom fiber stress at mid section at loading stage 4, effective depth are the most significant constraints for almost all the 14 parameters.

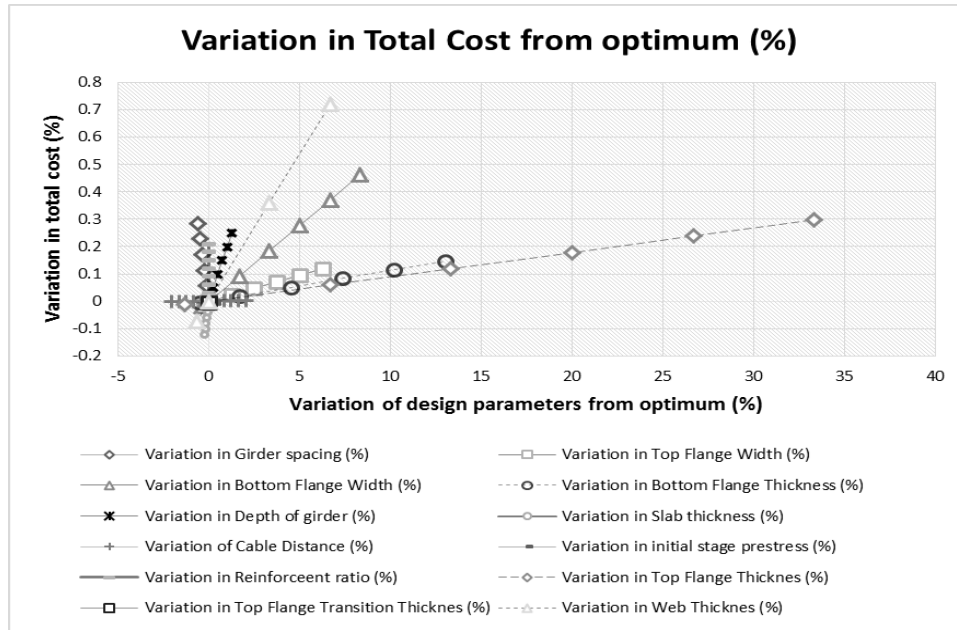


Figure 4 Sensitivity of 12 design parameters with respect to total cost of bridge

4. CONCLUSIONS

In this paper, sensitivity analysis is done for the cost optimized design of continuous PC girder bridge (30m span 3 lane) for a number of design variables required for the girders and the deck. Prior to that, cost optimized design of that bridge determined. To determine whether the cost optimized design is effective with regard to sensitivity of the design parameters, sensitivity analysis is done for the parameters for small deviations from the optimum. A modified C++ program is used for this analysis and output results are summarized. It has been found that slab thickness can be very sensitive for the optimum design solution since implicit constraints are violated for only 1mm increase or 1 mm decrease in the slab thickness. From further research it has been noted that slab thickness and reinforcement ratio are very sensitive with respect to total cost variation. Hence, it can be concluded that sensitivity can play a significant role in regard to structural safety. For this reason structural sensitivity analyses should be integral part in any of the design methodology.

5. REFERENCES

- Ahsan, R; Rana, S and Ghani SN. 2012. Cost optimum design of post-tensioned I-girder bridge using global optimization algorithm. *Journal of Structural Engineering. American Society of Civil Engineering*; 273-284.
- Becker, W; Rowson, J; Oakley, JE; Yoxall, A; Manson, G and Worden, K. 2011. Bayesian sensitivity analysis of a model of the aortic valve. *Journal of biomechanics*, 44(8), pp.1499-1506.
- Chen, X and Yang, H. 2017. Sensitivity analysis and optimization of a typical passively designed residential building with hybrid ventilation in hot and humid climates. *Energy Procedia*, 142, pp.1781-1786.
- Ghani SN. 1989. A versatile algorithm for optimization of a nonlinear nondifferentiable constrained objective function. *UKAEA Harwell report number R13714*. HMSO Publications Centre, PO Box 276, London SW85DT; ISBN: 0-7058-1566-8.
- Rana, S and Ahsan, R. 2010. Design of pre-stressed concrete I-girder bridge superstructure using optimization algorithm, *Journal of Bridge Engineering*
- Seferlis, P and Hrymak, AN. 1996. Sensitivity analysis for chemical process optimization. *Computers and Chemical Engineering*, 20(10), pp.1177-1200.
- Yue, H; Brown, M; He, F; Jia, J and Kell, DB. 2008. Sensitivity analysis and robust experimental design of a signal transduction pathway system. *International Journal of Chemical Kinetics*, 40(11), pp.730-741.

EFFICACY OF ORDINARY PLASTER TO INCREASE COMPRESSIVE STRENGTH OF BRICK MASONRY WALL

A. Mahmud¹, A. F. Mazumder^{2*}, M. T. Ahmad³ & S. A. Emon³

¹Bangladesh Water Development Board, Dhaka, Bangladesh.

E-mail: asifmahmud1348@gmail.com

²Department of Civil and Construction Engineering, Western Michigan University,
Michigan, USA.

E-mail: abul.f.mazumder@wmich.edu

³Department of Civil Engineering, Presidency University, Dhaka, Bangladesh.

E-mail: tanvir.ah248@gmail.com; emonsaha445@gmail.com

*Corresponding Author

ABSTRACT

Plaster is a mix of cement, sand, and water that is applied on the surface of masonry wall. The key purposes of providing plaster are to protect the masonry surfaces from moisture ingress, hide defective joints, and obtain a smooth and durable surface. Plaster also increases the axial capacity of the wall. Investigation of increase of axial capacity of masonry wall due to application of plaster is needed. Therefore, an experimental program is undertaken. The main objective of the work is to investigate the increase of axial load bearing capacity of a plastered masonry wall. Hence, six prisms ($234.95 \times 114.3 \times 63.5$ mm) are constructed. Three prisms are plastered on both sides with 12.5 mm thick plaster. The cement-sand ratio of the plaster is 1:2 and water-cement ratio is 0.6. All the prisms are tested under incrementally increased axial compressive load after 28 days curing period. The average compressive strength of the masonry wall without and with plaster is 3.48 and 4.23 MPa, respectively. Therefore, the 12.5 mm plaster could increase the axial capacity by 21.55% and the efficiency of the plaster is 25.28%.

Keywords: Brick; Masonry; Plaster.

INTRODUCTION

Masonry wall is one of the most popular and common type of structural component which is made from individual units laid in and bonded together using mortar. Aesthetic appearance, cost effectiveness, and ease of construction are main features of masonry wall. Thermal mass and fire protection of the building, reduced life cycle cost, and 30 to 100 times higher useful life cycle than structural steel are the key advantages of masonry wall (Wikipedia). Usually, masonry walls are used as partition wall, retaining wall, structural wall, and in heritage structures. The typical practice of using masonry walls as unreinforced. Portland cement mortar is used to plaster on both sides of unreinforced masonry wall (URM). Plaster is provided to protect the masonry wall surface from rough environmental exposure, to hide defective joints, to prevent moisture entrance, and to obtain clean, smooth, and durable surface. A 12.5 mm thick plaster is provided for inner surface and 18.75 mm plaster is provided for outer surface of the wall. This plaster makes the wall stronger, durable, and increases the load bearing capacity of the wall as well.

Unreinforced masonry (URM) walls are vulnerable to high axial and earthquake load. URM walls can be used as load-bearing wall, if proper strengthening materials are used. Some researchers used CFRP, GFRP sheet and bars, tensile reinforced mortar, ultra high performance concrete, and ordinary mortar

for strengthening (Basaran et al., 2013; Vasconcelos et al., 2012; Mahmood et al., 2008; ElGawady et al., 2006; Zhao et al., 2003; Mazumder, 2017; Mazumder et al., 2017) and found out axial capacity of masonry wall with and without strengthening techniques and schemes. Some researchers investigated the axial capacity of masonry wall using numerical simulations (Mazumder and Sarfin, 2017; Mazumder and Nishat, 2017). The axial capacity of the URM wall is also increased due to the application of plaster. Thus, an experimental study is needed to investigate the increase of compressive strength due to the application of plaster on the both sides of the wall. Therefore, a study is initiated. The main objective of this study is to investigate the increase of load bearing capacity of unreinforced masonry wall with the use of 12.5 mm thick plaster on both sides while keeping cement-sand ratio as 1:2 and water-cement ratio as 0.6.

METHODOLOGY

The load bearing capacity of unreinforced masonry wall prisms are evaluated using axial load tests. In this test, incrementally increased compressive load is applied to the prisms. Six specimens are tested in two categories – i) three unreinforced masonry prisms (UMP) and ii) three 12.5 mm thick plastered masonry prisms (PMP). The compressive strength of brick and mortar is also investigated. Six specimens are constructed and wet cured for 28 days. Specimens are tested under compressive load after curing period.

Material properties

Mechanical properties of wall components, brick and mortar, are investigated experimentally. Compressive strength of bricks is obtained following test procedure of Barbosa (2009). The average compressive strength of bricks is 6.61 MPa. The compressive strength of mortar is tested following ASTM C39. The 28-day compressive strength of mortar is 26.09 MPa. The water-cement and cement-sand ratio of mortar are 0.6 and 1:2, respectively.

Construction of prisms

Six prisms are constructed with bricks and Portland cement mortar is used as head and bed joints. The nominal size of a brick is $235 \times 110 \times 70$ mm, approximately. Three layers of bricks, containing one and a half bricks in each layer, are cast to form the prisms. 12.5 mm thick plaster is applied on the both sides of the three prisms. The aspect ratio for all walls is 0.9 and height to thickness of the wall is 2.10, approximately. After casting, specimens are wet cured for 28 days. After curing period, the specimens are tested.

Experimental setup, instrumentation, and procedure

According to ASTM C1314 and European Standard EN1052-1(1999), masonry prisms (UMP and PMP) are tested under uniaxial compressive load. To avoid eccentricity, the prisms are placed vertically and horizontally perfectly aligned on Universal Testing Machine (UTM). The axial compression forces are exerted on the prism through steel plate and rubber sandwich. The steel plate and rubber sandwiches are attached on the top and bottom of the prisms to ensure uniform distribution of the axial force without any stress localization. Fig. 1 shows the test setup for UMP and PMP.



a) Experimental setup of UMP



b) Experimental setup of PMP

Figure 1: Specimen and experimental setup

RESULTS

Six prisms are tested to evaluate compressive strength using UTM. An incrementally increased compressive load is applied on the prisms until failure. Table 1 shows the compressive strength of UMP prisms. The average compressive strength of UMP is 3.48 MPa. Compressive strength of each PMP is presented in Table 2. The average compressive strength of PMP is 4.23 MPa. The 12.5 mm plaster could successfully increase the compressive strength of UMP by 21.55%. The efficiency (η) of the plaster is found to be 25.28% as presented below.

$$\eta = \frac{(\text{Increase in compressive strength}) \times \text{Wall thickness}}{\text{Plaster thickness} \times \text{Compressive strength of mortar}} = \frac{(4.23 - 3.48) \times 111.67}{12.7 \times 26.09} \times 100 = 25.28\%$$

Table 1: Compressive strength of UMP

Serial no.	Dimension (L × B × H) (mm × mm × mm)	Load (kN)	Stress (MPa)	Average stress (MPa)
1	360 × 112.33 × 219	140	3.46	3.48
2	363 × 111 × 214.33	148	3.67	
3	365 × 111.67 × 219	135	3.31	

Table 2: Compressive strength of PMP

Serial no.	Dimension (L × B × H) (mm × mm × mm)	Load (kN)	Stress (MPa)	Average stress (MPa)
1	360 × 106.67 × 216.67	155	4.04	4.23
2	375 × 112.33 × 228	152	3.61	
3	369 × 110 × 218.33	205	5.05	

CONCLUSIONS

Ordinary Portland cement mortar is used to plaster the inner and outer surface of an unreinforced masonry wall. The main purpose of plastering is to protect the wall from deleterious moisture ingress and provide a smooth, clean, and durable surface. Plaster increases the axial capacity of the masonry wall. To evaluate the increase in axial capacity, six prisms are constructed and three of them are plastered. All the specimens are tested under compression in universal testing machine after 28 days wet curing period. The average compressive strength is 3.48 and 4.23 MPa for UMP and PMP prisms, respectively. Therefore, the axial capacity of masonry wall is increased by 21.55% approximately due to 12.5 mm plaster. The efficiency of the plaster is 25.28%.

ACKNOWLEDGEMENTS

The research work presented in the paper has been carried out at the Department of Civil Engineering, Presidency University (PU). The authors would like to thank PU authority for their continuous support.

REFERENCES

- Basaran, H; Demir, A and Bagci, M. 2013. The Behavior of Masonry Walls with Reinforced Plaster Mortar. *Advances in Material Science and Engineering*, 1-9.
- Barbosa, CS and Hanai, JB. 2009. Strength and Deformability of Hollow Concrete Blocks: Correlation of Block and Cylindrical Sample Test Results. *Ibracon Structures and Materials Journal*.
- ElGawady, MA; Lestuzzi, P and Badoux, M. 2006. A Seismic Retrofitting of unreinforced Masonry Walls Using FRP. *Science Direct, Composites: Part B (37)*: 148-162.
- Mahmood, H; Russell, AP and Ingham, JM. 2008. Monotonic Testing of Unreinforced and FRP-Retrofitted Masonry Walls Prone to Shear Failure in an Earthquake. *The 14th World Conference on Earthquake Engineering*, 214-220.
- Mazumder, AF and Sarfin, MAA. 2017. Numerical Investigation of Axial Capacity Assessment of UHPC Plastered Wall using ABAQUS. *Proceedings of the ICEIRE 2017*, 4: 45-48.

Mazumder, AF; Mahmud, A and Rafael, M. 2017. Investigation of the Contribution of the Plaster in Compressive Strength of Unreinforced Masonry Wall. *Proceedings of the ICEIRE 2017*, 4: 182-184.

Mazumder, AF. 2017. Axial Load Bearing Capacity of Unreinforced Concrete Masonry Wall and UHPC Block Wall. *Proceedings of the ICEIRE 2017*, 4: 25-28.

Mazumder, AF and Nishat, M. 2017. Numerical Investigation of Axial Capacity Assessment of UHPC Plastered Wall using ABAQUS. *Proceedings of the ICEIRE 2017*, 4: 33-36.

Vasconcelos, G; Abreu, S; Fanguero, R and Cunha, F. 2012. Retrofitting Masonry Infill Walls with Textile Reinforced Mortar. *15 WCEE, LISBOA*, 178-187.

Wikipedia. (Last visited May 2015)

Zhao, T; Xie, J and Li, H. 2003. Strengthening of Cracked Concrete Block Masonry Walls Using Continuous Carbon Fiber Sheet. *9th North American masonry conference, South Carolina, Clemson*, 9: 156-167.

DETERMINATION OF CHLORIDE ABSORPTION IN CONCRETE – AN ALTERNATIVE METHOD FOR ASSESSING THE DURABILITY OF CONCRETE IN LOW-BUDGET LABORATORIES

M. T. Islam*, M. A. Rahman & I. Ahmed

*Department of Civil Engineering, Bangladesh University of Engineering and Technology,
Dhaka, Bangladesh.*

E-mail: tariqulaunto.1993@gmail.com

**Corresponding Author*

ABSTRACT

Corrosion in concrete is an electro-chemical process that results in degradation of embedded steel as a consequence of reaction with environment. In coastal regions corrosion of rebar in concrete is largely associated to a degree of presence of chloride ion that is in contact with concrete. The amount of chloride ion in concrete is important as chloride ion plays a significant role in depletion of passive layer of rebar and in promoting corrosion of rebar in concrete in presence of moisture and oxygen. This procedure involves direct measuring of chloride ion concentration in curing water at 1st, 3rd, 7th, 14th and 28th days of curing period where concrete cube samples were submerged in a container for curing and chloride concentration of that curing water was measured. The curing water was 3.5% (by weight) sodium chloride solution which simulates the saline condition of coastal area. The test was conducted on concrete samples prepared from both OPC and PCC. The depletion of amount of chloride ion in the curing water will be the measure of absorbed chloride ion by concrete which may be used to interpret the corrosion rate of embedded steel as an alternate to Rapid Chloride Permeability Test (RCPT).

Keywords: Corrosion; Durability; Absorption; Chloride Ion; Curing;

INTRODUCTION

Concrete is the mostly used construction material all over the world (Islam et al., 2018). Concrete envelops the reinforcing bars which plays an important role in carrying the design loads. Concrete durability is referred to its ability to resist physical and chemical deterioration caused by interaction with the surrounding environment or by interaction between the constituents. When concrete is exposed to harsh environment like high salinity of coastal areas, it becomes susceptible to ingress of chloride ion. Despite having several benefits, reinforcing bars lack resistance against chloride induced corrosion and is vulnerable to degradation. The overall capacity of structure depends on the strength of the individual components of that structure (Rahman et al., 2017). Thus corrosion of the rebar results in reduction of service life of the structure. The durability of concrete structures depends on the surrounding environment and on the nature of the concrete construction (Iffat et al., 2014). Rapid Chloride Permeability Test (RCPT) was developed in FHWA research program (Iffat et al., 2014). The programme was aimed at developing techniques to measure the chloride permeability of concrete. The process of performing RCPT is specified in AASHTO T122 and ASTM C1202. There are instruments available in the market for performing RCPT but they are quite expensive. This situation has asked for an attempt to build a low cost experimental setup that will provide us an indication about the chloride absorption rate for various mixes of concrete which might help us to interpret the corrosion rate of the embedded steel similar to RCPT but with minimum possible costs.

METHODOLOGY

The test scheme included casting of total 8 numbers of 4 inch x 4 inch x 4 inch concrete cubes. Among them 4 cubes were cast with 3.5% (by weight) saline water and 4 cubes were cast with fresh water. Moreover, 4 of them were made by using OPC cement and 4 of them were made with PCC cement. The mix ratio for 1m³ concrete for all of the cubes are given below:

Cement = 402 kg

Stone Chips = 1119.8 kg

Sylhet Sand = 602.5 kg

Water = 160.8 kg

The details of the test scheme are presented in Table-1

Table 1: Details of the Cubes Tested

Designation		Cement Type	Casting Water	Curing Water
FSOC1	FSO	OPC	Fresh water	Saline Water
FSOC2		OPC	Fresh water	Saline Water
FSPC1	FSP	PCC	Fresh water	Saline Water
FSPC2		PCC	Fresh water	Saline Water
SSOC1	SSO	OPC	Saline Water	Saline Water
SSOC2		OPC	Saline Water	Saline Water
SSPC1	SSP	PCC	Saline Water	Saline Water
SSPC2		PCC	Saline Water	Saline Water

*First letter describes casting water, Second letter describes the curing water, third letter describes the cement type and fourth letter is for cube samples. Here, F=Fresh Water, S= Saline Water, O= OPC, P= PCC, C=Cube Sample

Here, four samples were both cast and cured with saline water in order to simulate the worst possible case where there is extreme scarcity of fresh water and there is no other alternative but to use saline water for casing and curing process.

Experimental Setup

After casting, the concrete cubes were placed on plastic containers and they were submerged under 3.5% (by weight) saline water shown in Fig. 1 which simulates the saline condition of the coastal areas (Rashid et al., 2013).



Fig. 1: Process of Curing

Titration

Chloride ion concentration of the curing water was evaluated by direct titration method using standard silver nitrate solution (0.0141 N) and potassium chromate as an indicator on the 1st, 3rd, 7th, 14th and 28th day of curing period. Chloride ion concentration of the curing water was determined using Eq. (1).

$$\text{Chloride Ion, Cl}^- (\text{mg/L}) = (\text{mL of AgNO}_3 \text{ used}) \times (\text{Multiplying Factor}) \quad (1)$$

Multiplying Factor = (Normality of AgNO₃) x (Equivalent weight of Cl⁻) x 1000 / (mL of sample taken)

With the progression of time the chloride ions were absorbed by the concrete cubes as a result there were a decline in the concentration of the chloride ion in the curing water. Thus the decline in the concentration of the chloride ion is equal to the absorption of chloride ion by cubes.

RESULTS AND DISCUSSIONS

The data obtained from the test are presented on Table 2 and in Fig. 2. From the result we can see that cubes made with PCC cement and casted with fresh water absorbed least amount of chloride ion and cubes made with OPC cement and casted with saline water absorbed the most amount of chloride ion.

Table 2: Chloride Ion Absorbed by Concrete

Designation	Chloride Ion Absorbed by Concrete (mg / sq.inch)				
	Day-1	Day-3	Day-7	Day-14	Day-28
FSO	0	136.7	195.3	204.2	252.7
FSP	0	130.2	148.7	154.4	196.3
SSO	0	138.4	206.5	284.2	484.9
SSP	0	134.8	184.9	243.8	402

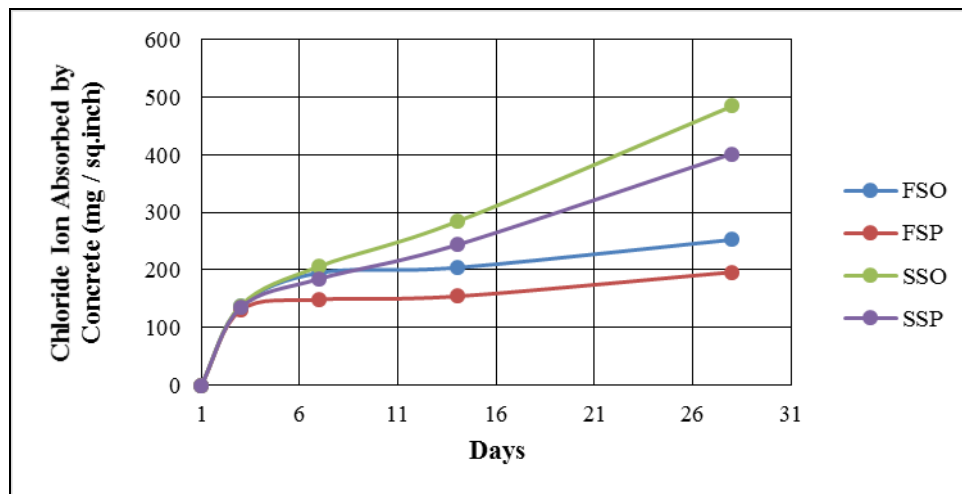


Fig. 2: Chloride Absorbed by Concrete for various mixes.

According to Faradays law, the amount of any substance deposited or liberated during electrolysis is proportional to the quantity of electric charge passed and to the equivalent weight of the substance

$$W=ZQ \quad (2)$$

Where, W= Weight of Substance

Z= Constant of proportionality called electrochemical equivalent

Q= Quantity of charged passed

In case of RCPT, charged is passed from one surface of a 4 inch diameter cylindrical disk. If we convert the value of charge described in AASHTO T277 and ASTM C1202 for the interpretation of RCPT results, then using Eq. (2) we can find the weight of chloride ion for that amount of passed charge and can compute the weight of chloride ion passing through per square inch of the surface of the 4 inch diameter cylindrical disk. Details are described in Table 3.

Table 3: Conversion of Charge to Weight Using Faraday Formulae

Charge Passed (Coulombs)	Weight of Chloride Ion per Area (mg/sq.inch)
>4000	>117.2
2000-4000	58.6-117.2
1000-2000	29.3-58.6
100-1000	2.93-29.3
<100	< 2.93

Using similar mix ratio as described earlier the average total charge passed through the concrete specimens were found to be 4719.5 coulomb in RCPT test for PCC cement (Iffat et al., 2014). If we convert this value by using Eq. 2 we found weight of chloride per area to be 138.2 mg/sq. inch. In our case we found this value to be 196.3 mg/sq.inch which is very close. The depth of chloride ion penetration was obtained on the 80th day by spraying AgNO₃ solution to the cross section which is presented in Table 4 and Fig. 3. From all of these data we can see that this concrete cubes will not be durable in marine conditions. Besides, RCPT and titration method give almost similar results.

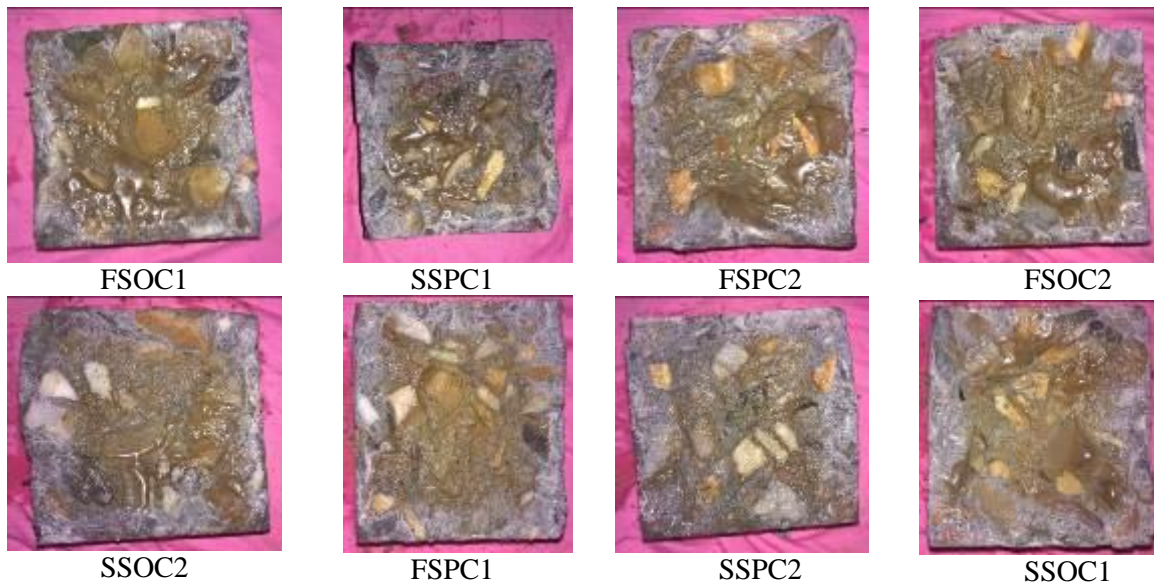


Fig. 3: Chloride Ion Penetration Depth on 80th Day

Here, the white portion of the above pictures denotes the chloride ion penetration in concrete cubes. Concrete is not a uniform material in nature and so the chloride penetration depth is also not uniform throughout the section. Therefore, the average depth of chloride ion penetration was evaluated by taking average of more than 16 data per cube.

Table 4: Average Chloride Ion Penetration Depth on 80th Day

Designation	Average Chloride Ion Penetration (mm)
FSO	13
FSP	10
SSO	15
SSP	14

Comparison of Cost

Total cost for the whole test procedure was less than 1000 BDT (12.5 USD). Whereas, the total cost for RCPT setup with locally available materials is 30,000 BDT (375 USD) (Iffat et al., 2014). Moreover, there are some ready apparatus available in the market for RCPT test which costs are more than 4000 USD. This comparison clearly shows how economically feasible this method can be.

CONCLUSIONS

The experimental setup requires less than 5% of the cost required to perform RCPT. Moreover, the test can be performed wherever there is facility for performing titration with ordinary apparatus. Comparing with the results of RCPT in literature (Iffat et al., 2014), it can be concluded that this method will provide reasonably good results if conducted properly. Concretes exposed to saline environment are highly subjected to chloride induced rebar corrosions. By performing this test, the probability of corrosion can be predicted at nominal cost. This method can become popular in construction sites of developing country like Bangladesh.

ACKNOWLEDGMENTS

The authors pay their profound thanks to Environment Engineering Laboratory, Concrete Laboratory, Inorganic Chemistry Laboratory, Department of Chemistry and Department of Civil Engineering, Bangladesh University of Engineering and Technology (BUET) for their assistance in this research work.

REFERENCES

- Iffat, S; Emon, AB; Manzur, T. and Ahmed, ST. 2014. An experiment on Durability Test (RCPT) of Concrete According to ASTM Standard Method using Low-Cost Equipments. *Advance Material Research.*, 974 (2014):335-340.
- Rahman, MA. and Begum, M. 2017. Comparative Study of RCC and Steel Framed Building Using Pushover Analysis. *International Conference on Disaster Risk mitigation.*
- Rahman, MA; Islam, MT. and Ahmed, I. 2018. Use of High Strength Concrete in Columns of RCC Building for Cost Effectiveness and Sustainability. *1st National Conference on Water Resources Engineering.*
- Rashid, T; Hoque, S. and Akter, F. 2013. Ocean Acidification in the Bay of Bengal. *Open Access Scientific Reports.*
- Understanding AASHTO T277 and ASTM C1202 Rapid Chloride Permeability Test: *Technical Bulletin TB 0100 (Concrete).*

PERFORMANCE OF PARTIALLY REPLACED PLASTIC PARTICLE AS COARSE AGGREGATE IN PRODUCING CONCRETE

M.S. Islam^{1*}, M.H.R. Himon², M.M. Hossain² & M.A. Islam²

¹*Department of Civil Engineering, Tennessee Tech University, USA
Email: mislam46@students.tntech.edu*

²*Department of Civil Engineering, World University of Bangladesh, Dhanmondi, Dhaka - 1205, Bangladesh.*

**Corresponding author*

ABSTRACT

Waste plastic has now been an important issue due to its non-biodegradable properties for all developing countries especially in Bangladesh. The amount is also growing at a fast rate day by day. So it has now become the most challenging concern in the recent times for environmental wellbeing. In the present study, waste PET which is a polymer compound of Polyethylene Terephthalate has been selected as the aggregate for partial replacement of coarse aggregate in producing concrete in the construction industry. The plastic particle obtained from PET bottle has been replaced 5% by volume of stone as well as brick aggregate in the concrete. After finding the data from all tests performed in the laboratory, results are compared among 4 types of concrete. However, water cement ratio is 0.40 for all cases having the same gradation of coarse aggregate, fine aggregate and cement content. Concrete cylinder having the diameter of 100 mm and height of 200 mm has been made for testing of compressive strength, splitting tensile strength and stress-strain diagram for 28 days. Beam specimen of dimensions 125mm X 125 mm X 600 mm is also made to understand the behaviour of flexural strength. In addition to that pull test out has been conducted to determine the shear strength of concrete. Research results show the prospect of using 5% plastic particles as the replacement of conventional aggregates in the concrete in order to save the green environment.

Keywords: Plastic waste; PET bottle; Compressive strength; Tensile strength; Bond strength; Flexural strength.

INTRODUCTION

Following a normal growth of population in Bangladesh, the amounts of plastic waste materials are also growing at a faster rate. Plastics have become an intimate and inseparable part of our lives. At present, there are a large number of plastic industries, are producing plastics in Bangladesh in order to make life easier. The factors behind the growth of plastic are low density, user-friendly designs, fabrication capabilities, long life, light weight, as well as low cost (Habib et al., 2017). In Bangladesh, due to the rapid increase in the use of plastic materials, a new problem is raised i.e. solid waste disposal problem. It needs a long time even more than a hundred years to degrade the waste plastics in the soil (Haque, 2015). In Dhaka, the capital of Bangladesh, around 3400 tons of solid waste is generated every day, of which 4.15% was composed of plastic materials during 2005 and 5.46% during 2014 (Haque 2015). These reports indicate that plastic waste generation rises at the rate of 10.43% per year in the amount of plastic waste (Rahman et al., 2012; Waste concern, 2016). Land filling is also not feasible with such waste plastic due to large area is needed moreover; it will lose the fertility of valuable lands as well as clogging in the drainage systems. So, plastic waste has now been

a serious environmental issue. On the other hand, Uses of concrete in the world are increasing day by day. As reported by Robinson et al. (2004), and Mehta (2009), concrete consumption in the world is estimated to 17.5 billion tons for 7 billion populations in the world. To make this huge amount of concrete, huge amount of coarse and fine aggregates are needed. The availability of coarse aggregates in Bangladesh has also become a serious issue in the recent years. In Bangladesh, around 147 tons plastic waste is generated every day and most of the volume is Polyethylene Terephthalate (PET) coming from different sizes and shapes of plastic bottles, toys, furniture and so on (Habib et al., 2017). If waste plastic is used as the partial replacement of coarse aggregate for new constructions, it will save huge amount of natural resources as well as the cost for new materials. Moreover, the disposal problem of waste plastic material will be solved (Himon et al., 2018; Youcef et al., 2009). So, using waste plastic as the partial replacement of coarse aggregate has been now an interesting solution in order to shorten the consumption of natural coarse aggregates and preservation of energy. The main objectives of this study are to identify the physical and mechanical properties of concrete made of partially replaced plastic particles as well as make comparison with fresh aggregate concrete and finally, to find out the potentialities of using plastic particles as the partial substitution of fresh coarse aggregate in producing concrete.

METHODOLOGY

Materials

In the present study, two types of coarse aggregate i.e. stone aggregate and crushed clay brick aggregate have been used. Besides, locally available Sylhet sand as fine aggregate and Portland composite cement (CEM II/B-M) have been used as the binding material.

Plastic particles as coarse aggregate (pp)

Plastic particles have been used as the partial replacement of coarse aggregate in the current study. Collected PET bottle were cut into pieces manually to have a size of 19 mm downgraded as shown in Fig. 1. The plastic particles were then sieved to control a standard grading as per ASTM C33-93.



Fig. 1: Plastic particles cut down from PET bottles

Fineness modulus of the plastic particle was obtained 6.35 in the laboratory and shown in Fig. 2. The unit weight and void content are calculated according to the ASTM standard requirements of specification C29. Rodding method is used to calculate the unit weight. Specific gravity and absorption capacity of the plastic particle are also determined according to the ASTM standard requirements of specification C127. Table 1 presents the physical properties of all materials.

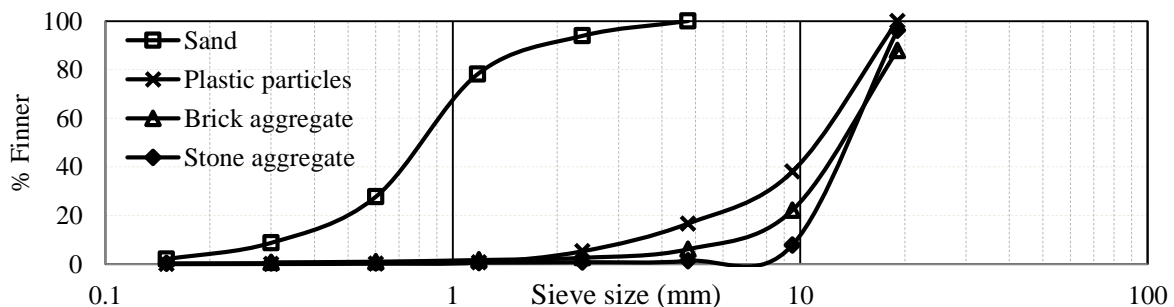


Fig. 2: Gradation curve of all materials

Coarse aggregate (CA) and Fine aggregates (FA)

Stone chips and Crushed brick is commonly used in Bangladesh as coarse aggregate. In the present study both types of coarse aggregates as well as sand found in Sylhet district in Bangladesh called Sylhet sand as fine aggregate have been used. The size of the collected coarse aggregate was 19 mm downgraded. The aggregates were then sieved to control a standard grading according to standard ASTM C33-93. The unit weight and void content, specific gravity were calculated according to the ASTM specification C29 and C27 respectively for all types of aggregates. Table 1 shows the physical properties of all types' aggregates that have been tested in the laboratory.

Table 1: Properties of all materials

Types of aggregates	Fineness Modulus (FM)	Unit Weight (Kg/m ³)	% Voids	Bulk Specific Gravity (SSD)	Bulk Specific Gravity (OD)	Apparent Specific Gravity (OD)	Absorption Capacity %
Plastic Chips	6.35	245	83.04	1.33	1.30	1.34	0.98
Stone chips	6.91	1623	38.25	2.66	2.64	2.70	1.23
Brick chips	6.76	1644	17.0	1.97	1.68	2.38	17.42
Fine aggregates	2.89	1674	33.81	2.54	2.47	2.64	2.63

Cement & Water

Portland composite cement (CEM II/B-M) has been collected from the local market in Dhaka city and its initial setting time and final setting time is determined according to the ASTM standard C191. In the present study, the used cement contains 70-79% clinker, 21-25% fly ash, slag, limestone and 0-5% gypsum. However, potable water is used in all cases for the casting of concrete.

Mixture proportion

In the present study, total 4 types of concrete have been produced. i.e. Brick aggregate concrete (BAC), Brick aggregate concrete made with partially replaced plastic particles (BACPP), Stone aggregate concrete (SAC), as well as Stone aggregate concrete made with partially replaced plastic particles (SACPP). The mixture proportions have been summarized in the Table 2. Water to cement ratio (w/c) of concrete is 0.44 for all cases and no admixtures are used. Sand to total aggregate volume ratio (s/a) is 0.44. However, 5% plastic particles have been replaced with the weight of coarse aggregate.

Table 2: Weight based mix proportion for 1 m³ of concrete

SL No.	Types of concrete	Cement (kg/m ³)	Brick Aggregates (kg/m ³)	Stone Aggregates (kg/m ³)	Plastic Particles (kg/m ³)	Sand (Kg/m ³)	Water (kg/m ³)
1.	BAC	400	818.5	-	0.0	489.5	489.5
2.	SAC	400	-	1083.5	0.0	689.5	689.5
3.	BACPP	400	778.4	-	40.1	489.5	489.5
4.	SACPP	400	-	1029.3	54.2	689.5	689.5

Sample preparation, Mixing, Casting, and Curing of Concrete

Fig. 3 shows the details of sample preparation, mixing, casting and curing of concrete. However, concrete cylinder with a dimension of 100 mm in dia and 200 mm in height has been made as specimen for determining the results of compressive strength, tensile strength as well as stress-strain pattern.



(a) (b) (c) (d)

Fig. 3: Preparation of sample (a) Preparation of mold (b) Concrete casting (c) Slump test (d) Concrete curing
 For bond strength of concrete, pull-out test has been conducted with 10 mm bar diameter. For flexural strength of concrete, 150 mmX150mmX600mm beams have been made as specimen. Here, 10 mm bar is used as main bar and 8 mm bar is used as tie bar having 100 mm spacing. An automated mixture machine has been used for mixing of concrete. Trial mix has been prepared for every case as mentioned earlier before the final mixing is done. In this study, under water curing method is applied with normal tap water to ensure adequate moisture and temperature as requirements of specification by ASTM C192/C192M-02.

2.7 Experimental test setup

Details investigation has been carried out to determine the mechanical properties of fresh and partially replaced plastic aggregate concrete. Experimental setup has been conducted for obtaining the results from compressive strength test, splitting tensile strength test, stress-strain behaviour, bond strength test, shear strength test as well as flexure strength test for 28 days. Compressive strength of concrete has been measured by using Universal Testing Machine (UTM) of 800 kN with a rate of loading controller as shown in Fig. 4(a). Compressive strength of the cylinder is determined as per ASTM C3 9M-03. Tensile strength of concrete is determined as per ASTM C496M-04 as shown in Fig. 4(b). In this study, a strain gauge is used having the gauge length of 75 mm to measure the strain of specimen under a uniform loading rate. In the present study, in order to determine the bond strength from pull out test a special arrangement is arranged with the UTM as per the instruction of ASTM C900. Here, a hollow steel ram is also used at the lower portion of the steel bar which is embedded into the concrete cylinder as shown in Fig. 4(c). Fig. 4(d) shows the flexural strength test by 3rd point loading setup.

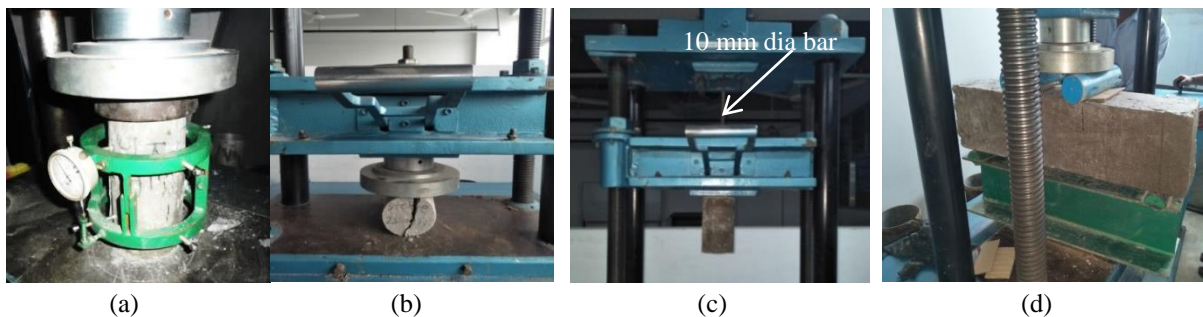


Fig. 4: Experimental setup (a) Compressive strength setup (b) Splitting tensile strength setup (c) Pull-out test setup (d) Flexural strength test setup

Here, the bonding depth is 200 mm with 10 mm dia steel bar. To measure the shear strength as well as flexure strength of beam, a 3rd point loading arrangement has been conducted as shown in Fig. 5. In this method, loading rate is controlled by using controlling regulator. The load is applied at a very slow rate and an initial load of about 10 kN is applied and then slowly increased until failure.

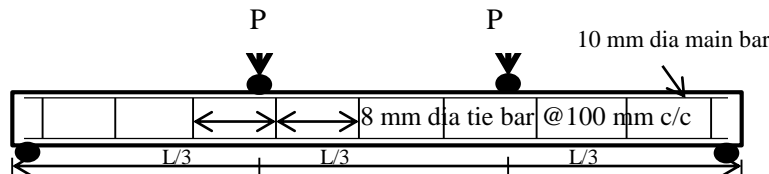


Fig. 5: Schematic diagram of third Point loading for flexural strength test

RESULTS AND DISCUSSIONS

In the present study, fresh and mechanical properties of hardened concrete have been determined to understand the behaviour of partially replaced plastic particles in producing concrete.

Compressive and Splitting Tensile Strength of concrete

Workability of fresh concrete has been decrease with the partial replacement of plastic particles as shown in Fig. 6. The result of using plastic particles on compressive & tensile strength of concrete is

tested at 28 days as shown in Figs. 7 and 8 respectively. No significant downfall is observed in compressive and tensile strength. A value of around 10% decrease in 28 days for both compressive and tensile strength is found for brick aggregate concrete made of partially replaced plastic particles (BACPP) compared to the concrete made of fresh brick aggregate (BAC). Similar trend is also found for SACPP compared to SAC.

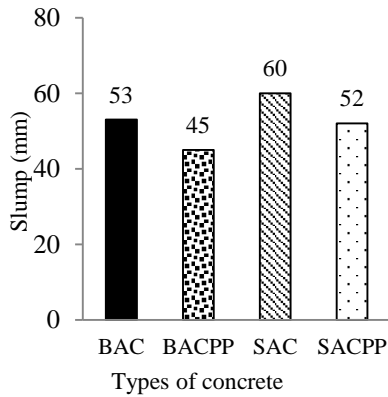


Fig. 6: Workability of concrete

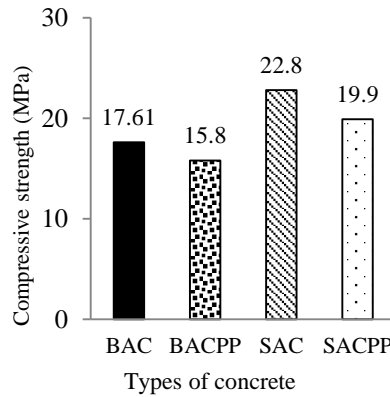


Fig. 7: Compressive strength

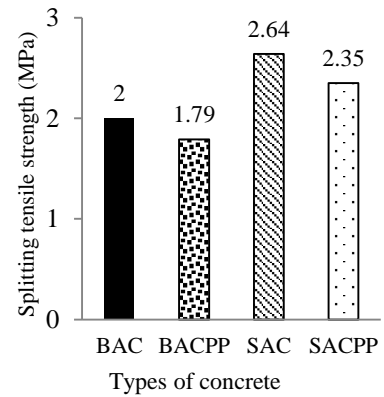


Fig. 8: Splitting tensile strength

Stress-Strain pattern and Modulus of elasticity of Concrete

Effect of partial replacement of plastic aggregate on the behaviour of stress-strain and modulus of elasticity of concrete made of both brick chips and stone chips are observed for 28 days and presented in Figs. 9 and 10 respectively. It is shown that rupture strain limit of BACPP and SACPP is 10 to 15 % lower than that of fresh brick and stone aggregate concrete. For modulus of elasticity, around 15-20% value is found lower for BACPP and SACPP compared to BAC and SAC.

Bonding and Shear Strength of Concrete

In all cases, it is seen that the concrete made of partially replaced plastic aggregate i.e. BACPP and SACPP is around 10 to 15% downfall compared to BAC and SACPP respectively as presented in Fig. 11 for bonding strength and Fig. 12 for shear resistance.

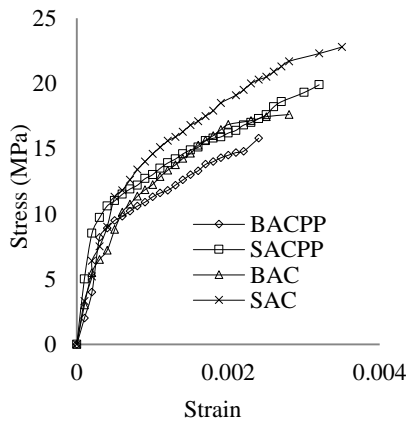


Fig. 9: Stress-Strain pattern

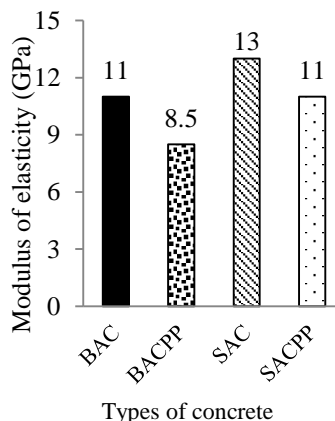


Fig. 10: Modulus of elasticity

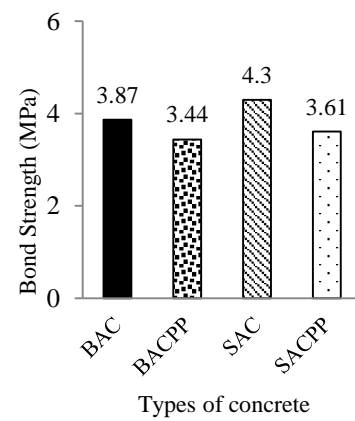


Fig. 11: Bond strength

Flexural Strength of and maximum midspan Deflection of Concrete Beam

Figs. 13 and 14 show the flexural strength of beam as well as the maximum deflection during testing at 28 days. Around 10-15% downfall in 28 days flexure strength is observed for both BACPP and SACPP compared to BAC and SAC. However, maximum mid span deflection is 12.5 mm for BACPP.

Fractured surface of the specimen

Fig. 15 shows the fractured surfaces of compressive strength test, tensile strength test, bond strength and flexural strength test. Failure mode of concrete cylinder for both compressive and tensile strength

is relatively brittle for BACPP and SACPP. In case of bond strength test by pull-out method both slip and grip failure is observed. However, in the flexural strength test of beam, shear failure is seen at an angle of about 45 degree.

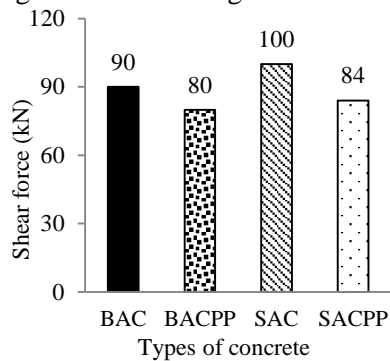


Fig. 12: Shear resistance

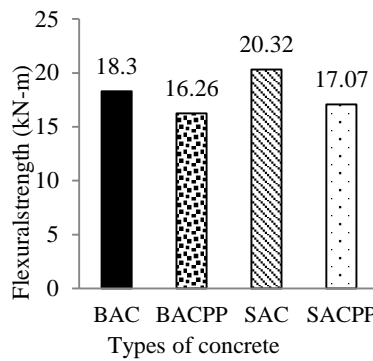


Fig. 13: Flexural strength

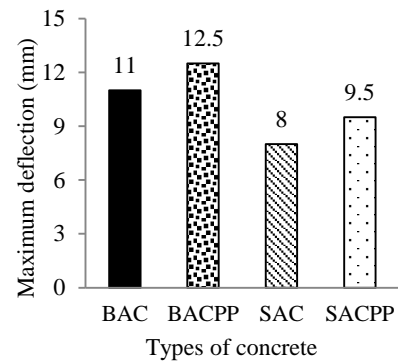


Fig. 14: Maximum deflection



Fig. 15: Fractured surface of all specimens tested in laboratory

CONCLUSIONS

The main conclusions that can be drawn from this experimental study are stated as below:

- 1) Around 10% to 12% decrease is found in 28 days compressive as well as splitting tensile strength of concrete made with partially replaced plastic particle compared to fresh aggregate concrete.
- 2) Rupture strain limit decreased around 10%-15% for partially replaced plastic aggregate concrete compared to fresh aggregate concrete. Similar trend is found for modulus of elasticity of concrete.
- 3) About 10%-15% downfall is found in 28 days shear strength as well as flexural strength of concrete made with partially plastic particle.
- 4) Around 15% more deflection is observed for partially replaced plastic aggregate concrete compared to fresh aggregate concrete. However, more brittle failure is seen for partially replaced plastic aggregate concrete due to less bonding among the aggregates.

ACKNOWLEDGMENTS

The authors are thankful to all lab technician/assistants of Civil Engineering Department, World University of Bangladesh (WUB), for their all sorts of assistance during the experimental study.

REFERENCES

- Habib Z. M, Alom M.M and Hoque M.M. 2017, Concrete production using recycled waste plastic as aggregate. *Journal of Civil Engineering (IEB)*, 45(1): 11-17.
- Haque M. A. T. 2015. Environmental challenges of plastics waste in Bangladesh, [online] available at <http://www.mpma.org.my/Documents/Bangladesh.pdf>. [Accessed 18 November 2018].
- Himon M.H.R., Hossain M.M., Islam M.A. 2018. *Behavior of partially mixed plastic particle as coarse aggregate*. B.Sc. thesis, Dept. of Civil Engineering, World University of Bangladesh.
- Mehta, P. K., 2009. Global Concrete Industry Sustainability”, *ACI Concrete International*, 45-48.
- Rahman, M., Islam, A., Ahmed, M. and Salam, A. 2012. Recycled polymer materials as aggregates for concrete and blocks. *Journal of Chemical Engineering, (IEB)*, 27(1): 53-57.
- Robinson Jr., G.R., Menzie, W.D., and Hyun, H. 2004. Recycling of construction debris as aggregate in the Mid-Atlantic Region. *Conservation and Recycling, USA Resources*, 24. 275-294.

Waste Concern Consultant, 2006. Report on composition of plastic waste and market assessment of the plastic recycling sector in Dhaka city. 1-79.

Youcef, G., Bahia, R., Brahim, S. and Rabah, C. 2009. Use of recycled plastic bag waste in the concrete. *Journal of International Scientific Publications*. 8(1): 480–487.

NUMERICAL SOLUTION OF ONE-DIMENSIONAL WAVE EQUATION BY FINITE DIFFERENCE METHOD

M. A. Islam^{1*}, N. A. Khan² & A. Rashid³

^{1,2}*Department of Mathematics, Uttara University, Dhaka-1230, Bangladesh.*

E-mail: amirul.math@gmail.com

³*Department of Mathematics, Jahangirnagar University, Dhaka-1342, Bangladesh.*

**Corresponding author*

ABSTRACT

In this article, we analyze a numerical algorithm for solving one-dimensional wave equation. The finite difference scheme is used for solving numerically the wave equation of second order partial differential equations. The proposed FDM is quite efficient for solving this type of linear second order partial differential equation (PDE). We examine approximate solution of wave equation with the analytic solution. The approximate solution using proposed FDM is satisfactory with the analytic solution. Finally we investigate numerical solution of proposed finite difference scheme for different space step size and time step size. Two examples are shown to verify the applicability and competency of the finite difference method.

Keywords: finite difference scheme, wave equation, application examples, etc.

INTRODUCTION

The finite-difference scheme is mainly used for finding approximate solution of the real life engineering problems. Finite difference scheme is the advanced numerical method. In technology, engineering and science fields finite difference technique is highly demand for solving second order partial differential equations. In many situations, findings an analytic solution to wave equation of second order partial differential equations (PDE) is impossible, where numerical method are applied to get computation solutions. In real world, most of the problems in science, engineering and technology are most complicated to find analytic solution. Then numerical method is applied to find approximate solution of the required problems. The wave equation is widely used in fields such as fluid dynamics, biomedical imaging, electromagnetics and acoustics. The wave equation of linear partial differential equation (PDE) is an important second order differential equation (DE), which is an extremely important evolution model in describing the propagation of water waves, electromagnetic waves, seismic waves, gravity waves, lights waves, sound waves, and oscillatory waves. Feng and Li (2013) discussed the stability of a one dimensional wave equation of partial differential equation. Wazwaz (1998) presented decomposition method to solve one-dimensional wave equation. Chun et al. (2009) discussed homotopy perturbation method for solving different type of partial differential equations. Szyszka (2017) presented finite difference method to solve one-dimensional wave equation. He (2005) discussed solution procedure of partial differential equations (PDE) applying homotopy perturbation method. Abbasbandy (2008) analyzed a numerical method to solve different type of partial differential equations. Noor and Mohyud-Din (2008) discussed solution of nonlinear higher-order boundary value problems using variational iteration method. Han *et al.* (2005) proposed a finite-difference method for

solving Schrödinger equation of one-dimensional. In this paper, we have applied developed finite difference method to solve wave equation of second order linear partial differential equation.

FINITE DIFFERENCE SCHEME

In this research, we consider wave equation of linear partial differential equation (PDE) with initial boundary conditions (IBC). Finite difference method (FDM) is a powerful numerical method to obtain computational solution of differential equation on the basis of mathematical discretization. The finite difference schemes are derived from truncated the Taylor's series method in which partial differential equation(PDE) and initial- boundary conditions are replaced by a set of algebraic equations. Finite difference method is also used to find approximate solution of the partial differential equations of engineering problems such as heat transfer problems, fluid dynamics problem, etc. The main purpose of this work is to find close approximate solutions of an initial boundary value problem for equation (1.1) using FDM. To explain the finite difference technique, we consider the general form of one dimensional wave equation defined by:

$$\frac{\partial^2 u}{\partial t^2} = a^2 \frac{\partial^2 u}{\partial x^2} \quad (1.1)$$

The given differential equation can be described as

$$a^2 u_{xx} - u_{tt} = 0 \quad (1.2)$$

with initial and boundary conditions (IBC):

$$\left. \begin{aligned} u(0,t) = 0, u(m,t) = 0; 0 < x < m \\ u(x,0) = f(x), u_t(x,0) = 0; t > 0 \end{aligned} \right\} \quad (1.3)$$

The central finite difference in space and time approximations of second derivatives are given by

$$\frac{\partial^2 u}{\partial x^2} \approx \frac{u(i+1, j) - 2u(i, j) + u(i-1, j)}{h^2} + O(h^2) \quad (1.4)$$

$$\frac{\partial^2 u}{\partial t^2} \approx \frac{u(i, j+1) - 2u(i, j) + u(i, j-1)}{k^2} + O(k^2) \quad (1.5)$$

Substituting (1.4) and (1.5) in (1.1) we get the following equation

$$\frac{u(i+1, j) - 2u(i, j) + u(i-1, j)}{h^2} = a^2 \frac{u(i, j+1) - 2u(i, j) + u(i, j-1)}{k^2} \quad (1.6)$$

$$\begin{aligned} u(i+1, j) - 2u(i, j) + u(i-1, j) &= \frac{a^2 h^2}{k^2} u(i, j+1) - 2u(i, j) + u(i, j-1) \\ \Rightarrow u(i, j+1) &= \delta^2 u(i+1, j) + 2(1 - \delta^2)u(i, j) + \delta^2 u(i-1, j) - u(i, j-1) \end{aligned} \quad (1.7)$$

where, $\delta = \frac{a\Delta t}{\Delta x} = \frac{ak}{h}$ is known as a Courant number and equation (1.7) is called the finite difference scheme for wave equation.

NUMERICAL SOLUTION PROCEDURE

Finite Difference Method (FDM) is the most important numerical method used to solve practical engineering problems where there exist a different type boundary conditions and shapes in the defined region of partial differential equations (PDE). The finite difference approximations to partial derivatives at a point (x_i, t_j) are described as : The xy -plane is divided into a network of rectangles of length $\Delta x = h$ and breadth $\Delta t = k$ by drawing the lines $x_i = i\Delta x = ih$ and $t_j = j\Delta t = jk$ parallel to x and y axes. The points of intersection of these lines are called grid points or mesh points or lattice points. The grid point (x_i, t_j) are denoted by $u(i, j)$. The approximate value of $u(i, j)$ can be

obtained by using equation (1.7) for all values of i and j . In this finite difference scheme has truncation error of spatial order $O((\Delta x)^2) = O(h^2)$ and temporal order $O((\Delta t)^2) = O(k^2)$.

APPLICATION EXAMPLES

In this section, we consider two examples of wave equations to verify accuracy of the proposed finite difference method (FDM). Numerical results are obtained and the approximate results of solution are described by graphically in figures 1(a)-1(d) & 2(a)-2(d).

Example 1: we consider one-dimensional wave equation, $\frac{\partial^2 u}{\partial t^2} = 16 \frac{\partial^2 u}{\partial x^2}$ with initial and boundary conditions (IBC): $u(x,0) = 6 \sin \pi x - 3 \sin 4\pi x, u(0,t) = 0, u(2,t) = 0, u_x(x,0) = 0; 0 < x < 2, t > 0$.

The exact solution is given by $u(x,t) = 6 \sin(\pi x) \cos(4\pi t) - 3 \sin 4\pi x \cos 16\pi t$ and shown in figure 1(a) and also approximate results are obtained using proposed finite difference method (FDM) and the graphs of the numerical solutions of wave equation are shown graphically in figures 1(b)-1(d).

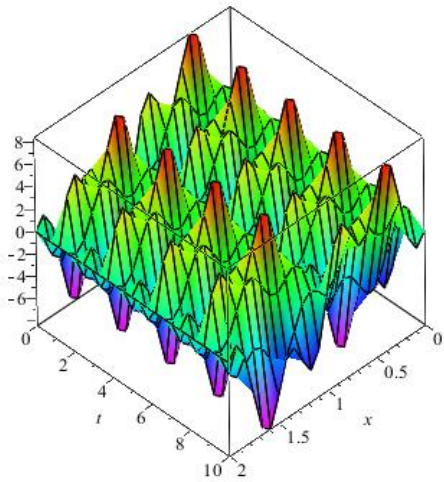


Fig1(a): Exact solution $u(x,t)$ for different values of x and t .

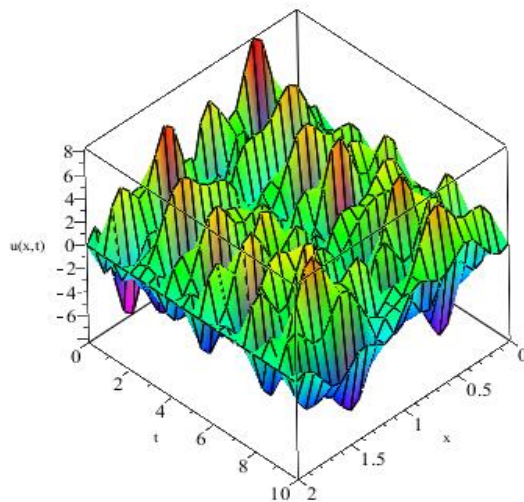


Fig1 (b): Approximate solution $u(x,t)$ for space step, $h=0.10$ and time step, $k=0.10$.

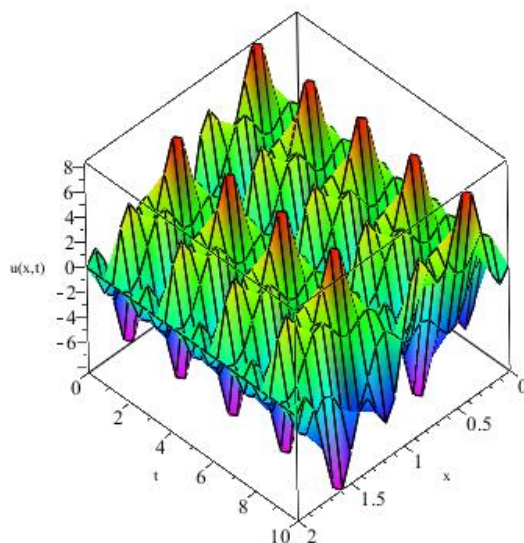
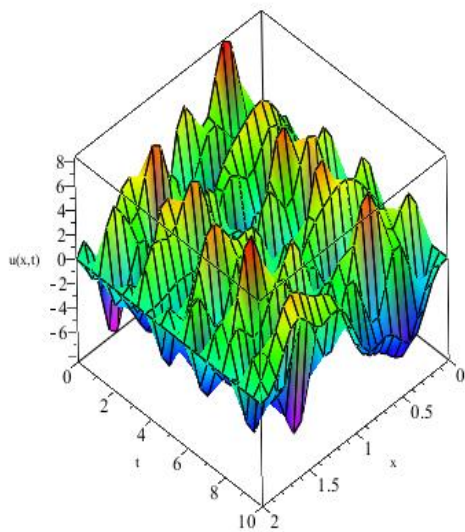


Fig1 (c): Approximate solution $u(x,t)$ for space step $h=0.05$ and time step, $k=0.05$.

Fig1 (d): Approximate solution $u(x,t)$ for space step $h=0.001$ and time step, $k=0.001$.

Example 2: we consider one-dimensional wave equation, $\frac{\partial^2 u}{\partial t^2} = 4 \frac{\partial^2 u}{\partial x^2}$ with initial and boundary conditions (IBC): $u(x,0) = \sin 4x, u(0,t) = 0, u(\pi,t) = 0, u_t(x,0) = 0; 0 < x < \pi, t > 0$.

The exact solution is given by $u(x,t) = \sin(4x) \cos(8t)$ and shown in figure 2(a) and also approximate results are obtained using proposed finite difference method (FDM) and the graphs of the approximate solutions of the wave equation are shown graphically in figures 2(b)-2(d).

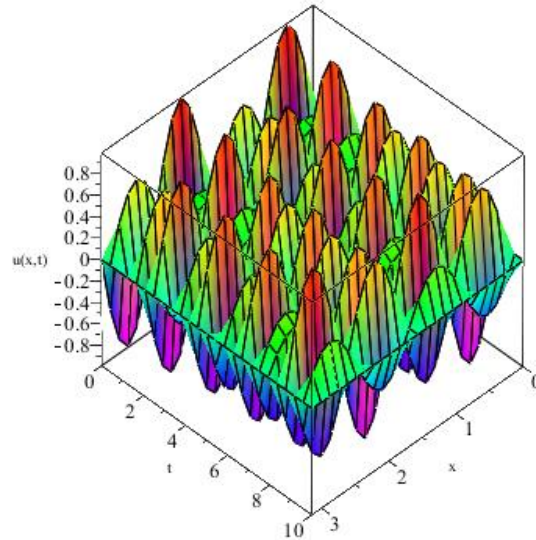
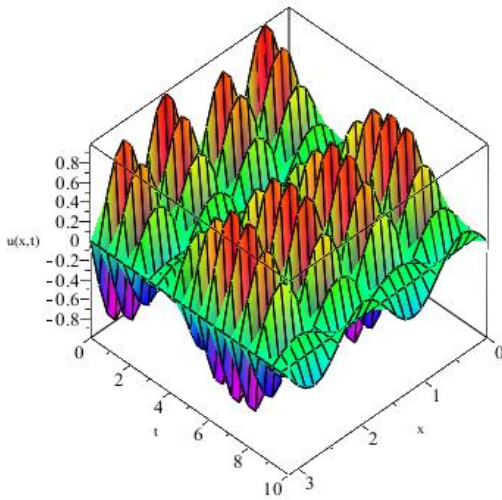


Fig2(a): Exact solution $u(x,t)$ for different values of x and t .

Fig2 (b): Approximate solution $u(x,t)$ for space step, $h=0.25$ and time step, $k=0.25$.

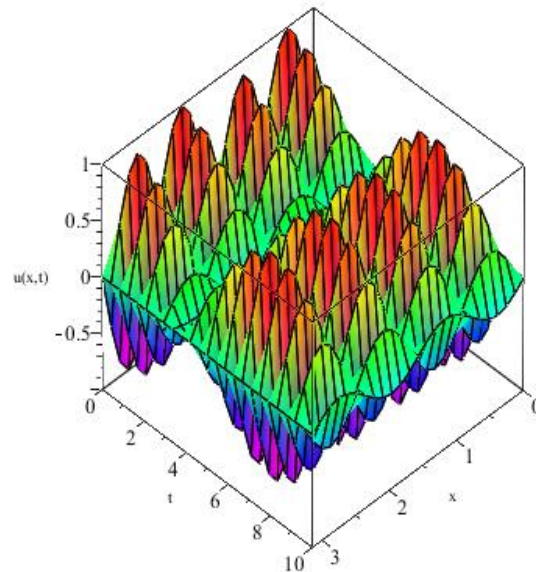
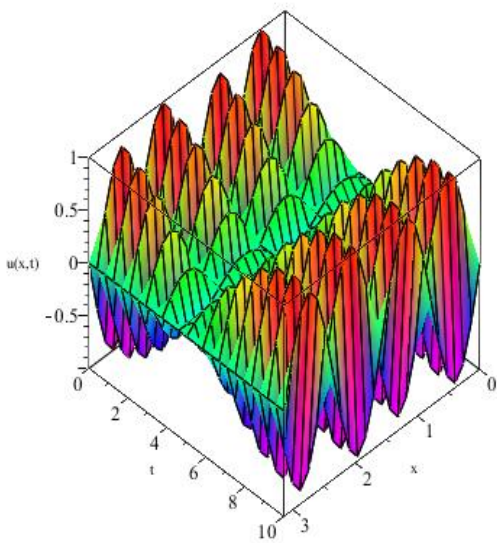


Fig2 (c): Approximate solution $u(x,t)$ for space

Fig2 (d): Approximate solution $u(x,t)$ for space step

step $h=0.05$ and time step, $k=0.05$.

$h=0.01$ and time step, $k=0.01$.

DUSCUSSION OF RESULTS

Accuracy of the solution will depend on step size, h and k . In order to compare the approximate solution with the exact solution we consider two numerical examples. The effect of the space step h and time step k in the solution is shown in all figures: 1(b)-1(d) and figures: 2(b)-2(d). To obtain more accurate results, h should be small and k is necessarily very small. A numerical method is said to be convergent if $|U(x_n, t_n) - u(x_n, t_n)| = 0$ for $h \rightarrow 0, k \rightarrow 0$. Where $U(x_n, t_n)$ denotes the exact solution and $u(x_n, t_n)$ denotes the approximate solution. The approximated solution is evaluated by using Maple software for proposed numerical method at different step sizes. Finally we observe that the proposed finite difference method (FDM) is converging faster if $\Delta x = h \rightarrow 0$ and $\Delta t = k \rightarrow 0$ and it is the more reliable method for finding the approximate solution of wave equation of initial boundary value problems for partial differential equations (PDE).

CONCLUSION

In this paper, we have applied the finite difference algorithm to develop numerical solution scheme for the wave equation. We present two numerical tests to show the convergence and efficiency of the proposed numerical method. To find more accurate results to need the space step size and time step size smaller for this proposed method. From the figures we can easily see that the accuracy of the solution of the problem is depending on the pace step size h and time step size k . The graph of the approximate solution approaches to the graph of the exact solution when $\Delta x = h \rightarrow 0$ and $\Delta t = k \rightarrow 0$. The computational solutions attained by the proposed finite difference method are in good agreement of the results with exact solutions. By the proposed method obtained result are generally more accurate and also the approximate solution converged faster to the exact solution.

ACKNOWLEDGEMENTS

The authors would like to express their sincere thanks to the referees for their valuable suggestions to enrich the quality of the paper. We would also like to show our gratitude to the Professor Dr. Moqbul Hossain and Dr. Shahansha Khan for their encouraging our research work.

REFERENCES

- Feng, H. and Li, S., 2013, "The stability for a one-dimensional wave equation with nonlinear uncertainty on the boundary", *Nonlinear Analysis*, 89, 202-207.
- Wazwaz, A.M., 1998 "A reliable technique for solving the wave equation in an infinite one-dimensional medium", *Appl. Math & Comp.*, 92(1), 1-7.
- Chun, C., Jafari, H. and Kim, Y., 2009, "Numerical method for the wave and nonlinear diffusion equations with the homotopy perturbation method", *Computers and Mathematics with Applications*, 57, 1226-1231.
- Szyszkla, B., 2017, "A nine-point finite difference scheme for one-dimensional wave equation", *AIP Conference Proceedings*, 1863(1), 56-78.
- J.H. He, 2005, "Application of homotopy perturbation method to nonlinear wave equations", *Chaos Solitons Fractals*, 26 (3), 695-700
- S. Abbasbandy, 2008, "Numerical method for non-linear wave and diffusion equations by the variational iteration method", *Int. J. Numer. Mech. Engrg.*, 73 (12), 1836-1843
- Noor, M.A., Mohyud-Din, S.T., 2008, "Variational iteration method for solving higher-order nonlinear boundary value problems using He's polynomials", *Int. J. Nonlinear Sci. Numer. Simul.*, 9 (2), 141-156.

Han, H., Jin, J., Wu, X., 2005, "A Finite-Difference Method for the One-Dimensional Time-Dependent Schrödinger Equation on Unbounded Domain", *Comp. & Math. with Appl.*, 50 ,1345-1362.

CHLORIDE DIFFUSION COEFFICIENTS OF SOME COMMON CONCRETE MIXES OF BANGLADESH

N. Mashrur*, N. A. Shishir¹, M. W. Islam², Z. H. Sehab³, M. J. Hasan⁴ & T. Manzur⁵

*Department of Civil Engineering, Bangladesh University of Engineering & Technology,
Dhaka-1000, Bangladesh*

E-mail: naqib.mashrur@gmail.com

**Corresponding Author*

ABSTRACT

Predicting service life is an essential aspect of long-term sustainability of any reinforced concrete (RC) infrastructure in a marine environment. The service life of RC is primarily affected by chloride induced corrosion of embedded reinforcement and the consequent degradation of concrete. One of the major factors that have a pronounced effect on the degree of chloride induced corrosion is the chloride diffusion coefficient of concrete which represents the ability of concrete to resist chloride penetration. The chloride diffusion coefficients for concrete with different types of cement are available in few codes and literature. Those values could be used for predicting service life for similar concrete structure. However, diffusion coefficient largely depends on concrete mix proportions, local construction practice and materials. Therefore, it is of immense importance to evaluate the diffusion coefficient of various local mixes for predicting the service life of concrete infrastructure of Bangladesh. This prompted an investigation of the diffusion coefficients of some common concrete mixes of Bangladesh. Rapid Migration Test (RMT) has been used to achieve this end. The code NT BUILD 492 has been followed to perform the non-steady state migration test. The coefficients thus determined demonstrate that cement mixes using PCC cement are superior to their OPC counterparts in terms of durability. Similarly mixes prepared with stone aggregates show better resistance to chloride diffusion than those prepared with brick aggregate.

Keywords: service life; sustainability; chloride diffusion coefficient; non-steady state migration test; durability.

INTRODUCTION

Concrete, in recent times, has emerged as a popular construction material as it is an economical, relatively durable and most importantly, an inert material. The constituents of the concrete themselves are often less affected by or in some cases, immune to the degrading impacts of a harsh surrounding. However, the steel rebar, often used to reinforce concrete elements, are highly reactive to such a harsh exposure and eventually, play a part in reducing serviceability of a RC element. One of the most noteworthy factors that is responsible for service life reduction of a RC element can be said to be chloride induced corrosion (Manzur et al., 2018; Baten et al., 2016; Maaddawy and Shoudki, 2003). In the southern region of Bangladesh, the salinity in groundwater is constantly growing and as per a study by Mott McDonald (2016), nearly 32% of the total area was found to be affected. Thus, effects of chloride ingress on durability aspect of a structure need to be considered while designing an RC structure, situated at or near coastal areas. The reactions among the constituents of concrete, create a high pH environment within the material (Moreno et al., 2004). This encourages

the development of a passive layer of oxide that surrounds and protects the embedded bar from corrosion (Verma et al., 2014). However, this is only possible by ensuring proper quality control while construction which is, often, neglected in our country (Afroz et al., 2015). Hence, results in permeable concrete. In addition, some mixes are inherently more permeable than others due to their mix constituents. In such cases of permeable concrete, chloride ions penetrate up to the passive layer around embedded reinforcement, reduce the pH level and stimulate the rust formation at a rate three orders of the magnitude faster (Portland Cement Association, 2002). The degree to which a particular mix of concrete is susceptible to the ingress of chloride ions depends, primarily, on the mix quality and can be expressed in terms of migration or diffusion coefficient values (NT BUILD 492, 1999). This paper focuses on studying the resistance to corrosion susceptibility of concrete mixes, prepared using commonly used and locally available aggregates (brick and stone) and cement types (Ordinary Portland Cement or OPC and Portland Composite Cement or PCC). The mixes were prepared following local mix practices and the water-cement ratios were also selected so as to reflect the contemporary practices of Bangladesh. Thereafter, the mixes were tested for chloride migration as per the specifications of NT BUILD 492 (1999). The test yields the depth of chloride penetration for a particular mix from which the degree of resistance of a particular mix can be determined. Based on the obtained values, the effects of aggregate and cement type variation were evaluated and presented in this paper. This comparative analysis can be hoped to give the field engineer a basic idea regarding selection of proper material for durable RC structure.

METHODOLOGY

Experimental Plan

The Rapid Migration Test is a method that uses an electric potential to accelerate the flow of chloride ion through concrete and a colorimetric indicator - in this case AgNO_3 - to measure the depth of penetration. This experiment prepares 9 different mixes of concrete; 3 variations of water-cement ratios using OPC cement and brick aggregate; 3 variations of water-cement ratios using PCC cement and stone aggregate and 3 more variations of water-cement ratio using PCC cement and brick aggregate. Compressive strength values were taken at 28 days. The RMT experiment was run after 45 days of casting the concrete.

Experimental setup

The experimental setup was prepared as per the specifications of NT Build 492. Rubber sleeve: with inner diameter 100mm and outer diameter 115 mm, of about 150 mm height were made for the experiment. The catholyte reservoir was a glass box having the dimensions of 370mm by 270mm by 280mm. Glass supports that would have a top surface bent at an angle of 32° were used as a stand for the specimen to be placed upon. The cathode was a stainless steel plate of 0.5 mm thick attached to the support with a rod attached for connection to the electric power source. The anode was a stainless steel mesh of 0.5 mm thick; it also had a rod attached for connection to the power source. A power source capable of supplying up to 30V DC voltage was used. Fig. 1 shows a complete experimental setup.

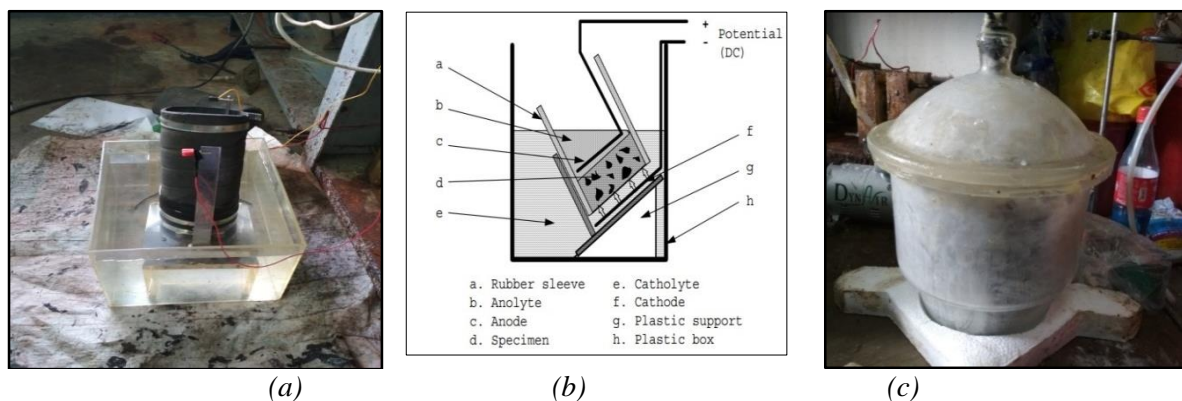


Fig. 1: a) and b) RMT Setup and c) Preconditioning of Concrete Slice

Preparation of specimen

Cylinders measuring 100mm in diameter and 200mm in height were produced for each concrete mix. After the concrete had set and hardened, one cylinder of every mix variation was cut into 3 sample specimen of 50 mm height each with the excess from each end being discarded. The middle piece of each set was used for the migration test run. Once the pieces were cut, they were washed off and the excess water was wiped off to make them surface dry. The curved faces of the specimen were coated with paint.

Preconditioning

Before the tests are run, it was required that the specimen be preconditioned by subjecting it to pressures and environments as specified by NT Build 492. This was done in order to simulate the worst case scenario for the concrete. First, the specimens were put inside a desiccator outfitted with a vacuum pump capable of reducing the pressure inside the desiccator chamber to 1kPa. The specimen was sealed inside the desiccator in an airtight manner and the pressure was brought down to 1-5kPa. This low pressure condition was maintained for 3 hours. At the end of the 3 hour period, saturated $\text{Ca}(\text{OH})_2$ was introduced into the chamber, completely immersing the specimen. The pressure was left at 1-5kPa after which the specimen was allowed to rest at atmospheric pressure for another 18 ± 2 hours.

Materials

Ordinary Portland Cement (OPC) and Portland Composite Cement (PCC) were the binding agents used for this study. Locally sourced stone and brick chips (3/4 inch downgrade) were used as coarse aggregates. The catholyte solution was prepared by mixing 100g NaCl in 900g tap water. The anolyte solution was prepared with 12g NaOH pellets dissolved in 1L distilled water (0.3N NaOH solution). Saturated $\text{Ca}(\text{OH})_2$ solution was for preconditioning and 0.1M AgNO_3 solution was used for chloride penetration depth measurement.

Test procedure

The catholyte reservoir was filled with the NaCl solution. The specimen was fitted into the rubber sleeve and secured with clamps. This was subsequently placed on a plastic dais within a tank containing the catholyte solution. The interior of the sleeve was fed with 300mL of the anolyte solution - up to 2/3 of the height of the sleeve. The electrodes were connected to their respective terminals and the electric switch was flipped. Initially the voltage was set to 30V. The initial current as well as the initial temperature of the anolyte solution was recorded. The voltage was adjusted according to the Table1 of NT Build 492. The new voltages and currents were also recorded. Current was run through the specimen for 24 hours after which the final current and temperatures were recorded and the power supply was turned off. The specimen was disassembled from the setup, washed with tap water and any excess water was wiped off to make it surface dry. The specimen was split axially into 2 pieces, taken to a dark room and the split surface of one of the pieces was sprayed with 0.1M AgNO_3 solution. Once the white precipitate had formed and was discernible, the depth of penetration was measured using a ruler upto a precision of 0.1mm. At least 7 readings were taken at 0.1mm intervals disregarding 0.1mm at the edges. Any place where the penetration front is blocked by an aggregate is also discarded.

The non-steady state chloride migration coefficient was calculated using Eq.(1). (NT Build 492, 1999)

$$D_{rcm} = \frac{0.239(273+T)L}{(U-2)t} (x_d - 0.0238 \sqrt{\frac{(273+T)Lx_d}{U-2}}) \quad (1)$$

Where,

D_{nssm} : non-steady-state migration coefficient, $\times 10^{-12}$, m^2/s ;

U: absolute value of the applied voltage, V;

T: average value of the initial and final temperatures in the anolyte solution, $^{\circ}\text{C}$;

L: thickness of the specimen, mm;

x_d : average value of the penetration depths, mm.

RESULTS AND DISCUSSIONS

The chloride diffusion coefficients calculated using Eq. (1) is shown in the Table 1 below along with the respective average compressive strengths of the concrete mixes.

Table 1: Experimental data summary

Cement Type	CA Type	W/C Ratio	Compressive Strength, psi	Chloride Diffusion Coefficient $\times 10^{-12}$, m ² /s
PCC	Stone	0.42	5880	11.9
	Stone	0.45	4880	15.7
	Stone	0.48	4520	17.5
OPC	Brick	0.42	3950	24.3
	Brick	0.48	3410	25.0
	Brick	0.5	2790	27.0
PCC	Brick	0.42	3860	20.1
	Brick	0.45	3610	21.7
	Brick	0.5	2570	24.0

From diffusion coefficient it is seen that the mix utilizing PCC as its cement type and stone as the coarse aggregate has the most satisfactory performance. An elementary idea of the resistance to chloride penetration of the mixes can be gathered from existing literature (Zych, T. 2014). It is ascertained that only the PCC stone mixes with w/c ratio below 0.45 are in the acceptable range while all other types are unacceptable.

Fig. 2 shows the variation of chloride diffusion coefficient for non-steady state migration against compressive strength (psi) for the OPC brick and PCC brick mixes. It is construed that there exists a linear correlation between strength and chloride diffusion rates; the diffusion coefficient changes inversely with strength. Comparison between OPC and PCC shows that PCC performs better in case of durability since for same strength OPC has higher diffusion coefficient than PCC. This can be accounted for by the fact that the fly ash (silica) in PCC cement reacts with calcium hydroxide to form more C-S-H gel at later ages and eventually refines pore distribution (Rumman, et al., 2015). This finding is momentous as it means locally produced PCC cements are better from a durability standpoint.

Fig. 3 displays the diffusion coefficient plotted against compressive strength of the PCC stone and brick mixes. When compared, it was observed that concrete using stone aggregates performed considerably better than those using brick. The least value of the coefficient for the brick samples is 20.1 whilst the worst one for stone samples is 17.5, meaning even the worst stone samples are better than the best brick ones. Bricks being more porous would allow for easier passage of chloride ions to it, jeopardizing the durability of the concrete (Amin and Choudhury, 2015).

Fig. 4 portrays the diffusion coefficient against water-cement ratio, juxtaposing the PCC stone mixes against the PCC brick mixes. It is observed that with the increase in w/c ratio, the value of the coefficient also seems to increase indicating the durability of concrete diminishes for higher water content mixes. The stone mix also shows greater resistance to ingress compared to the brick ones as was previously stated.

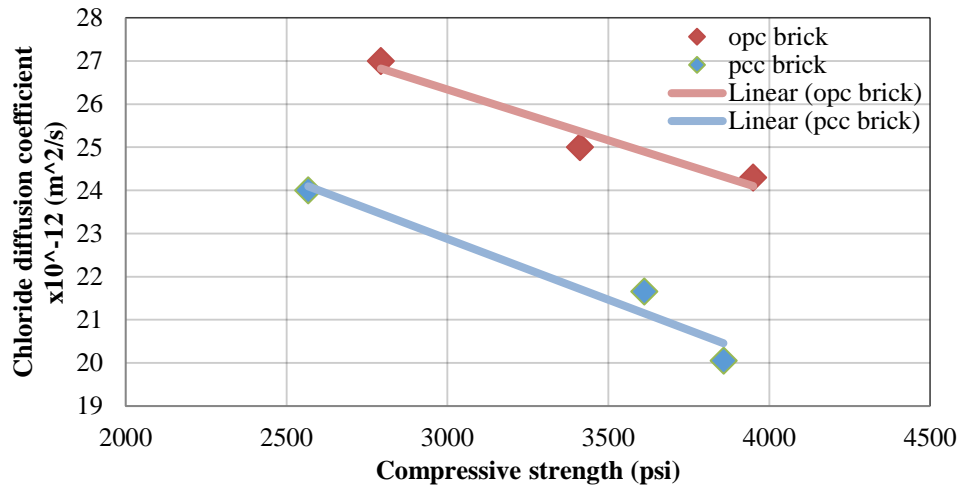


Fig. 2: Chloride diffusion coefficient vs. Compressive strength: Comparison between OPC brick and PCC brick

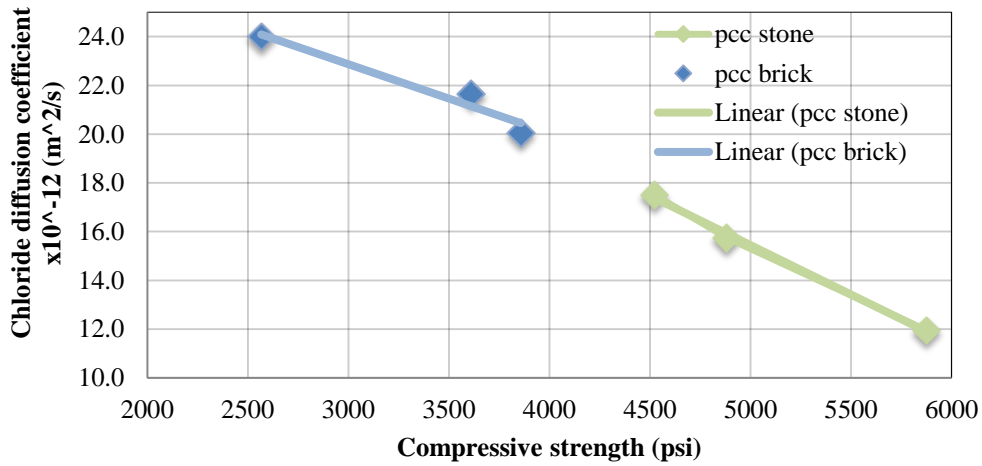


Fig. 3: Chloride diffusion coefficient vs. Compressive strength: Comparison between PCC stone and PCC brick

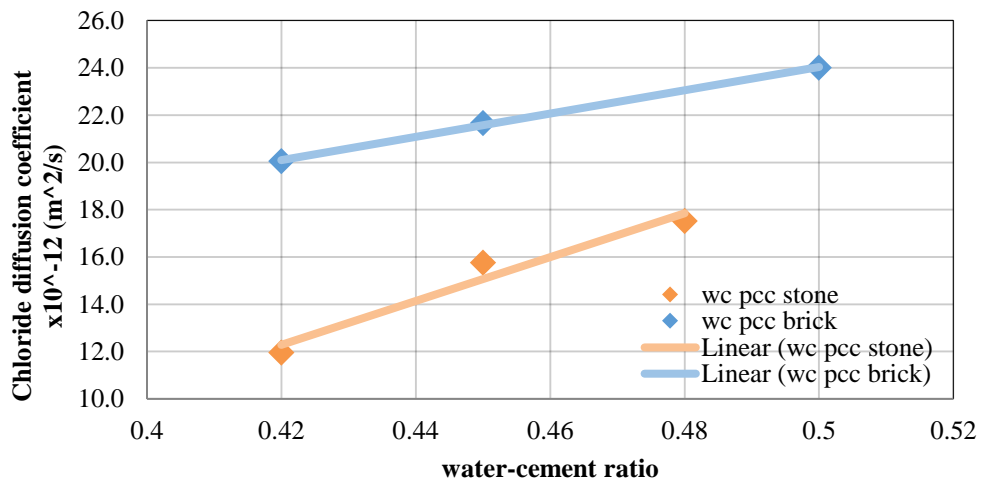


Fig. 4: Chloride diffusion coefficient vs. water-cement ratio: Comparison between PCC stone and PCC brick

CONCLUSIONS

From the present study, strong correlation between compressive strength and the rate of chloride diffusion is observed for the similar cement type. The susceptibility of concretes using brick aggregates to chloride ingress found to be greater than for conventional stone aggregates. Another significant observation is that locally produced PCC cements exhibited enhanced performance than OPC cements from durability perspective. It is also found that concrete using PCC cement and stone aggregates met the resistance to chloride penetration standards laid out NT Build 492. The outcome of the present study provides a preliminary idea on chloride resistivity of some common concrete mixes of the country prepared with available materials. It is obvious that further study will be required to obtain a more comprehensive understanding of the durability characteristics of concrete.

ACKNOWLEDGMENTS

The authors would like to acknowledge the kind help of Sumaiya Afroz, Lecturer, Department of Civil Engineering, Bangladesh University of Engineering and Technology during performing this research. The authors would also like express their gratitude toward the lab instructors of the concrete laboratory of Bangladesh University of Engineering and Technology (BUET) for their generous assistance.

REFERENCES

- Afroz, S; Rahman, F; Iffat, S and Manzur, T. 2015. *Sorptivity and Strength Characteristics of Commonly Used Concrete Mixes of Bangladesh*. International Conference on Recent Innovation in Civil Engineering for Sustainable Development (IICSD)
- Amin, A.F.M.S and Choudhury, Jamilur. 2015, *Intrinsic Properties of Brick Aggregate Concrete: A Review*. 1st International Conference on Advances in Civil Infrastructure and Construction Materials
- Baten, B; Hasan, M.J; Bose, B and Manzur, T. 2016. *Corrosion Potential of Stone and Brick Aggregate Concrete in the Context of Bangladesh*. BUET-ANWAR ISPAT 1st Bangladesh Civil Engineering Summit, BUET, Dhaka
- Maaddawy, T. A. El and Shoudki, K. A. 2003. *Effectiveness of impressed current technique to simulate corrosion of steel reinforcement in concrete*. Journal of Materials in Civil Engineering, ASCE, 1561(2003)15:1(41)
- Manzur, T; Baten, B; Hasan, M.J; Akter, H; Tahsin, A and Hossain, K. M. A. 2018. *Corrosion Behaviour of Concrete Mixes With Masonry Chips*. Construction and Building Material, 185: 20-19
- Moreno, M; Morris, W; Alvarez, M. G and Duffo, G. S. 2004. *Corrosion of reinforcing steel in simulated concrete pore solutions—Effect of carbonation and chloride content*. Corros. Sci., 46, 2681–2699
- Mott MacDonald and LGED. Inception Report, 2016. *Climate Resilient Concrete Structures in Marine Environment*. p.13. [online]. Available at <http://www.lged.gov.bd/AnnualReport/ReCAP/Inception%20Report-Climate%20Resilient.pdf>. [Accessed 31 August, 2018]
- NT Build 492, nordtest method, 1999-11. *Chloride Migration Coefficient From Non-steady-state Migration Experiments*. [online]. Available at <http://210.42.35.80/G2S/eWebEditor/uploadfile/20110819235419966.pdf> [Accessed, January 2018]
- Portland Cement Association. Concrete Information, 2002, *Types and Causes of Concrete Deterioration*, p.1-3. [online]. Available at http://www.cement.org/docs/default-source/fc_concrete_technology/durability/is536-types-and-causes-of-concrete-deterioration.pdf?sfvrsn=4 [Accessed 31 August, 2018]
- Rumman, R.; Kamal, M.R.; Manzur, T. and Noor, M. A. 2015. *Durability Performance of Locally Produced OPC and PCC Cement Concretes*. p.4
- Verma, SK; Bhadauria, SS and Akhtar, S. 2014. *Monitoring Corrosion of Steel Bars in Reinforced Concrete Structures*. The Scientific World Journal. [online] <http://www.ncbi.nlm.nih.gov/pmc/articles/PMC3914605/> [Accessed 16 June 2018]
- Zych, T. 2014. *Test Methods of Concrete Resistance to Chloride Ingress*. Technical Transactions, Civil Engineering. [online]. Available at <https://suw.biblos.pk.edu.pl/downloadResource&mId=1353955>. [Accessed 31 August 2018]

A STUDY ON COMPRESSIVE STRENGTH OF FIBER REINFORCED CONCRETE BY USING EARTH MATERIAL POWDER AND MARBLE DUST AS PARTIAL REPLACEMENT OF CEMENT AND SAND RESPECTIVELY

S.C. Malo^{1*} & M. N. Haque²

¹*Dept. of Civil Engineering, PUST, Pabna, Bangladesh <somirpust@gmail.com>*

²*Dept. of Civil Engineering, PUST, Pabna, Bangladesh <nazmul0pust131123@gmail.com>*

ABSTRACT

In this research the earthen material powder and marble dust are used as partial replacement of cement and sand respectively in varying percentage in order to investigate the compressive strength of fiber reinforced concrete. To fulfil this objective, physical and mechanical properties of raw materials are investigated as per ASTM code. At first control concrete is mixed with cement, sand, khoa (brick chips) and 2% GI wire of total weight of concrete (A-type) and then concrete is mixed with 5%, 10%, 15%, 20%, 25% and 30% EMP, keeping constant 5% MD and 2% GI wire which define B-type concrete. Further keeping constant 5% EMP and 2% GI wire, concrete is mixed with 2%, 4%, 6%, 8%, 10% and 12% MD which define C-type concrete. During mixing a variety of w/c is used to obtain medium degree of workability. After testing all types of cylindrical concrete specimen, the test result of G4-MD5-EMP15-GIW2-D28-WC50 specimen exhibits maximum compressive strength in B-type concrete and G9-MD4-EMP5-GIW2-D28-WC60 specimen exhibits maximum compressive strength in C-type concrete but not more than control concrete. So, it can be summarized that, concrete in which replacement of cement is done by 15% EMP and replacement of sand is done by 4% MD exhibits better performance.

Keywords: Fiber Reinforced Concrete (FRC), Compressive Strength, GI wire fiber, Low cost, Earth Material Powder (EMP), Marble Dust (MD).

INTRODUCTION

This study is regarded as one of the initial effort to incorporate earthen material as a substitute for cement in fiber reinforced concrete. Literature exhibits that there had never ever performed any task with earth material powder as partial replacement of cement. That's why, the research followed the guidelines and specifications available in the literature concerning partial replacement of ceramic waste as sand in concrete (Sivaprakash et al., 2016). Considering this study as pristine attempts, the present research attempts to move the current state of affairs forward and to lay the groundwork for future research in this field by exploring the prospects of earth material as a partial replacement of cement in fiber reinforced concrete.

Marble is a metamorphic rock resulting from the transformation of pure lime stone (Malpani et al., 2014). Marble sludge powder can be used as filler and helps to reduce the total voids content in

concrete (Hameed & Sekar, 2009). Marble dusts incorporation results in significant improvements in the compressive, flexural and split tensile strengths of concrete and this industrial bi-Product is capable of improving hardened concrete performance up to 10% (Ali & Hashmi, 2014). On the other hand, the maximum compressive and flexural strengths were observed for specimens containing a 6% waste sludge when compared with control and it was also found that waste sludge up to 9% could effectively be used as an additive material in cement (Corinaldesi et al., 2005). The maximum utilization of marble waste in various industrial sectors, especially the construction, agriculture, glass and paper industries would help to protect the environment.

Conventional concrete is normally weak in tension, bending, impact, fatigue, abrasion, deformation capacity, post crack load carrying capacity and toughness. The maximum cracking deformation in fibre reinforced concrete is much higher compared to traditional concrete. The main mechanism by which glass, synthetic, carbon, steel, etc. fibres make improvement in concrete performance is preventing the growth of cracks. It was observed that steel fibre content of 2.5-3.5% by weight produces relatively better results for the particular mix design used (Emon et al. 2017).

The replacement of these construction materials has a good impact in the field of engineering technology if following objectives are satisfied:

- i) The observation of compressive strength of fiber reinforced concrete (FRC) by partial replacement of cement and sand by earth material powder and marble dust respectively (with varying percentage).
- ii) Reduce the extra pressure on natural resource.
- iii) Protect environment from different environmental problems which results from those waste materials.

METHODOLOGY

In order to launch this experimental work, concrete were prepared using earth material, marble dust as partial replacement of cement and locally available dumar sand respectively, 2% GI wire and 25mm downgrade coarse aggregate. The whole research work has carried out under the following steps:

Step 1 Preparation of Materials

In this research, Brick chips and dumar sand are used as coarse and fine aggregate respectively. These materials are collected from local market. Earthen material powder and marble dust are used as the substitutes of cement and sand respectively. Earthen pot and marbles are collected from local market and then grinding these materials manually by hammer in order to obtain usable size. Since GI wire is used as fiber that's why wires are cut into small pieces one inch in length [Fig. 1].



Fig. 1: Prepared Materials

Step 2 Physical Property tests

Physical properties of coarse aggregate, fine aggregate, earth material, marble dust, OPC have been summarized in the following table

Table 1: Physical Properties of raw materials

Test Name	C.A.	F.A.	Cement	Marble Dust	Earth Material
Specific Gravity	1.946	2.675	2.96	2.48	2.65
Unit Weight(Kg/m ³)	953.207	1608.01	1440	1701.28	1701.28
Voids (%)	-	39.77	-	31.26	-
Water absorption (%)	-	0.185	-	0.28	-
Fineness Modulus	8.28	3.003	0	2.99	0
Setting Time (min)	Initial		96	-	-
	Final		542		
Normal Consistency (%)	29				

Step 3 Workability Test

The slump test does not measure the workability of concrete directly but it is an indirect measure of the same. A slump value of 50.8mm to 101.6mm (2"- 4") indicates medium degree of workability of concrete mixes (Aziz, 2012, p. 130-132). In this research, in order to obtain a medium degree of workability (slump value 2"-4") a variety of w/c ratio was used both in B-type & C-type concrete so that the w/c ratio was found be practical for the concrete mixes [Fig. 2].



Fig.2: Slump Test.

Step 4 casting of Cylindrical Specimen

Before casting Fiber Reinforced Concrete (A, B & C-type), Cement mortar cube were casted using w/c of 0.485 to know the compressive strength In this research, Concrete cylinder of size 100mm (4inch) diameter and 200mm (8inch) height for both B-type and C-type were cast using 1:2:4 mix (Binder : FA : CA) with variety of w/c ratio.



Fig. 3: Casting of Cylindrical Specimen.

The control concrete specimen was also cast using 1:2:4 mix (Binder: FA: CA) with w/c ratio of 0.65. Specimens with OPC replaced by earth material at 5%, 10%, 15%, 20%, 25% and 30% replacement levels and sand replaced by 5% marble dust were cast with 2% GI wire. Specimens with sand replaced by marble dust at 2%, 4%, 6%, 8%, 10% and 12% replacement levels and cement replaced by 5% earth material were cast with 2% GI wire [Fig. 3].

Step 5 Curing of Specimens

Curing is essential in the production of good quality and durable concrete. Water curing is the best method as it satisfies the entire requirement namely, promotion of hydration and elimination of shrinkage and absorption of the heat of hydration. In this study the test specimens were removed from the moulds after 24 hours and were shifted carefully to the place of curing for 28 days. Cylindrical specimens were then submerged into water tank and kept undisturbed there as shown in Figure () for the curing period designed [Fig. 4].



Fig. 4: Curing of Casted Specimen.

Step 6 Compressive Strength Test of Specimen

After the specified curing period, the concrete cylinders were subjected to compressive strength test by 2000KN capacity universal testing machine following the ASTM C39 (2003) specifications. An operational stage of the compression test is shown in Fig. 5(a). The compression was applied and the maximum or ultimate load carried by the specimen was recorded.



(a)

(b)

Fig. 5: Compressive Strength Test.

The compressive strength was calculated based on the ultimate load and the cross-sectional area of the cylinder and maximum from the results of three specimens. This load was increased gradually until the specimens failed as shown in Fig. 5(b). The crushing load was recorded at 28 days.

RESULTS AND DISCUSSION

Compressive strengths of B-type cylindrical specimen were represented in the following bar diagram [Fig. 6] at medium degree of workability using different replacements of EMP in fiber reinforced concrete:

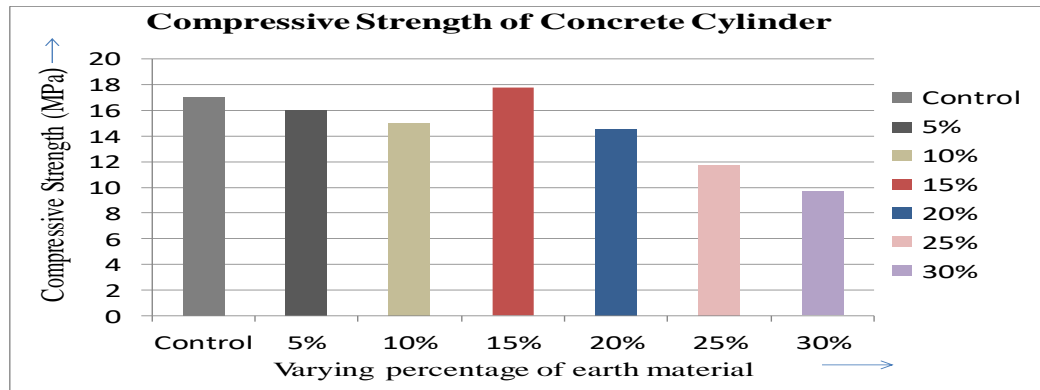


Fig. 7: Compressive strength of concrete for varying (%) of Earth Material with bar diagram.

Similarly compressive strengths of C-type cylindrical specimens were represented in the following bar diagram [Fig. 8] at medium degree of workability using different replacements of MD in fiber reinforced concrete:

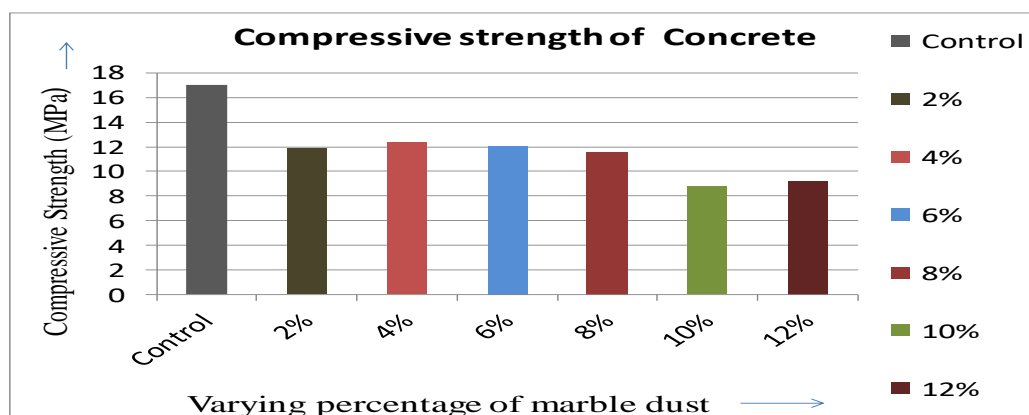


Fig. 8: Compressive strength of concrete for varying (%) of Marble Dust with bar diagram.

This results have reached that, replacement of 15% EM and 4% MD have better performance in case of compressive strength on fiber reinforced concrete than control concrete which is the reasons that maximum void filled at that percentage.

CONCLUSIONS

According to this research, we can reduce the extra pressure on raw materials like cement and sand as well as the material cost by keeping constant compressive strength. This type of materials will be helpful for constructing low rise building.

ACKNOWLEDGEMENTS

I acknowledge my absolute and ample gratitude and pleasure to almighty Allah for giving me enough faith, maturity in mind, health, time and patience to perform this research work. It is a great pleasure of the author to acknowledge his gratitude to his supervisor Tanmay Das, Lecturer, Department of

Civil Engineering, PUST, Pabna for his sincere guidance, kind co-operation, supervision, constant encouragement and valuable suggestions, intellectual discussions and patience throughout the period of this work. Without his whole-hearted supervision, this work would not have been possible. The author also pays his profound gratitude to his parents, close relatives, and friends for their inspiration towards the completion of this work.

REFERENCES

- Ali, M.M. & Hashmi, P.S.M. (2014). An Experimental Investigation on Strengths Characteristics of Concrete with the partial replacement of Cement by Marble Powder Dust and Sand by Stone Dust. *International Journal for Scientific Research & Development (IJSRD)*, 02(07), 360-368.
- AZIZ, D.M.A. (1973). *A Text Book of ENGINEERING MATERIALS*. Dhaka-1205: Hazi Book Centre 167, Dhaka New Market. Pp. 130-132
- Demirel, B. (2010). The Effect of the Using Waste Marble Dust as Fine Sand on the Mechanical Properties of the Concrete. *International Journal of the Physical Sciences*, 5(9), 1372-1380.
- Emon, M.A.B., Manzur, T. & Sharif, M.S. (2017). Suitability of Locally Manufactured Galvanized Iron (GI) Wire Fiber as Reinforcing Fiber in Brick Chip Concrete. *Case Studies in Construction Materials*, 7, 217–227.
- Hameed, M.S. & Sekar, A.S.S. (2009). Properties of Green Concrete containing Quarry Rock Dust and Marble Sludge Powder as Fine Aggregate. *APRN Journal of Engineering and Applied Sciences*, 04(04), 83-89.
- Malpani, R., Jegarkal, S.C., Shepur, R., Kiran, R., & Adi, V.K. (2014). Effect of Marble Sludge Powder and Quarry Rock Dust as Partial Replacement for Fine Aggregates on Properties of Concrete. *International Journal of Innovative Technology and Exploring Engineering (IJITEE)*, 4, 39-42.
- Sivaprakash, G., Kumar, V.S. & Saikia, L.J. (2016). Experimental Study on Partial Replacement of Sand by Ceramic Waste in Concrete. *International Journal for Chemical Sciences*, 14(S1), 266-274.
- Soliman, N.M. (2013). Effect of using Marble Powder in Concrete Mixes on the Behavior and Strength of R.C. Slabs. *International Journal of Current Engineering and Technology*, 3, 1863-1870.

PERMEABILITY MEASUREMENT OF A PERVIOUS CONCRETE

J. Rahman^{1*} & M. J. Islam²

¹*Department of Civil Engineering, Military Institute of Science and Technology, Dhaka, Bangladesh. E-mail: jesikarahman547@ce.mist.ac.bd*

²*Department of Civil Engineering, Military Institute of Science and Technology, Dhaka, Bangladesh. E-mail: mjislam@ce.mist.ac.bd*

**Corresponding Author*

ABSTRACT

As urbanization continues, the urge to introduce greener and more competent technologies is expanding. The pervious concrete (PC) belongs to the concrete ancestry and is composed of the same material requirements as that of a regular concrete, except that the high amount of interconnected void networks within it allow the passage of water through it and therefore prevent ground surfaces from inundation. Monitoring the rate of permeability of a PC helps to decide its applicability. Among the two American Concrete Institute (ACI) recommended methods, the falling head and constant head, this study used the falling head method in order to measure the rate of permeability of PC. Three mix proportions each having a different fine aggregate (FA) content, namely 0%, 10% and 20% FA, were prepared and the samples were then tested for permeability. The test results showed that there is an inverse relationship between the percentage of FA and the rate of permeability. The 0%FA sample having the lowest compressive strength, showed the highest rate of permeability unlike the 20%FA sample, having the lowest rate of permeability with the greatest compressive strength. Void content analyzed for each of the samples and a relationship drawn with the permeability rates indicate that an amount of permeability prevails even when the void content is negligible.

Keywords: Pervious concrete; Permeability; Falling head method.

INTRODUCTION

In recent years the World Risk Report 2011 (Birkmann, 2011) published that Bangladesh is highly vulnerable to unusual floods due to the lack of adaptive measures and coping ability leaving more than 30% of its land area inundated and affecting many people with health and occupational hazards. Developed countries like China, due to uncontrolled construction of impervious concrete land surfaces experienced extensive water pollution in Songhua River in 2005 (Haojie et al., 2018). To address this, the Sponge City is invented by the Ministry of Housing and Urban-Rural Construction of the People's Republic of China that uses the properties of PC (Hu et al., 2018).

The PC is termed as one of the Best Management Practices by the US Environmental Protection Agency (1999). To obtain the pervious nature, that its name already suggests, the aggregates are chosen to be of such a grading that allows a certain percentage of voids to be present within it. The typical void percentage in a PC ranges from 15% to 25% and the permeability within 100 to 750 l/min/m² (Tennis et al., 2004). The fine aggregate content are minimized in order to facilitate the porous structure. The water to cement (w/c) ratio is normally ranged from 0.28 to 0.45. The ACI Committee 522 (2010) recommends the use of coarse aggregates having sizes between 9.5mm to 19mm and that no fine aggregates to be incorporated in the mix proportion.

Numerous researches have been done to compute the rate of permeability using both falling head method and constant head method. Although the American Concrete Institute recommends it, the falling head method cannot identify the changes in porosity imparted by different materials used in the mixed design whereas the constant head method is sensitive to such variations (ACI, 2010 and Sandoval et al., 2017). Moreover, the constant head method is economical and has a less complicated procedure than the ones used in falling head method (Qin et al., 2015). Since PC consists of a design that uses minimal amount of FA, it is found to have lower compressive strength than that of a conventional concrete (Cui et al., 2016). Also, in PC, the permeability coefficient increases with the porosity and the rate of increment typically follows an accelerating trend. Schaefer et al (2006) proposed a linear correlation between void content and strength of PC which states that lower the void content, higher is the compressive strength.

The purpose of this study is to measure the rate of permeability of a PC by the falling head method and relate with the strength of concrete. In the present study, three types of mix designs were prepared and each mix had different amount of FA (0%, 10% and 20%, respectively) and the w/c ratio is kept constant to 0.4 throughout the study. The rate of permeability can be an effective indicator of the extent of porosity in the concrete. Although the relation is not directly proportional, the rate of permeability increases with the increase in porosity. However with increase in void content strength of concrete will reduce significantly. The significance of the test is to find out the water permeation capacity of a PC having a particular strength and thus to avail the decision about where can the PC be used basing on its capacity.

METHODOLOGY

Material Properties

The study has been done using ASTM Type I ordinary Portland cement (OPC) as the binding material (ASTM C 150, 2012). A w/c ratio of 0.4 was used, the amount of water needs to be adequate as too little of it would provide strength much lower than required whereas excess of it would not allow the consistency needed. The coarse aggregate selected were natural crushed stone aggregates complying to a size range with that of the ASTM C 33 size 67 (ASTM C 33, 2011). As permeability is the main output for the PC, the use of single-sized coarse aggregate would apparently seem beneficial but when strength is the concern, range of aggregate sizes is found to be more functional in terms of both permeability and strength. Sylhet sand was used as the FA having a fineness modulus of 3.2.

Mix design

The mix proportioning was done according to the ACI 211.3R-02 (2009) Guide for Selecting Proportions for No-Slump Concrete. Three mix designs were made having 0%, 10% and 20% FA to cast cylinders each having 100 mm diameter and 200 mm height. Each mix designs were used to cast 21 such cylinders making a total of 63 specimens to carry out the study and Table 1 below shows the proportions for a design void content of 15%.

Table 1 Mix proportion of PC for 1m³

Designation	Mass of Cement (kg)	Mass of Water (kg)	Mass of Coarse Aggregate (SSD) (kg)	Mass of Fine Aggregate (SSD) (kg)
0% FA	362.4	145	1567	0
10% FA	334.5	133.8	1472	145
20% FA	292.7	117.1	1361	301

Specimen preparation

All the cylinders were prepared according to the ASTM C 192 standard. The concrete mix was placed inside a steel mold conforming to the specifications of ASTM C470 and rodded 25 times in three layers. The samples were taken out of the mold after 24 hours and cured as per the ASTM regulations.

Permeability measurements

Permeability of the PC samples were measured at 28 days age by a falling head permeability apparatus shown in Figure 1 customized in such a way that it was similar to the one used in the permeability measurement of soil (ASTM D 5084, 2003).

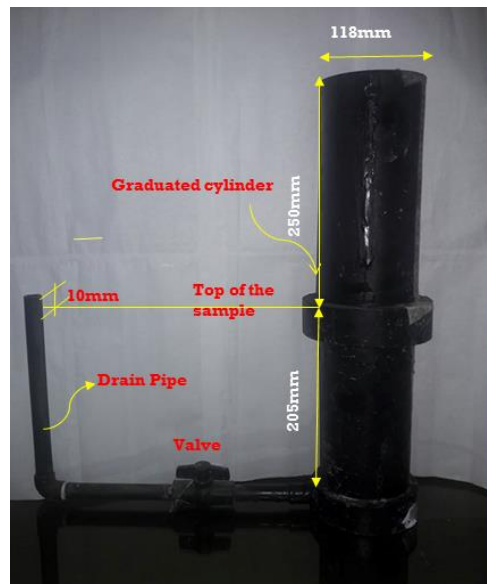


Fig. 1 Falling head apparatus

In order to limit the movement of water in only the vertical direction the surface of the cylindrical samples were coated with a waterproofing surface sealant leaving the top and bottom surfaces off. Nitobond EP, a two-component solvent free epoxy resin, was used as the sealant for this study. The sample was placed above a rubber pad in the bottom part of the graduated cylinder. The interface between outer surface of the PC samples and the inner surface of graduated cylinder of the apparatus was closed by wrapping the test samples with a sheet of synthetic rubber 3mm thick. The samples were saturated at the beginning in order to eliminate any air voids present within it. With the valve closed, the apparatus was filled with water to the top mark in the graduated tube and the initial height of water in the tube was noted as h_1 . The valve was then opened and a stopwatch started simultaneously to record the time t required for the water to drain down the specimen to a final height noted as h_2 . The process was repeated three times for each PC sample with the same initial and final water height and the average length of time calculated. The coefficients of permeability (K) of the samples were then calculated using Eq. (1) derived from the Darcy's law.

$$K = \frac{A_1 l}{A_2 t} \log \left(\frac{h_2}{h_1} \right) \quad (1)$$

Here A_1 and l denotes the cross-sectional area and length of the sample being tested respectively and A_2 being the cross-sectional area of the tube.

Void content analysis

Void content of the PC samples in this study were measured following the ASTM C 642 (2013) standard. This analysis was made on samples aged at 28 days. The code specification allows measuring the void content in a concrete sample by the determination of variation of its weight in different conditions.

RESULTS AND DISCUSSIONS

Compressive strength and tensile strength

Figures 2(a) and 2(b) present the compressive strength measured after 7 and 28 days and the tensile strength tested after 28 days of casting respectively. It can be observed that as the amount of FA increased both the compressive and tensile strength increased.

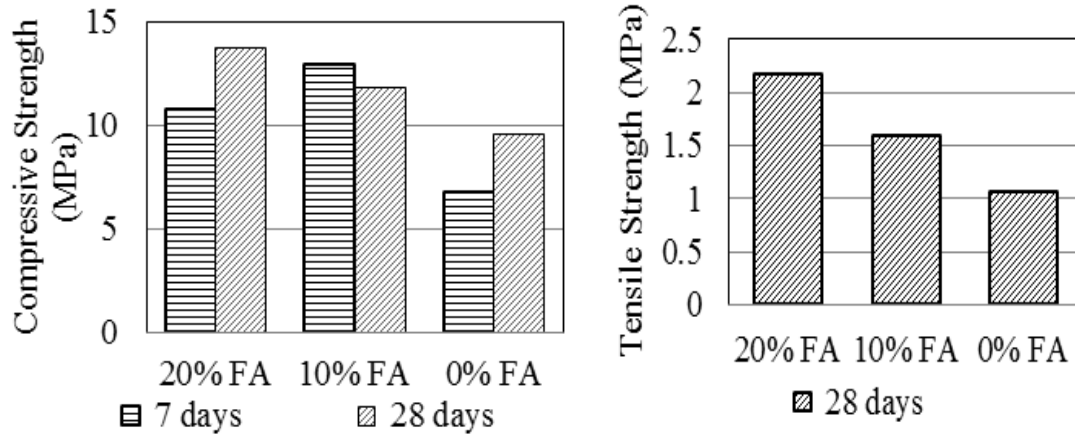


Fig. 2 (a) Compressive and (b) tensile strength of PC samples.

Coefficient of permeability

The PC samples were tested for permeability after 28 days of casting and the results are summarized in Table 2. The results show that the highest permeability observed was in 0% FA sample and the lowest at 20% FA sample meaning the permeability decreased with increase in percentage of FA in the mixture. Neithalath *et al.* (2006) conducted a similar experiment using falling head permeability apparatus and their results varied from 1mm/sec to 5mm/sec with a standard deviation of 0.3mm/sec to 0.8mm/sec. For comparison, the standard deviation in this research is found to be within 0.2mm/sec and 0.5mm/sec.

Table 2 Summary of permeability test results

Designation	Sample	A ₁ (mm ²)	A ₂ (mm ²)	l (mm)	t (sec)	h ₁ (mm)	h ₂ (mm)	K (mm/sec)	Avg. K <small>(mm/sec)</small>
0%FA	1	7524.9	10936	207	22.0	250	30	5.89	6.07
	2	8332.3	10936	204	23.4	250	30	6.03	
	3	7088.2	10936	196	18.4	250	30	6.29	
10%FA	1	7389.8	10936	204	35.0	250	30	3.58	3.96
	2	7238.8	10936	202	30.7	250	30	3.96	
	3	7088.2	10936	204	33.0	250	20	4.34	
20%FA	1	8332.3	10936	204	100	250	30	1.40	1.99
	2	7088.2	10936	205	46.9	250	30	2.58	
	3	7238.2	10936	207	63.0	250	30	1.98	

Fig. 3 represents the trend of compressive and tensile strengths with the rate of water permeability imparted by the amount of FA incorporated in the mix design. Both the strengths decreased as the permeability increased and vice versa which depicts that reducing the FA content improve permeability leaving lower strength which is often disadvantageous for structural uses.

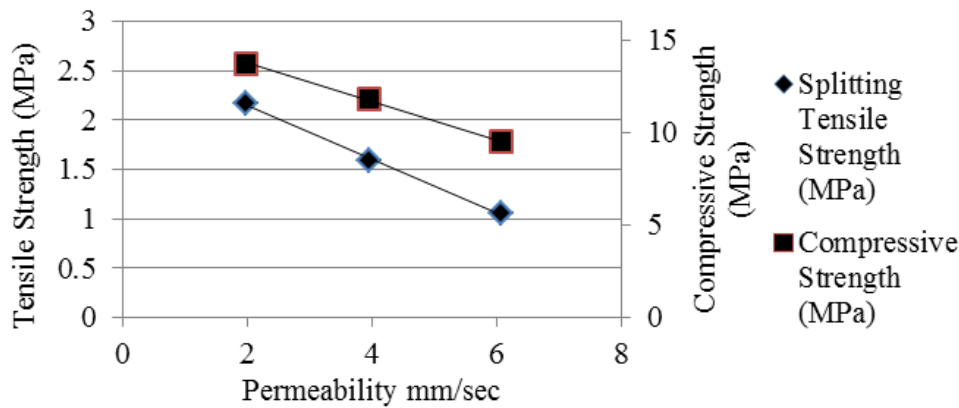


Fig. 3 Variation of the physical properties of the PC samples with the rate of permeability.

A speculation made on the comparison between void content and permeability (Fig. 4) signified that the rate of permeability increased with the void content in the PC samples. However, the increasing trend is found to be an accelerating one. This identifies the fact that permeability depends upon the interconnectivity between the voids that give access to the water for permeation but not the content of void and so it does not vary linearly with the void content in the PC. The proposed Eq. (2) presents that a PC has certain permeability even when the void content is 0%, where x and y present the void content (%) and rate of permeability in mm/sec respectively.

$$y = 0.2236e^{0.507x} \quad (2)$$

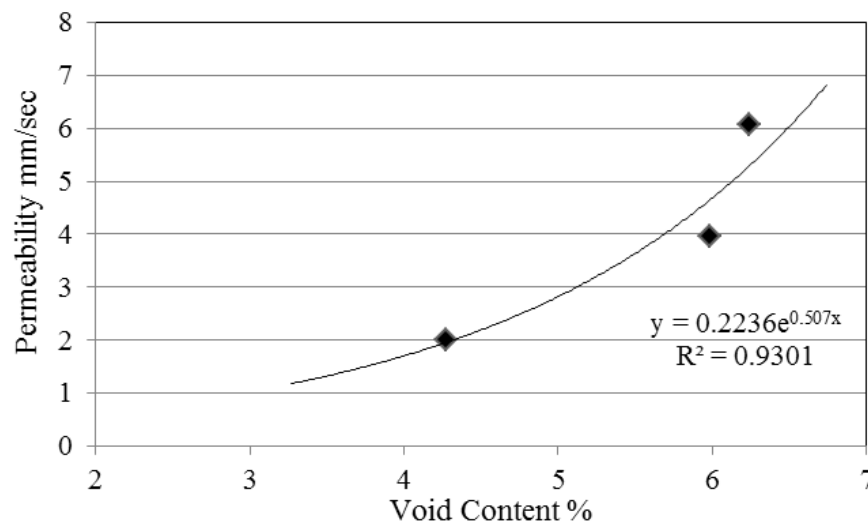


Fig. 4 Relationship between void content and permeability of PC

CONCLUSIONS

This study focuses on permeability measurements by the falling head method through an apparatus made specifically for the research. Using Darcy's law, the coefficient of permeability was determined and the results compared with the strength of PC varying with the amount of FA in the mix design. PC having 0%FA is found to have the lowest 28 days compressive strength (9.5 MPa) whereas its rate of permeability being the highest (6.07 mm/sec). On the other hand, PC containing 20%FA exhibited greatest 28 days compressive strength (13.70 MPa) which in turn has the lowest rate of permeability (1.99mm/sec). Both compressive and tensile strength decreased as the permeability of PC samples increased. Void content analyzed and plotted against the results of permeability to form an equation which indicates a direct relationship between these parameters. The equation proposed could therefore be used to determine the void content in a PC sample using the results of permeability.

REFERENCES

- ACI 211.3R, 2009 Guide for Selecting Proportions for No-Slump Concrete. *American Concrete Institute*, USA.
- ACI Committee 522, 2010. Report on Pervious Concrete 522R-10, *American Concrete Institute*, Farmington Hills, MI, USA.
- Agency, E.P.U.S 1999 *Storm water technology fact sheet porous pavement*. Washington, D.C: United States Environmental Protection Agency, Office of Water.
- ASTM C 33, 2011. Standard Specification for Concrete Aggregates, *ASTM International*, West Conshohocken, PA. www.astm.org.
- ASTM C 150, 2012 Standard Specification for Portland Cement *ASTM International*, West Conshohocken, PA. www.astm.org.
- ASTM C642, 2013. Standard Test Method for Density, Absorption, and Voids in Hardened Concrete, *ASTM International*, West Conshohocken, PA. www.astm.org.
- ASTM D 5084, 2003. Standard Test Methods for Measurement of Hydraulic Conductivity of Saturated Porous Materials Using a Flexible Wall Permeameter, *ASTM International*, West Conshohocken, PA, www.astm.org.
- Birkmann J. 2011. Global Risks Report 2011. *World Economic Forum* [online]. Available at <https://www.weforum.org/reports/global-risks-report-2011>. [Accessed 3 September 2018].
- Cui, X., Zhang, J., Huang, D., Gong, X., Liu, Z., Hou, F. and Cui, S. 2016. Measurement of Permeability and the Correlation between Permeability and Strength of Pervious Concrete. *1st International Conference on Transportation Infrastructure and Materials (ICTIM 2016)*. ISBN: 978-1-60595-367-0.
- Haojie, L., Rentai, L., Honglu, Y., Chenyang, M. & Heng, Z. 2018. Experimental study on the performance of pervious concrete. *IOP Conference Series: Earth and Environmental Science*, 113(1): 012126.
- Hu, M., Zhang, X., Siu Y.L., Li, Y., Tanaka, K., Yang, H. and Xu, Y. 2018. Flood Mitigation by Permeable Pavements in Chinese Sponge City Construction. *Molecular Diversity Preservation International (MDPI)*, 10(2): 172.
- Neithalath, N., Weiss, J. and Olek, J. 2006. Predicting the Permeability of Pervious Concrete (Enhanced Porosity Concrete) from Non-Destructive Electrical Measurements. *Proceedings of the 2006 Concrete Technology Forum on Pervious Concrete*. Nashville, USA.
- Qin, Y., Yang, H., Deng, Z., and He, J. 2015. Water Permeability of Pervious Concrete Is Dependent on the Applied Pressure and Testing Methods. *Advances in Materials Science and Engineering*, vol. 2015: 5-6.
- Sandoval, G. F. B., Galobardes, I., Teixeira, R. S. and Toralles, B. M. 2017. Comparison between the falling head and the constant head permeability tests to assess the permeability coefficient of sustainable Pervious Concretes. *Case Studies in Construction Materials*, 7: 317-328.
- Schaefer, V. R., Wang, K., Suleiman, M.T., and Kevern, J.T. 2006. Mix design development for pervious concrete in cold weather climates. Final Report, *National Concrete Pavement Technology Centre*, Iowa State University, Ames, IA. 16p.
- Tennis, P.D., Leming, M.L. and Akers, D.J. 2004. *Pervious Concrete Pavements, EB302.02*, Portland Cement Association, Skokie, Illinois, and National Ready Mixed Concrete Association, Silver Spring, Maryland, USA. 5p.

STRUCTURAL ANALYSIS OF SEMISUBMERSIBLE OFFSHORE PLATFORM

M. R. Karim*

*Department of Mechanical Engineering, University of Creative Technology Chittagong,
Chittagong, Bangladesh.*

E-mail: rezaukarim4307@gmail.com

**Corresponding Author*

ABSTRACT

This paper presents a case study of an offshore platform regarding the structural analysis. In search of oil and gas resources we need to approach to the deep sea, harsh environment and remote locations. One of the remarkable accomplishments of the petroleum industry is the development of technology that allows for exploring wells offshore to access additional energy resources. This offshore structures are largely exposed to stresses which induced more significantly by sea waves. Therefore, to provide structural safety and durability, the effects of wave induced loads have to be taken into consideration. One of the approaches for that is to perform a global structural analysis with the extreme hydrodynamic loading on the semisubmersible platform.

Keywords: Structural Analysis, Semisubmersible Platform, Hydrodynamic Load

INTRODUCTION

Despite an increase in complexity, improvements in offshore technology have allowed more complex well patterns to be explored to a greater depth such that additional petroleum resources can be discovered at a greater distance from the production structure, allowing more energy to be produced with less environmental impact. These offshore structures are greatly impacted by large wave loads. The repeated wave loads reduces the performance of the structural member. Structural analysis is one of the technic to quantify wave induced loads to ensure structural durability and safety of the offshore platform.

The main objective is to make structural analysis and identify critical locations of the offshore platform with respect to von Mises stress for different wave direction. A methodology has been developed for structural analysis of a Semisubmersible Offshore Platform with extreme environmental loading condition.

METHODOLOGY

For the Finite Element modelling and analysis of the offshore platform, DNV software Sesam GeniE has been used. The hydrodynamic simulation is carried out in the DNV software HydroD Wadam. The hydrodynamic simulations are performed in the frequency domain for the structure operating in north Atlantic. For the frequency domain, a Bret-Schneider spectrum with 26 frequencies and 8 wave directions are chosen. The global motion response of the structure was analysed using a post-processing software named POSTRESP. The FE-simulations are carried out in the DNV software SESTR for linear structural FE-analysis. Following are the steps taken for analysis

- 3D-Modelling (Sesam-GeniE)

- Hydrodynamic Analysis (HydroD-Wadam)
- Structural Analysis (Sestra)
- Global Response(Xtract)

3d Structural Modelling

Simplified model of a twin pontoon column stabilized semisubmersible unit is considered which consist of 4 sets of columns legs, 2 horizontal pontoons, 2 bracings and a derrick that has been chosen to perform structural analysis. Its characteristic length is 90 meter, Pontoon Height 9 meter, Width of Pontoon 18 meter, height of column 35 meter, Diameter of Column 15 meter and deck height is 10 m. St52 is used as a material which has following properties:

Table 1 Material Properties of the Structural Model (St52)

Material Property	Value	Unit
Yield Stress	2.35×10^8	Pa
Density	7850	Kg/m ³
Young's Modulus	2.1×10^{11}	Pa
Poisson's Ratio	0.3	
Thermal co-efficient	1.2×10^{-5}	delC ⁻¹
Damping co-efficient	0.03	N.s/m

Modelling has been done with Sesam GeniE software as shown below with color-coding:

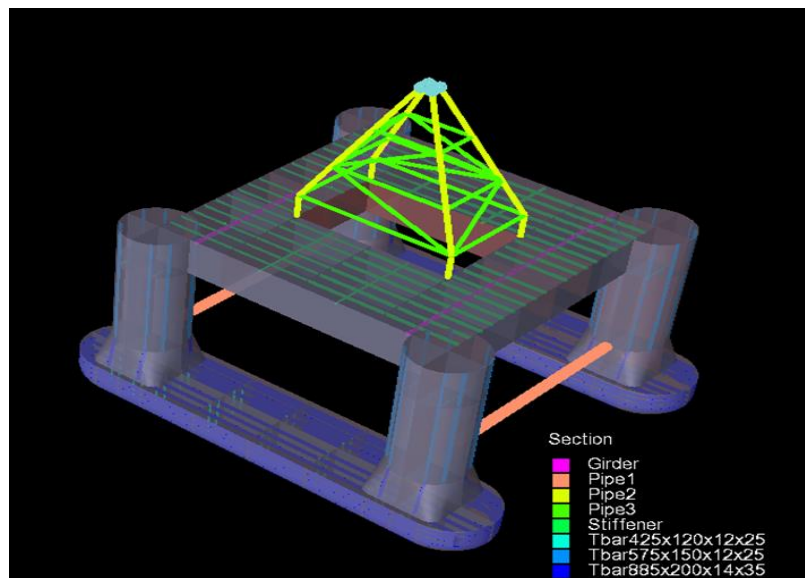


Fig.1: Structural Members

Global model includes following:

- the longitudinal stiffness of the pontoons,
- the axial and bending stiffness of the braces,
- the axial and bending stiffness of the columns,
- the in plane and vertical bending stiffness of the deck

Hydrodynamic Analysis

Extreme hydrodynamic loading condition of North Atlantic Ocean is considered. Wave loads are computed by HydroD Wadam using Morison’s equation and potential theory. Wadam is an integrated part of the SESAM suite of programs which is tailored to calculate wave loads on models created by the SESAM Genie. The results from the Wadam global response analysis stored on a Hydrodynamic Results Interface File (G-file) for statistical post processing in Postresp. Hydro model is shown in Figure below which is consisted of finite element model of the structure.

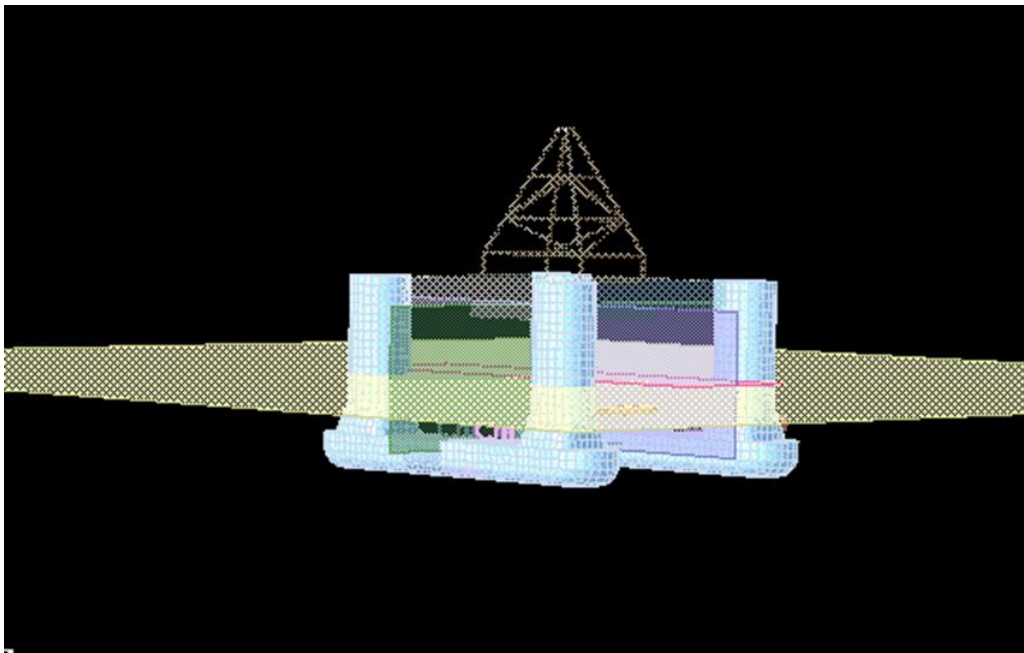


Fig.2: Hydro Model of the Offshore Structure

Mass Model properties for the Hydrodynamic Analysis is given below in Table 2

Table 2 Mass Model Properties of the Structure

Property	Value	Unit
Mass of structural Model	23.6×10^6	Kg
Buoyancy Volume	25.1×10^3	m^3
Centre of Buoyancy in coordinate(x,y,z)	(0, 0, -13.5)	m
Centre of Gravity in coordinate (x,y,z)	(0, 0, -10)	m
Radius of Gyration (x,y,z)	30.9, 29.7, 38.6	m
Roll-Pitch Centrifugal Moment (XYRAD)	-5.67×10^{-14}	m^2
Roll-YAW Centrifugal Moment (XZRAD)	0	m^2
Pitch-YAW Centrifugal Moment(YZRAD)	-4.63×10^{-15}	m^2

The response of the structure was measured in terms of its Response Amplitude Operators (RAOs) for the 6 degree of freedom

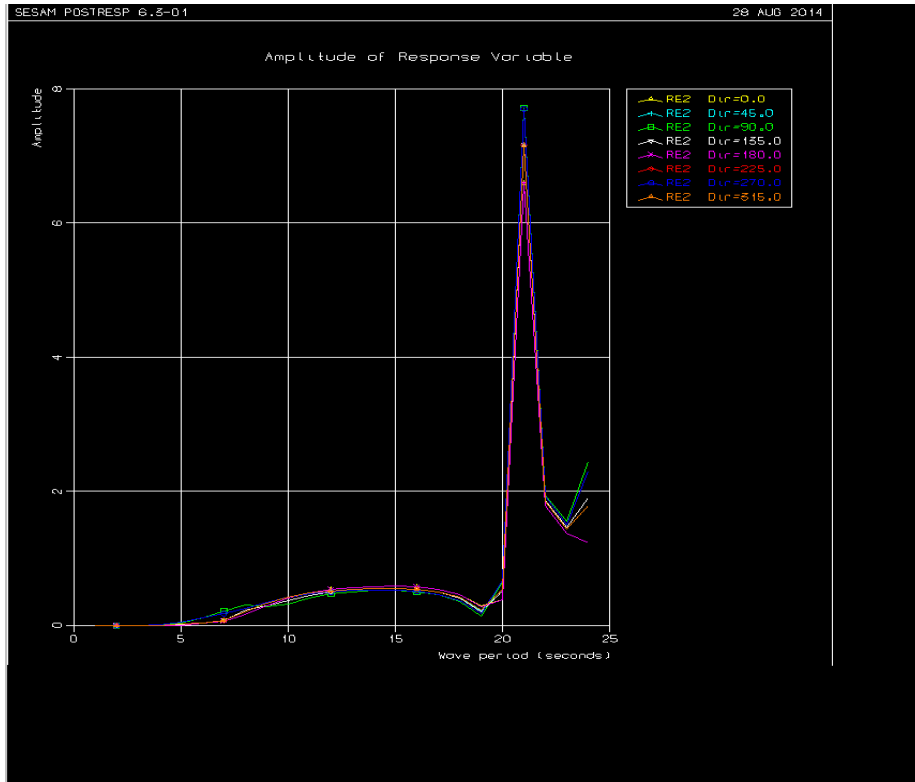


Fig.3: RAO -Relative motion at water surface (0, 0, and 40)

The RAO is shown above. There are two peaks, one at 21.5s (amplitude 7.8) which comes from the heave resonance mainly and one at 23.5s (amplitude 2.2) which comes from the roll resonance mainly. The worst wave direction is 270 and 45 degrees for both peaks. Wave loads applied on the structure is shown below.

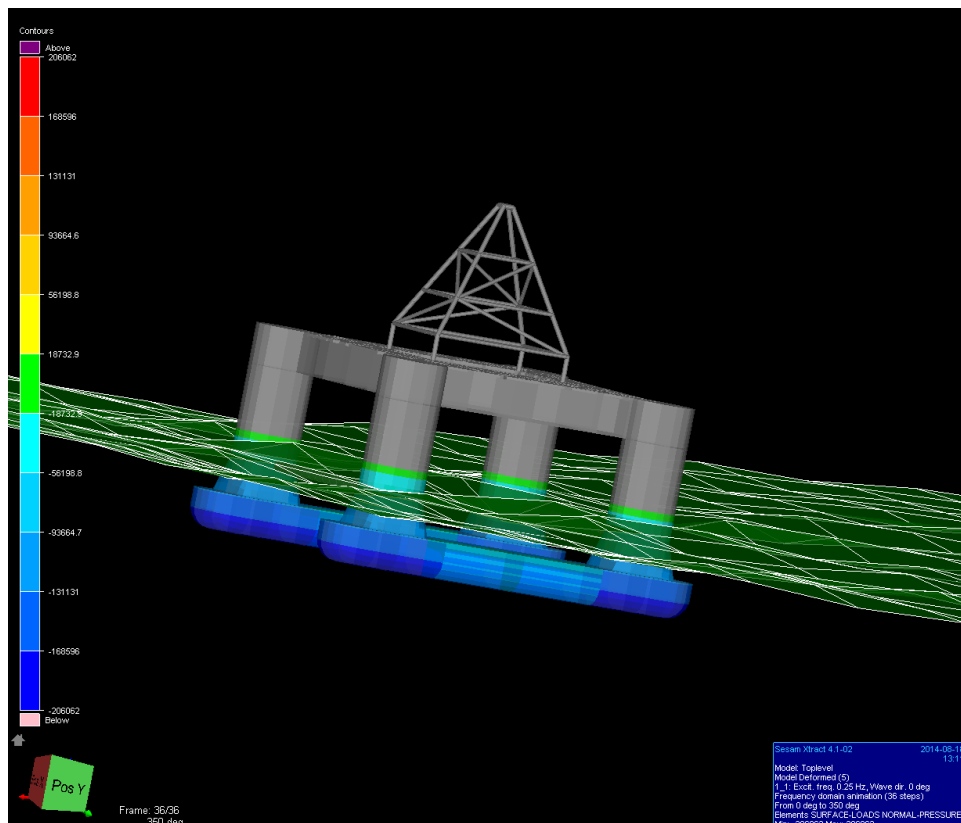


Fig.4: Surface loads of the structure in frequency domain

Structural Analysis

The hydrodynamic load is applied to the structural model for subsequent quasi-static analysis of the structure. To avoid rigid body motion of the global structural model 6 degrees of freedom have fixed with the following restraints:

- 3 vertical restraints (Z)
- 2 transversal horizontal restraints (Y)
- 1 longitudinal horizontal restraint (X).

Structural analysis is presented in following figures based on von-misses stress considering self-weight.

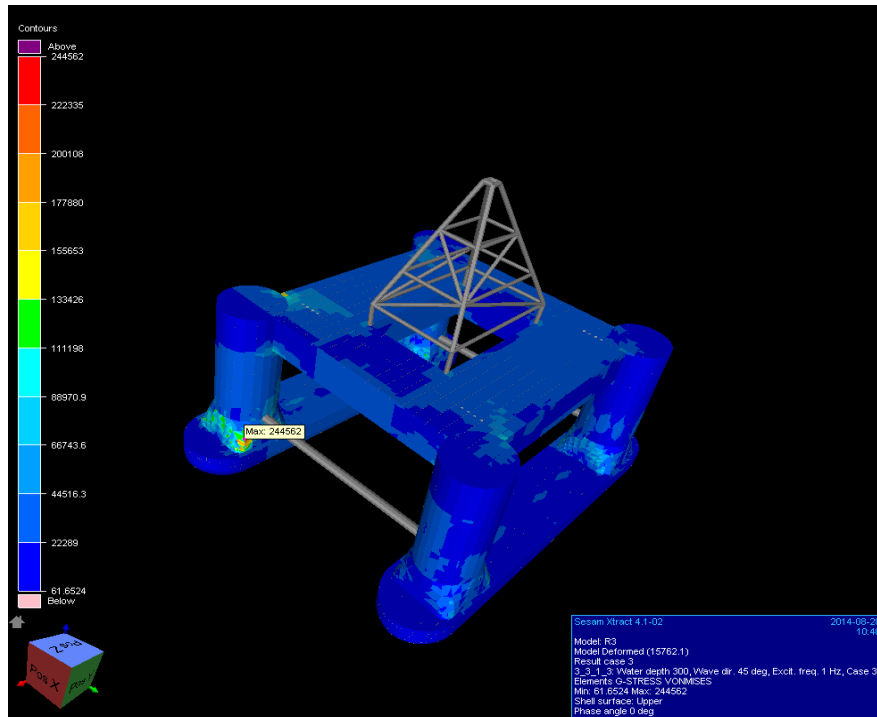


Fig.5: Von Mises Stress at Water depth 300, Wave dir. 45 deg, Excit. Freq. 1 Hz

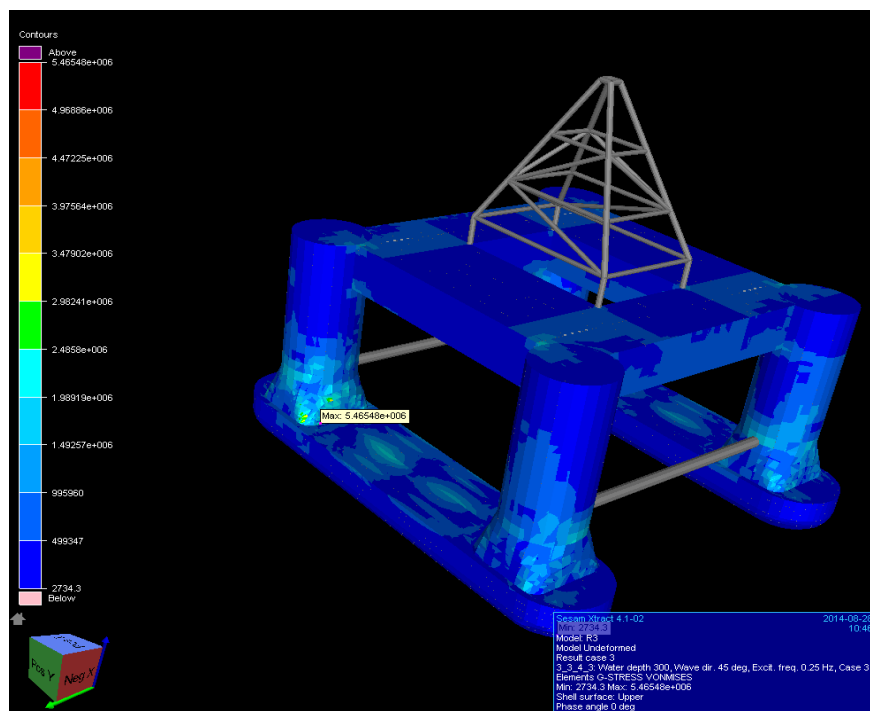


Fig.6: Von Mises Stress Water depth 300, Wave dir. 45 deg, Excit. Freq. 0.25 Hz

RESULT AND DISCUSSIONS:

The maximum stress level due to wave induced loading were found to be occurring at around similar wave frequency range ($f= 0.04-0.05$ Hz or $T= 20-25$ sec). The worst wave direction is found at 270 and 45 degrees. The analyses showed that the critical regions with respect to von-mises stress are located in the column to pontoon connections. Heave and roll are the most significant motion response for operations of Semisubmersible offshore structures.

CONCLUSIONS:

Structural analysis of a semisubmersible platform with extreme environmental conditions was depicted in this paper. First, a 3d structural model of the platform was created and then hydrodynamic loads are applied for subsequent hydro-analysis. Finally A linear structural FE-analysis was performed for the global model in order to find out the critical locations. To get more accurate result local sub-models can be created and analysis for local models can be performed as stress ranges could locally become significant

ACKNOWLEDGEMENTS:

The author would like to express deep appreciation to support of DNV-GL, Gdynia, Poland for allowing to use all software required for the analysis

REFERENCES:

- [1] Camilla Knifsvund and Andrea Tesanovic, *Global and Detailed Local Fatigue Assessment of a container vessel*. Chalmers University of Technology, 2012
- [2] DNV-GL, "Guidelines to Assess High-Frequency Hull Girder Response of Container Ships", 2014
- [3] G. Sigurdsson, "Probabilistic Fatigue of offshore structure," University of Aalborg, Sohngaardsholmsvej 51, DK-9000 Aalborgg, Denmark
- [4] Md Rezaul Karim, "Fatigue Analysis of Offshore Drilling Unit," *Article in Press*
- [5] Niraj Kumar Singh, "*Global Response Analysis for Semisubmersible Offshore Platform*," Thesis-EMSHIP, 2013
- [6] Philippe Rigo and Enrico Rizzuto, "Analysis and design of Ship Structure," *Chapter 18*

EFFICIENCY ANALYSIS OF NUMERICAL SOLUTION OF SAINT-VENANT TORSION PROBLEM BY FINITE ELEMENT METHOD

M. A. Islam^{1*} & M. S. Karim²

¹*Department of Mathematics, Uttara University, Dhaka-1230, Bangladesh*

²*Department of Mathematics, Shah Jalal University of Science & Technology, Sylhet-3114, Bangladesh.*

E-mail: amirul.math@gmail.com

**Corresponding Author*

ABSTRACT

This paper is devoted to the study of approximate solution of saint venant torsion problem using finite element method (FEM). The Finite element method is most popular for solving this type of problems. The finite element method is mostly used in the field of structural mechanics. We derived global stiffness matrix and load vector for four sided quadrilateral elements of mesh of two triangles and mesh of six triangles. In this paper, we consider 3 four-nodded quadrilateral elements and 3 eight-nodded quadrilateral elements to compute the Prandtl stress function values and the torsional constants k of Saint-Venant torsion problem for a square cross-section. The obtained finite element solution will be very nearest to exact solution if the domain of the body is splitted into smaller elements. We obtained finite element results which are compared with the exact torsion solutions to verify the accuracy of proposed FEM. The finite element solutions to reach the good agreement with the exact solutions of Saint venant torsion.

Keywords: Saint-Vennat torsion, stress function values ,torsional constant and application example.

INTRODUCTION

The finite-element method (FEM) is a popular numerical method used for solving a large range of science and engineering problems. Applications range of finite element method from stress and deformation analysis of automotive, spacecraft, shipbuilding and bridge structures to filed analysis of magnetic flux, heat and fluid flow, and other flow problems. In finite element method, the complex domain like a complicated structure is discretized into many numbers of finite elements and the solution like nodal displacements, element stresses are evaluated in the various locations of the structure. Nowadays, finite element analysis (FEA) is used in some biomechanical engineering problems typically include analysis of human spine, skull, hip joints, heart, eye, etc. In FEM, stiffness matrix, body force vector are to be determined numerically. In this paper, finite element method (FEM) is applied to calculation of torsional constants and stress function values of saint-venant torsion problem for a square cross section. In order to find the solution of saint vennat torsion problem for a square domain by FEM, the domain or continuum is divided into finite number of small elements of simple regular shapes. In finite element analysis, the size of the elements influences the convergence of the solution. In square cross-section has four axes of symmetry; therefore, only one –eighth of the cross-section has been analyzed. This fractional portion is divided into 4-noded and 8-noded three elements for finding accurate solution of saint venent torsion. The accuracy of the finite element solution depends on the finite element mesh. Li *et al.* (2000) discussed finite element based on Galerkin's method for the torsional rigidity of an arbitrarily shaped bar made of different materials.

Najera and Herrera (2005) presented a method to approximate the torsional rigidity of any cylindrical solid cross section. Darilmaz *et al.* (2007) developed a hybrid finite element method to calculate the torsional rigidity of arbitrarily shaped composite sections. Jog and Mokashi (2014) presented finite element solution of the Saint-Venant torsion and also shown finite element formulation based on the warping function of torsion and bending problems for prismatic beam. Islam and Karim (2017) presented finite element Solutions of Saint Venant torsion problem for a trapezoidal cross section. Baretta *et al.* (2015) analyzed closed form solution of the torsion problems. Teimoori *et al.* (2016) discussed the torsion for rectangular cross section of bars with effective coating layers. Taheri and Hematiyan (2017) analyzed accuracy of the developed algorithm for a torsion. Nguyen (1992) discussed straight and curved quadrilateral elements to find Prandtl stress function values for torsion problems. Ecsedi and Baksa (2010) discussed electric displacement potential function and Prandtl's stress function for the Saint–Venant torsional problems. In this paper, the accuracy and efficiency of the presented technique is demonstrated through the calculation of Prandtl stress function values and torsional constant of square cross section on the basis of finite element approach.

FINITE ELEMENT MODELLING

In this section, domain is divided number of finite elements. The set of finite elements is said to be mesh generation of the domain. In this model, we have discretized of the quadrilateral domain with triangular finite elements. To find the accurate finite element solution of required torsion problem, we needs higher order finite elements. Quadrilateral element of this model can be easily expressed to well-shaped triangles. In most of the engineering problems, the domain has irregular shapes. For this reason, the irregular shaped domain is splitted into convenient number of regular shaped finite elements. The finite element meshes shown in figs. 1(a) and 1(b).The finite element is a small portion of the system (or domain).

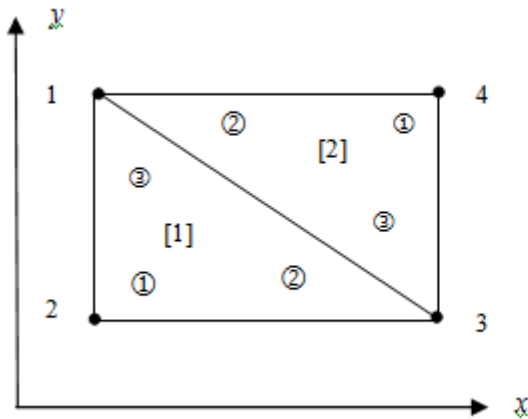


Figure 1(a): Mesh of two Triangular elements.

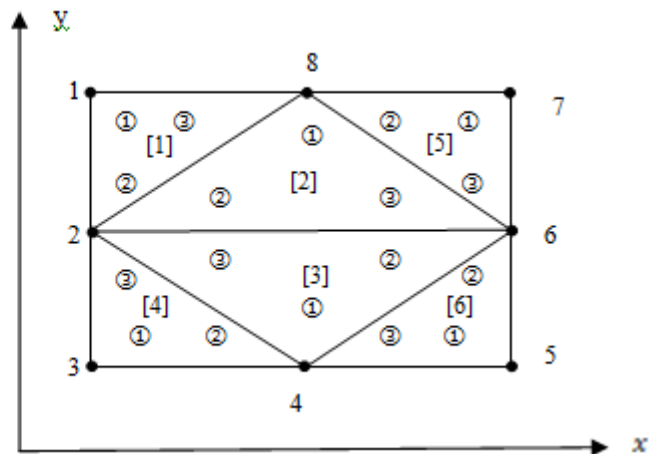


Figure 1(b): Mesh of six Triangular elements.

The transformation formulae between two coordinates systems are

$$x = \sum_{i=1}^3 x_i N_i; \quad y = \sum_{i=1}^3 y_i N_i \quad (1.1)$$

The shape functions of triangle elements are given by,

$$N_1 = 1 - \xi - \eta; \quad N_2 = \xi; \quad N_3 = \eta; \quad (1.2)$$

From (1.1) & (1.2), we have,

$$x = (x_2 - x_1)\xi + (x_3 - x_1)\eta + x_1, \quad (1.3)$$

$$y = (y_2 - y_1)\xi + (y_3 - y_1)\eta + y_1 \quad (1.4)$$

The corresponding Jacobean can be written as:

$$J^{[e]} = \frac{\partial(x, y)}{\partial(\xi, \eta)} = \frac{dx}{d\xi} \frac{dy}{d\eta} - \frac{dx}{d\eta} \frac{dy}{d\xi} \quad (1.5)$$

GLOBAL STIFFNESS MATRIX AND LOAD VECTOR EVALUATION SCHEMES

In this section, we have used four-noded and eight-noded quadrilateral elements for construct global stiffness matrix and load vector [see Fig.1 (a) & Fig.1 (b)]. A matrix formulation is also developed and applied to the problems in the analysis of Saint Venant torsion. The finite element formulation of the laplacian matrix defined by the equation:

$$K_{ij}^{[e]} = \iint_{\Omega} \left(\frac{\partial N_i}{\partial x} \frac{\partial N_j}{\partial x} + \frac{\partial N_i}{\partial y} \frac{\partial N_j}{\partial y} \right) dx dy = \int_0^1 \int_0^{1-\xi} \left(\frac{\partial N_i}{\partial x} \frac{\partial N_j}{\partial x} + \frac{\partial N_i}{\partial y} \frac{\partial N_j}{\partial y} \right) J^{[e]} d\xi d\eta$$

$$F_i^{[e]} = \iint_{\Omega} N_i(x, y) dx dy = \int_0^1 \int_0^{1-\xi} N_i(\xi, \eta) J^{[e]} d\xi d\eta$$

For Figure-1, we have global stiffness matrix and global load vector

$$K = \begin{bmatrix} k_{11} & k_{12} & k_{13} & k_{14} \\ k_{21} & k_{22} & k_{23} & k_{24} \\ k_{31} & k_{32} & k_{33} & k_{34} \\ k_{41} & k_{42} & k_{43} & k_{44} \end{bmatrix} \text{ and } F = \begin{bmatrix} f_1 \\ f_2 \\ f_3 \\ f_4 \end{bmatrix}$$

Where k_{ij} and F_i are the global coefficients, which can be written in terms of the element coefficients.

$$k_{11} = k_{33}^{[1]} + k_{22}^{[2]} ; k_{12} = k_{21} = k_{31}^{[1]} ; k_{13} = k_{31} = k_{32}^{[1]} + k_{23}^{[2]} ; k_{14} = k_{41} = k_{21}^{[2]} ; k_{22} = k_{11}^{[1]} ; k_{23} = k_{32} = k_{12}^{[2]} ; k_{24} = k_{42} = 0 ; k_{33} = k_{22}^{[1]} + k_{33}^{[2]} ; k_{34} = k_{34} = k_{31}^{[2]} ; k_{44} = k_{11}^{[2]} .$$

$$f_1 = F_3^{[1]} + F_2^{[2]} ; f_2 = F_1^{[1]} ; f_3 = F_2^{[1]} + F_3^{[2]} ; f_4 = F_1^{[2]} .$$

From figure-2, we have global stiffness matrix and global load vector

$$K = \begin{bmatrix} k_{11} & k_{12} & k_{13} & k_{14} & k_{15} & k_{16} & k_{17} & k_{18} \\ k_{21} & k_{22} & k_{23} & k_{24} & k_{25} & k_{26} & k_{27} & k_{28} \\ k_{31} & k_{32} & k_{33} & k_{34} & k_{35} & k_{36} & k_{37} & k_{38} \\ k_{41} & k_{42} & k_{43} & k_{44} & k_{45} & k_{46} & k_{47} & k_{48} \\ k_{51} & k_{52} & k_{53} & k_{54} & k_{55} & k_{56} & k_{57} & k_{58} \\ k_{61} & k_{62} & k_{63} & k_{64} & k_{65} & k_{66} & k_{67} & k_{68} \\ k_{71} & k_{72} & k_{73} & k_{74} & k_{75} & k_{76} & k_{77} & k_{78} \\ k_{81} & k_{82} & k_{83} & k_{84} & k_{85} & k_{86} & k_{87} & k_{88} \end{bmatrix} \text{ and } F = \begin{bmatrix} f_1 \\ f_2 \\ f_3 \\ f_4 \\ f_5 \\ f_6 \\ f_7 \\ f_8 \end{bmatrix}$$

Where k_{ij} and F_i are the global coefficients, which can be written in terms of the element coefficients.

$$k_{12} = k_{21} ; k_{13} = k_{31} ; k_{14} = k_{41} ; k_{15} = k_{51} ; k_{16} = k_{61} ; k_{23} = k_{32} ; k_{24} = k_{42} ; k_{25} = k_{52} ; k_{26} = k_{62} ; k_{27} = k_{72} ;$$

$$k_{28} = k_{82} ; k_{34} = k_{43} ; k_{35} = k_{53} ; k_{36} = k_{63} ; k_{37} = k_{73} ; k_{38} = k_{83} ; k_{45} = k_{54} ; k_{46} = k_{64} ; k_{47} = k_{74} ; k_{48} = k_{84} ;$$

$$k_{56} = k_{65} ; k_{57} = k_{75} ; k_{58} = k_{85} ; k_{67} = k_{76} ; k_{68} = k_{86} ; k_{78} = k_{87} ; k_{11} = K_{11}^{[1]} ; k_{12} = K_{12}^{[1]} ; k_{13} = k_{14} = k_{15} = 0 ;$$

$$k_{16} = k_{17} = k_{71} = 0 ; k_{18} = k_{81} = K_{13}^{[1]} ; k_{22} = K_{22}^{[1]} + K_{22}^{[2]} + K_{22}^{[3]} + K_{22}^{[4]} ; k_{23} = K_{31}^{[4]} ; k_{24} = K_{31}^{[3]} + K_{32}^{[4]} ; k_{25} = 0 ;$$

$$k_{26} = K_{23}^{[2]} + K_{32}^{[3]} ; k_{27} = 0 ; k_{28} = K_{23}^{[1]} + K_{21}^{[2]} ; k_{33} = K_{11}^{[4]} ; k_{34} = K_{12}^{[4]} ; k_{35} = k_{36} = k_{37} = k_{38} = 0 ;$$

$$k_{44} = K_{11}^{[3]} + K_{22}^{[4]} + K_{33}^{[6]} ; k_{45} = K_{31}^{[6]} ; k_{46} = K_{12}^{[3]} + K_{32}^{[6]} ; k_{47} = k_{48} = 0 ; k_{55} = K_{11}^{[6]} ; k_{56} = K_{12}^{[6]} ; k_{57} = k_{58} = 0 ;$$

$$k_{66} = K_{33}^{[2]} + K_{22}^{[3]} + K_{33}^{[5]} + K_{22}^{[6]} ; k_{67} = K_{31}^{[5]} ; k_{77} = K_{11}^{[5]} ; k_{78} = K_{12}^{[5]} ; k_{88} = K_{33}^{[1]} + K_{22}^{[2]} + K_{22}^{[5]} ;$$

$$f_1 = F_1^{[1]}; f_2 = F_2^{[1]} + F_2^{[2]} + F_3^{[3]} + F_3^{[4]}; f_3 = F_1^{[4]}; f_4 = F_1^{[3]} + F_2^{[4]} + F_3^{[6]}; f_5 = F_1^{[6]};$$

$$f_6 = F_3^{[2]} + F_2^{[3]} + F_3^{[5]} + F_2^{[6]}; f_7 = F_1^{[5]}; f_8 = F_3^{[1]} + F_1^{[2]} + F_2^{[5]};$$

PROBLEM FORMULATION

In this section, in order to find the reliability and accuracy of the finite element method, we consider a two-dimensional boundary value (Torsion) problem.

$$\frac{\partial^2 u}{\partial^2 x} + \frac{\partial^2 u}{\partial^2 y} = -2 \quad \text{in } \Omega$$

$$u = 0 \text{ on } c_1 \quad \text{and} \quad \frac{\partial u}{\partial n} = 0 \text{ on } c_2$$
(1.6)

in a square region[see Fig.2(a)]

$$\Omega = \{(x, y) : -0.5 < x < 0.5, -0.5 < y < 0.5\}$$

where $u(x, y)$ is the Prandtl stress function and c_1, c_2 are boundaries of the constitute the cross-section. The finite element model of equation (1.6) can be expressed as the matrix form as

$$[K]\{u\} = \{F\}$$

Where, $[K]$ = Global stiffness matrix.

$\{u\}$ = Nodal displacement vector.

$\{F\}$ = Nodal force vector/global load vector.

The torsional constant k is given by

$$k = \iint_{\Omega} u_i(x, y) dx dy$$

APPLICATION EXAMPLE

In this section, we consider one example to verify efficiency of our proposed finite element method (FEM). The approximate results of stress function values, torsional constant (k) and maximum errors (E_k) are obtained and shown in table-1:

Example1: The Finite Element (FE) models of the physical geometry are shown in figures-2(a), 2(b) and 2(c). This cross-section has four axes of symmetry; therefore, only one –eight of the cross-section needs to be analyzed. This fractional portion is partitioned into three elements as shown in the figure 2(b) and 2(c).

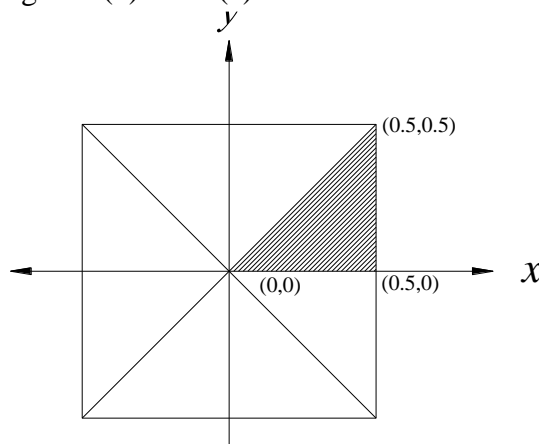


Figure 2(a): Axes of symmetry of a square cross-section

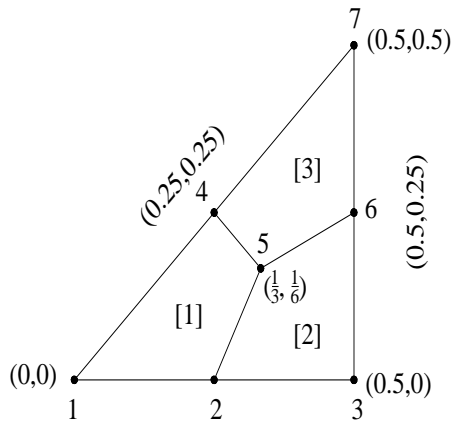


Figure 2(b): The FE model-1 with 3 four-nodded elements

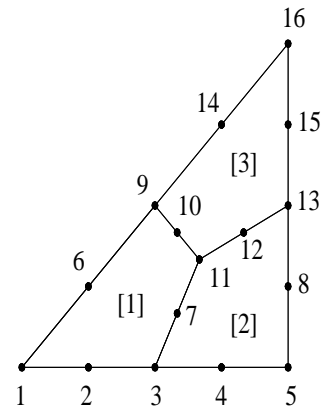


Figure 2(c): The FE model-2 with 3 Eight-nodded elements

Table-1: Computed stress function values, torsional constant k and Error a square cross section.

FE Model No	u_i values						Computed Torsional constant k	Error E_k
	i	u_i values	i	u_i values	i	u_i values		
1	1	0.1687704123	2	0.1098614665	4	0.07088683659	0.1209181652	14.01%
	5	0.07059626924	-	---	-	---		
2	1	0.1507258725	2	0.1403092055	3	0.1126971687	0.135182421	3.87%
	4	0.06759445117	6	0.1335117459	7	0.1008446742		
	9	0.08784755322	10	0.08585832250	11	0.07697950938		
	12	0.04150879918	14	0.03661101666	-	---		
Exact Torsional constant k= 0.140625								

RESULT AND DISCUSSION

The accuracy of the solution will depend on small element size. A measure of error $E_k = 100|1 - k/k_{exact}|$ is given when an exact solution of the torsional constant (k) is available. From the figure: 2(b) for FE model-1 using the developed element of this study computed torsional constant $k=0.1209181652$ and error (E_k) = 14.01%. We get also from the figure: 2(c) for FE model-2 using the developed element of this study computed torsional constant $k=0.135182421$ and error (E_k) = 3.87%. Finally we observe that the computed result is more efficient and it is expected that the torsional constant may be computed by increasing element numbers.

CONCLUSION

In this paper, we have used finite element method (FEM) to find numerical solution of saint Vennant torsion problem for a square cross section. An important part of finite element modelling is the mesh generation, which involves numbering the nodes and elements, and the generation of nodal coordinates and the connectivity matrix. The numerical solutions obtained by the proposed method are comparing with the exact solutions in good agreement. The finite element solutions obtained by two different meshes of triangular elements are compared in table-1. The finite element solution obtained by 6-triangular elements is most accurate when compare to the FE solution obtained by 2-triangular elements. Finally we may be concluded that numerical solution of saint-vennat torsion problem apply the higher order elements is more efficient.

ACKNOWLEDGEMENTS

The authors would like to thank the anonymous referees for their valuable suggestions to improve the quality of the paper. We would also like to express our deep gratitude to the Professor Dr. Moqbul Hossain and Dr. Nurul Alam Khan for their kind help to this research work.

REFERENCES

- Li, Z., Ko, J.M. and Ni, Y.Q., 2000, "Torsional Rigidity of Reinforced Concrete Bars with Arbitrary Sectional Shape", *Finite Elements in Analysis and Design*, 35, 349-361.
- Najera, A. and Herrera, J.M., 2005 "Torsional Rigidity of Non-Circular Bars in Mechanisms and Machines", *Mechanism and Machine Theory*, 40, 638-643.
- Darılmaz, K., Orakdogan, E. and Girgin, K., 2007, "Torsional Rigidity of Arbitrarily Shaped Composite Sections by Hybrid Finite Element Approach", *Steel and Composite Structures*, 7, 241-251.
- Jog, C. S., and Mokashi, I. S., 2014, "A Finite Element Method for the Saint-Venant Torsion and Bending Problems for Prismatic Beams", *Computers and Structures*, 135, 61-72.
- Islam, M.I and Karim, M.S, 2017, "Analysis of the Finite Element Solutions of Saint Venant torsion problem for a trapezoidal cross section", *International Conference on Mechanical, Industrial and Materials Engineering (ICMIME-2017)*, 1-6.
- Barretta, R; Feo,L and Luciano,R, 2015,"Some closed form solutions of functionally graded beams undergoing nonuniform torsion",*Composite structures*,123,132-136.
- Teimoori, H., Faal, R.T., Das, R, 2016 "Saint-Venant torsion analysis of bars with rectangular cross-section and effective coating layers", *Appl. Math. Mech.* , 37(2), 237–252 .
- Taheri, F., Hematiyan, M.R. 2017, "Torsional analysis of hollow members with sandwich wall, *J. Sandw. Struct. Mater.* **19**(3), 317–334 .
- Nguyen, H. S., 1992, "An Accurate Finite Element formulation for Linear Elastic Torsion Calculations. *Computers & Structures*, 42(.5), 707-711
- Ecsedi, S., Baksa, A., 2010, "Prandtl's formulation for the Saint-Venant's torsion of homogeneous piezoelectric beams", *International Journal of Solids and Structures*, .47(22-23), 3076-3083.

STUDY ON THE USE OF SUGARCANE BAGASSE ASH IN CONVENTIONAL CONCRETE AND IT'S IMPACT ON STRENGTH AND WORKABILITY

N.M. Khan & N.H.M. K.Serker*

*Department of Civil Engineering, Rajshahi University of Engineering & Technology,
Rajshahi, Bangladesh.*

E-mail: nafees111988@gmail.com

**Corresponding Author*

ABSTRACT

Sugarcane Bagasse Ash (SCBA) is one kind of waste which can be termed as the residue left over from burning sugarcane bagasse. The utilization of this waste may be very economical and can also solve the environmental problem. The partial replacement of cement and sand by SCBA can reduce the production of cement and also reduce the cost of making concrete.

SCBA has been chemically and physically characterized in this paper. From chemical test it shows that bagasse ash contains significant amount of silica. The effect of cement replacement by SCBA on the setting time was evaluated. Then cement was replaced by SCBA upto 25% in conventional concrete with a mix proportion of 1:2:4 and compressive strength at the ages of 7, 28 and 90 days was determined. Effect of addition of bagasse ash on the workability of concrete was also studied in this study. Results show that replacing cement by SCBA upto 25% in conventional concrete increases the slump value gradually from 0% to 15% and increasing more than 15% decreases the slump value. Replacement of 5% cement with SCBA gains more compressive strength than target strength, where as 10% cement replacement causes a slight reduction in compressive strength compare with target strength at 28 days. Finally sand was also replaced by SCBA upto 60% by volume in conventional concrete with same mix proportion and compressive strength at the ages of 7, 28 and 120 days was also evaluated. The test results show that upto 30% sand replacement causes strength gaining more than 100% of target strength at 28 days. Conventional concrete where sand replaced by SCBA at 10%, concrete gain more compressive strength than 0% sand replaced by SCBA at 7, 28 and 120 days test separately.

Keywords: Sugarcane Bagasse Ash; Workability; Compressive Strength.

INTRODUCTION

Bangladesh is a developing country. As a developing country focus are given on ways of utilizing the waste products. These wastes utilization would not only be economical, but may also help to create a sustainable and pollution free environment (Vyavhare, 2013; Modani, 2013). Sugar mill is one of the major sources of wastes in Bangladesh. There are several sugar mills in Bangladesh which produce 0.8 million ton Sugarcane Bagasse Ash (SCBA) approximately per year. These by products and wastes are not only difficult to dispose but also cause some health hazards. Disposal and management are the major tasks for this large amount of wastes. Today, the main aim of the environmental agencies and governments is to minimize the disposal problem. The productive use of these materials is one of the best ways to alleviate some of the problems of the solid waste management (Srivastava, 2014; Krishna, 2014). One of the key solutions is to utilize these wastes in the concrete.

There are several types of industrial wastes which can be utilized in the concrete either as a replacement of cement or as an additive material. Some of these wastes are Coal Fly Ash, SCBA, Ground Granulated Blast Furnace Slag, Waste Glass, Plastics, Wood Ash, Rice-husk ash etc. It has been identified that utilization of these wastes enhances some properties of the concrete (Ganesan et

al., 2007). Significant researches have been going on in various parts of the world related to these subjects.

Sugarcane bagasse is burned under controlled condition in high temperature which contains the large amount of silica which has pozzolanic properties. The use of SCBA in concrete can also reduce the environmental pollution and save the sources of natural raw materials used in the construction industry (Srinivasan, 2010; Sathiya, 2010). In this present study, investigation of the effect of SCBA in conventional concrete by partial replacement of cement at various ratios by weight was done. To study the effect of replacing the fine aggregate was also carried out. Concrete cylinders with different proportion of SCBA were cast to determine the compressive strength. Workability of the concrete mix was measured alongside using standard test. Determination of chemical composition of SCBA was done using the standard specifications. Determination of initial and final setting times of partially replaced cement by SCBA was also done.

METHODOLOGY

The workability and compressive strength of conventional concrete were determined experimentally where cement and sand were partially replaced with SCBA. The standard methods of testing the physical properties of aggregates and chemical properties of SCBA were used in this study and discussed in following sections.

Materials Used for the Research

Cement: The ordinary Portland cement of strength class: 52.5 N (as per BDS EN 197-1) was used in this research work. This cement has specific gravity of 3.15 and normal consistency of 28%.

Fine aggregate: Fine aggregate (commonly known as Domer sand) free from debris was used having specific gravity of 2.62, fineness modulus of 2.44 and unit weight 1521.62 kg/m³.

Coarse aggregate: Coarse aggregate (crushed black stone) was used having specific gravity of 2.66, fineness modulus of 7.09 and unit weight 1631.22 kg/m³.

Determination of Properties of SCBA

SCBA was collected during the cleaning operation of a boiler in the sugar factory, located in the town of Harian, Rajshahi. SCBA was used having specific gravity of 2.10; fineness modulus of 0.93 and unit weight 444.82 kg/m³.

Portland cement mainly content particle size of equal and less than 75 µm. When both cement and sand was partially replaced by SCBA the particle size of SCBA need to be close of cement or sand particle size. So SCBA was obtained after passing through 75µm standard sieve used for this thesis.

The chemical composition test was done in Central Science Lab, University of Rajshahi. The chemical test for the determination of different constituents in the SCBA sample was performed using EDXRF (Energy Dispersive X-ray Fluorescence) spectrometer.

Table 1 Chemical composition of Portland cement, Fly Ash and SCBA

Materials	SiO ₂	Al ₂ O ₃	Fe ₂ O ₃	CaO	MgO	MnO	Na ₂ O ₃	TiO ₂	K ₂ O	SO ₃	LOI
Portland Cement Type II	22.4	3.3	2.9	52.2	2.3	0.1	0.4	0.3	1	13.5	1.5
Fly Ash C class	48-68	18-34	2-8	15-39	3-6	-	-	-	-	1-5	0.1-12
SCBA (Rajshahi)	86.93	2.52	2.53	-	-	7.54	-	0.23	-	-	0.25

Results from the analysis of the chemical composition of SCBA are shown in table. The chemical composition of baggase ash was compared with type II Portland cement and class C fly ash. Data of type II Portland cement and class C fly ash were collected from Abbasi and Zargar's (2013) research work. It was observed that SCBA mainly content silica (SiO₂) which is larger in compare with

Portland cement and fly ash. Cement and fly ash content a fair amount of calcium oxide, where SCBA was not content any calcium oxide. Silica and lime are the two main compounds which play the major role in binding the concrete and strength development of concrete.

Experimental Work

First we determined the setting time of cement using SCBA upto 25%. Second experimental investigation was to partially replace cement with SCBA upto 25% on the basis of weight (0%, 5%, 10%, 15%, 20%, and 25%) and third experimental investigation was to partially replace sand with SCBA upto 60% on the basis of volume (0%, 10%, 20%, 30%, 45%, and 60%) to study the effect on strength and workability of conventional concrete.

The mix design of concrete was done according to Indian Standard guidelines, where the concrete grade was used M 20 for both case. Maximum nominal aggregate size was used 20 mm, mixing proportion of concrete was used 1:2:4 (cement: fine aggregate: coarse aggregate). For cement replacement with SCBA water cement ratio was used 0.50 and for sand replacement with SCBA the water cement ratio was used 0.55.

For M 20 grade = concrete grade strength = 20 MPa (cube) = 16 MPa (cylinder)

A total of 108 numbers of concrete specimens were casted in full study. The specimens considered in this study consisted 300 mm long and 150 mm diameter cylinders. A total of 54 numbers of cylinders were casted for each case and each of these six different percentages of both cases workability was found out by slump test as per Abram's law.

The ingredients of concrete were thoroughly mixed in mixer machine till uniform thoroughly consistency was achieved. Before casting, machine oil was smeared on the inner surfaces of the cast iron mould. Concrete was poured into the mould and compact thoroughly using vibrator. The top surface was finished by means of a trowel. The specimens were removed from the mould after 24h. All the cylinder specimens were cured for different time period. After curing each specimens were tested for compressive strength at different days of curing. The specimens were taken out from the curing tank just prior to the test. The test for compressive strength was conducted using universal testing machine.

RESULTS AND DISCUSSIONS

Our test results are divided into two parts. In first case cement was replaced by SCBA upto 25% by weight and in second case sand was replaced by SCBA upto 60% by volume. The results obtained from the experimental investigations are showed in tables. All the values of compressive strength are the average of the three trails in each case in the testing program of this study. The results are discussed as follows.

Table 2 initial & final setting times of cement using SCBA

Cement content % (by weight)	SCBA content % (by weight)	Initial Setting Time (minutes)	Final Setting Time (minutes)
100 %	0 %	64	250
95 %	5 %	40	240
90 %	10 %	29	210
85 %	15 %	20	205
80 %	20 %	14	181
75 %	25 %	11	172

SCBA has a tendency to absorbed water from cement paste, because of this tendency the setting times of cement decreased gradually with the increased percentage of SCBA in cement paste. As per Indian Standard (IS) minimum initial setting time of OPC cement should be 30 minutes and maximum final setting time of OPC cement should be 600 minutes. Upto 10% SCBA used cement give initial setting time close to minimum value given by IS. For final setting time all the values are within the limit of IS.

Cement Replacement by SCBA

Target strength or grade strength of cylinder at 28 days = 16 MPa

Table 3 Slump value, compressive strength, and percentage strength gain of target strength by concrete where cement replaced by SCBA upto 25% at 7, 28 and 90 days.

Cement replacement by weight (%)	Slump value (mm)	Compressive strength at 7days (MPa)	Compressive strength at 28 days (MPa)	Compressive strength at 90 days (MPa)	Strength at 7 days compared to target strength (%)	Strength at 28 days compared to target strength (%)	Strength at 90 days compared to target strength (%)
0	10	14.14	21.25	23.80	88.38	132.81	148.75
5	13	13.12	19.51	23.18	82.00	121.94	144.88
10	24	11.11	15.71	19.54	69.44	98.19	122.13
15	38	9.82	13.22	18.09	61.38	82.63	113.06
20	6	9.30	11.18	16.01	58.13	69.88	100.06
25	8	7.77	10.19	13.86	48.56	63.69	86.63

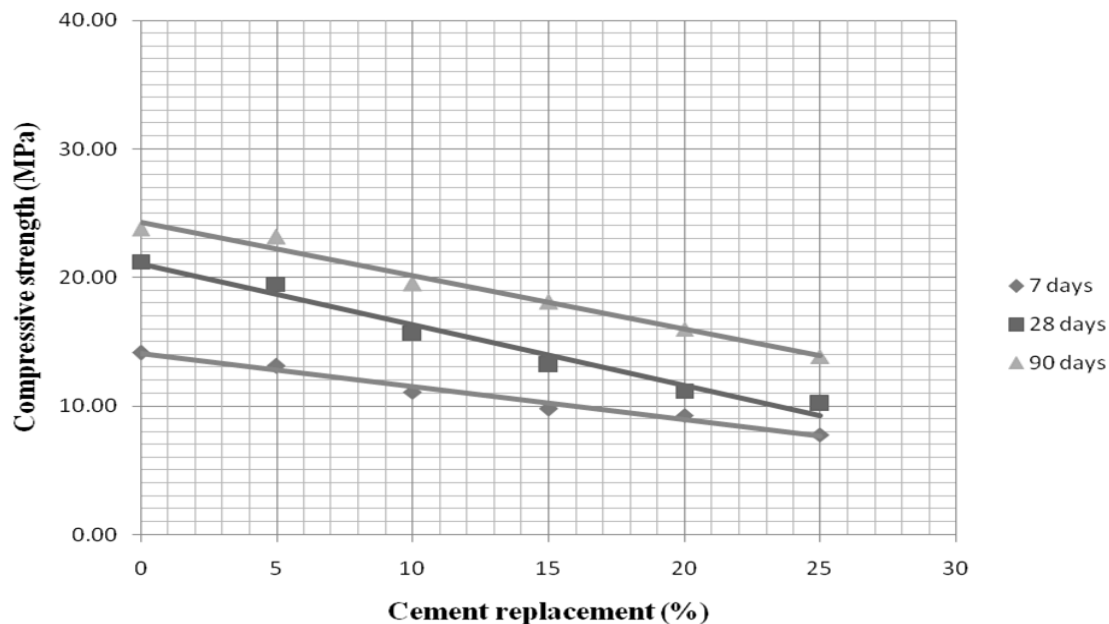


Figure 1 Compressive strength (MPa) vs Cement replacement in percentage

In normal condition where cement was not replaced with SCBA has an average compressive strength = 21.25 MPa at 28 days, which is greater than concrete grade strength = 16 MPa. Slump value increased gradually upto 15% when cement was partially replaced by SCBA. Upto 10% cement replaced with SCBA concrete gain over 69% of target strength at 7 days which is greater than desire strength of 65%. At 5% cement replaced with SCBA concrete gain 121.92% of target strength and at 10% cement replaced with SCBA gain over 98% of target strength at 28 days. Also upto 20% cement replaced with SCBA, concrete gain compressive strength more than 100% of target strength at 90 days.

Sand Replacement by SCBA

Target strength or grade strength of cylinder at 28 days = 16 MPa

Table 4 Slump value, compressive strength, and percentage strength gain of target strength by concrete where sand replaced by SCBA upto 60% at 7, 28 and 120 days.

Sand replacement by volume (%)	Slump value (mm)	Compressive strength at 7days (MPa)	Compressive strength at 28 days (MPa)	Compressive strength at 120 days (MPa)	Strength at 7 days compared to target strength (%)	Strength at 28 days compared to target strength (%)	Strength at 120 days compared to target strength (%)
0	27	14.01	21.24	29.20	87.56	132.75	182.50
10	24	14.20	23.03	30.55	88.75	143.94	190.94
20	19	12.49	19.23	22.38	78.06	120.19	139.88
30	12	11.06	18.21	21.88	69.13	113.81	136.75
45	10	6.60	9.63	10.50	41.25	60.19	65.63
60	12	5.91	7.63	10.09	36.94	47.69	63.06

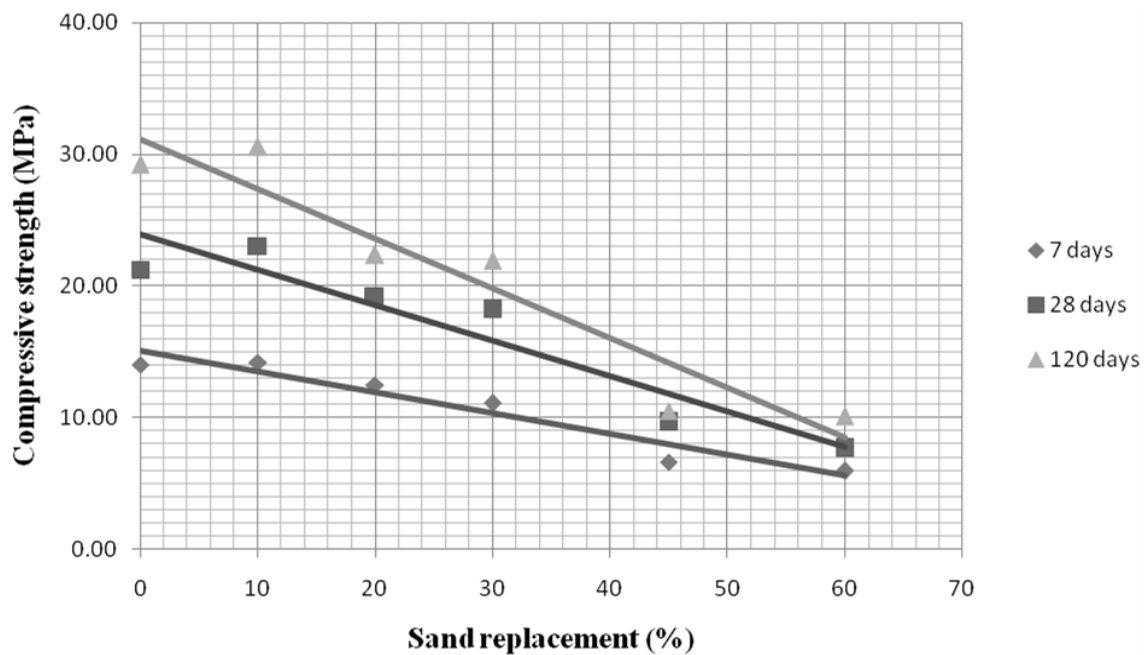


Figure 2 Compressive strength (MPa) vs Sand replacement in percentage

In normal condition where sand was not replaced with SCBA has an average compressive strength = 21.24 MPa at 28 days, which is greater than concrete grade strength = 16 MPa. By replacing sand with SCBA upto 45% volume wise, the workability of concrete decreased gradually with the increased of SCBA in the concrete. Upto 30% sand replaced with SCBA concrete gain over 69% of target strength at 7 days which is greater than desire strength of 65%. Upto 30% sand replaced with SCBA volume wise, concrete gain compressive strength over 113% of target strength at 28 days and at this point concrete also gain compressive strength over 136% of target strength at 120 days.

CONCLUSIONS

SCBA was chemically and physically characterized and then it was used as partial replacement of cement upto 25% to determine the effect on setting time of the binding material. After that SCBA was used in conventional concrete which was divided into two parts. First, Cement replaced by SCBA upto 25%. Second, Sand replaced by SCBA upto 60%. From the experimental investigation and discussion of results, the following conclusions are drawn-

- SCBA has a tendency to absorb water from cement paste, because of this tendency the initial and final setting times of cement decreased when the percentage of SCBA increased in cement.
- When cement partially replaced with SCBA in conventional concrete upto 25% by weight, workability of the concrete increased gradually from 0% to 15%. But when sand replaced

with SCBA upto 60% volume wise, the workability of concrete decreased gradually with the increased of SCBA from 0% to 45% in the concrete.

- Conventional concrete where cement was replaced by SCBA at 10%, concrete gain compressive strength close to target strength at 28 days.
- When sand was replaced by SCBA at 10% in conventional concrete, concrete gain more compressive strength than 0% sand replacement with SCBA occurs at 7, 28 and 120 days test separately. Also at 10% when sand was replaced by SCBA in conventional concrete 28 days strength gain more than 143% of target strength.
- When cement was replaced by SCBA from 5% to 25% by weight and sand was replaced by SCBA from 10% to 30% by volume in conventional concrete, long-term strength gain by concrete for each condition was more than 115% compare to 28 days strength which was significant.
- From chemical composition test it was observed that SCBA mainly contain siliceous and some aluminous materials which in the presence of water react with calcium hydroxide (Portland cement) to form compound possessing cementitious properties. So SCBA can be used as mineral admixture or filler material in concrete which has some pozzolanic properties.

REFERENCES

- Abbasi, AK and Zargar, A. 2013. Using baggase ash in concrete as pozzolan. *Middle- East Journal of Scientific Research*, 13 (6): 716-719.
- ASTM, American Society for Testing and Materials, Annual Book of ASTM Standards.
- Ganesan, K; Rajagopal, K and Thangavel, K. 2007. Evaluation of bagasse ash as supplementary cementitious material. *Cement and Concrete Composites*, 29 (6): 515-524.
- IS 456 : 2000, Code of practice plain and reinforced concrete. Bureau of Indian Standards, New Delhi.
- IS 10262 : 2009, Concrete mix proportioning – guidelines. Bureau of Indian Standards, New Delhi.
- Srinivasan, R and Sathiya, K. 2010. Experimental study on bagasse ash in concrete. *International Journal for Service Learning in Engineering*, 5 (2): 60-66.
- Srivastava, AP and Krishna, V. 2014. Potential of industrial wastes and by- products in concrete: an innovative embodiment to sustainability. *International Journal of Civil Engineering and Technology*, 5 (8): 101-113.
- Vyavhare, M and Modani, P. 2013. Utilization of bagasse ash as a partial replacement of fine aggregate in concrete. *Procedia Engineering*, 51 (2013), 25-29.

APPLICABILITY OF RICE HUSK BIOCHAR AS A PARTIAL REPLACEMENT OF CEMENT

M.A. R. Shuvo*, M. A. N. Hasan, M. M. Atiya & E. R. Latifce

Civil Engineering Department, Ahsanullah University of Science and Technology, Dhaka, Bangladesh.

E-mail : ashifrshuvo@gmail.com

**Corresponding Author: ashifrshuvo@gmail.com*

ABSTRACT

Worldwide cement industry emits 5% of the total annual CO₂ emitted by man-made causes. Carbon emission can be reduced by replacing cement with an alternative material in the preparation of concrete. ‘Carbon sequestration’ which is a natural or artificial process by which carbon dioxide is removed from the atmosphere and held in solid or liquid form. Carbon savings come from carbon sequestered for the long-term (100's to 1000's years) in biochar. If we are able to confine the carbon in the form of biochar in concrete, it will remain there for a long time even after the disposal of concrete. This study focused on determining the optimum amount of Rice husk biochar that can be replaced in cement-concrete without losing much its strength and durability. The mechanical properties, i.e., compressive strength, water retention rate & workability were measured using sample mortar mixes that contained rice husk biochar as a replacement of cement at 0%, 5% & 10% replacement rate. 27 specimens of 2" mortar cubes were tested for compressive strength after 28 days of water curing, 28 days of air curing & 56 days of water curing. To examine the water retention rate, the weight losses of the specimens were measured at different intervals up to 49 days. To measure the workability, flow test of mortar mixes was conducted. It was found that biochar can be used as a replacement of cement up to 5% without significantly reducing the workability and strength. Another significant observation is that biochar mixed sample continues to gain strength at a moderate rate even after 28 days of curing, whereas the increase rate for ordinary concrete mixes is very low after 28 days.

Keywords: Rice husk biochar; carbon sequestration; compressive strength; curing; cement replacement

INTRODUCTION

Cement is a must material for present day's construction industry. But its production requires a highly energy-intensive process and this process produces about 5% of man-made carbon dioxide annually (Choi et al., 2012). On the other hand, a large amount of dry waste is being disposed by burning them into ash and this process also emits a large amount of carbon dioxide. According to a study, in Germany, the incineration of 1 Mg of municipal waste in MSW incinerators is associated with the production/release of about 0.7 to 1.2 Mg of carbon dioxide (Johnke, 2001). One possible solution to these two problems is – try to turn the dry waste into biochar (not ash) and this biochar will be stored in the concrete and thus the carbon will be stored in the concrete instead of releasing carbon dioxide in the atmosphere. This sequestration process using biochar would reduce the release of carbon dioxide back into the atmosphere, but it is a challenge to consume the high carbon content of biochar in concrete. Because the carbon itself increases the water demand in the concrete and causes a reduction of compressive strength with an increase in replacement rate (Choi et al., 2012). But if it is possible to produce such biochar which has a some kind of cementitious property, then the reduction of compressive strength may be less. A study suggests that rice husk has the chemical compositions that

are required for pozzolanic activity (Cordeiro et al., 2009). So, rice husk can be used for producing biochar and replacing this biochar as a supplementary to cement and observing the negative effects and finally trying to find the optimum amount of replacement rate is our intention.

METHODOLOGY

Preparation of rice husk biochar

Rise husk biomass was first put in pyrolysis process (using an aluminium pot and cover the pot with a lid) through stove to convert it into biochar. At the beginning, the white smoke was emitting that is actually the moisture evaporating from the biomass. Heating has been stopped when the grey smoke starts to emit because the grey smoke creates when the carbon in the biomass is burnt. Then grind the biochar into fine particle when it has been cooled down.

Compressive strength test

This test method conforms to the ASTM standard requirements of specification C109. To make 2" cube mortar specimens, all the materials needed as per requirement was mixed to prepare a mixture of cement & sand having ratio of 1: 2.75. It goes on to say that 0%, 5% and 10% biochar is mixed (as the replacement of cement) separately for different samples. Water/cement ratio of 0.50 is controlled for all samples. In accordance with given specifications, tamping and water/air curing was done. For this test, 3 cubic specimens have been made for each batch (total 27 Nos.) and their compressive strength is measured under UTM and finally, the average strength of each batch was taken.

Water retention / weight loss test

To compare the water retention rate, weight loss has been measured by filling cylindrical containers (4" inside diameter & 5" height) with mortar mixes with 0%, 5% & 10% biochar variation as the replacement of cement. The mortar was put into the cylinders in three steps with uniform tamping. Once all the mixes were made, the weights were recorded in the following intervals: 0 hr, 1 hr, 2 hrs, 3 hrs, 5 hrs, 1 day, 3 days, 7 days, 10 days, 14 days, 20 days, 31 days, 39 days, and 49 days.



Fig. 1: Sample placing, tamping and measuring weight

Flow / workability test

In order to determine the workability of the mortar mix samples, a flow test was conducted by measuring the percentage of mortar flow in accordance with ASTM C1437. The test utilizes a specially designed table that repeatedly raises and drops a known quantity of mortar 25 times (Choi et al., 2012). A higher w/c ratio of 1.5 was used due to the unavailability of the shaking table. For this test a mold of 4 cm height, 6 cm top dia, 7 cm bottom dia was used. All the materials needed as per requirement was mixed to prepare a mixture of cement & sand having ratio of 1: 2.75. As usual three batches of sample mixes were prepared with 0%, 5% & 10% biochar variation as replacement of cement. First the mold was put on a smooth surface, then the mixes were poured into the mold up to top level & then the mold was taken away to allow the mortar to spread and finally the largest dimension was recorded.



Fig. 2: Mortar paste, Molding & measuring diameter after demolding sample

RESULTS AND DISCUSSIONS

Compressive strength test

Table 1: Compressive strength data

Sample ID	Crushing Load (lb)	Avg. Compressive Strength (psi)
NW28D	2378.92823	606.8694462
5% W28D	2084.74325	538.1371314
10% W28D	1207.87597	311.86896
NA28D	1605.11337	427.805605
5% A28D	1596.70551	412.1593995
10% A28D	862.187256	222.5573712
NW56D	2354.42405	617.6322592
5% W56D	2199.48573	567.8988127
10% W56D	1438.86716	377.4556967

Note:

- N, 5% & 10% = cement replacement rate by biochar (0%, 5% & 10% respectively);
- W & A = Curing condition (Water curing & Air curing respectively);
- 28D & 56D = Curing period (in days)

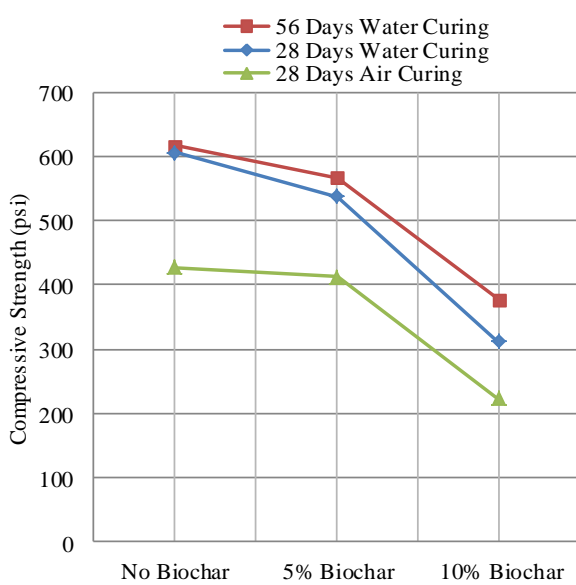


Fig. 3: Development of compressive strength

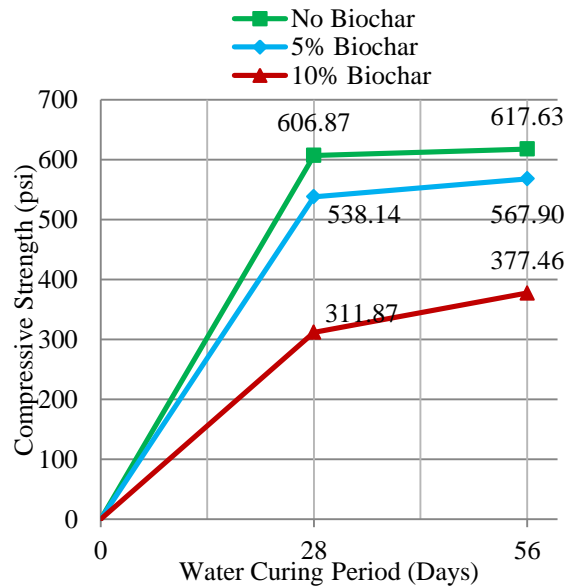


Fig. 4: Compressive strength development due to water curing for more than 28 days

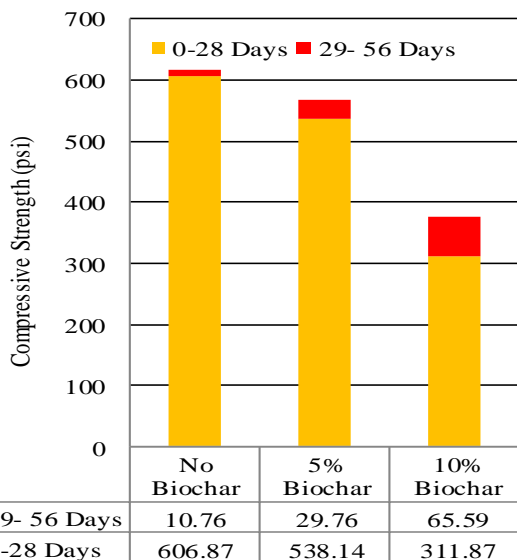


Fig. 5: Compressive strength development due to water curing for more than 28 days

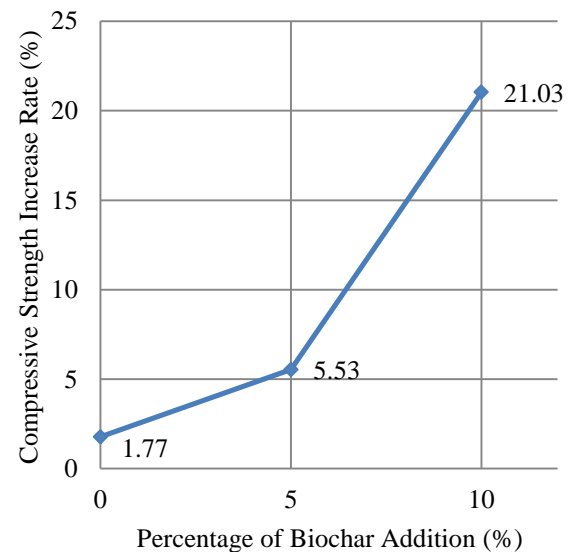


Fig. 6: Compressive strength increase between 28 to 56 days due to water curing

From Fig. 4-6, it can be concluded that –

- Normal concrete gains 99% of its total strength in 28 days.
- Due to addition of biochar into concrete, it continues to gain strength even after 28 days.

- For normal concrete the rate of gain of compressive strength is much slower after 28 days. Whereas for biochar mixed concrete, the rate is much higher.

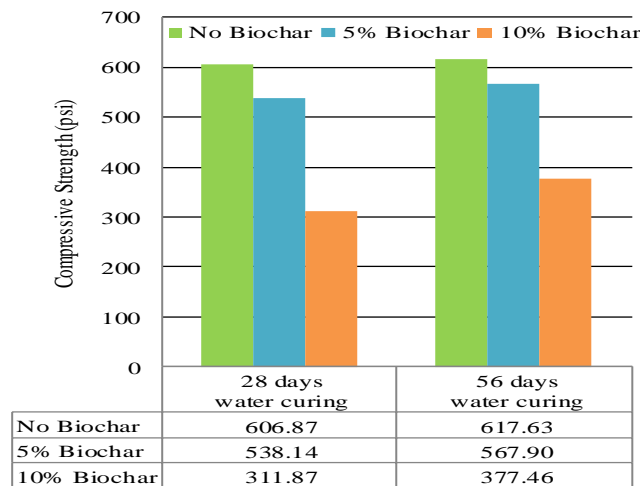


Fig. 7: Effect of biochar addition on strength depending on water curing period

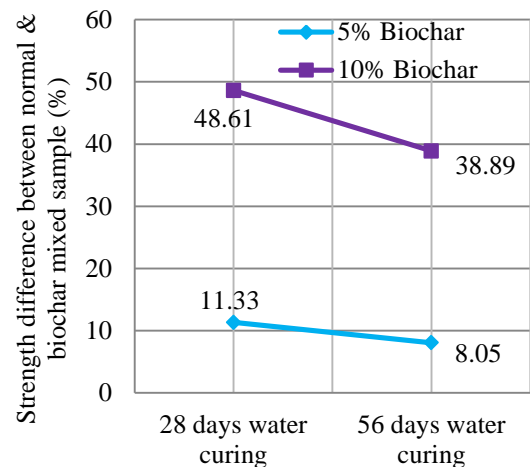


Fig. 8: Strength difference of biochar mixed sample w.r.t. normal mix with varying water curing period

From Fig. 7-8, it can be concluded that –

- According to the test result, compressive strength is reduced with the addition of biochar. The more the biochar is added, the more the strength is reduced.
- But if the biochar mixed sample is water cured for a long period, its strength might be equal to conventional mixed sample at a point.

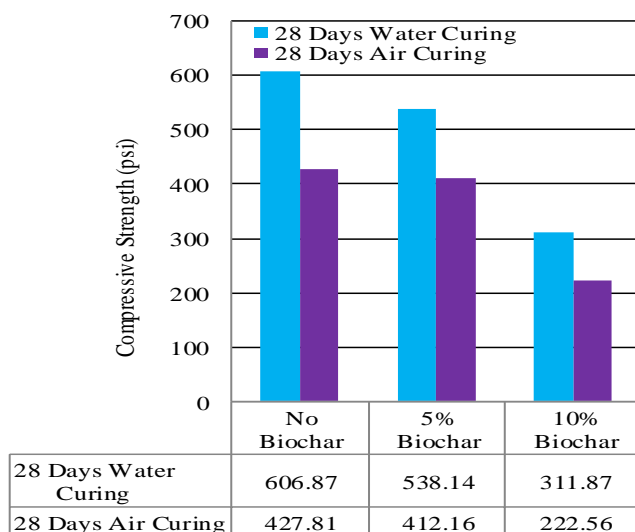


Fig. 9: Effect of biochar addition on strength depending on curing condition

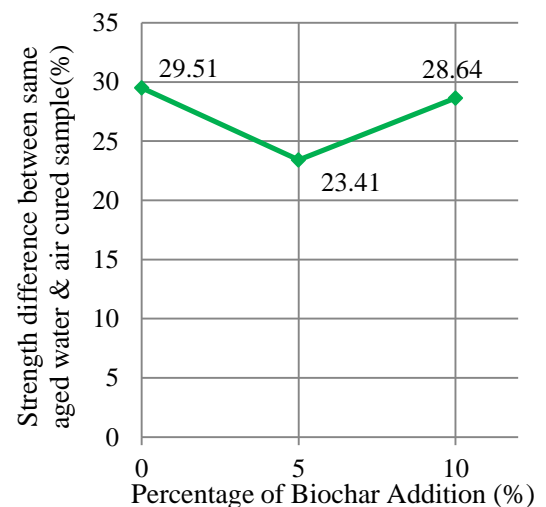


Fig. 10: Strength difference of air cured sample w.r.t. water cured with varying biochar addition

From Fig. 9-10, it can be concluded that –

- In normal practice, most of the time it is unable to continue the water curing regularly. Between these gaps, the concrete is mainly cured by air. That's why the strength gained is lower than the desired strength.
- But if the biochar mixed sample is used in normal practice, the strength will not be such lowered than that for normal concrete due to irregular water curing.

Water retention / weight loss test

Table 2: Percentage of weight loss with respect to initial weight

Time (hr)	Weight (g)			Weight Loss (g)			Percent of Weight Loss (%)		
	No Biochar	5% Biochar	10% Biochar	No Biochar	5% Biochar	10% Biochar	No Biochar	5% Biochar	10% Biochar
0	2258	2369	2536	0	0	0	0.000	0.000	0.000
1	2255	2366	2534	3	3	2	0.133	0.127	0.079
2	2253	2364	2532	5	5	4	0.221	0.211	0.158
3	2253	2363	2531	5	6	5	0.221	0.253	0.197
5	2251	2362	2530	7	7	6	0.310	0.295	0.237
24	2238	2349	2516	20	20	20	0.886	0.844	0.789
72	2220	2331	2496	38	38	40	1.683	1.604	1.577
168	2203	2312	2481	55	57	55	2.436	2.406	2.169
240	2194	2303	2476	64	66	60	2.834	2.786	2.366
336	2191	2302	2472	67	67	64	2.967	2.828	2.524
480	2185	2296	2469	73	73	67	3.233	3.081	2.642
744	2181	2291	2463	77	78	73	3.410	3.293	2.879
936	2174	2285	2459	84	84	77	3.720	3.546	3.036
1176	2171	2282	2457	87	87	79	3.853	3.672	3.115

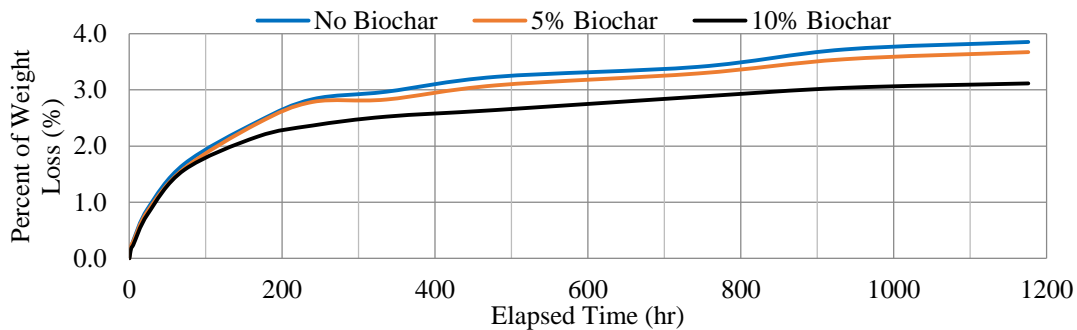


Fig. 11: Percentage of weight loss with time

Workability / flow test

Table 3: Determination of flow rate

Biochar Addition	Initial Average Diameter (inch)	Diameter After Flow (inch)	Difference in Diameter (inch)	Flow Rate (%)
0%	$(2.55+2.57)/2 = 2.56$	6.9	4.34	169.53
5%		6.7	4.14	161.72
10%		6.5	3.94	153.91

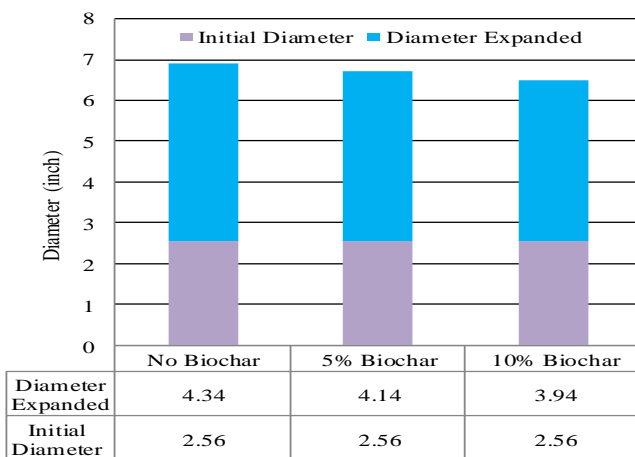


Fig. 12: Variation of workability due to biochar addition shown by column-chart

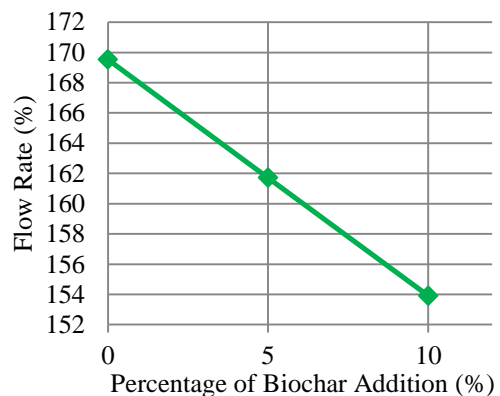


Fig. 13: Variation of flow rate due to biochar addition

Table 4: Result summary

Findings

Compressive Strength Test:

1. Carbon emission from cement industry can be reduced by reducing the use of cement. Biochar can be used as a replacement of cement in concrete upto 5% without significantly reducing the concrete strength. Thus the concrete can be a source for carbon sequestration.
2. The more the biochar-mixed concrete is water cured, the more the possibility that it gains the strength equal to normal concrete.
3. For biochar replaced mixes, it is found that concrete continues to gain strength at a moderate rate even after 28 days curing, whereas the increase rate for normal mixes is very low after that period. The reason is – biochar has a high water holding capacity and it holds the water that is added during casting.
4. If it is not possible to perform continuous water curing, the strength will not be such lowered for biochar-mixed concrete than that for normal concrete.

Weight Loss Test:

1. The weight loss over time due to moisture evaporation is less for the mortar mixes that include biochar than that for the conventional mix. It might be happened because biochar holds the water in it, that's why less moisture evaporates and thus the biochar mixed samples loose less weight than normal concrete.

Flow Test:

1. A negative effect of biochar addition is that – the more the replacement rate is, the less the workability of the mixture is.
2. For 5% biochar replacement, this problem is not that much effective.

CONCLUSIONS

Hazardous greenhouse gas emission from cement industry which is responsible for global warming can be reduced by using biochar as a partial replacement of cement in concrete upto 5 percent without significantly reducing its strength and in this process carbon will also be stored in concrete for a long term in the form of biochar instead of releasing into atmosphere as a gas. Alongside biochar can also be used as a self-curing agent in concrete due to its high water holding capacity. As a result, for conventional mixes of concrete, the increase rate of strength is significantly reduced after 28 days. But for biochar mixed mixtures, even after 28 days the increase rate is much better. Finally, a negative side of biochar addition is that – the more the biochar is used as a replacement of cement, the more the workability of the mix is reduced.

REFERENCES

- ASTM C109 / C109M-16a, Standard Test Method for Compressive Strength of Hydraulic Cement Mortars (Using 2-in. or [50-mm] Cube Specimens), ASTM International, West Conshohocken, PA, 2016
- ASTM C1437-15, Standard Test Method for Flow of Hydraulic Cement Mortar, ASTM International, West Conshohocken, PA, 2015
- Choi, Won Chang; Yun, Hyun Do; Lee, J. Y. (2012). Mechanical Properties of Mortar Containing Bio-Char From Pyrolysis. *Journal of the Korea institute for structural maintenance and inspection*, 16(3), pp.67–74.
- Cordeiro, G. C.; R. D. T. Filho; E. M. R. Fairbairn. 2009. Use of ultrafine rice husk ash with high-carbon content as pozzolan in high performance concrete. *Materials and Structures*, vol. 42, No. 7, 2009, pp.983-992.
- Johnke, Bernt. 2001. Emissions from waste incineration. *IPCC Good Practice Guidance and Uncertainty Management in National Greenhouse Gas Inventories*, Chapter 5, pp.463.
- Latifee, E. R. 2007. *An Introduction to Properties and Evaluation of Engineering Materials*. ISBN: 984-300-000839

EXPERIMENTAL INVESTIGATION ON THE EFFECT OF SUBSTRATE MOISTURE ON THE INTERFACIAL BOND STRENGTH BETWEEN SUBSTRATE AND OVERLAY CONCRETE

A. Rahman* & M. M. Hoque

*Department of Civil Engineering, Dhaka University of Engineering and Technology,
Gazipur, Bangladesh.*

E-mail: arifurrahmanbd@yahoo.com

**Corresponding Author*

ABSTRACT

This study aims at investigating the effect of substrate moisture content on the interfacial bond between substrate and overlay concrete. Several parameters were studied in this study such as: type of overlay concrete, moisture content and specimen shapes. A total 24 slant shear specimens made with brick and stone aggregate concrete (12 half prismatic + 12 half cubic) were tested. The substrate concrete surface was chipped with conventional metallic chisel and then the overlay concrete was bonded on it. In order to investigate the effect of moisture content, the substrate specimens were pre-wetted in potable water for 0, 8, 12, 24, 36 and 72 hours before adding overlay concrete. Afterwards, the slant shear test was conducted using the universal testing machine. Experimental results reveal that bond strength increases with moisture content up to 24 hours pre-wetted condition, when specimens were submerged more/less than 24 hours, bond strength found decreasing. The maximum bond strength was obtained 8.72 MPa and 7.11 MPa with prismatic (P) specimens whereas 8.41 MPa and 11.74 MPa with cubic (C) specimens for Brick to Brick (BB) and Brick to Stone (BS) specimens, respectively. The maximum bond strength was observed at 24 H pre-wetting SSD condition for both prismatic and cubic specimens.

Keywords: Substrate, overlay, interfacial bond strength, pre-wetting.

INTRODUCTION

Strengthening of existing structures is very common all over the world due to its financial viability and environmental friendliness as compared to reconstruction. In Bangladesh, a large scale strengthening have been being executed after the disastrous collapse of Rana Plaza at Savar, Dhaka especially, in the Ready-Made Garments (RMG) factory Buildings with a view to avoid manmade disaster. Strengthening are usually required to address a number of conditions of the existing structures; restorations, vertical extensions and horizontal expansion beyond the design limit, change of function of structures, change of load(s), inferior quality construction, improper structural design, deterioration of concrete due to aggressive environment or age and so on. There are several techniques of strengthening for instance, RC jacket, steel jacket, Fibre Reinforced Polymer (FRP) jacket, externally bonded reinforcement. Among different techniques of strengthening, RC jacket is very commonly used in Bangladesh accounting for the technical skill of the construction workers and cost of strengthening. In RC jacketing are accompanied by adding new concrete layer termed as overlay next to old concrete layer termed as substrate represents a common strengthening practice in all over the world. In most of the cases of RC strengthening, substrate concrete made from brick and/or stone aggregate are strengthened by stone aggregate concrete which reveals that composite member are made with non-homogenous or homogenous properties. The RC jacketing consists of wrapping overlay concrete with required reinforcements next to substrate concrete introducing different surface preparation techniques. The load transfer mechanism of substrate concrete (brick or stone) to overlay concrete (stone or brick) is different due to having different mechanical properties of brick and stone aggregates. The mechanical

properties; surface texture, moisture absorption capacity, unit weights, modulus of elasticity and mechanical interlocking capabilities of brick aggregate and stone aggregate are different. The bond developed at the interface of substrate to overlay concrete is largely influenced by several parameters: surface roughness, use of adhesives, moisture of the substrate surface, presence of micro-cracks, numbers of shear connector, and compressive strength of concrete (Julio et al., 2004; Beushausen, 2010; Talbot et al., 1994; Saucier et al., 1991; Silfwerbrand, 1990).

However, disagreement among the researchers have been observed on substrate pre-wetting before applying overlay concrete and the optimum moisture content to ensure proper bonding between substrate and overlay concrete interface. Even in codes of practice recommendations regarding substrate pre-wetting are shown contradictory. These controversial opinions are based on dry substrate concrete and wet substrate concrete resulting the formation of a harsh mix concrete and dilute overlay mix concrete respectively that affect the bond strength as stated by Beashausen & Alexander (2009). Talbot et al. (1994) stated that pre-wetting the substrate concrete (i.e., saturated surface dry surface) before applying overlay is the most appropriate solutions. Saucier and Pigeon (1991) refer to the AASHTO-AGC-ARTBA joint committee that recommends a dry substrate concrete except in dry and hot summer days, and the Canadian standard association A23.1 recommends that wetting the substrate surface for at least 24 h before applying overlay concrete.

In the contrast, Silfwerbrand (2003) and Zhu (1992) have reported that the moisture content does not play a major role in affecting bond strength of the repaired concrete specimen as long as there is no free water on the substrate surface. In connection to, Cleland and Long (1997) conducted an experimental study on four moisture condition of substrate concrete and found lower bond strength for oven dry and saturated substrate wet condition while a similar bond strength for laboratory dry and saturated substrate wet condition. In addition, Emmons (1994) mentioned that moisture level of the substrate surface may be critical in achieving bond and an excessively dry substrate may absorb too much water from the overlay while excessive moisture in the substrate may clog the pores and prevent absorption of the overlay concrete. In addition to, Silfwerbrand & Beushausen (2006) established a graph which represented the effect of moisture improving interfacial bond.

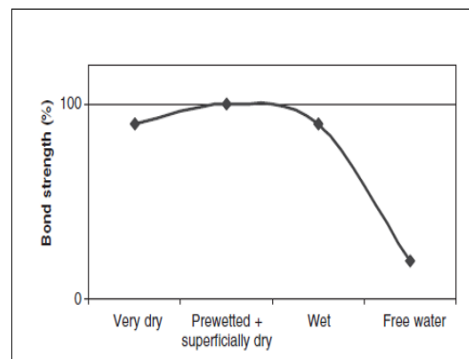


Fig.1: Effect of moisture condition on interfacial bond strength

Finally, conclusion can be drawn based on study conducted by Chorinsky (1996). He specified that excessively dry or excessively wet of substrate concrete dependably results in feeble of the interfacial bond. With this background, the present study aims to achieve the objectives;

- 1) To conduct literature review and
- 2) To investigate the effect of substrate moisture on the interfacial bond strength;

Methodology

In this study, a total number of 24 slant specimens were made where, 12 numbers prismatic specimens and 12 numbers cubic specimens. Adopted Prismatic and cubic specimens' dimensions were 200mmx200mmx450mm and 150mm x150mm x150 mm, respectively. In the first phase of constructing substrate specimens, first had the 12 nos. half prismatic and 12 nos. half cubic specimens with 30-degree inclination of having mixing ratio; cement: sand: brick aggregate are 1:15:3 and water: cement ratio is 0.45, specimens were cured for 30 days. After cured aforesaid days, these specimens were kept open to the air for 120days and substrate concrete have been made roughen by conventional

metallic chisel. On the second phase of adding overlay concrete, overlay concrete having mixing ratio; cement: sand: stone aggregate is 1:1.25:2.5 and water: cement ratio is 0.40 were added next to substrate concrete. Prior to adding overlays, substrate specimens have been pre-wetted to vary the moisture condition of the substrate. These substrate specimens were submersed before adding overlay for 0H, 8H, 12H, 24H, 36H and 72Hours, respectively. Adding overlay concrete, again these specimens were kept for curing for 30 days. Finally, these specimens were sent to laboratories for the evaluation of interfacial bond strength by Slant shear test as per ASTM C882 (1999). The water absorption capacity of brick and stone aggregates, compressive strength of both concretes and interfacial bond strength obtained for all situations are shown in Table 1, Table 2 and Table 3, respectively.



Fig.2: Monolithic failure (P); Fig.3: Substrate failure (P); Fig.4: Shear failure (P); Fig.5: monolithic failure (C);

Table -1: Water absorption capacity of brick aggregate and stone aggregate.

Type	Mass (SSD), gm.	Mass (oven dry at 105°C), gm.	Water absorption capacity %
Brick aggregate	3036	2796	9.00
Stone aggregate	3900	3732	5.00

RESULTS AND DISCUSSIONS

Table 2 represents the average values obtained with tests performed on standard specimens to evaluate the compressive strength of the substrate concrete and overlay concrete. In table 3, the interfacial bond strength in shear determined with the Slant shear test for prismatic and cubic specimens are given for different moisture conditions. The interfacial bond strength, illustrated in fig 6-11, shows that bond strength increases with the pre-wetted hours up to 24H, and when the specimens are pre-wetted more than 24H, interfacial bond strength is decreased. It is to be mentioned that the failure mode, observed in all specimens, tested for both prismatic and cubic specimens were found ambiguous with the relevant results. The maximum bond strength was obtained 8.72MPa and 7.11Mpa with prismatic specimens whereas 8.41Mpa and 11.74Mpa with cubic specimens for Brick to Brick (BB) and Brick to Stone (BS) specimens, respectively. In case of Prismatic specimens, illustrated in Fig 7 and Fig 9, bond strength were found increasing of 32%, 142%, 187%, 152%, 96% for BB and 62%, 85%, 99%, 91%, 75% BS specimens compared to 0H pre-wetting condition to each situations, respectively. And in case of cubic specimens, illustrated in Fig. 6 and Fig 8, bond strength were found increasing of 23%, 47%, 74%, 68%, 55% for BB and 19%, 38%, 57%, 51%, 15% for BS specimens compared to 0H pre-wetting condition to each situations, respectively. The maximum bond strength, in both cases, was observed for the 24H substrate pre-wetted SSD (saturated surface dry) condition.

Table -2: Strength of substrate and overlay concrete.

Type	Cylinder size	Avg. compressive strength, Mpa		Loading rate
		Substrate	Overlay	
BB(P)	100mmx200mm	22	26.6	2KN/S
BS(P)		22	36.2	
BS(C)		22	37.3	
SS(C)		37	40	

Table -3: Interfacial bond strength (Slant shear test results).

Parameters		Prismatic specimens			Cubic Specimens			
SL no.	Pre-wetted Hours, H	Type of specimen	Failure Load, KN	Bond strength Mpa	Name	Failure Load, KN	Bond strength Mpa	Type of Failure
		BB (Brick to brick bond)			BS (Brick to stone bond)			
1	0	BB-0H	156	3.04	BS-0H	248	4.83	Shear failure
2	8	BB-8H	206	4.01	BS-8H	305	5.94	Bond failure
3	12	BB-12H	378	7.36	BS-12H	364	7.09	substrate failure
4	24	BB-24H	448	8.72	BS-24H	432	8.41	Monolithic failure
5	36	BB-36H	393	7.65	BB-36H	416	8.10	Monolithic failure
6	72	BB-72H	306	5.96	BS-72H	384	7.48	Bond failure
		BS (Brick to stone bond)			SS (Stone to stone bond)			
7	0	BS -0H	184	3.58	SS-0H	384	7.48	Shear failure
8	8	BS-8H	298	5.80	SS-8H	457	8.90	substrate failure
9	12	BS-12H	340	6.62	SS-12H	529	10.30	substrate failure
10	24	BS-24H	365	7.11	SS-24H	603	11.74	Monolithic failure
11	36	BS-36H	352	6.85	SS-36H	580	11.29	Monolithic failure
12	72	BS-72H	321	6.25	SS-72H	455	8.86	Bond failure

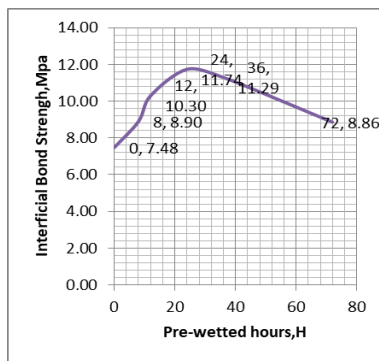


Fig. 6: SS Bond strength (C);

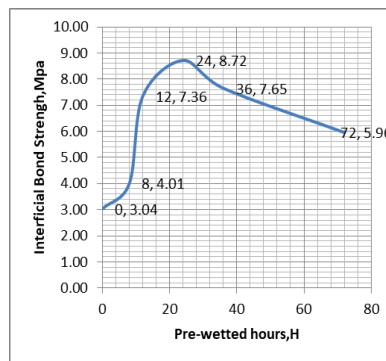


Fig. 7-BB Bond strength (P);

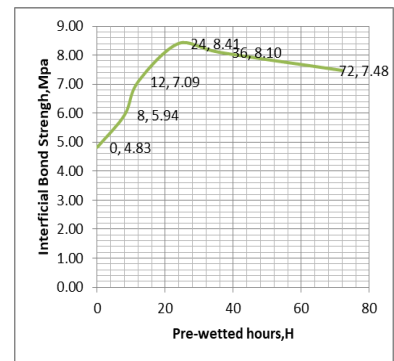


Fig. 8-BS Bond strength (C)

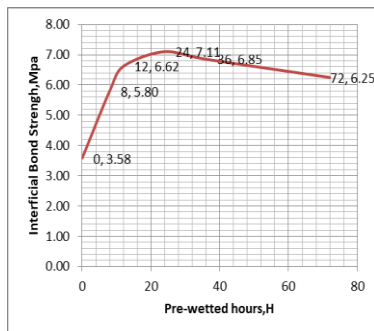


Fig.9: BS Bond strength (P);

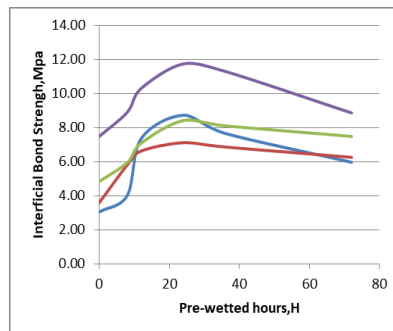
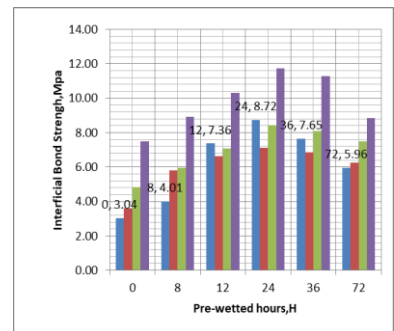


Fig.10-11. Comparisons of bond strength for all situations;



It is noted that maximum bond strength was observed for 24 H pre-wetted SSD condition in all situations considered in the study. In case of substrate pre-wetting more than 24H and lower than 24H, lower bond strength were observed as free surface water has been tended to dilute the overlay mix resulting in the increase of the water binder mix ratio and a dry substrate concrete absorbed the water from the overlay material resulting in the formation of a harsh mix concrete which cannot provide a proper interlocking mechanism.

CONCLUSIONS

The main conclusions drawn from this experimental study are that moisture of the substrate concrete greatly influences the interfacial bond strength. The maximum bond strength, in all cases, was observed at 24H pre-wetting SSD condition. With this adequate pre-wetting hour, the maximum bond strength were observed increasing of 187%, 99% for BB (P) and BS (P) and 74%, 57% for SS (C) and BS (C) specimens compared to 0H pre-wetting condition, respectively. In case of BB and SS specimens, superior bond strength were found compared to BS specimens due to having the same surface texture, moisture absorption capacity and monolithic behaviour of two layer concrete. Finally, lower bond strength was observed for poorly pre-wetting (lower than 24 H) and over pre-wetting condition (more than 24 H) as a dry substrate concrete absorbed the water from the overlay material resulting harsh mix concrete and free surface water tended to dilute the overlay mix resulting increase the water binder mix ratio.

ACKNOWLEDGMENTS

The experimental work described in this study was supported by and executed at the Department of Civil Engineering, Dhaka university of Engineering & Technology (DUET), Gazipur-1700, Bangladesh. The authors express their gratitude to DUET for supporting this study. The support is greatly appreciated by the authors.

REFERENCES

- ASTM C 882, 1999. Standard test method for bond strength of epoxy-resin systems used with concrete by slant shear, American Society for Testing Materials, 100 Barr Harbor Dr., West Conshohocken, PA 19428, USA, 1999, doi:10.1520/C0882_C0882M-05E01.
- Beushausen, H. & Alexander, M. 2009. Concrete repair. In *Fulton's Concrete Technology*. G. Owens, Ed. ninth ed. Midrand, South Africa: Cement and Concrete Institute. 393-412 P.
- Beushausen, H. 2010. The influence of concrete substrate preparation on overlay bond strength. *Magazine of concrete research*. 62(11):845-852.
- Chorinsky E. G. F. 1996. Repair of concrete floors with polymer modified cement mortars. RILEM Symposium Adhesion between polymers and concrete. *Chapman and Hall, London* 230-234 P.
- Cleland DJ; Long AE.1997. The pull-off test for concrete patch repairs. In: Proceedings of the Institution of Civil Engineers. *Structures and Buildings*. vol. 122. November 1997: 451–60 P.
- Emmons PH. 1994. Concrete Repair and Maintenance. In: Part Three: Surface Repair, Section 6: Bonding Repair Materials to Existing Concrete. MA: R.S. Means Company; 1994:154–63 P.
- Júlio, E.N.B.S., Branco, F.A.B. & Silva, V.D. 2004. Concrete-to-concrete bond strength. Influence of the roughness of the substrate surface. *Construction and building materials*. 18(9):675-681.
- Lukovic, M., Savija, B., Ye, G. & Zhou, J. 2012. Modelling water absorption of the concrete substrate in concrete repairs. (Concrete Repair, Rehabilitation and Retrofitting III – Alexander et al. (eds)).
- M. Talotti. 2014. *Influence of substrate moisture preparation on concrete overlay bond strength*. Master's thesis, Department of Civil Engineering, University of Cape Town.
- Santos, P., Júlio, E. and Silva, V.D.2007 .Correlation between concrete-to-concrete bond strength and the roughness of the substrate surface, *Elsevier, Construction and Building Materials*, 21(8):1688-1695.
- Saucier, F. & Pigeon, M. 1991. Durability of new-to-old concrete bondings. ACI special publication. 128 P.
- Silfwerbrand J. 1990. Improving concrete bond in repaired bridge decks. *Concrete Int* 1990 :121 (6).
- Saucier F, Pigeon M, 1990. Durability of new-to-old concrete bonding. In: Proceedings of the ACI International Conference Evaluation and Rehabilitation of Concrete Structures and Innovations in Design, Hong Kong, 1:689–707.

- Silfwerbrand, J. 2003. Shear bond strength in repaired concrete structures. *Materials and Structures*. 36(6):419-424.
- Talbot C, Pigeon M, Beaupre D, Morgan DR, 1994. Influence of surface preparation on long-term bonding of shotcrete. *ACI Mater J*, 560–6 P.
- Zhu, Y. 1992. Effect of surface moisture condition on bond strength between new and old concrete. Department of Structural Mechanics and Engineering, Royal Institute of Technology, Stockholm, Bulletin No. 159.

PERFORMANCE OF WASTE PLASTIC BOTTLES AS SUBSTITUTE OF BRICK ON MASONRY WALL

M.R. Awall*, S.M. Minhaz, G. Biswas, J. Anar & M.N. Parves

Department of Civil Engineering, Rajshahi University of Engineering & Technology, Rajshahi, Bangladesh.

E-mail: robi95@gmail.com

**Corresponding Author*

ABSTRACT

This study is to investigate the possibility of using plastic bottles in masonry wall. Plastic bottle is considered as useless items but it has sustainability characteristic that can be helpful for masonry building construction instead of some conventional material such as brick. Disposal of plastic bottle has become an issue of major concern in modern days. A suitable approach for this situation is using some part of plastic bottle waste as required materials for building construction. Therefore, in this study compressive strength, temperature susceptibility test on masonry wall are made with plastic bottles and are experimentally investigated. Also cost analysis and weight comparison between brick masonry and bottle brick masonry block are investigated. A total of 24 specimens are prepared with various combinations of plastic bottles and then tested in accordance with ASTM recommendations. This study utilized 500ml MUM plastic bottle, those are placed inside the masonry block specimens and then analyze the resultant weight and compressive strength. Different temperatures (300C and 400C) are applied to investigate the compressive strength due to the effect of temperature on the specimens. The test results revealed that compressive strength of the bottle brick masonry is come to close to the standard brick masonry and the compressive strength decreases with the increase of temperature on the specimen. The use of waste plastic bottle in masonry wall is cost effective. Moreover, it also reduces the weight of the masonry wall and it may provide an easy outlet of the efficient disposal of this environmental hazard.

Keywords: Plastic bottles; masonry wall; building construction; compressive strength; temperature susceptibility; environmental hazard.

INTRODUCTION

At the present time, urbanization is very rapid with the population growth in Bangladesh. It offers modernization for human life but changes the environmental aspects. Today, cost effective materials is very essential for construction industry to increasing the strength of concrete structures. The need to the building has increased and to respond this demand, the country tends to use the industrial building materials. But these building materials in spite of increasing the energy consumption in the industry section, they can also increase the cost of homes and are considered as the barrier for users to obtain the basic needs of the human life. So, now it is time to use of indigenous, locally available and cost effective waste materials which can be recycled or reused for the purpose of building construction.

Plastics are non-biodegradable substance in nature and takes more than 300 years to degrade if left unhandled without proper disposal (Pappu et al. 2007). Every second 22,000+ empty bottles are discarded in this world (Bezeau, 2016). Among different waste materials, plastic waste justifies special attention on account non-biodegradable property which is creating a lot of problems in the environment.



Fig.1 Clogging of drainage system



Fig.2 Disposal of plastic bottles

Now-a-days, plastic bottle is common in packing some liquid foods such as mineral drinking water, juice, milk, medicine etc. After use, only a few amounts of bottles are disposed to the trash bin which then gets collected by municipality and transported for recycle or final disposal. But most of the plastic bottles are disposed here and there which cause considerable damage to the environment such as clogging of drainage system, soil pollution etc. Figure 1 shows the clogging of drainage system by waste plastic bottles and Fig. 2 shows waste plastic bottles around the dustbin that are responsible for soil pollution because of its non-biodegradable nature.

In many parts of the world, a considerable amount of research is carried out in the field of masonry work, but only a few publications in this field are available. Safinia and Alkalbani (2016) examined the possibility of using plastic bottles in concrete block. They utilized 500-ml plastic bottles that were placed inside the concrete masonry units and checked the compressive strength. The testing results were supposed to be reasonable as a control of compressive strength for the concrete blocks. Mojtaba et al. (2013) studied the purpose of using plastic bottle as a sustainable material in the building construction. It has been confirmed that the plastic bottles can be used in some parts of building construction. Reusing the plastic bottles as the building materials can have significant effects on saving the building embodied energy by using them instead of bricks in walls. Also it is reducing the CO₂ emission in manufacturing the cement by reducing the percentage of cement used in construction. Ramadevi and Manju (2012) investigated the mechanical behaviour of concrete with using plastic bottle fibers as fine aggregates. The concrete with mortar of plastic bottle fibers as fine aggregates reduced the weight of concrete. It was observed that the compressive strength increased up to 2% replacement of the fine aggregate with plastic bottle fibers and it gradually decreased for 4% and 6% replacements. Raghatate (2012) studied the properties of concrete containing different percentages of plastic were tested for compressive strength. The testing results show that an appreciable improvement in tensile strength of concrete can be achieved by introducing cut pieces of plastic bags. Compressive strength of concrete is exaggerated by addition of plastic pieces and it is decreasing as the percentage of plastic increases. In addition about 1% of plastic used in concrete causes about 20% reduction of compressive strength after 28 days curing. Therefore, it is concluded that the use of cut pieces of plastic can be feasible to increase the tensile strength of concrete. Khilesh (2014) studied the compressive strength behaviour of concrete by using steel fiber with waste plastics. The use of plastics in concrete lowered the compressive strength of resultant concrete. Rahman (2016) studied the use of waste plastic bottle in mortar block for bank protection work. The compressive strength of mortar block filled with waste bottle decrease with the increase of bottle content. From the above study it is observed that in most cases people are less concentrated on using plastic bottle as replacement of brick on masonry wall. Therefore, in this study waste plastic bottle is used to observe the compressive strength of masonry wall and the temperature susceptibility of plastic bottles on masonry block are investigated thoroughly. Also cost analysis and weight comparison between brick masonry and bottle brick masonry block are investigated.

METHODOLOGY

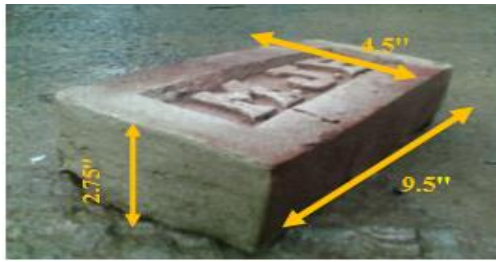


Fig.3. Standard brick (9.5"x4.5"x2.75").

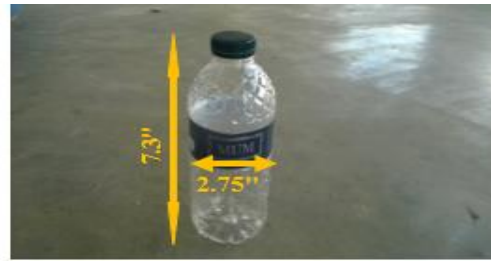


Fig.4. 500ml MUM PET bottle.

In this study, PET plastic bottles (MUM 500ml mineral drinking water PET bottle) are used as the substitute of bricks for the making of masonry wall. MUM mineral drinking water is the most popular and available mineral drinking water in our country. According to Partex Beverage Limited (PBL), yearly production of MUM 500ml bottle in our country is 31,04,64,000. The dimension of MUM 500ml bottle is nearly equal to the dimension of a standard brick. The dimension of the standard brick is 9.5"x4.5"x2.75" shown in Fig.3. The diameter and height of a MUM 500ml bottle is 2.75" and 7.3" respectively shown in Fig.4. Moreover, its uneven surface helps to create bond with the mortar.

Specimen Preparation

For compressive strength test, temperature susceptibility test and weight comparison, total 24 specimens were prepared using different dimensional cubical steel mould. The MUM 500ml bottles were bind using G.I. wire and nylon rope and placed into steel mould. The mortar mixing was prepared by taking cement-sand ratio of 1:3 and water cement ratio is 0.50. The specimens were systematically placed in curing tanks after 24 hours for 28 days. After that the weight of the specimens were taken. The masonry specimens were tested in the universal testing machine according to ASTM C1314-11. Some pictures are shown in Fig. 5, which represents the different size, alignment and connection type of block specimens. From which A1 and A2 consists of 4 bottles that are vertically alignment and connected with G.I. wire and nylon rope respectively. A3 consists of 6 bottles that is horizontally alignment and connected with G.I. wire. Type B1 and B4 specimens consist of 12 bottles that are vertically alignment and connected with G.I. wire. But the filling sand used in B1 type is wet and in type B4 is dry. Also in B2 type specimen bottles are connected with nylon rope and B3 type specimen bottles are horizontally

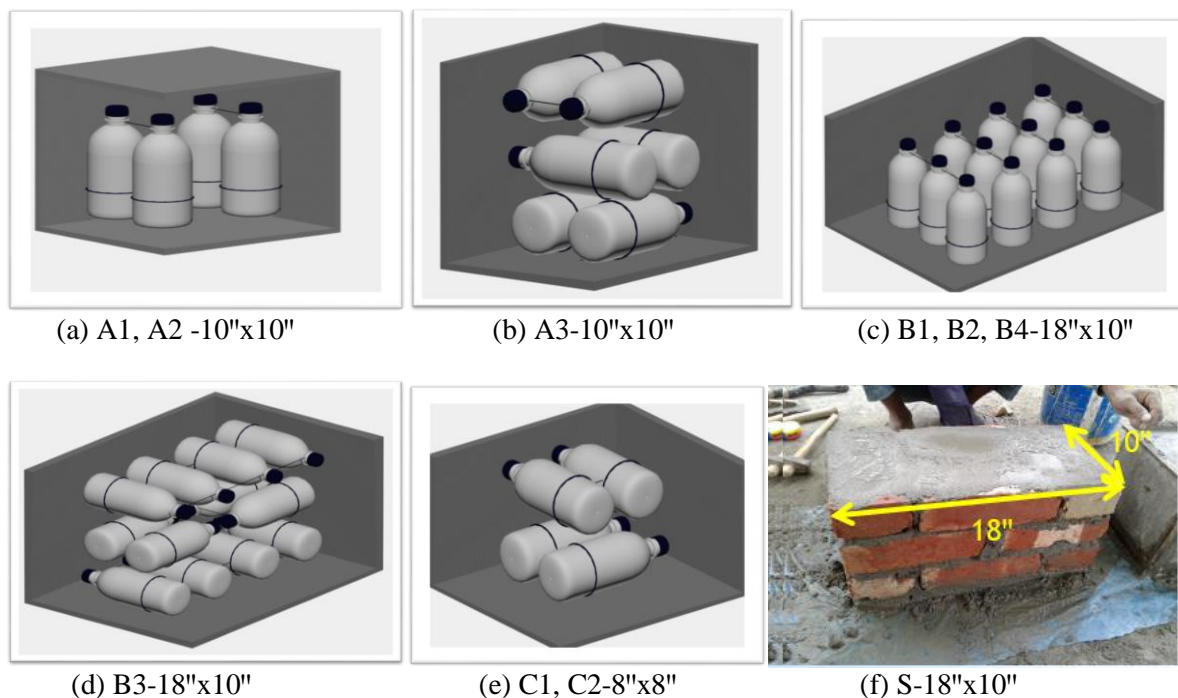


Fig.5. (a), (b), (c), (d), (e), (f) shows different type of block specimens.

alignment and connected with G.I. wire. Type C1 and C2 specimens are horizontally aligned and connected with G.I. wire and type S is standard specimen made with standard brick.

RESULTS AND DISCUSSIONS

Compressive strength test

The graphical representation of average compressive strength of type A1, A2 & A3 specimens (10"×10") are shown in Fig. 6. This figure shows that type A1 specimen has obtained comparatively larger compressive strength than type A2 and A3 specimens because of vertical bottles alignment connected with G.I. wire. Compressive strength of G.I. wire connected specimen and nylon rope connected specimen are 697.18 psi and 618.92 psi respectively. Therefore, bonding is increased with G.I. wire connection. Also the graphical representation of average compressive strength of type B1, B2, B3 and B4 specimens (18"×10") are shown in Fig. 7. This figure shows that type B1 specimen (501.78psi) has obtained comparatively larger compressive strength than other types B2, B3 and B4 specimens because of vertical bottle alignment connected by G.I. wire and fill with wet sand.

Average compressive strength of type C1 specimen (8"×8") is 1070.82 psi that is connected with G.I. wire shown in Fig. 8 and average compressive strength of type S specimen (18"×10") is 544.64 psi shown in Fig. 9. Different temperatures (300C and 400C) were applied to investigate the compressive strength due to the effect of temperature on the specimens. Results of compressive strength before and after applying temperature between type C1 and type C2 (avg.) specimens (8"×8") are shown in Fig. 10. This figure shows that compressive strength decreases with the increase of temperature. It was occurred because of the fact that melting point of PET plastic is about 255C to 265C (Raut et al., 2015). Polyethylene terephthalate is a semi crystalline polymer resin of the polyester in which polymer chains are parallel and closely packed. When heat was applied into the specimens above the melting point, the polymer chains became flexible and plastic bottles inside the specimens could not withstand its original

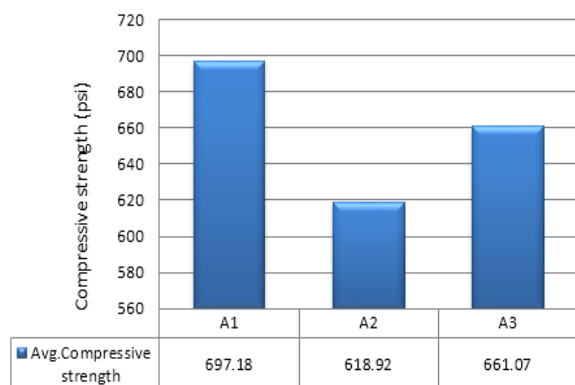


Fig.6. Avg. compressive strength of type A1, A2 and A3 specimens.

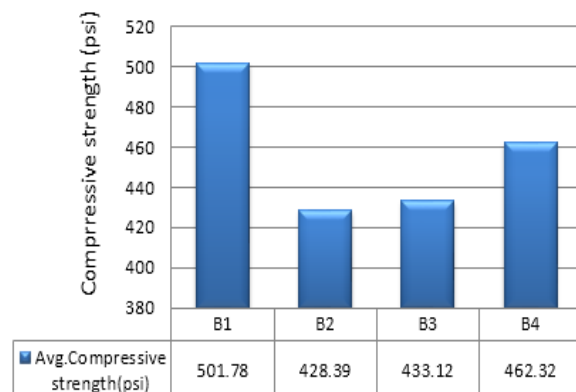


Fig.7. Avg. compressive strength of type B1, B2, B3 and B4 specimens.

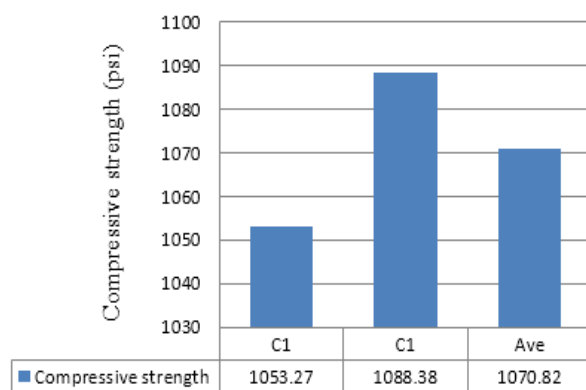


Fig.8. Compressive strength of type C1 specimen.

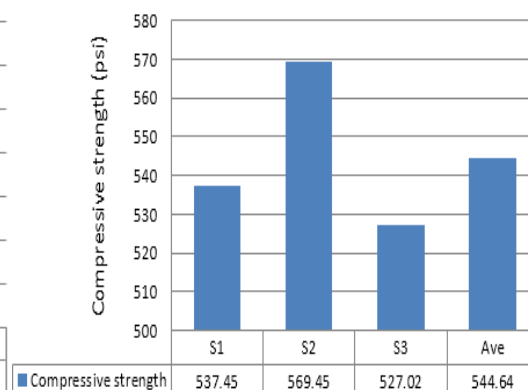


Fig.9. Compressive strength of type S specimen.

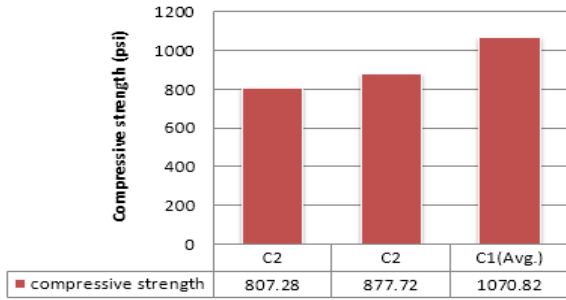


Fig.10. Temperature effect on compressive strength of type C2 and type C1 (avg.).

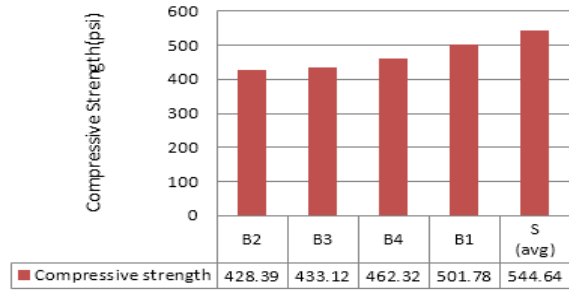


Fig.11. Comparison of compressive strength of type B1, B2, B3, B4 and S specimens.

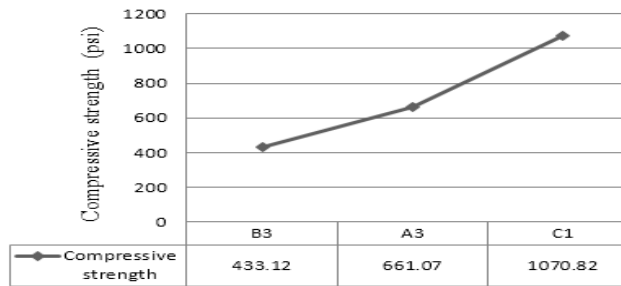


Fig.12. Comparison of compressive strength of type A3, B3 and C1 specimens.

properties which caused decrease of compressive strength of the specimen. So, it can be conclude that temperature is an important factor on which the compressive strength depends. The graphical representation of compressive strength of type B1, B2, B3, B4 and S specimens (18"×10") are shown in Fig. 11. This figure shows that the compressive strength of bottle brick specimen is nearly equal to the standard brick specimen. But between type B1 and B4 the compressive strength is high in B1 which is filled with wet sand than type B4 which is filled with dry sand. Also it is seen that the compressive strength of bottle brick specimen is increasing with the decrease of the size of specimen shown in Fig. 12, as plastic bottles are closely and properly oriented in small block specimens. Therefore, use of each small block specimen as masonry unit is more effective.

Weight comparison

The weight of the same size specimens of B1, B2, B3, B4 and S types were calculated to compare the weight among these specimens shown in Fig. 13. The weight of the standard brick specimen is 70.5 kg, however the weight of the bottle brick specimen is less than the brick specimen. Therefore, use of bottle brick will be suitable to build a lite weight structure.

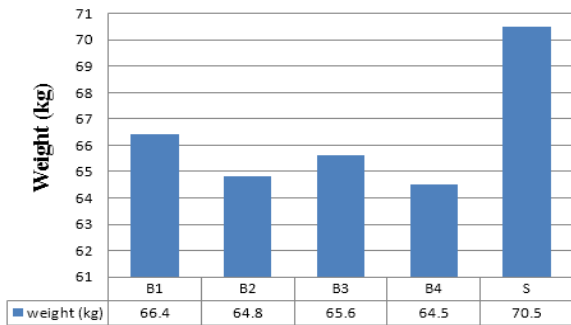


Fig.13. Comparison of weight of B1, B2, B3, B4 and S specimens.

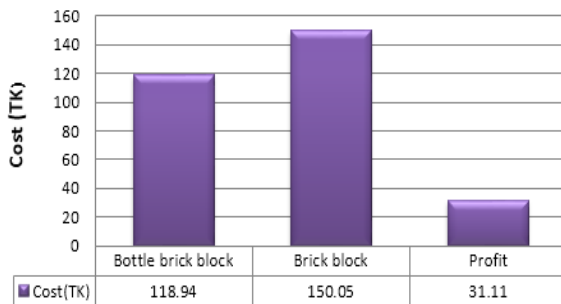


Fig.14. Comparison of cost between bottle brick block and brick block specimens.

Cost analysis

Cost is calculated of a single bottle brick block and a single brick block and compared with them shown in Fig.14. The cost for making each bottle brick specimen is 118.94 taka and the cost for making each brick block specimen is 150.05 taka. So, the cost for making each bottle brick specimen is 20.73% less than for making brick block specimen. Therefore, the use of bottle brick in masonry wall can be substitute of brick and it is economical.

CONCLUSIONS

This paper attempts to highlight the potential of waste plastic bottle used as an alternative material in construction and its low cost specialty. Experimental investigations were carried out to observe the compressive strength behaviour of the bottle brick masonry with variation of number of bottle use, their alignment and connection type. On the basis of results and subsequent discussion, it is conclude that the compressive strength of bottle brick masonry block is decrease with increase the temperature. Also the compressive strength of bottle masonry wall is nearly equal to the brick masonry wall, bottle brick can be used for building construction purposes mainly as partition wall. So, using the concept of bottle brick is cost effective, light weight than brick, energy efficient and available as compared to other conventional building materials. Therefore, it is consider as one of the low cost potential green project and has immovable attention of the architecture and construction firms.

REFERENCES

- Bezeau, R. 2016. The Founder of Plastic Bottle Village. *Renaissance Forum*. [online]. Available at: <https://www.plasticbottlevillage.com>.
- Khilesh, S. 2014. Study of Strength Property of Concrete Using Waste Plastics and Steel Fiber. *The International Journal of Engineering and Science (IJES)*. 3(5): 09-11.
- Mojtaba, VS; Masoud, VS; and Azin, SB. 2013. Investigating the Application of Plastic Bottle as a Sustainable Material in the Building Construction. *International Journal of Science, Engineering and Technology Research (IJSETR)*. 2(1): 28-34.
- Pappu, A; Saxena, M and Asolekar, RS. 2007. Solid wastes generation in India and their recycling potential in building materials. *Building and Environment*, 42(6): 2311-2320.
- Partex Beverage Limited. *Renaissance Forum*. [online]. Available at: www.partexbeverage.com
- Raghatate, AM. 2012. Use of Plastic in a Concrete to Improve Its Properties. *International Journal of Advanced Engineering Research and Studies*. 1(3): 109-111.
- Rahman, S. 2016. Study on Plastic Waste Bottle in Mortar Block for Bank Protection Work. *Thesis for Graduation of Bachelor of Science Degree*, Department of Civil Engineering, RUET, Rajshahi.
- Ramadevi, K; and Manju, R. 2012. Experimental Investigation on the Properties of Concrete with Plastic PET (Bottle) Fibres as Fine Aggregates. *International Journal of Emerging Technology and Advanced Engineering*. 2(6): 42-46.
- Raut, A; Patel, MS; Jadhwar, NB; Khan, U and Dhengare, SW. 2015. Investigating the Application of Waste Plastic Bottle as a Construction Material. *Journal of Advance Research in Mechanical and Civil Engineering*. 2(3): 86-99.
- Safinia, S; and Alkalbani, A. 2016. Use of Recycled Plastic Water Bottles in Concrete Blocks. *Creative Construction Conference*. Pages 115-119.

IMPROVEMENT OF CONVENTIONAL FERROCEMENT JACKETED COLUMN USING WIRE MESH & STEEL ANGLES AT CORNERS

K. I. M. Iqbal*, P. Nahian & D. M. Begum

Department of Civil Engineering, Bangladesh University of Engineering & Technology,
Dhaka, Bangladesh.

E-mail: iqbal.buet11@gmail.com; promy.nahian@gmail.com; shuma92@gmail.com

**Corresponding Author*

ABSTRACT

Ferrocement jacketing is used to rehabilitate the deficient RC column in order to increase its strength. This is comparatively easier to implement than other available methods of jacketing. In this study, the conventional ferrocement jacketing method is improved using both wire mesh and steel angle plates at four corners of the RC column. Total four RC columns were prepared, among which one was kept as reference column & rest three were jacketed. Each column was tested under concentric axial load. The results of the study have indicated a significant improvement in axial capacity and failure behavior of RC columns with the implementation of improved techniques of ferrocement jacketing. Conventional ferrocement jacketed column (using single wire mesh layer) showed 11% increase with respect to the reference column. Additionally, it has been found that ferrocement jacketed columns with additional mesh layers at corners showed 70% improvement in capacity with respect to reference RC column. On the other hand, provision of steel angles at corners of ferrocement jacketed column has resulted in 98% enhancement in capacity with respect to reference RC column. The ferrocement confined RC columns have shown improved ductility at failure as compared to the unconfined RC column.

Keywords: Ferrocement, Jacketing, Confinement, RC Column, Strengthening.

INTRODUCTION

A. Background:

Columns are the most important elements of the structural system to carry the vertical load as well as to provide lateral resistance and transfer total loads to the foundation (D. Sen et al. 2016). Reinforced columns capacity is lessened due to various reasons like overloading, corrosion of steel, earthquake, higher wind loads, fire, impact loads, etc. Therefore, the strengthening of deficient columns is necessary to increase the load carrying capacity and prevent spalling which can be achieved by confinement of column externally (M. Salih & C. Arunkumar, 2016). Columns have to be locally strengthened to ensure life safety using one of the following approaches, e.g. additional reinforced concrete layer, ferrocement jacketing, steel jacketing, FRP jacketing etc. (D. Sen & M. Begum, 2016). Ferrocement jacketing is found to be such an attractive technique due to its properties such as good tensile strength, lightweight, overall economy, water tightness, easy application and long life of the treatment (Prem Pal. & Dr. Manik Kumar). Ferro-cement jacketing consists of using different wire mesh layer throughout the column surface. The gaps between installed ferrocement wire mesh layer and existing concrete surfaces are filled with mortar to ensure a continuous contact. This type of improved column is known as a conventional ferrocement jacketed column. Researchers have indicated that this type of column often used to fail at corner due to having rich mixes of mortar at corner. To overcome this failure pattern A.B.M.A. Kaish (et al. 2015) proposed different techniques to improve conventional ferrocement jacketed column. Among which, two improvements are to be brought by using wire mesh layers and

angle plate at four corners. However, in his study, he only tested improved column using wire mesh layer at four corners. So, the behavior of column with ferrocement wire mesh layer & angle plate at corner needs to be investigated.

In this study, the column is improved using angle plates as well as wire mesh layer at four corners of the columns. These columns have been tested under axial compressive load to evaluate the behavior of improved ferrocement techniques.

B. Objectives:

The objectives of this study are as follows-

- a. To investigate the effect of ferrocement confinement on RC columns under axial compressive loads.
- b. To study the effect of corner improvement of ferrocement jacketed RC column by wire mesh & steel angles.
- c. To investigate the failure behavior of RC columns confined with ferrocement.

METHODOLOGY (SECTIONS)

A. Description of test Specimens:

In this study, four RC columns were constructed, among which three columns were jacketed with ferrocement wire mesh layer and one column was kept as a reference column. All the columns were tested under axial compressive load. Jacketing of columns consists of adding wire mesh layer, using angle plate & wire mesh at corner. This type of strengthening improves the axial and shear strength of columns. The reference column was constructed by brick chips, sand, cement, and steel. The micro concrete jacket was constructed by sand & cement. The drinkable water was used during the casting period. Four half scale RC columns measuring 152mm x 152mm in cross sections were constructed. Each column height was 1524mm. Among them, three columns were jacketed by using wire mesh of (8.5mm x 12.5mm) opening and 20 gages of wire was used. Wire mesh layers were bonded with the sides of RC column with cement mortar of 19 mm. In order to improve the corner, additional wire mesh and angle plate were used at corner in two of columns. In order to avoid local failure, the top and bottom of the column were constructed with high strength concrete and with closely spaced ties. 10mm diameter longitudinal reinforcement along with 8mm diameter ties at an interval of 150mm had been embedded in RC core. Details of the column jacketing techniques have been described in Table 1. & 2, and cross sections are illustrated in figure 1.

Table 1. Model Specimen Configurations Before Jacketing

Column Designation	Cross Section Dimension (mm ²)	Height (mm)	Reinforcement Details	
			Longitudinal Bar	Stirrup
C1A	152 × 152	1524	4 No. #10 mm	#8 mm tie bar @ 150 mm c/c
C2A	152 × 152	1524		
C3A	152 × 152	1524		
C6B	152 × 152	1524		

B. Material Properties:

Standard Portland Composite cement (CEM IIA) was used to construct all test columns. Locally available brick chips of 0.75-inch downgrade and sand were used as coarse aggregate and fine aggregate respectively. Total two batches of concrete were prepared for the initial casting of the column. Batches were designated by A & B, and concrete compressive strength obtained was 11.10 MPa & 9.63 MPa after 28 days cylinder test. Properties of steel, angle plate & wire mesh are given in Table 3 & 4.

Table 2. Model Specimen Configurations After Jacketing

Column Designation	Cross Section Dimension (mm ²)	Height (mm)	Jacketing Details	
			Wire Mesh Configuration	No. of wire mesh layer
C1A	152×152	1524	None	None
C2A	190×190	1524	(8.5mm × 12.5 mm) opening with 0.8mm diameter wire	Single layer & double layer at corner
C3A	190×190	1524		Single layer
C6B	190×190	1524		Single layer with (50mm×50mm×5mm) angle plate at corner.

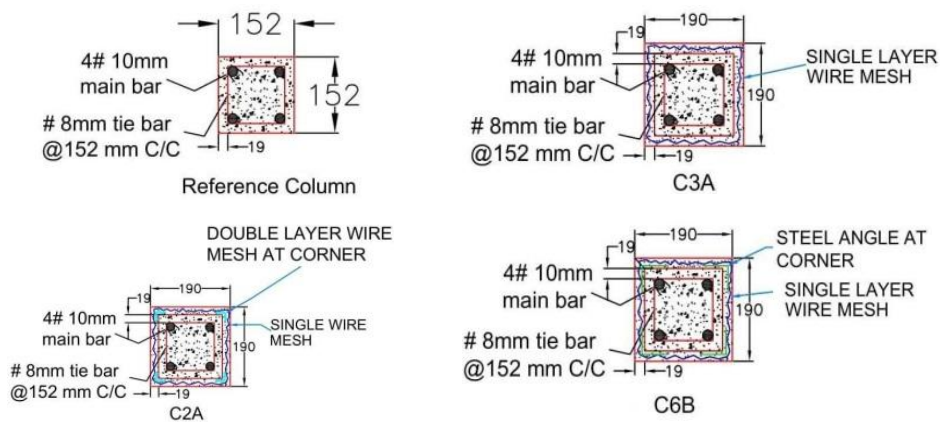


Fig. 1. Cross sectional details of four columns (dimensions are in mm)

Table 3. Properties of Steel Elements Used in Jacketing

Properties	Reinforcement		Angle
	10mm φ	8mm φ	50mm×50mm×5mm
Yield stress (MPa)	409	576	449
Ultimate stress (MPa)	556	647	624

Table 4. Properties of Ferrocement Wire Mesh

Gauge	Dia (mm)	Cross sectional area (mm ²)	Wire mesh type	Mesh opening (mm ²)	Yield strength (Mpa)	Ultimate strength (Mpa)
20	0.86	0.581	Woven square	(8.5×12.5)	401	448

C. Strengthening of RC Columns:

After 28 days of curing, surfaces of hardened columns, except C1A had been chipped off to get an uneven surface. Afterward, ferrocement wire meshes were attached in round throughout the column specimen. Mortar is necessary for perfect bonding between existing RC column and ferrocement wire

mesh. According to BNBC 2015[5] for brick jointing, the ratio 1:2 (cement: sand) should be used in mortar. And water-cement ratio should be 0.45. The mix ratio was controlled perfectly. Strengthening of three RC columns and also a complete jacketing are shown in figure 2.

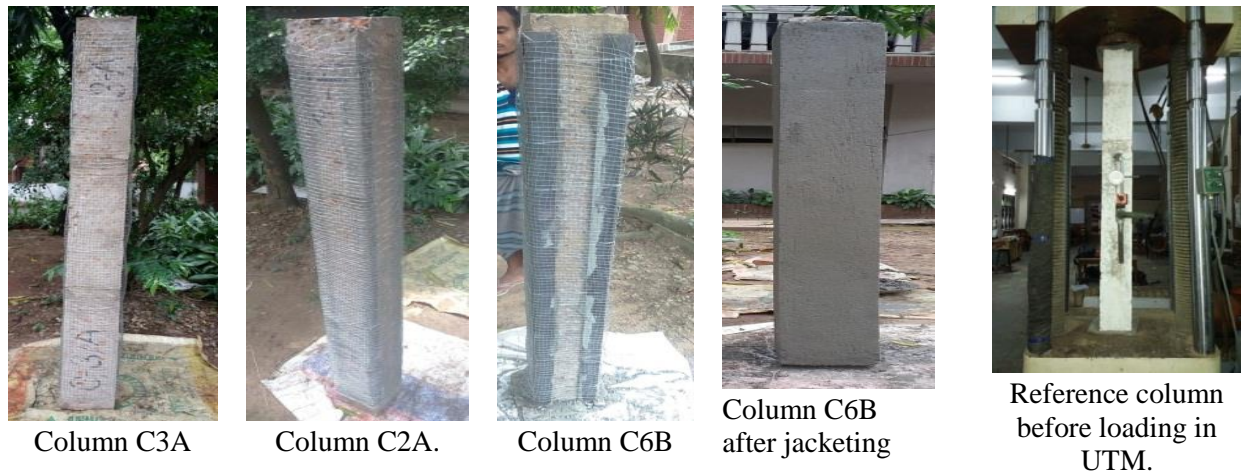


Fig. 2. Different types of ferrocement jacketing techniques applying on RC columns and loading column during test.

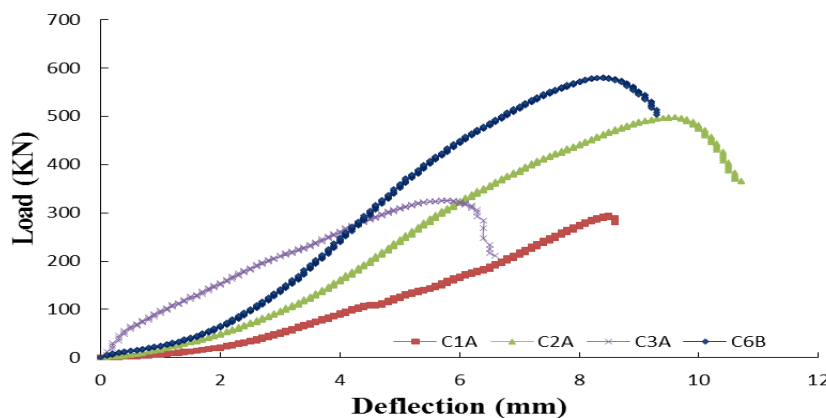
D. Test Set Up:

The specimens were placed in the Universal Testing Machine (UTM) of capacity 2000kN between the upper cross-head and the fixed crosshead. Loading was done at a rate of 3 mm/min and the load-displacement data were recorded by data-acquisition software. The specimens were mounted on the machine and at two ends geotextile were placed on both ends of the specimens to ensure uniform load distribution on the specimens. The loading condition during the experiment is shown in figure 2.

RESULTS AND DISCUSSIONS

A. Load- Deflection Behavior:

Reference Column is very weak in its capacity. Different kinds of jacketing were performed in order to increase its capacity using ferrocement wire mesh. It is observed that column with a single wire mesh jacket has more capacity than the column with no wire mesh layer. However, the column with a single wire mesh layer without improving corner can be regarded as the conventional ferrocement jacketed column. In this case, there is a huge probability that the failure will be initiated at the corner. This type of failure will occur without reaching the column’s ultimate capacity. In order to prevent this failure in the column, new techniques should be adopted. In this study, jacketing had been done at the corner using wire mesh layers and also by using angle plates. From these two improved strategies, it has been seen that the capacity of columns is increased as well as prevented its failure in the corner. The Load-deflection curves of these columns are shown in figure 3.



4.

Fig 3. Load vs Deflection curve of column C1A, C2A, C3A, C6B

From the above curve, it can be seen that the capacity of core column is 294 KN and column with single wire mesh layer is 325 KN. The capacity of column with improving corner using double wire mesh is 498 KN and column with improving corner using angle plate is 580 KN. Histogram of ultimate axial capacities of four columns are shown in figure 4 & their percentage increase are provided in Table 5.

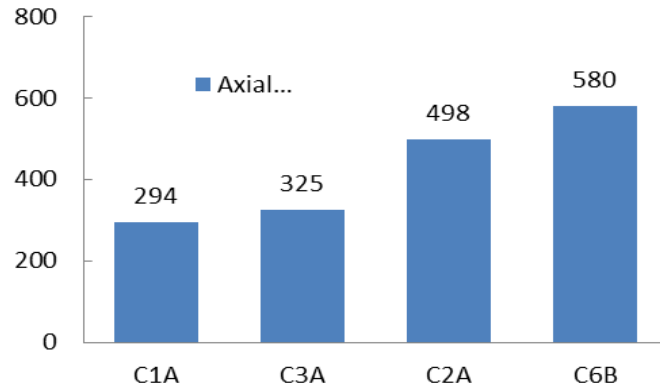


Fig 4. Histogram showing Axial Capacity (KN) of column C1A, C2A, C3A, C6B

Table 5. Ultimate Capacity of Each Column & Percent Increase in Capacity

Types	Ultimate Capacity (KN)	Percentage Increase in Capacity with respect to Core Column (%)	Axial Deflection (mm)	% Increment of Axial Deflection
Control Column / No Wire Mesh (C1A)	294		8.6	0
Column with Single Wire Mesh Layer (C3A)	325	11%	6.6	-23
Column with Single Wire Mesh Layer & Double wire mesh layer at corner (C2A)	498	70%	10.7	25
Column with Single Wire Mesh Layer & Angle Plate at corner (C6B)	580	98%	9.3	9

It is also evident that the column with a single wire mesh layer is increased its capacity by 11% with compare to the reference column. Column with single wire mesh and double wire mesh at corner is increased its capacity by 70% with compare to reference column. The conventional jacketed column improved by using steel angle plates at corner is increased its capacity by 98%, which indicates an increase in the confinement of the column as well as an increase in the strength of the column. Moreover, column improved by using angle plate at corner is increased its capacity by 26.67% than that compare to column improve using double wire mesh layer at corner. Axial deflection of each column and their increment with respect to the reference column is provided in Table 5.

It can also be seen that before rupture the column with a single wire mesh layer and having double wire mesh layers at corner shows more deflection. And the deflection pattern of angle improved column is much higher. Thus, it can be concluded that both corner improved columns have more ductility than that of the other two columns.

B. Failure Mode:

The axial shortening increased in a linear manner till failure would occur in the column. In order to distribute the load uniformly to the column, jute fiber was used in the top and bottom of every column. The failure modes that took place are shown in figure 5. It is observed that column C2A & C6B has prevented its failure at corner, while C1A & C3A has shown corner failure.

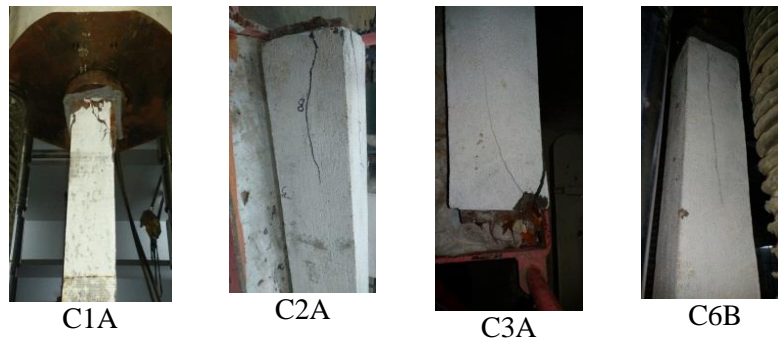


Fig 5. Failure pattern of columns C1A, C2A, C3A, C6B

CONCLUSIONS

The conclusions of the study can be summarized as,

- The axial capacity and failure behaviour of the reference RC column is observed to be improved significantly with the application of ferrocement jacketing.
- Columns with improvement in the four corners showed higher (about 50% more) capacity than that of only conventional single wire mesh layer column without corner improvement. However, corner improvement columns not only increased column capacity, but it also prevent the brittle failure that occurred at the corner of conventional ferrocement confined columns.
- Provision of steel angles at the corners resulted in significant improvement in capacity as well as failure behavior as compared to double layer mesh at corners of conventional ferrocement column. About 98% increase in capacity was found in comparison to the reference column, almost twice with the reference column

ACKNOWLEDGMENTS

The authors acknowledge the financial support provided by the Bangladesh University of Engineering & Technology (BUET), Dhaka, Bangladesh. In addition, first author would like to express his gratitude to Engr. Md. Tariqul Islam Aunto & Rubel Ahmmed who helped us during the research project.

REFERENCES

- A.B.M.A. Kaish, M. Jamil (2015), "An approach to improve conventional square ferrocement jacket for strengthening application of short square RC column", *Materials and Structures*, DOI 10.1617/s11527.
- BNBC —Bangladesh National Building Code, *an acronym for Bangladesh National Building Code*, Volume 2, Part 6 - —Structural Design", chapter 12 – —Ferrocement structures", pp. 6-703 to 6-711, 2015.
- D. Sen& M. Begum, (2016), "A Comparative Study of Steel Angles and Strips Strengthened RC Columns", *AJCE*, Vol. 18, No.3 (2017).
- M. Salih & C. Arunkumar (2016), "Strengthening of Reinforced Concrete Column using Jacketing Technique", *ICEIS-2016*.
- Prem Pal, Dr. Manik Kumar, Dr. S.K. Kaushik, "Effect of Wire Mesh Orientation on Strength of Beams Retrofitted using Ferrocement Jackets.", *IJE*, Vol-2, Issue-1, pp-9.

A NUMERICAL STUDY BY CONSTRUCTING A FINITE ELEMENT MODEL OF A SIMPLY SUPPORTED BEAM WITH COLD-FORMED STEEL SECTION

T.M. Raka* & K.M. Amanat

*Department of Civil Engineering, Bangladesh University of Engineering and Technology,
Dhaka 1000, Bangladesh.
E-mail: raka12.c.e@gmail.com*

**Corresponding Author*

ABSTRACT

In recent time sections which are cold-formed are commonly used in a wide range in different roof and wall system. The sections are found in various shapes such as lipped C and Z plain sections, Supa-Cee sections etc. Since the sections are cold-formed which means they are formed at room temperature usually by bending, they are usually thin sections. The paper provides the behaviour of the cold-formed plain lipped C-sections in shear and combined bending and shear by constructing a finite element (FE) model of cold-formed plain lipped C-sections using ANSYS. A simply supported beam was investigated through this numerical analysis. An investigation on the Direct Strength Method (DSM) which was carried out by this FE model has been provided in this paper. The influence of section depth in DSM nominal shear capacity is explained by constructing graphs in this numerical study.

Keywords: purlins; finite element model; buckling; ultimate capacity; shear

INTRODUCTION

The DSM was extended to purlin systems for shear and for combined bending and shear by Pham (2010). The vacuum rig tests on continuous lapped cold-formed purlins at the University of Sydney over a 10-year period were used to calibrate DSM design proposals for shear and combined bending and shear (Pham and Hancock 2009). The experimental investigation consisted of three different test series on high strength cold-formed C-section purlins. The test series were known as predominantly shear .V/, combined bending and shear .MV/ and bending only .M/ test series. The influence of torsion/distortion restraint straps screwed on the top flanges adjacent to the loading points were also considered in that research. In this paper, a numerical non-linear simulation, based on the finite element method (FEM) using the software package ANSYS, of high strength plain lipped C-section which could be recognized as cold-formed steel purlins can be found. The behaviour of this FE model is investigated in shear, combined bending and shear, and bending only. The evaluation of the performance of this FE model was carried out by comparing to the previous experimental tests conducted by Pham(2010) as described earlier. Material and geometric non-linearities were used to develop this model in ANSYS. A detailed FE model has been developed to study the structural behaviour of high strength cold-formed purlins in shear, combined bending and shear, and bending only. In order to obtain realistic models for the finite element nonlinear analysis, plastic strains are included. The results of this numerical study are discussed in this paper. The accuracy of the DSM was examined in this study. It is found from this study that The DSM nominal shear capacity with considering tension field action (TFA) can be used where the section is developing such behaviour in reality. Thinner and higher depth sections are tend to develop this behaviour in real case. For this case the formula can be used. The DSM nominal shear

capacity without considering tension field action (TFA) gives more conservative results in this regard. For thicker and shorter depth sections the DSM nominal shear capacity with considering tension field action (TFA) cannot be used since the real capacity is lower here. The details are explained in this paper by proper graphical representations.

TEST RIG CONFIGURATION AND SPECIMEN BOUNDARY CONDITIONS (PHAM 2010)

V and MV series (Pham 2010)

Fig. 1 shows both the V and MV series test set up by Pham (Pham 2010). The only difference between the V and MV tests is the ratio of shear span to depth. The shear span here was the distance between the lines of bolts at the loading and support points. With the V series, the ratio of shear span to depth was 1:1 whereas that of MV series was 2:1.

M series (Pham 2010)

Fig. 2 shows the detailed test configuration of the bending only series used by Pham (Pham 2010). The four point bending arrangement provided a central region of uniform bending moment and zero shear force.

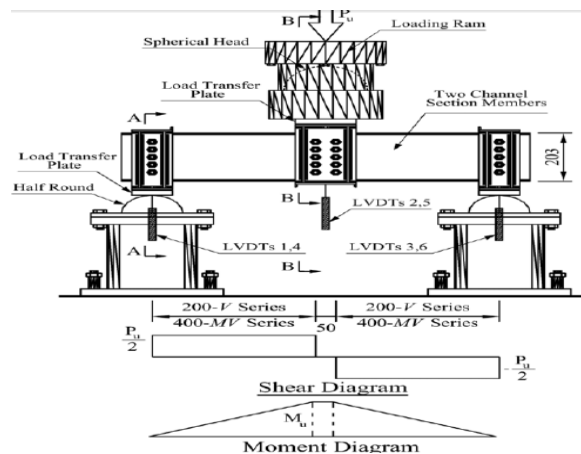


Fig. 1 *V and MV Test Set-up and Actual Experimental Test (Pham 2010)*

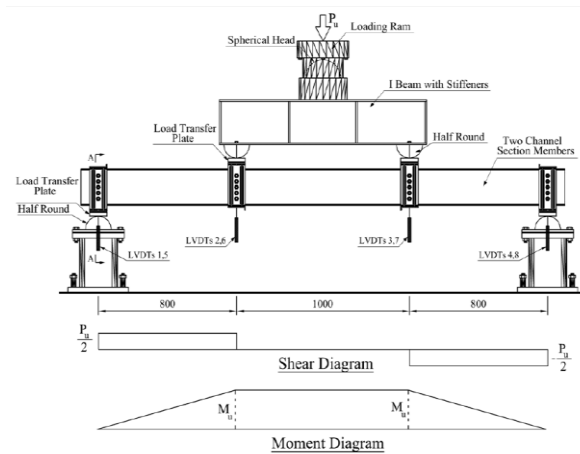


Fig. 2 *M-Test Set-up and Actual Experimental Test (Pham 2010)*

FINITE ELEMENT MODELING OF PLAIN C-SECTION

Element modelling

In ANSYS shell elements are special type of elements that are designed to efficiently model thin structures. SHELL181 is used for the model generation.

Material modelling

Cold-formed steel display linear behaviour in the stress versus strain study until the load exceeds the yield load, after that the material deformation is no longer fully recoverable. The Young's modulus and Poisson's ratio are included in this FE model to incorporate the linear behaviour of the material. In this FE model material behaviour is described by bilinear kinematic hardening (BKIN command in ANSYS) to get the full stress versus strain behaviour of this material.

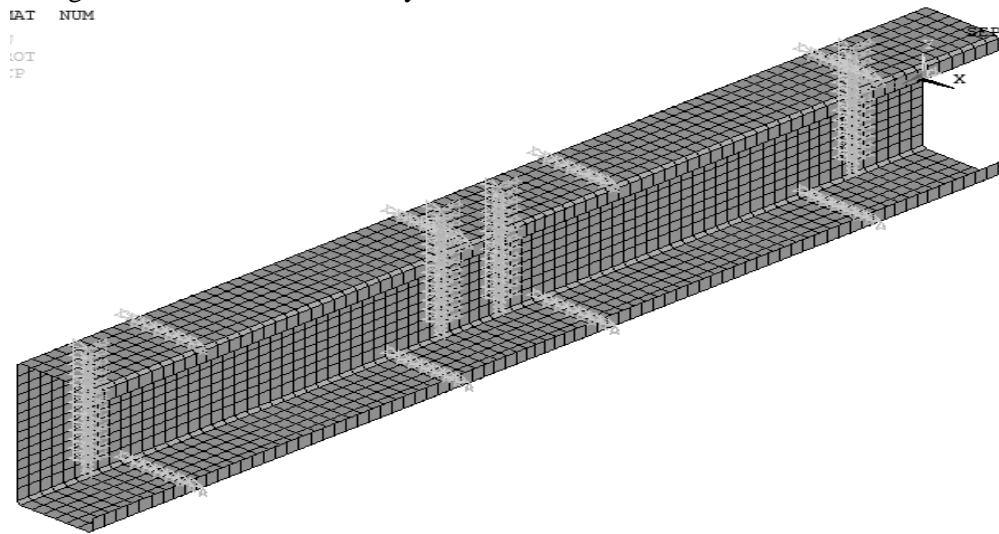
Meshing

Optimum meshing is done to get good results.

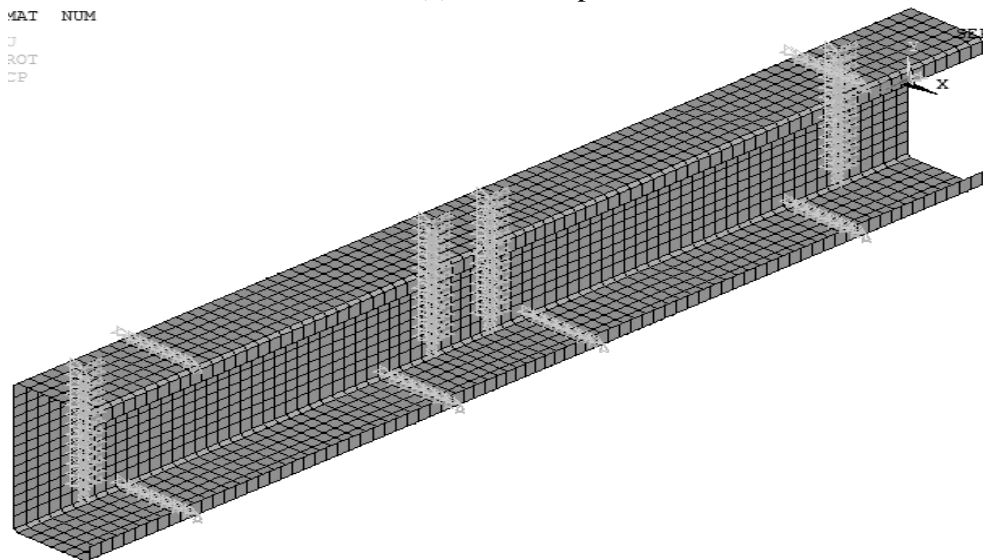
Boundary conditions and load application

Here the Z axis direction is defined along the span, the Y axis direction is defined along the depth of this section, The X axis is defined along the flange of the section. The nodes along depth excluding two lips

at support are selected and then translation in X and Y direction and rotation in Y and Z direction are restrained at these nodes . The origin (0,0,0) is selected at the mid depth of the section starting from one end and the translation in Z direction of this node is kept restrained . The nodes along depth excluding two lips at loading points are selected and the translation in X direction and rotation in Y and Z direction are restrained at these nodes . A displacement in Y direction is applied at these nodes .These boundary conditions are same for shear series (V-series) ,combined bending and shear series (MV-series) and only bending moment series(M-series) in this numerical study. The nodes along width of flange excluding two corners are selected at strap location and then the translation in X direction are restrained at these nodes. The displacement in Y direction of these nodes at any strap location are kept same by defining a set of coupled degrees of freedom in ANSYS. But in only bending moment test series the translation in X direction of nodes at strap location away from support and loading points are not kept restrained . Fig.3 and 4 shows the boundary conditions.



(a) With straps



(b) Without straps

Fig. 3 Support conditions and displacement application at nodes for shear test series (V-series) and combined bending and shear test series (MV-series): (a) With straps, (b) Without straps

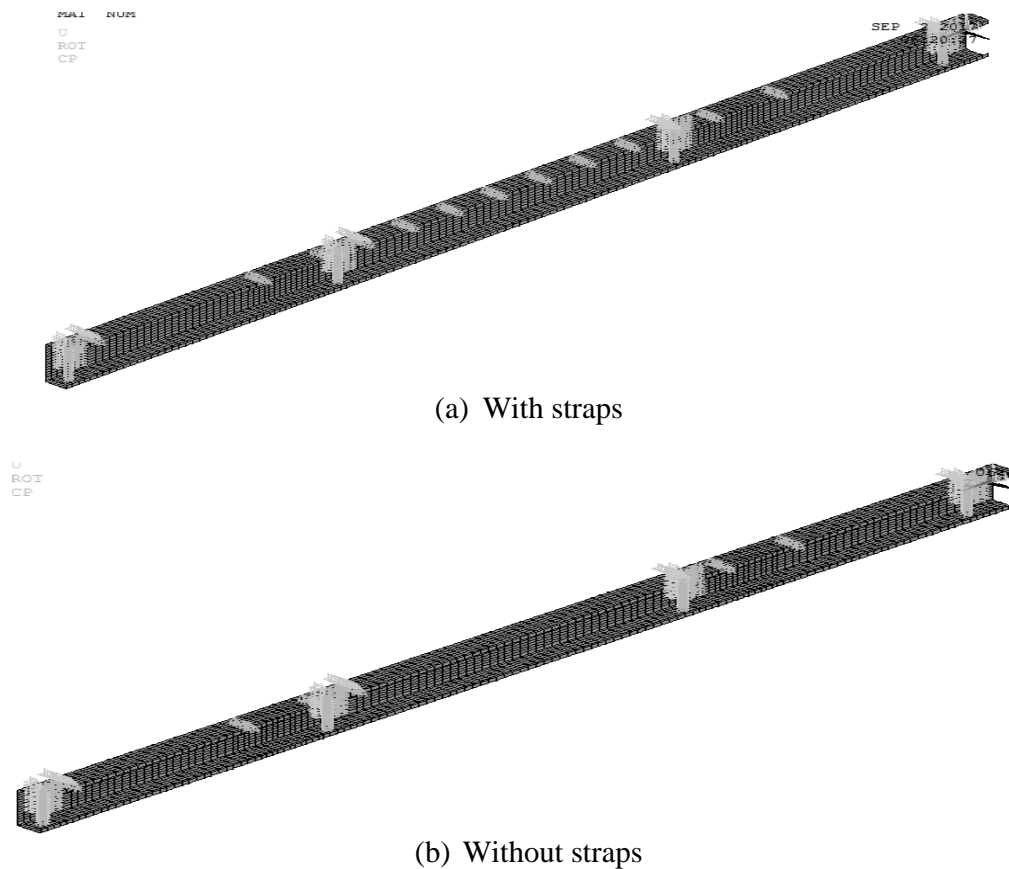


Fig. 4 *Boundary conditions and load application at nodes for only bending*): (a) *With straps*, (b) *Without straps*

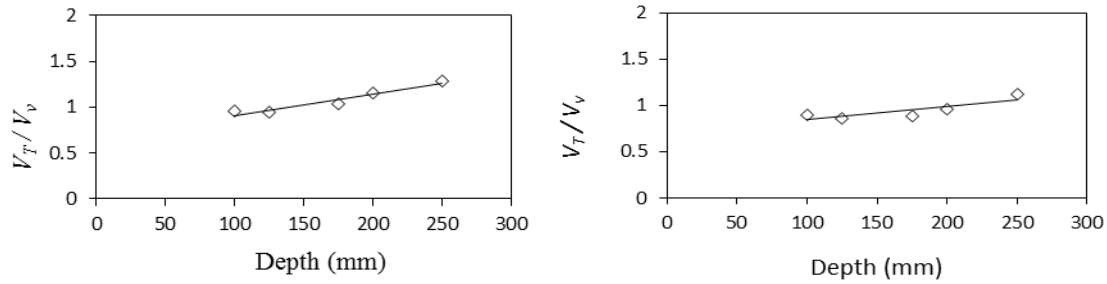
ANALYSIS RESULTS OF PLAIN C- SECTIONS

Figure 5 shows V_T / V_v vs. depth for thickness 2.4 mm where V_v is the DSM nominal shear capacity without considering TFA. Figure 6 V_T / V_v vs. depth for thickness 2.4 mm where V_v is the DSM nominal shear capacity with considering TFA. Here V_T is the shear at the support which is found from the analysis.

In fig.5 for only shear test with thickness 2.4 mm and V_v without considering tension field action the ratio V_T / V_v increases with depth which is shown from regression line. In fig.6 for only shear test with thickness 2.4 mm and V_v with considering tension field action the ratio V_T / V_v increases with depth which is shown from regression line but the slope of regression is not higher than the slope of regression line for only shear test with thickness 2.4 mm and V_v without considering tension field action. This shows the ultimate capacity is getting higher than the nominal capacity when depth is increasing. With increasing depth which means with more buckling potential DSM gives reduced capacity than the ultimate capacity remaining in conservative side and DSM is more conservative where tension field action is not considered. Where tension field action is developing more, there DSM capacity can be taken. But in case of with lower buckling potential for sections with lower depths DSM capacity cannot be used since DSM gives higher capacity than the Ultimate capacity.

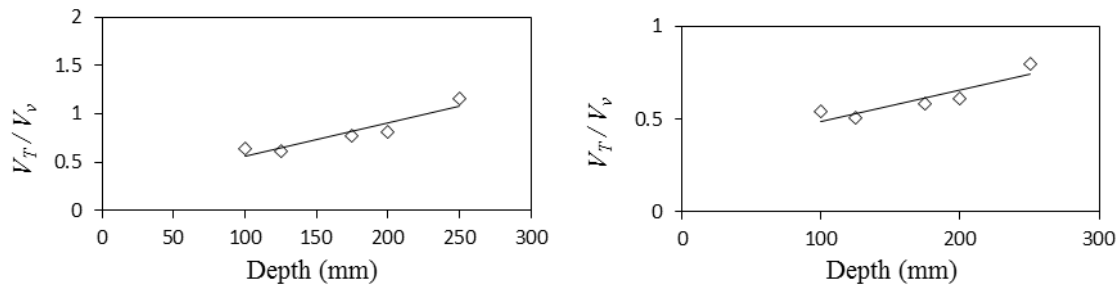
In fig.5 for combined shear and bending moment test with thickness 2.4 mm and V_v without considering tension field action the ratio V_T / V_v increases with depth which is shown from regression line. In fig.6 for combined shear and bending moment test with thickness 2.4 mm and V_v with considering tension field action the ratio V_T / V_v increases with depth which is shown from regression

line. In MV tests the span is longer which leads to lower buckling potential. The ultimate capacity is higher than the nominal capacity when depth is increasing. Since tension field action is not developing in MV tests V_T / V_v is always less than 1 when DSM capacity is used with considering tension field action. DSM capacity with considering tension field action cannot be used where tension field action is not developed.



(a) V-C with straps

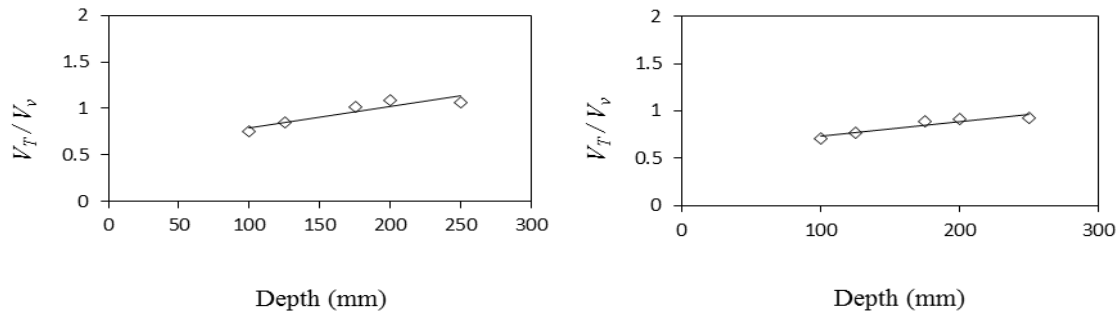
(b) V-C without



(c) MV-C with straps

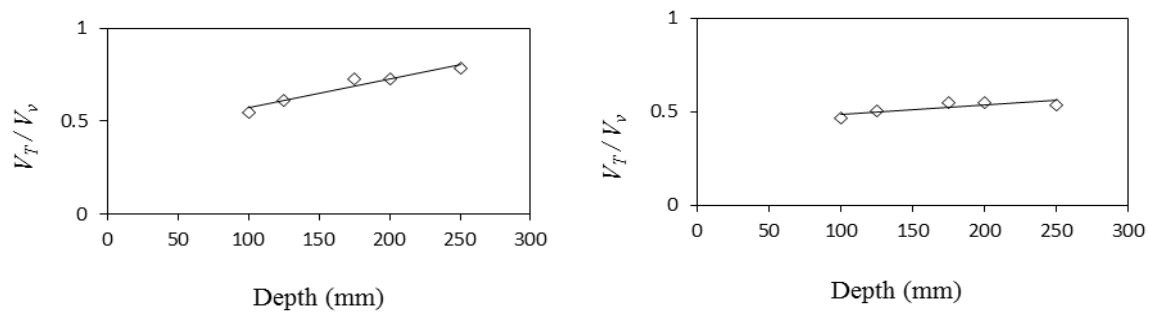
(d) MV-C without straps

Fig. 5 V_T / V_v vs depth for thickness of 2.4 mm without TFA



(a) V-C with Straps

(b) V-C without straps



(c) MV-C with straps

(d) MV-C without Straps

Fig. 6 V_T/V_v vs depth for thickness of 2.4 mm with TFA

CONCLUSIONS

For this investigation, a finite element model of cold-formed plain C- lipped sections has been developed using ANSYS with reference to the past experimental program conducted by Pham. The limitations of DSM was examined in this study. The behaviour of the FE model was studied by constructing the graphs the ratio V_T/V_v vs. depth where V_v is the DSM nominal shear capacity and V_T is the shear at the support which is found from the analysis. The influence of the depth to develop tension field action was investigated in this research. The applicability of the DSM is determined by the structural behaviour of the FE model. The findings of the study is included in this conclusion in short. When tension field action tends to develop more in the structural behaviour, DSM nominal shear capacity without considering tension field action remains in more conservative side than DSM nominal shear capacity with considering tension field action. When tension field action does not tend to develop in the structural behaviour, DSM nominal shear capacity without considering tension field action and DSM nominal shear capacity with considering tension field action cannot be used. For thinner and higher depth sections which tend to develop more tension field action, DSM nominal shear capacity without considering tension field action remains in more conservative side than DSM nominal shear capacity with considering tension field action. For thicker and lower depth sections which do not tend to develop tension field action we have to be careful in using DSM nominal shear capacity without considering tension field action and DSM nominal shear capacity with considering tension field action.

REFERENCES

- AISI (2007). North American Specification for the Design of Cold-Formed Steel Structural Members. 2007 Edition, AISI S100-2007
- Pham, C. H., and Hancock, G. J. 2009a. Direct Strength Design of Cold- Formed Purlins. *Journal of Structural Engineering*, American Society of Civil Engineers, Vol. 135, Issue 3, pp. 229-238.
- Pham, C. H., and Hancock, G. J. 2009b. Shear Buckling of Thin-Walled Channel Sections. *Journal of Constructional Steel Research*, Vol. 65, No. 3, pp. 578-585.
- Pham, C. H., and Hancock, G. J. 2009c. Experimental Investigation of High Strength Cold-Formed C-Section in Combined Bending and Shear. *Research Report No R894*, School of Civil Engineering, The University of Sydney, NSW, Australia, April, 2009.
- Pham, C. H. 2010. Direct Strength Method (DSM) of Design of Cold-Formed Sections in Shear, and Combined Bending and Shear. *PhD Thesis*, School of Civil Engineering The University of Sydney Australia.

SEISMIC VULNERABILITY ASSESSMENT OF PRIMARY SCHOOL BUILDINGS AT CHITTAGONG CITY CORPORATION, BANGLADESH USING FEMA 154

M. R. Mahmud¹, S. B. Ali^{1*} & M. A. R. Bhuiyan²

¹*Institute of Earthquake Engineering Research, Chittagong University of Engineering and Technology, Chittagong-4349, Bangladesh. E-mail: mahmudraihan270@gmail.com*

²*Department of Civil Engineering, Chittagong University of Engineering and Technology, Chittagong-4349, Bangladesh. E-mail: arbhuiyance@cuet.ac.bd*

**Corresponding Author*

ABSTRACT

The seismic performance of primary schools is of high importance because of their exceptional occupancy and their significant role after any natural disaster. Bangladesh is highly vulnerable to earthquake because of her proximity to the boundary of tectonic plates and fault lines. Chittagong is a major leading city and business capital of Bangladesh which is positioned in the south-eastern part of the country, falls in the moderate seismic zone according to Bangladesh building code (BNBC, 2015 draft) with a seismic zone coefficient of 0.28 g based on 2% probability in 50 years. In this city most of the government primary schools were built before implementation of seismic code. Therefore, it is necessary to investigate the seismic performance of existing buildings in government primary schools in Chittagong City. In the present study, a structural record of existing government primary school buildings in Chittagong City Corporation area has been developed. The seismic vulnerability of these buildings has been evaluated by using FEMA 154. The result of the study represents that the total 107 buildings of government primary school in Chittagong City Corporation are safe against probable earthquakes and 216 buildings are required more specified analysis to evaluate the level of actual risk.

Keywords: Rapid Visual Screening; Primary School Buildings; Vulnerability Assessment; Chittagong City Corporation.

INTRODUCTION

Bangladesh is a highly populated and developing country in the world. It is a naturally disaster prone country and most affected region due to global climate change over last decades (Kreft et al., 2014). Recently, the country affected by numerous disasters such as floods, cyclones, landslides, earthquakes, droughts and etc. As a result, each year the country faces thousands of casualty and lots of economic lose. Moreover, the proximity of the country to the edge of two energetic plates, i.e., one of them Indian plate and another is the Eurasian plate causes more vulnerable to earthquake. Though, there is no evidence of great earthquake happened in these faults for several years, repeatedly occurring small to medium earthquakes in this region makes us conscious about happening of serious earthquakes in the future. In 2009, CDMP has proposed five major fault zone, i.e., Madhupur fault (MF), Dauki fault, Plate boundary fault (PBF) -1, Plate boundary fault (PBF) -2 and Plate boundary fault (PBF) -3 (Fig. 1). Chittagong is second major city and business principal consists of 41 administrative wards with numerous important lifeline structures. This region falls in the moderate seismic zone according to Bangladesh National Building Code (BNBC, 2015 draft) with a seismic zone coefficient is 0.28g based on 2% probability in 50 years.

Chittagong has an extended evidence of earthquakes. Serviceability of lifeline facility is of high importance for emergency response after natural disasters especially earthquakes. This lifeline facility includes school buildings, hospital, fire service station, electrical power station, road network, bridges, gas lines etc. The school buildings are the most important structures and serious human concern and their safety needs to be ensured first. Any kind of slight collapse of any component of those buildings will cause loss of many lives. Most of the government primary school buildings in Chittagong city were constructed to be used as cyclone shelter and relief centre also. So, it is necessary to investigate the seismic performance of existing school buildings.

Thought, some of the researchers conducted research on evaluation of seismic vulnerability of important buildings in Chittagong city (Sarraz et al., 2015, Mazumder et al., 2018), none of them focused on school buildings. The present study has been carried out to evaluate seismic safety assessment of government primary school buildings in Chittagong City Corporation. In this study, main objective is to prepare a seismic vulnerability database of government primary school buildings in CCC. The result of this present study can be used for further seismic risk mitigation plan.

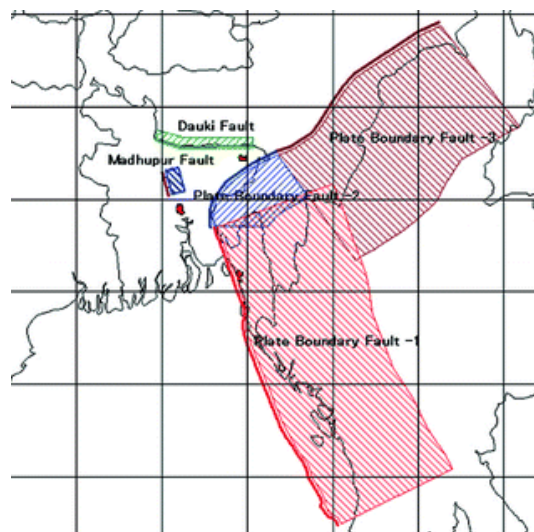


Fig. 1: Proposed earthquake fault zones by CDMP (CDMP, 2009)

SEISMICITY OF BANGLADESH

The past seismic data and recent seismic activities in and around Bangladesh indicate that the country is at seismic risk. The earthquake specialists are expecting severe earthquakes in this area in near future which can cause serious human casualties and damage of infrastructures. Bangladesh is highly vulnerable to earthquake because of its location in reasonable seismic region in the world seismic map prepared by Global Seismic Hazard Assessment Program (GSHAP, 1992) and proximity to the border of two energetic plates such as the Indian plate and the Eurasian plate. Attendance of existing fault lines in and surroundings the nation, are capable to produce damageable earthquake. The largest earthquake event occurred surroundings this region was Assam Earthquake in 1897 with magnitude 8.7 (Jain, 1998). This is broadly known as Great Indian Earthquake. There are hundreds of evidences of tremors that jolted Chittagong and its nearby areas. One of the largest earthquake in history happened in 1762 at Arakan in the southern part of Chittagong division which caused huge damage. It also triggered the earliest documented Tsunami in the Bay of Bengal. Another big earthquake occurred in 1869 with a surface-wave magnitude of 7.5 at Cachar, Assam. This was powerfully felt in the entire Chittagong division. Another citable earthquake known as Srimangal Earthquake (7.6 magnitude) was occurred around Sylhet in 1918 (Sabri, 2001). Epicentre of this earthquake was about 130 km from Dhaka. In 2003, a 5.2 magnitude earthquake shock the Barkal area of Rangamati district which causes damaged to several buildings, killed 2 people and injured more than 100 hundred people (Ansary and Sadek, 2006). No major earthquake has been take place in this region during last century. But regularly occurring small to medium earthquakes in this region makes us concern about future seismic risk.

STUDY AREA

Chittagong City Corporation (C.C.C.) area covers 185 square kilometres consisting 41 administrative wards and around 14000 persons live in per square kilometres. Total number of government primary schools in the Chittagong City Corporation is 215. Among them 14 schools are under construction. Most of the schools are comprised of several buildings. Total 343 independent school buildings are existed where 16 buildings are under construction, 2 are Tin shed and 2 are unused. Different buildings at each site have different characteristics. Most of the primary school buildings were constructed to use as cyclone shelter and relief centre. The condition of most of the government primary school buildings is poor due to becoming old and lacking of repair and maintenance.

METHODOLOGY

At present, a number of evaluation procedures are available to assess the safety level of a structure during an earthquake. Rapid visual screening (RVS) is one kind of procedure which use to identify record and class building structures that are potentially seismic hazardous during earthquake (FEMA 154, 2002). FEMA 154 RVS methodology is encapsulated in a one-page format that joins an explanation of a building structure. This method is planned to be applied without performing any structural computations. The Fig. 2 shows the score modifier for the assessment of the vulnerability of building structures according to FEMA 154.

Score Modifier

BASIC SCORE, MODIFIERS, AND FINAL SCORE, S															
BUILDING TYPE	W1	W2	S1 (NRF)	S2 (BR)	S3 (LM)	S4 (RC SW)	S5 (URM INF)	C1 (NRF)	C2 (SW)	C3 (URM INF)	PC1 (TU)	PC2	RM1 (FD)	RM2 (RD)	URM
Basic Score	4.4	3.8	2.8	3.0	3.2	2.8	2.0	2.5	2.8	1.6	2.6	2.4	2.8	2.8	1.8
Mid Rise (4 to 7 stories)	N/A	N/A	+0.2	+0.4	N/A	+0.4	+0.4	+0.4	+0.4	+0.2	N/A	+0.2	+0.4	+0.4	0.0
High Rise (> 7 stories)	N/A	N/A	+0.6	+0.8	N/A	+0.8	+0.8	+0.6	+0.8	+0.3	N/A	+0.4	N/A	+0.6	N/A
Vertical Irregularity	-2.5	-2.0	-1.0	-1.5	N/A	-1.0	-1.0	-1.5	-1.0	-1.0	N/A	-1.0	-1.0	-1.0	-1.0
Plan Irregularity	-0.5	-0.5	-0.5	-0.5	-0.5	-0.5	-0.5	-0.5	-0.5	-0.5	-0.5	-0.5	-0.5	-0.5	-0.5
Pre-Code	0.0	-1.0	-1.0	-0.8	-0.6	-0.8	-0.2	-1.2	-1.0	-0.2	-0.8	-0.8	-1.0	-0.8	-0.2
Post-Benchmark	+2.4	+2.4	+1.4	+1.4	N/A	+1.6	N/A	+1.4	+2.4	N/A	+2.4	N/A	+2.8	+2.6	N/A
Soil Type C	0.0	-0.4	-0.4	-0.4	-0.4	-0.4	-0.4	-0.4	-0.4	-0.4	-0.4	-0.4	-0.4	-0.4	-0.4
Soil Type D	0.0	-0.8	-0.6	-0.6	-0.6	-0.6	-0.4	-0.6	-0.6	-0.4	-0.6	-0.6	-0.6	-0.6	-0.6
Soil Type E	0.0	-0.8	-1.2	-1.2	-1.0	-1.2	-0.8	-1.2	-0.8	-0.8	-0.4	-1.2	-0.4	-0.6	-0.8

Fig. 2: Basic score modifiers for final score calculation (FEMA 154, 2002)

The method has been developed for a broad audience. The audience are including building officials and superintendents, government organization and private-sector building structure owners to recognize, record and order buildings that are potentially seismically dangerous during an earthquake. Although rapid visual screening is appropriate to all building structures. Its principal purpose is to investigate (i) older buildings that were planned and constructed earlier than the adoption of sufficient seismic design, (ii) building structures on soft or poor soils, (iii) building structures having performance features that harmfully influence their earthquake response. According to FEMA 154/ATC-21 process the vulnerability factors are: apparent quality of building, vertical irregularity, short column effect, pounding effect, post benchmark, soft story, age of construction of building, torsion effect of building and structural system.

DATA ANALYSIS AND RESULTS

The number of Government Primary Schools (G.P.S.) in the Chittagong City Corporation is 215. In the present study total 323 buildings are analyzed to assess the seismic vulnerability by considering rapid visual screening method of FEMA 154. There are mainly two types of structures exist in the school buildings in Chittagong City Corporation, such as, Unreinforced Masonry (URM) structure with rigid diaphragm and Reinforced Concrete frame (C3) structures with masonry infill. Fig. 3(a) represents the percentage of schools according to thana. Most school buildings are low rise; about 83% buildings are 3 storeys or less. Among the building stock the highest building is five storeys which is around 7%. Government primary school buildings can be categorized as variety of three important phase of development of NBC code. Study found that about 19% buildings were built before the year of 1993, 51% were built from 1993 to 2006 and 30% were built after the year of 2006.

To assess the seismic vulnerability of primary school buildings in the CCC area, rapid visual screening of FEMA 154 is used. Information of every building structure are collected by walking around the building.

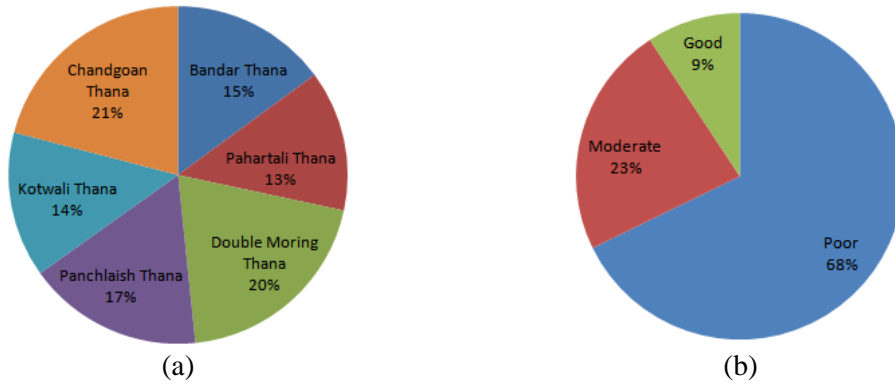


Fig. 3: Percentage of building (a) according to thana (b) according to physical condition

Fig. 3(b) represents the existing physical visible condition of the buildings in percentile form. From figure it is found that about 68% buildings are in poor condition and 23% and 9% buildings are in moderate and good condition respectively.

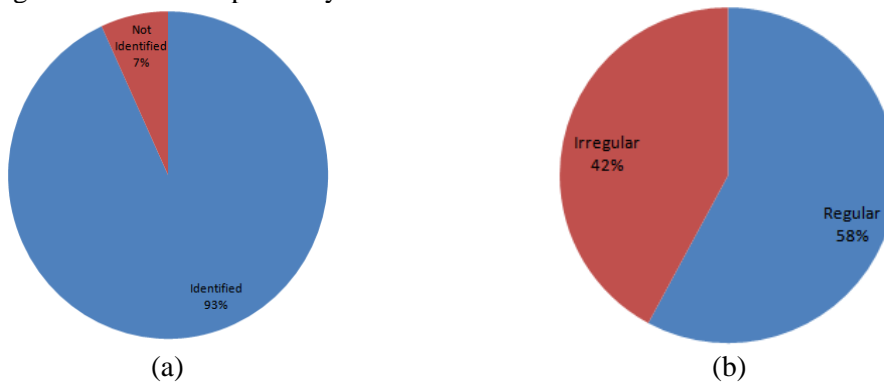


Fig. 4: Percentage of building having (a) short column effects (b) plan irregularity

Short columns carries shear force which is much higher than the shear carried by the lateral members. Short column can be described as the relation of the clear height of the column to depth of the column and is less than 2. Fig. 4(a) represents the percentage of buildings having short column effects in the government primary schools in CCC. It is observed that total 93% building having the short column. Complex structural feature is another key parameter responsible for poor seismic performance of school buildings. These irregular features are identified among the studied buildings. Total 187 buildings have no plan irregularity and 137 buildings have some irregularity especially with the re-entrant corners. Fig. 4(b) shows the percentage of presence of plan irregularity in government primary school buildings. It is seen that total 42% buildings are irregular in plan. Another type of irregular feature is vertical irregularity. The vertical irregularity is an important vulnerability factor which attributed in buildings by adopting setbacks, soft stories etc. The study found that total 117 buildings possess vertical irregularity which around 37% (Fig. 5(a)).

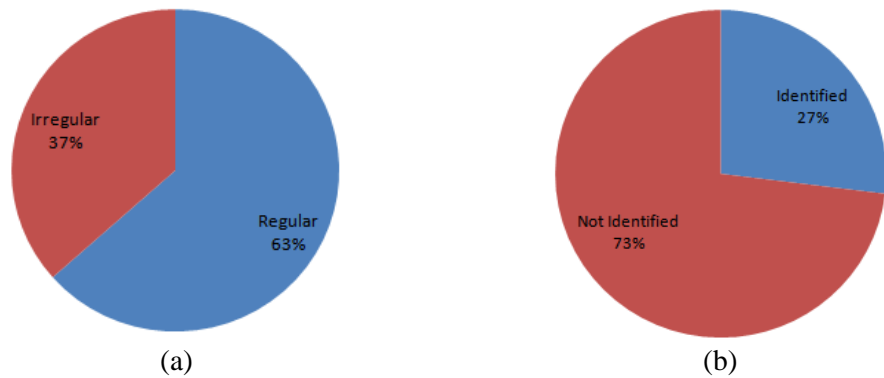


Fig. 5: Percentage of building having (a) vertical irregularity (b) pounding effects

Pounding effect of building is considered due to missing of enough space among the adjacent building structures which is significant vulnerable factor during earthquake. Fig. 5(b) shows that pounding effect is identified among 27% buildings of government primary school in CCC.

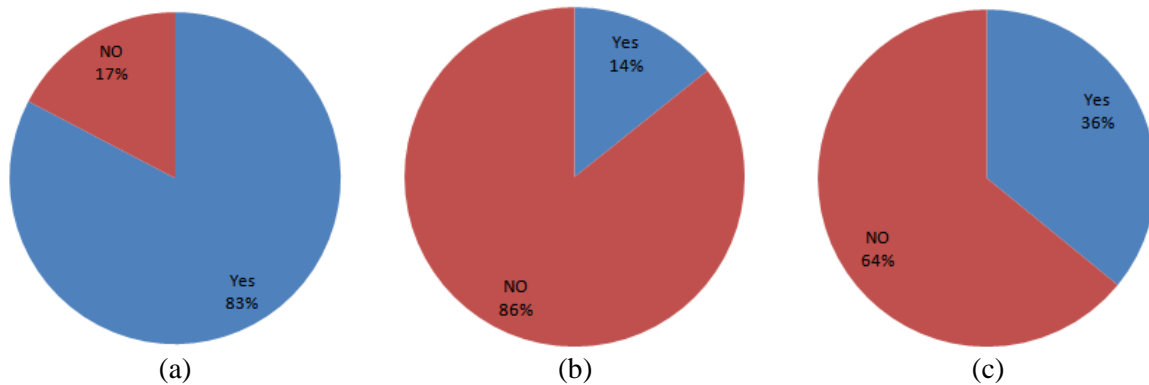


Fig. 6: Percentage of building having (a) parapet (b) cladding (c) other falling hazard

Non-structural masonry components of buildings such as parapets, chimneys, cladding and other falling hazards are prone to fall in earthquakes. Parapet indicates any low wall along the roof of a building which is defensive mini-wall made of bricks or other materials and cladding is extra glass work in a buildings. Other falling hazards are considered as chimneys, walls, appendages, tanks, signs, or any other building components that could fall during ground shaking. Fig. 6(a), 6(b) and 6(c) show the percentage of presence of falling hazard in the government primary school buildings in studied area. It is seen that total 267 buildings contain parapet, 46 buildings have cladding and 116 buildings constructed with other falling hazard which are around 83%, 14% and 36% respectively.

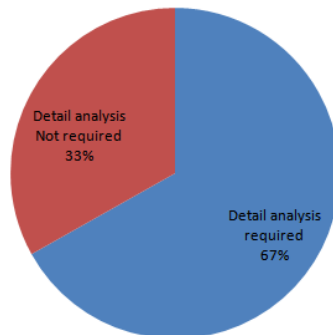


Fig. 7: Percentage of building that required detail Analysis

In the present study the cut off value of final structural score is considered as 2.0 which indicates that below this score seismically hazardous and detailed seismic evaluation of the building is required. This study summarized that total 216 buildings have score below cut off score and remaining 107 buildings have passed the score. It can be concluded that about 67% buildings required more detailed investigation to decide the level of actual seismic risk (Fig. 7).

CONCLUSIONS

In the present study, a structural record of existing government primary school buildings in Chittagong City Corporation area has been developed. The total number of government primary school in Chittagong City Corporation is 215. Among them 14 schools are under construction. Most of the schools are comprised with several buildings. In this study total 323 buildings are analysed to assess the seismic vulnerability of the schools. The final structural scores (S) of school buildings are determined by applying rapid visual screening suggested by FEMA 154. The parameters contributing the scoring system are mainly, the height, irregularities of the buildings, type of the soil underneath, Pre-Code and Post-Benchmark. From the results it can be concluded that total 107 buildings (around 33%) of government primary school in Chittagong City Corporation are safe against probable earthquakes and 216 buildings (around 67%) required further detailed analysis to determine the level of actual risk. These results are expected to be useful for administrative body who are going to conduct pre-disaster planning and capital investment planning.

REFERENCES

- Ansary, MA and Sadek, A. 2006. Assessment of 2003 Rangamati Earthquake, Bangladesh. Proceedings of 8th U.S. National Conference on Earthquake Engineering, San Francisco, USA.
- BNBC, 1993. Bangladesh National Building Code.
- BNBC, 2015 (draft). Bangladesh National Building Code.
- CDMP, 2009. Seismic Hazard & Vulnerability Assessment of Dhaka, Chittagong & Sylhet City Corporation. Comprehensive Disaster Management Program. Bangladesh
- FEMA 154, 2002. A Hand Book on Rapid Visual Screening of Buildings for Potential Seismic Hazards. Federal Emergency Management Agency, Washington DC, USA
- GSHAP, 1992. World Seismic Map. Global Seismic Hazard Assessment Program. Seismo.ethz.ch/GSHAP
- Jain, SK. 1998. Indian earthquakes: An overview. The Indian Concrete Journal, 72(11).
- Kreft, S.; Eckstein, D.; Junghans, L.; Kerestan C. and Hagen U. 2014. Global climate risk index 2015. German Watch, 3-59.
- Mazumder, RK; Utsob, MTU and Bhuiyan, MAR. 2018. Seismic vulnerability assessment of medical facilities: A GIS based application for Chittagong, Bangladesh. Malaysian Journal of Civil Engineering, 30(1): 97-112.
- Sabri, MSA. 2001. Earthquake intensity-attenuation relationship for Bangladesh and its surrounding region. A thesis of master in engineering in civil engineering, BUET, Bangladesh.
- Sarraz, A; Ali, MK and Das, DC. 2015. Seismic vulnerability assessment of existing building stocks at Chandgaon in Chittagong city, Bangladesh. American Journal of Civil Engineering, 3(1), 1-8.

SEISMIC VULNERABILITY ASSESSMENT OF PRIMARY SCHOOL BUILDINGS AT CHITTAGONG CITY CORPORATION, BANGLADESH USING FEMA 310

M. F. Shahriar, A.A. Walid, S. B. Ali*& M. A. R. Bhuiyan

Department of Civil Engineering, Chittagong University of Engineering and Technology, Chittagong-4349, Bangladesh.

E-mail: shafayatce@yahoo.com; fahimshahriar314159@gmail.com; abdullahwalid1301019@gmail.com; arbhuiyance@cuet.ac.bd*

**Corresponding Author*

ABSTRACT

Bangladesh is extremely vulnerable to seismic events because of its position near the boundary of tectonics plates. In this country, the primary school buildings have distinguished structural characteristics which cause them more vulnerable to earthquakes. Many existing government primary school buildings in Chittagong City Corporation were designed only to resist the gravity loads without seismic provisions. Also the seismic awareness among the tender-hearted children is not that much high. Therefore, it is necessary to investigate the vulnerability of these buildings to avoid serious damage and casualties in the future. In this paper, the seismic vulnerability of primary school buildings in Chittagong City Corporation (CCC) area has been evaluation by two phase, i.e., Tier 1 & Tier 2 analysis. Tier 1 analysis is done according to FEMA-154 guideline and Tier- 2 analysis has been conducted on the basis of FEMA-310 guideline. Total ten school buildings in Ward no.3 and Ward no.4 of the CCC area have been investigated. These results are expected to be helpful for administrative body who are going to conduct pre-disaster planning.

Keywords: Seismic Vulnerability; FEMA- 154; FEMA- 310; Soft Story; Chittagong City Corporation.

INTRODUCTION

Bangladesh which is situated in south-asia region, is one of the most seismic vulnerable countries in the world. Even a moderate seismic event can be cause a devastating consequence in the major cities of the country, particularly Chittagong, Sylhet and Dhaka (Alam et al., 2011). The main criteria for assessing an earthquake prone region are geology, topography, density of population and infrastructure and so on. Bangladesh is located in the moderate seismic region in the world seismic map prepared by Global Seismic Hazard Assessment Program (GSHAP, 1992). Geographically the country is situated near the boundary of two active continental plates, i.e., the Indian plate and the Eurasian plate. This country is encompassed by the regions of high seismicity including the northern Shillong Plateau and Himalayan Arc, eastern Arakan Yoma anticlinorium and Burmese Arc and northeast complex Naga-Disang-Jafong thrust zones. Moreover, the country is located in the Dauki Fault system where numerous subsurface active faults are existed. The largest earthquake event was occurred surroundings this region was Assam Earthquake in 1897 with estimated magnitude 8.7 (Jain, 1998) broadly known as Great Indian Earthquake. Another citable earthquake with an estimated magnitude was 7.6 (Sabri, 2001) in 1918 around Sylhet known as Srimangal Earthquake. Epicenter of this earthquake was about 130 km from Dhaka. In 2003, a 5.2 magnitude earthquake shock the Barkal area of Rangamati district which causes damaged to several buildings, 2 people were killed and more than 100 hundred people were

injured (Ansary and Sadek, 2006). No major earthquake has been take place in this region during last century.

Chittagong City Corporation is roughly 70 km away beyond the above described fault zones in the Bangladesh-Myanmar border zone. The Chittagong–Tripura folded belt experiences recurrent earthquakes (Alam et al., 2006). According to BNBC (BNBC, 2015 draft), Bangladesh has divided into four generalized seismic zones as shown in Fig. 1. The Chittagong region falls in the moderate seismic zone with a seismic coefficient of 0.28g based on 2 percent probability of exceedance in 50 years. The region has a long history of earthquakes. In 1762, one of the most devastating earthquakes occurred at Arakan which caused heavy damage in the southern part of Chittagong division. It also produced Tsunami in the Bay of Bengal. Another big earthquake occurred in 1869 with a surface-wave magnitude of 7.5 at Cachar, Assam. This was powerfully felt in the entire Chittagong division. The 1912 Mandalay earthquake with a surface-wave magnitude of 7.9 strongly felt in this region. The 1950 Assam earthquake with a magnitude of 8.6 was also felt in the same region with a strong shaking. During any natural disasters, the serviceability of lifeline facilities is very important. This lifeline facility includes school buildings, hospital, fire service station, electrical power station, road network, bridges, gas lines etc. The school buildings are the most important structures and any kind of slight collapse of any component of those buildings will cause loss of many lives.

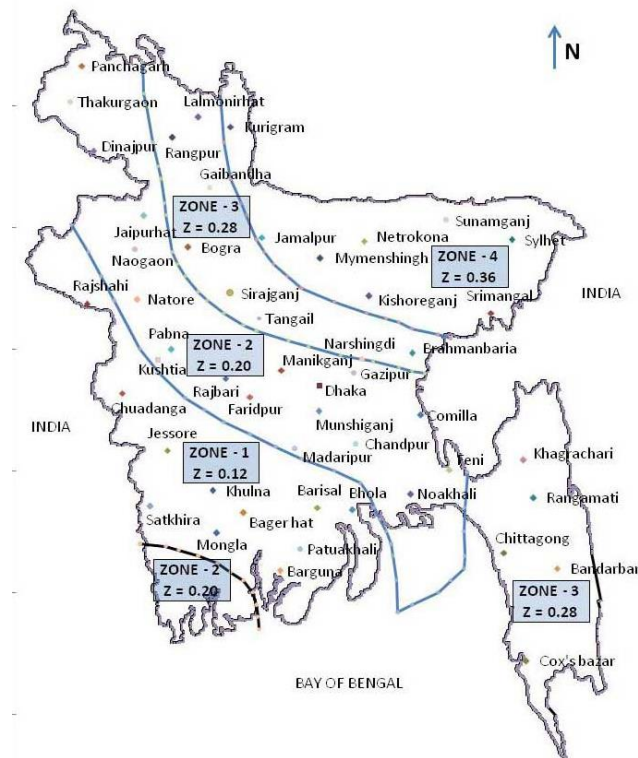


Fig. 1: Seismic zoning map of Bangladesh (BNBC, 2015 draft)

The seismic performance evaluation of the primary school buildings should have a crucial importance as they can be used as a temporary shelter after the occurrence of a major earthquake. However, most of these buildings have inadequate seismic resistance because of not maintaining any seismic provision in construction phase or poor seismic provision and also continuous processes of deterioration. Though, some of the researchers conducted research on evaluation of seismic vulnerability of important buildings in Chittagong city (Sarraz et al., 2015, Mazumder et al., 2018), none of them focused on school buildings. The present study has carried out to evaluate seismic safety assessment of government primary school buildings in Chittagong City Corporation using FEMA 310. In this study, main objective is to prepare a seismic vulnerability database of government primary school buildings in CCC.

STUDY AREA

Chittagong City Corporation (CCC) area covers 160 square kilometres where 41 administrative wards are existed and around 14,000 persons live in per square kilometres. Total number of government primary schools in Chittagong City Corporation is about 215. Among them 14 school are under construction. Most of the schools are comprised of several buildings. The survey areas of this research work are Panchlaish at ward-3 and Chandgoan at ward-4 of the CCC which are located on the edge of the river named Karnaphuli. Total 11 and 15 government primary school buildings are located in ward-3 and in ward-4 respectively. Most of the school buildings established as a reconstruction project under the Saudi financing.

METHODOLOGY

Earthquake is one of the most demolishing natural disasters which cause destructive effect on human lives as well as in infrastructures. There are several methods to determine seismic vulnerability assessment such as (FEMA-154, 1988), (FEMA-310, 1998), EURO CODE 8, New Zealand Guideline, Modified Turkish Method, IITK-GSDM etc. In this study, seismic vulnerability assessment procedure is conducted by two tiers. Tier 1 analysis is done according to FEMA-154 guideline and Tier- 2 analysis has been conducted on the basis of FEMA-310 guideline.

Rapid Visual Screening (RVS)

The Rapid Visual Screening has been thoroughly described in FEMA-154. This method is one of the quickest procedures to identify the seismically vulnerable buildings without the use on any expensive detailed evaluation of any particular building. In Rapid Visual Screening a scoring system has been developed that enables the users to identify the primary lateral load resisting system of structure and the seismic performance of the structures. The observation of the building will take an average of 15 to 30 minutes. Moreover, the surveyors can categorize the buildings into two types using a cut off score i.e., buildings safe against probable seismic events or buildings which are seismically hazardous.

FEMA-310

For the evaluation in Tier-2 phase, the professional design engineer can carry on a complete analysis of the building that has been identified as non-compliant, i.e., further evaluation of the individual deficiency of an unsafe building is needed according to Tier-1. This analysis is limited to simplified linear analysis methods and it could be done using one of the common linear static or dynamic analysis methods. After the seismic evaluation has been performed, a final assessment report shall be prepared.

RESULTS AND DISCUSSIONS

In Tier-1, total 10 numbers of primary school buildings have been evaluated using Rapid Visual Screening (RVS) method. Considering Chittagong City Corporation as moderate seismic risk zone, the cut off value is taken as 2.0. Buildings having cut off value less than 2.0, needed to be evaluated further in Tier-2 phase. The following Table 1 shows of the RVS scores of different primary school buildings.

Table 1: Final scores of RVS

Name of the school building	RVS Score	Detailed Evaluation Required
WAPDA colony govt. primary school building-1	1.7	Yes
WAPDA colony govt. primary school building-2	2.2	No
Shamsher para haji chand miya govt. primary school building-1	-0.8	Yes
Shamsher para haji chand miya govt. primary school building-2	2.2	No
Ekhlasur Rahman govt. primary school building	-0.1	Yes
Wajediya govt. primary school building	1.7	Yes
Taiyebiya govt. primary school building	1.7	Yes
Shahed para govt. primary school building	2.2	No
Chandgaon board govt. primary school building	2.2	No
Hajir pul govt. primary school building	2.2	No

Tier-2 evaluation has been conducted using FEMA-310 guideline. FEMA-310 guideline basically focuses on the features like soft story, geometry, mass & torsional irregularity etc. In the following Table 2 the summary of the deficiency of the individual has been shown.

Table 2: Summary of the deficiency exist

Name of the school building	Deficiency
WAPDA colony govt. primary school building-1	Re-entrant corners, torsional irregularity
Shamsher para haji chand miya govt. primary school building-1	Soft story, torsional irregularity
Ekhlasur Rahman govt. primary school building	Soft story, plan irregularity, vertical geometric irregularity, mass & torsional irregularity.

CONCLUSIONS

Seismic vulnerability assessment of the primary school buildings at the Panchlaish ward (No. 3) and Chandgaon ward (No. 4) has been conducted by two tiers. Tier 1 evaluation process has been done by FEMA-154 which has the combined description of a building, its layout, occupancy and a rapid evaluation of seismic hazard related to structural elements. In the study 10 primary school building has been screened out. Among them 3 school buildings have been investigated further using Tier 2. Tier 2 evaluation has been conducted using FEMA-310 guideline. FEMA-310 guideline basically focuses on the features like: soft story, geometry, mass & torsional irregularity. From the study it has been found that WAPDA colony govt. primary school at 3 no. ward has the vulnerability parameters, i.e., re-entrant corners and torsional irregularity. Shamsher para haji chand miya govt. primary school building at 4 no. ward, has the soft story and torsional irregularity. Ekhlasur Rahman govt. primary school building has severe irregularity problem like soft story, plan irregularity, vertical geometric irregularity, mass irregularity and torsional irregularity. As the vulnerability parameters exist at these three buildings, it can be said that WAPDA colony govt. primary school building-1, Shamsher para haji chand miya govt. primary school building-1 and Ekhlasur Rahman govt. primary school building are required further detailed analysis to determine the actual seismic risk level.

REFERENCES

- Alam, MJ; Hossain, E and Islam, ABMT. 2011. Seismic Vulnerability Assessment of Existing RC Buildings in GIS Environment of 16 no. Chawkbazar ward. Undergraduate thesis paper, Department of Civil Engineering, CUET.
- Alam, MJ; Bhuiyan, AR and Islam, MR. 2006. Seismic Structural Assessment of Damaged Chittagong Public Library Building during 27 July 2003 Earthquake. 4th International Conference on Earthquake Engineering, Taipei, Taiwan.
- Ansary, MA and Sadek, A. 2006. Assessment of 2003 Rangamati Earthquake, Bangladesh. Proceedings of 8th U.S. National Conference on Earthquake Engineering, San Francisco, USA.
- BNBC, 2015 (draft). Bangladesh National Building Code.
- FEMA-154. 1988. A Rapid visual screening of buildings for potential seismic hazards: A Handbook FEMA-154. Federal Emergency Management Agency, Washington DC, USA.
- FEMA-310. A handbook for the seismic evaluation of buildings. Federal Emergency Management Agency, Washington DC, USA.
- GSHAP. 1992. World Seismic Map. Global Seismic Hazard Assessment Programme. seismo.ethz.ch/GSHAP.
- Jain, SK. 1998. Indian earthquakes: An overview. The Indian Concrete Journal, 72(11).
- Mazumder, RK; Utsob, MTU and Bhuiyan, MAR. 2018. Seismic vulnerability assessment of medical facilities: A GIS based application for Chittagong, Bangladesh. Malaysian Journal of Civil Engineering, 30(1): 97-112.
- Sabri, MSA. 2001. Earthquake intensity-attenuation relationship for Bangladesh and its surrounding region. A thesis of master in engineering in civil engineering, BUET, Bangladesh.
- Sarraz, A; Ali, MK and Das, DC. 2015. Seismic vulnerability assessment of existing building stocks at Chandgaon in Chittagong city, Bangladesh. American Journal of Civil Engineering, 3(1), 1-8.

SEISMIC VULNERABILITY ASSESSMENT: A CASE STUDY OF CUET CAMPUS

S. Das¹, S. B. Ali^{2*}, R. K. Mazumder² & M. A. R. Bhuiyan³

¹Department of Civil Engineering, University of Louisiana, Lafayette, Louisiana, USA.

E-mail: shagata.joy@gmail.com

²Institute of Earthquake Engineering Research, Chittagong University of Engineering & Technology, Chittagong, Bangladesh. Bangladesh.

E-mail: shafayatce@yahoo.com^{*}; rkmazumder@cuet.ac.bd

³Department of Civil Engineering, Chittagong University of Engineering & Technology, Chittagong, Bangladesh.

E-mail: arbhuiyan@yahoo.com

**Corresponding Author*

ABSTRACT

Chittagong University of Engineering and Technology (CUET) campus is located in the Zone III of BNBC 2015 Draft with a seismic zoning coefficient 0.28g based on a maximum credible earthquake of 2 percent probability of exceedance of 50 years. In this University, many of the buildings including academic and residential were constructed before building code adaptation and seismic code provision enforcement. The present study has been carried out to assess the seismic vulnerability of existing buildings in CUET campus. Multi-level performance assessment techniques, i.e., FEMA 154, Turkish Preliminary Assessment and FEMA 310 are used to evaluate the seismic performance of the buildings. In this present study, total 25 buildings of CUET campus including 11 reinforced concrete and 14 masonry structures are assessed in the level 1 investigation. The structural information found in walk-down assessment procedure is presented in the Geographic Information System (GIS). Among them, 11 buildings which are student hostels and residential buildings are selected for level two investigation based on their level of importance in building use. Finally, detailed investigation was performed for those reinforced buildings.

Keywords: CUET; Seismic Assessment; FEMA 154; FEMA 310; Turkish Method.

INTRODUCTION

Bangladesh is highly vulnerable to earthquake because of her proximity to the boundary of tectonic plates (Eurasian plate and Indo-Australian Plate) and fault lines. The country and its surrounding areas have a long history of earthquakes. The last big event surrounding these region, The Great Indian Earthquake (Yeats et al., 1997) was happened due to the rupture of the Dauki fault (Morino et al., 2014) in 1897. Bangladesh is in the moderate seismic zone in the world seismic map which was developed by Global Seismic Hazard Assessment Program (GSHAP, 1992). In 2009, Comprehensive Disaster Management Program (CDMP) study proposed five major fault zones in Bangladesh, i.e., Madhupur fault (MF), Dauki Fault (DF), Plate Boundary Fault-1 (PBF-1), Plate Boundary Fault-2 (PBF-2) and Plate Boundary Fault-3 (PBF-3). Chittagong is located close to the PBF-2 and the city falls into zone II in the Bangladesh National Building Code (BNBC, 1993) with a seismic coefficient of 0.15g, considering a return period of 200 years. In proposed Bangladesh National Building Code (BNBC, 2015 draft) seismic map, Chittagong city region falls into zone III with a coefficient of 0.28g. In the

proposed seismic map where MCE was corresponded to a return period of 2475. That means in 50 years 2% probability of exceedance.

A project has been conducted by the Institute of Earthquake Engineering Research to evaluate the seismic vulnerability and develop a structural database of existing building at CUET Campus. Initially, under this project a total number of 80 buildings including 26 Reinforced Concrete and 54 Masonry structures were assessed in the level 1 investigation. Most of the buildings were found to be perform well during first level investigation. In this present study, total 25 buildings are assessed by FEMA 154 and FEMA 310. The structural information found in walk-down assessment procedure is presented in the Geographic Information System (GIS). Finally, detailed investigation was performed for the selected reinforced buildings which have high level of importance in building use.

STUDY AREA IN GIS MAP

The study area (Fig. 1) is situated in the Tripura-Chittagong Fold Belt (Alam et al., 1990). This region has a thick sedimentary sequence deposited through the Tertiary to Pleistocene age. During the Himalayan orogenic movements, this sedimentary sequence has been folded. This region has experienced a varied environment during the long geological time. The transgression and regression of sea were the reasons behind this variation of environment. Sitakunda fault, Tigerpass fault and Kamaphull fault cut this the plunge area.

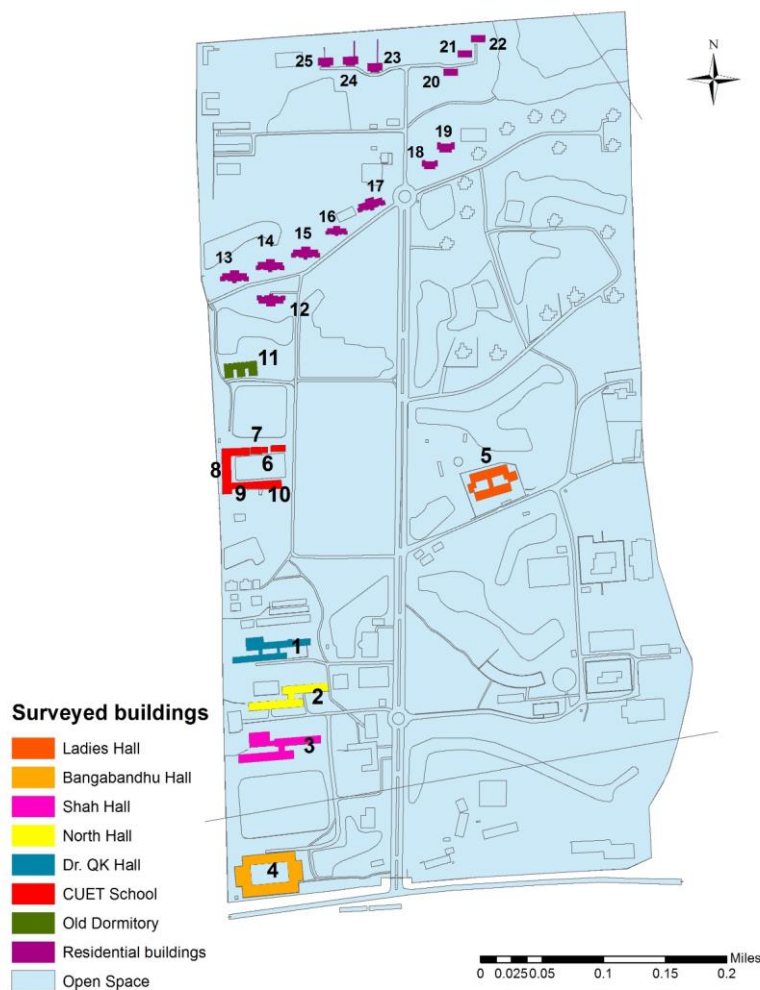


Fig. 1: Surveyed buildings with identification number in GIS

METHODOLOGY

To evaluate the seismic condition of the existing buildings, three level of risk assessment procedures have been applied based on importance level of the structures. There are two major types of structures are existed in CUET campus, i.e., Reinforced Concrete (RC) Frame Structures with unreinforced masonry infill wall and Unreinforced Masonry Buildings.

Ozcebe et al. (2006) employed the discriminate analysis technique for developing a preliminary evaluation methodology. Using this methodology seismic vulnerability of several existing RC buildings with low to medium has been assessed in Turkey. Identification of the buildings which are highly vulnerable to seismic events is the main objective of the procedure. This technique can only be applied up to seven stories RC frames and frame-wall structures.

In 1988, Federal Emergency Management Agency (FEMA) published a report (FEMA 154) on Rapid visual screening (RVS) of buildings for potential seismic hazards. RVS provides a procedure to identify, record and rank buildings considering potential seismic hazard (FEMA 154, 2002). RVS can be applied to both RC and masonry structures.

The third level detailed evaluation procedure is based on the determination of the anticipated strength of lateral load resisting elements. This probable strength can be compared with the expected seismic demands. The procedures in the level 3 employ linear analyses of the building according to FEMA 310. It requires the as built dimensions of all structural elements for performing this analysis. The linear static and non-linear static methods are applied to evaluate the capacity demand analysis of structure.

RESULTS AND DISCUSSIONS

Table 1 represents the summary of final score of different student halls and residential buildings at CUET campus obtained from RVS using FEMA 154. According to RVS (FEMA 154, 2002), score in between 0.7 to 2.0 has a high probability of Grade 3 damage and very high probability of Grade 2 damage (Rahman, N., 2014). On the other hand, score in between 2.0 to 3.0 have the high probability of damage grade 2 and very high probability of damage grade 1. Almost all the surveyed buildings have the score in the range of 0.7 to 2.0. So, masonry buildings may face cracks in many walls. Moreover, fall of plaster, and partial failure of chimneys of the buildings can also be occurred. On the other hand, RC buildings may face cracks in beams and columns of frames, and in partition and infill walls.

Table 1. Summary of final score using FEMA 154

Building Name	Building Type	Final Score
BANGABANDHU HALL	C3(URM INF)	1.9
Q.K.HALL	C3(URM INF)	0.9
TAREQ-HUDA HALL	C3(URM INF)	0.9
SHAH HALL	C3(URM INF)	0.9
LADIES HALL	C3(URM INF)	0.9
CUET SCHOOL PART 1	C3(URM INF)	1.2
CUET SCHOOL PART 2	C3(URM INF)	1.2
CUET SCHOOL PART 3	C3(URM INF)	1.2
CUET SCHOOL PART 4	C3(URM INF)	1.2
CUET SCHOOL PART 5	C3(URM INF)	2.2
Old Dormitory	C3(URM INF)	1.9
14 Residential Buildings	URM	1.7

Q.K. HALL, SHAH HALL, TAREQ-HUDA HALL and LADIES HALL, these have the lowest RVS score among the other buildings and have high probability of Grade 3 damage. That means these buildings may face cracks in columns and beam-column joints of frames, at the base and at joints of coupled walls. It is seen that most of the residential building configuration are somewhat similar.

Therefore, the obtained performance for single story residential URM represents a similar result in first level assessment.

Second level assessment is conducted for the RC buildings following Turkish level 2 guideline prepared by Ozcebe et al. in 2006. Eleven buildings are analyzed based on building importance level considering building use. From the summary of all the surveyed buildings in second level assessment (Turkish Preliminary Assessment) procedure lies in the low-risk group.

The structural model is developed using structural software ETABS for level 3 assessment. There are basically five buildings. We are assuming that these buildings are separated in different segments. So, each separated segments of these buildings are considered as distinct structure. That is why there are 11 C3 (URM INF) type structures. Firstly, the linear analysis is carried out for the models of the buildings. Finally, non-linear static (inelastic) procedure is applied for the model to evaluate the capacity analysis of the structure by plotting pushover analysis. Fig. 2 represents the story response plot and pushover curve of Dormitory building.

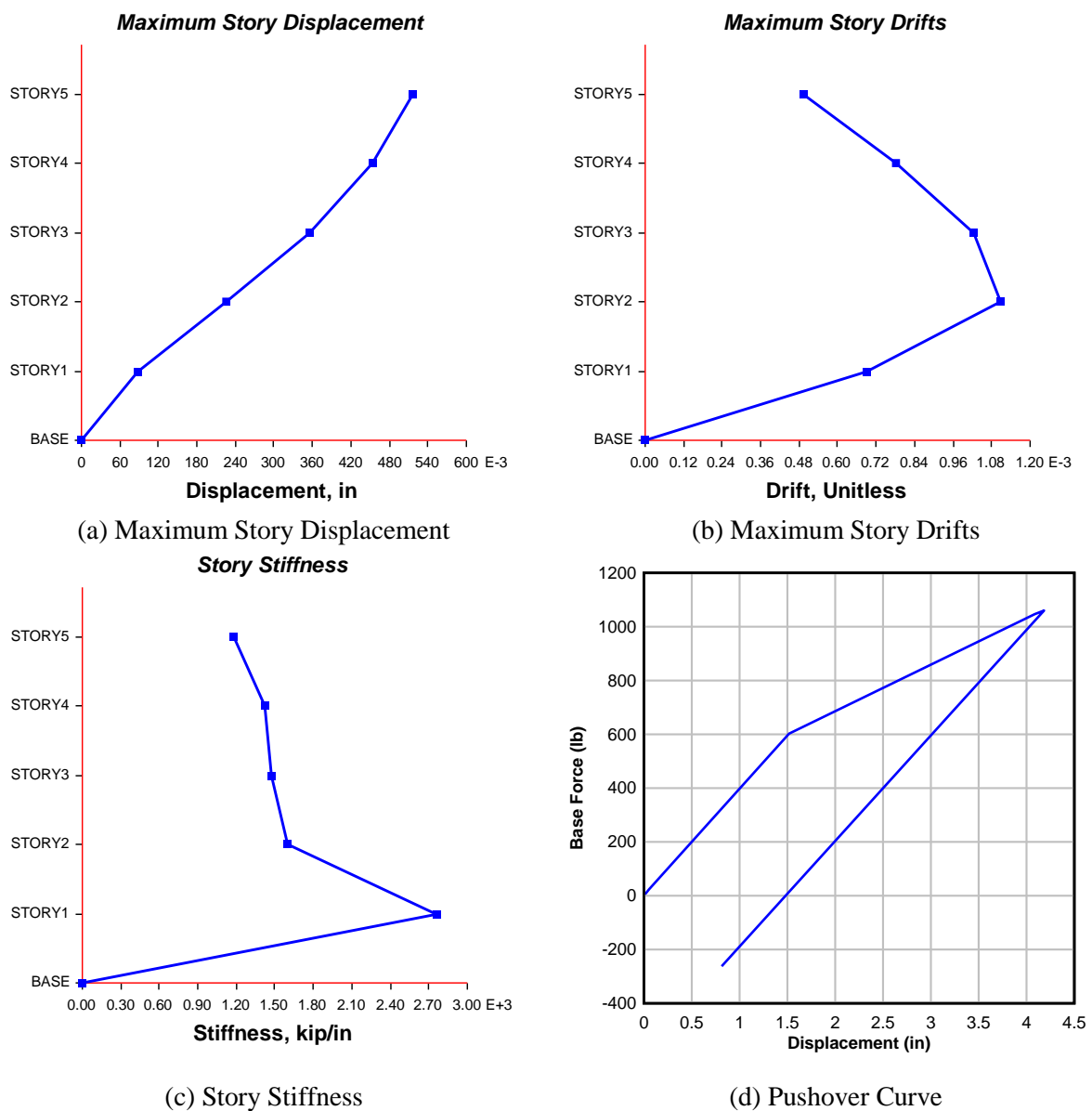


Fig. 2: Story response plot and Pushover curve of Old Dormitory Building.

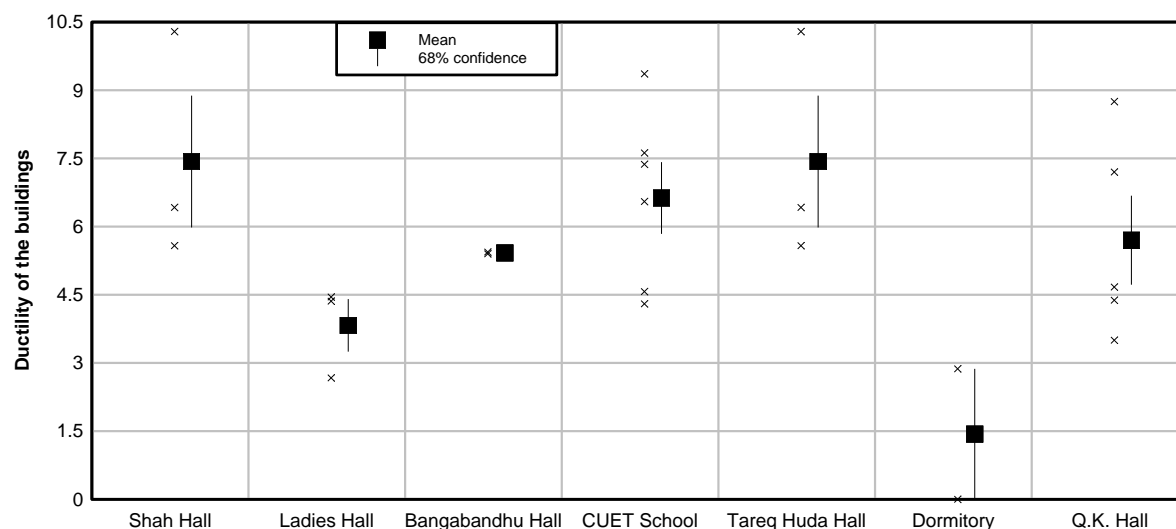


Fig. 3: Ductility of the residential and school buildings

In the third level assessment, the structural responses of the eleven RC buildings are checked to confirm that the conditions are within the acceptable limit according to BNBC. The drift values of all the buildings showed that the drift limit in both X and Y direction conform the story drift limitation as mentioned in Bangladesh National Building Code. Fig. 3 is showing the ductility of the different segments of the major buildings. This graph is giving a fair idea of the relative ductility and stiffness of the buildings. Shah hall and Tareq Huda hall are showing maximum ductility. On the other hand, the old dormitory building is showing less ductile behaviour.

CONCLUSIONS

A total of 25 buildings were investigated using Rapid Visual Screening (FEMA 154) assessment approach. Q.K. HALL, SHAH HALL, TAREQ-HUDA HALL and LADIES HALL have the lowest RVS score among the other buildings and have high probability of having cracks in beam-column joints and columns of frames. Moreover, these buildings may face cracks at the base, and at joints of coupled walls. Detail investigation was performed by using structural software ETABS for 11 reinforced buildings based on their level of importance in building use. The results of non-linear static analysis show that the response of structures was found within acceptable range according to BNBC. However, Masonry buildings need to be assessed in detail for more consistent results. Furthermore, Shah Hall and Tareq Huda hall show maximum ductility, whereas the old dormitory building represents less ductile behavior.

REFERENCES

- Alam, M. K., Hasan, A. K. M., Khan, M. R., & Whitney, J. W. (1990). Geological Map of Bangladesh. Geological Survey of Bangladesh. US Geological Survey, Dhaka.
- BNBC, (1993). Bangladesh National Building Code.
- BNBC, (2015). Bangladesh National Building Code.
- CDMP (2009). Seismic Hazard & Vulnerability Assessment of Dhaka, Chittagong & Sylhet City Corporations, Comprehensive Disaster Management Program, Bangladesh.
- FEMA 154 (2002). A Hand Book on Rapid Visual Screening of Buildings for Potential Seismic Hazards. Federal Emergency Management Agency, Washington DC, USA.
- GSHAP (1992). World Seismic Map. Global Seismic Hazard Assessment Program. Seismo.ethz.ch/GSHAP.
- Morino, M., Kamal, A. M., Akhter, S. H., Rahman, M. Z., Ali, R. M. E., Talukder, A. & Kaneko, F. (2014). A paleo-seismological study of the Dauki fault at Jaflong, Sylhet, Bangladesh: Historical seismic events and an attempted rupture segmentation model. *Journal of Asian Earth Sciences*, 91, 218-226.
- Rahman, N. (2014). Vulnerability Assessment of Earthquake and Fire Hazard and Formulating Risk

Reduction Strategies at Community Level. Graduate Thesis, Bangladesh University of Engineering and Technology, P-37.

Ozcebe, G., Sucuoglu, H., Yucemen, M. S., Yakut, A., & Kubin, J. (2006, April). Seismic Risk Assessment of Existing Building Stock in Istanbul a Pilot Application in Zeytinburnu District. In Proceedings of 8th US national conference on earthquake engineering, San Fransisco.

Yeats, R. S., Sieh, K. E., & Allen, C. R. (1997). The geology of earthquakes. Oxford University Press, USA.

EFFECT OF SSI ON SEISMIC RESPONSE OF FLYOVER: A CASE STUDY

M. R. Mukhlis¹* & M. A. R. Bhuiyan²

¹*Institute of Earthquake Engineering Research, Chittagong University of Engineering and Technology, Chittagong-4349, Bangladesh. E-mail: raihan.ieer@cuet.ac.bd*

²*Department of Civil Engineering, Chittagong University of Engineering and Technology Chittagong-4349, Bangladesh*

**Corresponding Author*

ABSTRACT

The soil structure interaction (SSI) has become an important measure in the seismic response evaluation of engineering structures with the emergence of massive constructions on soft soils such as dams, flyovers, tunnels, etc. This study investigates the effects of SSI on the non-linear seismic response of flyover pier for different far field ground motion history. Yield and ultimate displacements of pier have been evaluated by developing the force-displacement relationship through pushover analysis of a pile supported typical pier of a multispan simply supported flyover. Effect of SSI has been included in the study by calculating the stiffness of equivalent soil springs for pile foundation recommended by Japan Road Association (JRA). The non linear time history analysis has been adopted to measure the seismic response of the pier. Finally, maximum displacement of the pier top and corresponding displacement ductility demand has been used to evaluate the damage state of the pier with and without considering the effect of SSI in the modeling of flyover pier. From the analytical investigation, it can be concluded that, consideration of SSI in the modeling of flyover pier increases the seismic response.

Keywords: flyover pier; soil structure interaction; displacement ductility; seismic response.

INTRODUCTION

Flyover is one kind of bridge, which is an elevated structure carrying highway over roads, railways and other features. Since bridges are one of the most critical components of highway systems, it is necessary to evaluate the seismic safety of highway bridges (Hwang et al., 2001). Most of the structures involve some type of contact with ground. When the external forces, such as earthquakes, act on these systems, neither the structural displacements nor the ground displacements, are independent of each other. Conventional structural analysis neglect the SSI effects, while neglecting SSI is reasonable for light structures in relatively stiff soil such as low rise buildings but effect of SSI, however, becomes prominent for heavy structures resting on relatively soft soils for example high-rise buildings and elevated-highways on soft soil (Wolf, 1985). Methods that can be used to evaluate the SSI effects can be categorized as direct and substructure approaches. In a direct analysis, the soil and structure are included within the same model and analyzed as a complete system. In a substructure approach, the SSI problem is partitioned into distinct parts that are combined to formulate the complete solution.

Based on the above background, the study aims at evaluating the seismic response of a pile supported typical pier of Kadamtali flyover, constructed in Chittagong city of Bangladesh, with and without considering SSI. Initially, the yield and ultimate displacement of pier from pushover analysis and maximum displacement of pier tops from non linear time history analysis for three different ground motion history have been evaluated for both considerations of SSI. Effect of SSI has been included in the study through direct approach by calculating the stiffness of equivalent soil springs for pile

foundation recommended by JRA (2002). Finally, the seismic performance of the pier has been evaluated based on displacement ductility demand expressed in terms of damage states.

MODELING OF PIER

Physical Model

Kadamtali flyover (22.34°N; 91.82°E) was constructed to reduce traffic jam in Chittagong city of Bangladesh. Figure 1 shows a 3D view of the flyover. The flyover is approximately 1127 m long and 8.54 m wide. The reinforcement with yield strength of 413 N/mm² and concrete with compressive strength of 30 N/mm² are used to construct the flyover. It is spanning around 630 m with 22 spans of variable length from 21.3 m to 42.0 m. There are 21 piers with variable heights ranging from 4.66 m to 8.5 m. Figure 2 shows the transverse section of the typical pier of the flyover. The deck of the flyover is comprised of four pre-stressed concrete girders with 200 mm reinforced concrete slab. The girders rest on elastomeric neoprene bearing over concrete bearing pad installed on top of each pier. Each elastomeric neoprene bearing with a cross-section of 500 mm × 350 mm consists of 4 numbers of 3 mm steel plates with a total thickness of 70 mm. For this study, a typical pier (Pier 7 as shown in Figure 1) of the flyover has been selected for analysis purpose. Geometric dimensions of the typical pier are presented in Table 1.

Table 1: Geometric dimensions of a typical pier of Kadamtali flyover

Pier No.	Pier height, H (m)	Pier Dimension (m x m)	Longitudinal Reinforcement
7	8.27	1.2 x 2.5	66-Y25 bar

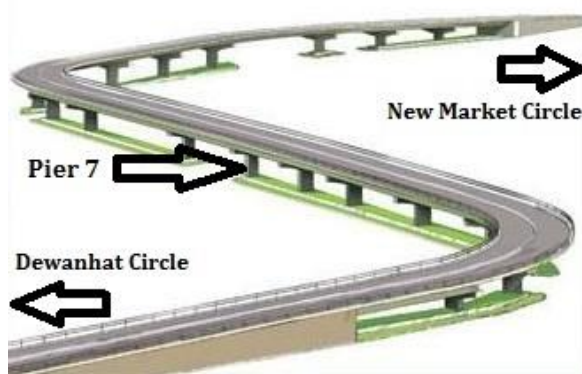


Fig. 1: 3-D view of Kadamtali flyover (Mukhlis and Bhuiyan, 2017)

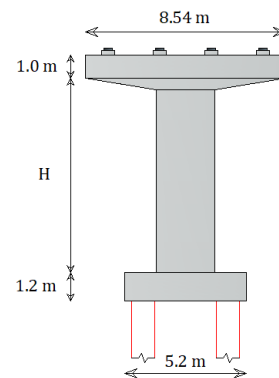


Fig. 2: Transverse section of typical pier

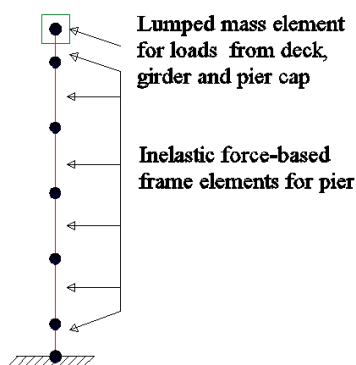


Fig. 3: Analytical model of typical pier without considering SSI

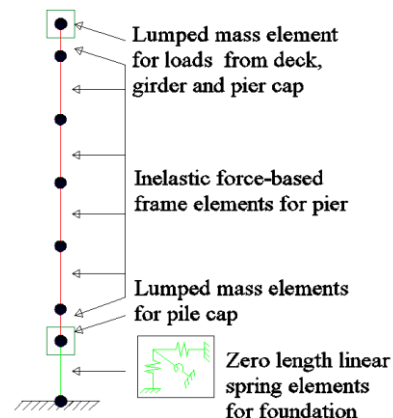


Fig. 4: Analytical model of typical pier considering SSI

Analytical Model

The pier-girder system is approximated as a continuous 2-D finite element frame using the SeismoStruct nonlinear analysis program. The superstructure and substructure of the system are modelled as a lumped mass system divided into a number of small discrete segments. The mass of each segment is assumed to be distributed between two adjacent nodes. The body of the flyover pier is modelled using fiber elements. The loads from deck, prestressed concrete girders and pier caps are calculated and modelled as lumped mass element on the pier top. The base of the pier is assumed to be fixed neglecting the foundation movement effect when SSI is not considered in the analysis. On the other hand, the base of the pier is modeled with zero length spring elements when SSI is considered in the analysis. At that case, the mass of the pile cap are simply put on the base node of the pier using lumped mass element in SeismoStruct. Analytical model of the typical pier without and with considering SSI are shown in Fig. 3 and Fig. 4 respectively.

PUSHOVER ANALYSIS OF PIER

The sectional analysis has been conducted by response 2000 to obtain the moment-curvature ($M-\Phi$) relationship of pier cross section as shown in Fig. 5 which is used to derive the force-displacement relationship of the pier. In addition, SeismoStruct 2016 is used to conduct the pushover analysis to derive the force-displacement relationships of the pier. This typical pier is modelled as single degree of freedom system with a lumped mass on the pier top carrying all the seismic dead load coming from deck, girder and pier cap. Fig. 6 shows the pushover model of the typical pier in SeismoStruct 2016 and Fig. 7 shows the force displacement relationship of the typical pier obtained from pushover analysis. This bilinear idealization of force displacement relationship can be easily found in the analysis result in SeismoStruct 2016, from which yield displacement (δ_y), ultimate displacement (δ_u) and ultimate strength (P_u) are obtained as shown in Fig. 8 and tabulated in Table 2 for the typical pier.

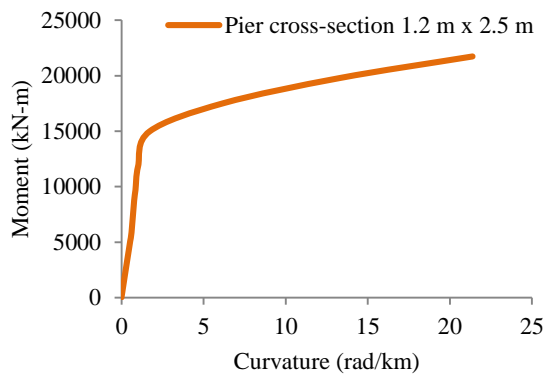


Fig. 5: Moment-curvature ($M-\Phi$) relationship for the typical pier cross-section



Fig. 6: Pushover model of the typical pier (SeismoStruct 2016)

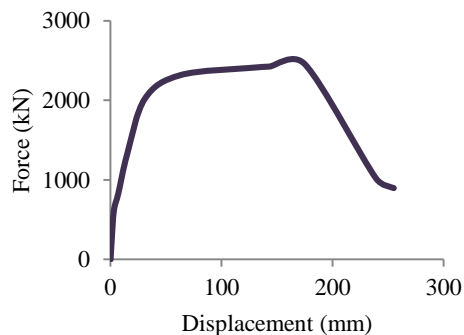


Fig. 7: Force-displacement relationship of typical pier

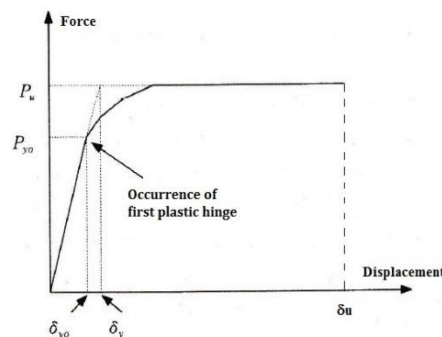


Fig. 8: Bilinear idealization of force-displacement relationship

Table 2: Ultimate strength of typical pier

Pier no.	Yield displacement, δ_y	Ultimate displacement, δ_u	Ultimate strength, P_u
----------	--------------------------------	-----------------------------------	--------------------------

	(mm)	(mm)	(kN)
7	37	175	2454

SEISMIC RESPONSE EVALUATION OF PIER

Seismic performance of bridge components are generally expressed in terms of damage conditions of those components subjected to seismic ground motions. Piers are generally the most critical components of bridges and different forms of engineering demand parameters (EDP) such as displacement ductility demands (μ_d) are generally used to measure the damage state (DS) of the bridge piers (Bhuiyan and Alam 2012, Bhuiyan and Alim 2017). Table 3 summarizes the definitions of various damage states and their corresponding damage criteria available in the literature.

Table 3: Damage states of bridge pier

Bridge Component	EDP (Displacement Ductility, μ_d)	Damage States (DS)	Physical Phenomenon
Pier	$\mu_d < 1.0$	No Damage	No Physical phenomenon
	$1.0 < \mu_d < 1.2$	Slight (DS 1)	Cracking and spalling
	$1.2 < \mu_d < 1.76$	Moderate (DS 2)	Moderate cracking and spalling
	$1.76 < \mu_d < 4.76$	Extensive (DS 3)	Degradation without collapse
	$\mu_d > 4.76$	Collapse (DS 4)	Failure leading to collapse
Reference	Hwang <i>et al.</i> 2001	FEMA 2003	FEMA 2003

Displacement ductility demand (μ_d) has been estimated from the results of time history analysis (THA) for specific ground motion history with and without considering soil structure interaction (SSI) using Eq. (1), where, d_u = maximum pier displacement from THA, d_y = yield displacement of pier.

$$\mu_d = \frac{d_u}{d_y} \quad (1)$$

Selection of Ground Motions

As sufficient seismic data is not available for this region, the time history analysis is conducted by applying three selected earthquake ground motion records with different peak ground acceleration (PGA) as shown in Table 4. The time histories of these three earthquakes are shown in Fig. 9.

Table 4: Earthquake ground motions for time history analysis

Earthquake No.	Earthquake Name	Magnitude, M_w	PGA (g)	Occurrence time of PGA (s)
EQ-1	El Centro-1940	6.9	0.35	2.12
EQ-2	Northridge-1994	6.7	0.45	4.06
EQ-3	Kobe-1995	6.9	0.24	15.16

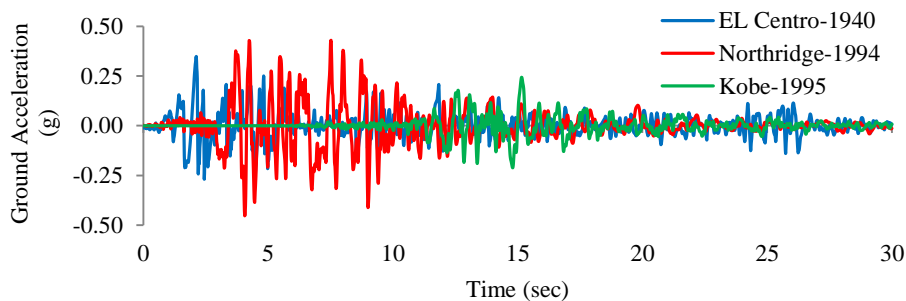


Fig. 9: Selected earthquake ground motion records for THA

THA without Considering Soil Structure Interaction (SSI)

Rayleigh damping has been chosen for THA of the pier with 5% damping using two fundamental modes in transverse and longitudinal direction with a period of 0.525 s and 0.252 s respectively found in the eigenvalue analysis. THA has been conducted by applying three selected ground motions shown in

Fig. 9 at the base of the pier in three separate models. The displacement response at the top of piers are represented with respect to time as shown in Figure 10 with peak displacements of 86 mm at 2.86 s, 154 mm at 7.28 s and 89 mm at 15.42 s for EQ-1, EQ-2 and EQ-3 respectively without considering SSI.

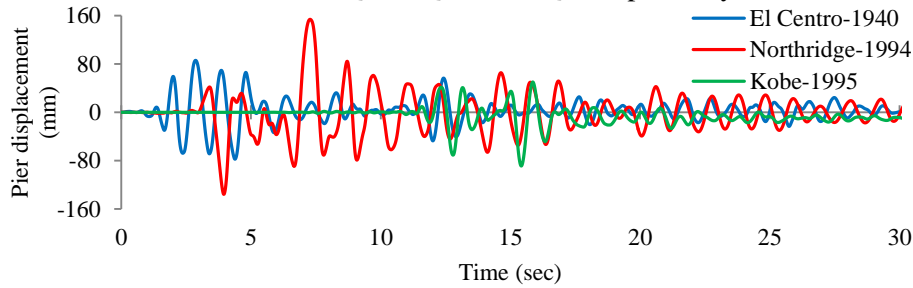


Fig. 10: Displacement response at pier top (without considering SSI)

THA Considering Soil Structure Interaction (SSI)

Soil structure interaction is considered in seismic analysis by modeling the soil medium. According to JRA (2002), spring constants for ground can be evaluated using the geometric properties of pile foundation and physical properties of underlying soil layer by following equations.

$$K_x = nk_1; K_z = nk_{vp}; K_{\theta y} = nk_4 + k_{vp} \sum_{i=1}^n x_i^2; K_{x\theta y} = -nk_2$$

when, pile head is assumed to be hinged, $k_1 = \frac{2E_p I_p}{\beta^3}; k_2 = k_3 = k_4 = 0$

where, $k_{vp} = \frac{aA_p E_p}{L_p}$ (tf/m); $\beta = \sqrt[4]{\frac{k_H D_p^4}{4E_p I_p}}$ (m⁻¹); $k_H = k_{H0} \left(\frac{B_H}{30}\right)^{-\frac{3}{4}}$ (kgf/cm³); $B_H = \sqrt{\frac{1}{\beta} D_p}$ (cm);

$$k_{H0} = \frac{E_D}{30} \text{ (Kgf/cm}^3\text{)}; E_D = 2(1 + \nu_D) \frac{\gamma_S}{10g} V_{SD}^2 \text{ (kgf/cm}^2\text{)}; V_{SD} = 0.8 \left(100N^{1/3}\right) \text{ (m/s)}$$

here, K_x = translational constant of ground along x-axis (tf/m); K_z = vertical constant of ground along z-axis (tf/m); $K_{\theta y}$ = rotational constant of foundation around the y-axis (tf-m/rad); $K_{x\theta y}$ = coupling constant of foundation of the displacement along x-axis and rotation around the y-axis (tf-m/m); $n = 4$, representing the total number of piles. Coefficient for distribution of soil vertical stiffness along the length of pile (a) is assumed to be 1. Poisson's ratio of soil (ν_D) is taken as 0.5, considering saturated clay & also the maximum value. Unit weight of soil (γ_S) is taken as 1.27 (tf/m³), considering soft silty clayed sand layer. Finally, K_x , K_z and $K_{\theta y}$ are found to be 1.93×10^9 kN/m, 6.03×10^6 kN/m and 1.95×10^7 kN-m/rad respectively. These spring constants of ground and foundation in longitudinal direction have been used at the base of the piers as zero length spring elements in the modeling of piers followed by THA by applying three selected ground motions shown in Fig. 9 at those spring elements of the pier in three separate models. The displacement response at the top of piers are represented with respect to time as shown in Figure 11 with peak displacements of 88 mm at 2.88 s, 158 mm at 7.29 s and 93 mm at 15.43 s for EQ-1, EQ-2 and EQ-3 respectively considering SSI.

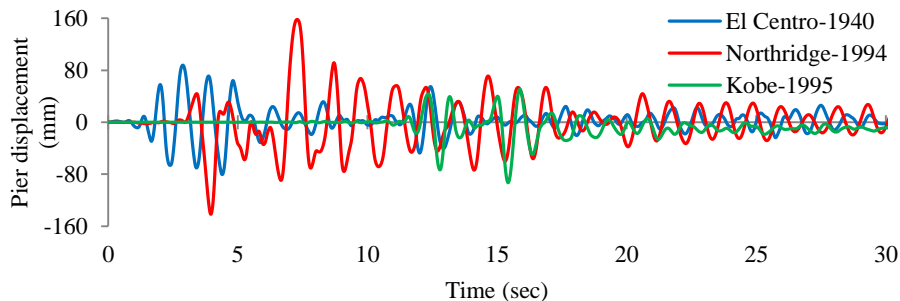


Fig. 11: Displacement response at pier top (considering SSI)

Damage State Evaluation of Pier

Damage states of the pier are evaluated based on displacement ductility demand (μ_d). Displacement ductility demands of pier models with and without considering SSI are shown in Table 5 using Eq. (1) and comparison of displacement ductility demands are shown in Fig. 12. It has been observed that μ_d

values increases up to 4.49% for EQ-3 due to SSI considerations though the physical damage state remains the same with extensive damage state (DS 3) representing degradation without collapse in response to all applied ground motions for both modeling considerations.

Table 5: Displacement ductility demand (μ_d) of typical pier

Earthquake No.	Earthquake Name	Displacement Ductility Demand (μ_d)		Increase in μ_d considering SSI (%)
		Without Considering SSI	Considering SSI	
EQ-1	El Centro-1940	2.32	2.38	2.33
EQ-2	Northridge-1994	4.16	4.27	2.60
EQ-3	Kobe-1995	2.41	2.51	4.49

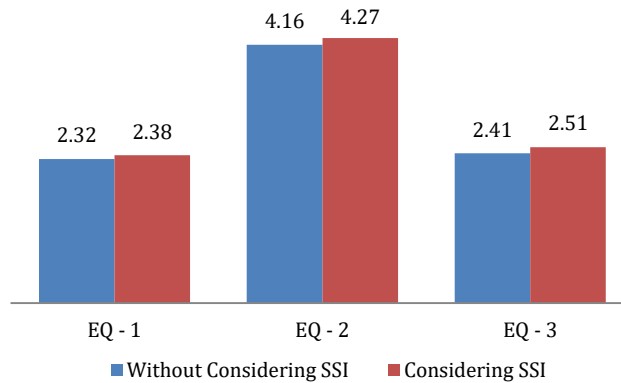


Fig. 12: Comparison of displacement ductility demand (μ_d) of typical pier

CONCLUSIONS

Interaction between soil and structure is considered in the modeling procedure of a typical pier of a flyover through equivalent spring constants. Pushover analysis of the pier has been conducted to determine the yield and ultimate displacement of the pier. Three selected earthquake ground motions of different PGA are used to compare the response of the pier models through time history analysis with and without considering SSI. From the time history analysis maximum top displacement of the pier models are used to determine the displacement ductility demands. These displacement ductility demands are used to evaluate the seismic performance of piers in terms of damage states. For all three earthquake ground motions, displacement ductility demands of piers show higher value when SSI is considered in the pier model though, physically the pier indicating towards damage with degradation without collapse with extensive damage state (DS-3) for both type of model. Hence, from the analytical results, it has been revealed that soil structure interaction has great impact on seismic response analysis of bridge piers and should be carefully taken into account in the modeling procedure.

REFERENCES

- Bhuiyan, MAR and Alam, MS. 2012. Seismic Vulnerability Assessment of a Multi-Span Continuous Highway Bridge Fitted with Shape Memory Alloy Bars and Laminated Rubber Bearings. *Earthquake Spectra*, 28(4): 1379-1404.
- Bhuiyan, MAR and Alim, H. 2017. Seismic Safety Evaluation of Abdul Mannan Overpass in Chittagong, Bangladesh. *Malaysian Journal of Civil Engineering*, 29(3): 250-272.
- FEMA. 2003. *HAZUS-MH MRI: Technical Manual, Earthquake Model*. Federal Emergency Management Agency, WA, USA.
- Hwang, H; Liu, JB and Chiu, Y. 2001. Seismic Fragility Analysis of Highway Bridges. *Technical Report of MAEC RR-4 project*. Mid-America Earthquake Center, USA.
- JRA. 2002. *Specifications for Highway Bridges - Part V: Seismic design*. Japan Road Association, Tokyo, Japan.
- Mukhlis, MR and Bhuiyan, MAR. 2017. Lateral Strength and Safety Evaluation of Piers of Kadamtali Flyover in Chittagong, Bangladesh. *International Journal of Advanced Structures and Geotechnical Engineering*, 6(2): 45-56.
- Wolf, JP. 1985. *Dynamic Soil-Structure Interaction*. Prentice-Hall, Inc., Englewood Cliffs, New Jersey, USA.

COMPARISON OF FORCE-BASED DESIGN AND DISPLACEMENT-BASED DESIGN METHODS FOR SEISMIC RESPONSE OF MULTISPAN BRIDGES

M. A. Hoque¹, M. R. Mukhlis^{2*} & M. A. R. Bhuiyan¹

¹*Department of Civil Engineering, Chittagong University of Engineering and Technology
Chittagong-4349, Bangladesh.*

²*Institute of Earthquake Engineering Research, Chittagong University of Engineering and Technology,
Chittagong-4349, Bangladesh.
E-mail: raihan.ieer@cuet.ac.bd*

**Corresponding Author*

ABSTRACT

Multispan bridges are very common structures in transportation system. Generally, all the bridges are designed using force-based design (FBD) method. Though displacement correlates damage better than strength does, FBD assumes damage in the structure is controlled by the provision of strength and uses displacement as the final check to determine the structural performance. Although current FBD method is considerably improved, there are some fundamental problems in its procedure. Displacement-based design (DBD) methods have been developed overcoming deficiency associated with FBD method. In this study, two DBD methods, direct displacement-based design (DDBD) and alternative displacement-based design (ADBBD), have been compared with FBD method for the seismic response of multispan bridges. Two different configurations of bridge models are considered here to compare their seismic response. Base shear and displacement are taken as primary seismic response parameter for this study. From the numerical evaluation it can be concluded that, DBD methods have shown better performance in calculating seismic responses than FBD method. Base shear calculated by DDBD and ADBBD methods are less than that calculated by FBD method, whereas displacement estimated by DDBD and ADBBD methods are more than that estimated by FBD method.

Keywords: multispan bridge; force-based design; direct displacement-based design; alternative displacement-based design; seismic response.

INTRODUCTION

Bridges are very important structures for safe and smooth passage of vehicles over rivers, roads, railways and other features. Bridges also connect islands to mainland (Bhuiyan and Alam 2012, Bhuiyan and Alim 2017). Since bridges are one of the most critical components of highway systems, it is necessary to evaluate the seismic safety of highway bridges in terms of seismic response (Hwang et al., 2001). Multi-span bridges are generally used when width of the obstacle is large. These bridges can be simply supported or continuous. Continuous bridges are more economical because less thickness can be provided due to less bending moment in midspan. They are suitable where there is no possibility of uneven settlement of foundations. But analysis of continuous bridges is more complex and they need more detailing (Chen and Duan, 2000). Bridges can be considered as simple structures as they possess little number of elements. At the same time this simplicity makes bridge structure less redundant. Failure of one element or connection between elements can cause collapse due to lack of alternate load path (Ghosn and Yang, 2014). Any kind of damage of bridges will destroy the transportation system. So, special care should be given in designing bridges.

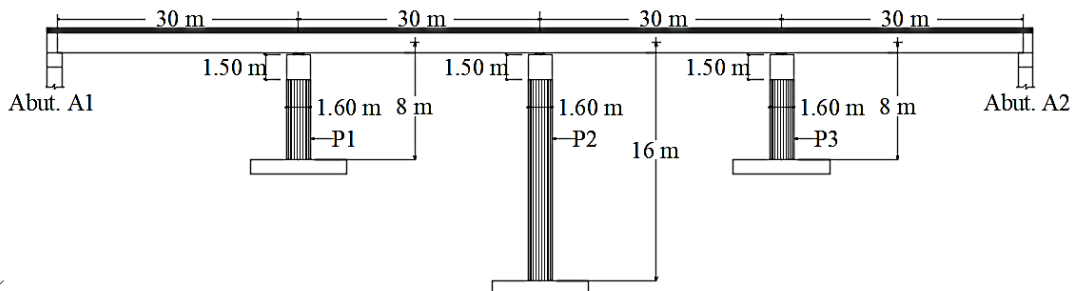
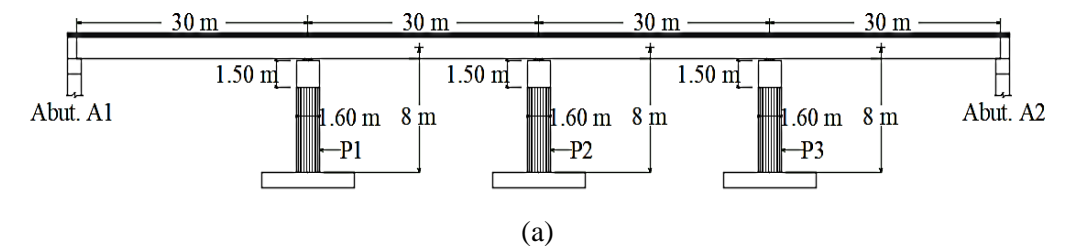
On the basis of above background, the study aims to evaluate analytically the seismic response of multispan bridges of two different configurations based on the variation of pier height to compare the estimation of seismic response by force-based Design (FBD) method with those by direct displacement-based design (DDBD) and alternative displacement-based design (ADBD) method. Base shear and displacement are taken as seismic response parameter for this study. Design response spectrum of Bangladesh National Building Code (BNBC Final draft, 2015) is used for the analysis in this study. Finally, these three methods have been compared for evaluating base shear and displacement in both of the longitudinal and transverse direction.

MODELING OF MULTISPAN BRIDGES

Multispan continuous bridges of two different configurations shown in Fig.1 are taken into consideration for this study with the variation of pier height. The geometric dimensions of pier-girder system are shown in Fig. 2. Each configuration of bridge models consists of spans with 30 m length. Bridge model 1 shown in Fig. 1(a) consists of three piers with equal height of 8 m whereas; Fig. 1(b) shows bridge model 2 with two equal outer piers of 8 m with a central pier of 16 m height. The diameter of each circular pier is taken as 1.60 m for both models (Fig. 1 and Fig. 2). Both of the bridge models also consist of similar span width of 12 m (Fig. 2). The layout of the superstructure is straight and continuous over the pier cap of size 1.6 m × 1.5 m for both models (Fig. 1 and Fig. 2). A hollow continuous box girder is considered for the deck of the bridge models (Fig. 2). Connection between pier top and box girder is considered as pinned. The superstructure is free to move both in the longitudinal and transverse direction. Pier longitudinal and transverse reinforcements are calculated for the critical case and used for all other cases. In addition to dead load, an area load of 1.7 kN/m² is taken in consideration for wearing surface. The bridge models are considered to be situated in a region with PGA value of 0.28g (BNBC Final draft, 2015). Site class is taken as B and importance category of the bridge is taken as critical and response reduction factor is taken as 1.5 (AASHTO, 2006). Both bridge models are analytically modelled in CSI Bridge software and analyzed by FBD, DDBD and ADBD method. Reinforcement details and material properties of piers for all models are described in Table 1.

Table 1: Pier reinforcement and material properties

Clear cover to longitudinal reinforcement	50 mm
Percentage of longitudinal reinforcement, ρ_l (92 nos., $d_b=32$ mm)	3.74 %
Strain to ultimate stress of longitudinal reinforcement	0.10
Percentage of transverse reinforcement, ρ_t ($d_b=16$ mm, $s=90$ mm)	0.59 %
Strain to ultimate stress of transverse reinforcement	0.12
Concrete compressive strength, f_c'	27.5 MPa
Reinforcement yield strength, f_y	414 MPa



suitable values of the maximum displacement and maximum drift. After calculating yield displacements from the geometry of the elements, displacement ductility demands may be directly calculated from target displacements (Δ_d). Starting with this ductility and with a set of response displacement spectra, the effective period (T_e) of an equivalent linear SDOF system is determined at peak displacement, considering an equivalent damping ratio (ξ_e). The effective stiffness (K_e) of the equivalent SDOF system at maximum displacement can be found from Eq. (1) using effective mass (m_e) of the structure participating in the fundamental mode of vibration. Finally, design base shear force, is calculated by Eq. (2).

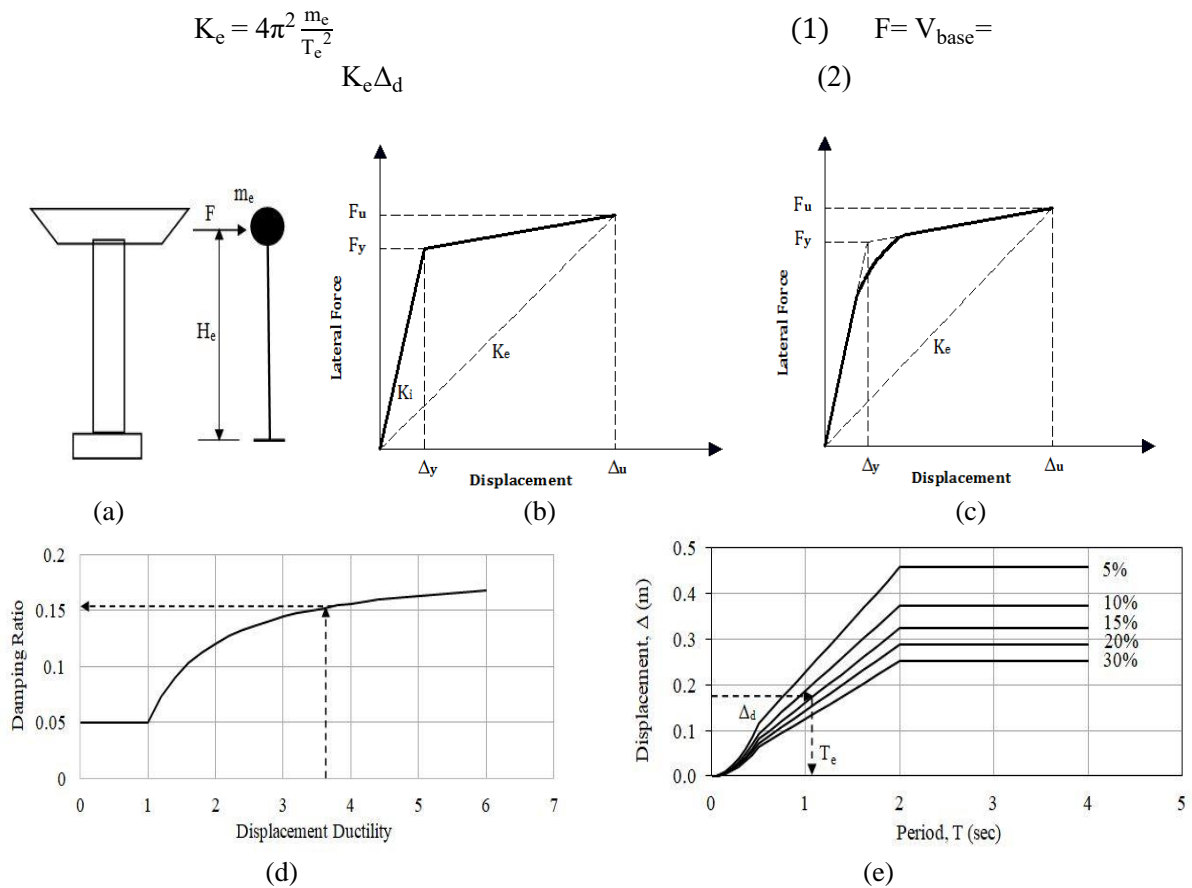


Fig.4: DBD methods; (a) SDOF simulation (b) effective stiffness for DDBD (c) effective stiffness for ADBD (d) Effective damping ratio estimation (e) effective period estimation from displacement spectra

The only difference between DDBD and ADBD is that, ADBD utilizes pushover analysis to determine yield displacement (Δ_y), ultimate displacement (Δ_u) and ultimate force (F_u), from which effective stiffness is calculated. The main philosophy of DBD methods are shown in Fig. 4. The bridge models (Fig. 1) are also analyzed by DDBD and ADBD methods in this study.

NUMERICAL RESULTS

Design Base Shear

The base shear for both models in longitudinal and transverse direction is determined by FBD, DDBD and ADBD methods. Figure 5 shows the comparisons of the base shear in both directions. In the longitudinal direction, DDBD and ADBD estimated 54% and 35% less total base shear respectively than that calculated by FBD for bridge model 1 (Fig. 5a). DDBD and ADBD have estimated 40% and 30% less total base shear respectively than that calculated by FBD for bridge model 2 (Fig. 5b). In the transverse direction, DDBD and ADBD have estimated 38% and 12% less total base shear respectively than that calculated by FBD for bridge model 1 (Fig. 5c). DDBD and ADBD have estimated 38% and 34% less total base shear respectively than that calculated by FBD for bridge model 2 (Fig. 5d).

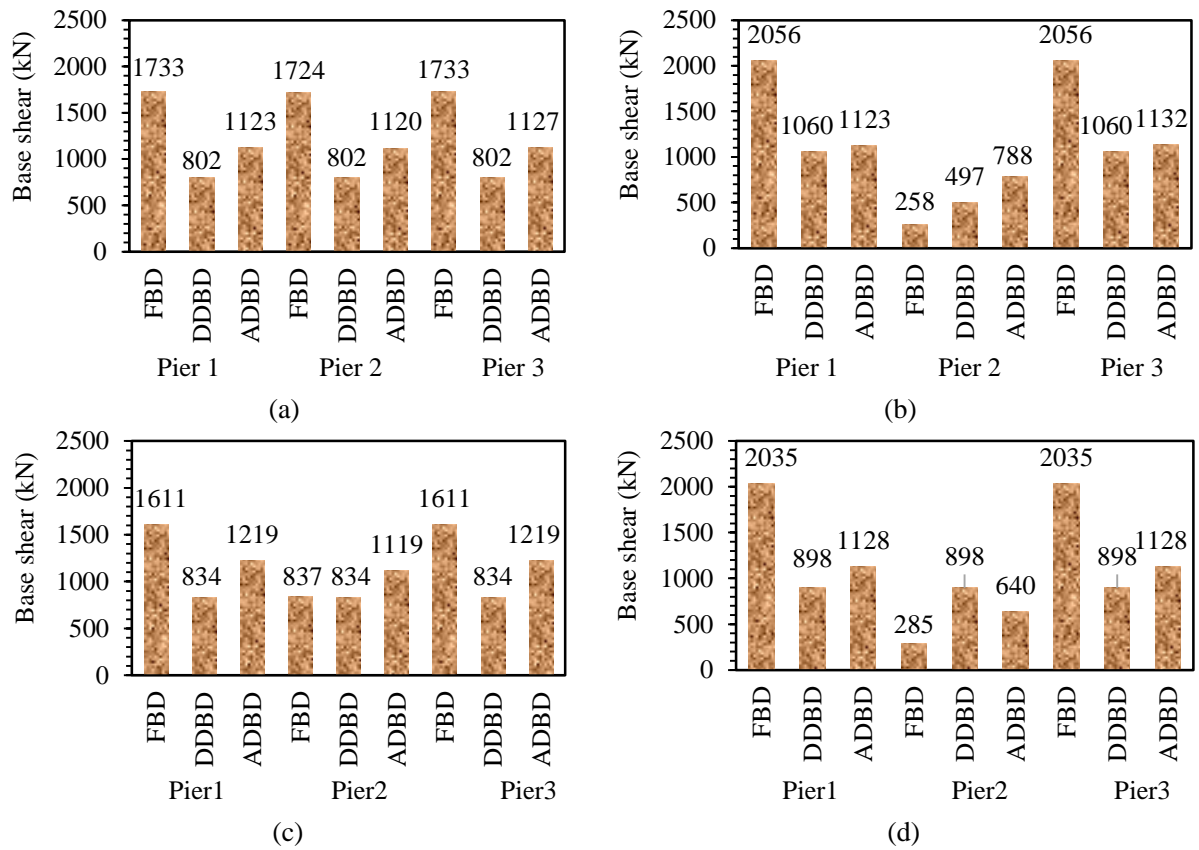


Fig. 5: Comparison of design base shear of bridge models; (a) Model 1 - longitudinal direction (b) Model 2 - longitudinal direction (c) Model 1 - transverse direction (d) Model 2 - transverse direction

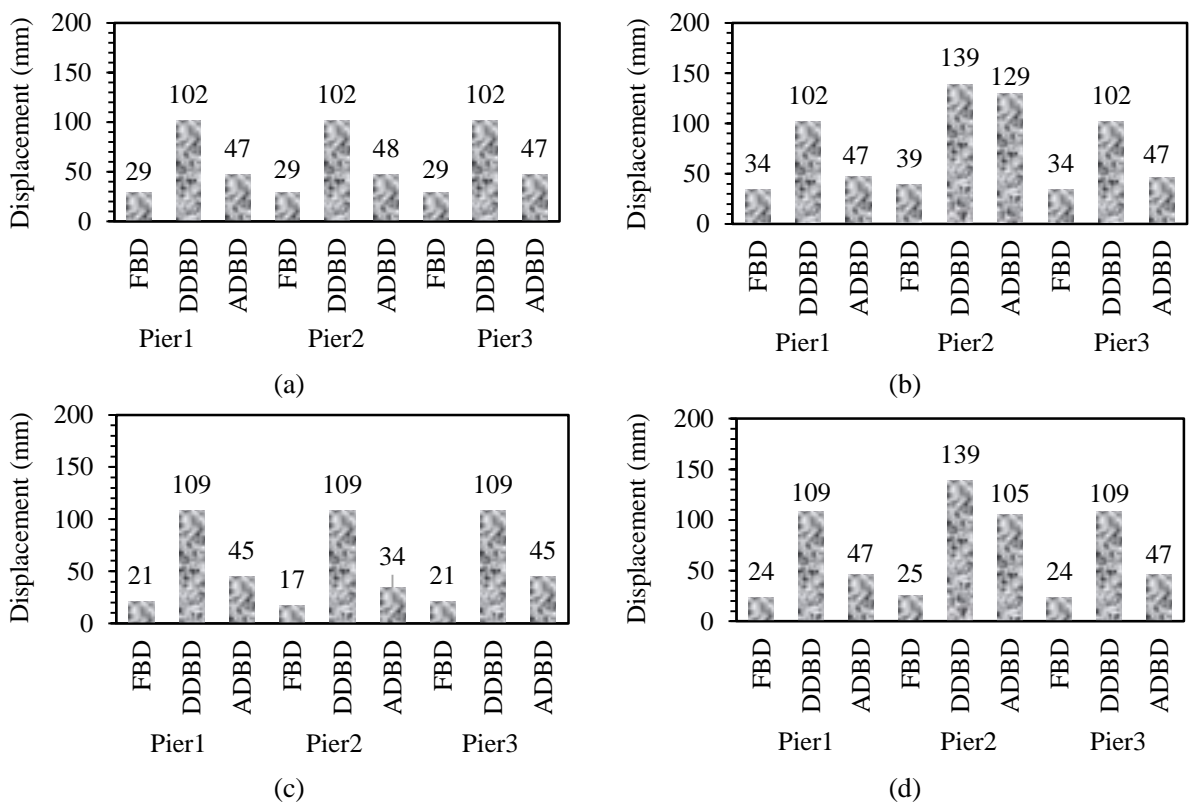


Fig. 6: Comparison of design displacement of bridge models; (a) Model 1 - longitudinal direction (b) Model 2 - longitudinal direction (c) Model 1 - transverse direction (d) Model 2 - transverse direction

Design Displacement

The displacement at pier tops for both models in longitudinal and transverse direction is determined by FBD, DDBD and ADBD methods. Figure 6 shows the comparisons of the displacements in both directions. In the longitudinal direction, FBD and ADBD have estimated 72% and 54% less design displacement respectively than that calculated by DDBD for all three piers of equal height in bridge model 1 (Fig. 6a). But FBD and ADBD have estimated 67% and 54% less design displacement respectively than that calculated by DDBD for two outer piers of small height, though FBD and ADBD have estimated 72% and only 7% less design displacement respectively than that calculated by DDBD for the central pier of large height in bridge model 2 (Fig. 6b). In the transverse direction, FBD and ADBD have estimated 81% and 59% less design displacement respectively than that calculated by DDBD for two outer piers of equal height, though FBD and ADBD have estimated maximum of 84% and 69% less design displacement respectively than that calculated by DDBD for the central pier of equal height in bridge model 1 (Fig. 6c). FBD and ADBD have estimated 78% and 57% less design displacement respectively than that calculated by DDBD for two outer piers of small height, though FBD and ADBD have estimated 82% and 24% less design displacement respectively than that calculated by DDBD for the central pier of large height in bridge model 2 (Fig. 6d).

CONCLUSIONS

Displacement-based methods use the displacement spectrum for calculating the base shear force. It is observed that using displacement spectrum needs less step of calculation than using acceleration spectrum of FBD method which makes the calculation easier. From numerical evaluation of two bridge models, it is observed that base shear calculated by DDBD and ADBD is as much as 54% and 35% lesser than that calculated by FBD which makes the pier having less dimension and reinforcement. Again, design displacement estimated by FBD and ADBD is as much as 82% and 59% lesser than that calculated by DDBD. Eventually, FBD method estimates low fundamental period of structures which determines high acceleration resulting high base shear. On the other hand, DBD methods estimate high fundamental period of structures using effective stiffness in place of initial stiffness resulting low base shear and from displacement spectra for high fundamental period high design displacement is obtained. It can be summarized that, DBD methods are more effective than FBD in predicting seismic demand of multispan bridges. DBD methods are introduced with better performance than FBD method in predicting seismic demand of the structure as it designs the structure to achieve a given performance limit state depending on design displacement. In compare to that, FBD requires repetitions of several design steps to achieve desired performance specified by the code.

REFERENCES

- AASHTO. 2006. *AASHTO Guide Specifications for LRFD Seismic Bridge Design*. American Association of State Highway and Transportation Officials, Washington, D.C. (2006)
- Bhuiyan, MAR and Alam, MS. 2012. Seismic Vulnerability Assessment of a Multi-Span Continuous Highway Bridge Fitted with Shape Memory Alloy Bars and Laminated Rubber Bearings. *Earthquake Spectra*, 28(4): 1379-1404.
- Bhuiyan, MAR and Alim, H. 2017. Seismic Safety Evaluation of Abdul Mannan Overpass in Chittagong, Bangladesh. *Malaysian Journal of Civil Engineering*, 29(3): 250-272.
- BNBC Final Draft. 2015. *Bangladesh National Building Code*. Housing and Building Research Institute, Dhaka, Bangladesh.
- Chen, WF and Duan, L. 2000. *Bridge Engineering Handbook*. CRC Press, Washington, D.C., USA.
- Ghosn, M and Yang, J. 2014. *Bridge System Safety and Redundancy*. NCHRP Report 776, National Academy of Sciences, Washington, D.C., USA.
- Hwang, H; Liu, JB and Chiu, Y. 2001. Seismic Fragility Analysis of Highway Bridges. *Technical Report of MAEC RR-4 project*. Mid-America Earthquake Center, USA.
- Priestley, MJN. 1993. Myths and Fallacies in Earthquake Engineering - Conflicts Between Design and Reality. *Bulletin of the New Zealand National Society for Earthquake Engineering*, 26(3): 329-341.

PERFORMANCE EVALUATION OF SHAPE MEMORY ALLOY IN SEISMIC RETROFITTING OF RC BUILDING

E. Roy¹, P. Ghose¹, M. R. Mukhlis^{2*} & M. A. R. Bhuiyan¹

¹*Department of Civil Engineering, Chittagong University of Engineering and Technology, Chittagong-4349, Bangladesh*

²*Institute of Earthquake Engineering Research, Chittagong University of Engineering and Technology, Chittagong-4349, Bangladesh.*

E-mail: raihan.ieer@cuet.ac.bd

**Corresponding Author*

ABSTRACT

Recent earthquakes have clearly demonstrated an urgent need to upgrade and strengthen seismically deficient structures. Retrofitting is one of the best options to make an existing inadequate building safe against future probable earthquake or other environmental forces. Any technology or material has its limitations and to meet the new requirements, new technologies have been invented and used over ages. Recently, an active confinement technique using Shape Memory Alloys (SMAs) has been proposed as a more effective alternative to conventional passive confinement methods. This study focuses on the seismic vulnerability of an existing RC building in Chittagong city. Two analytical models have been generated to make a comparison between the existing building in ETABS 2015 and SMA retrofitted building in SeismoStruct 2018. Nitinol (Nickel titanium) is used as a SMA material for retrofitting the columns of the RC building. Linear static analysis of the two analytical models has been performed to compute the structural responses according to Bangladesh National Building Code (BNBC Final Draft, 2015). Demand Capacity Ratio (DCR) is taken as the primary parameter to measure the structural response. Based on the analytical evaluation, SMA retrofitted building using Nitinol has shown better seismic performance.

Keywords: demand capacity ratio; retrofitting; seismic performance; shape memory alloy.

INTRODUCTION

Practically no building can be made earthquake proof. The engineering intention is to make buildings earthquake resistant, such buildings resist the effects of ground shaking, although they may get damaged severely but would not collapse during the strong earthquake. Old buildings have been structurally designed for much lesser seismic actions when compared to buildings that are designed today. Structurally rehabilitation brings a structure or a structural member to a specified safety and performance level. Depending on state of a structure or structural member, rehabilitation can be divided into two categories: Repairing and Strengthening. Repair is the rehabilitation of a damaged structure or a structural member, on the other hand strengthening is upgrading an undamaged structure or the member. Re-strengthening of reinforced concrete members has become very common in the modern world. But the failure of columns is a major concern for structural engineers because the failure of a column may lead to global failure of a structure. One popular solution to the problem of strengthening old reinforced concrete (RC) structure is to place jackets around the structure elements. Jackets have been constructed using concrete jacketing, steel jacketing, precast concrete jacketing, external pre-stressing, FRP wrapping and SMA wrapping. Each method has its own advantage and disadvantages.

This study focuses on retrofitting by SMA material. SMA is a unique class of alloy that undergoes large deformation as well as energy dissipation capacities while maintaining a super-elastic response and return to its original shape through stress removal (super-elasticity) or heating (shape memory effect). There are various components of SMAs such as Ni-Ti, Cu-Zn-Al, Cu-Al-Ni, Fe-Mn, Mn-Cu etc. The copper-based and NiTi-based shape-memory alloys are considered to be engineering materials. These compositions can be manufactured to almost any shape and size (Awan and Khan, 2018). In this study Ni-Ti alloy is used as a SMA material. When a SMA is in martensite form at lower temperatures, the metal can easily be deformed into any shape. When the alloy is heated, it goes through transformation from martensite to austenite. In the austenite phase, the memory metal remembers the shape it had before it was deformed. Superelastic and shape memory effect of SMA material is shown in Fig. 1 (Alam et al., 2005).

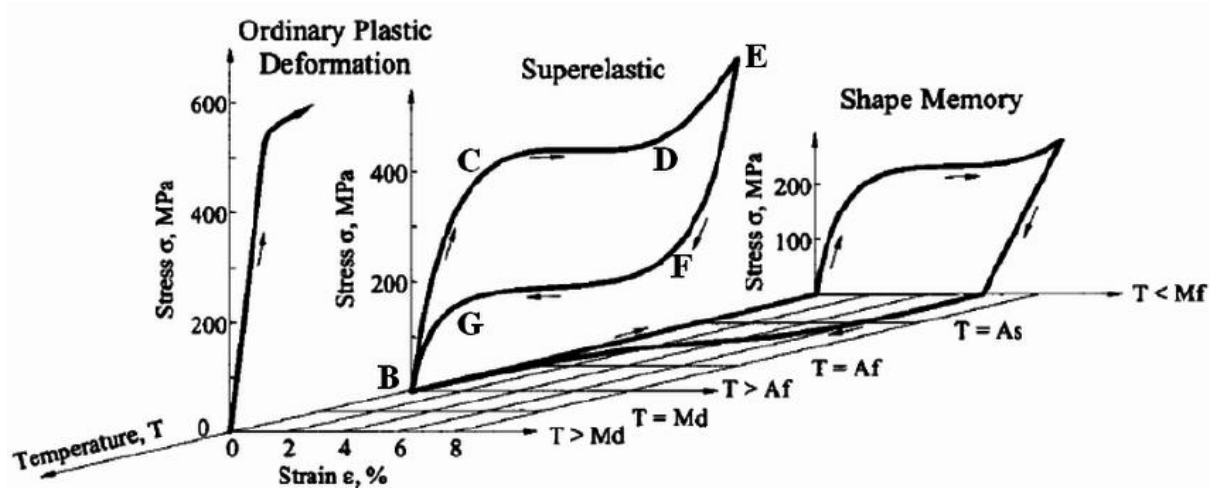


Fig.1: 3D stress-strain-temperature (σ - ϵ - T) diagram of SMA showing SME in martensite state, PE during austenite/martensite phase transformation and elastic-plastic behavior of austenite at higher temperature (Alam et al., 2005)

In this figure we can see that, an ordinary plastic material goes through deformation with the stress increment but it cannot regain its original phase after stress removal. In case of smart materials; as the stress increases the material goes through deformation. But after the removal of stress the material returns to its original position; which is called the superelastic property of SMA materials. The shape of a smart material deforms when the temperature reaches martensite finish state. But when the temperature reaches the austenite finish state the material returns to its original phase; which is called the shape memory property of smart materials (Christian, 2018). In this study Nitinol is used as a SMA material. Properties of Nitinol are listed below in Table 1 (Alam et al., 2012).

Table 1: Properties of Nitinol

Parameter	SI Unit	English Unit
Modulus of Elasticity	28000 MPa	4061362 psi
Austenite to Martensite starting stress	410 MPa	59477.832 psi
Austenite to Martensite finishing stress	470MPa	68181.907 psi
Martensite to Austenite starting stress	170 MPa	24661.545 psi
Martensite to Austenite finishing stress	140 MPa	20309.514 psi

An existing 7 storey garments building JEANS 2000 LTD, located at Plot #67, Sector #7, CEPZ, Chittagong, shown in Fig. 2 is analyzed in this study. Equivalent static analysis is performed according to Bangladesh National Building Code (BNBC Final Draft, 2015). C/D method (Capacity-Demand) is followed in this study taking demand capacity ratio (DCR) as the primary parameter to measure the structural response. Jacketing with SMA is performed analytically in this study for retrofitting under strength or weak columns. Finally DCR values of column from both retrofitted and nonretrofitted

model are compared to understand the influence of SMA retrofitting in the seismic performance of structure.

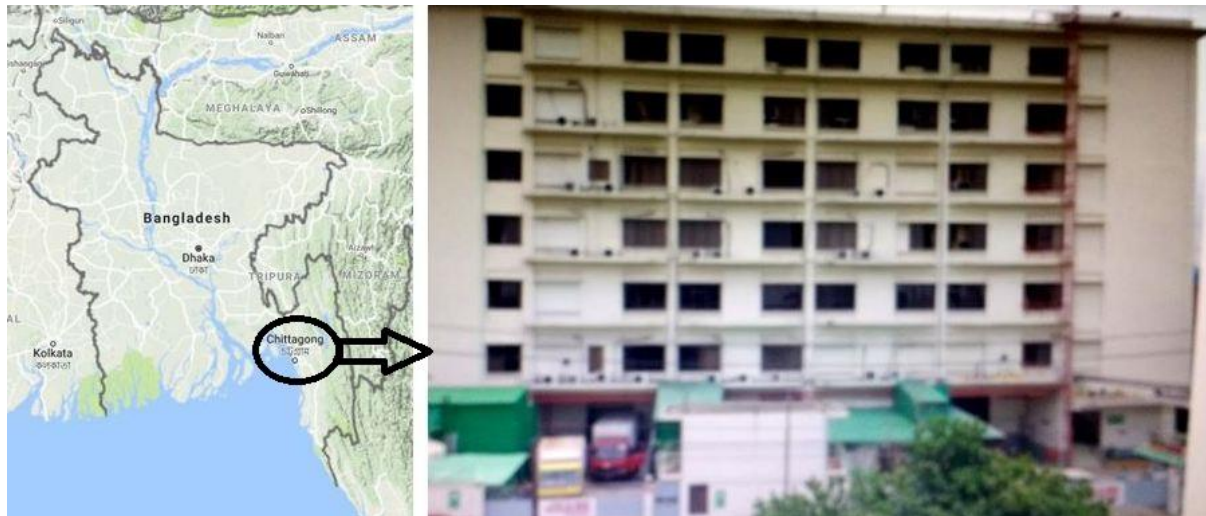


Fig. 2: Existing garments building under study

METHODOLOGY

Concrete material of 2500 psi compressive strength and grade 60 steel is used in the analysis. The reinforcement details of the columns and beams are listed in Table 2 and Table 3.

Table 2: Reinforcement detailing of column

Types of column	Size	Longitudinal bars	Transverse bars	No. of stirrup		Clear cover thickness
				Along height	Along width	
C1	24''*24''	12-22mm Ø	10mmØ @7-12''	4	4	2.5''
C2	24''*24''	14-22mm Ø	10mmØ @7-12''	4	4	2.5''
C3	24''*24''	20-22mm Ø	10mmØ @7-12''	4	4	2.5''
C4	24''*24''	24-22mm Ø	10mmØ @7-12''	4	4	2.5''

Table 3: Reinforcement detailing of beam

	Size	Longitudinal bars		Transverse bars
		Top	Bottom	
Support-section	25''*12''	3-22mmØ and 3-22mm Ø E.T.	3-22mmØ	10mmØ @ 5-8''
Mid-section	25''*12''	3-22mmØ	3-22mmØ and 3-22mm Ø E.B.	10mmØ @ 5-8''

Load Calculations

For the building under study, dead load and live loads are estimated according to Bangladesh National Building Code (BNBC Final draft, 2015). Floor finish, beam wall, partition wall, RC water tank, PVC water tank loads are taken into account as dead loads. Roof live load, slab live load having storage and machineries, slab live loads without storage and machineries are taken as live loads. Calculations for earthquake loads and wind loads for both X and Y-direction is also performed according to Bangladesh National Building Code (BNBC Final Draft, 2015). The analytical method is used here to calculate the wind loads. All the coefficients and load combinations are taken according to Bangladesh National Building Code (BNBC Final Draft, 2015). Using the base shear, part of shear force at each storey of the building is calculated. Seismic weight of the structure is used to calculate the base shear force which is found from the ETABS analysis.

Modelling and Analysis of Existing Structure

Modelling of Existing Structure is performed by ETABS 2015. After generating an ETABS model, seismic weight, W is calculated from the axial force diagrams of each elevation. Seismic weight is determined according Bangladesh National Building Code (BNBC final draft, 2015). The total dead load of a building, including partition walls and applicable portions of other imposed loads listed below:

- (a) For live load up to and including 3kN/m^2 , a minimum of 25 percent of the live load shall be applicable.
- (b) For live load above 3kN/m^2 , a minimum of 50 percent of the live load shall be applicable.
- (c) Total weight (100 percent) of permanent load or retained water or any imposed load sustained in nature shall be included.

After determining the seismic weight; earthquake loads are calculated. Then earthquake and loads are applied in both X and Y-direction. From a lot of methods of analysis static analysis is performed in this section. A total number of 9 load combinations were used in this analysis. For different load combinations, there are different values for AFD (axial force diagram), SFD (shear force diagram) and BMD (bending moment diagram). The load combinations are used according to Bangladesh National Building Code (BNBC final draft, 2015). The maximum values for axial force and moment are found from the envelope. Selecting the preferences ACI-318-11 the model is checked. There are total of 448 columns from which 210 columns cannot withstand the assigned loads. Demand Capacity Ratio of those columns exceeded 1.0. CSI Column software is used in this study to check the DCR values found from ETABS. A hand calculation is also performed to double check the DCR values. DCR value of a defected column will be discussed in the result and discussion section.

Modeling and Analysis of Retrofitted Structure

A SeismoStruct model is generated to retrofit the weak columns. After creating the building model, dead load, live load, earthquake and wind loads are applied. A total number of 9 load combinations were used in this analysis to apply the nodal loads. The columns which showed DCR value greater than 1.0 are retrofitted here with Nitinol SMA. Static analysis is performed in this study. At first a wrapping of 1.25 mm thickness was applied to the defected columns. Using the AFD, BMD and SFD from the SeismoStruct software demand capacity ratio at top and bottom is calculated through the CSI Column software. 184 columns showed DCR value less than 1.0 after retrofitting. Then 1.5 mm thickness wrapping was applied to other 26 columns. Those columns also showed better result after retrofitting with SMA wrapping of 1.5 mm. DCR value of a retrofitted column will be discussed in the result and discussion section.

RESULTS AND DISCUSSIONS

To make a comparison between a retrofitted and non-retrofitted column, a column of C3 property of storey 4 is taken. Two DCR value will be considered in this case. One for the retrofitted DCR which will be found from SeismoStruct analysis and the other form the nonretrofitted column which will be found from ETABS analysis. Static analysis is considered in both of the cases.

DCR value of a Non-Retrofitted column

To determine the DCR value of that column, axial load, M_{ux} -Bottom, M_{ux} -Top, M_{uy} -Bottom, M_{uy} -Top is determined from ETABS. The values of the corresponding column are listed below in Table 4.

Table 4: Moments of the column

Storey	Column Profile	M_{ux} -Bottom (k-ft)	M_{ux} -Top (k-ft)	M_{uy} -Bottom (k-ft)	M_{uy} -Top (k-ft)
S4	C30-3	322.13	328.56	214.26	235.59

Using these values, DCR value of both top and bottom of the column is calculated using CSI column software and the maximum of those two is listed below in Table 5.

Table 5: DCR value of the Non-Retrofitted column

Storey	Column profile	Demand capacity ratio	Remarks
--------	----------------	-----------------------	---------

S4	C30-3	1.28	Not safe
----	-------	------	----------

All the columns are checked by the same process and 210 columns were found having a DCR value greater than 1.0. Those columns were retrofitted using SeismoStruct software.

DCR value of a Retrofitted column

To determine the DCR value of that column, axial load, M_{ux} -Bottom, M_{ux} -Top, M_{uy} -Bottom, M_{uy} -Top is determined from SeismoStruct. The values of the corresponding column are listed below in Table 6.

Table 6: Moments of the column

Storey	Column profile	M_{ux} -Bottom (k-ft)	M_{ux} -Top (k-ft)	M_{uy} -Bottom (k-ft)	M_{uy} -Top (k-ft)
S4	C30-3	483.06	461.43	63.08	58.21

Using the values of axial force, moment at top and moment at bottom from SeismoStruct analysis; DCR value was determined using the CSI Column software and listed below in Table 7.

Table 7: DCR value of the Retrofitted column

Storey	Column profile	Demand capacity ratio	Remarks
S4	C30-3	0.67	Safe

A comparison between the moment carrying capacities of the columns and their demand capacity ratio is shown in Fig. 3 and Fig. 4 respectively.

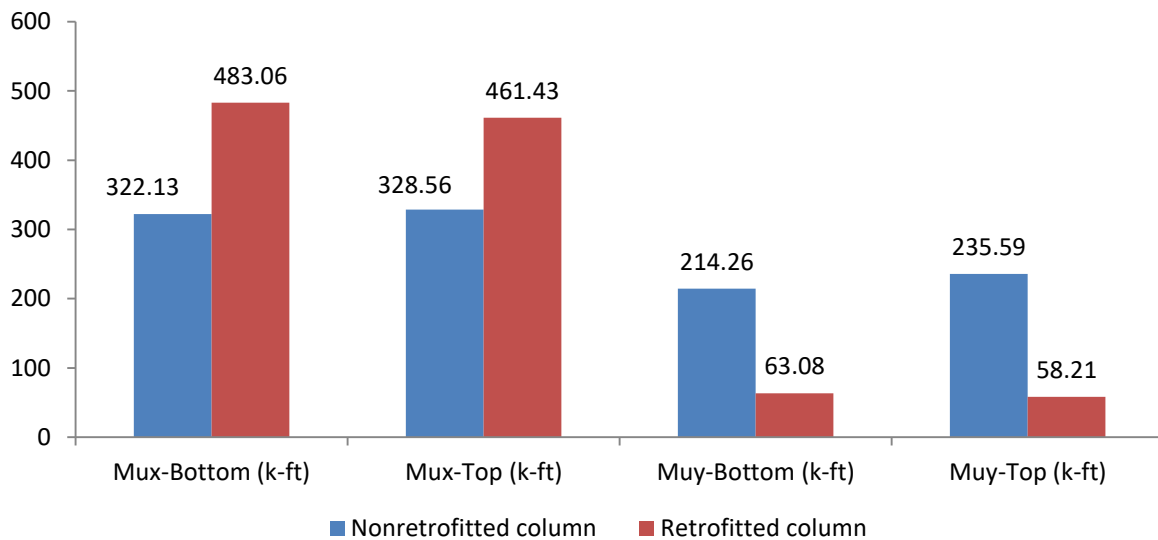


Fig. 3: Comparison between moment carrying capacities of retrofitted and nonretrofitted column.

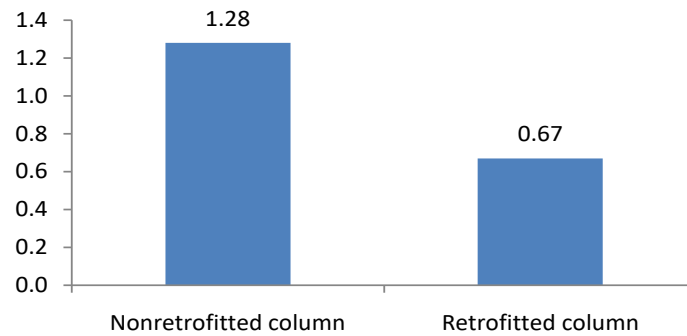


Fig. 4: Comparison between the DCR values of retrofitted and nonretrofitted column.

This process is repeated to check DCR values for all columns retrofitted with Nitinol SMA of 1.25 mm thickness. After this step, 26 columns showed DCR values greater than 1.0. Then they were retrofitted using 1.5 mm wrapping. After the comparison, it is clear that columns retrofitted with SMA will show better performance in the future. As SMA is a corrosion resistive material, those columns will have this advantage. After the assessment of the outcome of the investigation some recommendations can be stated for future research. In this project only static analysis was considered. But dynamic analysis should be performed to make the structure fully restrained against seismic loads. In this study foundation was not considered. The support of every frame was fixed support. But foundation analysis should be performed to get more accurate result. This study didn't consider the permanent weight of machine and equipment because of lack of information. Instead of that the largest live load for garments building from BNBC was assigned in those particular slabs. For better result, permanent weight of machine and equipment should be estimated clearly.

CONCLUSIONS

The building analyzed in this study is a garments building (Jeans 2000 Ltd.) located in CEPZ, Chittagong, Bangladesh. The type of analysis considered here is static analysis according to BNBC. The primary parameter considered in this study is Demand-Capacity-Ratio (DCR). DCR value of 210 columns of the existing structure analyzed in ETABS 2015 exceeded 1.0, which means higher demand of columns than allowable capacity. To retrofit these defected columns, Nitinol SMA of 1.25 mm thickness wrapping is used for 184 columns and 1.5 mm wrapping is used for the remaining 26 columns by the assistance of SeismoStruct 2018 software. DCR values of the retrofitted columns were less than 1.0 which means that those columns can withstand the existing loads. These conclusions indicate that Nitinol SMA can be used as a more effective retrofitting material. The numerical results have revealed that responses of RC columns are significantly reduced after retrofitting it by SMA material.

REFERENCES

- Alam, MS; Nehdi, M and Youssef, MA. 2005. Shape Memory Alloy as a New Construction Material. *International Workshop on Smart Materials and Structures*, Toronto, Ontario, Canada.
- Alam, MS; Bhuiyan, MAR and Billah, AHMM. 2012. Seismic fragility assessment of SMA-bar restrained multi-span continuous highway bridge isolated by different laminated rubber bearings in medium to strong seismic risk zones. *Bulletin of Earthquake Engineering*. 10(6): 1885-1909.
- Awan, IZ and Khan, AQ. 2018. Fascinating Shape Memory Alloys. *Journal- Chemical Society of Pakistan*, 40(01):1-23.
- BNBC Final Draft. 2015. *Bangladesh National Building Code*. Housing and Building Research Institute, Dhaka, Bangladesh.
- Christian, L. 2018. *Linear and Non-linear Mechanical Behaviour of Solid Materials*. Springer.

EXPERIMENTAL AND NUMERICAL INVESTIGATION ON FLEXURAL BEHAVIOR OF HIGH STRENGTH REINFORCED CONCRETE BEAM

S. Bhowmick¹, M. J. Alam¹, M. R. Mukhlis^{2*} & M. A. R. Bhuiyan¹

¹Department of Civil Engineering, Chittagong University of Engineering and Technology
Chittagong-4349, Bangladesh.

²Institute of Earthquake Engineering Research, Chittagong University of Engineering and Technology,
Chittagong-4349, Bangladesh.
E-mail: raihan.ieer@cuet.ac.bd

*Corresponding Author

ABSTRACT

The use of high strength concrete has become popular in construction work because of its improved strength and durability. High-strength concrete can be used as a substituting material over conventional concrete for structural members. This study describes the flexural behaviour of high strength reinforced concrete beam. The variation of flexural ductility with concrete compressive strength is quite complicated and thus sincerely reviewed in this paper. An experimental and numerical investigation of high strength reinforced concrete beam has been conducted in the present study. Four simply supported beams, having compressive strength of 27.50 MPa, 43.85 MPa, 54.05 MPa and 62.01 MPa, reinforced in top and bottom edges of the beam have been investigated in this study. The beams were tested under two-point loading to reveal their flexural behaviour. Load-deflection diagram and ductility index are the primary parameters that were considered in this study. The ultimate loads that obtained from the experimental results were found to be in good agreement with the numerical results. In addition, this study also compared the theoretical and experimental deflection at the mid-point of the beam. The cracking behaviour of all the beams and the crack width is also reviewed in this paper.

Keywords: high strength concrete; flexural ductility; load-deflection; crack width.

INTRODUCTION

In recent years, because of the advancement of concrete technology, the use of high strength concrete has increased and high strength concrete has been now used in many countries around the world. They also raised the upper limit of the concrete strength in their building code (Pam et al., 2001) to consider the higher strength of modern concrete. The use of high strength concrete can improve the durability of concrete, decrease the shrinkage and creep of the concrete, and reduce the size of the structural member (Lin et al., 1992). Although, in many cases the behaviour of high strength concrete is different from normal strength concrete, therefore high strength concrete should not be treated as normal strength concrete with greater strength. Another problem of high strength concrete i.e. generally more brittle in nature compared to that of normal-strength concrete (Pam et al., 2001). As high-strength concrete is more brittle in nature, their crack does not always occur in aggregate-hardened cement paste interfaces (Ho et al., 2002). It has been found that reinforced concrete beams made of high-strength concrete, if not properly designed, could fail in a brittle manner (Sarkar et al., 1997). As a consequence, in the design of reinforced concrete integrating high strength concrete, meticulous checking of ductility, cracking, and shear strength of the structure is ineluctable.

METHODOLOGY

Four beams were tested under simply supported condition. The dimensions of each beam were 915 mm × 152.4 mm × 139.7 mm. The span length of each beam was 813 mm with 51 mm clearance from the each end to the support. The span depth ratios taken in this study is around 6 which are lower than the previous studies available in the literature. To facilitate the cracking patterns on beam during the application of load, gridding was done. Each unit was 10 mm × 10 mm. The beams were tested under two concentrated loads with a constant moment region. The distance between the two point loads was 305 mm. The deflections were measured at mid-point. The beams were tested under load control condition. The deflection was recorded for each 10 kN increment of load up to failure and their crack pattern was also recorded. The experimental setup of the beam under two point loading are shown in Fig.1. Material properties and the geometric dimensions of the tested beams are shown in Table 1.

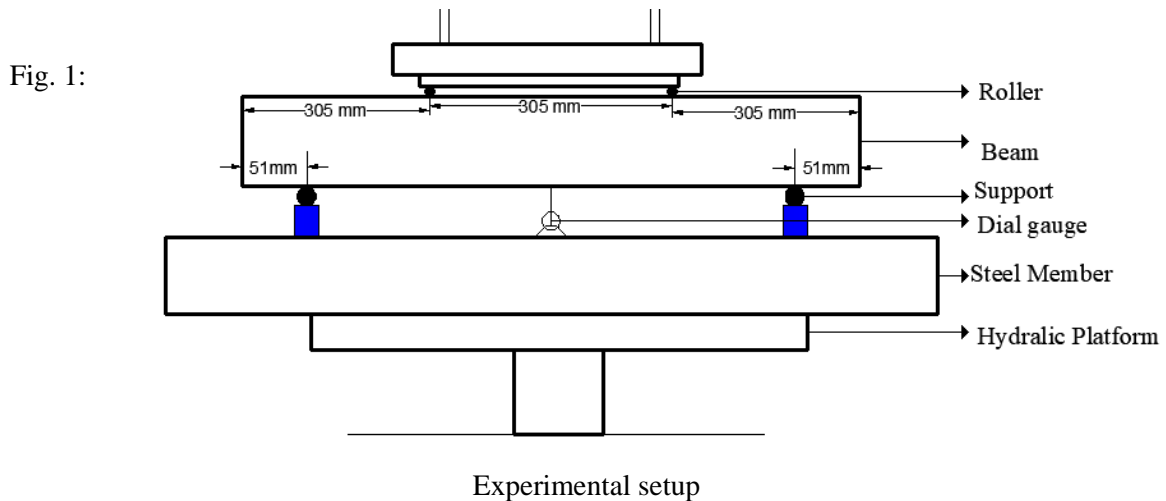


Table 1: Material properties and the geometric dimensions of the tested beams

Beam no.	Compressive strength, f'_c (MPa)	Depth of the centre of bottom Steel layer, d (mm)	Depth of the centre of top Steel layer d' (mm)	No. of Bottom Steel, A_s	No. of Top Steel A'_s
B1	27.50	96.3	25.4	2#16	2#12
B2	43.85	96.3	25.4	2#16	2#12
B3	54.05	96.3	25.4	2#16	2#12
B4	62.01	96.3	25.4	2#16	2#12

Experimental Investigation

The main objective of this experiment program is to investigate the flexural behavior of reinforced concrete beam. A total of four small-scale rectangular concrete beams were tested. All of them were reinforced with grade 60 steel. A total of four batches of concrete were used for this study. The designed compressive strengths for four batches were 27.50 MPa, 43.85 MPa, 54.05 MPa and 62.01 MPa. Development of first crack in the beam and fracture of the beam during experiment are shown in Fig. 2 and Fig. 3 respectively.



Fig. 2: Development of first crack in the beam

Fig. 3: Fracture of the beam during experiment

All specimens were loaded up to failure using a four-point flexural test under monotonic loading condition. The main variables are the compressive strength of concrete. The overall performance of the tested specimens was evaluated based on the overall flexural behavior.

Numerical Investigation

In this study the beam is analysed by static pushover analysis method due to incremental load application. The reinforcement detailing of the beam is carefully maintained and material property that is used in this program are tried to be synchronized with the experimental result. The properties of concrete and reinforcement details used for experiment program were put in SeismoStruct software as shown in Table 2. The two point loading was set in the model of the beam by applying two incremental loads of 10 kN from 305 mm distance of each end of the beam. The two hinge support was placed at the bottom of the beam at 51 mm from both ends. The analytical model of the beam and development of first crack in the analytical model of the beam is shown in Fig. 4 and Fig. 5 respectively.

Table 2: Material properties of the beams for numerical investigation

Material name	Material type	Material properties	Remarks
Concrete 1	Con_ma	$f'_c = 15 \text{ MPa}$ up to 45 MPa	Used in beam B-1 and Beam B-2
Concrete 2	Con-hs	$f'_c = 50 \text{ MPa}$ up to 120 MPa	Used in beam B-3 and Beam B-4
Steel	Stl_bl	$E = 200071.60 \text{ MPa}$ $F_y = 462 \text{ MPa}$	Used in all four beams

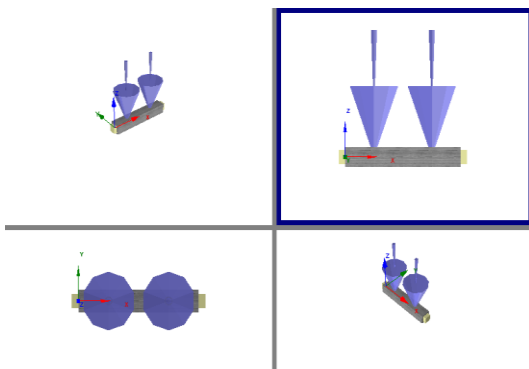


Fig. 4: Analytical model of the beam

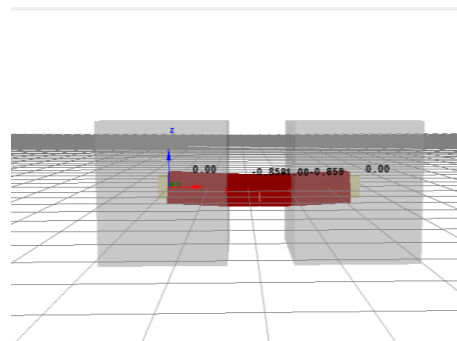


Fig. 5: Development of first crack in the analytical model of the beam

RESULT AND DISCUSSION

The parameters used to evaluate flexural performance were flexural cracking load and ultimate load under the load deflection behaviour, cracking width, ductility index, flexural capacity and deflection under service load.

Load deflection behaviour

Four separate load deflection curves were obtained experimentally and numerically and they are shown in Fig. 6 and Fig. 7. From Fig. 6 and 7 it can be shown that experimental load deflection curve slightly varies from numerical load deflection curve and numerical result shows larger deflection than experimental result except from beam B-1 where the experimental result shows larger value than numerical one.

The comparison of development of first crack loading and ultimate loading between experimental results and numerical evaluation are shown in Fig. 8 and Fig. 9. As seen in Fig. 8 and 9 the cracking load increases with the increase of concrete compressive strength both experimentally and numerically but numerical results showed larger value than experimental results. But the opposite phenomenon occurred in case of ultimate load. Here, experimental results showed larger value than numerical results except for beam B-1 which showed the similar value for both experimental and numerical.

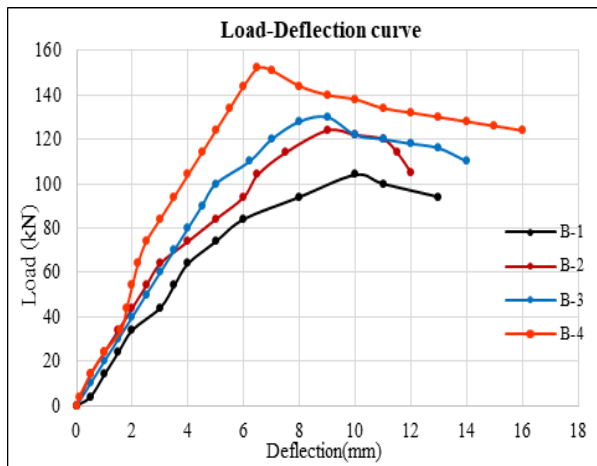


Fig. 6: Load-deflection curve from experimental results

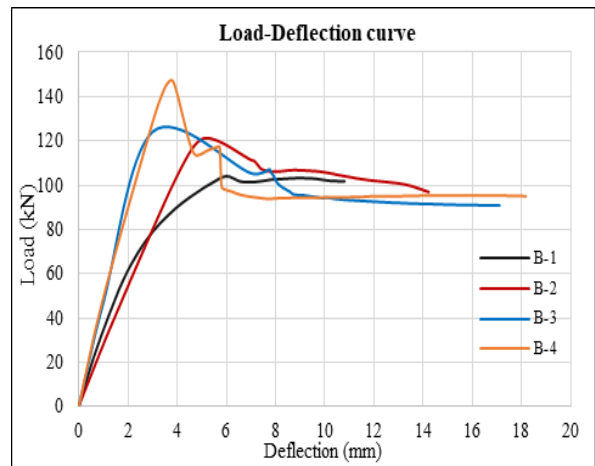


Fig. 7: Load-deflection curve from numerical results

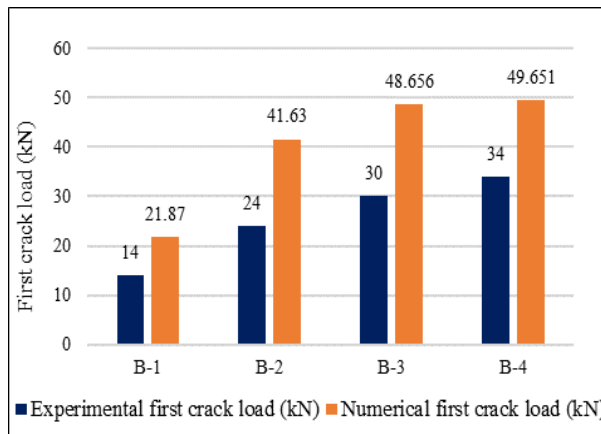


Fig. 8: Comparison of first crack load

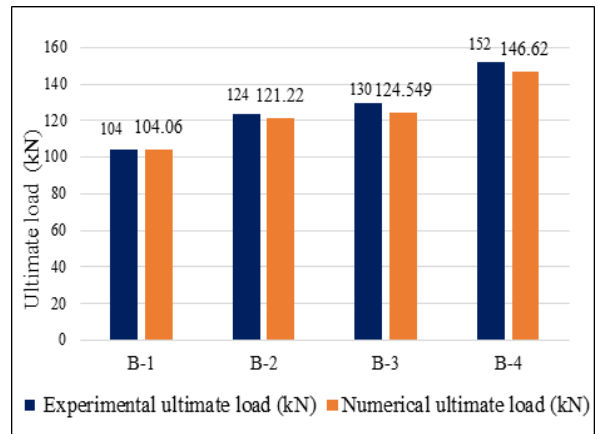


Fig. 9: Comparison of ultimate load

Cracking behaviour

Crack widths were measured at every load interval at the tension steel level and the crack formations were marked on the beam. The crack width at the tensile face was measured at every load stage in all the tests. The cracks forming on the surface of the beams were mostly vertical, suggesting failure in flexure. From experimental investigation it is observed that the crack widths are increasing for higher strength concrete. Though in most codes of practice, the maximum allowable crack width lie in the range of 0.10

to 0.40 mm (Vidivelli and Subbulakshmi, 2016), all crack widths found from the experiments exceed the value recommended in codes.

Table 3: Crack width and numbers of cracks for beam

Beam no	Max crack width (mm)	No. of crack between loading points
B-1	1.0	2
B-2	1.3	3
B-3	3.1	5
B-4	3.9	6

Ductility index

The ductility index (μ_d) was calculated depending on (Δ_{max}/Δ_y) , where the deflection at ultimate load (Δ_{max}) is the deflection when the load reached 85% of the ultimate load and (Δ_y) is the deflection when the applied load reached 75% of the ultimate load (Pam et al., 2001). The variation of ductility index of beam both experimentally and numerically are shown in Fig. 10.

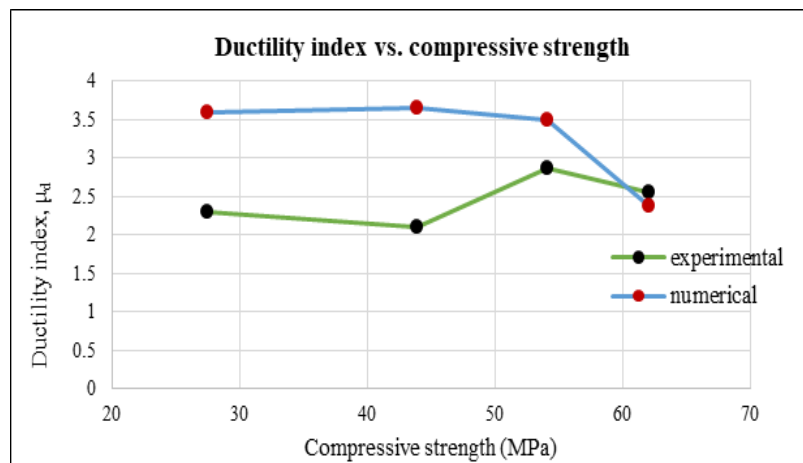


Fig. 10: Variation of ductility index with concrete compressive strength

From Fig. 10 it has been observed that the ductility index of beam showing large variation between the experimental and numerical results and opposite trend in the results. The main reason behind this variation and opposite trend in the result is the inaccuracy in casting of beam with lack of adequate clear cover and lack of required no. of dial gauge to measure the deflection under two point loading. It is known that concrete becomes less deformable and more brittle when its compressive strength increases especially when it is heavily reinforced. This might be the reason behind the decrease in ductility index for higher compressive strength of concrete.

Flexural capacity

Flexural strength of beams are shown in Table 4. From Table 4 it has been observed that the flexural strength of beam increases with the increase in the compressive strength of concrete both experimentally and numerically. This increase in flexural strength is rapid in case of beam B-2 and beam B-4.

Table 4: Flexural strength of beams

Beam no.	Compressive strength (MPa)	Flexural strength (MPa)	
		Experimental	Numerical
B-1	27.5	31.98	32.0
B-2	43.85	38.12	37.27
B-3	54.05	39.97	38.29

B-4	62.01	46.73	45.08
-----	-------	-------	-------

Maximum deflection at service load

Comparison between the calculated ($\delta_{ser,ACI}$), the corresponding experimental deflection ($\delta_{ser,exp}$) and numerical ($\delta_{ser,num}$) at service load are shown in Table 5. From the Table 5 it is observed that ACI 318-11 code expression for E_c value leads to a highly unconservative prediction of ($\delta_{ser,ACI}$) in terms of experimental result. But ACI 318-11 code overestimates the predicted deflection in terms of numerical result except for beam B-3.

Table 5: Experimental, numerical and predicted deflection at service load

Beam No.	$\delta_{ser,exp}$ (mm)	$\delta_{ser,num}$ (mm)	$\delta_{ser,ACI}$ (mm)	$\delta_{ser,exp}/\delta_{ser,ACI}$	$\delta_{ser,num}/\delta_{ser,ACI}$
B-1	3.90	2.00	2.66	1.47	0.75
B-2	3.95	2.30	2.67	1.48	0.86
B-3	4.00	3.80	2.59	1.54	1.47
B-4	3.40	1.90	2.87	1.18	0.66

CONCLUSIONS

The effect of concrete compressive strength on the flexural behaviour of reinforced concrete beam was investigated in this study. The load-deflection curves from the beams obtained experimentally are slightly different from numerical analysis. As concrete compressive strength increases the flexural strength of reinforced concrete beam also increases. The ductility index increases as concrete compressive strength increases for the same ρ up to some limit in terms of experimental results thereafter decreases as f_c' increases. ACI 318-11 code expression for E_c leads to a highly unconservative prediction of deflection at service ($\delta_{ser,ACI}$) in terms of experimental result. The maximum crack width lies in the range of 1.0 mm to 4.0mm which is larger than code suggested value.

ACKNOWLEDGMENTS

The authors gratefully acknowledge the support from the Department of Civil Engineering, Chittagong University of Engineering and Technology, Chittagong for carrying out this research. Also special thanks to industrial partners Confidence Cement Limited and BASF, Bangladesh for their material support in this research.

REFERENCES

- Ho, JCM; Kwan, AKH and Pam, HJ. 2002. Effects of Using High-strength Concrete on Flexural Ductility of Reinforced Concrete Beams. *The Hong Kong Institute of Engineers Transactions*, 9(1): 14-21.
- Lin, CH; Ling, FS and Hwang, CL. 1992. Flexural Behaviour of High Strength Fly Ash Concrete Beams. *Journal of the Chinese Institute of Engineers*, 15(1): 85-92.
- Pam, HJ; Kwan, AKH and Islam, MS. 2001. Flexural Strength and Ductility of Reinforced Normal and High Strength Concrete Beams. *Proceedings of the Institution of Civil Engineers: Structures and Buildings*, 146 (4): 381-389.
- Sarkar, S; Adwan, O and Munday, JGL. 1997. High Strength Concrete: An Investigation of the Flexural Behavior of High Strength RC Beams. *Structural Engineer*, 75 (7): 115-121
- Vidivelli, B and Subbulakshmi, T. 2016. Flexural Behaviour of High Performance Concrete Beams Subjected to Bending. *American Journal of Engineering Research*, 5(11): 326-332.

EFFECTS OF LEACHING ON THE PROPERTIES OF MORTAR

J.C. Kuri, S. Akter* & A. Choudhury

*Department of Civil Engineering, Chittagong University of Engineering & Technology,
Chittagong-4349, Bangladesh.*

E-mail: u1301121@student.cuet.ac.bd

**Corresponding Author*

ABSTRACT

Leaching of calcium and other ions from hydrates increases the porosity of cement based materials which has a negative effect on strength and durability. This study investigated the effects of leaching on the properties of mortar. Compressive strength and weight of the mortar and pH of leached water at different leaching periods were evaluated. The mortar specimens were subjected to tank leaching test where samples were exposed to demineralized water for 15, 30 and 90 days. The experimental results demonstrate that after leaching, the alkalinity of leached water increased due to the dissolution of calcium and other ions from mortar samples. Generally, for the first 30 days leaching there was no significant negative effect on the properties of mortar, rather leachant act as a curing medium. Due to the dissolution of hydration products, after 90 days leaching period, weight of the mortar specimen was decreased by 0.75% compared to without leaching sample. On the other hand, after 90 days leaching compressive strength of mortar increased by 72.60% compared to without leaching sample. In addition, after 90 days leaching period, compressive strength and weight decreased by 23.48% and 1.48% respectively compared to 30 days leached specimens.

Keywords: Leaching; dissolution; demineralized water; hydration products; mortar.

INTRODUCTION

Dissolution and alteration of cementitious materials occur due to long term contact with water. Concrete structures such as hydraulic structures, underground structures, radioactive waste containers, water purification plants, tunnels etc. when contacted with water leaching occurs. Leaching is a diffusion reaction phenomenon which takes place when cementitious materials are exposed to poorly mineralized or demineralized water (Rozière et al., 2009). The mechanism of leaching is very slow but can be a risk at longer periods (Kamali et al., 2003).

Hardened cement concrete is a porous material which contains solid hydration products such as portlandite (CH), calcium silicate hydrates (C-S-H), monosulfate (AFm), ettringite (Aft), etc. as well as pore space. Pore space is filled up with interstitial solution which is highly charged with Ca^{2+} , OH^- , Na^+ , K^+ , etc. (Faucon et al., 1998). Normally solid hydration products and the interstitial solutions remain in thermodynamic equilibrium condition. However, when concrete contacts with demineralized or poorly mineralized water the thermodynamic equilibrium condition does not exist. Leaching is accelerated with soft or demineralized water. Water creates concentration gradients which lead to the diffusion of ions from the highly concentrated interstitial solution to demineralized water and progressively dissolution or precipitation of the solid product occurs (Burlion et al., 2006; Faucon et al., 1998; Planel et al., 2006). The rate of attack depends on the quality and shape of the concrete, the rate at which the water percolates through or flows over it, the temperature, pH and the concentration of solutes in the water (Taylor, 1997; Kamali et al., 2003).

Porosity and transport properties of concrete increased due to leaching. Porosity of concrete has great influence on strength, toughness, durability and overall performance of concrete. Pore of the concrete leads to the cracks in concrete structures and degrade the performance. Moreover, other aggressive chemical such as chloride, sulphate, magnesium, etc. can penetrate into the concrete structure during the leaching process (Moranville et al., 2004). Chemical properties of pore water, such as pH, Eh (oxidation potential) and element concentration are also affected due to the process of leaching (Carde and Francois, 1999; Haga et al., 2005). Therefore, deterioration due to leaching causes severe damages on concrete structures such as cracking, delamination, spalling or even fracture (Weiting et al., 2011).

METHODOLOGY

Materials

Ordinary Portland Cement (OPC) was used as the binding material in this study. The specific gravity and specific surface area of cement were 3.15 and 3600 cm²/gm, respectively. Natural silica sand was used as a fine aggregate. The physical properties of the sand are shown in Table 1.

Table 1: Physical properties of fine aggregate

Property	Sand
Bulk specific gravity (OD basis)	2.60
Absorption capacity (%)	2.48
Fineness modulus (FM)	2.7

Mix Proportions and test methods

The sand to cement ratio of the mortars was 2.75. The water to cement ratio was kept constant at 0.55. The mortar mixture was prepared on a water tight platform. First, the fine aggregates and cement were dry mixed thoroughly. Then the required amount of water was added carefully so that no water was lost during mixing. The fresh mortar was then put into the 50 mm sides cube moulds and compacted using the standard temping method. The specimens were allowed to remain in the mould for the first 24 hours at ambient condition. After that these were demoulded with care so that no edges were broken and were placed in the curing tank at the ambient temperature for curing of 28 days until the leaching process began.

Tank leaching test was conducted in order to evaluate the effect of leaching on mortar. To conduct the tank leaching test, after 28 days curing period, hardened mortar was exposed to demineralized water in accordance with NEN 7345 (1995) standard. To prepare the leachant, 5 ml of the demineralized water was used per 100 mm² of the surface area of the specimen. The properties of leachant and leached mortar specimen were evaluated at 15, 30 and 90 days leaching periods.

pH of leached water was recorded at different leaching periods. Compressive strength tests were performed following the ASTM C109/C109M (2016) standard. First compressive strength tests were conducted after 28 days curing of sample in normal water before leaching process. After that the compressive strength of mortar was determined at 15, 30 and 90 days leaching periods. Three specimens were tested at each leaching period and an average value of the compressive strength is reported. In addition, the weight of the mortar specimen was accumulated at 0, 15, 30 and 90 days leaching periods in order to evaluate the change of weight after different leaching periods.

RESULTS AND DISCUSSION

pH variations of leached water

Fig. 1 shows the variation of pH of leached water at different leaching periods. From the Fig. 1 it is observed that the pH of the pure water was 6.6 and pH of the leached water varies from 6.9 to 9.2 which suggests the alkalinity of leached water. Alkalinity of leached water increased compared to pure water due to the dissolutions of ions such as Ca^{2+} , Na^+ , K^+ , OH^- , etc. from the mortar specimen. It is also seen that pH variation is not so high for the different leaching period because pH also depends on many factors such as temperature, CO_2 in the surrounding environment, etc.

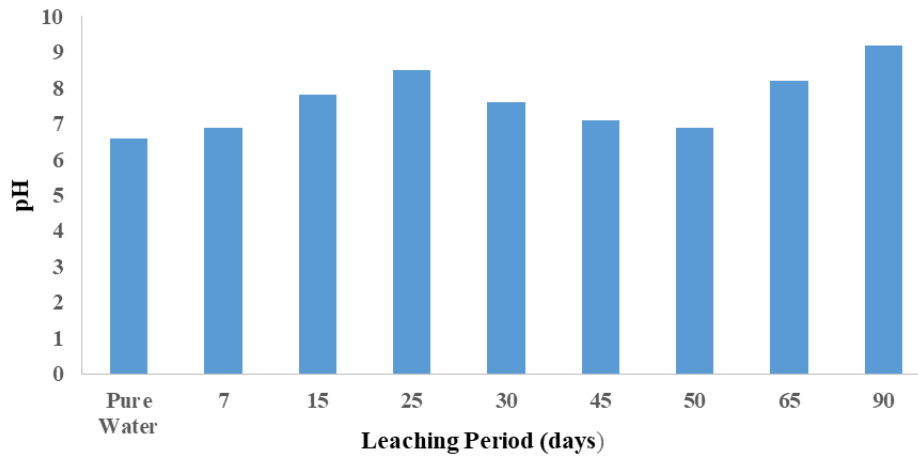


Fig. 1: pH of leached water at different leaching periods

Compressive strength variations

Fig. 2 illustrates the change of the compressive strength of mortar at different leaching periods. It is noticed that after 28 days curing period (0 days leaching period), the compressive strength of mortar was 21.9 MPa. The compressive strength of mortars were 27.9, 49.4, 37.8 MPa for 15, 30 and 90 days leaching periods, respectively. After 15 and 30 days leaching, the compressive strength of mortar specimens was increased by 27.39% and 125.67%, respectively compared to without leaching sample. This result suggests that up to 30 days leaching, there was a formation of solid products which might come from further curing and leads to increase compressive strength. In contrary, after 90 days leaching, the compressive strength was decreased by 23.48% compared to 30 days leaching specimens. This result indicates that dissolution of hydration products was happened due to 90 days leaching and consequently compressive strength was decreased.

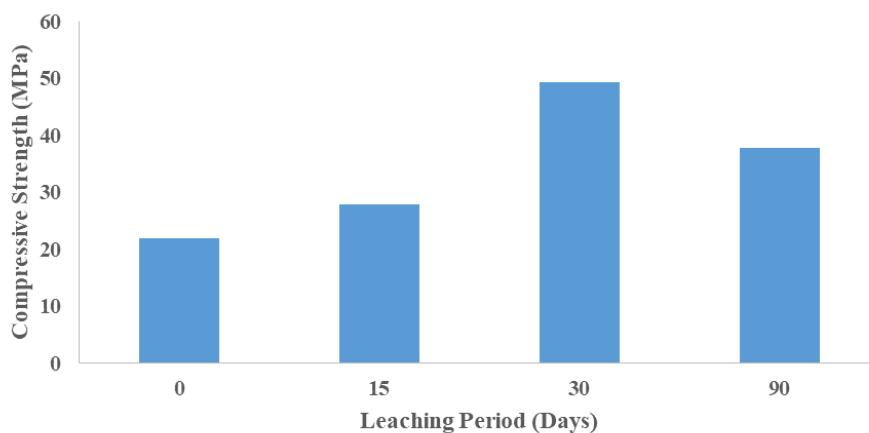


Fig. 2: Compressive strength of mortar at different leaching periods

Weight variations

The weight variations of the mortar specimen due to leaching are shown in Fig. 3. The weight of the specimen were 268, 268, 270 and 266 gm for 0, 15, 30 and 90 days leaching periods, respectively. It can

be seen that after 15 days leaching, weight of mortar specimen is same as without leaching sample. However, after 30 days leaching the weight of mortar increased by 0.75% compared to without leaching sample. This result also indicates that there was a formation of solid products for up to 30 days leaching period, which might come from further curing and leads to increase the weight of mortar. On the other hand, after 90 days leaching the weight of mortar decreased by 0.75% and 1.48% compared to without leaching and 30 days leaching specimens, respectively. This result suggests that dissolution of hydration products due to leaching leads to decrease the weight of mortar.

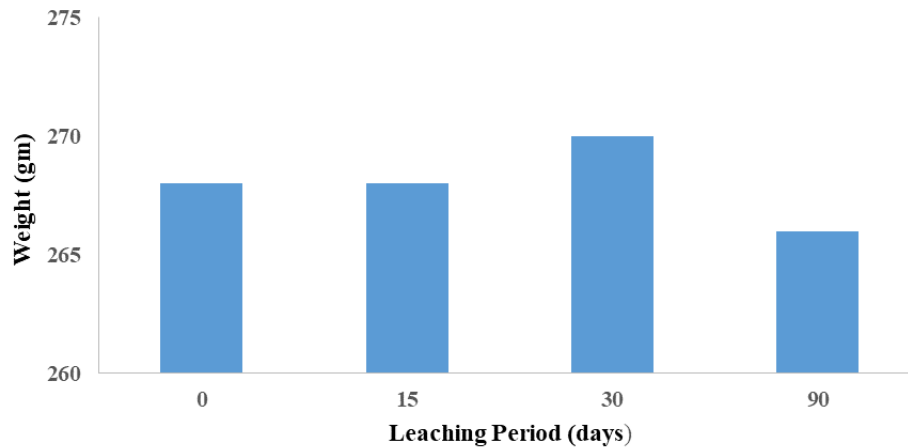


Fig. 3: Weight of mortar at different leaching periods

CONCLUSIONS

In this study the effect of leaching on mortar specimens was investigated. Leaching was conducted using tank leaching test. Based on the experimental analysis of this study, the following conclusions could be drawn:

- Alkalinity of leached water increased due to the dissolution of ions such as Ca^{2+} , Na^+ , K^+ , and OH^- etc. from the mortar specimen.
- After 15 and 30 days leaching the compressive strength of mortar was increased by 27.39% and 125.67%, respectively compared to without leaching sample. In contrary, after 90 days leaching, the compressive strength was decreased by 23.48% compared to 30 days leaching specimens.
- After 30 days leaching the weight of mortar increased by 0.75% compared to without leaching sample. On the other hand, after 90 days leaching the weight of mortar decreased by 0.75% and 1.48% compared to without leaching and 30 days leaching specimens, respectively.
- In general, for the first 30 days leaching there was no significant negative effect on the properties of mortar, rather leachant act as a curing medium. However, after 90 days leaching period, performance of mortar gradually deteriorated.

ACKNOWLEDGMENTS

The laboratory support provided by Chittagong University of Engineering & Technology (CUET) is gratefully acknowledged.

REFERENCES

ASTM C109/C109M. 2016. Standard Test Method for Compressive Strength of Hydraulic Cement Mortars

- Burlion, N; Bernard, D and Chen, D. 2006. X-ray microtomography: Application to microstructure analysis of a cementitious material during leaching process. *Cement and Concrete Research*, 36, 346–357.
- Carde, C and Francois, R. 1999. Modelling the loss of strength and porosity increase due to the leaching of cement pastes. *Cement and Concrete Research*, 21, 181–188.
- Faucon, P; Adenot, F; Jacquinet, JF; Petit, JC; Cabrillac, R and Jorda, M. 1998. Long-term behaviour of cement pastes used for nuclear waste disposal: review of physico-chemical mechanisms of water degradation. *Cement and Concrete Research*, 28, 847-857.
- Haga, K; Shibata, M; Hironaga, M; Tanaka, S and Nagasaki, S. 2005. Change in pore structure and composition of hardened cement paste during the process of dissolution. *Cement and Concrete Research*, 35, 943–950.
- Kamali, S; Gerard, B; Moranville, M. 2003. Modelling the leaching kinetics of cement-based materials—influence of materials and environment. *Cement & Concrete Composites*, 25, 451–458.
- Moranville, M; Kamali, S; Guillon, E. 2004. Physicochemical equilibria of cement-based materials in aggressive environments — experiment and modeling, *Cem. Concr. Res.* 34, 1569–1578.
- Nederlands Normalisatie Instituut (NEN), 7345. 1995. Leaching Characteristics of Solid Earthy and Stony Building and Waste Materials - Leaching Tests – Determination of the Leaching of Inorganic Components from Buildings and Monolithic Waste Materials with the Diffusion Test.
- Planel, D; Sercombe, J; Bescop, PL; Adenot, F and Torrenti, JM. 2006. Long-term performance of cement paste during combined calcium leaching-sulfate attack: kinetics and size effect. *Cement and Concrete Research*, 36, 137–143.
- Rozière, E; Loukili, A; El Hachem, R; Grondin, F. 2009. Durability of concrete exposed to leaching and external sulphate attacks. *Cement and Concrete Research*, 39, 1188-1198.
- Taylor, HFW. 1997. *Cement Chemistry*. London: Tomas Telford Publishing.
- Weiting, L; An, C; Ran, H; Chuntao, C and Xingang, Z. 2011. Effect of Calcium Leaching on the Properties of Cement-based Composites. *Journal of Wuhan University of Technology-Mater Sci Ed*, 26(5), 990-997.

COMPARATIVE STUDY ON THE ENGINEERING PROPERTIES OF LOCALLY AVAILABLE BRICKS & SAND IN EASTERN REGION OF CHITTAGONG

*M. M. Hossain¹, M. A. Islam², O. C. Debanath¹ & M. S. Islam¹

¹ Department of Civil Engineering, Chittagong University of Engineering & Technology, Chittagong-4349, Bangladesh, mosaddek.cuet08ce@gmail.com.

² Department of Sustainable Mining and Remediation Management, TU Bergakademie Freiberg, 09596 Freiberg, Germany, md-ariful.islam@student.tu-freiberg.de.

ABSTRACT

Bricks & sand are used in various types of construction work such as partition wall, reservoir, road & building. Problems frequently occur due to the use of low-quality bricks & sands. Bricks & sand that do not fulfil the quality standards make structures weak & faulty. Different field and laboratory tests are needed for quality control of these engineering materials. This study covers the experimental investigation sand and brick samples collected from ten different local areas of Chittagong district. These materials were tested through field and laboratory tests to assess their engineering properties in order to compare with standard limiting values. Unit weight, Fineness modulus, Salinity, Water Absorption Capacity, Specific gravity and Chloride tests were conducted for sand. Whereas Field Test, Size & Shape, Salinity, Chloride, Unit Weight, Water Absorption and Crushing Strength tests were performed for Bricks in the laboratory of Chittagong University of Engineering and Technology. The properties of brick and sand samples are observed to vary for different sources. However, the test data may provide necessary information to ensure quality of construction works in this region.

Keywords: Bricks; Sand; Engineering properties; Laboratory test; Field test

INTRODUCTION

Soil is the upper layer of earth containing inorganic particles and organic substance covering most of the land surface. Sand has been defined as a loose granular substance and various organic matter having liquid and gas in the empty space between the soil particles. Soil is also considered to be harsh grained particle with particle size between 0.07 mm to 4.75 mm (Lambe, 1951) and is an engineering material that plays a significant part in civil engineering works. Soils vary mostly in their chemical and physical properties depending on their age and states (parent material, climate, topography and vegetation) under which they are shaped. The major component of the most soils is inorganic material. It comprises mostly of mineral particles having particular physical and chemical properties that differ on the basis of the parent material conditions under which the soil was formed. The texture of soil is a feature that is ascertained mostly by the relative ratio of inorganic particles of various sizes. Grit particles are larger than 2mm in diameter, frieze sand-particles less than 2 mm and larger than 0.2 mm in diameter, fine sand-particles are either 0.2mm or 0.02mm in diameter, silt-particles between 0.02 mm and 0.002 mm in diameter (Das and Sobhan, 1998). Quartz is the remarkable mineral in the sand fraction of a large number of soils. On the other hand, sand particles have a relatively small surface area per unit weight, less water retention with little chemical activity in comparison with silt and clay. So, it is essential to know about physical and chemical properties of soil so as to know whether the soil is chemically active or not (Zaman and Islam, 2010). Soil engineering has wide application in the construction of different civil engineering structure like foundations, retaining structures, stability of

slopes, underground structures, pavement design, earth dam etc. The properties defining sand as standard quality would be well graded, coarse and clean, free from all types of detrimental substances, and does not contain any uncleanliness like iron pyrite acidic and basic, mica etc.

Meanwhile, Brick is the small building material in the form of a rectangular block which was first produced in a sun-dried form at least 6,000 years ago. Clay is the basic component that is mined from open pits, formed, and then fired in a kiln in order to produce strength, hardness, and heat resistance. Brick was the major building material in the ancient Near East and its multi-dimensionality was extended in shale ancient Rome by developments in manufacture and by new techniques of bonding. Little amounts of manganese, barium, and other additives are mixed with the clay to produce various shapes and barium carbonate is used to develop brick's chemical resistance to the components. Many other additives such as byproducts from papermaking, ammonium compounds, wetting agents, flocculants causing particles to form loose clusters and deflocculants dispersing clusters have been used in brick and some clays need the addition of sand or grog (pre-ground, pre-fired material like scrap brick). Various types of coating materials and procedures are needed to produce brick of a certain color or surface texture. The flux lowers the melting temperature of the sand in order to be bonded to the brick surface. There are some other materials such as graded fired and unfired brick, nepheline syenite and graded aggregate can also be used. The primary step in producing brick is crushing and grinding the raw materials in separator and a jaw grinder. Then, the mixture of components desired for each particular batch is selected and filtered before it was sent on to one of the three brick shaping processes. They are extrusion, molding or pressing. Among the three processes the first one is the most adaptable and it is the most common. Once the bricks are shaped and they are dried to remove excess moisture which may cause cracking during the ensuing firing process. Firing in ovens and then cooling, they are detached-automatically stacked, wrapped with steel bands and padded with plastic corner protectors. The bricks which are used in construction works are burnt bricks. They are classified as the first-class bricks, second class bricks, third class bricks and fourth-class bricks. So, the optimum properties which make quality bricks are well burnt with copper colored. They are free from cracks having square and sharp edges. They produce audible metallic sound at time of struck. These types of bricks absorb minimum water when they are submerged in water. These bricks do not break although they are dropped from 1-meter height (Aziz, 1995). The main objectives of this study are to assess the quality of the locally available bricks and sand by field test and relevant laboratory tests. Thereafter the properties of brick & sand will be compared with standard value.

EXPERIMENTAL PROGRAM

Materials used

Sand

Sand samples were collected from the following areas: Karnaphuly (bahirerchor), CUET balurchora, Shilok sand, Karnaphuly river (vitorerchor), Modunaghat, Bangalkhali, Tarabuniar chora, Ranir hat, Ichamoti river, Raojankhal.

Brick

Bricks samples were collected from different brick fields of Raozan and Rangunia Upazila. The various frog marks were BBC, SBM, EBM, FM, BBM, MBI, KBM, MBM, BBI, PBM. For each source sample No.1 (first class), No.2 (second class) and No.3 (picket) were collected.

Test conducted

Sand

The following laboratory tests were performed to assess the quality of the collected sand sample. Standard test procedure (ASTM C29, ASTM C128-15, ASTM C136, ASTM D1411-09) were followed for the relevant test:

- Sieve Analysis
- Specific Gravity
- Unit Weight
- Salinity
- Chloride

Bricks

The various tests were performed in the laboratory according to relevant standard procedure (ASTM C67 / C67M-18):

- Compressive Strength
- Water Absorption
- Unit Weight
- Efflorescence Test
- Field Test of Brick

RESULT AND DISCUSSION

As stated earlier, brick and sand samples were collected from the locally available sources. For each test, average of at least 03 samples test results were taken. The test results are shown in graphical and tabular forms. Fig. 1 to Fig. 5 shows the F.M., unit weight, specific gravity, chloride content and salinity respectively of sand samples collected from various sources. Also, Table 1 shows the comparison of results with the standard values. On the other hand, Fig. 6 to Fig. 10 show the crushing strength, salinity, unit weight, water absorption and chloride content respectively of brick samples collected form different brick fields. Likewise, Table-2 shows the brick field test results. Also, Table 3 shows the comparison of results with standard values for brick samples. From the Figures and tables, it is seen that engineering properties of the brick and sand samples vary form source to source. However, after detail analysis of the test results, a few conclusions and recommendations are made therefrom.

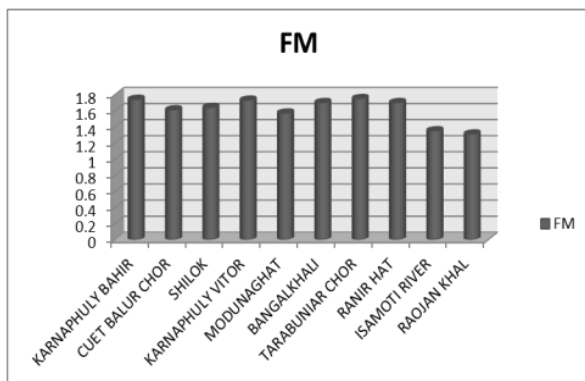


Fig. 1: Fineness Modulus of Sand

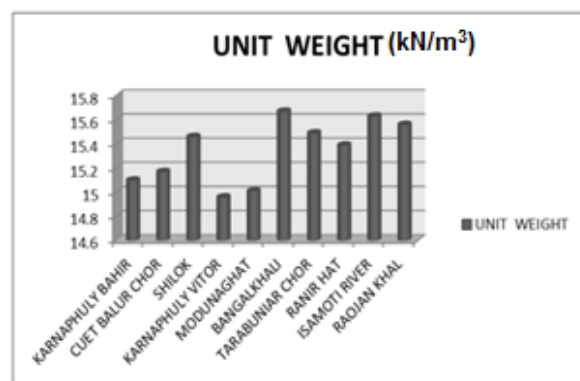


Fig. 2: Unit Weight of Sand

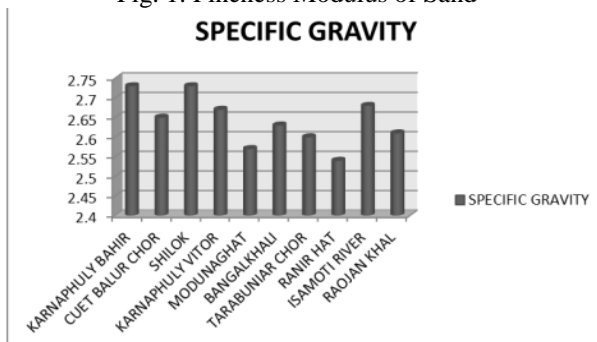


Fig. 3: Specific Gravity of Sand

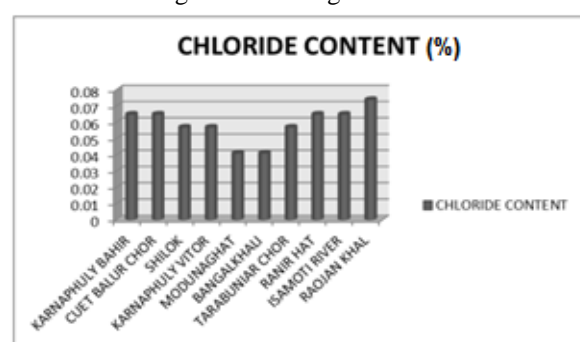


Fig. 4: Chloride Content of Sand

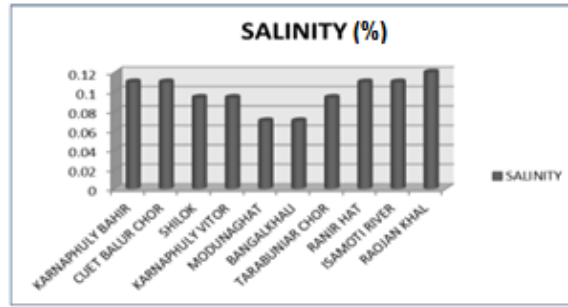


Fig. 5: Salinity Content of Sand

Table 1: Comparison of Results with Standard values (Sand)

Parameters	Results	Standard Values
Fineness modulus	1.57-1.74	2.3-3.1
Specific gravity	2.54-2.73	2.65-2.68
Unit weight	14.97-15.67	14-19
Salinity	0.072-0.12	0.074-.099
Chloride content	0.042-0.07	0.045-0.060

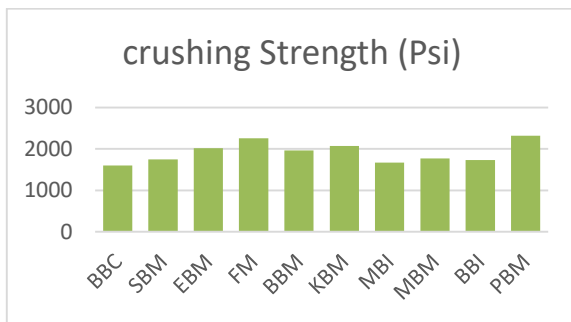


Fig. 6: Crushing Strength of Bricks

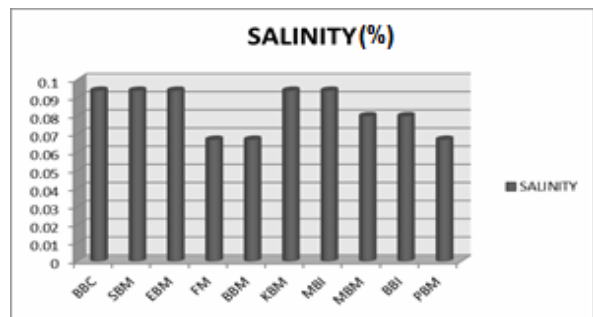


Fig. 7: Salinity of Bricks

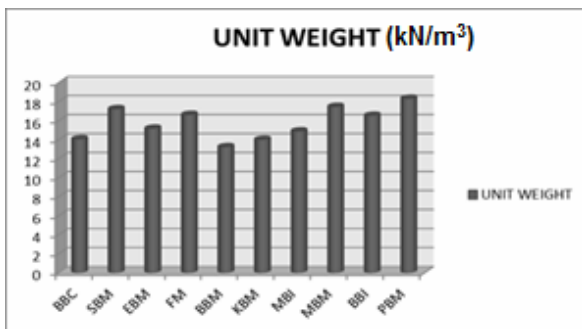


Fig. 8: Unit Weight of Brick

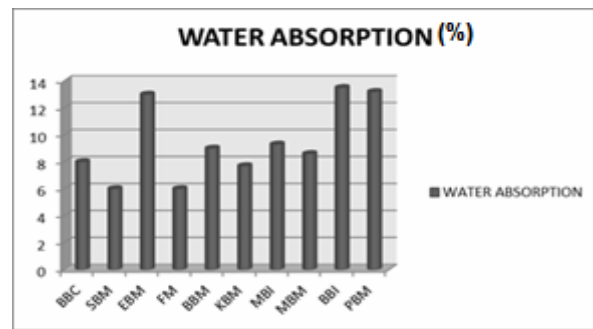


Fig. 9: Water Absorption of Brick

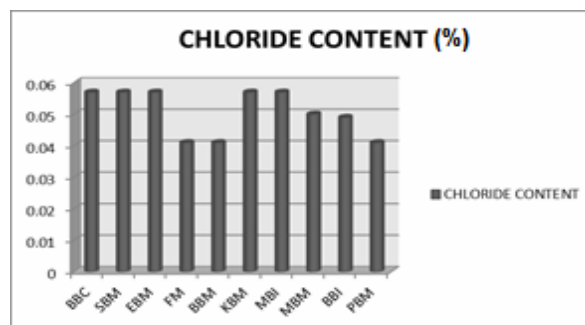


Fig. 10: Chloride Content of Bricks

Table 2: Field test of brick

Test Name	Sample	BBC	SBM	EBM	FM	BBM	KBM	MBI	MBM	BBI	PBM
T-Test	1	S	S	S	S	S	S	S	S	S	NS
	2	NS	S	S	S	S	NS	S	NS	NS	S
	3	NS	S	NS	S	S	S	NS	S	S	S
Nail Test	1	S	S	S	S	S	S	S	S	S	NS
	2	NS	NS	S	S	S	NS	S	S	S	S
	3	NS	S	NS	S	S	S	NS	S	S	S
Sound Test	1	S	S	S	S	S	S	S	S	S	S
	2	S	S	S	S	S	S	S	NS	S	S
	3	NS	S	S	S	S	S	NS	S	S	S

* S- satisfactory; NS- not satisfactory

Table 3: Comparison of Results with Standard values (Brick)

Parameters	Results	Standard Values
Field test	Satisfactory	
Unit weight (kN/m ³)	13.22-17.46	18.84
Water absorption (%)	0.06- 0.21	15-20
Salinity (%)	0.067-0.094	
Crushing strength (psi)	1600-2400	

CONCLUSIONS

In this study, samples of brick & sand from ten different sources of sand & brick fields were collected, tested and analyzed with regard to assess the various aspects of engineering properties. It is clear that for locally available sand and bricks, test results for different engineering properties vary with the sources location. The key findings are:

- (i) The Fineness Modulus of sand collected from different sources falls below the standard limit, but the other properties including specific gravity, unit weight, salinity, chloride content of sand lies within standard limiting values.
- (ii) Among all the sources Shilok sand is found satisfactory as it mostly complies with the standard limiting values.
- (iii) The field test of first-class bricks collected from the various sources are found satisfactory. But for 2nd class and picket brick, the quality doesn't satisfy in maximum cases.
- (iv) The unit weight, salinity and chloride content of bricks collected from different sources lies within the standard limit in most of the cases.
- (v) Water absorption capacity of bricks lies within standard limit. However, 2nd class and picket bricks absorb more water and exceed the limiting value.
- (vi) The crushing strength of bricks collected from all the sources falls below the standard limit.

REFERENCES

- Aziz, MA and Rahman, KM. 1995. *Engineering material*. Hafiz Book center. pp. 28-46
- ASTM C29/C29M-17a, *standard test method for bulk density ("unit weight") and voids in aggregate*, ASTM International, West Conshohocken, PA.
- ASTM C67 / C67M-18, *standard test methods for sampling and testing brick and structural clay tile*, ASTM International, West Conshohocken, PA.
- ASTM C128-15, *standard test method for relative density (specific gravity) and absorption of fine aggregate*, ASTM International, West Conshohocken, PA.
- ASTM C136 / C136M-14, *standard test method for sieve analysis of fine and coarse aggregates*, ASTM International, West Conshohocken, PA.
- ASTM D1411-09, *standard test methods for water-soluble chlorides present as admixtures in graded aggregate road mixes*, ASTM International, West Conshohocken, PA.
- Das, BM. and Sobhan K. 1998. *Principles of geotechnical engineering*. PWS Publishers
- Lambe W. 1951. *Soil testing for engineers*. New York: Wiley And Sons.
- Zaman, MAU and Islam, MM (2010) *Study on physical, chemical and engineering properties of coastal sand.*, Undergraduate Thesis, Department of Civil Engineering, CUET

USE OF JUTE FIBER TO IMPROVE CONCRETE PROPERTIES AGAINST FIRE

N. Anjum*, N. Akter & G. M. Sadiqul Islam

*Department of Civil Engineering, Chittagong University of Engineering and Technology,
Chittagong-4349, Bangladesh.*

E-mail: u1301075@student.cuet.ac.bd, nazmaaktermitu2017@gmail.com; gmsislam@cuet.ac.bd*

**Corresponding Author*

ABSTRACT

Fire resistance needs to be considered carefully during concrete structures' design which could be improved by addition of discrete fibers. As a local and ecofriendly biodegradable natural fiber, jute could be an effective material to improve concrete properties under elevated temperature. This experimental research studied residual compressive strength, crack and spall of jute fiber concrete exposed to different elevated temperatures (200°C, 400°C, 600°C, and 800°C). Properties of C35 strength concrete composites containing 15 mm and 20 mm length jute fibers were compared with plain concrete without fiber. With addition of jute fiber, compressive strength of concrete increased up to 16% and 6% respectively for 15mm and 20 mm fibers. Up to 200°C strength increased for both plain and 15mm fibered concrete, where the latter gained more strength (max 25%). At 400°C, 600°C and 800°C, strength reduction in control concrete is more than 15mm fibered concrete (max 20%). At any elevated temperature, 20mm fiber reduced the compressive strength than both control and 15mm fibered concrete. Crack area (max 71%) and width (max 20%) reduced using 15 mm jute fiber at elevated temperature than control while 20 mm jute fibered concrete produces higher density thinner micro-crack. Both 15 mm (max 43%) and 20 mm (max 65%) could resist spalling better than control concrete. Overall, 20mm length jute fiber was found to be more effective in reducing crack width and spalling.

Keywords: jute fiber; residual compressive strength; crack area; spall area.

INTRODUCTION

Because of large number of fire accidents, design of building structures against fire became more and more important. On November 24, 2012 a fire broke out in Tazreen Fashions garment factory in Ashulia, Bangladesh that led to the death of at least 112 workers trapped in a building and almost 200 were injured without emergency exits (The Daily Star, 2012). During terrorist attack, accidental break out and different type of explosions, properties of concrete undergo a rapid change within a short period. At elevated temperature, strength of concrete decreases owing to its physical and chemical changes; excessive cracking, decrease of bond and anchorage between the concrete and reinforcement or spalling of concrete cover can also be seen. Moreover, premature collapse of the whole structure can happen due to faster warm up the reinforcements situated below the detached concrete layers (Czoboloy *et al.*, 2016). To mitigate this losses, different types of fiber was used to improve the fire resistant properties of concrete. Use of jute fiber in construction could increase the exploration field for the material and restrict the utilization of polymer which is environmentally detrimental. Moreover, in Bangladesh, jute is locally available and hence less expensive (Zakaria *et al.*, 2016). The main aim of the proposed study is to evaluate the residual compressive strength, cracking and spalling of jute fiber concrete exposed to high temperature.

METHODOLOGY

Materials

Processed jute fiber was used for this study. To process, raw jute was mixed with jute batching oil (JBO), emulsifier (liquid soap) and noni det P40 and was run through *Spreader Machine*. Jute batching oil increased flexibility and smoothness of the raw jute surface. Main purpose was to remove gammy substance by forming bacteria and softening the surface. Secondly, the producer from first step was driven through *Carding Breaker Machine* to make the fiber more separable from each other. These fine and slicer fiber used in this study was collected from Karnafuli Jute Mills Limited, Chittagong. The processed jute fiber prepared in 15 mm and 20 mm length to use in concrete. Bundle form and desired length are shown in Figs. 1, 2 and 3. Properties of the processed jute fiber are given in Table 1.

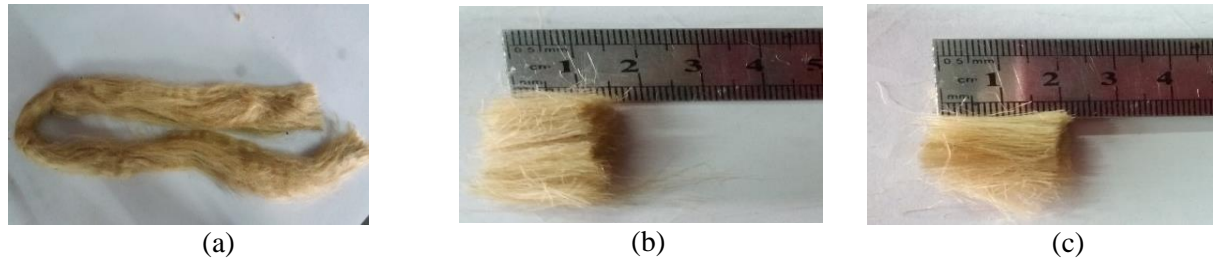


Fig. 1: (a) Processed Jute Fiber, (b) 15 mm length jute fiber and (c) 20 mm length jute fiber

Table 1: Properties of Jute Fiber

Property	Value	Property	Value
Length (mm)	15, 20	Density (g/cm ³)	1.3-1.46
Diameter (μm)	15	Elongation (%)	1.5-1.8
Aspect ratio (l/d)	1000, 1333	Young's modulus (GPa)	10-30

CEM I was used as binding material. Graded crushed stone chips according to ASTM C33 with 20 mm nominal maximum size was used as coarse aggregate. Coarse sand with fineness modulus 2.70 was used as fine aggregate. PCE based superplasticizer (0.9% by weight of cement) was used as water reducing agent. In addition Viscosity Modifying Agent (VMA) (0.3% by weight of cement) was used.

Concrete Mix Design

Concrete mix was designed as per ACI 211.1-91 (2009) to obtain target strength of 35 MPa (w/c = 0.45) at 28 days curing considering slump value of 125 mm. Three mixes were prepared; control mix was without fiber and the other two with same fiber content but varying length (15mm and 20 mm). Previous researches found concrete with higher jute fiber content has discontinuous distribution of materials which produces low strength areas in the composite. Remarkable enhancement in compressive strength of concrete was observed with 0.1% volumetric content (Zakaria *et al*, 2016; Asaduzzaman, 2018). Therefore, fiber content was kept 0.1% of total concrete volume for this study. The detailed concrete mix proportions of constituent materials (SSD condition where applicable) of concretes used for the study are presented in Table 2.

Table 2: Mix proportion for 1 m³ fresh concrete (target strength 35 MPa)

Constituents	Amount, kg
Water	170
Cement	455
Super Plasticizer	4.09
VMA	1.36
Coarse aggregate (SSD)	1000
Fine aggregate (SSD)	785
Jute fiber (0.1%)	0.241

Preparation of the test specimen

In total 162 (4 inch) concrete cubes with (15 and 20mm) fiber and control samples were prepared. The fibers were cut to specified length manually by a hand scissor. Jute fibers were dispersed in three layers. One-third of jute fiber was placed over stone chips (SSD), over that sand (SSD) was placed and over sand again one-third of jute fiber was placed (Fig. 2 (a) and (b)). Then after packing cement rest of the fiber was placed (Fig. 2(c)). Dry mixing of stone chips, sand, cement and jute fiber was done uniformly. Mixing water with admixtures was added to concrete and mixed uniformly (Fig. 2(d)). Fresh concrete was casted in cube moulds. These were demoulded after 24 hours and cured underwater for 28 days.

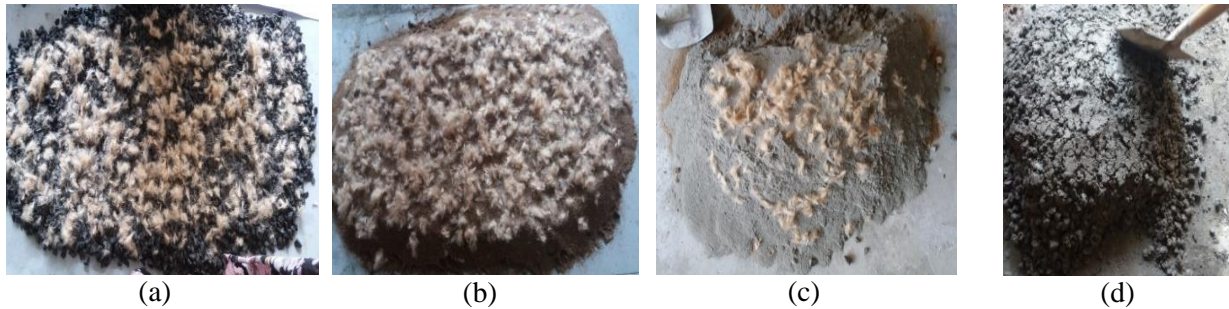


Fig. 2: (a) fibers placed over coarse aggregate, (b) 1/3 fibers placed over fine aggregate, (c) Fibers placed over cement and (d) Mixed fiber concrete

Experimental Program

After underwater curing for specified period, the samples were surface dried. These were then heated in an electric furnace (Fig. 3(a)) at 200°C, 400°C, 600°C and 800°C for 2 and 4 hours. The heated samples were cooled at room temperature and surface images were captured using a digital camera. Cracks and spalls were drawn and scanned from printed images of cubes surfaces. By using Image J software crack area, average crack width and spall area were measured (Fig. 3(c) and (d)). Compressive strength test (Fig. 3(b)) was conducted according to BS 1881-116:1983.

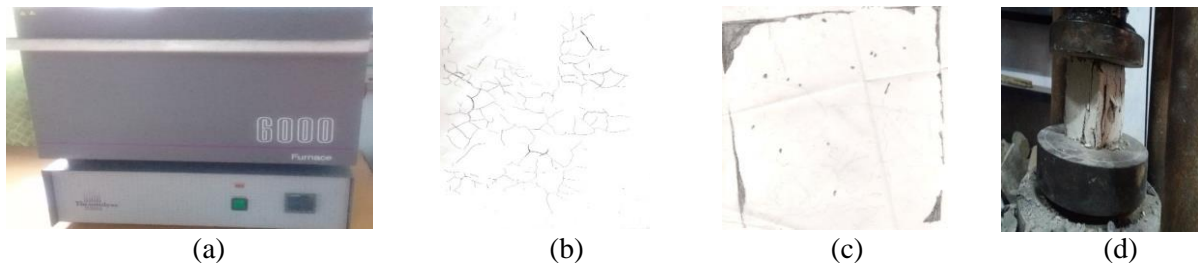


Fig. 3: (a) Electric furnace for sample heating, (b) 800°C- 4 hours cracking, (c) 600°C -2 hours spalling and (d) Compressive strength testing set up of concrete block

RESULTS AND DISCUSSIONS

Compressive strength test

Fig. 4 shows that compressive strength of control concrete and 15 mm jute fibered concrete increase at 200°C, where 15 mm jute fibered concrete gained more strength than plain concrete (max 25%). With further increase in exposure duration, compressive strength was also increased. This increase might be due to removal of free water with temperature increasing surface forces between gel particles (Lankard *et al*, 1971). Residual compressive strength decreased for both plain and 15mm fibered concrete at 400°C, 600°C and 800°C due to removal of chemical water for bonding. However, 15mm fibered concrete gave better performance than control concrete due to Poisson's effect initiates cracks at micro levels. With increment of applied load, these cracks keep growing. When the advancing crack approaches the fiber, the fiber blocked the forward propagation of the crack and diverting the path of crack. This permits the fiber reinforced concrete to withstand additional compressive strength over the control specimen with no fibers (Srikar *et al*, 2016).

In case of 20 mm jute fibered concrete, residual compressive strength were found to be in decreasing trend. Longer length of fibers is more effective to make well connected network with pre-existing pores (Heo *et al*, 2011). At elevated temperature, well connected bigger pore creates due to melting or degradation of longer fiber. The presence of higher porosity and small channels might reduce the mechanical strength of the composites (Alomayri *et al.*, 2014).

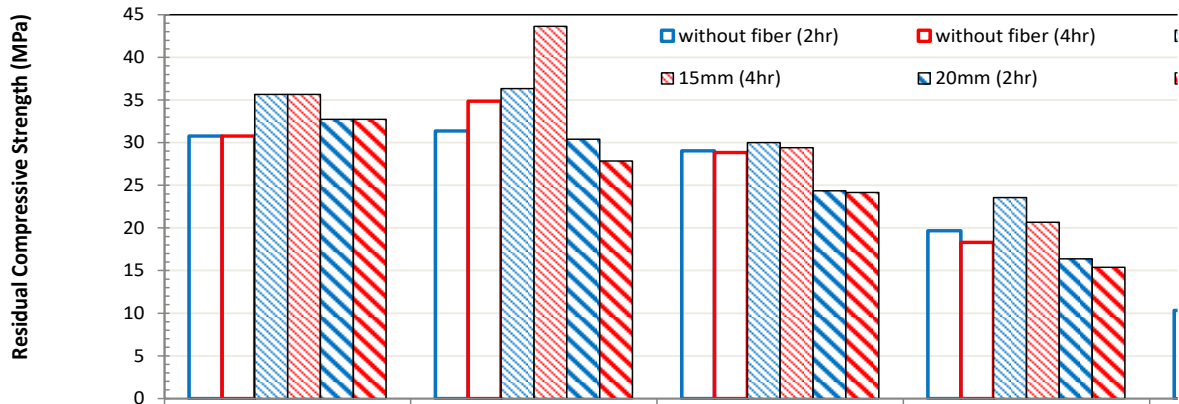


Fig. 4: Residual compressive strength of concrete exposed to high temperature

Crack area and width

At high temperature (600°C and 800°C) crack occurred on the concrete surface. Use of 15 mm jute fiber reduced both crack area (max 71%) and average crack width (max 20%) compared to control concrete. This indicates that jute fibers are effective in prevention of cracking caused by high temperatures. Crack occurrence was reduced due to the formation of small cavities inside the matrix created by the char and burnt fiber. (Alomayri *et al*, 2014) used cotton fibers and found results similar to this study. However, in the case of 20 mm length jute fibered concrete exhibits a much higher crack density than the control concrete. At 800°C, very thin cracks with a dense network were found between and around the sand and aggregate skeleton. Micro cracking occurs due to thermal dilation or shrinkage gradients between cement and aggregates. At high temperature such as 800°C, aggregates dilate whereas paste shrinks as a result of dehydration. As the fiber dilates during melting, this might create a tensile stress in the matrix that favors nucleating cracks (Khalifa *et al.*, 2001). Shorter fibers are less effective than longer fibers in concrete at elevated temperatures. Crucial connectivity of pores inside of concrete to evacuate vapours is assumed to be dependent on the length of fiber. The passage created by inclusion of longer length of fibers build up well connected network with pre-existing pores, particularly cracks induced by thermal incompatibility of cement and aggregate (Heo *et al*, 2011). Jute fiber concrete shows better result in reducing crack width in this study where 20 mm length acts better than 15 mm due to its longer length. Every case, crack area and width increased for 4 hours than 2 hours exposure.

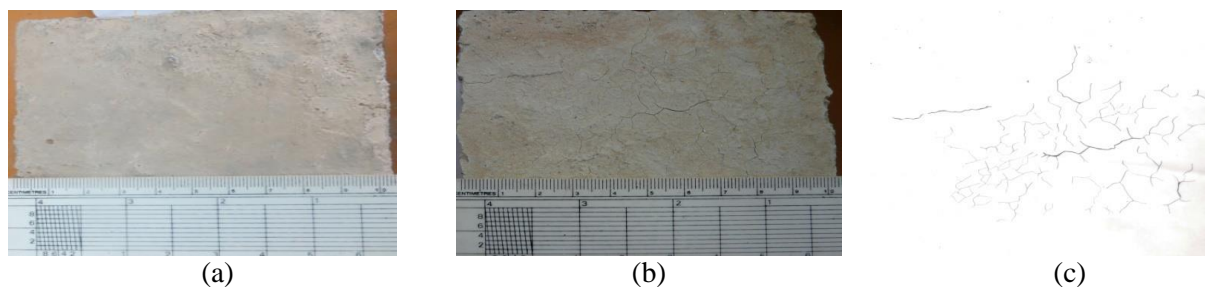


Fig. 5: (a) cracking at 200°C for 4 hours, (b) cracking at 800°C for 4 hours (raw image) and (c) cracking at 800°C for 4 hours (drawn on tracing paper)

Spall area

At high temperature (600°C and 800°C) crack and spalling occur on the surface of concrete (with and without fiber). Study shows jute fiber is effective in reducing spalling. No explosive spalling occurred in any case. At high temperature burnt fibers increase the porosity in concrete which results in the escape of vapour pressure and thereby lower the risk of spalling (Srikar *et al*, 2016). Using 15 mm (max

43%) and 20 mm (max 65%) jute fiber spall area reduced. Moreover, longer length (20 mm) fiber improves the performance of spalling protection as found by (Heo *et al*, 2011). Therefore, 20 mm jute fiber reduced spall than 15 mm jute fiber. Every case, spall area was increased with the exposure period.

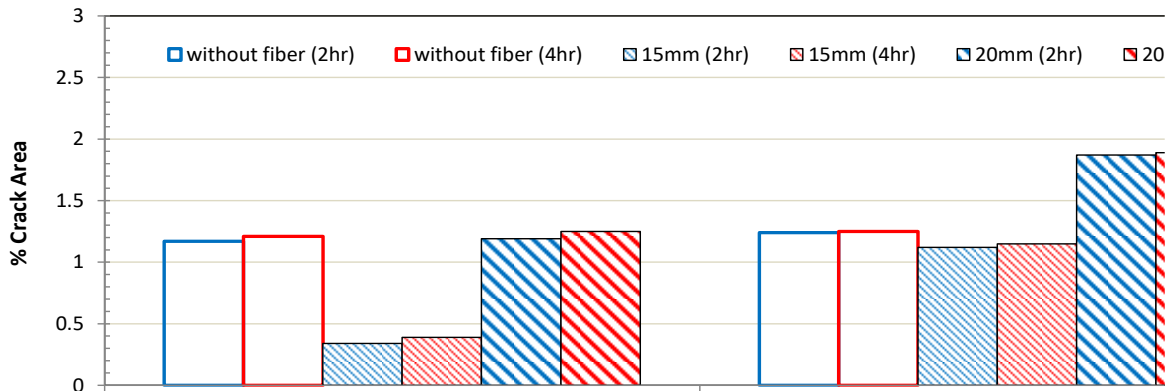


Fig 6: Crack area of concrete exposed to 600°C and 800°C

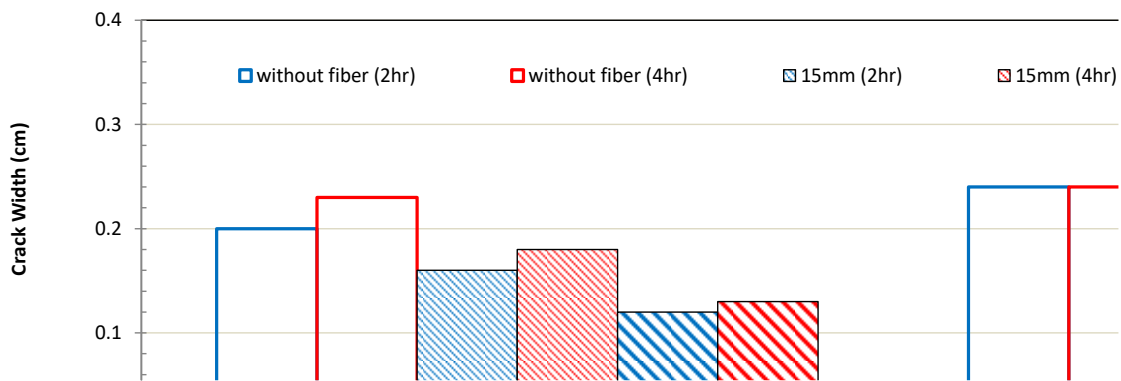


Fig 7: Crack width of concrete exposed to 600°C and 800°C



Fig 8: Spalling at 800°C for 4 hours



Fig 9: Tracing of spalling

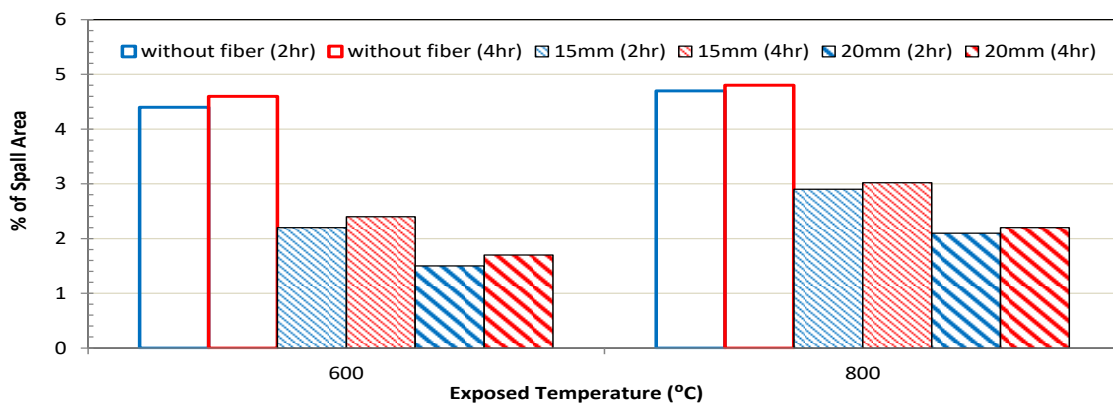


Fig 10: Spall area of C35 concrete exposed to 600°C and 800°C

CONCLUSIONS

From the experimental result of compressive strength and software analysis of crack area, width and spalling area of 0.1% jute fiber concrete exposed to fire the following conclusion can be drawn:

- With addition of 0.1% jute fiber, compressive strength of concrete increased up to 16% and 6% for 15 mm and 20 mm length jute fiber respectively;
- At elevated temperature up to 200°C, compressive strength increased for both control and 15 mm jute fibered concrete, where 15 mm jute fibered concrete gained more strength than control concrete (max 25%) but strength decreased for 20 mm jute fibered concrete. Above 200°C compressive strength reduced for all concrete samples. It was observed that exposing to 400°C, 600°C, 800°C, residual compressive strength of 15 mm jute fibered concrete was better than control concrete (max 20%). The residual compressive strength was found lower for 20 mm jute fibered concrete compared to other two samples;
- At high temperature (600°C, 800°C) crack and spalling occur on the surface of concrete (with and without fiber). Crack width reduced using both 15 mm (max 20%) and 20 mm length (max 43%) jute fibered concrete compared to control concrete. Crack area reduced for 15 mm jute fibered concrete (max 71%) but in 20 mm jute fibered concrete higher density thinner micro crack was produced. Reduced spalling was obtained for both 15 mm (max 43%) and 20 mm (max 65%) jute fibered concrete; and
- Overall, 20 mm length jute fiber was found more effective in reducing crack width and spalling.

ACKNOWLEDGEMENTS

The laboratory support provided by Chittagong University of Engineering & Technology (CUET) is gratefully acknowledged. Thanks also extended to industrial partners CEM Ready Mix Concrete and BASF, Bangladesh for material support.

REFERENCES

- ACI 211.1-91 (Reapproved 2009): Standard Practice for Selecting Proportions for Normal, Heavyweight and Mass Concrete, *American Concrete Institute*, MI, 48331-3439 USA.
- Alomayri, T; Vickers, L; Shaikh, FUA and Low, IM. 2014. Mechanical properties of cotton fabric reinforced geopolymer composites at 200- 1000 C. *Journal of advanced ceramics*, 3(3): 184-193.
- Asaduzzaman, SM. 2018. A study on the properties of jute fiber reinforced concrete, MEng Thesis, *Department of Civil Engineering, CUET*, 120p.
- Czoboly, O; Lubloy, E; Hlavicka, V; Balazs, GL; Keri, O; and Szilagyi, IM. 2016. Fibers and fiber cocktails to improve fire resistance of concrete. *Journal of Thermal Analysis and Calorimetry*, 128: 1453–1461.
- Heo, YS; Sanjayan, JG; Han, CG and Han, MC. 2011. Critical parameters of nylon and other fibers for spalling protection of high strength concrete in fire. *Materials and Structures*, 44: 599-610.
- Kalifa, P; Chene, G; Galle, C. 2001. High temperature behavior of HPC with polypropylene fibers from spalling to microstructure, *Cement and concrete research*, 31: 1487-1499.
- Lankard, DR; Birkimer, DL; Fondfriest, F and Snyder, MJ. 1971. Effects of Moisture Content on the Structural Properties of Portland Cement Concrete Exposed to Temperatures up to 500F”, *Temperature and Concrete*, SP-25: 59-102.
- Srikar, G; Anand, G and Prakash, SS. 2016. A study on residual compression behavior of structural fiber reinforced concrete exposed to moderate temperature using digital image correlation. *International Journal of Concrete Structures and Materials*, 10(1): 75-85.
- The Daily Star, November 27, 2012.
- Zakaria, M; Ahmed, M; Hoque, MM and Islam S. 2016. Scope of using jute fiber for the reinforcement of concrete material, *Textiles and Clothing Sustainability*, 2(11): 1880-1886.

PERFORMANCE OF REINFORCED CONCRETE SHORT COLUMNS INCORPORATING CERAMIC WASTE POWDER WITH PARTIAL REPLACEMENT OF CEMENT

M. M. Rana^{1*}, I. Saifullah¹, M. H. Islam² & T. Sakib¹

¹*Department of Civil Engineering, Khulna University of Engineering & Technology, Khulna-9203, Bangladesh.*

Email: mdmasudrana8594@gmail.com; saifullah@ce.kuet.ac.bd; masudkuet14@gmail.com*

²*Department of Building Engineering & Construction Management, Khulna University of Engineering & Technology, Khulna-9203, Bangladesh.*

Email: hamidcekuet@gmail.com

**Corresponding Author*

ABSTRACT

Sustainability of concrete as well as eco-friendly construction materials that make the pollution free environment are currently an innovative focus in concrete industries. A huge amount of waste ceramics are generated enormously all over the world. These wastages of ceramic are generally dumped at nearby places resulting in the environmental pollution causing harmful effect to inhabitant and agricultural lands. With increasing constraints on landfills, it is crucial to find alternative effective ways for recycling of ceramic wastes. Moreover, there is a large amount of greenhouse gas (CO₂) emitted in the atmosphere due to the manufacture of cement, and hence, reduction of uses of cement in concrete can play an important role to save the energy and protect the environment resulting makes the world more sustainable. This research highlighted the possibilities of using ceramic waste powder as effective partial replacement of cement in concrete. This research is mainly concerned with the experimental investigation of the performance of reinforced concrete short columns under axial compression loading. Test results indicated that the use of ceramic waste powder in concrete is one of the best possible option for solid waste management.

Keywords: Sustainability; recycling; ceramic waste powder; short columns; compression loading; solid waste management.

INTRODUCTION

The production of industrial wastes have been increasing gradually because of the continuous demands of resources use. However, due to increase of limitations of disposal industrial wastes on landfills, industries have to discover new effective approaches for recycling by-products as well as their wastes. A large quantity of wastes are generated in the production stage. From the perspective of the sustainability, recycle of waste ceramic from ceramic industries as well as electric power companies is one of the most significant methods to control global environmental problems (Higashiyama et al. 2010). Senthamarai and Devadas (2005) reported that approximately 30% of the daily manufacturing volume in the ceramic industries converted into wastes. In Europe, the quantity of wastes in the several production stages of the ceramic industries extents about 3 to 7% of its global production (Fernandes et al. 2004). Liu et al. (2015) stated that wastes ceramic have produced critical issues to environment, particularly in ceramic producing regions because of its poor biodegradability. Moreover, the practices of dumping or scarce management of waste from the numerous manufacturing sectors have a prominent effect on the receiving environment, leading to air, soil, water and noise pollution, amongst other problems in addition to current environmental complications. Therefore, recycling of ceramic wastes can provide the pronounced economic, social, and environmental profits (Liu et al. 2015).

Construction consumes huge quantities of building materials. Due to widespread use, concrete has attracted the attention of research all over the world. It is comprised of three major constituents such as aggregate, binder and water. The major component of concrete from the embodied energy point of view is the binder. A material that appears to have the potential to partially substitute of both binder and aggregate is ceramic waste. The production of one ton of Portland cement produces around an equal amount of CO₂ (Sadek et al., 2014). This contributes to approximately 8% of the yearly global green-house gas emissions to the atmosphere (Najim et al., 2016). Besides, advance technologies, it is often solved by the incorporating of various secondary or waste materials (Vieira et al. 2016; Hela et al. 2016). The philosophy of utilization of waste materials in the building materials denotes one of the current issues of materials engineering.

Ceramic waste can be used securely in the production of concrete because of its numerous satisfactory properties. It is durable, hard and highly resistant to biological, chemical and physical composition. It can originate from the production or demolition of a multitude of products such as wall and floor tiles, bricks and roof tiles, household ceramics, refractory products, sanitary ware, technical ceramics, expanded clay aggregates, inorganic bonded abrasives, therefore the chemical composition and physical properties vary considerably. Aggregate with ceramic electrical insulator has good resistance to the chemical attacks such as sulphate attack and chloride attack by inhibiting penetration of these chemicals (Dhavamani and Gobinatha, 2013) and the compressive strength suffers a very slight decrease (Senthamarai et al. 2011). The negative impact of industrial solid waste have on environment has led researchers (Halicka et al. 2013) to examine the use of ceramic sanitary ware waste as coarse and fine aggregate. The utilization of waste ceramic powder as a filler for self-compacting concrete has been investigated by Subasi et al. (2017), especially when the fresh state properties were improved. The addition of waste ceramic powder only slightly affects final mechanical properties (maximal dosage used in was 25%) (Subasi et al. 2017).

A classification of ceramic waste can be divided into two categories according to the source of its raw materials. In every category, the fired ceramic waste can be classified in accordance with the production procedures differentiating them by the use of red or white ceramic pastes. Nevertheless, the usage of red paste is more common and much greater in volume. Reuse of ceramic waste also provides advantageous in the perspective of energy, predominantly when the waste is from kiln industry (the ceramic industry) where highly endothermic decomposition reactions have already taken places, thus improving the energy formerly incorporated during production. In the ceramic industry several types of waste are generated, among them cement and concrete production can contribute a significant percentage of the total produced waste materials which can ease the serious environmental impact of these materials and also partially assist to attain the much needed sustainability in cement and concrete production and greener environment. In view of environmental issue and by-product waste disposal problems made the researches to investigate and to explore the possibility to utilize it for construction activities. Most researches concrete with waste ceramic powder deal with the characterization of fresh and hardened concrete properties, with the lack of information regarding the structural performance of sections cast with concrete containing waste ceramic powder. Therefore, this study explores the experimental observation of the performance of short column using waste ceramic powder as replacement of cement subjected to axial loading.

METHODOLOGY

Sample Preparation

The concrete constituents were mixed in a revolving drum in approximately three to five minutes to obtain uniform consistency. After mixing, 6 numbers of 900 x 150 x 150 mm reinforced concrete short columns were prepared with 12 mm bar as longitudinal reinforcement and 8 mm bar as tie reinforcement. During the preparation of short columns, the cement is replaced by ceramic powder by an amount of 20%. The optimum percentage of replacement of cement by ceramic waste powder has been selected based on the investigation of the mechanical properties of concrete using ceramic waste powder performed by Hamid (2018). After casting, the specimens were left in the casting room for 24 hours. After that, the specimens were demolded and cured. An initial curing for 28 days in water, then

specimens were kept inside the lab under ambient conditions until testing. Figure 1 shows the prepared sample reinforced concrete short column sample.



Figure 1: Preparation of reinforced concrete short column sample

Compressive Strength Test of Column Specimens

Several researchers, for instance, Niang et al. (2015) performed reinforced concrete short columns test incorporating glass powder subjected to compression loading. The test strategy of this research is almost identical to other researchers like as Niang et al. (2015) as presented in Figure 2. The complete test setup of reinforced concrete column under axial load is illustrated in Figure 3. It should be mentioned that compressive strength test was carried out after curing the specimens for 28 days in water bath.

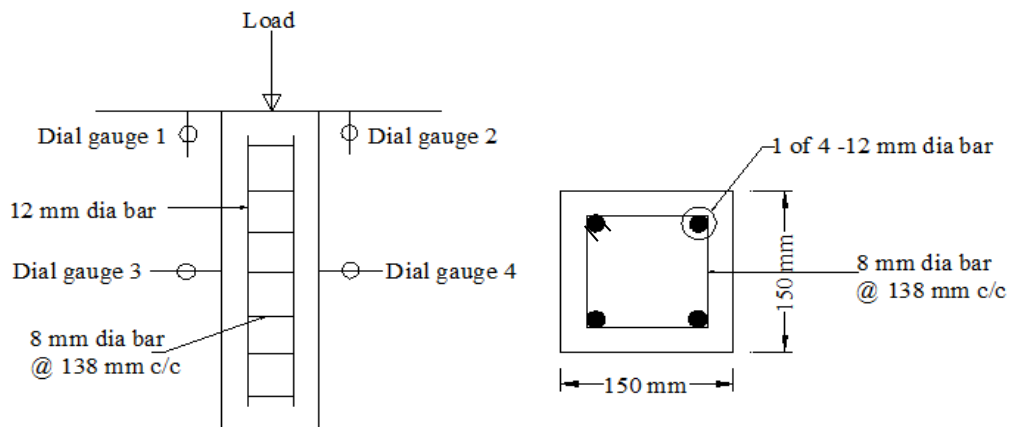


Figure 2: Schematic diagram of test set-up

A geotextile was used on the floor parallel to the fixed support. The fixed support has a center point so along that point a center point was kept on the floor. Then the column was set up there and geotextile was used again with the setup of a circular and long plate. The long plate was used to measure vertical deformation. Dial gauges were set at the center point of the column to measure lateral deformation. The average value of two dial gauges positioning the opposite faces of the column was taken as the lateral deformation of this direction. Two dial gauges were set at the top of the column to quantity the axial strain. The average value of this two dial gauges was taken as the axial strain for the specimens. It should be noted that the capacity of the dial gauge was 0.01-30 mm. There was a setup of load cell over the long plate.

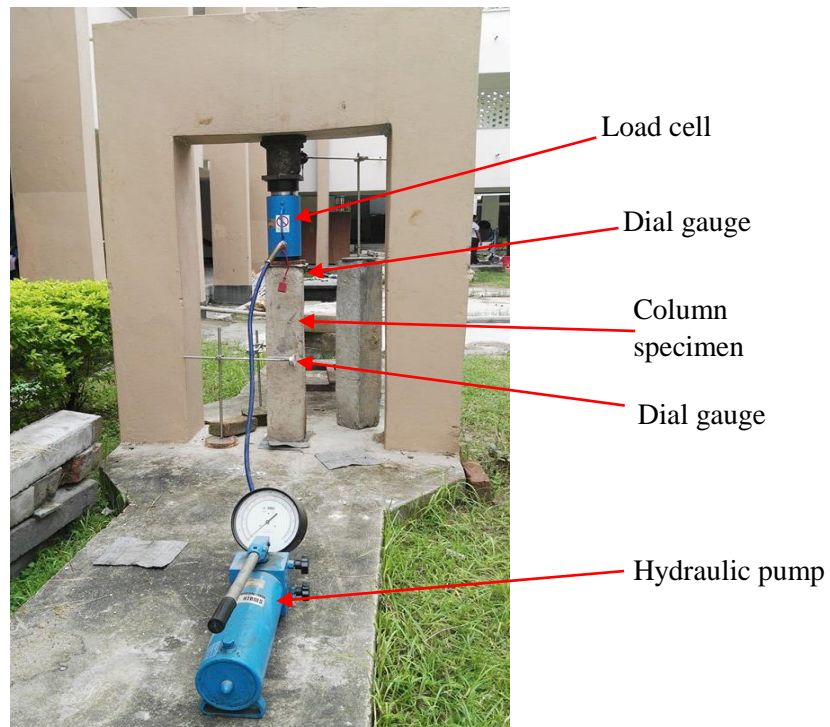


Figure 3: Test setup of reinforced concrete column under axial load

The capacity of the hydraulic jack was 500 KN. After setting everything the empty space was covered with plate of steel. Then hydraulic jack was pumped to obtain zero reading. Reading was taken for every 10 kN of load. The load was applied continuously until failure of the specimen. This process was repeated for each specimen.

RESULTS AND DISCUSSIONS

Six column specimens (three specimens with cement referred as control specimen; and three specimens containing 20% replacement of cement by ceramic waste powder) were prepared and tested after 28 days curing condition. The compressive strength of columns was determined under axial loading. Figure 4 shows the variation of capacity of reinforced concrete short column due to 20% replacement of cement by ceramic waste powder.

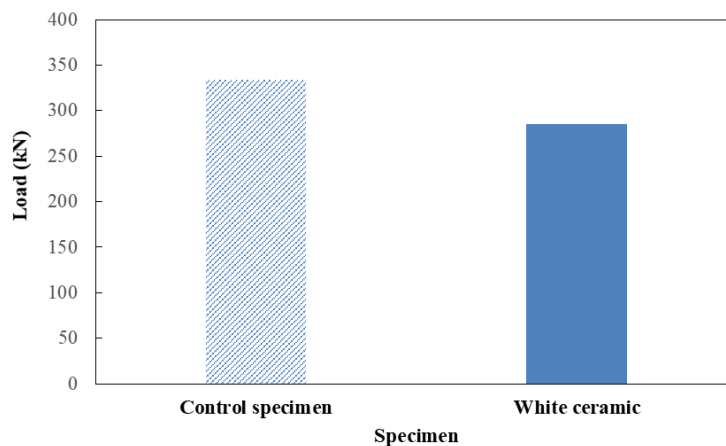


Figure 4: Variation of capacity of reinforced concrete columns with 20% replacement of cement using ceramic waste powder

From Figure 4, it is observed that the capacity of columns is 334.1 kN and 284.7 kN for cement and 20% red ceramic powder replacement respectively. There is approximately 15% variation of capacity

observed due to the 20% replacement of cement using ceramic powder which provides satisfactory results for using ceramic waste powder in concrete as a better alternative option of cement. Figure 5 shows the stress-axial strain relationships for columns incorporating waste ceramic powder and column containing cement only. It can be stated that column containing cement only provides higher stiffness compared to column incorporating ceramic waste powder. However, column containing ceramic waste powder shows higher ductility with respect to cement containing column only. The development of higher ductility may be occurred due to the crystals of ceramics since they have no inherent grain boundaries to interfere with dislocation motion as supported by researcher Pelleg (2014). However, some others factor like as grain size, additional second phase, structural modification (preferably to nanostructure) can be responsible for the ductility of concrete containing ceramic powder (Pelleg, 2014).

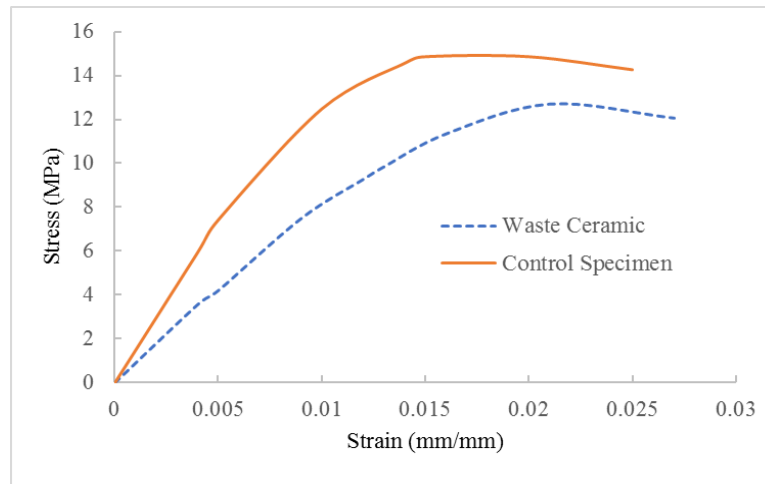


Figure 5: Stress vs. strain relationships for columns incorporating waste ceramic powder.

As the reinforced concrete columns were axially loaded, the reinforcement steel and concrete experienced stresses. When the loads were high compared to the cross area of the column, the steel and concrete reached the yield stress and column failed without undergoing any significant lateral deformation. The concrete column was crushed and collapse of the column was due to the material failure. In both columns, failure occurred due to crushing of concrete (shown in Figure 6) that corresponds to general failure criteria of short columns.



(a) Failure pattern for column containing cement only



(b) Failure pattern for column containing 20% replacement of cement using ceramic waste powder

Figure 6: Observation of cracks for different reinforced concrete columns

SUMMARY AND CONCLUSIONS

This research highlighted the possibilities of using ceramic waste powder as effective partial replacement of cement in concrete. This research is mainly concerned with the experimental investigation of the performance of reinforced concrete short columns under axial compression loading. From the illustrated results it can be concluded that the 20 percentile replacement of red ceramic waste showed good agreement with the concrete containing cement only and hence it becomes more economical without compromising concrete strength than the standard concrete. Therefore, test results indicated that the use of ceramic waste powder in concrete is one of the technically and economically feasible and viable option for safe disposal of ceramic waste, and hence, maintain towards the sustainability of concrete construction. Moreover, utilization of ceramic waste and its applications can be beneficial in the construction industries.

ACKNOWLEDGEMENTS

The authors are highly acknowledged to the authorities of Seven Rings Cement Company who supplied the required amount of materials to prepare the test specimens and accomplish the research work properly. We are also grateful to all the laboratory technicians of the Department of Civil Engineering, Khulna University of Engineering & Technology for their warmth co-operation during the project work.

REFERENCES

- Dhavamani, DS. And Gobinnatha, D. 2013. Chemical Resistance of Concrete with Ceramic Waste Aggregate. *International Journal of Current Engineering and Technology*, 3(3).
- Fernandes, M., Sousa, A., and Dias, A. 2004. Environmental Impact and Emissions Trade Ceramic Industry, A case study. *Portuguese Association of Ceramic Industry APICER*.
- Halicka, A., Ogrodnik, P., and Zegardlo B. 2013. Using ceramic sanitary ware waste as concrete aggregate. *Construction and Building Materials*, 48: 295-305.
- Hamid. 2018. *Mechanical & microscopic investigation of concrete incorporating ceramic waste powder as partial replacement of binding material*. M.Sc. thesis, Khulna University of Engineering & Technology, Bangladesh.
- Higashiyama, H., Yagishita, F., Sano, M., and Takahashi, O. 2011. Compressive Strength and Resistance to Chloride Penetration of Mortars Using Ceramic Waste as Fine Aggregate. *Construction and Building Materials*, 26:96-101.
- Hela, R., Tazky M. and Bodnarova, L. 2016. Possibilities of determination of optimal dosage of power plant fly ash for concrete. *Jurnal Teknologi*, 78:59-64.
- Liu, F., Liu, J., Ma, B., Huang, J. and Li. H. 2015. Basic properties of concrete incorporating recycled ceramic aggregate and ultra-fine sand. *Journal of Wuhan University of Technology-Mater. Sci.* 30(2): 352–360.
- Najim, KB, Al-Jumaily I. and Atea AM. 2016. Characterization of sustainable high performance/self-compacting concrete produced using CKD as a cement replacement material. *Construction and Building Materials*, 103:123-129.
- Niang, A., Roy, N. and Tagnit-Hamou, A. 2015. Structural behavior of concrete incorporating glass powder used in reinforced concrete columns. *Journal of Structural Engineering*, 141(3).
- Pelleg, J. 2014. *Mechanical properties of ceramics, Solid mechanics and its applications*, Springer International publication, Switzerland.
- Sadek, DM; Amin, SK and Youssef NF. 2014. Blended cement utilizing ceramic wall tile waste. *Construction Materials and Structures*, 152 - 161
- Senthamarai, RM and Manoharan, PD. 2005. Properties of Concretes Produced with Waste Ceramic Tile Aggregate. *Asian Journal of Civil Engineering*. 14(3):369-382.
- Subasi, S., Ozt'urk, H. and Emiroglu, M. 2017. Utilizing of waste ceramic powder as filler materials in self-consolidating concrete, *Construction and Building Materials*, 149:567–574.
- Vieiera, T., Alves, A., De Brito J., Correia J. R. and Silva RV. 2017. Durability-related performance of concrete containing fine recycled aggregates from crushed bricks and sanitary ware. *Materials and Design*, 90:767-776.

EFFECT OF FIBRE DIRECTION ON DIRECTIVITY PATTERN OF A₀ MODE LAMB WAVE SCATTERED AT THROUGH-HOLE DAMAGE REGION IN UNIDIRECTIONAL LAMINATES: A COMPUTATIONAL STUDY

M. S. Rabbi^{1*}, K. Teramoto² & M. Hasan¹

¹*Department of Mechanical Engineering, Chittagong University of Engineering & Technology, Chittagong 4349, Bangladesh. E-mail: rabbi@cuet.ac.bd*

²*Department of Advanced Technology Fusion, Saga University, Japan.*

E-mail: tera@me.saga-u.ac.jp

**Corresponding Author*

ABSTRACT

An investigation of the scattering behavior of A₀ mode Lamb wave at a subsurface cylindrical hole in unidirectional composite laminates is presented. A three-dimensional finite element method is used in this study to discuss the influence of the fiber direction in the wave propagation. The excitation frequency of 30 kHz is allowed to propagate with plane strain condition along a defected squared shape laminate. Four different specimens, based on the fiber direction (0°, 30°, 60°, and 90°) with an identical defect are considered. It is found that the Lamb wave scattering is complicated in other fibre directional laminates than the horizontal (0°) and vertical (90°) fibre directional laminate. The results depict that the amplitudes and directivity pattern of the scattered wave is considerably influenced by the fibre direction. The outcomes of this computational study help to the use of the A₀ mode Lamb wave for damage characterization and detection in composite laminates.

Keywords: A₀ mode Lamb wave; unidirectional laminate; scattering characteristics; fibre direction.

INTRODUCTION

Health Monitoring of the infrastructure based on Non-destructive Evaluation (NDE) becomes popular to the researchers from the last several decades as it increases the reliability and reduces the life-cycle cost for infrastructure. Among the various NDE techniques, Lamb waves based technique proved sensitive and efficient to detect the most type of defects (Guo, 1993; Rose, 2002). The perception regarding the scattering behavior of Lamb wave is an essential part in the application for detecting anomalies in structures. Number of researches has been carried out to investigate the Lamb wave interaction at various types of damage for isotropic material (Lowe, 2002; Cegla, 2008; Moreau, 2008). In recent years, Composite Laminates (CL) draws more attention in a wide spectrum of industries, especially in safety-critical applications such as aircraft primary structures, constructional structures, cars, rail vehicles, etc. Better strength & stiffness-to-weight ratios, controllability in fibre alignment, good acoustic and thermal insulation, low fatigue are the dominating advantages of CL. CL could be damaged during manufacturing as well as in long-term use in many ways and could be generated by fatigue, overload or impacts, which further leads to delamination, fibre breakage, voids, and matrix cracking. Due to the anisotropic nature of CL, researchers are yet to found the effective analytical solutions of Lamb waves scattering at defected region. Numerous investigations have been carried out through numerical simulation to understand the scattering of Lamb wave at through holes in the structure. Guo and Cawley (1993) studied the reflection of the S₀ mode Lamb wave in CL with plane strain assumption and it was shown that such type of mode is not useful to detect the delamination at the

through-thickness locations. The reflection behavior of fundamental mode Lamb waves from delamination of CL was studied by Hayashi and Kawashima (2002). It was found that A_0 mode Lamb wave is extensively responsive to the delamination type defect at all through-thickness locations.

In recent years, an analytical model based on the Poisson theory is proposed by Zhang et al. (2014) to predict the reflection of S_0 mode Lamb wave from a cylindrical flaw in a TI composite plate. The outcomes of the research suggest that in low frequency the Poisson theory can precisely illustrate the behaviour of the S_0 wave. Hai et al. (2015) offered an analytical study of the S_0 Lamb mode reflection from a blind hole in a plate-like structure using the 3D theory. They described the interaction of the high frequency Lamb waves with defects. Reza and Ng (2015) investigated guided wave (GW) based scattering behavior at delamination in composite beams and the mode conversion phenomena as well. They conducted the 3D FE simulation and the result was verified by experimental studies. It was reported that, sizes and location of the flaw have crucial influence on the reflecting behavior of GW.

A NDE method using the A_0 mode to spot the position of the delamination along the thickness of a CL has been presented by Singh et al. (2017) by means of numerical and experimental studies. Chiu et al. (2017) studied the reflection of the A_0 mode by delamination at the edge of a quasi-isotropic CL. To interrogate the delamination, located at the mid-plane of the structure, they carried out the computational as well as the experimental studies. They concluded that the scattering behavior and amplitude remarkably influence by the ratio of flaw size to the wavelength. The interaction of A_0 mode Lamb waves with delamination using finite element simulations have been analyzed by Feng et al. (2018). Lamb waves propagation in a multiple layer laminate was compared with propagations obtained in a delaminated. Based on the comparison of the scattering characteristics between multi-layer laminate and single layer sub-laminate, they proposed a reference-free localization technique for damage identification.

This paper studies the A_0 mode Lamb wave scattering at a subsurface cylindrical flaw in unidirectional composite laminate, focusing on the effect of the fibre direction on the scattering behavior. The exciting features of A_0 mode compared to its counterpart are (i) relatively easy to generate at low frequency, and (ii) shorter wavelength at the entire range of frequency. These leading characteristics of A_0 mode Lamb wave attracted considerable interest in quantitative damage evaluation (Diamanti, 2007; Belanger, 2009; Ng, 2009).

MATERIAL CHARACTERISTICS

Generalized Hooke's Law for anisotropic material can be denoted as

$$[\sigma] = [C][\varepsilon] \quad (1)$$

In the aforementioned equation, the 4th order stiffness matrix [C] defines the behaviour of the material. Unidirectional laminate with 0° fibre direction [Fig. 1] known as the transversely isotropic media and is the building block of composite laminated structures. The engineering constants of each layer is determined by micromechanical modelling (Chamis, 1989) and given as $C_{11}=96.0$, $C_{22}=9.60$, $C_{12}=3.60$, $C_{23}=7.01$, $C_{55}=3.30$ (all values are in GPa).

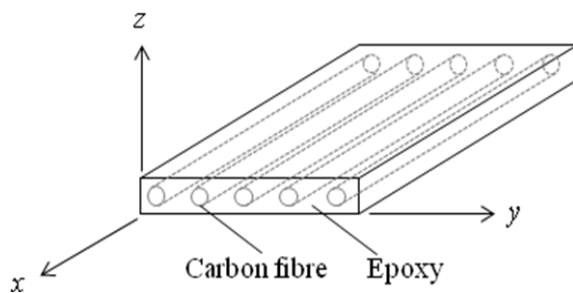


Fig. 1: Orientation of carbon fibre in 0° laminate

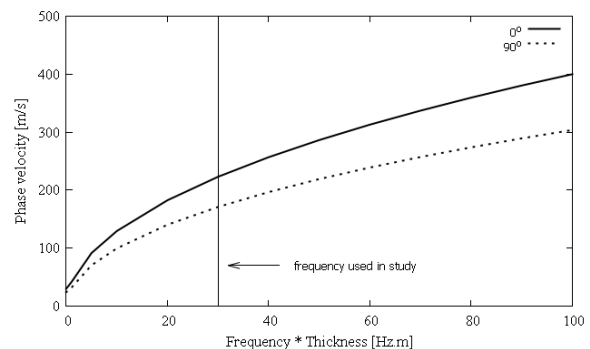


Fig. 2. Theoretically calculated phase velocity dispersion curves for A_0 mode Lamb wave propagating along the fibre axis (solid plot) and the perpendicular direction (dots plot) in HTI material of 1.0 mm in thickness.

Dispersion curve of A_0 mode Lamb wave for such laminate is depicted in [Fig. 2]. In this study, 4 unidirectional laminate with the fibre direction of 0° , 30° , 60° , and 90° is considered. Directional dependence of the phase velocity is a key property of an anisotropic material. To investigate these criteria, the fibre orientation must be transformed to the new coordinate system. Any cartesian coordinate system into a new coordinate system (consider both coordinate system share same origin), is obtained by rotating the coordinate axes through an angle θ about the vertical (z) axis and for a 4th order stiffness matrix $[C]$, transformed components of new stiffness matrix can be formulated by (Bao, 2005):

$$[C'] = [T][C][T'] \quad (2)$$

These transformed components are directly involved to calculate the characteristics of unidirectional laminate with any fibre direction. Based on this criterion a polar diagram is constructed showing the angular dependency of phase velocity will be discussed on the next section.

FINITE ELEMENT MODEL

A 3D FE simulation is conducted to study the propagation of the A_0 mode Lamb wave in a unidirectional laminate with the subsurface cylindrical defect. Generation of the geometry and meshing are done in explicit type software LS-DYNA (LS, 2007) and the simulations were done using the same platform. The laminates considered in this study consisting of the eight-ply unidirectional lamina with a stacking pattern of $[0]_8$, $[30]_8$, $[60]_8$, and $[90]_8$. The density of each lamina is considered 1500 kg/m^3 . The dimension of the model is 6 mm in length and width having 1 mm of thickness where each lamina has a thickness of 0.125 mm. The theoretically calculated wavelengths at the fibre direction and perpendicular to it are 7.36 mm and 5.70 mm respectively. To ensure the number of nodes per wavelength for perfect prediction of wave propagation, a fine mesh with dimension $0.1 \text{ mm} \times 0.1 \text{ mm}$ (20 nodes) is used for the entire model (Alleyn, 1992). The eight-node 3D reduced integration solid brick [Fig. 3] elements with hourglass control are considered to generate the flawless region of the 3D model whereas the surrounding of the cylindrical defect modelled using the combination of six-node wedge element.

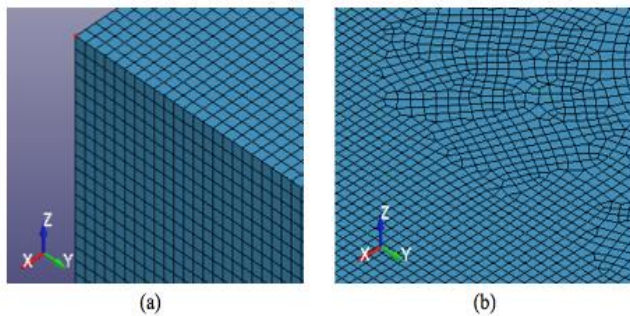


Fig. 3 3D model plate meshing (a) flawless region, (b) surrounding of defected region

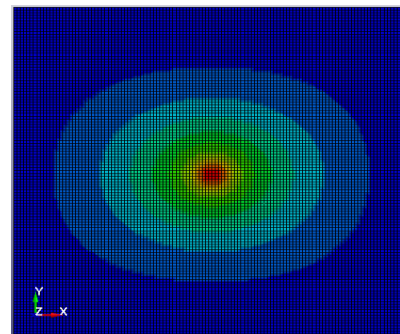


Fig. 4 Wave propagation in $[0]_8$ unidirectional laminate for $f=30 \text{ kHz}$, after $7 \mu\text{s}$ of irradiation

To validate the model for experiment, a sample run carried out in a $[0]_8$ flawless plate allowing the wave propagation from a circular transducer diameter of 0.9 mm source with a frequency of 30 KHz and located at the centre of the model. Contours of normal displacement of the particles taken into account and [Fig. 4] clearly illustrates that the wave frontal profile follows the information considered in this study according to “Eq. 1”. At any particular location, the A_0 mode Lamb wave signal can be obtained by monitoring the normal (z) displacement of the elements located at the mid-section of the 3D model in the vertical direction. This guaranteed that only A_0 mode is detected as the S_0 and SH_0 mode have zero normal displacements at that location. [Fig. 5] illustrates the angular dependence of the A_0 mode Lamb wave phase velocity from the theoretical calculation and FE simulation which resembles good agreement. Each value of the phase velocity is normalized by its maximum value. It can be said that the wave propagation is solely focused the fibre direction of the laminate.

To generate the subsurface laminate, elements are removed from the 3D model and the geometrical configuration considered in this study is illustrated in [Fig. 6]. During the experiment, Lamb wave is excited by applying the 30 kHz mono-cycle tone burst nodal displacement pulse to the surface nodes in the out-of-plane direction at the ‘L’ part of the 3D model. The time step is approximately 100 ns, which

is sufficient to satisfy the conditions for the explicit type of finite difference numerical analysis (Courant et al., 1967). The hourglass energy is found less than 2% of the internal energy for all carried out studies which sufficiently helpful to predict the Lamb wave field accurately. After excitation from the ‘L’ end of the model, Lamb wave strikes at the boundary of the defect, reflection and transmission immediately occurred throughout the entire defected area. Next section will discuss these interactions of A_0 mode Lamb wave with the defect.

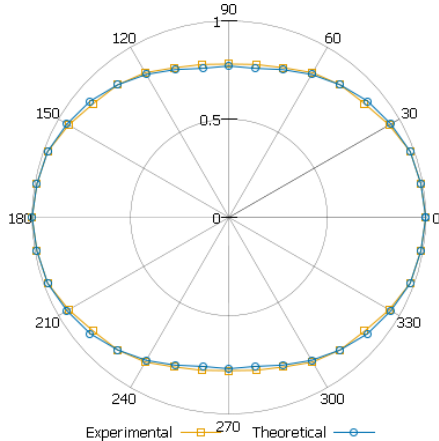


Fig. 5 Angular dependence of phase velocity from theoretical calculation and FE simulations for $\theta = 0^\circ$ at $f=30$ kHz

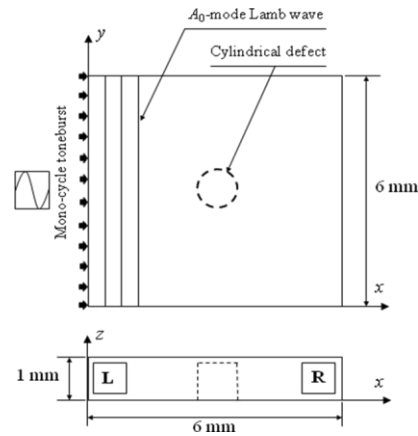


Fig. 6 Geometrical specification of the model used in the FE simulations with the considered coordinate system.

INTERACTION OF LAMB WAVE WITH SUBSURFACE DEFECT

Reflection and Transmission Characteristics

In this subsection, the reflection as well as the transmission characteristics of the A_0 mode Lamb wave at the defect is studied. To measure the reflection, measurement points are taken at the periphery of the defect and $140 \leq \theta \leq 220$ with a 10° interval. In contrast, $0 \leq \theta \leq 30$ and $330 \leq \theta \leq 350$ with the same interval, transmission behavior is measured. [Fig. 7] illustrates the amplitude of the reflection and transmission at the defected region, respectively (values are normalized by the maximum amplitude measured on the surface at that instant). As illustrated in the figure, $[0]_8$ laminate shows the maximum whereas $[90]_8$ laminate shows the minimum amplitude of the reflection and the variation is assumed to be symmetric along the axis passing through the centre of the defect. On the other hand, it is also depicted that $[60]_8$ and $[90]_8$ laminate shows the negative amplitude in case of the transmission and in both cases the $[30]_8$ and $[60]_8$ laminate shows that the amplitude pattern is not symmetric.

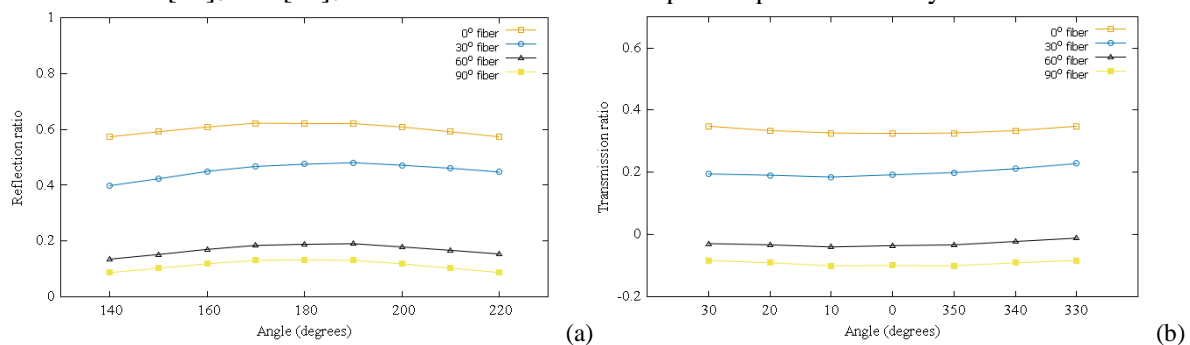


Fig. 7 Amplitude of the (a) reflection and (b) transmission from a subsurface flaw as a function of θ by the interaction of 30 kHz wave (normalized with its maximum value).

Directivity Pattern of the Scattered Wave

This subsection is employed for quantitative analysis of the scattered normal displacement in the vicinity of the defected region for unidirectional laminate through plotting the Directivity Pattern (DP). For DP analysis, the additional out-of-plane displacement due to the interaction of the incident wave is extracted using the baseline subtraction technique. This can be done by conducting two simulations

(each for the defected and intact laminate) with identical meshing. The normal displacement of the scattered wave $u_z^S(x, y, t)$ is evaluated by

$$u_z^S(x, y, t) = u_z^T(x, y, t) - u_z^I(x, y, t)$$

where $u_z^T(x, y, t)$ and $u_z^I(x, y, t)$ are the out-of-plane displacement components at measuring points of a particular time, of the defected and intact laminates, respectively. The pattern is generated by calculating the absolute normalized value taken from the experiment (normalized by maximum absolute amplitude of the incident wave at the defect centre location of the intact laminate). [Fig. 8] depicts the DP of the 30 kHz incident wave at the 1 mm diameter circular subsurface defect. DP for each laminate on the boundary of the defect indicates that there is a definite variation in amplitude almost in every angle. The zero value in [Fig. 8(a)] is quite understandable as in those points; both of the values nullify each other which are also illustrated in [Fig. 7]. Another point of interest to be noted, the DP is not symmetric concerning the 0° direction for the symmetric subsurface defect although it looked like symmetry in [Fig. 7]. This phenomenon is another differentiable criterion of anisotropic material from the isotropic as in case of isotropic material the scattering DP is perfectly symmetric (Cegla et al., 2008). This characteristic suggests that the DP of CL is complicated than that in the isotropic material.

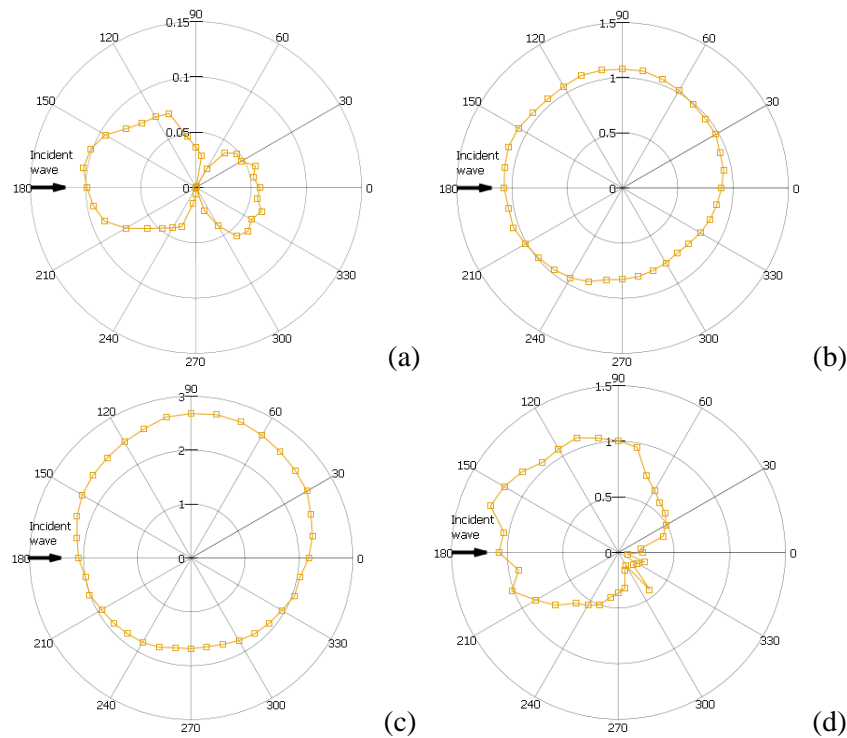


Fig. 8 DP for (a) $[0]_8$, (b) $[30]_8$, (c) $[60]_8$, and (d) $[90]_8$ unidirectional laminates at the boundary of the subsurface defect after interaction with 30 kHz incident wave.

[Fig. 8] displays that with the same geometrical configuration of the subsurface defect, the scattering characteristics are dependent on the fibre direction. The sensitivity of the DPs on the subsurface cylindrical defect demonstrates that scattering behavior in composite laminates is in general much more complicated and fibre direction is playing a significant role on that.

CONCLUSION

This paper investigated the effect of fibre direction on scattering characteristics of the fundamental mode antisymmetric (A_0) Lamb wave at a subsurface cylindrical flaw in unidirectional CL. The details of 3D FE modeling and analysis on the prediction of Lamb wave propagation as well as scattering behavior have been demonstrated concisely. Angular dependence of the phase velocity dispersion curve found by computational study showed quite decent agreement with that from the analytical. Unidirectional laminates with four different fibre directions (0°, 30°, 60°, and 90°) have been

investigated where the shape and size of the defect remained identical. The results depicted that, the amplitude and directivity distribution significantly influenced by the fiber direction. Outcome of the computational study provides the idea of the influence of fibre orientation on the scattering phenomena of A_0 mode Lamb wave at subsurface cylindrical flaw, leads to further development in damage detection technique for CL.

REFERENCES

- Alleyne, DN and Cawley, P. 1992. The interaction of Lamb waves with defects. *IEEE transactions on ultrasonics, ferroelectrics, and frequency control*, 39(3): 381-397.
- Bao, M. 2005. *Analysis and design principles of MEMS devices*. Elsevier.
- Belanger, P and Cawley, P. 2009. Feasibility of low frequency straight-ray guided wave tomography. *NDT & E International*, 42(2): 113-119.
- Cegla, FB.; Rohde, A and Veidt, M. 2008. Analytical prediction and experimental measurement for mode conversion and scattering of plate waves at non-symmetric circular blind holes in isotropic plates. *Wave Motion*, 45(3): 162-177.
- Chamis, CC. 1989. Mechanics of composite materials: past, present, and future. *Journal of Composites, Technology and Research*, 11(1): pp.3-14.
- Chiu, WK.; Rose, LRF and Nadarajah, N. 2017. Scattering of the fundamental anti-symmetric Lamb wave by a mid-plane edge delamination in a fiber-composite laminate. *Procedia Engineering*, 188: 317-324.
- Courant, R.; Friedrichs, K and Lewy, H. 1967. On the partial difference equations of mathematical physics. *IBM journal of Research and Development*, 11(2): 215-234.
- Diamanti, K.; Soutis, C and Hodgkinson, JM. 2007. Piezoelectric transducer arrangement for the inspection of large composite structures. *Composites Part A: Applied science and manufacturing*, 38(4): 1121-1130.
- Feng, B.; Ribeiro, AL and Ramos, HG. 2018. Interaction of Lamb waves with the edges of a delamination in CFRP composites and a reference-free localization method for delamination. *Measurement*, 122: 424-431.
- Guo, N and Cawley, P. 1993. The interaction of Lamb waves with delaminations in composite laminates. *The Journal of the Acoustical Society of America*, 94(4): 2240-2246.
- Hai-Yan, Z.; Jie-Cong, Y.; Rui, W and Shi-Wei, M. 2014. S_0 Lamb Wave Scattering from a Cylindrical Inhomogeneity in a Transversely Isotropic Composite Plate. *Chinese Physics Letters*, 31(8): 084301.
- Hai-Yan, Z.; Jian, X and Shi-Wei, M. 2015. High-Frequency Guided Wave Scattering by a Partly Through-Thickness Hole Based on 3D Theory. *Chinese Physics Letters*, 32(8): 084301.
- Hayashi, T and Kawashima, K. 2002. Multiple reflections of Lamb waves at a delamination. *Ultrasonics*, 40(1-8): 193-197.
- Lowe, MJ.; Cawley, P.; Kao, JY and Diligent, O. 2002. The low frequency reflection characteristics of the fundamental antisymmetric Lamb wave a_0 from a rectangular notch in a plate. *The Journal of the Acoustical Society of America*, 112(6): 2612-2622.
- Manual LD, Volume I. Version 971.2007. Livermore Software Technology Corporation. May;7374:354.
- Moreau, L and Castaings, M. 2008. The use of an orthogonality relation for reducing the size of finite element models for 3D guided waves scattering problems. *Ultrasonics*, 48(5): 357-366.
- Ng, CT and Veidt, M. 2009. A Lamb-wave-based technique for damage detection in composite laminates. *Smart materials and structures*, 18(7): 074006.
- Rose, JL. 2002. A baseline and vision of ultrasonic guided wave inspection potential. *Journal of pressure vessel technology*, 124(3): 273-282.
- Singh, RK.; Ramadas, C.; Shetty, PB and Satyanarayana, KG. 2017. Identification of delamination interface in composite laminates using scattering characteristics of lamb wave: numerical and experimental studies. *Smart Materials and Structures*, 26(4): 045017.
- Soleimanpour, R and Ng, CT. 2015. Mode conversion and scattering analysis of guided waves at delaminations in laminated composite beams. *Structural Monitoring and Maintenance*, 2(3): 213-236.

SALINITY REMOVAL AND FEASIBILITY STUDY ON SEA SAND IN GEOPOLYMER CONCRETE

S. Sarker^{1*}, M. M. Islam¹ & R. Hasan¹

¹*Department of Civil Engineering, Chittagong University of Engineering and Technology, Chittagong-4349, Bangladesh.
E-mail: s.sarkerce@gmail.com*

**Corresponding Author*

ABSTRACT

The rapid growth in the expansion of the construction work is leading to a depletion of natural resources like river sand. This overuse should be balanced by introducing certain abundantly available other natural materials which can replace the river sand. On the other hand, the production of every ton of cement contributes to the production of one ton of CO₂. The coal-based power plant produces a huge amount of fly ash that creates disposal problems but at the same time, it can be utilized as a partial substitution of cement. The alkali-activated fly ash concrete (Geopolymer Concrete) shows considerable promise for application in the construction industry as an alternative to OPC. In this experimental work, the chloride content of sea sand from different region of Chittagong & Cox's Bazar is determined and its removal techniques are discussed. The sea sand (washed and unwashed) has been used as an alternative to river sand and strength properties of OPC and geopolymer concrete are studied. The results show that washed sea sand gives satisfactory strength compared to river sand in case of OPC. Unwashed sea sand affects the compressive strength in OPC concrete but gives similar results as of washed sea sand in geopolymer concrete.

Keywords: Geopolymer Concrete, Fly Ash, River Sand, Sea Sand, Chloride content etc.

INTRODUCTION

The annual Cement consumption of Bangladesh was 27.1 million tons in 2017. This means that every year more than 20 million tons sand and rock are used. River sand has been widely used in the production of concrete in Bangladesh. However, river sand is expensive. Its cost of transportation to construction sites and excessive erosion associated with excavation from the natural sources are additional burdens. Large-scale depletion and over consumption of naturally occurring building material have also indirectly created numerous environmental problems. Therefore, it is an immediate requirement to seek an alternative to river sand in production of concrete. Available alternative fine aggregate resources for producing concrete in Bangladesh are coastal sand or sea sand from different coastal beach of Cox's bazar and Chittagong side. Due to large scale availability, ease of extraction and low cost, sea sand has the greatest potential to replace river sand as an alternative. The chloride ion present in the sea sand makes its application potentially threatening to the durability of concrete structures. Therefore, it is important to remove chloride ions from the sea-sand by washing them either natural rainfall or artificial washing plants prior to use for the concrete. Besides the chloride problem, consumers are much concerned about shell contents and textural suitability of sea sand. Therefore, sea sand usage in Bangladesh is limited and only rarely used for concrete work. This study examines the suitability of sea sand as an alternative fine aggregate for the river sand in concrete production by reducing salt concentration within the permissible value & by increasing its strength with the help of geopolymer concrete.

In Bangladesh, one of the major sources of material for power generation is coal and its by-product- fly ash- is an environmental threat to the public, if not disposed of properly. Therefore the safe disposal of

fly ash is still a major concern. So, the use of geopolymer concrete with fly ash as aluminosilicate material not only helps to reduce the release of CO₂ emission (by reducing the production of cement), but also effectively disposes off fly ash, an industrial waste produced in large quantities.

The sea sand is available in abundant quantity but due to presence of salt and chloride it can't be used as fine aggregate in concrete as the salt and chlorides both affect the strength and durability of Portland cement concrete. But in geopolymer concrete the case is different. In cement concrete the reaction is hydration and in geopolymer concrete the reaction is polymerization. The nature of these two reactions is not same. The work is carried out to study the effect of treated and untreated sea sand in cement concrete as well as geopolymer concrete. The present research work also focuses on the influence of geopolymer concrete using sea sand, both at ambient temperature and after exposure to elevated temperatures, and makes a comparison of strength with the concrete made with river sand.

METHODOLOGY

Based on the literature study, the research was done in two phases:

Phase 1: Salinity Concentration of local sea sand and salt removal techniques:

Aggregate properties such as grading and dry density, along with determination of soluble chloride content in sea sand were carried out. Leaching, Retained water washing test, simulated rain test and influence of temperature were conducted to study the salinity removal characteristics (Samraj and Nagarajan, 2013).

Phase 2: Strength development characteristics of concrete made with sea sand

100 mm cubical OPC Concrete and Geopolymer Concrete specimens were incorporated with Alkali activator (Sodium Hydroxide flakes and Sodium Silicate solution) and Fly Ash as a partial replacement of cement were cast. Washed and unwashed sea sand was used in this process. Some concrete cubes were also cast using River sand for comparison. The 100 mm concrete cubes were cast for compressive strength test at 1, 7, 28 and 90 days. Temperature curing was followed for geopolymer concrete whereas for OPC cubes water curing was done (Shinde & Kadam, 2016).

MATERIALS

SEA SAND

Samples were collected from five different coastal regions of Chittagong – Guliakhali, Bashbaria, Potenga and Parki sea beach and also from Kolatoli point, Cox's Bazar. Sample was collected in wet state and it was dried in Oven before determining the parameters.

FLY ASH

Fly ash was obtained from Premier Cement Mills limited, Chittagong, Bangladesh. From this **Table 1** it could be observed that, the fly ash has low calcium content. In this experiment 0%, 20%, 40%, 60% of fly ash is used as a partial replacement of cement in geopolymer concrete cube preparation.

Table 1: Chemical composition of Fly ash (Mass %)

SiO ₂	Al ₂ O ₃	Fe ₂ O ₃	CaO	Na ₂ O	TiO ₂	MgO	Mn ₂ O ₃	SO ₃	Loss of ignition
60.78	28.36	4.57	2.1	0.04	1.82	0.83	0.04	0.40	1.06

ALKALINE ACTIVATORS

In geopolymer concrete, to activate the fly ash, a combination of sodium hydroxide solution and sodium silicate solution was chosen as the alkaline activator. NaOH pellets of 98% purity and the Na₂SiO₃ solution had 34.64% SiO₂, 16.27% Na₂O, and 49.09% water. Sodium silicate relative density was 2.13gm/cm³. The sodium hydroxide (NaOH) solution was prepared by dissolving either the flakes or the pellets in water. In this experiment 35% of alkaline activators with respect to binder was used.

CEMENT

The properties of cement used in this experiment are given in **Table 2**.

Table 2: Physical properties and Chemical composition of cement

Blaine's Specific surface (cm ² /gm)	Normal Consistency	Specific gravity	Setting Time (min)		28 days Compressive Strength (MPa)
			(a) Initial	(b) Final	

3500	26%	3.15	70	175	30.4
CaO	SiO ₂	Al ₂ O ₃	Fe ₂ O ₃		
64%	21%	6%	3.50%		

AGGREGATES

Coarse aggregate with nominal sizes of 12.5 mm were used. Fine aggregates were used in the form of River sand from Fatikchori and Sea sand from Kolatoli point. Aggregates were prepared in saturated-surface-dry (SSD) condition to avoid the absorption of the alkaline solution by the aggregates which reduce the polymerization of the fly ash. **Table 3** shows the physical properties of aggregates

Table 3: Physical properties of aggregates

Properties	Coarse Aggregate	Fine Aggregate (River sand)	Fine Aggregate (Sea sand)
Specific Gravity	2.59	2.35	2.56
Unit Weight	1560 kg/m ³	1580 kg/m ³	1612kg/m ³
Fineness Modulus	6.77	2.57	1.17

SOLUBLE CHLORIDE CONCENTRATION DETERMINATION

The amount of chlorides present in the sea sand was determined using Silver Nitrate method (Karthikeyan and Nagarajan, 2017). First 50 grams samples of each location were immersed in 100 mL water separately. Then 25 mL solutions for each sample were used to titrate with 0.0141N Silver Nitrate solution. Silver Nitrate reacts with chloride ions to form Silver Chloride. The completion of reaction was indicated by the red colour produced by the reaction of Silver Nitrate with Potassium chromate solution which was added as an indicator. The reduction of soluble Chloride concentration of sand after washing was also determined by the same method. **Fig.1** displays the Experimental Setup for determination of soluble chloride in sand



Fig.1: Experimental Setup for determination of Soluble Chloride in sand

SOLUBLE CHLORIDE REMOVAL TECHNIQUE

LEACHING TECHNIQUE

After determining the initial chloride concentration of different samples collected from various sources, (Parki, Potenga, Cox's Bazar-Kolatoli point), sand samples having higher Chloride concentration were taken for Chloride removal. 500 grams sample of each source were taken in separate 5L volume container filled with normal water. They were retained in a large tank having 140 L capacity. The whole tank was filled with water.

SIMULATED RAIN TECHNIQUE

Fresh water was allowed to pass through the sand which leached out water soluble Chloride and Chloride content was measured after every 30 minutes time intervals. In this process, sample was kept in a tank of space area 63cm X 63cm. It was washed with water having a controlled flow of 1.60cm³/hr that resembles with the normal rainfall intensity in Bangladesh during Monsoon. Samples were collected after 30 minutes time interval up to 2 hours simulated rain and Chloride concentration was measured by Silver Nitrate Method. Cox's Bazar Kolatoli Point sand has the highest soluble Chloride concentration and also the highest Chloride removal rate in Leaching technique. So Simulated rain washing was only done for the sand collected from Cox's Bazar Kolatoli Point.

RETAINED WASHING TECHNIQUE

Sand collected from Cox's Bazar Kolatoli point was immersed in full depth of water in a tank of 140L capacity. Samples were collected at each day interval and continued for 3 days.

BOILED WATER WASHING TECHNIQUE

5L water was added to 500 grams untreated sand in a pan. Solubility is a property that is affected by temperature, so more salt dissolves in hot water than cold water. The water was heated until the salt present in sand dissolved. Then salt water was poured into a separate container and Chloride concentration of sand was measured by Silver Nitrate Method.

PREPARATION OF ALKALI SOLUTIONS

The NaOH solution was first prepared at the required molarity of 12M. For this, 12X40=480 grams Sodium Hydroxide flakes are dissolved in 1 litre water. The exothermic reaction was continued for some time. 30 minutes before casting, sodium silicate was added and thoroughly mixed.

CASTING & CURING OF GEOPOLYMER CONCRETE SPECIMENS

Coarse and fine aggregates in saturated surface dry condition were well mixed with required percentage of fly ash and cement in a pan mixture. Premixed alkaline activator solution was then added gradually in the mixer. Mixing was continued for further 4-6 minutes. All geopolymer concrete specimens were cast using standard molds of 100 mm cubical shape. The geopolymer concrete was compacted in 3 layers with the help of a tamping rod. The fresh fly ash-based geopolymer concrete was dark in color and shiny in appearance. Samples were demolded 72 hours after casting. Three different curing approaches are adopted for the samples (Hardjito et al., 2004; Wallah and Rangan, 2006). Some are left in 28-35°C for air curing until testing and some are kept under water for water curing. Dry air curing at elevated temperature of 60°C for one day was adopted for the rest of the sample

RESULTS AND DISCUSSIONS

SALINITY REMOVAL

The result of Chloride ion removal varies with collected sand location. **Table 4** shows the initial Chloride ion concentration was maximum (1320 ppm) for raw sand collected from Cox's Bazar-Kolatoli point. **Table 5** shows the highest Chloride ion removal rate and lowest concentration of Chloride ion after treatment (29 ppm) for this sand. This sand was used for the following salinity removal techniques.

Table 4: Salinity concentration of sand collected from different coastal region

Source	Parki	Guliakhali	Potenga	Bashbaria	Cox's Bazar (Kolotoli)
Conc. In ppm	610	478	726	99	1320

Table 5: 1st, 2nd & 3rd Leaching data of 500gm sand sample (using Normal water):

Source	Raw sample conc. in ppm	1 st wash (4 days)	2 nd wash(8 days)	3 rd wash (22days)
Parki	610	87	76	34
Potenga	726	75	61	40
Cox's Bazar	1320	66	52	29

In leaching technique, 500 grams samples were taken in circular 5L oil container separately. Retained water washing result was analogous to Leaching technique using normal water. But the tank used in retained water washing had a surface area almost 30 times greater than that of circular oil container used in leaching technique. So with the increase of surface area of washing, salinity removal at a high rate was achieved. This is because of larger surface area coming in contact with water in retained water washing technique. For simulated rain technique, a 2 hours continuous rainfall in Monsoon shows better salinity removal than all other retained washing processes. Because of continuously washing away the water, the solubility of Chloride ion was always less than its solubility limit in water. As a

result, more Chloride ion got dissolved in continuous washing than retained water washing process. In endothermic reaction, increasing temperature increases the solubility of the solute. Therefore, lowest of all Chloride ion concentration has been achieved only after 3 times washing of sea sand sample with boiled water. A maximum 99% chloride ion has been removed in this process. **Table 6** shows the final chloride ion content for various methods.

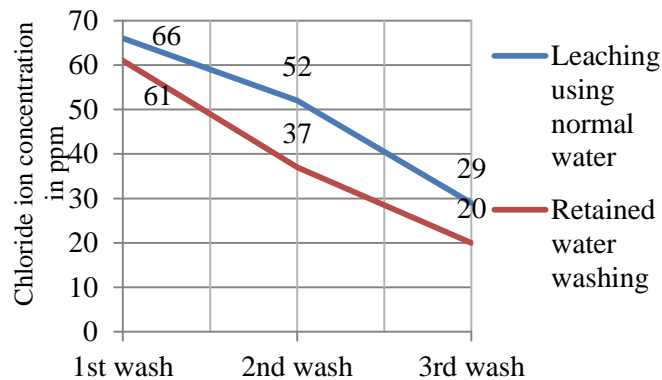


Fig. 2: Influence of surface area in Chloride ion removal.

Table 6: Final Chloride ion content of 500 grams sand sample

Method	Leaching	Retained water washing	Simulated rain washing	Boiled water washing
Final Cl ⁻ conc. in ppm	29	20	15	13

COMPRESSIVE STRENGTH

Results of compressive strength of cement concrete and geopolymer concrete are presented in **Table 7**, and the graphical variation is shown in following **Fig.3, 4 and 5**

Table 7: Details of Mix and Compressive Strength

Notation	Types of curing	Fly Ash (%)	28 days Comp. Strength (MPa)	Types of curing	1 day Comp. Strength (MPa)
B1RSF00(OPC)	Water	--	31.2		
B2TSSF00(OPC)	Water	--	27.2		
B3USSF00(OPC)	Water	--	25.8		
B4TSSF20(GP)	Ambient temp.	20	26.4	Temp. curing at 60°C	25.9
B5TSSF40(GP)	Ambient temp.	40	27.0	Temp. curing at 60°C	26.8
B6TSSF60(GP)	Ambient temp.	60	26.6	Temp. curing at 60°C	29.8
B7USSF20(GP)	Ambient temp.	20	25.1	Temp. curing at 60°C	24.5
B8USSF40(GP)	Ambient temp.	40	26.4	Temp. curing at 60°C	26.3
B9USSF60(GP)	Ambient temp.	60	26.5	Temp. curing at 60°C	29.1

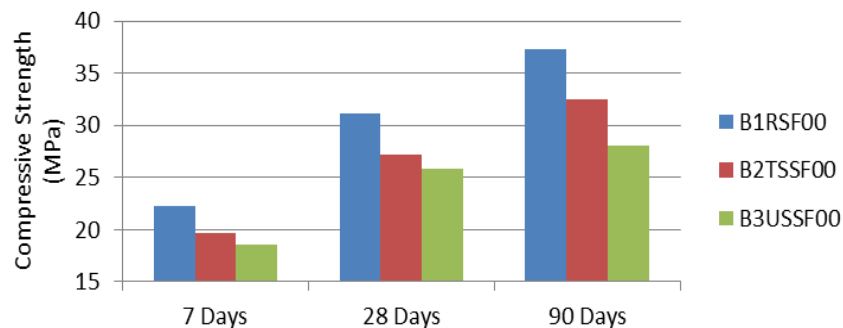


Fig. 3: Comparison of OPC concrete compressive strength results in Water curing using river sand, treated and untreated sea sand.

Ordinary Portland Cement concrete strength using river sand (RS) is always greater than the strength using treated (TSS) and untreated sea sand (USS). The lowest compressive strength is seen for OPC

concrete using untreated sea sand and the most important fact is that, as time goes on, the difference in strength between treated and untreated sea sand becomes more and more.

From **Table 7**, it can be said that with the increase of Fly ash content from 40 to 60%, 1 day elevated temperature curing strength of geopolymer cube has become greater than 28 days ambient temperature curing strength for both Treated (B6TSSF60) and untreated sand geopolymer concrete (B9USSF60). For other batches, with lower Fly ash content 28 days ambient temperature curing strength is quite similar to 1 day elevated temperature curing strength.

Variation of strength between Ordinary Portland Cement and Ambient temperature cured Geopolymer Concrete having varying percentage of Fly ash (20%, 40% and 60%) are shown in **Fig.4** and in **Fig.5**. For 20% Fly ash geopolymer concrete, the early strength is a little smaller than that of Ordinary Portland Cement concrete but greater than 40 and 60% Fly ash geopolymer concrete. Though early strength was smallest, 90 days strength is the greatest for 60% Fly ash geopolymer concrete. The difference in 90 days strength between 20% Fly ash containing geopolymer concrete with treated sea sand (B4TSSF20) and OPC with treated sand (B2TSSF00) is 2.9 MPa. This difference has increased to 6.8 MPa when 60% Fly ash containing geopolymer concrete is used. So, with the increase of Fly ash content, the strength becomes higher and higher than the Ordinary Portland Cement concrete in the long run.

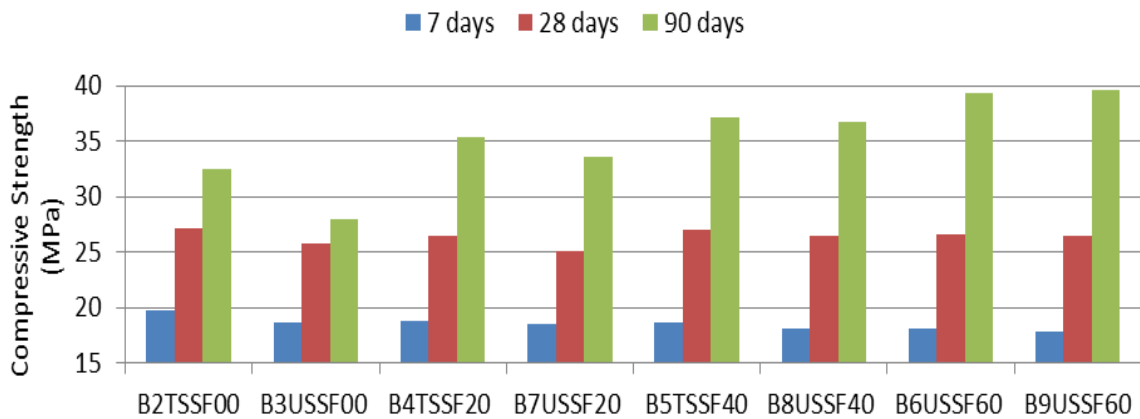


Fig. 4: Comparison of Compressive strength of OPC and Geopolymer Concrete with 20, 40 & 60% FA

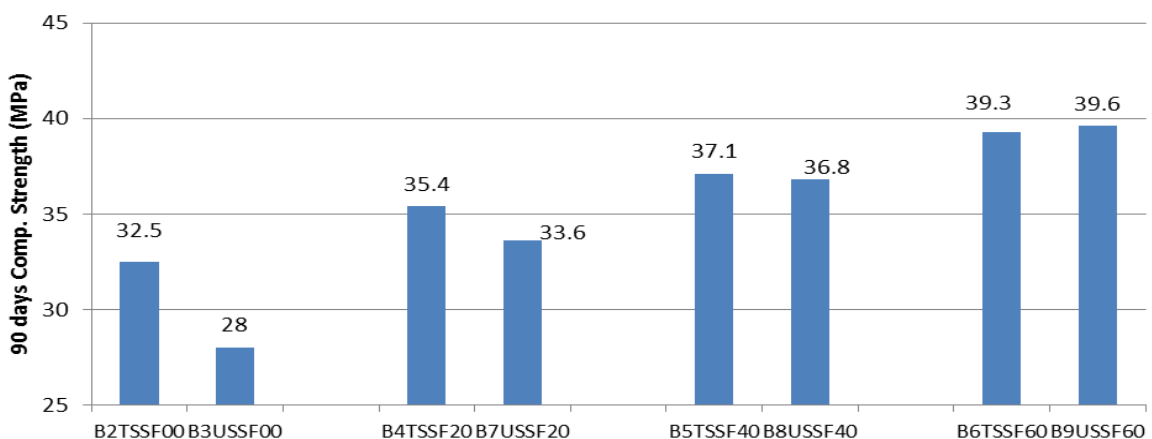


Fig.5: Comparison between 90 days compressive strength results

For OPC concrete specimens made from treated sand obtained by washing showed better performance than concrete specimens using untreated sea sand. The strength of OPC concrete with river sand

(B1RSF00) is 4.8 MPa higher than that with Treated sea sand (B2TSSF00).

This difference has increased to 9.3 MPa when unwashed sea sand is used (B3USSF00). So, washing sea sand before using is recommended to improve the strength of OPC concrete. The difference in variation of strength using Treated and Untreated sea sand gets reduced with increasing Fly ash content in geopolymer concrete. And the most important observation is that, for 60% fly ash content untreated sea sand showed better strength performance than the treated one. Even 90 days treated sea sand contained OPC concrete (B2TSSF00) strength is smaller than untreated sea sand contained geopolymer concrete. If only strength is considered, geopolymer concrete is a better approach than treated sea sand containing OPC concrete (**Ref. Fig.5**)

CONCLUSIONS

Based on the variables considered, experimental techniques and results, the conclusions can be summarized as follows:

- (i) The chloride ion removal rate depends on the collected sea sand source. Removal rate depends largely on the surface area of tank and not much affected by retention period. Larger surface area shows better removal rate even having lower retain period. A maximum 99% chloride ion was removed by boiled water washing techniques.
- (ii) Treated sea sand shows better strength performance than untreated sea sand in OPC concrete. With the increase of curing period and Fly ash percentage, strength increment rate for geopolymer concrete is higher than OPC.
- (iii) Considering strength only, geopolymer concrete shows better performance than treated sea sand in OPC concrete.
- (iv) Chloride ion removal rate using continuous washing rain is satisfactory and also becomes economic if rain water can be utilized. Stockpiling of sea sand in an open space before Monsoon is an effective process for salinity removal (Ratnayake et al., 2014). An onshore washing plant can be established, for large scale production.
- (v) The chloride content can be removed by continuous washing combined with the use of warm water to make de- salting more effective.

REFERENCES

- Hardjito, D; Wallah, SE; Sumajouw, MJ and Rangan, BV. 2004. *The Compressive Strength of Fly Ash Based Geopolymer Concrete*. Research Gate.
- Karthikeyan, M and Nagarajan V. 2017. *Chloride Analysis of Sea Sand for making Concrete*. Springer.
- Ratnayake, NP; Puswewala, UGA; Chaminda, SP; Ekanayaka, EMTM and Jayawardene, MN. Evaluation of the Potential of Sea Sand as an Alternative to River Sand for Concrete Production in Sri Lanka, *Journal of Geological Society of Sri Lanka*, 16: 109-117.
- Samraj, P and Nagarajan, V. 2013. Sea Sand as Fine Aggregate for Concrete Production, *National Symposium for Recent Trends in Civil Engineering*, P.S.G college of Technology, Coimbatore, India.
- Shinde, BH and Kadam, DKN. 2016. Strength Properties of Fly Ash Based Geopolymer Concrete with Sea Sand. *American Journal of Engineering Research (AJER)*, 5(7): 129-132.
- Wallah, SE and Rangan, BV. 2006. *Low-Calcium Fly Ash-Based Geopolymer Concrete: Long-Term Properties*. Research Report GC 2, Faculty of Engineering, Curtin University of Technology, Perth, Australia.

AN EXPERIMENTAL INVESTIGATION ON IMPROVEMENT OF CONCRETE STRENGTH USING BACTERIAL APPROACH

M.S. Islam^{1*}, T. Sinha², M.S. Islam³ & M.K Uddin⁴

¹Department of Civil Engineering, Chittagong University of Engineering and Technology, Chittagong, Bangladesh. E-mail:msislam.cuet@gmail.com

²Department of Civil Engineering, Chittagong University of Engineering and Technology, Chittagong, Bangladesh. E-mail:tsinha@mun.ca

³Department of Civil Engineering, Chittagong University of Engineering and Technology, Chittagong, Bangladesh. E-mail:msislam@cuet.ac.bd

⁴Department of Microbiology, Chittagong University, Chittagong, Bangladesh. E-mail:kamal.mbio@cu.ac.bd

*Corresponding Author

ABSTRACT

Concrete is an absolutely essential element of infrastructure throughout the world. Concrete though is able to carry high compressive load but very weak in case of tensile forces, for which steel bars are embedded in the concrete. Again, cracks are inevitable in concrete that allows the ingress of corrosive materials and consequently deterioration of the structural concrete starts with the corrosion of embedded steel. This leads to the reduction in strength and durability of concrete. The aim of the study is to investigate the performance of bacterial concrete. Concrete specimens of 100 mm cubical size were cast and cured for different ages in plain water to study the strength aspect of bacterial concrete. Concrete specimens having different bacterial concentrations have been studied. From the investigation it is found that concrete specimens containing bacterial species show better performance than the identical conventional concrete. Among them, concrete specimens of bacterial concentration 6.39×10^8 cells/ml showed better result regarding strength development due to microbial activities in concrete.

Keywords: *Bacillus subtilis*; Compressive Strength; Tensile Strength; Microbial Concrete; MICP

INTRODUCTION

Concrete is the most essential element that is an absolutely ingredient component of public infrastructure including most of the buildings. It can get destroyed for a variety of reasons including the material limitations, design gap and construction practices, as well as exposure conditions. The durability of concrete is related to the characteristics of its pore structures. The more open the pore structure, the more vulnerable the material is liable to degradation mechanism caused by penetrating substances.

A major concern to concrete is that it is subjected to cracking due to its relatively low tensile strength (Wiktor & Jonkers, 2011, Khaliq et al, 2016). Various mechanisms could cause the formation of concrete cracks, e.g. tensile and compressive forces, freeze-thawing reactions and shrinkage. The presence of cracks not only reduces the strength of concrete and hampers the structural integrity and durability of material but also makes concrete particularly vulnerable to a deleterious environment (Jonkers & Schlangen, 2007).

Aiming to extend the service life of concrete structures, various man-made repairs have been developed; these approaches mainly followed a procedure of monitoring, detection and repairing. When cracks are detected in concrete, repairing agents are normally applied to the outside and they gradually penetrate

to the cracks. It is generally known that man-made repairs are mostly applicable to repair the large cracks. However, these repairs usually have relatively high operation costs and it is particularly difficult to repair small and deep cracks (Wang et al, 2012, Muhammad et al, 2016). In addition, it is difficult for the implementation of continuous-time inspection and maintenance, especially in the case of underground concrete structures and large scale construction and infrastructures (Xu & Yao, 2014). Therefore, in order to timely improve the strength and durability of concrete, once cracks appear, an innovative and promising approach is to implement automatic repair, i.e the Microbiologically Induced Calcite Precipitation (MICP) approach.

When a concrete structure is damaged, water starts to seep through the cracks due to the ingress of water and nutrients and the bacteria go to the active state from dormant state. Then the spores of the bacteria germinate and the bacteria start to feed on the calcium lactate. As the bacteria feed, oxygen is consumed and the soluble calcium lactate is converted to insoluble limestone (CaCO₃). The limestone solidifies on the cracked surface and the cracked surfaces are sealed up. Tests have shown that when water seeps into the concrete, the bacteria germinate and increase their concentration by binary process. They convert the nutrients into limestone within seven days as per laboratory investigation. The calcification process takes several weeks in lower temperature.

In this study, spores of specific alkali-resistance bacteria related to genus *Bacillus* are added to the concrete mixture. This study shows a significant increase in strength due to the addition of bacteria.

METHODOLOGY

2.1 Materials

2.1.1 Bacteria used for the investigation: *Bacillus subtilis* ATCC-6633 was utilized as an experimental bacterium in this investigation. This bacterium was supplied from the Department of Microbiology, University of Chittagong. *Bacillus subtilis* is a Gram-positive and catalase-positive bacterium, commonly found in soil. The cells are typically rod-shaped and are about 4-10 micrometers (µm) long and 0.25–1.0 µm in diameter. With other members of the genus *Bacillus*, it can form an endospore to survive extreme environmental conditions of temperature and desiccation. It is considered as an obligate aerobe and *B. subtilis* is found to be alive at -3°C low temperature to 70°C high temperature. The detail of its temperature sustainability is summarized in **Table 1**.

Table 1: *Bacillus subtilis* bacteria temperature sustainability test

Temperature	-3°C	10°C	20°C	30°C	40°C	50°C	60°C	70°C	80°C	90°C
Bacteria alive condition	Alive	Alive	Alive	Alive	Alive	Alive	Alive	Alive	Alive	Dead

2.1.2 Cement: Ordinary Portland Cement (OPC) ASTM Type-1, conforming to ASTM C-150 was used as binding material. Its physical properties and chemical compositions are given in **Table 2**.

Table 2: Physical properties and chemical composition of OPC

Serial No	Characteristics	Value
1	Blaine's Specific surface (cm ² /gm)	2900
2	Normal Consistency	26%
3	Soundness by Le Chatelier's Test (mm)	4.5 mm
4	Specific gravity	3.15
5	Setting Time	
	(a) Initial (min)	70
	(b) Final (min)	175

2.1.3 Aggregates: Locally available natural sand passing through 4.75 mm sieve and retained on 0.075 mm sieve was used as fine aggregate. The coarse aggregate was crushed stone with a nominal size of 12.5 mm. Physical properties of the aggregate are given in **Table 3**.

Table 3: Physical properties of aggregates

Properties	Coarse Aggregate	Fine Aggregate
Specific Gravity	2.59	2.55
Unit Weight	1560 Kg/m ³	1580 Kg/m ³
Fineness Modulus	6.77	2.57
Absorption Capacity	0.6%	1.45%
Moisture Content	0.57%	1.12%

2.1.4 Water: Water conforming to the requirement of IS456-2000 was used with p^H value 7 and at zero turbidity.

2.2 Variables

2.2.1 Concrete quality: Two different grades of microbial concrete having bacterial concentration of 2.12×10^8 cells/ml, 2.12×10^7 cells/ml, 3.25×10^8 cells/ml, 3.25×10^7 cells/ml, 6.39×10^8 cells/ml, 6.39×10^7 cells/ml, 7.91×10^8 cells/ml and 7.91×10^7 cells/ml were used. Control concretes of similar grades were cast for comparing its properties with that of microbial concrete.

2.2.2 Exposure period: Specimens were tested periodically after the specified curing period of 28 days in plain water.

2.2.3 Size of Specimens: 100 mm x 100 mm x 100 mm cube specimens were prepared following ASTM standard procedure.

2.2.4 Curing environment: A total of 850 concrete specimens were cast in the laboratory. After casting, the specimens were kept at 27°C temperature and 90% relative humidity for 24 hours. After demoulding, all the specimens were cured in plain water for different curing ages at room temperature.

2.2.5 Specimen preparation: 100 mm x 100 mm x 100 mm cube specimens were prepared following ASTM standard procedure. Mixed design was carried out following ACI guidelines that was based on material properties. Required amount of microorganisms with media were mixed and added to concrete matrix. All specimens are cured in plain water for different exposure periods. **Table 4** shows the details of concrete mix design.

Table 4: Mix ratios for specimen preparation

Designed Strength	Cement	Fine aggregate	Coarse aggregate	w/c ratio
20 MPa	1	2.56	2.71	0.592
40 MPa	1	1.28	1.73	0.38

2.3 Test procedures:

2.3.1 Compressive strength test: After specific curing, strength tests were performed using compression testing machine. Compressive strength and tensile strength of concrete is defined as the

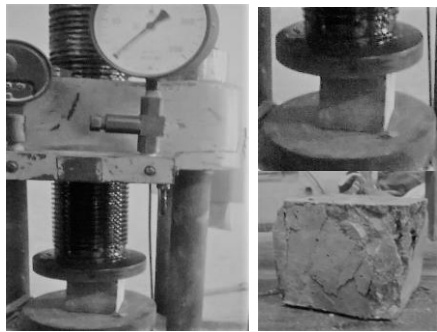


Figure 1: Compressive strength test performed by applying a true line load along the top and bottom face of the specimen. To prevent very high local compressive stresses at the load line, narrow strips of relatively soft material such as hard

load which causes the failure of a standard specimen divided by the area of cross section under uniaxial compression load at a given rate (7 KN/sec). 100 mm x 100 mm x 100 mm cube specimens were placed in the compressive testing machine as shown in **Fig.1**. The load was applied gradually at a constant rate and ultimate load was noted down for each specimen. The average stress value of 5 test specimens was considered as representative strength.



Figure 2: Tensile strength test

2.3.2 Tensile Strength test: Tensile strength of concrete is calculated through indirect tension test known as Splitting Tension Test. This test was performed by applying a true line load along the top and bottom face of the specimen. To prevent very high local compressive stresses at the load line, narrow strips of relatively soft material such as hard board or ply wood are interposed between the specimen and the plate (Ref. Fig-2). Under this condition due to a high horizontal compressive stress at the top and bottom of the specimen, failure is initiated by the horizontal uniform tensile stresses acting over the remaining cross section of the cubes. In this test the load was applied at a constant rate of increase in tensile stress of 0.02-0.04 MPa/sec. The tensile splitting strength was calculated by using the following equation:

$$\text{Tensile Strength} = \frac{2P}{\pi a^2} \quad (1)$$

Here,

P= Maximum load carried by the specimen during test

a= side of the cube

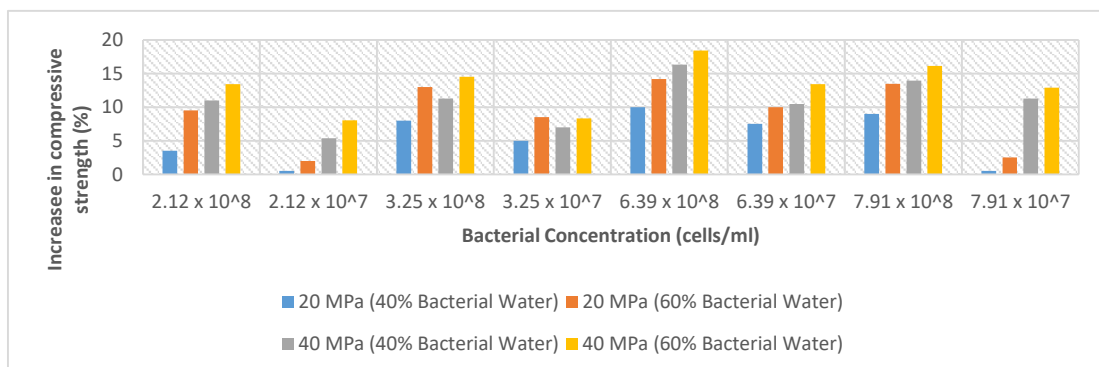
RESULTS AND DISCUSSIONS

Compressive Strength Test Results:

The test results for both control and microbial concrete specimens were analysed critically to observe the variation of concrete strengths between normal and bacterial concrete. It is seen that, for each curing periods, the strength of microbial concrete is higher than that of control concrete. The (%) increase in strength of microbial concrete after 28 days exposure period are shown in **Table 5 and 6**.

For compressive strength test, **Table-5** represents the variation of compressive strength as compared to control concrete at 28 days curing period. From table, it is clear that the compressive strength for all bacterial concrete is higher than control concrete and for the bacterial concentration 6.39×10^8 cells/ml, the maximum increase in strength was observed. The **Fig.3** illustrates graphical representation for the increase in compressive strength as compared to control concrete.

Table 5: % Increase in compressive strength as compared to control concrete (28days)



Bacterial Conc (cells/ml)	Increase in compressive strength (%)			
	20 MPa (40% Bacterial Water)	20 MPa (60% Bacterial Water)	40 MPa (40% Bacterial Water)	40 MPa (60% Bacterial Water)
2.12×10^8	3.5	9.5	11.02	13.44
2.12×10^7	0.5	2	5.38	8.06
3.25×10^8	8	13	11.29	14.52
3.25×10^7	5	8.5	6.99	8.33
6.39×10^8	10	14.2	16.35	18.44
6.39×10^7	7.5	10	10.48	13.44
7.91×10^8	9	13.5	13.98	16.13
7.91×10^7	0.5	2.5	11.29	12.9

Figure 3: Increase in compressive strength as compared to control concrete (28 days)

Tensile Strength Test Results:

Similarly, from **Table 6**, for tensile strength test results, the increase of the tensile strength is observed to be higher for all bacterial concrete group as compared to control concrete. In this case, it is also found that 6.39×10^8 cells/ml is the optimum value that provide highest increment as compared to other bacterial groups.

The Fig.4 illustrates the graphical presentation of the increase in tensile strength of microbial concrete over controlconcrete. From the above tables and figures, it is clear that (%) increase in both the strengths i.e. compression as well as tensile one are relatively higher in higher grade concrete (M40) as compared to lowre grade concrete (M20) that ranges from 2 to 10%. Moreover, among all the microbial groups, concrete specimens made with bacterial concentration of 6.39×10^8 cells/ml showed the maximum increase in strength which is around 10 to 18% at 28 days of curing. Also concrete specimens made with 60% bacterial water showed higher increase in strength as compared to specimens made with 40% bacterial water in case of both higher grade (M40) and lower grade (M20) concrete.

Table 6: % Increase in tensile strength as compared to control concrete (28days)

Bacterial Concentration (cells/ml)	Increased in compressive strength (%)			
	20 MPa (40% Bacterial Water)	20 MPa (60% Bacterial Water)	40 MPa (40% Bacterial Water)	40MPa (60% Bacterial Water)
2.12×10^8	2.61	6.34	6.92	11.32
2.12×10^7	0.75	1.87	2.08	2.31
3.25×10^8	12.69	21.64	23.09	25.64
3.25×10^7	4.85	5.22	12.47	13.86
6.39×10^8	22.76	26.36	28.48	30.33
6.39×10^7	19.4	25.75	22.86	26.1
7.91×10^8	4.85	14.55	15.7	20.1
7.91×10^7	1.49	13.06	12.93	16.17

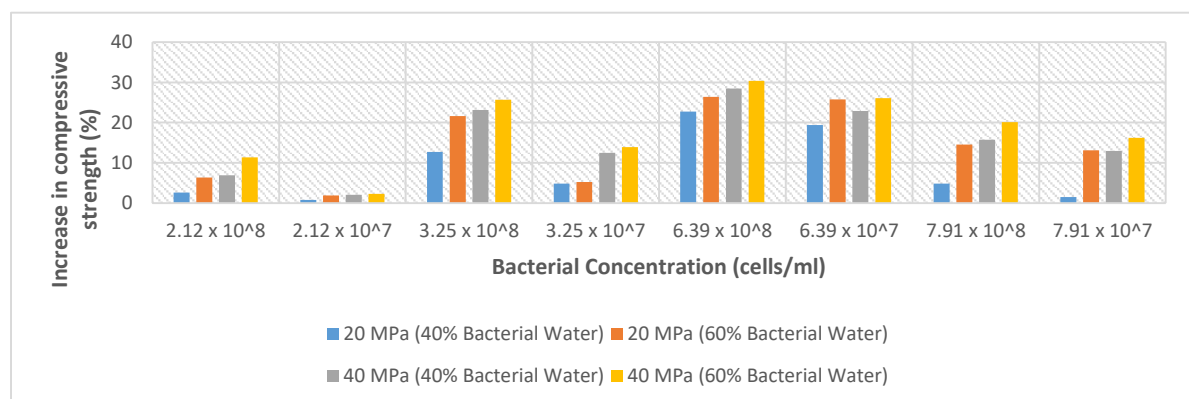


Figure 4: Increase in tensile strength as compared to control concrete (28 days)

CONCLUSIONS

Based on the limited number of variables and strength results studies, the following conclusions can be drawn.

- The increase in compressive strength is higher for all bacterial concrete as compared to control concrete with curing ages.
- The rate of strength increment is higher for 40 MPa bacterial concrete as compared to 20 MPa bacterial concrete ranging from 2% to 10%.
- Among all microbial groups, concrete specimens with bacterial concentration of 6.39×10^8 cells/ml is found to be most effective in increasing compressive strength i.e. around 10% to 18 % for 28 days of curing.
- Concrete specimens with 60% bacterial water shows more increase in strength as compared to that of 40% bacterial water in cases of both lower grade (20 MPa) and higher grade (40 MPa) of concrete.

ACKNOWLEDGMENTS

The authors gratefully acknowledge the support provided by the department of Civil Engineering, Chittagong University of Engineering and Technology (CUET) in the form of laboratory facilities for completion of this project. Authors also expressed their deep gratitude to **Prof. Dr. Md. Moinul Islam**, the Head, CE Dept., CUET, and to **Prof. Dr. Wahhida Shumi**, Department of Microbiology, University of Chittagong, for providing all kinds of support. Authors would also express their special thanks to **Royal Cement Limited**, Chittagong, for supplying cement for the works.

REFERENCES

- Jonkers, H. M., & Schlangen, E. (2007, April). Crack repair by concrete-immobilized bacteria. In *Proceedings of the first international conference on self healing materials* (pp. 18-20).
- Khaliq, W., & Ehsan, M. B. (2016). Crack healing in concrete using various bio influenced self-healing techniques. *Construction and Building Materials*, 102, 349-357.
- Muhammad, N. Z., Shafaghat, A., Keyvanfar, A., Majid, M. Z. A., Ghoshal, S. K., Yasouj, S. E. M., ... & Shirdar, M. R. (2016). Tests and methods of evaluating the self-healing efficiency of concrete: A review. *Construction and Building Materials*, 112, 1123-1132.
- Wang, J., Van Tittelboom, K., De Belie, N., & Verstraete, W. (2012). Use of silica gel or polyurethane immobilized bacteria for self-healing concrete. *Construction and building materials*, 26(1), 532-540.
- Wiktor, V., & Jonkers, H. M. (2011). Quantification of crack-healing in novel bacteria-based self-healing concrete. *Cement and Concrete Composites*, 33(7), 763-770.
- Xu, J., & Yao, W. (2014). Multiscale mechanical quantification of self-healing concrete incorporating non-ureolytic bacteria-based healing agent. *Cement and concrete research*, 64, 1-10.

EFFECTS OF DEICING SALTS ON STRENGTH PROPERTIES OF CONCRETE

M. A. Hossain*¹ & M. S. Islam²

¹ Department of Civil Engineering, Chittagong University of Engineering & Technology, Chittagong 4349, Bangladesh. E-mail: altafsunny@cuet.ac.bd

² Department of Civil Engineering, Chittagong University of Engineering & Technology, Chittagong 4349, Bangladesh. E-mail: msislam@cuet.ac.bd

*Corresponding Author

ABSTRACT

In order to keep the winter highways, clear of snow and ice deicers are applied. Deicers usually contain chlorides of salts containing mostly sodium chloride, calcium chloride, magnesium chloride etc. The increasing usage of deicers has upraised concerns over their use and are stated to have harmful effects on concrete structure through their reactions with the paste of cement and thereby reducing concrete strength and integrity. This study is aimed to investigate the effect of NaCl and CaCl₂ solutions on the compressive and tensile strength of concrete. A total of 210 nos. of 100 mm concrete cube specimens were cast and exposed to different concentrations of NaCl and CaCl₂ solutions as well as in plain water over a period of 6 months. The effects of deicing salts on concrete were evaluated based on the decrease in compressive and tensile strength of concrete as compared to plain water cured concrete of similar age and condition. Although at the early age, both the salts had a minor negative impact on concrete strength, specimens in CaCl₂ environment showed higher losses in strength (6 to 20%) than that exposed to NaCl solutions after 6 months' exposure period under identical curing conditions.

Keywords: De-icing salts, Sodium Chloride, Calcium Chloride, Compressive strength, Tensile strength.

1. INTRODUCTION

Ice and snow control processes are critical for maintaining roadways that endure the snowy and cold weather in the cold-climate zone. Deicers (chiefly chloride-based salts) are frequently used on winter streets to either break down the bond between ice and the roadway or prevent the bonding of ice to the highway. Parking places, roadway pavements, wayside hardware, and other non-highway items close to winter maintenance actions are exposed to the damaging effects of deicing salts. Deicers may also impose damaging effects on concrete structure through their reactions with cement paste or aggregates and thus lessen concrete strength and integrity, which may foster the entrance of moisture, oxygen and other aggressive agents onto the reinforcement layer promoting corrosion in reinforcement. The harmful mechanism appears to be occurred due to chemical reactions, distillations, and emulsification,

as well as the generation of further stress in the bituminous concrete (Shi et al., 2009). Expansion of concrete is a major reason for damaging concrete structure such as pavements, bridge decks, retaining walls, parking structures, and other similar structures which is a result of freezing and thawing cycling. Spalling and cracking are also the consequences of the expansion of concrete (P. K. Mehta and Paulo J. M. Monteiro, 1993). These problems are intensified due to the application of deicing salts. In the presence of moisture and deicer chemicals, freezing and thawing causes surface scaling of concrete slabs. The concentration of deicer solutions is directly related to the quantity of scaling loss to an individual concrete under freezing and thawing cycling.

2. LITERATURE REVIEW

There has been a gradual rise in the practice of using ice control products (chloride based) for winter time maintenance operations (Shi et al., 2013). The increasing use of deicing salts has raised up concerns about the harmful effects of deicers on vehicles, transport infrastructure, and the surrounding environment. Each year, substantial amounts of ice and snow control products are applied to roadways, the ecological effects of these deicing products have been questioned by regulatory and environmental organizations (Watson et al., 2007). A study investigated the ecological impacts of deicing chemicals used for ice and snow control, counting those on the ground, surface, and drinking waters (Fay and Shi, 2012).

Many researchers concentrated their study to find out the causes of deterioration of concrete due to the application of deicing chemicals. Damage of concrete by deicing salts is linked to complex processes associated with the chemical and physical change in aggregates and cement paste. In an experimental study the effects of various deicing salts on concrete weakening was investigated (Lee et al., 2000). Environmental situations (freeze/thaw and wet/dry cycling) on highway concrete samples with various deicing chemicals were simulated in the laboratory. The study reported that there had been physical and chemical effects of each deicer on the concrete samples altering the properties of dolomite coarse aggregate, the dolomite coarse aggregate-paste interface, and cement paste. Solutions of chloride usually stimulated decalcification of cement paste and transformed ettringite to chloroaluminate. Magnesium-bearing deicers initiated severe paste deterioration by developing brucite as well as non-cementitious magnesium silicate hydrate. The effects due to Mg-bearing acetates on the deterioration of concrete was more severe than those caused by Ca-acetates. It is also observed that the NaCl solution showed the least deterioration to the aggregate-cement paste. Another study reported three main ways of damaging effects of deicing solutions on Portland Cement Concrete (PCC): i) physical deterioration such as “salt scaling”; ii) chemical reactions between deicers and cement paste; and iii) deicers aggravating cement- aggregate reactions (Shi et al., 2009). A research work was devoted to finding the effects of concentrated brines of NaCl, CaCl₂, MgCl₂, and CMA on PCC and decided that both chemical and physical interactions take place within concrete when it was exposed to de-icers and freeze/thaw conditions (Sutter et al., 2008).

The chemical process through which the salt-scaling happens has been described by Neville (Neville, 1969). It was stated that saturated calcium chloride solutions were deleterious to concrete, even without freezing and thawing cycling. The saturated solution of calcium chloride resulted in mass gains, increased volume expansions, and losses in dynamic modulus of elasticity of concrete at a high w/c of 0.7. Neville further theorized that at the low w/c, degradation of concrete occurred due to leaching which resulted in loss of strength, whereas at the high w/c it happened principally from deposition and crystallization in the voids left by water molecules.

The key objective of this study was to evaluate the effects of two de-icers, namely NaCl and CaCl₂, on concrete based on variation in the compressive and tensile strength of concrete as compared to plain water cured concrete of similar age and condition.

3. STUDY DESIGN AND METHODOLOGY

In this study, the effects on concrete cured in solutions containing sodium chloride (NaCl) and calcium chloride (CaCl₂) were evaluated based on variation in the compressive strength and tensile strength of concrete as compared to plain water cured control specimens of similar age and condition. Three concentrations are tested for each de-icing chemical and the compositions of the solutions are shown in Table 3.1. The concrete mix used in the study contained a commercial brand of Portland Composite Cement (PCC) with strength class 42.9 N. The percentage of clinker, gypsum and slag, limestone, fly ash in the cement were 65–79%, 0–5% and 21–35% respectively and the specific gravity was 3.15. Concrete mix proportions are shown in Table 3.2. Coarse size sand was selected as fine aggregate and 20 mm downgraded crushed stone chips meeting the requirements of ASTM C33 was selected as coarse aggregate. Both of the aggregates were collected from the Sylhet district of Bangladesh. Table 3.3 depicts the physical characteristics of aggregates.

Table 3.1: De-icing Solutions

Deicing salt	Percentage of salt in water	Molal ion concentration
NaCl	3	1.06
	6	2.18
	9	3.38
CaCl ₂	3	0.84
	6	1.73
	9	2.67

*Distilled water used for all solutions

Table 3.2: Concrete Mix Proportions (SSD Basis)

Cement content	Sand	Coarse aggregate	Free w/c ratio
425kg/m ³	446kg/m ³	1422kg/m ³	0.40

Table 3.3: Physical Properties of Aggregates

Property	Sand	Stone Chips
Bulk specific gravity (OD basis)	2.52	2.64
Absorption capacity, %	1.32	0.78
Fineness Modulus (FM)	2.53	---
Unit weight (Dry rodded), kg/m ³	1576	1518

In the study, the effects of strength on concrete exposed to solutions containing NaCl and CaCl₂ were evaluated. Various increased percent of salt concentration in solutions was used to have the accelerated environmental effects within a short period. The study also includes control specimens that were exposed to tape water throughout the test period. The concrete ingredient materials were mixed manually poured in mould (size 100mmx100mmx100mm) and compacted. After 24 hours, the specimens were demoulded and then cured in deicer solutions at 25°C for 1, 2, 4, 13 and 26 weeks. Concrete cubes cured in tape water were used as control specimens.

A total of 210 concrete cubes (105 for compressive strength and 105 for splitting tensile strength test) were cast. The compressive strength of concrete cube specimens was determined by following EN 12390-3 (BS EN, 2009) while the splitting tensile strength of concrete was determined as per EN 12390-6 (BS EN, 2000). The splitting tensile strength is calculated by using the following formula:

$$f_{ct} = 2F / \pi Ld$$

Where, f_{ct} is the splitting tensile strength, in N/mm² or MPa; F is the maximum observed load, in Newtons; d is the cross-sectional dimension in mm; L is the length of the line of contact of the specimen in mm.

4. RESULT AND DISCUSSION

Figure 4-1 and Figure 4-2 represent the compressive strength and splitting tensile strength test results of concrete specimens cured under different de-icing salt solutions respectively. The results show that compressive and tensile strength of concrete cube specimens loss progressively with the increases of NaCl and CaCl₂ concentration at 90 and 180 days; however early strength increase is found to be marginal at 7, 14 and 28 days. In both solutions, the strength values of specimens are observed to be increased at early ages followed by gradual decrease at longer ages.

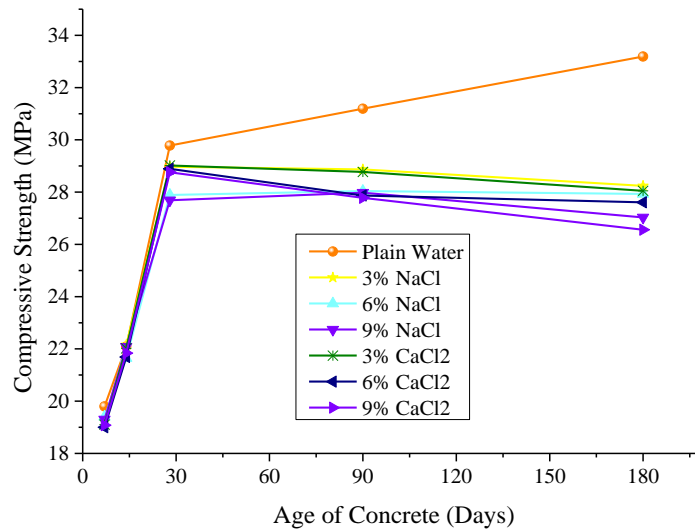


Figure 4-1: Effect of Curing Medium on the Compressive Strength of Concrete

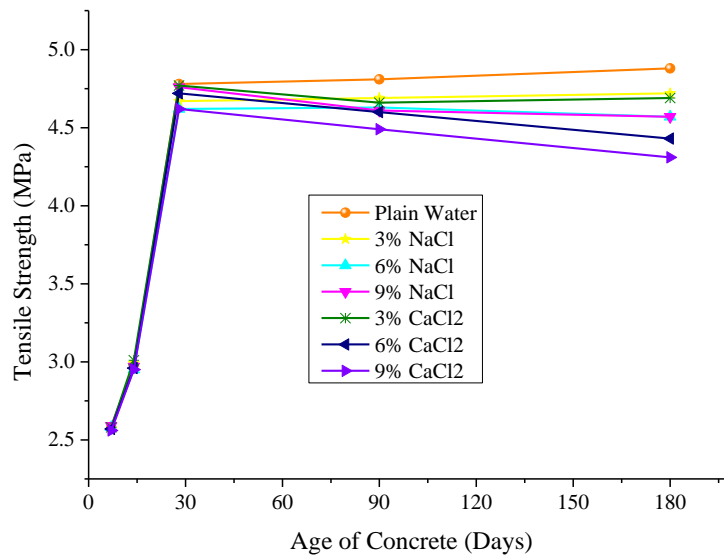


Figure 4-2: Effect of Curing Medium on the Tensile Strength of Concrete

Percentage loss in compressive strength of concrete in the deicing environment as compared to plain water concrete is shown in Figure 4-3 and percentage loss in tensile strength of the same is shown in Figure 4-4. With the effect of the different solution, the losses in the strength of concrete specimens are different. In both solutions, losses in strength show increasing trend with the increase in the study period despite some strength gain in concrete is observed at early ages. For example, at 180 days, the losses in compressive strength of concrete cured under NaCl and CaCl₂ solutions range from 14.9 to

20.0 % as compared to control concrete, whereas, there were no remarkable losses in the strength of concrete up to 28 days. However, at later ages, losses in the compressive and tensile strength of the concrete cured under CaCl_2 are much higher than the concrete cured under NaCl solutions.

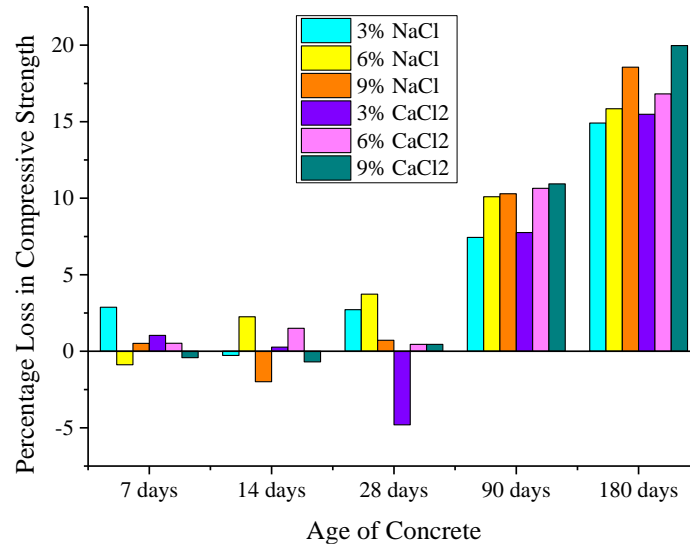


Figure 4-3: Percentage Loss in Compressive Strength of Concrete

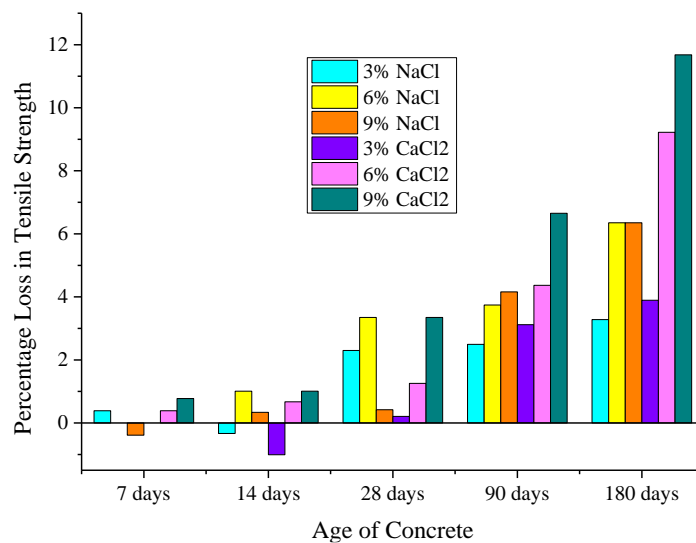


Figure 4-4: Percentage Loss in Tensile Strength of Concrete

Pore size distribution of hardened cement paste is altered in presence of chloride ions and chloroaluminate salts are the product of chloride solutions. Chloride solutions also deteriorate concrete integrity by decalcifications which is much evident at later ages. Chloride presence in pore solution, either is held to the surface of the products of hydration physically or bound to the products of hydration chemically. Chlorides act together with calcium silicate hydrate (CSH) at three dissimilar levels as a chemisorbed layer on CSH, in the CSH interlayer places or are bound in the CSH lattice intimately. Chlorides are also recognized to promote the leaching of $\text{Ca}(\text{OH})_2$ and promote the development of porous CSH including complex reactions. The formation of porous CSH, the leaching of calcium hydroxide and the decalcification effects of NaCl and CaCl_2 all play their own toll on strength deterioration of concrete.

5. CONCLUSION

Laboratory study results suggest that deicers have strength accelerating properties at initial ages which discontinue at later ages. Also, the strength development patterns indicate that due to the presence of chloride environment, concrete specimens experience long-term compressive and tensile strength losses. However, based on the limited number of scope and variables studied, the following conclusions can be drawn;

- The strength of concrete specimens in both NaCl and CaCl₂ solutions increases at early ages i.e. up to 28 days followed by losses in strength at later ages.
- The losses in compressive strength are observed to vary in the range of 14 to 19 % at 180 days whereas the losses in tensile strength are found to vary in the range of 3 to 11 % at the same age.
- Compressive strength losses of concrete in CaCl₂ were around 4 to 8 % higher than that of concrete in NaCl solutions at 180 days. Whereas the tensile strength losses of concrete in CaCl₂ were about 19 % to approximately 84 % higher than that of concrete in NaCl solutions at 180 days.

ACKNOWLEDGMENTS

The authors would like to express their gratitude to the Civil Engineering Department, Chittagong University of Engineering & Technology (CUET) for providing additional funding and laboratory services for performing this research work. The material support provided by industrial partners Diamond Cement and Planning and Development (P&D), CUET is gratefully acknowledged.

REFERENCES

- BS EN, 2009. Testing hardened concrete, part-3: compressive strength test of concrete. Eur. Comm. Stand.
- BS EN, 2000. Testing hardened concrete: Tensile splitting strength of test specimens. Eur. Comm. Stand.
- Fay, L., Shi, X., 2012. Environmental impacts of chemicals for snow and ice control: State of the knowledge. *Water. Air. Soil Pollut.* 223, 2751–2770. <https://doi.org/10.1007/s11270-011-1064-6>
- Lee, H., Cody, R.D., Cody, a M., Spry, P.G., 2000. Effects of Various Deicing Chemicals on Pavement Concrete Deterioration. *Proc. Mid-Continent Transp. Symp.* 151–155.
- Neville, A.M., 1969. Behaviour of concrete in saturated and weak solutions of magnesium sulphate or calcium chloride. *Jounal Mater. Sci.* 4, 781–816.
- P. K. Mehta and Paulo J. M. Monteiro, 1993. *Concrete: Structure, Properties, and Materials*, Second ed. Pearson College Div; Subsequent edition.
- Shi, X., Akin, M., Pan, T., Fay, L., Liu, Y., Yang, Z., 2009. Deicer impacts on pavement materials: Introduction and recent developments. *Open Civ. Eng. J.* 3, 16–27.
- Shi, X., Veneziano, D., Xie, N., Gong, J., 2013. Use of chloride-based ice control products for sustainable winter maintenance: A balanced perspective. *Cold Reg. Sci. Technol.* 86, 104–112. <https://doi.org/10.1016/j.coldregions.2012.11.001>.
- Sutter, L., Peterson, K., Julio-Betancourt, G., Hooton, D., Van Dam, T. Van, Smith, K., 2008. The deleterious chemical effects of concentrated deicing solutions on Portland cement concrete. *South Dakota Dep. Transp. Off. Res.* 5, 216. <https://doi.org/Final Report SD2002-01-F>.
- Watson, C.H.L.S., Central, L., Regional, F., Authority, T., Irector, E.X.D., Skinner, R.E., Barker, J.B., Authority, T., Behrens, M.W., Dot, T., Biehler, A.D., Dot, P., Brown, L.L., Dot, M., Canby, A.P., Transportation, S., Partnership, P., Kanafani, A.K., Engineering, C., Linnenkohl, H.E., Dot, G., 2007. Guidelines for the Selection of Snow and Ice Control Materials to Mitigate Environmental Impacts. <https://doi.org/10.17226/23178>.